Characterising microsporidian host-parasite interactions

Andrew Watson

PhD Thesis

Institute for Cell and Molecular Biosciences

Newcastle University

June 2016

Thesis submitted for the degree of doctor of philosophy at Newcastle University

Abstract

Microsporidia are an enormously successful group of obligate intracellular fungal parasites that infect most eukaryotes including humans. In my thesis I have analysed and compared microsporidian genomes to identify which genes have been conserved, and which lost, during the transition of the group to parasitism, sequenced the transcriptome of a mixed infection of *Trachipleistophora hominis* in a rabbit kidney cell line, and provided a description of the *T. hominis* intracellular lifecycle. My results demonstrate that microsporidian genome evolution is extremely dynamic; with huge loss of genes in the microsporidian common ancestor balanced by group and lineage-specific gene family expansion and innovation. Genes that are conserved among microsporidians are generally expressed at higher than average levels in the transcriptome of *T. hominis*. Lineage-specific genes show greater variation in expression, but some are very highly expressed suggesting that they play important roles in *T. hominis* biology. The transcriptomics data for *T. hominis* confirmed that it contains one of the largest microsporidian genomes in terms of gene content and also identified previously unannotated genes, some of which may have important roles in the parasite. Detailed analysis of my gene expression data demonstrated that differential expression of duplicate genes is a general feature of *T. hominis* gene families, including nucleotide transport proteins that are already known to have important roles in the microsporidian lifestyle. A method for partially synchronising the *T. hominis* infection was established and used to investigate the development of the infectious cycle using light microscopy and antibodies to *T. hominis* proteins. My observations suggest that the infection proceeds in a reproducible and predictable pattern under the experimental conditions used; providing a tool for future detailed study of how *T. hominis* infects and exploits eukaryotic host cells.

Acknowledgements

This PhD project was generously funded by the BBSRC. I am indebted to my supervisors Martin Embley, Robert Hirt and Tom Williams for their support and patience throughout this project. They have often gone out of their way to help and to guide me when I most needed it and none of this would have been possible without them.

All of my colleagues in the Embley/Hirt lab have contributed to my project. I would like to thank Sirintra Nakjang, Kacper Sendra, Alina Goldberg, Sarah Heaps, Peter Major, Cedric Bicep, Will Lewis, Svetlana Cherlin and Shaojun Long. I would especially like to thank Alison Gregory and Paul Dean who provided some of my early training, Eva Heinz, who supervised my first project as an undergraduate and continues to send me excellent fantasy books, and again Tom Williams who introduced me to programming and coffee. Perhaps most importantly, thanks go to our lab technicians Ekaterina Kozhevnikova and Maxine Geggie, who support all of our work and somehow manage to keep us all in check. I would also like to thank all of the support staff in ICaMB, and particularly Louise Campbell who has put up with my barrage of emails. Outside of the Embley/Hirt lab I would like to thank my collaborators in Exeter, Bryony Williams, Scott Campbell and Karen Moore, who were hugely supportive during my visit. I would also like to thank Trevor Booth at Newcastle University Bioimaging Unit, Tracey Davey at Newcastle University Electron Microscope Research Service and the Exeter Sequencing Facility.

My friends have provided a huge support base in the last four years. While there are too many people to mention, I would particularly like to thank Phil for coping with living with me for the majority of the period, Elizabeth, Anna, Clare, Keith, Jonathan and Adam, and my fellow PhD students Chris. I would also like to thank all of my friends in various north east Gilbert and Sullivan societies who persevered to drag me out of the lab to their strange world and teach me to sing despite my initial protests.

Of course my final thanks go to my family; especially Mam, Dad, Sarah and Tom, but also my extended family, who will never tire of making Sherlock Holmes jokes at my expense.

Table of Contents

Table of figures

List of abbreviations

ACS	Acetyl-CoA synthetase
AIDS	Acquired immune deficiency syndrome
AMP	Adenosine monophosphate
AOX	Alternative oxidase
AsnA	Asparagine synthetase A
ATP	Adenosine triphosphate
BLAST	Basic Local Alignment Search Tool
CDA	Chitin deacetylase
CHS	Chitin synthase
CoA	Co-enzyme A
DNA	Deoxyribonucleic acid
ds	Double stranded
KOG	Eukaryotic orthologous groups
FPKM	Fragments per kilobase per million mapped reads
GFA1	Glutamine-fructose-6-phosphate aminotransferase
GNA1	Glucosamine-6-phosphate N-acetyltransferase 1
GSH	Glutathione
GTP	Guanosine triphosphate
HGT	Horizontal gene transfer
HIV	Human immunodeficiency virus
HK	Hexokinase
HSP	Heat shock protein
LCMA	Last common microsporidian ancestor
LOESS	Local regression
MCL	Markov Clustering
MEM	Minimal essential medium
MPS	Monopolar Spindle
Msc	Mechanosensitive channel

NTT	Nucleotide transport protein
NudC	Nuclear distribution protein
Nup	Nucleoporin
ORF	Open reading frame
PBS	Phosphate buffered saline
PCM	Phosphoacetylglucosamine mutase
PDK4	Pyruvate dehydrogenase lipoamide kinase isozyme 4
PPARGC1A	Peroxisome proliferator-activated receptor gamma co-activator 1-alpha
PPI	Protein-protein interaction
PRKAA2	AMP-activated protein kinase catalytic subunit alpha-2
PTP	Polar tube protein
PV	Parasitophorous vacuole
RK	Rabbit Kidney
RNA	Ribonucleic acid
RNAi	RNA inhibition
RNAseq	RNA sequencing
rRNA	Ribosomal RNA
SE	Standard error
SNP	Single nucleotide polymorphism
SOD	Superoxide dismutase
SPB	Spindle pole body
ss	Single stranded
SWP	Spore wall protein
TEM	Transmission electron microscopy
TMD	Transmembrane Domain
tRNA	Transfer RNA
Tyr	Tyrosine
UDP	Uracil diphosphate

UGP1	UDP-N-acetylglucosamine pyrophosphorylase
UTR	Untranslated region
YNK	Nucleotide diphosphate kinase
µm	Micrometer

Chapter 1 : Introduction

1.1 A general introduction to Microsporidia

Microsporidia are a successful group of obligate endoparasitic fungi which infect eukaryotes (Hirt et al., 1999; James et al., 2013; Vávra and Lukeš, 2013). Since the initial identification of Microsporidia by Carl Wilhelm von Nägeli in 1857 the size and diversity of the group has increasingly become apparent (Franzen, 2008; Vávra and Lukeš, 2013). Current estimates suggest that there are over 1300 distinct species of Microsporidia (Vávra and Lukeš, 2013). The size of the group is paralleled by the breadth of its Eukaryote host range, spanning all major vertebrate groups and most invertebrate groups (Vávra and Lukeš, 2013). These hosts include species of economic and ecological significance, such as the honeybee where *Nosema ceranae* has been implicated in colony collapse syndrome (Vidau et al., 2011), or commonly farmed species of fish such as salmonids (Kent, 2000).

Documented cases of human microsporidiosis have risen sharply since the onset of the acquired immune deficiency syndrome (AIDS) pandemic, and fourteen species of Microsporidia have been described as causing opportunistic infection in immunocompromised humans (Didier and Weiss, 2011, 2006; Didier, 2005), including *Trachipleistophora hominis*. In addition to human immunodeficiency virus (HIV)/AIDS patients, microsporidian infections have been identified in transplant patients undergoing immunosuppressive therapy, diabetics, and ocular infections in wearers of contact lenses (Didier and Weiss, 2011). The symptoms of infection vary from species to species, and are dependent on the localisation of infection. Many of these species infect the gut, where they cause diarrhoea-like symptoms, while some, such as *Trachipleistophora hominis*, also infect muscle tissue where they are associated with muscle wasting (Didier and Weiss, 2011, 2006).

Human microsporidiosis was highlighted by the increase in immunocompromised individuals during the HIV and AIDS epidemic, however a number of recent surveys have challenged the view of Microsporidia as purely opportunistic parasites of humans (Didier and Weiss, 2011). Microsporidian infection has been associated with outbreaks of diarrhoea from contaminated cucumber (Decraene et al., 2012). Microsporidian spores were also identified in the stools of apparently healthy individuals who tested seropositive for the parasites, suggesting that they may be a more common component of the gut microbiome

than previously anticipated (Sak et al., 2011). In one recent survey in Cameroon, incidents of microsporidian spore detection in stool samples were actually higher in apparently healthy subjects compared to immunocompromised people (Nkinin et al., 2007). This suggests that Microsporidia are present in the population at higher levels than commonly appreciated.

Aside from their importance as Eukaryotic pathogens, Microsporidia have proven a valuable model for the study of basic evolutionary processes. The lack of typical mitochondrial structures in Microsporidia and their phylogenetic placement at the base of eukaryotes in early molecular sequence analyses meant that Microsporidia were proposed to belong to a group of basal eukaryotes called the "Archaezoa" which primitively lacked a mitochondrion, having diverged from other eukaryotes before the gain of the mitochondria by alpha-proteobacterial endosymbiosis (Cavalier-Smith, 1987a, 1987b). If true this would have profound implications on our understanding of Eukaryotic origins, suggesting that the development of characteristic eukaryotic features such as a nucleus and a complex cytoskeleton, predate the mitochondrial endosymbiosis.

Subsequent work to test the archaezoa hypothesis demonstrated that the apparent basal position of Microsporidia was an artefact of long-branch attraction (Hirt et al., 1999). This is a phenomenon where faster evolving sequences tend to group together in phylogenies when phylogenetic models do not appropriately deal with heterogeneity in rates of evolution. Analysis using models that account for rate heterogeneity have suggested that Microsporidia are the sister group to fungi (James et al., 2013), meaning that if Microsporidia did lack mitochondria it must be through secondary loss of the organelle. Further work identified homologues of mitochondrial proteins encoded by Microsporidia (Germot et al., 1997; Hirt et al., 1997; Peyretaillade et al., 1998), and in *T. hominis* confirmed that these proteins localise to small double-membrane bounded organelles, mitochondrial remnants called mitosomes (Williams et al., 2002). Mitochondrial proteins have since been identified in other microsporidian genomes, predominantly proteins involved in mitochondrial iron-sulphur cluster biogenesis (Goldberg et al., 2008; Hjort et al., 2010). Rather than primitively amitochondrial eukaryotes, this work demonstrated that Microsporidia are fungal pathogens (James et al., 2013) whose mitochondria have undergone extreme secondary reduction, potentially as part of the adaptation to their obligate intracellular lifecycle. The sequencing of microsporidian genomes has confirmed

that this reduction is not restricted to their mitochondria, but that the microsporidian common ancestor underwent an extreme reduction in overall coding capacity compared to its free living relatives (Corradi and Slamovits, 2011; Heinz et al., 2012; Katinka et al., 2001). Understanding the nature and extent of this reduction, and the study of Microsporidia from an evolutionary perspective, could thus help us to understand how Microsporidia adapted to their parasitic lifestyle.

Despite growing evidence of the prevalence of Microsporidia as parasites of Eukaryotes, including humans, and the importance of Microsporidia as models for reductive evolution, many aspects of the molecular basis of microsporidian infection remain uncharacterised (Vávra and Lukeš, 2013; Williams, 2009). In part this may be due to the inherent difficulty in studying the organisms. As obligate intracellular parasites the majority of the microsporidian lifecycle occurs inside its host (Cali and Takvorian, 2014). This presents barriers to genetic manipulation of the parasites both in terms of transfection and selection for transformants. Currently no tools for genetic manipulation of model Microsporidia exist. Core components of splicing machinery, Argonaute and Dicer, are present in several species including *Trachipleistophora hominis* (Heinz et al., 2012), however so far the use of this system to knockdown gene expression has only been tested in *Nosema ceranae* (Paldi et al., 2010). There are generally no methods for extracellular culture or purification of intracellular stages of the parasite lifecycle, meaning that the parasite must be co-cultured with a host organism and cell line, and that the only stage of the lifecycle that it is possible to purify is the spore. Understanding this complex life-cycle and the behaviour of the parasite in its different life-cycle stages including its morphology and gene expression, would provide a crucial framework to understanding how Microsporidia interact with their host cell.

1.2 The microsporidian lifecycle

1.2.1 Spores and Inoculation

Microsporidian spores are the vectors for transmission of the parasite. They are surrounded by a spore wall with two main layers, the endospore and the exospore (Weiss et al. 2014). In *Encephalitozoon hellem*, a close relative of *E. cuniculi*, it was shown that the exospore itself is made up of multiple layers (Biglardi et al., 1996). The exospore is thought to be primarily composed of Microsporidia-specific structural proteins. Some of these proteins have been identified and characterised, however the role they may play beyond structural integrity is

unclear (Weiss et al., 2014). *Encephalitozoon intestinalis* spores appear to adhere to host glycans, anchoring them to the cell. Removing these glycans *in vitro* has been shown to reduce spore adherence and level of infection (Hayman et al., 2005). The *E. intestinalis* endospore includes Microsporidia specific glycan binding protein Enp1, which was characterised in *E. intestinalis* (Southern et al., 2007), however this inner layer is primarily composed of alpha chitin (Weiss et al., 2014).

The mechanism by which a spore infects its host is a unique feature of microsporidian biology. Microsporidian spores contain a highly coiled proteinaceous "polar tube" (Weiss et al., 2014). The prevalent view for microsporidian infection describes the physical penetration of the host cell membrane by the explosive eversion of the polar tube during spore germination (Weiss et al., 2014). The coiling of the polar tube inside the spore means that the ejected polar tube is typically significantly longer than the spore itself. *Trachipleistophora hominis* has a spore size of just 4µm x 2.4µm but its polar tube is coiled 11.5 times inside the spore, meaning on ejection it can reach 75µm in length, approximately 19x the total length of the spore (Hollister et al., 1996). The contents of the microsporidian spore (the sporoplasm) pass through this polar tube and directly into the host cell where it can grow and replicate (Weiss et al., 2014).

Three components of the polar tube have been identified in *Encephalitozoon spp.* (including *E. cuniculi*) polar tube proteins (PTP) 1, 2 and 3 (Delbac et al., 2001, 1997; Peuvel et al., 2002). All of these proteins are unique to Microsporidia, with no significant sequence similarity to proteins from other Eukaryotes (Polonais et al., 2005). Strikingly, though homologues of the *Encephalitozoon* polar tube proteins can be identified in other species of Microsporidia they show low similarity at the primary sequence level between different species (Polonais et al., 2005), meaning a combination of features such as amino acid composition, presence of a signal peptide and genomic context have been used to identify polar tube proteins outside of *Encephalitozoon* (Cornman et al., 2009). In *Trachipleistophora hominis* only two polar tube proteins have been identified, both in the parasite genome and in spore proteomics, PTP2 and PTP3 (Heinz et al., 2012). The absence of PTP1 would be surprising considering it is considered the major polar tube protein where it has been identified (Weiss et al., 2014), and it is possible that this protein is either highly divergent in *T. hominis* or else was missed during the sequencing of the *T. hominis* genome.

1.2.2 Intracellular proliferation (merogony) and spore formation (sporogony)

The intracellular nature of the replicative stages of the parasite makes them difficult to study compared to spores. Whilst live spores can be purified from stool and tissue samples from infected individuals this is not generally true of intracellular stages of the parasite lifecycle. The only method for enriching for intracellular stages of the parasite life-cycle was developed for *Encephalitozoon cuniculi* sporonts, but this is untested for other species (Chavant et al., 2005; Taupin et al., 2006). Systems to co-culture Microsporidia *in vitro* with a host cell line to study the intracellular stages of the parasite lifecycle have only been developed for a small number of species (Cali and Takvorian, 2014). This does not include most prevalent human pathogen, *Enterocytozoon bieneusi*, which is usually isolated from the stool of infected individuals. *Trachipleistophora hominis* can be cultured with commonly used rabbit kidney cell lines (Field et al., 1996; Hollister et al., 1996), making it a valuable model for studying intracellular stages of infection in a human pathogen.

There are two defined intracellular phases of the microsporidian life-cycle. These life-cycle phases are usually localised to the host cytoplasm, however several species predominantly grow and divide within the host nucleus (Cali and Takvorian, 2014). The initial phase, merogony, involves proliferation of the parasite. Cells in this proliferative stage are called meronts. The mode of replication includes a combination of plasmotomy and binary division which can vary from species to species (Cali and Takvorian, 2014). The mode of replication in *Trachipleistophora hominis* is thought to be predominantly by binary division of binucleate to uninucleate meronts (Field et al., 1996; Hollister et al., 1996), however this is based on studies undertaken prior to the availability of specific molecular markers for the parasite.

The second phase of the intracellular lifecycle, sporogony, is the process of differentiation of cells into spores. Cells undergoing sporogony are known as sporonts. The transition between merogony and sporogony is marked by the deposition of an electron-dense material on the parasite membrane (Cali and Takvorian, 2014). In a single *T. hominis* infected cell, individual meronts from the same initial infection will differentiate to sporonts at different times, meaning that merogony and sporogony run alongside each other in the same infected cell (Field et al., 1996; Hollister et al., 1996). *T. hominis* sporonts develop within a compartment called a parasitophorous vacuole (PV). In *T. hominis* the PV appears to

form during sporogony (Field et al., 1996; Hollister et al., 1996), contrasting other species which grow within a PV throughout infection (*Encephalitozoon cuniculi*) (Cali and Takvorian, 2014; Rönnebäumer et al., 2008), or in direct contact with the host cytoplasm throughout infection with no PV formation (*Enterocytozoon bieneusi*) (Cali and Owen, 1990; Cali and Takvorian, 2014). Inside the vacuole Microsporidia undergo further binary divisions during sporogony before the differentiation into mature spores (Cali and Takvorian, 2014). In *T. hominis* there is a variation both in the total number of spore bags in an infected cell and the number of mature spores which develop from a single spore bag (Hollister et al., 1996). A maximum of ten spore bags has been observed in a single *T. hominis* infected cell, and each spore bag can contain between two and thirty-two spores, though most often eight or sixteen (Hollister et al., 1996).

1.2.3 Transmission of infection

The microsporidian spore is responsible for the dissemination of infection. This includes transmission of infection to neighbouring cells or systemic spread to new organs within the parasites host, as well as the infection of new host organisms through excretion of spores into the environment (Cali and Takvorian, 2014). Microsporidian lifecycles can be extremely complex, requiring successful transmission between multiple hosts or vertical transmission to the progeny of their host cell (Smith, 2009). While mature spores can germinate within their spore bags and infect neighbouring cells, to spread to new organs in their host or to new organisms the spores must be released from their host cell. This could occur by the lysis of the host cell, or by a non-lytic route (Cali and Takvorian, 2014). *Nematocida parisii* is the only microsporidian in which an active process of exit has been described in any detail. *N. parisii* is a parasite of *Caenorhabditis elegans*, infecting the intestinal epithelium (Troemel et al., 2008). Its host specificity means that the parasite can be co-cultured with *C. elegans in vivo*, providing a powerful model system in which to study host-parasite interactions (Troemel et al., 2008). In this system *N. parisii* was shown to interact with the host cytoskeleton, opening gaps in a cytoskeletal structure at the apical side of *C. elegans* epithelial cells called the terminal web. Spores can exit the cell without through these gaps without causing lysis (Estes et al., 2011). In both *T. hominis* and *E. cuniculi* the mechanism of release is another unknown aspect of the infectious cycle.

1.3 The impact of microsporidian genomics

In an organism that is not amenable to genetic manipulation the availability of molecular sequence data has opened up new avenues for research in Microsporidia. The first microsporidian genome sequenced was that of *Encephalitozoon cuniculi* (Katinka et al., 2001). At the time of publication this was the smallest identified eukaryotic genome at 2.9Mb in size (Katinka et al., 2001), suggesting that microsporidian genomes, in addition to their mitochondrion, are highly reduced. Since the sequencing of the *E. cuniculi* genome a flood of new data from different sequencing projects has been made available (Campbell et al., 2013; Cornman et al., 2009; Corradi et al., 2010, 2009; Cuomo et al., 2012, 2011; Desjardins et al., 2015; Heinz et al., 2012; Katinka et al., 2001). Recent comparative analysis of these genomes has revealed that the extreme levels of genome reduction observed in *Encephalitozoon spp.* are not typical for Microsporidia (Heinz et al., 2012). Genome sizes varied between 2.3Mb - 51.3Mb, however the largest source of this variation was in genome size and the quantity of non-coding DNA (Desjardins et al., 2015; Heinz et al., 2012). In terms of coding capacity, Microsporidia show reduction in both the number of genes (generally less than ~3000) and average protein size compared to their free living relatives (Heinz et al., 2012). *Trachipleistophora hominis* has one of the largest protein coding capacities of any microsporidian at 3266 proteins (Heinz et al., 2012), exceeded only by the recently sequenced *Edhazardia aedis* genome at 4190 proteins (Desjardins et al., 2015).

With access to molecular sequence data from the parasite the function of proteins can be predicted based on similarity to characterised proteins in other organisms or on sequence properties (such as presence or absence of signal peptides (Petersen et al., 2011) or transmembrane domains (Krogh et al., 2001; Sonnhammer et al., 1998). Comparing which genes are present in microsporidian genomes to their free living relatives has revealed what kind of genes were lost during the groups extreme genome reduction. Genome analysis has demonstrated that the reduced protein coding capacity of Microsporidia includes the loss of enzymes in crucial biosynthetic pathways for a free-living non-parasitic lifestyle (Heinz et al., 2012; Katinka et al., 2001). An example is provided by the absence of pathways for oxidative phosphorylation and *de novo* biosynthesis of nucleotides in Microsporidia *E. cuniculi* and *T. hominis* (Heinz et al., 2012; Katinka et al., 2001). ATP is required by the parasite, both as a vital cellular energy resource and as a precursor for nucleotide biosynthesis. While *T. hominis* and *E. cuniculi* retain the pathways for glycolysis for substrate level production of

ATP from ADP, this relies on a net supply of ADP and is unlikely to meet the replicating parasites energy demands (Heinz et al., 2012; Katinka et al., 2001). As *T. hominis* and *E. cuniculi* are unable to synthesise these molecules themselves they must acquire them from their host. Candidate ATP transport proteins were identified in microsporidian genomes based on their homology to characterised *Chlamydia* nucleotide transport proteins (NTTs) (Katinka et al., 2001; Tsaousis et al., 2008). Phylogenetic analysis indicates that an NTT was acquired a single lateral gene transfer to the common ancestor of Microsporidia from bacteria (Tsaousis et al., 2008), where they play a similar role in ATP acquisition. The lateral gene transfer event was followed by lineage specific expansions of the family by gene duplication (Heinz et al., 2014). The activity of candidate transporters from two species, *Trachipleistophora hominis* and *Encephalitozoon cuniculi*, have been characterised by heterologous expression in *Eschericha coli*, where they were able to transport purines (Heinz et al., 2014; Tsaousis et al., 2008). This could fulfil the parasites energy demands during infection, compensating for their own reduced metabolisms. Microsporidia lack pathways required to convert purines to pyrimidines, which would still be required for DNA synthesis. Recently a promising candidate for pyrimidine transport was identified in *Nematocida parisii*, a NupG-like protein (Cuomo et al., 2012). Similar to the *NTTs,* the NupG family is conserved in all sequenced Microsporidia and has undergone independent expansion events by gene duplication in different microsporidian lineages (Cuomo et al., 2012).

Despite lacking pathways for mitochondrial ATP production by oxidative phosphorylation, Microsporidia have retained a reduced form of the organelle called the mitosome, originally identified in *Trachipleistophora hominis* (Williams et al., 2002). Microsporidian homologues for proteins in the iron-sulphur cluster biogenesis pathway have been shown to localise to the mitosome in *Trachipleistophora hominis* and *Encephalitozoon cuniculi* (Goldberg et al., 2008; Hjort et al., 2010; Williams et al., 2002). The proteins required for this pathway are conserved in the majority Eukaryotes, with iron-sulphur clusters required for the function of a broad range of essential cytosolic and nuclear metalloproteins (Lill and Mühlenhoff, 2008). It is the only known mitochondrial pathway essential for yeast viability (Lill and Mühlenhoff, 2008). Several microsporidian iron-sulphur cluster biogenesis proteins were able to functionally compliment deletions of their homologues in yeast (Goldberg et al., 2008; Hjort et al., 2010), demonstrating they are likely

to retain their ancestral function in the microsporidian mitosome. One of the few homologues of mitochondrial genes retained by Microsporidia but not directly associated with iron-sulphur biogenesis, alternative oxidase (AOX), has been predicted to play a role in substrate level ATP production by glycolysis, however it is unclear when this pathway is active in Microsporidia (Dolgikh et al., 2011; Williams et al., 2010).

As Microsporidia are characterised by an extreme reduction in protein coding capacity, much post-genomics research has focused on which genes pathways have been lost or retained in the group. In *T. hominis* this reduction was recently shown to be a more dynamic process than previously appreciated, balanced by the expansion and gain of protein families by *de novo* gene formation, duplication events, and lateral gene transfer (Heinz et al., 2012). These expanding gene families include the previously discussed transporter families, NupG and NTT (Cuomo et al., 2012; Heinz et al., 2014). Other gene family gains or expansions against the background of genome reduction in Microsporidia are likely to play important roles in the lifecycle of the parasite. Furthermore, those genes which are retained in all species of Microsporidia despite the reduction in protein coding capacity are likely to play roles in the core biology of the parasite, including its pathogenesis. The availability of several microsporidian genomes means that identification of core and expanded microsporidian genes is now possible.

1.4 Transcriptomics as a tool to study microsporidian-parasite interactions

RNA sequencing (RNAseq) is a powerful tool for the quantitative study of gene expression, which can be used to examine differential expression of genes between treatment groups or time points. The single nucleotide resolution means that it is also possible to compare the quantity of different RNA isoforms in the sample, for example the quantity of different splice isoforms, or quantity of different isoforms resulting from expression in a heterozygous organism (Mortazavi et al., 2008; Nagalakshmi et al., 2008). In Microsporidia the majority of molecular level characterisation to date is based on the sequencing and annotation of genomes. Important microsporidian proteins have been identified and functionally characterised in *Trachipleistophora hominis*, including ATP transport proteins and the iron-sulphur cluster biogenesis machinery (Goldberg et al., 2008; Heinz et al., 2014, 2012; Hjort et al., 2010). Layering transcriptome data on to this data can help to confirm the validity of

these genome annotations, as well as to provide data on the level and timing of expression of these genes, which is important if we are to understand their function in the cell more fully.

Recently the transcriptomes of several microsporidian species have been studied. These include *Edhazardia aedis* (Gill et al., 2008), *Encephalitozoon cuniculi* (Grisdale et al., 2013), *Nematocida parisii* (Cuomo et al., 2012)*, Spraguea lophii* (Campbell et al., 2013), and a combined study of *Edhazardia aedis* and *Vavraia culicis* (Desjardins et al., 2015). The studies used similar techniques; however the experimental design and the analysis of the transcriptome data from each study had markedly different focuses and so have contributed differently to our understanding of microsporidian molecular biology. Collectively the *Spraguea lophii, Encephalitozoon cuniculi* and *Nematocida parisii* transcriptomes were used to improve genome annotation, study gene splicing patterns and efficiency, and to examine the nature of transcript UTRs (Campbell et al., 2013; Cuomo et al., 2012; Grisdale et al., 2013). In *S. lophii* RNA was purified from *in vitro* germinated spores. This, in combination with secretion proteomics data, allowed the group to identify sets of highly expressed hypothetical microsporidian proteins that may play important roles in the spore or early infection (Campbell et al., 2013). The recently published transcriptomes of *V. culicis* and *E. aedis* focusing on host parasite-interactions, including genes expressed during the parasite lifecycle and interestingly the host response to infection (Desjardins et al., 2015). *Trachipleistophora hominis* has been used as a model microsporidian for the study of gene function in Microsporidia, as previously discussed. Coupling this functional data with a transcriptome of the parasite may help to expand on this functional characterisation. Further, no previous study has explored how the transcriptome of a microsporidian relates to the evolutionary history of the organism. *T. hominis* has a relatively large genome compared to other Microsporidia, despite genome reduction in the microsporidian ancestor (Heinz et al., 2012). This large genome includes a range of ancestrally inherited genes and *T. hominis* lineage -specific innovations (Heinz et al., 2012), providing an opportunity to explore how these different sets of genes are expressed in the parasite.

Chapter 2 : Materials and Methods

2.1 Genome and gene family analysis

2.1.1 Homologous gene family construction

Homologous microsporidian gene families were constructed in collaboration with Dr. Sirintra Nakjang. Dr. Sirintra Nakjang performed the clustering while I was involved in the experimental design and assessment of cluster quality; including the selection of species and parameters used in the analysis. Briefly; all available protein sequences from eleven microsporidian (Table 2.1), six fungal, and three animal genomes were classified into clusters of homologs using Markov Clustering (MCL) (Enright et al., 2002). This method uses similarity results provided by all vs all Blast searches to generate clusters. BlastP (Altschul et al., 1990) with a low complexity mask was used for sequence similarity searches. The input values for MCL were e values (cut-off ≤ 10−5) from all-against-all BlastP searches with an alignment length cut-off as follows: 0.5 for both query and target sequences if both sequences are from non-microsporidian genomes, 0.5 for either query or target sequence if they both are from microsporidian genomes, and 0.45 for microsporidian sequence if searches against sequences from non-microsporidian genomes. Less strict alignment length cut-off values were applied to microsporidian protein sequences, because they are often shorter and more divergent than their homologs in fungal or animal genomes.

The key parameter for MCL clustering is the inflation value, which controls the tightness (granularity) of clusters. The procedure for selecting inflation rate for MCL is the same procedure as used by Carman and Han (2011) and Heinz et al. (2012) (Carman and Han, 2011; Heinz et al., 2012). Inflation rates between 1 and 10 in increments of 0.2 were tested for clustering. The F-measurement (Paccanaro et al., 2006) was used to assess the quality of clusters generated with each inflation value. This measurement describes the results of a comparison between the clusters generated by MCL clustering and a reference set of clusters. The references cluster set was made up of 15 well-characterised proteins with different levels of conservation in Microsporidia and in other opisthokonts. Broadly conserved proteins included in the reference dataset included DNA polymerase alpha and delta, RNA polymerase, nucleoporin (Nup) 170, members of the TCP-1 ring complex chaperone family, pyruvate kinase, glycerol-3-phosphate dehydrogenases, phosphoacetyl-glucosamine mutase, superoxide dismutase 2, and iron sulphur cluster assembly protein

Isd11. Reference protein families that had no homologues in microsporidians but were broadly conserved in other opisthokonts included nucleoporins Nup84, Nup188, and Nup192. Polar tube protein 2 (PTP2) was used as a representative of a microsporidian-specific protein family. I additionally manually explored the clustering of gene families that were not included in the calculation of the F-measurement but were the focus of research in the host laboratory, including the nucleotide transport proteins (NTTs) and Nucleoside permease (NupG) families. I also explored cluster properties such as the number of "core" microsporidian genes (defined below) under different parameters. An inflation rate of I = 1.2 yielded the best F-measurement value of 0.4 and was used for further analysis.

Microsporidian sequences are often highly divergent from their fungal and animal homologs, and therefore the Blast cut-off values described above are too strict for some of these divergent sequences to form a cluster with homologs from outside the Microsporidia. As a result, an exclusive cluster is formed that contains only microsporidian sequences despite the inclusion of known opisthokont homologues in the dataset, which form a separate cluster. To reconcile fungal and animal homologs of these microsporidian sequences, the microsporidian-only clusters were merged with another cluster if at least one member from each of the two clusters were reciprocal best BlastP hits, that is, two sequences, one from each cluster, that are each other's respective top BlastP hit (e value cut-off: 0.001). The resultant protein family clusters were used in all subsequent analyses.

Microsporidian species	Known hosts	Estimated genome size	Number of predicted protein-coding genes	%GC content	Reference
***Encephalitozoon cuniculi* GB-M1**	Mammals	2.9 Mb (11 chromosomes)	1996	47	(Katinka et al. 2001)
***Encephalitozoon intestinalis* ATCC 50506**	Mammals	2.3 Mb (11 chromosomes)	1833	41.4	(Corradi et al. 2010)
***Encephalitozoon hellem* ATCC 50504**	Mammals, birds	2.5 Mb (11 chromosomes)	1848	43.4	(Pombert et al. 2012)
***Encephalitozoon romaleae* SJ-2008**	Insects	2.5 Mb (11 chromosomes)	1831	40.3	(Pombert et al. 2012)
***Nosema ceranae* BRL01**	Insects	7.86 Mb of 8.6 Mb	2060	25.27	(Cornman et al. 2009)
***Vittaforma corneae* ATCC 50505**	Mammals	3.21 Mb	2248	36.47	*
Trachipleistophora hominis	Mammals, insects	8.5 Mb	3266	31.91	(Heinz et al. 2012)
Vavraia culicis floridensis	Insects	6.12 Mb	2780	39.75	*
***Nematocida sp1* ERTm2**	Nematodes	4.7 Mb	2770	38.3	(Cuomo et al. 2012)
***Nematocida parisii* ERTm1**	Nematodes	4.07 Mb	2661	34.4	(Cuomo et al. 2012)
***Nematocida parisii* ERTm3**	Nematodes	4.15 Mb	2726	34.5	(Cuomo et al. 2012)

Table 2.1: Species included in the comparative analysis of microsporidian genomes.

* Data from the Microsporidia Comparative Sequencing Project, Broad Institute of Harvard and MIT (http://www.broadinstitute.org/)

Outgroup Species	Estimated genome size	Number of predicted protein-coding genes	%GC content	Reference
Homo sapiens	3231.3 Mb (23 Chromosomes + MtDNA)	70,076	47	(Venter et al., 2001)
Apis mellifera	246.9 Mb (16 chromosomes + Mt DNA)	21777	34.1	(Consortium, 2006)
Tetraodon nigroviridis	342.4 Mb	27,918	46.6	(Crollius et al., 2000)
***Saccharomyces cerevisiae* S288c**	12.3 Mb (16 chromosomes)	5404	38.42	(Goffeau et al., 1996)
***Schizosaccharomyces pombe* 972h**	12.6 Mb	5133	36.0	(Wood et al., 2002)
***Coprinopsis cinerea* okayama7#130**	36.1 Mb	13356	51.6	(Stajich et al., 2010)
Candida albicans	8.5 Mb (Haploid version)	6276	33.7	(Inglis et al., 2012; van het Hoog et al., 2007)
***Rhizopus oryzae* strain RA 99-880**	39 Mb	17459	35.4	(Ma et al., 2009)
***Neurospora crassa* OR74A**	40.7Mb	11390	48.6	(Galagan et al., 2003)
***Batrachochytrium dendrobatidis* JEL423**	23.7Mb	8794	39.3	*

Table 2.2: Summary of opisthokont outgroups to Microsporidia included in the comparative analysis.

* Data from the *Batrachochytrium dendrobatidis* Sequencing Project, Broad Institute of Harvard and MIT (http://www.broadinstitute.org/)

2.1.2 Identification of core gene families

A custom Python script was used to mine gene family data and identify “core” microsporidian gene families from the dataset generated in 2.2.1. “Core” gene families were defined those conserved across nine of eleven microsporidian species included in the analysis rather than in all eleven species. Several of the genomes included in the analysis are either in a draft or partial state. The relaxation of the parameters in the definition of the core microsporidian genome to those in nine of eleven genomes allows for the potential absence of gene family members in individual species due to missing sequence data. The script used in the analysis is described below.

2.1.3 Identification of expanded microsporidian gene families

Gene families that may have expanded in Microsporidia were identified using the same custom Python script. Potential expansions were defined as those gene families present in higher numbers in at least one microsporidian than any of the opisthokont outgroup species included in the analysis. Those gene families predicted to be expanded in the common ancestor of Microsporidia using Dollo parsimony were focused on in the analysis; and particularly those that had seemingly retained both duplicate copies of the gene throughout Microsporidia. Dollo parsimony assumes that something lost in a particular lineage cannot be regained, allowing simplification in the reconstruction of evolutionary history. Under Dollo parsimony, gene families predicted to expand in the LCMA were those which included more members in at least one species on either side of the root of Microsporidia than in any of their free living relatives. Phylogenies for candidate gene families were constructed based on Bayesian analysis using PhyloBayes (Lartillot et al., 2009). Protein sequences in each family were aligned using two different methods, MAFFT (Katoh, 2002) and MUSCLE (Edgar, 2004). A consensus alignment was then generated using T-Coffee (Notredame et al., 2000), and the resulting alignment was trimmed using trimAl (Capella-Gutiérrez et al., 2009) with the automated1 option to remove regions of low confidence alignment. Automated1 applies a heuristic to automatically select the trimming mode based on the properties of the multiple sequence alignment, choosing between from three different modes; gappyout, strict and strictplus. The CAT60 model (Le et al., 2008) implemented in PhyloBayes (Lartillot et al., 2009) was used on trimmed multiple sequence alignment. A consensus tree of trees generated from two independent Markov chain Monte Carlo chains was constructed.

Convergence was assessed using the criteria of 1) a maximum bipartition discrepancy (maxdiff) < 0.1 and 2) a minimum effective size > 100 for all sampled parameters.

2.1.4 Script used for the identification of gene families

Below is a summarised version of the script used to identify gene families with specific patterns of distribution in Microsporidia, including those identified in the core microsporidian genome, those predicted as expanded in Microsporidia, and those co-segregating with the microsporidian RNAi machinery. Identifying different features was achieved by varying the output options; of which three examples are included below. Comment lines starting with # are placed before elements of the script to explain the role of each step, as per standard practice in python.

```
# Step 1: Import python modules containing functions used later in the script.
import sys
import re
import os

# Step 2: Define file handle to an output file.
result = open("output.txt", “w")

#Step 3: Define file handle to read the file containing information on gene family clusters.
This is a text file in which each line in a tab delimited list of unique gene identifiers
corresponding to the genes assigned to a cluster. These identifiers include a unique four
letter species specific tag (listed below) which can be searched for using regular expressions.

clusters = open("clusters_final.txt")

#Note: A list of species included that are included in the clusters and their corresponding
unique identifiers are included for reference.

#hosa   [Homo sapiens]
#apme [Apis mellifera]
#teni    [Tetraodon nigroviridis]
#caal    [Candida albicans]
#rhor    [Rhizopus oryzae]
#coci    [Coprinopsis cinerea]
#sace    [Saccharomyces cerevisiae S288c]
#sapo   [Saccharomyces pombe]
#trho    [Trachipleistophora hominis]
#enbi    [Enterocytozoon bieneusi H348]
#noce   [Nosema ceranae BRL01]
#encu   [Encephalitozoon cuniculi GB-M1]
#enin    [Encephalitozoon intestinalis ATCC 50506]
#ocba   [Octosporea bayeri]
```

#necr [Neurospora crassa]
#nep1 [Nematocida parisii ERTm1]
nep3 [Nematocida parisii ERTm3]
nesp [Nematocida sp.]
vacu [Vavraia culicis]
enhe [Encephalitozoon hellem]
enro [Encephalitozoon romalae]
vico [Vittaforma corneae]

#Step 5: Read each line in the cluster file one by one; which equates to considering one cluster at a time.

for line in clusters:

#Step 6: For each cluster, create a counter starting at zero for each individual species included in the analysis. Three species are shown below but this is repeated for all species in the analysis.

```
homo_count = 0
cere_count = 0
coci_count = 0
```

#Step 7: For each cluster, create additional counters for other elements of the analysis, such as the total number of fungal, animal or microsporidian species represented in a cluster.

```
fungi_count = 0
animal_count = 0
microsporidia_count = 0
```

#Step 8: Use a regular expression to search for each instance of the unique species identifier within a cluster for each species included in the analysis individually. Whenever the identifier is found the count for that species is increased by one. This traces the number of genes from any given species within a cluster.

```
for match in re.finditer("trho", line):
        thom_count = thom_count + 1
for match in re.finditer("hosa", line):
        homo_count = homo_count + 1
```

#Step 9: Use the counts of the number of genes within a cluster for each species to generate additional metrics for the number of microsporidian, animal and fungal species represented in each gene family. The number of microsporidian species represented in a gene family was used to identify core microsporidian genes. The number of animal or fungal genes was used to determine whether genes were microsporidia specific or present in other opisthokonts.

#Step 9a: Repeat for all microsporidian species to count the number of microsporidian species represented in a gene family.

```
if thom_count > 0:
        microsporidia_count = microsporidia_count + 1
```

#Step 9b: Repeat for all fungal species to count the number of animal species represented in a gene family.

```
if sace_count > 0:
        fungi_count = fungi_count + 1
```

#Step 9c: Repeat for all animal species to count the number of animal species represented in a gene family.

```
if sace_count > 0:
        fungi_count = fungi_count + 1
```

#Step 10: Define conditions for data output, which allows the extraction of different gene family sets such as core gene families or gene families particular to specific lineages. Three different output options are listed below as examples.

#Step 10a: Identification of core microsporidian gene families – those conserved in nine or more microsporidians included in the analysis.

```
    if microsporidia_count > 8:
```

#Step 10b Identification of *T. hominis/V. culicis* lineage specific genes:

```
    if thom_count > 0 and vacu_count > 0 and microsporidia_count < 3 and fungi_count
    < 1 and animal_count < 1:
```

#Step 10c: Identifying clusters that, within microsporidia, exclusively include species that also encode the RNAi machinery.

```
    if thom_count > 0 and noce_count > 0 and vacu_count > 0 and vico_count > 0 and
    cuni_count  < 1 and inte_count < 1 and nep1_count < 1 and nep3_count < 1 and
    enhe_count < 1 and enro_count < 1 and nesp_count < 1:
```

#Step 11: Write a file containing the identifier for each cluster that is identified under the selected conditions and the number of genes in each species. This can be edited to include the unique identifiers of genes within the clusters for all or select species.

```
        lines=line.split()
        result.write (lines[0] + "\t" + str(homo_count) + "\t" + str(cere_count) + "\t" +
        str(teni_count) + "\n")
clusters.close()
result.close()
```

2.1.5 Analysing the effect of core membership on level of expression in E. cuniculi and N. parisii

To estimate the effect of core membership on expression level, we fit a linear mixed-effects model in a Bayesian framework using OpenBUGS (Lunn et al., 2009) and the "BRugs" R package to avoid complications with ML parameter estimation for unbalanced data (e.g., differing numbers of genes per gene family). Estimates are posterior medians and effects are judged to be significant when the 95% Bayesian credible interval does not overlap zero. The reported results were robust to the choice of prior. We investigated the relationship between $\log_e$ transformed expression levels (FKPM values), core status (binary fixed effect), time point (continuous covariate), and nested random effects for gene family in core status and gene in gene family.

2.2 Transcriptome analysis

2.2.1 Culture of T. hominis infected RK-13 cells

T. hominis was grown in co-culture with RK-13 cells (Hollister et al. 1996) grown in complete minimal essential medium (MEM); which contains 10% heat inactivated foetal calf serum and antibiotics (Penicillin/Streptomycin (0.1mg/ml), Ampicillin B (1µg/ml) and Kanamycin sulphate (0.1mg/ml)).

For the RNAseq study in chapter 4 a single 175cm^2 flask of RK-13 cells was grown to confluence (defined as a continuous cell monolayer) and split into three separate flasks. These flasks were incubated in parallel until confluence, when each was again split into two centrifuge tubes (~1.5x10^6 RK-13 cells per tube). Samples were spun at 400g and trypsin removed. The cells were resuspended in 5ml completed MEM. Spores were freshly harvested from the culture media of 20 flasks of *T. hominis*-infected RK-13 cells by centrifugation, followed by two washes in PBS (Heinz et al., 2012). The final spore pellet was resuspended in 400µl PBS (~2.3x10^7 spores/ml), and 100µl of this spore suspension was added to one of the two centrifuge tubes containing RK-13 cells, giving a multiplicity of infection of ~2 spores per host cell. Cells were incubated for 10 minutes at room temperature before seeding to a new 175cm^2 flask containing 40ml completed MEM. Flasks of uninfected and *T. hominis* infected RK-13 cells were raised in parallel for 7 days post inoculation. As the multiplicity of infection was relatively low, cells were trypsinised and split twice as previously described. Unpublished data from the host laboratory suggests that

splitting the cell culture in this way is effective in boosting overall levels of infection. Two days after the final trypsinisation the cells were harvested in 6ml of RNAprotect, which was collected in 3ml aliquots and immediately frozen at -20^{o}C. Frozen cells were later transferred to -80^{o}C. At this stage, approximately 60% of cells in flasks to which spores had been added exhibited signs of infection by *T. hominis*.

2.2.2 Preparation of RNA for sequencing

One of the 3ml aliquots of cells suspended in RNAprotect (Qiagen) was thawed for each sample and pelleted by centrifugation at 400g. All RNAprotect was removed by pipetting and cells were resuspended in 1ml TRIZol reagent (Invitrogen). The TRIzol cell suspension was exposed to three rounds of bead beating for 20s at 5 m/s in order to lyse cells and spores, after which total RNA was purified from each sample using the standard TRIzol (Invitrogen) extraction protocol. This includes chloroform based phase separation of RNA from proteins and DNA, RNA precipitation in 100% isopropanol, and RNA washing in 75% ethanol. An additional clean-up step was performed using the GeneJet RNA column purification kit (ThermoScientific) to remove residual organic solvents and genomic DNA from the purified total RNA. RNA was eluted from the GeneJet column in 50µl of nuclease free water. A 10ul aliquot of total RNA was taken for assessing RNA concentration, purity and degradation, while the remaining sample was stored at -80^{o}C until submission for sequencing. Initial RNA concentrations and purity were assessed on the Nanodrop 2000.The RNA integrity and final RNA concentrations were assessed using the Agilent RNA 6000 Nano Kit on the Agilent 2100 BioAnalyser. All samples yielded 50µl of RNA of concentrations between 400 and 600 ng/µl, providing sufficient material for RNA sequencing (with 5µg of RNA requested for submission for RNA sequencing). The RNA integrity values of these samples were >6.5, suggesting only minor RNA degradation may have occurred during RNA purification. All subsequent sequence library preparation and sequencing was carried out by Exeter Sequencing Facility in collaboration with Karen Moore. Briefly, Poly A RNA was enriched from 5µg of purified total RNA. Libraries were prepared using the ScriptSeq™ v2 RNA-Seq Library Preparation Kit (Epicentre Biotechnologies) and sequenced on the Illumina HiSeq 2500 in Rapid-Run mode; producing non strand specific 100bp single-ended reads. Each library was sequenced on two different lanes of the sequencer, providing technical replication.

2.2.3 Processing and analysis of RNAseq data

The *Trachipleistophora hominis* genome and annotation (Heinz et al., 2012) were obtained from NCBI, whilst the genome and annotation of the European rabbit (*Oryctolagus cuniculus:* GCA_000003625.1) were obtained from the Ensembl database. Bowtie2 (Langmead and Salzberg, 2012) was used to separately index the genomes of *T. hominis* and *O. cuniculus.* Quality control on the raw RNA sequencing reads was performed using FastQC (Andrews, 2010) and Illumina sequencing adapters and low quality bases were trimmed using fastq-mcf (Aronesty, 2011) with default settings. In order to quantify the expression levels of *T. hominis* transcripts, and for novel transcript discovery, TopHat2 (Kim et al., 2013) was used to map quality-filtered reads from each infected sample to the *T. hominis* genome using default parameters. Transcripts were assembled and quantified using cufflinks (Trapnell et al., 2010). The final transcriptome assembly was generated using cuffmerge (Trapnell et al., 2010). All sequence data associated with this project has been deposited at NCBI under the BioProject ID PRJNA 278775. Linear mixed-effect models were used to assess differential expression between different categories of genes within the parasite transcriptome. We fit functional category as a fixed effect, with random effects for gene, technical replicate, and biological replicate, and used $\log_e$ FPKM values as the response variable.

Transcripts that mapped to unannotated regions of the *T. hominis* genome were screened for potential ORFs by using BLASTx to search against the nr database with an E-value threshold of 0.01. SNPs were identified using SamTools mpileup and bcftools (Li et al., 2009). Vcfutils.pl varFilter was applied under default settings to remove low quality SNPs, with the addition of a minimum read depth of 10 (Danecek et al., 2011). An additional filter was applied to remove bases with low mapping quality scores. Values of 20, 40, 60 and 80 were tested. In all cases application of the filter reduced non-peak (0.5 frequency) signals while retaining the overall distribution of the allele frequency spectrum. We used a value of 60 as a balance between stringently filtering out low quality mapping and retaining data. The location of SNPs relative to annotated *T. hominis* genes and the impact of SNPs on annotated protein-coding sequences were assessed using SNPeff (Cingolani et al., 2012b) and processed using SNPsift (Cingolani et al., 2012a).

To maximise the data available for intron detection, reads from all samples including *T. hominis*-infected cells were pooled and mapped onto the *T. hominis* reference genome

using TopHat2 (Kim et al., 2013). Junctions mapping to the same region of the *T. hominis* genome were merged. The intron junctions identified from this mapping were manually filtered so as to retain only those junctions covered by more than one read and that did not span a gap in the *T. hominis* genome assembly.

For quantification of *O. cuniculus* transcripts, TopHat2 (Kim et al., 2013) was used to map reads from all samples from one lane of the sequencer to the *O. cuniculus* genome, and transcripts were assembled and quantified using cufflinks as described above. The abundance of transcripts in the three flasks of uninfected RK-13 cells was compared to that in the three flasks of *T. hominis* infected RK-13 cells using cuffdiff to test for differential expression (Trapnell et al., 2013). All RNA sequencing results were analysed in R using the cummeRbund package (Trapnell et al., 2012). Reciprocal best blast of rabbit genes against the KEGG (Kanehisa and Goto, 2000) reference protein dataset and the KOBAS 2.0 pipeline (Xie et al., 2011) were used was used to annotate the rabbit genome with KEGG categories and to test for enrichment of different KEGG pathways in the set of differentially expressed genes identified in cummeRbund. Enrichment was tested using Fischer's exact test with Benjamini and Hochberg correction for the false discovery rate (Benjamini and Hochberg, 1995).

2.2.4 Phylogenetic analysis of PiggyBac elements

T. hominis PiggyBac elements THOM_1159, THOM_1429 and the additional family member newly identified in our transcriptome were BLASTed against the nr database, retrieving the top 100 significant hits with an E-value of less than 0.05. Duplicate hits were manually removed before sequences were aligned using M-Coffee (Wallace et al., 2006), combining the results of alignments using Muscle (Edgar, 2004), Mafft (Katoh, 2002), ProbCons (Do et al., 2005), PCMA (Pei et al., 2003), and Fsa (Bradley et al., 2009). Poorly-aligning regions were identified and removed using trimAl with settings as previously described (Capella-Gutiérrez et al., 2009). The phylogeny was inferred using the C20 model (Quang et al., 2007) implemented in PhyloBayes 3.3 (Lartillot et al., 2009), with tests for chain convergence as previously described.

2.2.5 Assessing heterogeneous expression in duplicated gene families

A phylogenetic screen was implemented by Sirintra Nakjang, Tom Williams and Peter Foster to identify expanded gene families in *T. hominis* and other Microsporidia (Nakjang et al., 2013). I screen these gene families for those including at least two genes from *T. hominis*; suggesting that they may have arisen from a duplication event. The expression levels of genes within these families were then explored in the *T. hominis* transcriptome. To identify the gene families showing the greatest level of between-paralogue expression level divergence in *T. hominis*, the expression level of each gene was normalised by the average level of expression for the family to which it belonged, then the standard deviation of these values was taken for each family. Families were ranked by this score to identify those families with the greatest within-family divergence.

2.3 Tracing the infectious cycle of *T. hominis*

2.3.1 Cell culture for time course

Basic culture was carried out as described in 2.2.1; however with some small differences. The results from two separate time course studies are presented here; the same protocol was followed in each case however samples were taken at different post infection time points and different antibody markers were explored (see 2.3.2).

For each time course a single 175cm^2 flask of uninfected RK-13 cells was grown to sub-confluence (80% confluence where confluence is defined as a continuous cell monolayer) and split into 24 well plates, with a seeding density of around 1x10^5 cells per well. Cells in 24 well plates were raised in parallel until ~80% confluence, where they contain ~1.9x10^5 cells per well. At this point, fresh spores were harvested from 20 flasks of *T. hominis* infected RK-13 cells. The protocol for spore purification was modified from the RNAseq experiment. Instead of harvesting spores from the media of *T. hominis* infected RK-13 cells, heavily *T. hominis* infected RK-13s were scraped from the flask. The scraped cells were pooled into a centrifuge tube and resuspended in 10ml of PBS. Cells in suspension were lysed by three one minute long rounds of sonication, with five minutes of incubation on ice between rounds. Observations from the host laboratory suggest that this liberates mature spores from host cells and spore bags, and that these are more abundant than spores floating freely in the culture media. While the previous protocol liberated ~1x10^7

spores from 20 flasks of *T. hominis* infected cells, the new approach recovers ~10x as many free spores. Harvested spores were cleaned twice in PBS, as previously described, before being diluted in from complete media and added to RK-13 cells to initiate infection. The combination of scaling down the number of host cells in the 24-well plate format increased the multiplicity of infection to ~11 spores per host cell (two full 24 well plates were used in each time course). The addition of spores to RK-13 cells is the point of inoculation, representing time zero in the time course. In both time courses RK-13 cell were washed three times in PBS 30 minutes after inoculation. This was to remove excess spores from the surface of the RK-13 cells.

2.3.2 Markers and time points for time course

Samples in time courses were prepared for immunofluorescence (see 2.3.3). All experiments used anti-HSP70 antibodies raised in rat by Kacper Sendra at 1:300 concentrations. All experiments were carried out in biological duplicate and included a control to which no primary antibody was added at each time point. The following describes other antibodies, and the time course in which they were used:

Time course A

This time course was undertaken in collaboration with Kacper Sendra in his study of the segregation and localisation of mitosomes. Slides were prepared for microscopy together due to the intensive nature of sampling every 2 hours, but were imaged and analysed independently. The anti-MPS-3 antibody was raised and characterised by Kacper Sendra in rabbit, and is used at a dilution of 1:300 for immunofluorescence. The anti-HSP70 antibody was raised by Kacper Sendra in rat and used at a dilution of 1:300 for immunofluorescence. This combination of antibodies was used for the semi-quantitative tracing of infection from 0.5 to 40 hours post infection. The first sample was taken shortly after inoculation, immediately after washing excess spores from the surface of the monolayer at 0.5h post infection. The next sample was taken at 2h post infection and subsequently a sample was taken every two hours until 40 hours post infection; though not all time points were included in the quantitative analysis.

Time course B

This time course was undertaken independently. Anti-NTT1, NTT3 and NTT4 antibodies were the same as those used in the recently published characterisation of *T. hominis* nucleotide

transport proteins (Heinz et al., 2014) raised by Dr. Alina Goldberg in rabbit. The antibodies were used at dilutions of 1:20, 1:30 and 1:50 respectively. These antibodies were used in conjunction with the anti-HSP70 antibody described above to explore NTT expression across the parasite lifecycle. Samples were taken at 2h, 15h, 22h, 46h and 69h post infection.

2.3.3 Microscopy of T. hominis infected RK-13 cells

For immunofluorescence assays, at each time point glass slides were removed from the cell culture 24 well plates and placed into clean wells in a new plate containing PBS. After two additional PBS washes, cells were fixed in 50% methanol 50% acetone pre-cooled to -20^{o}C. After fixation, slides were cleaned three times in PBS to remove excess methanol/acetone before blocking in 5% milk/PBS for a minimum of 1 hour. Slides were inverted on to a drop containing two primary antibodies diluted in 1% milk/PBS and incubated overnight at 4^{o}C. Following overnight incubation, slides were washed 3 times for 10 minutes in PBS before the addition of secondary antibodies in 1% milk/PBS. Secondary antibodies were a mixture of Alexa Fluor 488 anti-rabbit IgG raised in goat, and Alexa Fluor 594 anti-rat IgG raised in goat (LifeTechnologies), each at a 1:300 dilution. Following the secondary antibody incubation, slides were washed 3 times in PBS before the addition of DAPI at a concentration of 1µg/ml for 5-10 mins. Slides were mounted in ProLong Gold antifade mountant (ThermoFisher) which was allowed to set overnight at room temperature. Microscopy was performed using the Zeiss Axio Imager II (Upright) in structured illumination (apotome) mode at the Newcastle University Bio-Imaging unit.

For transmission electron microscopy (TEM), a 175cm^2 flask of *T. hominis* infected RK-13 cells was washed 3 times with 10ml of ice cold 0.1M cacodylate buffer (cacodylic acid in H_2O, pH 6.5) before fixation overnight at 4^{o}C in 2.5% glutaraldehyde. Following fixation cells were washed 3 times in ice cold 0.1M cacodylate buffer. Cells were then scraped off and centrifuged at 16,000g. The samples were submitted to Newcastle University Electron Microscope Research Service for processing. Briefly, these underwent secondary fixation in 1% osmium tetraoxide before dehydration in increasing acetone concentrations. The samples were then impregnated with increasing concentrations of TAAB epoxy resin using the TAAB epoxy resin kit. Finally, samples were embedded in 100% fresh resin. Ultrathin sections (~70nm) were cut on a RCM MT-XL ultramicrotome and collected on pilioform coated copper grids. Grids were examined using a Philips CM1000 Compustage (FEI)

transmission electron microscope, and images were collected using an AMT CDD camera (Deben).

2.3.4 Image analysis

All images were analysed using commercially available software, Volocity from PerkinElmer. Parasite length and width were respectively defined as the longest and shortest diameter through the parasite that was measured in the phase contrast image of the cell. The number of HSP70 signals per parasite was estimated using Volocity fluorescence point detection, searching for the brightest spots within a 0.1µm radius (the approximate size of the *T. hominis* mitosome (Williams et al., 2002)). The number of nuclei per parasite and the number of parasites infecting a single host cell were counted manually. Images were prepared for presentation using Fiji (Schindelin et al., 2012).

Chapter 3 : Comparative genomics of Microsporidia

3.1 Introduction

Since the sequencing of the first microsporidian genome, that of *Encephalitozoon cuniculi* (Katinka et al., 2001), many new microsporidian genomes have been published. Individually these studies have provided valuable insights into microsporidian biology and evolution. At the time of publication the *Encephalitozoon cuniculi* genome was the smallest identified eukaryotic genome; highly reduced both in protein coding capacity and average intergenic region size compared to free living relatives (Katinka et al., 2001). Microsporidia are often typified by this extreme reduction, and while several newly identified microsporidian genomes are much larger than those of the *Encephalitozoon* (Campbell et al., 2013; Cornman et al., 2009; Corradi and Slamovits, 2011; Cuomo et al., 2012; Heinz et al., 2012; Katinka et al., 2001) the largest source of variation in genome size in these species is in the amount of non-coding DNA and lineage-specific proteins (Corradi and Slamovits, 2011; Heinz et al., 2012). All sequenced Microsporidia encode a similar number of genes, suggesting that the extreme reduction in protein coding capacity occurred in the last common microsporidian ancestor (LCMA) (Corradi and Slamovits, 2011; Heinz et al., 2012). Considering this predominant genome reduction in the microsporidian LCMA, gene families that were retained both in the LCMA and subsequent microsporidian lineages following the radiation of the group are likely to play important conserved roles in the biology of the parasites. Comparative genomics will allow us to identify these “core” conserved genes and gene families. Where functional predictions for genes and gene families are available based on sequence similarity to characterised homologues, identifying conserved core genes will have an immediately valuable role in understanding basic elements of the parasites molecular biology.

Whilst a large proportion of the reduction in microsporidian protein coding capacity occurred in the common ancestor of the group, some gene families and pathways retained by the LCMA have been lost independently in multiple microsporidian lineages (Heinz et al., 2012; Williams et al., 2010). The central elements of the RNAi pathway, argonaute and dicer, make up one such pathway (Heinz et al., 2012). Previous studies have demonstrated that the microsporidian genomes which encoded the RNAi machinery also included transposable elements (Heinz et al., 2012). The RNAi machinery is associated with the defence of the

genome against transposable elements, repressing the expression of repetitive DNA and transgenes (Girard and Hannon, 2008; Obbard et al., 2009), leading to the suggestion that this may be the main role of the RNAi machinery in Microsporidia (Heinz et al., 2012). The core elements of the RNAi machinery carry out a broad range of roles in other organisms, with a wide range of interaction partners and interlinked pathways RNAi (Castel and Martienssen, 2013). It is possible that interaction partners closely linked to the function of the RNAi machinery in Microsporidia have also been exclusively retained in genomes encoding the RNAi machinery. Identifying these gene families and the roles of their homologues in other organisms may help to understand whether the RNAi machinery has functions beyond transposable element defence in Microsporidia.

Recent analysis has suggested that although there was an overall extreme reduction in protein coding capacity in the LCMA; this has been partly balanced by the gain of novel protein families (Heinz et al., 2012). A small number of gene family gains were predicted in the microsporidian LCMA, but the majority were predicted to have occurred in specific microsporidian lineages (Heinz et al., 2012). A gene family can be gained in the group by *de novo* formation or by horizontal gene transfer into Microsporidia from another organism. In individual microsporidian genomes many identified genes were found to be microsporidia-specific, with no detectable homologues outside the group and containing no conserved domains or motifs to help to predict their functions (Corradi and Slamovits, 2011; Heinz et al., 2012; Peyretaillade et al., 2014). In contrast relatively few horizontal gene transfers into Microsporidia have been identified; though there has been no published systematic screen for HGT. One gene family gained by horizontal gene transfer in Microsporidia is also the only transporter family to be functionally characterised in the group, the nucleotide transport protein (NTT) family. Microsporidia are thought to have acquired the NTTs from bacteria in a single horizontal gene transfer into the LCMA (Heinz et al., 2014, 2012; Richards et al., 2003; Selman and Corradi, 2011; Tsaousis et al., 2008), and NTTs from both *E cuniculi* and *T. hominis* have been demonstrated to transport ATP (Heinz et al., 2014; Tsaousis et al., 2008), suggesting that Microsporidia may use these proteins to acquire ATP from their host cell. The replacement of native metabolic pathways with transporters able to steal substrates from the host cell is an important step in the adaptation to an obligate intracellular lifestyle,

and we may expect other gene families gained by the LCMA or by specific microsporidian lineages to play roles in niche adaptation.

In addition to being acquired by HGT, the nucleotide transport protein family has expanded in size in Microsporidia through a series of lineage-specific gene duplications (Heinz et al., 2014). Gene duplication events are another way in which genomes can expand and potentially mediate adaptation to a given habitat. Ohno's evolution by genome duplication describes three potential fates for a pair of genes produced by a gene duplication event; neofunctionalisation, subfunctionalisation or gene loss (Ohno, 1970). A potential example of neofunctionalisation in Microsporidia is provided by the NTT gene family in *Encephalitozoon cuniculi*. The family has undergone three independent duplications in the *Encephalitozoon* lineage, which all encode four NTTs. In *E. cuniculi* three of these localise to the parasite plasma membrane, where they may steal nucleotides from their host cell, however one NTT (NTT3) is targeted to the mitosome (Tsaousis et al., 2008), suggesting the development of a novel localisation and role for this gene family member. As with microsporidian gene-family gain, we may expect gene families that have expanded in Microsporidia against the backdrop of extreme genome reduction to contribute to adaptation to new niches. Those gene family expansions which occur in the LCMA are of particular interest, as they may include adaptations to the obligate intracellular niche during the transition from a free living to a parasitic lifestyle. Currently there has been no systematic screen for such gene families in Microsporidia.

To explore the dynamics of gene family gain, loss, expansion and contraction in Microsporidia, a phylogenetic birth-death model was implemented in Count (Csurös, 2010) by Sirintra Nakjang (Figure 3.1). The results of this model support the extensive gain and loss of gene families in the ancestral microsporidian, consistent with previous parsimony analysis (Heinz et al., 2012), but also suggested extensive lineage specific genome evolution. The results are consistent with a bottleneck of gene family loss in the LCMA followed by expansion of gene families in microsporidian lineages either by gene family expansion through gene duplication, *de novo* gene formation or HGT at different rates in different lineages. While this method gives an estimate for the number of gene families present, gained and lost at different ancestral nodes in Microsporidia; it does not identify these gene families or identify the mode of genome or gene family expansion. To explore the dataset

further it is necessary to perform a detailed bioinformatic identification and characterisation of gene families with respect to their evolutionary history (Figure 3.1).

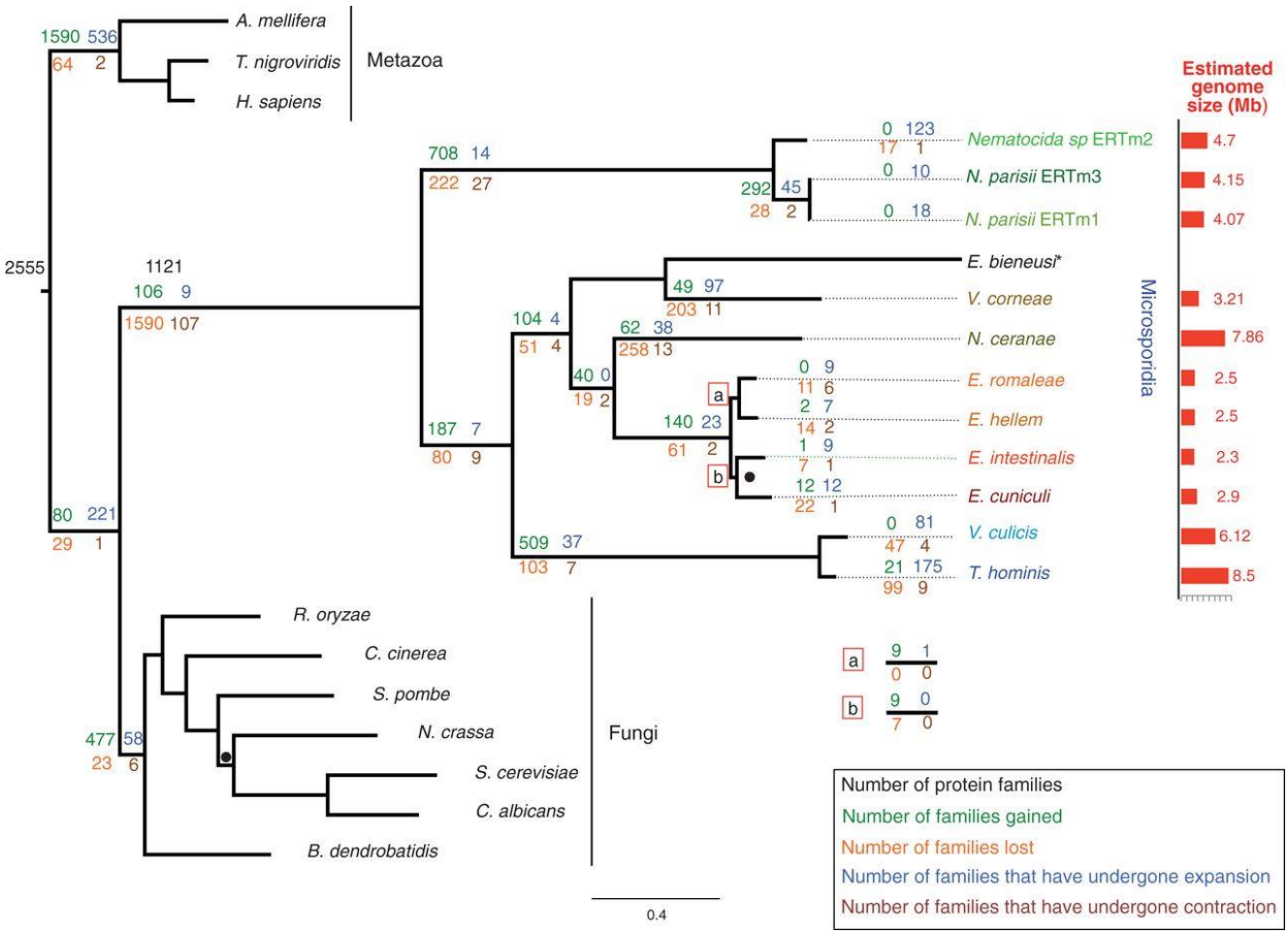

Figure 3.1: Gain, loss, expansion, and contraction of protein families during the evolution of microsporidian genomes from (Nakjang et al., 2013).

Gene family gains (green), losses (orange), expansions (blue) and contractions (brown) mapped on to a concatenated protein phylogeny of the Microsporidia and outgroup fungi and animals. The tree is artificially rooted between Fungi and Metazoa. *Enterocytozoon bieneusi* (marked with a *) is included in the tree but not included in further analysis due to level of contamination in its assembled genome. This phylogeny forms the basis of further analysis of microsporidian gene family evolution.

The data from this chapter contributed to the below publication, which is freely available at:

http://gbe.oxfordjournals.org/content/5/12/2285

Nakjang S, Williams TA, Heinz E, Watson AK, Foster PG, Sendra KM, Heaps SE, Hirt RP, Martin Embley T: **Reduction and expansion in microsporidian genome evolution: new insights from comparative genomics.** Genome Biol Evol 2013, 5:2285–303.

3.2 Aims

Analysis of microsporidian gene family data generated by Dr. Sirintra Nakjang, and integration of this data with published datasets to:

1. Identify core conserved microsporidian gene families
2. Identify gene families acquired by Microsporidia
3. Identify gene families that expanded in the common ancestor of Microsporidia.
4. Explore the distribution of the RNAi machinery and transposable elements in Microsporidia, and identify any gene families co-distributing with the RNAi machinery.

3.3 Results

3.3.1 The core microsporidian genome

From a total of 3,204 gene families that included microsporidian sequences, my analysis revealed a "core" microsporidian gene set of 802 gene families; that is, 802 gene families conserved in 9 of 11 analysed microsporidian genomes (Figure 3.2). The parameters defining the core gene set were relaxed in this way in order to allow for the inclusion of partial genomes in the dataset. Ninety-five percent (767/802) of the core gene families have homologs in other opisthokonts and are likely to have been inherited vertically from their opisthokont common ancestor (Figure 3.2).

The conservation of core microsporidian gene families against a backdrop of extreme genome reduction means that they may be expected to be of greater functional importance than non-core families. To assess whether this was reflected in the available functional data for Microsporidia, the expression levels of *N. parisii and E. cuniculi* genes in the core set were compared to those in the rest of their genomes using data from published transcriptome analyses (Cuomo et al., 2012; Grisdale et al., 2013). In *E. cuniculi* (Grisdale et al., 2013) the level of expression of core genes was significantly higher than that of other genes across all three experimental time points (±0.239 for core/noncore genes, 95% Bayesian credible interval [0.1818, 0.2975] for the effect of core genes), and the same effect

was observed in the *Nematocida* transcriptomic data (±0.7909 for core/noncore genes, 95% Bayesian credible interval [0.716, 0.865] for the effect of core genes). These results suggest that genes in core microsporidian gene families play important roles in the parasites lifestyle.

3.2.2 Recently acquired gene families in Microsporidia

Of the 3,204 gene families including Microsporidian sequences, 2033 were specific to one or more microsporidian lineage, with no homologues in any opisthokonts sampled in the dataset (Figure 3.2). 2019 of these had no significant hits to any species outside of the Microsporidia based on BlastP and HHSearch results. Recently it has been suggested that the *Trachipleistophora hominis* genome includes a proportion of false-positive ORFs (Peyretaillade et al., 2014) due to the abundance of short lineage-specific genes in its annotation. If true then microsporidia-specific gene families would be expected to be inflated by these falsely annotated ORFs, however 76% of microsporidia-specific gene families had a member whose expression is supported by either transcriptomics (Cuomo et al., 2012; Grisdale et al., 2013) or proteomics (Brosson et al., 2006; Heinz et al., 2012); suggesting that false ORFs had a limited impact on gene family analyses.

Thirty-two gene families only found in Microsporidia are also "core" microsporidian gene families; that is, they are conserved in 9 of 11 sampled microsporidian genomes; suggesting they may have been acquired in the LCMA (Figure 3.2). Ancestrally derived core microsporidian genes are predicted to play particularly important roles in the groups' parasitic lifestyle, and it is tempting to speculate these 32 core microsporidia-specific gene families may play a similarly important roles. Further, as novel genes in the LCMA they could be important genes for the adaptation of Microsporidia to their obligate intracellular niche. Only two core microsporidia-specific gene families have been characterised in Microsporidia, a polar tube protein (Delbac et al., 2001; Peuvel et al., 2002; Polonais et al., 2005) and a spore wall protein family (Brosson et al., 2006; Peuvel-Fanget et al., 2006; Southern et al., 2007; Xu et al., 2006). The identity of these two families seems to be consistent with the prediction of functional importance, since both families play key roles in the microsporidian lifecycle. Polar tube proteins (PTPs) are components of the microsporidian infection apparatus; a unique microsporidian structure used to penetrate the host cell in spore germination (Williams, 2009). Spore wall proteins (SWPs) are integral to the construction of

the microsporidian spore wall, allowing microsporidia to survive in an environmentally resistant state and acting as a vector for infection (Williams, 2009). None of the remaining core microsporidia-specific gene families have been characterised, however the expression of members of each family was detected in *E. cuniculi* and *N. parisii* transcriptomics (Cuomo et al., 2012; Grisdale et al., 2013) during infection of their respective host organisms, consistent with their playing a role during infection.

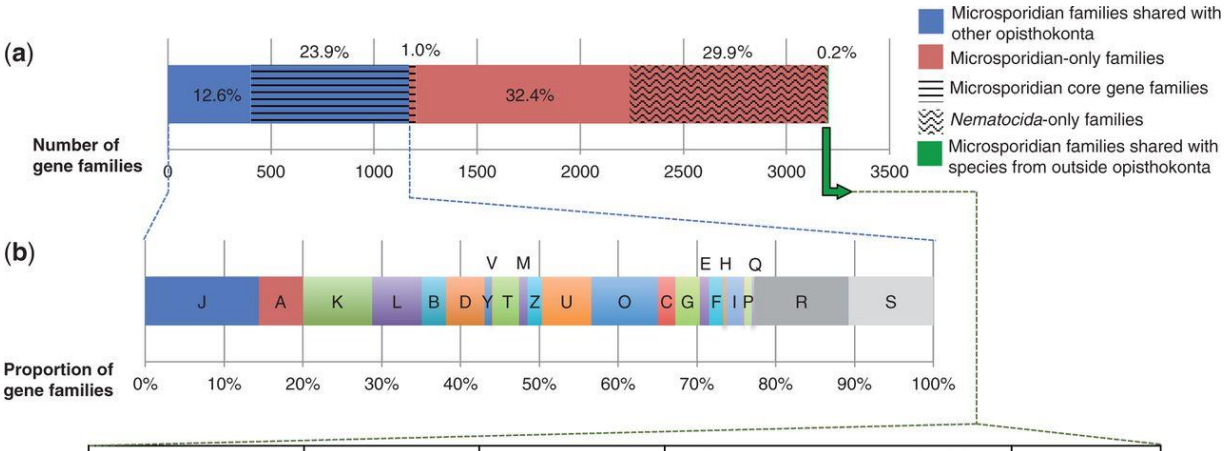

(c)

Annotation of protein families derived from outside the opisthokonta	Number of microsporidian taxa in cluster	N-terminal signal peptide (SP) or transmembrane domain (TMD)	Taxonomic distribution from BLASTP searches	Identified as an HGT
ATP/ADP translocase (NTTs)	11	No SP, 10-12 TMDs in all microsporidian sequences	*Chlamydia*, *Rickettsia*, Streptophyta (green plant), Chlorophyta, Bacillariophyta	Tsaousis et al. 2008
Small conductance mechanosensitive ion channel (MscS)	11	No SP, 1 TMD for *Nematocida* homologues	Streptophyta, Korarchaeota, Euryarchaeota, Crenarchaeota and many bacterial phyla	This study
Cysteine-rich secretory proteins (CAP) domain-containing protein (Pfam:PF00188)	11	SP predicted for most of the sequences , No TMD	Bacteria, Parabasalia (*Trichomonas vaginalis*)	This study
Aspartate-ammonia ligase (asnA; Pfam:PF03590)	3 (*T. hominis*, *V. culicis*, *N. ceranae*)	No SP or TMD detected	Apicomplexa, Amoebozoa, Parabasalia, Bacteria	Heinz et al. 2012
Phosphoribosyl transferase domain protein	2 (*E. romaleae*, *E. hellem*)	No SP or TMD detected	Euryarchaeota, Korarchaeota, Bacteria	Pombert et al. 2012
Putative glycosyltransferase	3 (all three *Nematocida spp.*)	SP predicted	Viridiplantae, Kinetoplastids, Crenarchaeota, Bacteria	This study

Figure 3.2: The origin of protein families identified in Microsporidia

The analysis presented in this chapter provided the evolutionary history of protein families described in A), while functional analysis and screening for HGTs in B) and C) was carried out by Sirintra Nakjang.

A) The proportion of microsporidian gene families that have homologues in other opisthokonts (blue), are microsporidia-specific (red) or only have homologues in species outside of the opisthokonts (green – identified by Sirintra Nakjang). Gene families that are conserved in at least 9 of 11 microsporidian genomes are “core” microsporidian gene families (horizontal striped background). Many of the gene families were specific to only one microsporidian; *Nematocida* (wavy background), consistent with its large phylogenetic distance from other Microsporidia included in the analysis (Figure 3.1). B) Functional classification of microsporidian gene families shared with opisthokonts based on COG category (Tatusov et al., 2000) identified by Sirintra Nakjang. C) Gene families with no

homologues in other opisthokonts that are hypothesised to have been gained in Microsporidia by horizontal gene transfer. Those highlighted as being identified in this study were identified in a systematic screen implemented by Sirintra Nakjang, Tom Williams and Peter Foster.

3.2.3 Gene family expansion in reduced microsporidian genomes

Expansion of opisthokont-related gene families

A Dollo parsimony based approach was used to identify gene families that have expanded in Microsporidia, focusing on expansions occurring in the common ancestor of Microsporidia. This method identified five gene families which were predicted to be expanded in the common ancestor of Microsporidia (Table 3.1); however the retention of duplicate copies of the genes in all Microsporidia following the ancestral expansion event was only predicted for two gene families, MscS and Ste24. The MscS gene family is made up of mechanosensitive ion channels, while the Ste24 gene family includes zinc metalloproteases; their roles are discussed in more detail in below.

	Fungi			**Microsporidia**				
Gene family description	***S. cerevisiae***	***C. cinerea***	***N. crassa***	***T. hominis***	***N. ceranae***	***E. cuniculi***	***E. intestinalis***	***E. bieneusi***
Metalloprotease (similar to STE24)	2	1	1	2	6	3	3	3
Small Conductance Mechanosensitive Ion Channel Family	0	3	2	8	6	5	5	6
Haloacid dehalogenase-like hydrolase	2	1	1	5	6	1	1	1
Protein containing Rho GTPase activating protein domain	0	0	0	4	2	2	2	1
dUTPase (similar to DUT1)	1	1	1	3	1	2	2	6

Table 3.1: Gene families predicted as expanded in the microsporidian common ancestor by Dollo parsimony.

Gene families predicted as expanded in the LCMA by Dollo parsimony. The number of gene family members encoded by a reduced selection of microsporidians and several fungal relatives are included.

In addition to the identification of gene families expanding in the microsporidian common ancestor, systematic screening of phylogenies of gene families by Dr. Sirintra Nakjang, Dr. Tom Williams and Dr. Peter Foster identified 222 families with strong support for gene duplication in one or more microsporidian lineages or the microsporidian LCMA. These gene families are predicted to play a broad range of roles in Microsporidia, including all KOG functional categories. I found that the majority of the expanded gene families (176 of 222) were also core microsporidian gene families; suggesting that a proportion of those gene families that were retained in the LCMA have subsequently expanded and contributed to microsporidian adaptation. These include the MscS gene family, supporting the results from my initial screen. The expansion of transport protein families in the common ancestor of Microsporidia is particularly interesting considering the overall backdrop of genome reduction in this period of microsporidian evolution. Diversification in the function of paralogues following gene duplications may have contributed to the adaptation of Microsporidia to their intracellular lifestyle. The biological context and the phylogeny of McsS and Ste24 metalloprotease gene families with an expanded sample set are discussed below.

Ste24 membrane-spanning metalloprotease

The microsporidian Ste24 homologs identified share common features with yeast Ste24, which has the zinc metalloprotease catalytic motif HEXXH and multiple TMDs (Tam et al., 2001), suggesting that they are membrane-spanning proteases. All microsporidian genomes sampled in the initial screen for ancestral duplications encode at least two copies of Ste24; compared to one copy in sampled opisthokonts. The phylogenetic analysis of the Ste24 gene family included an expanded sampling of both microsporidia and outgroups compared to the gene family analysis. One microsporidian clade is highly divergent from other eukaryotic Ste24 sequences in the cluster; as indicated by its long branch length (Figure 3.3). The top Blast hits of sequences from this clade include bacterial sequences, but HGT from bacteria is not supported by phylogenetic analysis. Instead, the phylogeny is consistent with a duplication of Ste24 followed by high levels of sequence divergence in one copy of the duplicated pair in the LCMA. This is the classic observation for gene fate following gene duplication. There is also evidence for independent lineage-specific expansions in both *Nosema* and *Encephalitozoon.*

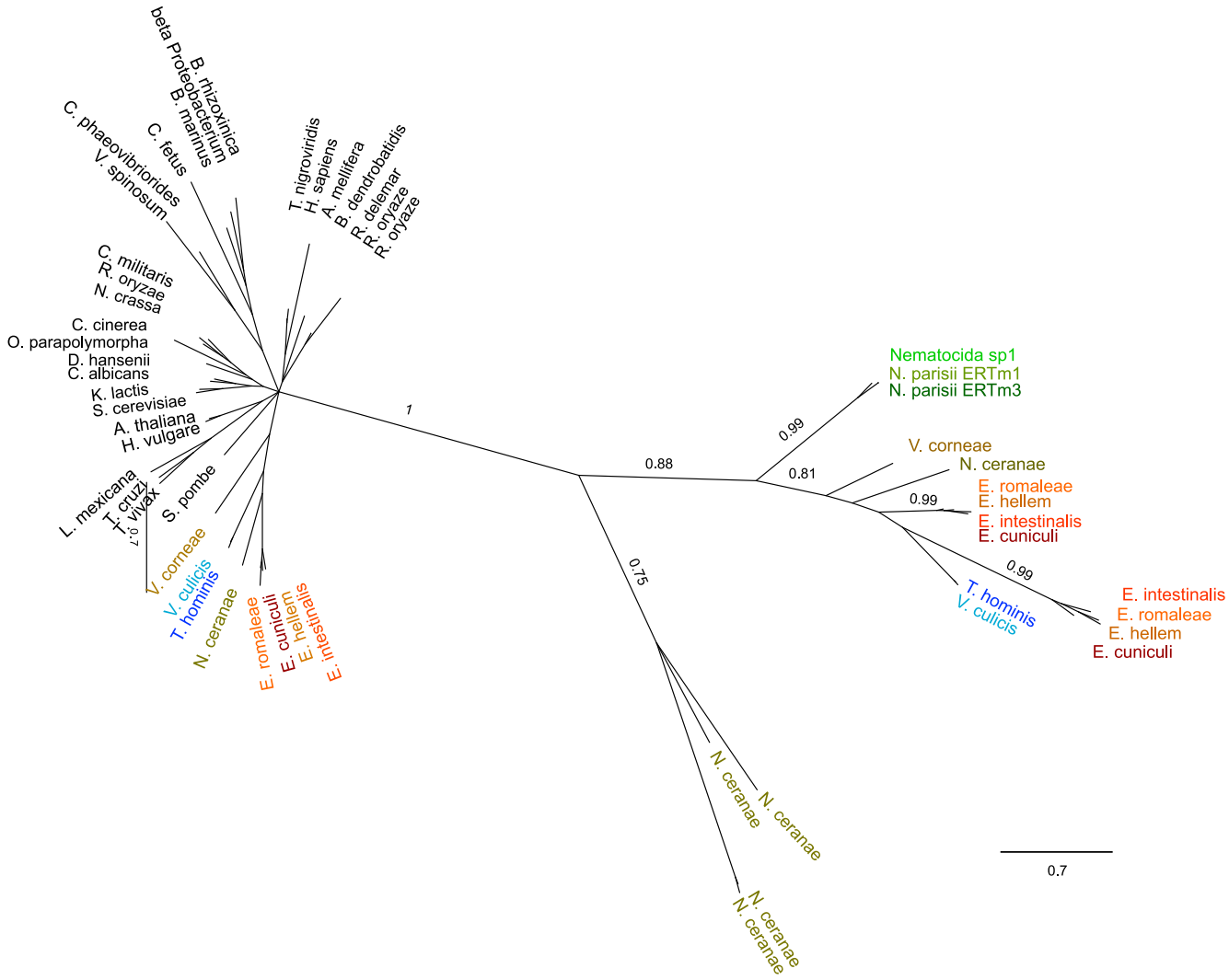

Figure 3.3: Phylogeny of the Ste24 gene family.

The phylogeny of the Ste24 gene family. Microsporidian gene family members are coloured. Additional Ste24 homologues from species not sampled in the gene family construction were added based on BLAST results. The phylogeny is consistent with duplication of the gene family followed by divergence at the sequence level, as indicated by the extremely long branch lengths of members of this family compared to conserved homologues.

In *Saccharomyces cerevisiae*, Ste24 also plays a role in the localization of chitin synthase 3 (Chs3) to the plasma membrane at the bud neck during cell division (Meissner et al., 2010). Chs3 is required for the synthesis of chitin in yeast (Meissner et al., 2010), and this is the primary component of the inner layer of the microsporidian spore (the endospore) (Williams, 2009). Interestingly, the expression of all three *E. cuniculi* Ste24 genes increased significantly (ECU02_1380: P = 2.29 × 10−11; ECU05_1370: P = 0.035; ECU05_1390: P = 1.99 × 10−10) as the infectious cycle progresses, similar to the expression pattern of genes coding for spore components (Grisdale et al., 2013). Expression of the single copy of Ste24 in *N. parisii* (NEPG_00127) also increased with the first observation of spores (Cuomo et al., 2012). These findings suggest that Ste24 may have retained this role in the regulation of chitin synthesis in Microsporidia, thus contributing to spore formation. The function of the highly divergent copy is unknown, but it is interesting to note that proteases in many pathogens have been identified as virulence factors (Yike, 2011).

McsS mechanosensitive ion channel family

MscS proteins are a family of mechanosensitive ion channels. These regulate osmotic homeostasis by opening or closing a channel permeable to water and small ions in response to mechanical deformation of the cell membrane, such as that caused by physical or osmotic pressure (Haswell et al., 2011; Kung et al., 2010); MscS also function in the septum ring formation of bacteria and plastids (Wilson and Haswell, 2012). The MscS gene family (MscS1) was predicted to have expanded in the microsporidian LCMA in my initial analysis. Further analysis by Dr Eva Heinz and Dr Sirintra Nakjang identified an additional gene family containing divergent microsporidian McsS family members (MscS2); however this does not contradict my initial analysis. All microsporidian genomes encode at least four copies of MscS1 and only one copy of MscS2. Phylogenetic analysis incorporating both gene families indicates that they have two distinct origins. The MscS1 subfamily is related to Eukaryotic MscS proteins. The phylogeny suggests that five copies of MscS1 were present at the LCMA following repeated gene duplications, consistent with the predictions of Dollo parsimony (Figure 3.4). One of these copies was then lost in the *Nematocida* spp lineage. MscS2 was likely acquired in a single horizontal transfer event into the common ancestor of Microsporidia from bacteria. The only other eukaryotes in which MscS2 is found are plants; however these genes appear to have been acquired independently from their microsporidian homologues. The expression of all MscS genes identified in *N. parisii* ERTm1

and *E. cuniculi* were detected in the transcriptomic analyses of cells infected with these parasites (Cuomo et al., 2012; Grisdale et al., 2013). In *E. cuniculi*, the two distinct MscS families were expressed differently across the infectious cycle of the parasite (Grisdale et al., 2013). Four of the five *E. cuniculi* eukaryotic-like MscS1 genes significantly increased in expression between 24 h and 48 h post infection (ECU01_1240: P = 0.01; ECU01_1170: P = 1.17 × 10−3; ECU10_1360: P = 1.14 × 10−7; ECU03_1000: P = 1.02 × 10−6) (Grisdale et al. 2013). In contrast, the level of expression of bacterial-like MscS2 significantly decreased during the same time period (ECU09_0470: P = 1.02 × 10−6). This coincides with the timing of spore formation in the *E. cuniculi* lifecycle, suggesting that MscS1 may play a role in spores or spore formation, while MscS2 is active earlier in the parasite lifecycle. Consistent with this, the only MscS protein detected in *T. hominis* spore proteomics analysis was an MscS1 protein (locus tag: THOM_1684) (Heinz et al., 2012).

In *Escherichia coli*, MscS is characterized by three TMDs (Bass et al., 2002), the C-terminal domain and the third TMD are important for channel function and gating (Edwards et al., 2005; Koprowski and Kubalski, 2003). Comparing the domain architecture of the two microsporidian MscS families, the MscS1 family resembles a “canonical” MscS protein, whereas the bacterial-like MscS2 sequences are extremely reduced in length. Compared with the structure of *Escherichia coli* MscS (Bass et al., 2002), the MscS2 sequences have lost the C-terminal domain and most, or all, of the TMDs, with only the beta-domain being retained. It is therefore unclear whether any of the microsporidian MscS2 proteins are membrane bound, and if so, whether they function as ion channels. The presence of two distinct MscS families in Microsporidia, one potentially obtained by horizontal transfer and the other by lineage-specific expansion, coupled with their expression in both the spore and meront stages and throughout the parasite life cycle, suggests that MscS proteins play important but so far unrecognized roles in microsporidian biology. Based on what is known about the function of these proteins in model organisms, these roles may be related to the regulation of osmotic stress at the cell surface during different life stages (e.g., during the germination process), as well as during cell or organelle division (Wilson and Haswell, 2012).

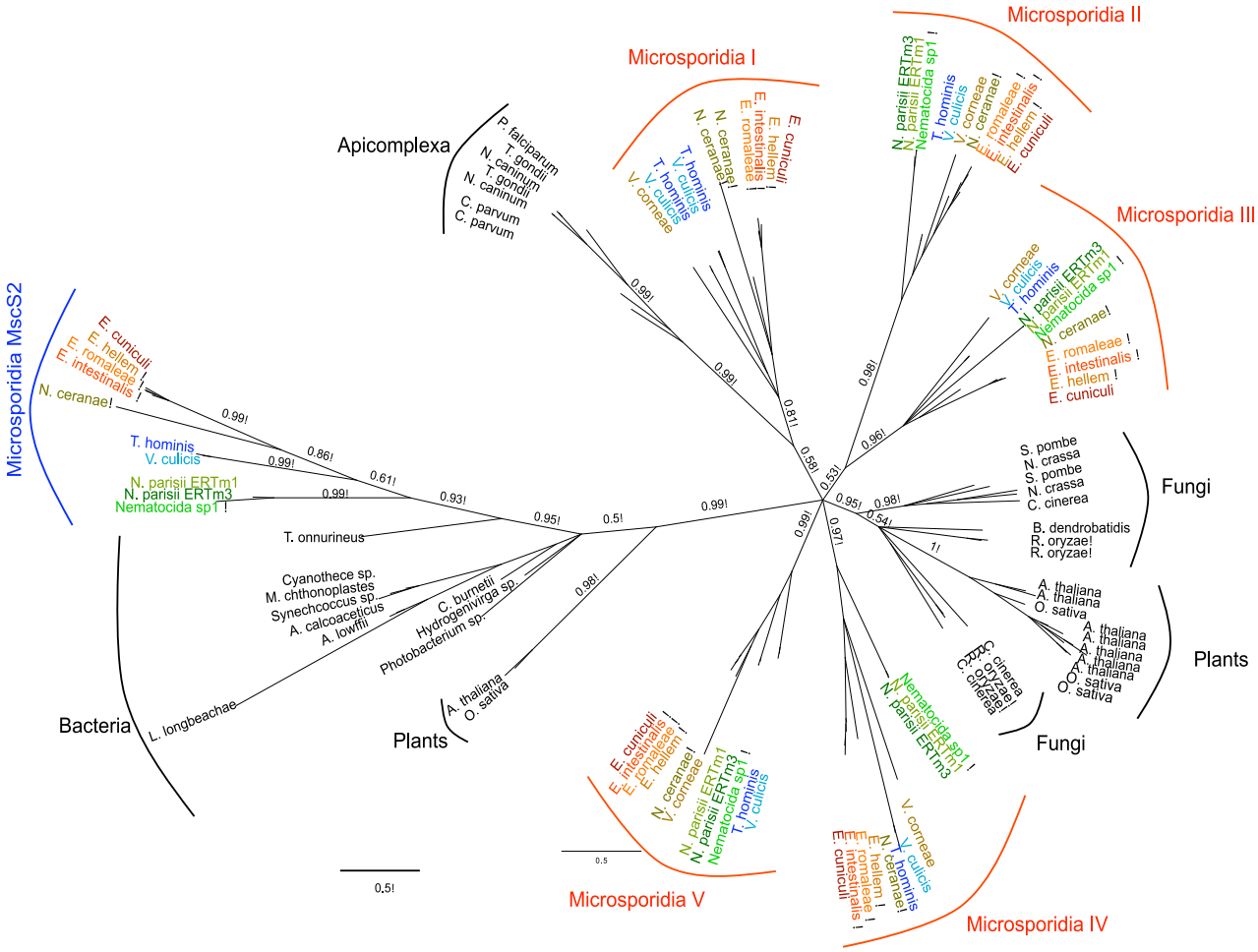

Figure 3.4: The phylogeny of the MscS gene family.

The phylogeny of the MscS gene family including microsporidian MscS1 (red) and MscS2 (blue)with homologues outside of the sampled dataset identified by blast. The MscS2 gene family (blue) emerges from with bacteria, suggesting that Microsporidia have gained this by lateral gene transfer. The MscS1 members of the gene family have expanded multiple times within the microsporidian lineage.

Expansion of new microsporidian gene-families

Gene families acquired by Microsporidia in the sampled dataset for the construction of microsporidian gene families include both unique microsporidia-specific gene families and those where no homologues were detectable in free living fungal relatives of Microsporidia, but are hypothesised to have been acquired by horizontal gene transfer based on Blast results in distantly related organisms. These gene families can be described as expansions of the microsporidian genome in that they are relatively recent acquisitions by the group; however their lack of opisthokont homologues mean they are excluded from both the Dollo parsimony and phylogenetic screens for prediction of gene family expansion by gene duplication. The simplest assumption is that each gene family that was gained by

Microsporidia was gained in a single independent event; either an ancestral microsporidian lineage acquired a single gene from this gene family from another organism by horizontal gene transfer, or else a single new gene formed *de novo* in an ancestral microsporidian lineage, generating a novel gene family. Making this assumption, any gene family acquired by Microsporidia that includes more than one member in a species is likely to have undergone expansion by gene duplication. 408 of the 2033 gene families predicted to be microsporidian acquisitions were also predicted to have expanded at in at least one microsporidian lineage; suggesting that after their acquisition they continue to contribute to increasing microsporidian genome diversity. No gene families acquired by Microsporidia were identified as expanded in all microsporidian genomes included in the study, and only one was expanded in 9 of 11 species; the nucleotide transport protein (NTT) family, however this gene family has been shown to have expanded independently in multiple microsporidian lineages (Heinz et al., 2014). Assuming no lineage-specific loss of duplicate gene copies (which is unlikely to hold true for all gene families included in the analysis) our data suggests that none of these core microsporidia-specific gene families also expanded in the LCMA. This is perhaps unsurprising considering the majority of gene family acquisitions are lineage-specific; only 32 microsporidia-specific gene families are "core" gene families, suggesting acquisition in the LCMA.

3.2.4 Distribution of RNAi machinery and transposable elements in sequenced Microsporidia

Four microsporidians were identified which encoded members of the dicer and argonaute gene families; *Trachipleistophora hominis*, *Vavraia culicis, Vittaforma cornaea* and *Nosema ceranae*. The *Edhazardia aedis* genome was not available at the time of gene family construction; however blast searches identify homologues of dicer, argonaute and transposable elements (Figure 3.5). All of the species encoding the RNAi machinery also encode transposable elements (Figure 3.5); leading to the suggestion that the pathway may have been retained by these species as a defence against transposable elements (Heinz et al., 2012). The recently published genome of *Nematocida parisii* breaks this trend (Cuomo et al., 2012). *N. parisii* encodes transposable elements (Cuomo et al., 2012; Parisot et al., 2014) whilst apparently lacking the RNAi machinery (Figure 3.5), and the expression of some of these transposable elements was detected in the *N. parisii* transcriptome (Cuomo et al., 2012) suggesting they may be active. Further, no single type of transposable element is

uniquely shared by those Microsporidia encoding the RNAi machinery to the exclusion of *N. parisii* (Parisot et al., 2014). This suggests that Microsporidia may be able to cope with the burden of transposable elements without the RNAi machinery; and that the RNAi machinery may play additional roles to defence against transposable elements in those genomes where it is retained.

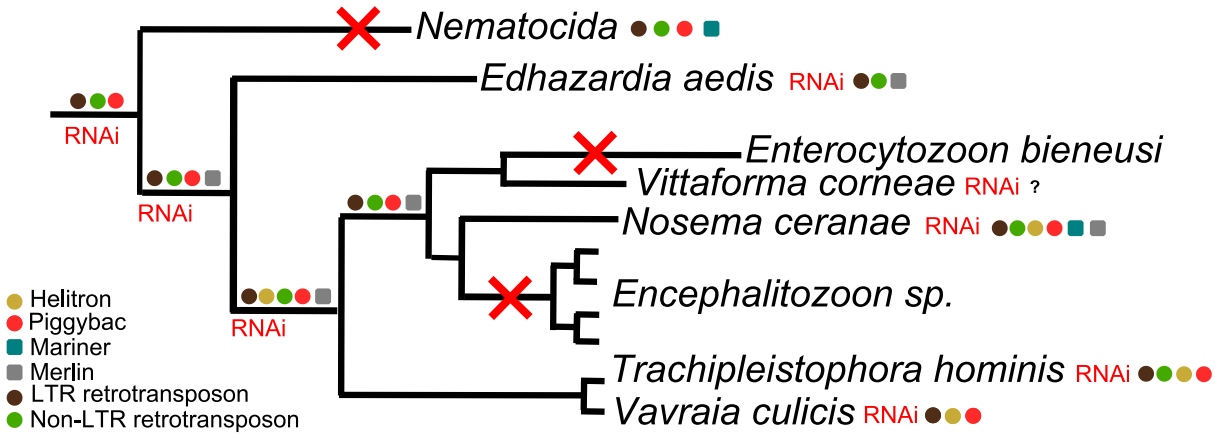

Figure 3.5: The distribution of the elements of the RNAi machinery and transposable elements in Microsporidia.

The distribution of the RNAi machinery (based on the presence of Dicer and Argonaute) and transposable elements identified in Microsporidia (Parisot et al., 2014) mapped on to a dendrogram representative of the rRNA phylogeny of microsporidian genomes included in this analysis (Adapted from (Heinz et al., 2012)). Loss of the RNAi machinery during microsporidian evolution is indicated by a red cross on a branch of the dendrogram. Prediction of transposable element distribution on ancestral microsporidian branches is based on Dollo parsimony. *Nematocida* is the only microsporidian lineage that encodes transposable elements but lacks the RNAi machinery that is hypothesised to defend the genome against their influence.

Gene families that co-distribute with the RNAi machinery

Trachipleistophora hominis, *Vavraia culicis, Vittaforma cornaea* and *Nosema Ceranae,* which all encode the core elements of the RNAi machinery argonaute and dicer, also exclusively share 11 other gene families amongst the Microsporidia in the sampled dataset. BlastP searches against the *Edhazardia aedis* genome detected homologues of all but three of these gene families. The three gene families absent from the *E. aedis* genome all include hypothetical proteins of unknown function, though one contains an YVNT-type WD40 repeat domain (IPR015943). Only gene families which also have homologues in *Edhazardia aedis* are discussed below (Table 3.2). Intriguingly the majority of these remaining gene families share

a common hypothesised role in the defence against cellular stress, and the yeast homologues of three gene families also directly interact with RNA.

T. hominis locus tag	Annotation
THOM_2863	Dicer*
THOM_2705	Argonaute*
THOM_1262	putative SNase-like domain protein
THOM_0711	putative ubiquitin---protein ligase
THOM_0606	Serine/threonine protein kinase and endoribonuclease ERN1/IRE1
THOM_3010	D-Try-tRNA deactyase
THOM_1560	Deoxyribodipyrimidine photolyase/cryptochrome
THOM_1050-1051	RNA-directed RNA polymerase QDE-1
THOM_0280	putative Pso2p interstrand cross-link repair protein
THOM_1443	Leucine rich repeat domain containing protein

Table 3.2: Gene families that co-distribute with the RNAi machinery in microsporidian genomes

The annotations of gene families based on BLAST searches and Interpro domain searches are provided alongside the locus tag of gene family members from one representative microsporidian included in the analysis, *Trachipleistophora hominis*. Two gene families, labelled as hypothetical proteins, are Microsporidia specific and contain no identifiable protein domains.

Three of the gene families co-distributing with the RNAi machinery in Microsporidia are hypothesised to interact with RNA, and one has been proposed to play a direct role in the RNAi pathway; the QDE1 RNA directed RNA polymerase gene family. In *Neurospora crassa,* QDE1 is proposed to initiate the RNAi response by binding ssDNA to synthesise ssRNA, and converting this ssRNA to the dsRNA substrate of the RNAi machinery (Forrest et al., 2004; H. C. Lee et al., 2010; Lee et al., 2009). This mode of RNAi initiation is important in the quelling of the expression of repetitive DNA elements and transgenes (e.g. transposable elements) (Forrest et al., 2004). This is consistent with the role of the core RNAi machinery in some Microsporidia as a defence against transposable elements proposed by (Heinz et al., 2012); however the model for QDE1 function suggests an additional role for the RNAi machinery in Microsporidia in the repair of DNA damage (H. C. Lee et al., 2010; Lee et al., 2009).

QDE1 produces dsRNA from a ssDNA starting template (H. C. Lee et al., 2010). Recent research in *Neurospora crassa* has demonstrated that dsRNA is produced in the vicinity of double stranded breaks in DNA, with QDE1 required for this response (Lee et al., 2009).

dsRNA is hypothesised to recruit the RNAi machinery to the double stranded break site, which in turn recruits the double stranded break repair complex and induces DNA repair (H. C. Lee et al., 2010; Lee et al., 2009). This provides a link between the DNA damage response and the role of the RNAi machinery in *N. crassa*, and the exclusive co-distribution of QDE1 with the RNAi machinery in Microsporidia suggests that this link is conserved in the group. Beyond QDE1, the response to DNA damage is one of the cellular stress responses represented by two additional gene families co-distributing with the RNAi machinery in Microsporidia; a Pso2p-1 like and a deoxyribodipyrimidine photolyase/cryptochrome like gene family. Pso2p is a conserved nuclease required for the repair of interstrand crosslinks and ds breaks (Brendel et al., 2003; Cattell et al., 2010). Interestingly the Pso2 has also been shown to preferentially cleave hairpin structured DNA, the formation of which can be induced in a number of ways including following a transposition event (Tiefenbach and Junop, 2012). Deoxyribodipyrimidine photolyase is an enzyme that repairs pyrimidine dimers in the presence of light following DNA damage (Weber, 2005). Another gene family contains a SNase-like domain (IPR016071), indicative of a potential nuclease function; however the precise role of this domain in eukaryotes is unknown (Callebaut and Mornon, 1997; Ponting, 1997). The conservation of these gene families in those microsporidians also encoding the RNAi machinery suggests that in addition to being required for transposon defence, the RNAi machinery may play a more direct function in the response to DNA damage, giving it a broader role in the maintenance of microsporidian genome integrity.

Yeast homologues of the remaining two gene families hypothesised to bind RNA, D-Try-tRNA deacylase and ERN1/IRE1, are involved in RNA editing that is independent of both the RNAi and splicing machineries. They are also both involved in cellular stress defence, however rather than DNA repair these respectively play a role in preventing the accumulation of truncated or misfolded proteins. D-Tyr-tRNA deacylase prevents the toxic accumulation of D-Tyr-tRNA.; a tRNA that naturally forms in cells by the misincorporation of D-Tyr to tRNA by Tyr-tRNA synthetase instead of L-Tyr (Calendar and Berg, 1967; Soutourina, 2000). D-Tyr-tRNA deacylase detects and cleaves D-Try-tRNA, liberating free tRNA which can be recycled (Calendar and Berg, 1967). Previous studies have suggested have suggested that organisms unable to synthesise L-Tyrosine themselves generally lack D-Try-tRNA deacylase (Soutourina, 2000); however Microsporidia lack genes for the *de novo* synthesis of tyrosine. ERN1/IRE1 is an endoribonuclease which splices transcription factor XBP1, leading to

activation of the cellular response to misfolded proteins (Calfon et al., 2002). Misfolded proteins are often polyubiquitylated, targeting them for degradation by the proteasome (Goldberg, 2003). One gene family that co-distributes with the RNAi machinery is annotated as an ubiquitin-protein ligase, and may be a part of this proteolytic response to misfolded proteins. Similar to the DNA damage response, recent studies have revealed potential links between the RNAi pathway and the proteolytic turnover of misfolded proteins in *C. elegans*, though more research is required to elucidate the molecular basis of this link (Long et al., 2014). The finding that these gene families co-distribute exclusively with the RNAi machinery in Microsporidia seems to support the hypothesised link between RNAi and misfolded protein turnover (Long et al., 2014).

3.4 Discussion

The identified core microsporidian gene set represents those gene families encoded by 9 of 11 currently sequenced microsporidians for which genome data is available. While it is likely that the addition of new genome data to this analysis would reduce the size of the predicted core gene set; the minimal difference in gene set size after the addition of four genomes to the dataset, including from the highly divergent microsporidian *N. parisii* (Cuomo et al., 2012), suggests this gene set is robust and representative for the group as a whole. The definition of a core gene set allows us to explore important facets of microsporidian biology such as what core metabolism is retained by the group is (Nakjang et al., 2013), or what transport protein families are present in all microsporidian genomes that may allow them to compensate for their reduced metabolism. The conservation of highly expressed core gene families in Microsporidia despite the extreme genome reduction in the LCMA raises the question of why these particular gene families have been retained. The high levels of expression of members of these gene families in two distinct microsporidian lineages (Cuomo et al., 2012; Grisdale et al., 2013) across the lifecycle of the parasite suggests that they may play an important role in the biology of the parasite. The majority of core microsporidian gene families (767/802) were also identified in other opisthokonts, suggesting they were vertically inherited from their common ancestor. Many of these are eukaryotic genes that are essential for cell-viability, including ribosomal proteins, transcription and translation factors and polymerases. The functional properties of core microsporidian gene families were investigated by Dr. Nakjang using functional data

available for their orthologues in the model fungi *S. cerevisiae* (Cherry et al., 2012). Yeast genes with an orthologue in the core microsporidian gene set were found to be significantly more likely to be essential (Fisher's exact test, P = 2.47 × 10−73,) and have a significantly higher number of interaction partners (Wilcoxon rank-sum test, P = 2.5 × 10−25) than those without. As in Microsporidia, the yeast genes were expressed at significantly higher levels under normal yeast growth conditions (Wilcoxon rank-sum test, P = 2.5 × 10−25) (Ghaemmaghami et al., 2003). Fitting a generalised linear model to this data indicated that no single factor was sufficient to explain the retention of these genes in Microsporidia, but all three factors had an influence on the process. These data demonstrate that during the extreme reduction in protein coding capacity in the microsporidian common ancestor, genes with high expression, connectivity and essentiality were preferentially retained, similar to the pattern of gene loss and retention observed in bacterial endosymbionts (McCutcheon and Moran, 2012) and bacterial intracellular pathogens (Williams and Fares, 2010).

Further analysis by Dr. Nakjang demonstrated that the core microsporidian genome is enriched for archaeal derived gene families, which are also preferentially retained in other reduced eukaryotic genomes (Alvarez-Ponce et al., 2013). This pattern of gene conservation and loss draws interesting parallels to the "complexity hypothesis" for gene flow during eukaryogenesis (Cohen et al., 2011; Jain et al., 1999). Based on current hypotheses for eukaryogenesis, the host for the mitochondrial endosymbiont is most likely to have been an archaeon (Williams et al., 2013). Following the acquisition of the mitochondrial endosymbiont, many archaeal genes were replaced by their bacterial homologues by horizontal gene transfer from the endosymbiont to its host. The complexity hypothesis explores the likelihood of horizontal gene transfer leading to successful gene replacement in this scenario. In network theory, for a network where connections between nodes represent interactions, the removal of a single highly connected node in the network is significantly more likely to disrupt the overall network structure than removal of one with relatively few connections. The same principle can be applied to protein-protein interaction (PPI) networks. Thus, replacement of those proteins with more interactions in a PPI network is more likely to cause a disruption to the overall network and lead to a loss of viability. Archaeal genes replaced by bacterial homologues during eukaryogenesis can be considered as being lost from a network; though their bacterial homologues may partially or fully compensate for original function. In model eukaryotes, genes with high connectivity in

protein-protein interaction networks tend to be of archaeal origin (Cohen et al., 2011). Their conservation suggests they were more resistant to gene replacement by horizontal gene transfer during eukaryogenesis than genes with fewer interactions. The same set of biases in protein-protein interaction network connectivity is observed in the pattern of gene loss observed in reduced Eukaryotes including Microsporidia in our analysis, suggesting that the constraints of minimising disruption to interaction networks affect to both gene replacement in the proto-eukaryote, and gene loss in the LCMA.

Patterns of distribution of core elements of the RNAi machinery, dicer and argonaute, suggest that the RNAi machinery was retained in the microsporidian LCMA, but subsequently lost independently in multiple microsporidian lineages. While it was hypothesised that the RNAi machinery is required for defence against the damaging effects of transposable elements on genome stability, the finding that *Nematocida parisii* encodes transposable elements without the RNAi machinery suggests that it may play additional roles in those genomes where it is retained. The gene families that co-distribute with the RNAi machinery in Microsporidia are involved in the response to different cellular stresses; DNA damage and misfolded/truncated protein accumulation. Both pathways have previously been linked to the RNAi pathway, and this link seems to be conserved in Microsporidia. The molecular mechanism linking the RNAi machinery and DNA repair has been studied in *N. crassa* (H. C. Lee et al., 2010). A direct link between the RNAi machinery and the response to DNA damage, the QDE1 gene family (H. C. Lee et al., 2010), is exclusively shared between those Microsporidia retaining the RNAi machinery. In contrast there is no direct molecular link characterised between RNAi and the turnover of misfolded proteins (Long et al., 2014). If a link between the two pathways is present in Microsporidia, the reduced nature of microsporidian genomes may be useful in focusing this research. Similar to the RNAi and DNA repair pathways, the gene family responsible for this link between RNAi and misfolded protein turnover may co-distribute with the RNAi machinery. The role of ERN1/IRE1 in transcription factor activation is a one potential link, though XBP1 has not been identified as upregulating expression of the RNAi machinery. Together our results suggest that, in addition to a potential role in defence of the microsporidian genome against transposable elements, the RNAi machinery may play a more general role in maintaining genome integrity

in response to cellular stress in those species it is retained. It remains unclear why additional pathways for defence against cellular stress may be required in these microsporidians.

A similar approach to that taken in the study of the RNAi machinery could be useful the study of other gene families which were present in the LCMA and independently lost in different microsporidian lineages. For example, alternative oxidase (AOX) has been lost independently on multiple microsporidian lineages. The enzyme has been hypothesised to allow the regeneration of NAD+ from NADH in the microsporidian mitosome in combination with the glycerol-3-phosphate shuttle (Williams et al., 2010). Identifying which gene families co-distribute AOX in Microsporidia, or which are only found in those Microsporidia lacking AOX, could help us to learn more about its role in those species where it is retained.

The gain of new gene families in Microsporidia against the backdrop of genome reduction in Microsporidia highlights the dynamic nature of microsporidian genome evolution, and raises questions about what roles they may play in the cell. These new gene families include genes gained by horizontal gene transfer, and microsporidia-specific genes with no homologues in other organisms. 32 microsporidia-specific families are also core-microsporidian gene families, suggesting that they were acquired in the microsporidian common ancestor. Based on the properties of vertically inherited core microsporidian genes, we may expect members of core microsporidia-specific gene families to be expressed at high levels, have high essentiality, and have a high number of interactions with other proteins. The only two such gene families which have been characterised appear to fit with this profile. Both polar tube and spore wall proteins are part of universally conserved features of the Microsporidian cell (Williams, 2009); suggesting they are essential to the parasite. They also have the potential to have a high number of different interaction partners as part of linked multi-protein complexes; all polar tube components of *Encephalitozoon cuniculi* interact with one another (Bouzahzah et al., 2010; Peuvel et al., 2002) and two polar tube proteins in *Nosema bombycis* interact with the spore wall (Li et al., 2012), though the polar tube is highly divergent between different lineages (Polonais et al., 2005) making it difficult to generalise these results to Microsporidia as a whole. In addition, specific interactions with host cell antigens have been identified in examples of both polar tube proteins and spore wall proteins (Southern et al., 2007). Finally, upregulation of the expression of members of both gene families is detected in the later stages of infection in the transcriptomes of *E.*

cuniculi (Grisdale et al., 2013) and *N. parisii* (Cuomo et al., 2012), coinciding with the onset of spore formation and consistent with their characterised role in Microsporidia. The polar tube is unique and universal to Microsporidia. As the method of penetrating a host cell to initiate an intracellular infection, the acquisition of the polar tube can be seen as an important step in the adaptation of Microsporidia to their obligate intracellular niche. Other microsporidia-specific genes gained in the LCMA may be important in this ancestral adaptation, while genes specific to different microsporidian lineages may play roles in the adaptation to different host cell or spore environments.

Similar to the gain of novel gene families, expansion of gene families in Microsporidia by gene duplication provides an opportunity for adaptation and the acquisition of new functional diversity against a backdrop of predominant reduction. For those genes expanding in the common ancestor of Microsporidia, this may include genes involved in core aspects of the transition of Microsporidia from a free living ancestor into their parasitic niche (Vogel and Chothia, 2006). Recent work has suggested that genes at the centre of protein-protein interaction networks are likely to be more resistant to successful gene duplication events than those at the periphery (Korbel et al., 2008). Similar to the biases affecting the complexity hypothesis, this is because the short term dosage effect of a duplication event on a protein in the centre of a PPI network is more likely to have a destabilising effect on protein complex formation, and so the network as a whole. The prediction of this theory is that gene duplication events are predominantly successful in gene families at the periphery of PPI networks. Thus; core microsporidian genes would also be predicted to be resistant to expansion by gene duplication due to the enrichment for gene families with a large number of interaction partners. Contrasting this prediction, the majority (176 of 222) of gene families predicted as expanding in Microsporidia in the phylogenetic screen implemented by Nakjang et al, were core microsporidian gene families. The proportion of genes predicted as expanded in all core-microsporidian genes (176 of 802; ~22%) is similar to those predicted in microsporidian acquisitions (408 of 2033; ~20%). This could be explored further by determining whether those genes predicted as expanded in the core set generally have fewer connections in PPI networks than other core gene families.

Of the gene families recently acquired by Microsporidia that are predicted to have expanded in the group, only the NTT family is predicted as having expanded in the majority

of microsporidians; another transport protein family (Heinz et al., 2014; Tsaousis et al., 2008). Whilst the simplest explanation for this would be an expansion of the gene family in the LCMA, the published phylogeny of the gene family is not consistent with this view. Intriguingly the gene family has independently expanded in multiple lineages (Heinz et al., 2014); suggesting that in addition to a core function common to all Eukaryotes the gene family has undergone lineage-specific adaptations. This is held out by functional data for microsporidian NTTs; all NTTs in *E. cuniculi* and in *T. hominis* have been characterised as purine transport proteins (Heinz et al., 2014; Tsaousis et al., 2008), however in *T. hominis* all NTTs localised to the plasma membrane (Heinz et al., 2014), while in *E. cuniculi* one NTT appears to have specialised in its localisation to the mitosome following a lineage-specific gene duplication (Tsaousis et al., 2008).

3.5 Conclusions

Work presented in this chapter compares the available genomes of microsporidians in detail, allowing the categorisation of gene families in these genomes by their evolutionary history. While previous work focuses on the reduced nature of microsporidian genomes; here the groups' dynamic expansion and gain of new gene families is explored. Core microsporidian gene families that were retained in 9 of 11 microsporidian genomes are predicted to play important roles in the parasite. The core gene families have similar properties to archaeal gene families that were resistant to replacement by the mitochondrial endosymbiont during eukaryogenesis. Some core gene families are unique to Microsporidia, and likely formed *de novo* in the LCMA. These include microsporidian innovations that play important roles in their obligate intracellular lifestyle, polar tube proteins and spore wall proteins. In addition to the gain of unique microsporidian gene families, the expansion of opisthokont gene families by gene duplication is identified in the LCMA. These include a metalloprotease family and a mechanosensitive ion channel family. Mechanosensitive ion channel families are typically involved in response to external stimuli, and may play a role in the response of Microsporidia to different environments they are exposed to in their lifecycle. Finally, while the RNAi pathway was present in the LCMA it has been lost independently in different microsporidian lineages. The co-distribution of the RNAi machinery with genes involved in RNAi linked DNA repair in *N. crassa* suggests the pathway may play a general role in the defence of genome integrity in those genomes where it is

retained, and a similar strategy could be used to explore the function of gene families that have differentially lost in microsporidian lineages.

Chapter 4 : Transcriptomic profiling of host-parasite interactions in the microsporidian *Trachipleistophora hominis*

4.1 Introduction

RNA sequencing (RNAseq) is a powerful tool for the quantitative study of gene expression, which can be used to examine differential expression of genes between treatment groups or time points (Costa et al., 2010; Trapnell et al., 2013). The advent of RNA-sequencing provides the opportunity to investigate microsporidian gene expression during the intracellular stages of infection on a genome-wide scale. Gene expression analyses of *Edhazardia aedis*(Gill et al., 2008), *Encephalitozoon cuniculi* (Grisdale et al., 2013), *Nematocida parisii* (Cuomo et al., 2012), *Spraguea lophii* (Campbell et al., 2013) and *Nosema bombycis* (Ma et al., 2013) have already shown that this technology can be used for microsporidians, highlighting the potential of this technique for studying a group of parasites that cannot be genetically manipulated in the laboratory. Discoveries range from the first confirmation that microsporidian transposons are transcribed, and so may be active (Gill et al., 2008), to inefficient splicing of introns (Campbell et al., 2013; Grisdale et al., 2013); all contributing to an improved understanding of microsporidian biology. *Trachipleistophora hominis* has been used as a model for the study of conserved aspects of microsporidian biology; including the identification and characterisation of a mitochondrial remnant (the mitosome) (Goldberg et al., 2008; Hjort et al., 2010; Williams et al., 2002), genome biology (Heinz et al., 2012) and microsporidian nucleotide transport proteins (Heinz et al., 2014). This prior work makes *T. hominis* an ideal candidate study by transcriptomics, which provides the first transcriptome of a microsporidian with a large genome that has been shown to infect humans.

All microsporidian transcriptome projects have significantly contributed different aspects of our understanding of microsporidian biology (discussed in 1.4); however there are some limitations to previous studies. The transcriptome of *Nematocida parisii* traces the stage of infection inside the host at its post infection time points; however lack of biological replication of samples makes it impossible to assess whether observed changes in transcript abundance between time points are statistically significant (Cuomo et al., 2012). Conversely the post-infection time course for *Encephalitozoon cuniculi* was carried out in triplicate,

however only three post infection time points were examined, with the second and third time points showing very similar expression profiles (Grisdale et al., 2013), and the progression of infection was not traced. The recently published transcriptomes of *V. culicis* and *E. aedis* represent the most in depth study to date focusing on host parasite-interactions, including replicated samples, and different post-infection stages (Desjardins et al., 2015). As these are both exclusively insect pathogens they were grown *in vivo*, so different time points also reflect different stages in their host's lifecycle (Desjardins et al., 2015), and interestingly the host response to infection was explored at the transcriptome level. When these microsporidian transcriptomes were published there had been no detailed comparison of the available microsporidian genome diversity. Work discussed in chapter 3 and more broadly in (Nakjang et al., 2013), combined with other recent publications (Cuomo et al., 2012; Desjardins et al., 2015; Heinz et al., 2012), has contributed to a growing understanding of microsporidian genome evolution. Its dynamic nature is highlighted in the dramatic gene loss in the LCMA and subsequent lineage specific genome expansion, and factors potentially affecting patterns loss and expansion of gene families have been identified. Transcription is another factor that has been implicated as playing a role in gene family evolution. Following a gene duplication event subfunctionalisation and neofunctionalisation can both occur by shifting protein function, or by changing the timing and level of its expression (Conant and Wolfe, 2008; Ohno, 1970). *T. hominis* is a microsporidian with a relatively large genome meaning compared to other microsporidians; however much of this size is due to the lineage specific expansion and acquisition of gene families subsequent to reduction in the LCMA. As such the parasite provides an interesting model in which to study gene expression in the context of microsporidian genome evolution.

Recent studies have also highlighted strategies by which host cells respond to microsporidian infections, including defence responses mediated by ubiquitination (Bakowski et al., 2014), the production of antimicrobial peptides and the perturbation of metabolic pathways (Ma et al., 2013), and the differential response of an insect host to microsporidian infection under different methods of transmission (Desjardins et al., 2015). In the present study we have used RNA sequencing to investigate gene expression by *Trachipleistophora hominis* infecting a mammalian (rabbit kidney) cell line, and we compare

host expression under infected and non-infected conditions. This allows us to also probe the host response to infection at the molecular level.

4.2 Aims

- Investigate gene expression by *Trachipleistophora hominis* infecting a mammalian (rabbit kidney) cell line.
- Combine analysis of the *T. hominis* transcriptome with information gained from comparative genomics (chapter 3) to investigate gene family evolution.
- Compare expression in the RK-13 host line under infected and non-infected conditions to identify changes in expression in response to infection.

This chapter is the basis of the following manuscript in press at BMC genomics:

Transcriptomic profiling of host-parasite interactions in the microsporidian *Trachipleistophora hominis*: Andrew K. Watson, Tom A. Williams, Bryony A. P. Williams, Karen A. Moore, Robert P. Hirt, T. Martin Embley.

All sequence data associated with this project has been deposited at NCBI under the BioProject ID PRJNA 278775.

4.3 Results and Discussion

4.3.1 Reproducibility of host-parasite transcriptomics

T. hominis is an obligate intracellular parasite grown in laboratory co-culture within rabbit kidney (RK) cells (Hollister et al., 1996). Total RNA was harvested from three biological replicates of infected RK cells seven days post inoculation, at which point ~60% of RK cells in each flask were infected with *T. hominis*. At this stage the community of *T. hominis* cells was a mixture of different life cycle stages including thick walled spores and pre-spore stages (sporonts and sporoblasts) as well as the intracellular sporoplasm (newly geminated parasites inside the host cell) and replicative or meront stages (Figure 4.1). A bead beating method similar to one previously shown to lyse *T. hominis* spores (Heinz et al., 2012) was used to lyse cells for RNA extraction. In parallel, total RNA was also isolated from three biological replicates of uninfected RK cells in order to compare patterns of host expression under the two conditions. 2.3×10^7 sequencing reads were obtained from *T. hominis* infected cells, with 7.7% of the reads mapping to the *T. hominis* genome. The reproducibility

between biological and technical replicates was very high, both for pairwise comparisons of the expression of individual genes between replicates and the overall distribution of expression levels across all transcripts (Figure 4.2 (*T. hominis*); Figure 4.3 (rabbit)). These results indicate that the analysis of the *T. hominis* and host transcriptomes was highly reproducible; allowing their potential biological implications to be explored in a meaningful way.

While our sample included a heterogeneous mixture of different stages of the *T. hominis* lifecycle, there are differences in the abundance of markers for spore formation compared to parasite proliferation (discussed in 4.3.5). These could be explained in a number of different ways. One possibility is that, despite the heterogeneous infection, there may be a higher proportion of meronts in the parasite population. This is supported by the description of the *T. hominis* lifecycle, in which merogony and sporogony occur concurrently in the same host cell; suggesting that most infected cells will include either only meronts, or a combination of both sporonts and meronts (Hollister et al., 1996). Alternatively, the spore stages of the parasite lifecycle may be more quiescent, with an overall reduction in levels of gene expression and thus number of transcripts per parasite cell, as observed in the non-replicating stages of the fission yeast cell cycle (Marguerat et al., 2012), so that they will naturally be represented at lower levels in the total RNA pool; however spore specific markers such as PTP2 were amongst the most highly expressed genes in the later stages of a time course of *E. cuniculi* infection (Grisdale et al., 2013). Another possibility is that the lysis procedure (Heinz et al., 2012) may not lyse *T. hominis* sporonts, sporoblasts and spores as efficiently as meronts for the extraction of RNA. If so, then the extracted RNA would be enriched for transcripts from replicative stages of the parasite lifecycle despite the mixed infection. This seems less likely due to the relatively harsh lysis conditions used in the experiment. Exploring the expression of RNA across a post-infection time course may help to resolve these questions, and the results presented in Chapter 5 lay a potential foundation for such studies.

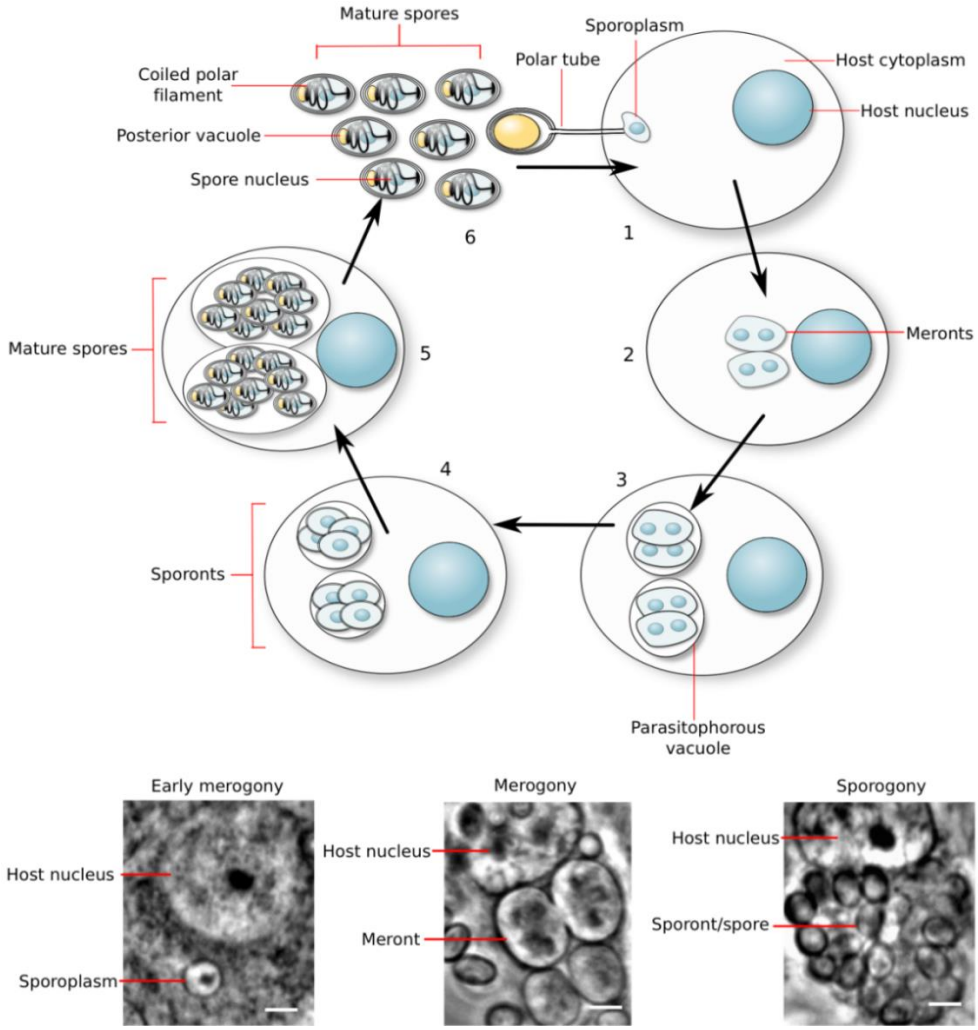

Figure 4.1: A schematic lifecycle of *Trachipleistophora hominis.*

A schematic lifecycle of *Trachipleistophora hominis* with phase contrast images of representative intracellular stages. In stage 1, the *T. hominis* spore injects its contents into the host cell via a proteinaceous polar tube. This uninucleate sporoplasm is the earliest stage of infection of the host cell (Cali and Takvorian, 2014). Following injection, the parasite – now called the meront - grows and begins to proliferate in the host cell (merogony, the second stage of the parasite lifecycle) (Field et al., 1996; Hollister et al., 1996). It is unknown how many cycles of proliferation meronts undergo in the host cell before stage three of the lifecycle begins, the transition from meronts to spore-forming sporonts. In Microsporidia this transition is marked by the deposition of an electron-dense material on the surface of the parasite, and in *T. hominis* this is correlated with the formation of the parasitophorous vacuole, an additional membrane surrounding the parasite within the host cell (Cali and Takvorian, 2014; Field et al., 1996; Hollister et al., 1996). During spore formation (sporogony) the microsporidian spore wall is assembled, and *T. hominis* undergoes a further round of proliferation (Field et al., 1996; Hollister et al., 1996). Eventually mature spores form inside the host cell (stage 5). These spores may either eject their polar tubes from within their host cell and infect neighbouring cells, or else be released from the cell in stage 6 of the parasite lifecycle, allowing dissemination of the infection to new cells or new organisms (Cali and Takvorian, 2014).

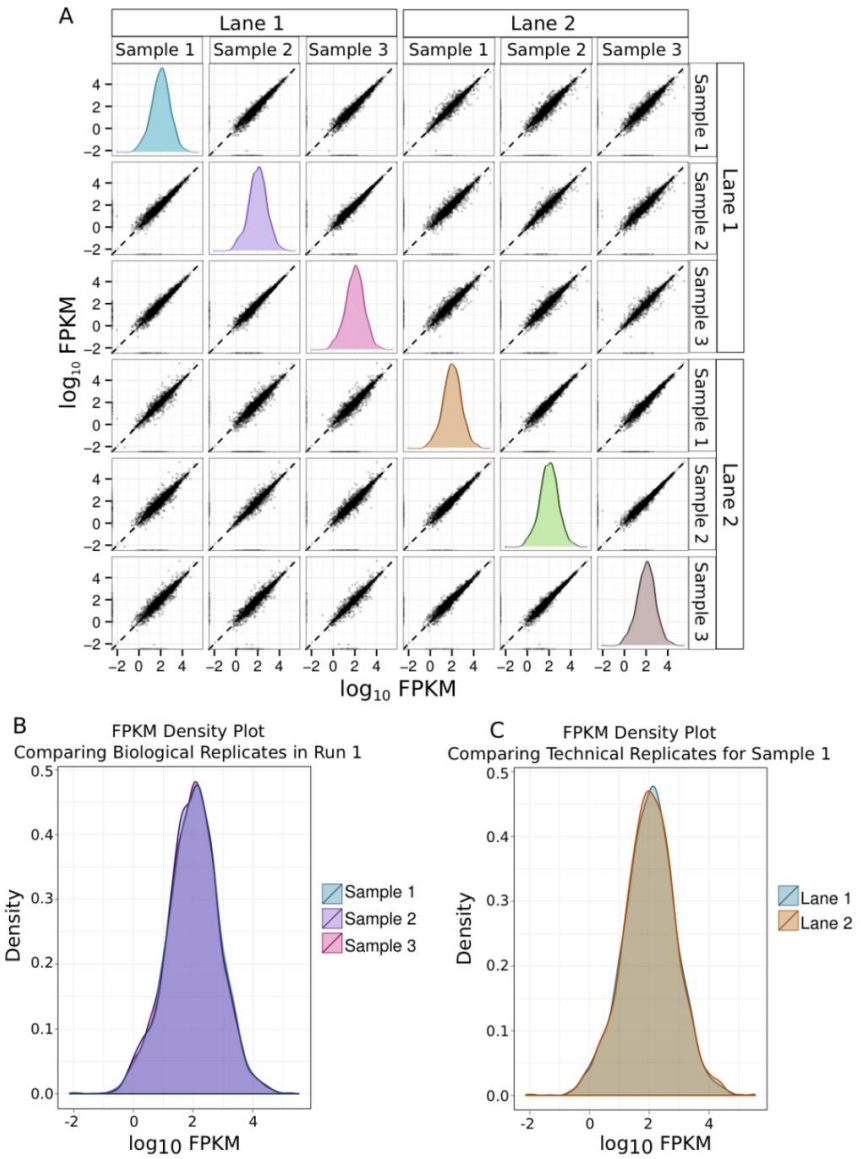

Figure 4.2: Robustness and reproducibility of transcriptomic analysis for *T. hominis*.

Each sample is an individual biological replicate of *T. hominis* infected RK-13 cells from which total RNA was purified. All of these samples were sequenced on two different lanes of the Illumina sequencing chip to provide technical replication. The strong positive correlation of transcript abundance, as measured by Fragments Per Kilobase per Million mapped reads (FPKM) between replicates in all cases is indicative of high levels of reproducibility between both biological and technical replicates. A) Pairwise comparisons of *T. hominis* transcript $\log_{10}$ FPKM values between biological replicates (samples) and technical replicates (sequencing lanes); density plots generated in cummerbund (Trapnell et al., 2012) represent the distribution of $\log_{10}$ FPKM values for that replicate. B) FPKM density plot overlay comparing the distribution of *T. hominis* transcript FPKM values between individual biological replicates (samples) from a single sequencing lane. C) FPKM density plot overlay comparing the distribution of *T. hominis* transcript FPKM values between technical replicates (different sequencing lanes) from a single sample (Sample 1). The levels of reproducibility between replicates for the expression of host genes were equally very high (Figure 4.3).

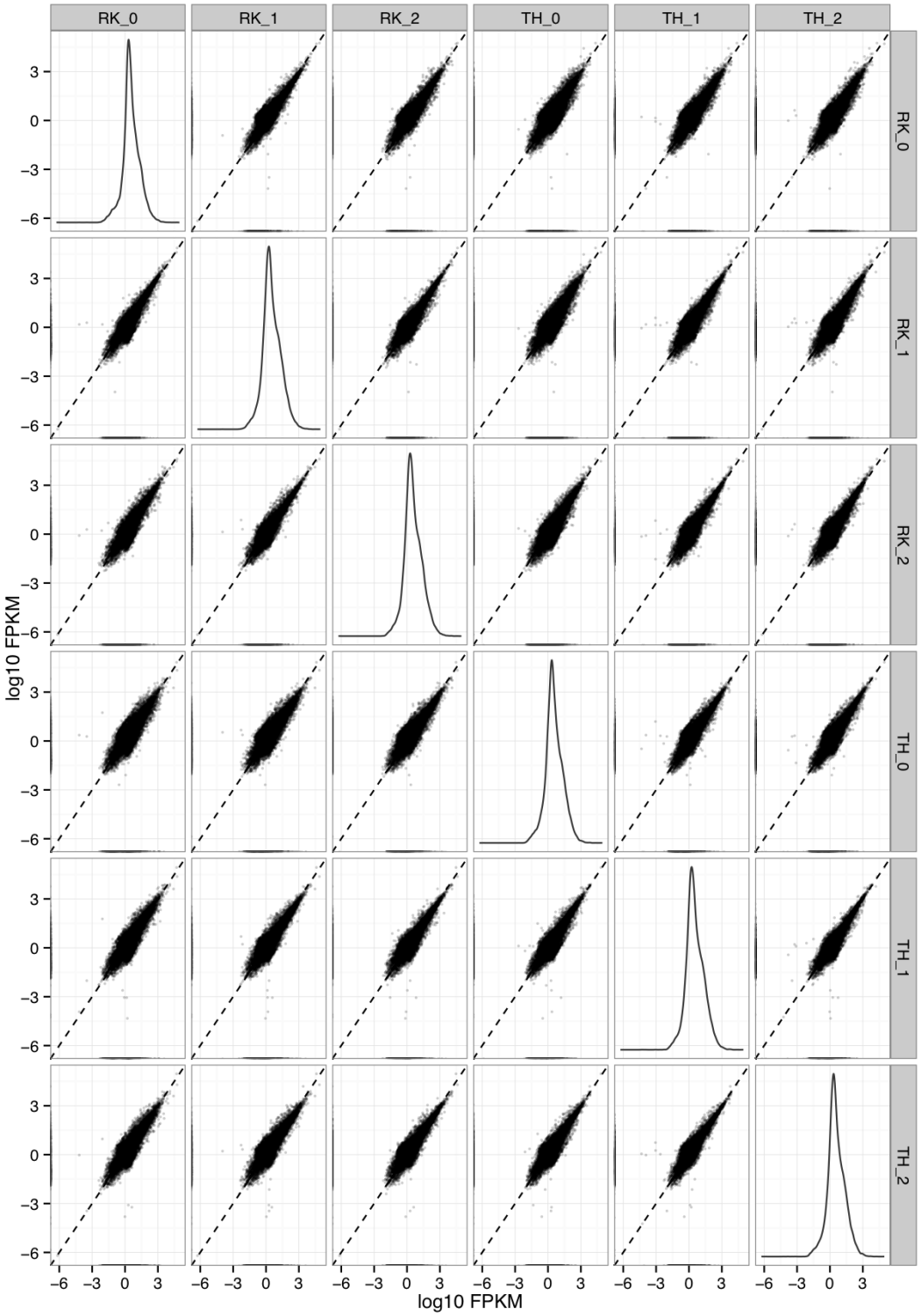

Figure 4.3: Robustness and reproducibility of transcriptomic analysis for RK-13 cells during intracellular infection.

Pairwise comparison of $\log_{10}$ FPKM values in rabbit kidney cell transcript quantification, as outlined in Figure 4.2 for parasite transcripts. In this case biological replicates of uninfected RK-13 cells (samples labelled RK) are compared to those for *T. hominis* infected RK-13 cells (samples labelled TH).

4.3.2 T. hominis has more genes than small-genome microsporidians

The *T. hominis* genome (~11.6 Mbp haploid genome size) was initially reported to contain 3,266 predicted open reading frames (ORFs) (Heinz et al., 2012), which is over 1000 more genes than the ~2000 open reading frames predicted for the best studied small genome (~2.3-2.5 Mbp haploid genome size) species of *Encephalitozoon* (Heinz et al., 2012; Katinka et al., 2001; Peyretaillade et al., 2014). It has been suggested that the predicted number of *T. hominis* genes may be an overestimate due to over-prediction of small genes (Peyretaillade et al., 2014). Indeed, some ORFs (113) appear to be unique to *T. hominis*, with no homologues identified in its closest sequenced relative *Vavraia culicis* (Cuomo et al., 2011; Vávra and Becnel, 2007), or any other microsporidian (Heinz et al., 2012; Nakjang et al., 2013). Additionally, *T. hominis* encodes a large family of novel leucine rich repeat proteins (117 ORFs) that includes many fragmented ORFs, indicative of ongoing pseudogenisation (Heinz et al., 2012). It is therefore possible that the estimated coding capacity of *T. hominis* includes some false positives, particularly given the highly derived nature of most microsporidian gene sequences (Heinz et al., 2012; Peyretaillade et al., 2014). Evidence was obtained for the expression of 2,958 (90%) of the 3,266 annotated *T. hominis* ORFs (Appendix A), including 85% of the leucine-rich repeat genes, suggesting that most are genuine ORFs. However, expression was detected for fewer (73%: 83 of 113) *T. hominis*-specific genes. This is consistent with the idea that some of these may be false-positive calls; however they may also be expressed in a condition specific manner. Balancing this reduction in the predicted gene count based on transcription, evidence was obtained for an additional 292 transcripts that were not predicted as ORFs in the original genome project. One hundred and fifty-five (80%) of these transcripts are located within regions of ambiguous genomic sequence or near the ends of scaffolds; the difficulty in annotating these regions may explain their absence from the original *T. hominis* genome annotation (Heinz et al., 2012).

Ninety seven of the 292 novel transcripts lacked an ORF suggesting that they might be *T. hominis* noncoding RNAs, however they did not give significant matches to the noncoding RNAs already included in the Rfam database (Burge et al., 2013; Nawrocki et al., 2009). They also appear to be missing from other microsporidian genomes as searched using BLASTN. Despite this, one of the transcripts, XLOC_000764, was in the upper 95th percentile

of overall expression levels; that is, its expression level was higher than 95% of detected transcripts, suggesting that it plays a physiologically relevant role. The remaining 195 transcripts are predicted to contain ORFs of which 89 had significant hits to the nr protein database at a BLASTX E-value cut-off of 0.01. The two most highly expressed of the 89 shared significant similarity to partial ORFs (VCUG_01670 and VCUG_016701) annotated in the *Vavraia culicis* genome (Cuomo et al., 2011), the closest sequenced relative of *T. hominis* (Vávra and Becnel, 2007). The putative *T. hominis* protein is 564 amino acids in length and contains a series of 12 tandem glycine-asparagine repeats. A search using HHPred (Söding, 2005; Söding et al., 2005) suggests that these are similar to a class of repeats present in over 30% of *Plasmodium falciparum* genes. Their function in *Plasmodium falciparum* is unknown, but it has been suggested that they may interact with host proteins (Muralidharan and Goldberg, 2013). Consistent with this idea, the *T. hominis* gene has an N-terminal signal peptide (Petersen et al., 2011), suggesting that it might be secreted or localised on the surface of the parasite.

Twenty-five of the newly identified transcripts show significant similarity to genes outside of the microsporidian clade, including several broadly-distributed eukaryotic genes previously thought to be absent from the genome of *T. hominis*. These include exportin, a component of the nuclear export machinery, as well as homologues of deoxyhypusine hydroxylase (Park et al., 1993), the Rea1 AAA-ATPase (Bassler et al., 2010), and the 60S ribosomal protein L29 (DeLabre et al., 2002). We found transcript evidence for three new transport proteins, including an amino acid/auxin permease of the AAAP family, a putative cation transporting P-type ATPase, and a member of the DMT superfamily of drug and metabolite transporters that includes a UAA transporter family domain (pfam:08449) associated with UDP-N-acetyl-glucosamine:UMP antiporter activity. Published data demonstrate that microsporidians can import purine nucleotides using nucleotide transport (NTT) proteins (Heinz et al., 2014; Nakjang et al., 2013; Tsaousis et al., 2008) but as yet there is no evidence for the transport of pyrimidine nucleotides by these transporters. Based upon *in silico* predictions it appears that microsporidians cannot make pyrimidines *de novo* so there is a transport gap that needs to be filled (Heinz et al., 2014; Nakjang et al., 2013; Tsaousis et al., 2008). UDP-N-acetylglucosamine is the direct monomeric precursor for chitin synthesis, an integral component of the microsporidian spore wall (Weiss et al., 2014), but it is also biosynthesised by the mammalian host cell in which it plays roles as a co-enzyme,

signalling molecule, and precursor for glycosylation (Slawson et al., 2006; Zachara and Hart, 2004). The pyrimidine UDP is liberated from UDP-N-acetylglucosamine during chitin polymerisation by chitin synthase and during glycosylation, so as well as providing chitin precursors this novel transporter could potentially provide the starting substrate to make pyrimidines needed for *T. hominis* DNA and RNA biosynthesis (Figure 4.4). Genes within the chitin biosynthesis pathway in *T. hominis* are generally expressed at similar levels in our analysis (600-900 fpkm), however expression of the terminal components of the pathway, chitinase and chitin synthases, were much lower (20-30fpkm) (Figure 4.5). These observations suggest that in the proliferative stages of the microsporidian lifecycle, UDP-N-acetylglucosamine is either being used primarily for UDP-liberating glycosylation reactions, or being accumulated for chitin production during sporogony. We also obtained transcriptomic evidence for a previously unannotated *T. hominis* homologue of a UDP-N-acetylglucosamine pyrophosphorylase, an enzyme also encoded on the genomes of *Vavraia*, *Encephalitozoon*, *Anncalia*, *Edhazardia* and *Vittaforma.* This enzyme catalyses the conversion of UTP and N-acetyl-alpha-D-glucosamine 1-phosphate to UDP-N-acetylglucosamine and diphosphate. This means that, in addition to potential acquisition of UDP-N-acetylglucosamine from the host, *T. hominis* encodes a complete pathway for its biosynthesis (Figure 4.5). The potential importance of this enzyme for spore wall formation in Microsporidia makes it a potential target for therapeutic intervention. Thus, recent studies have shown that UDP-N-acetylglucosamine pyrophosphorylase is essential for the survival of *Trypanosoma brucei* in its bloodform lifecycle stage (Stokes et al., 2008), and chemicals that can selectively inhibit the *Trypanosoma brucei* UDP-N-acetyl pyrophosphorylase have been identified (Urbaniak et al., 2013).

In conclusion, the transcript data from our experiments appear to be very reproducible for both host and *T. hominis*. The data validate the majority of gene models originally predicted from the *T. hominis* genome sequence and identify some previously missed genes, providing evidence for a total of 3,153 transcribed genes and making the *T. hominis* gene compliment one of the largest identified for microsporidians so far (Peyretaillade et al., 2014).

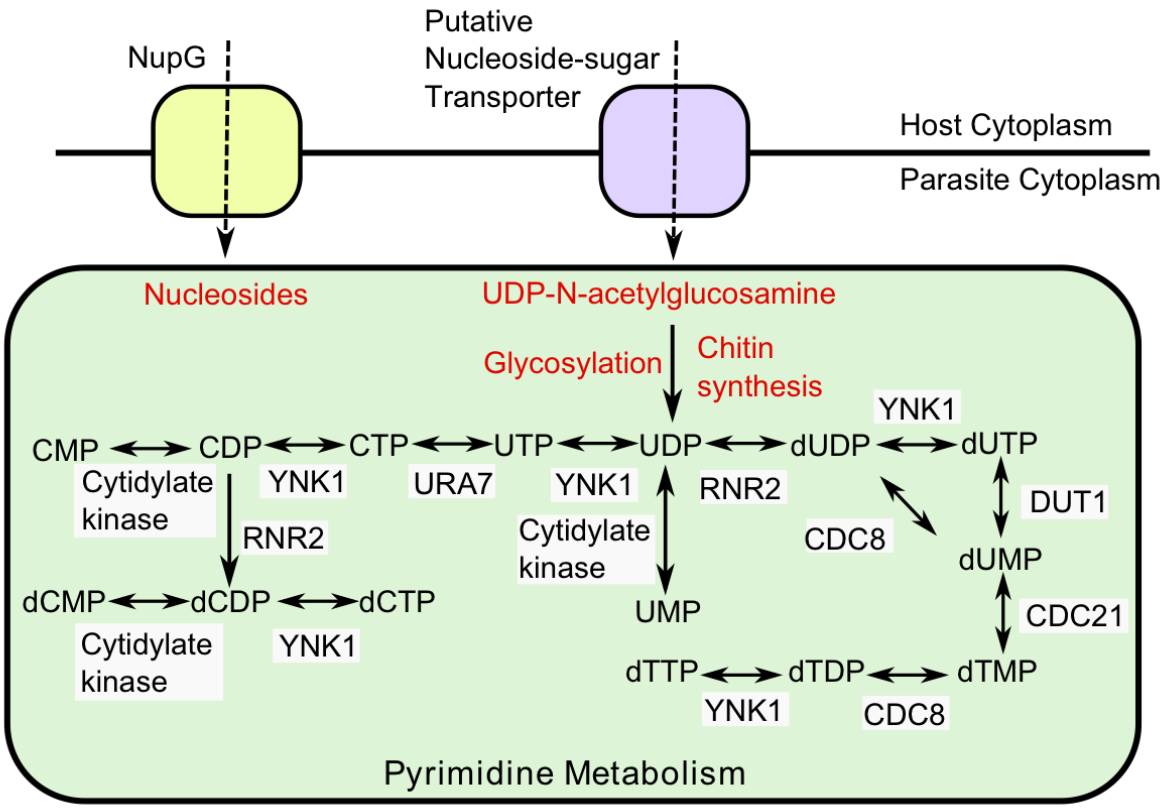

Figure 4.4: A potential route for pyrimidine and chitin precursor acquisition by *T. hominis.*

De novo routes for pyrimidine biosynthesis are not present in Microsporidia, but scavenger pathways allow conversion between different pyrimidines (Nakjang et al., 2013). The import of only one pyrimidine from the host cell would, in principle, enable the biosynthesis of other pyrimidines via scavenger pathways, because interconversions between bases are possible. NupG-like transport proteins have been hypothesised to transport nucleosides and thus act as a source of pyrimidine precursors (Cuomo et al., 2012), but the specificity and subcellular localisation of these genes are currently unknown. A putative UDP-N-acetyl glucosamine transporter provides another potential source of pyrimidines in *T. hominis* and V. culicis: the imported metabolite can feed into chitin synthase and glycosylation pathways, both of which may liberate free pyrimidine.

Key: YNK1, nucleotide diphosphate kinase; URA7, CTP synthase; RNR2, ribonucleotide-disphosphate reductase; CDC8, thymidylate/uridylate kinase; DUT1, Deoxyuridine triphosphate diphosphatase (dUTPase); CDC21, Thymidylate synthetase.

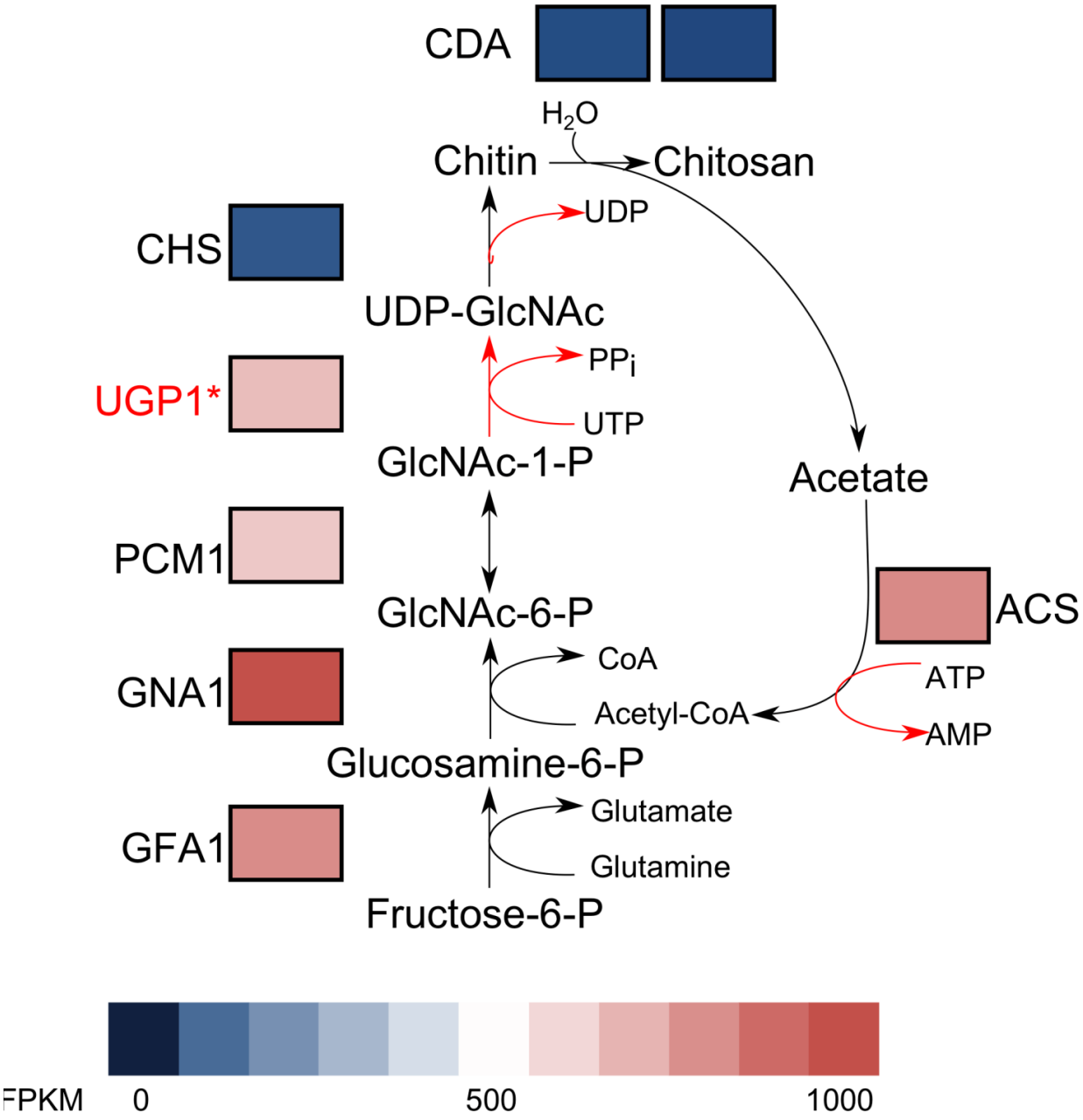

Figure 4.5: Expression of genes in the *T. hominis* chitin biosynthesis pathway during infection.

The heatmap shows the levels of expression of genes within the chitin biosynthesis pathway, with blue representing low levels of expression and red as high. The significantly lower expression levels of chitin synthases compared to the rest of the pathway leading to UDP-N-acetylglucosamine production suggests a drive for UDP-N-acetylglucosamine biosynthesis occurs despite low chitin synthesis. A low chitin synthesis activity is consistent with the low expression of other enzymes involved in spore wall formation in this sample.

Key: GFA1, glutamine-fructose-6-phosphate aminotransferase; GNA1, glucosamine-6-phosphate N-acetyltransferase 1; UGP1, UDP-N-acetylglucosamine pyrophosphorylase; PCM, phosphoacetylglucosamine mutase; CHS, chitin synthase; CDA, chitin deacetylase; ACS, acetyl-CoA synthetase.

4.3.3 Overlapping transcription in a gene-sparse microsporidian genome

140 *T. hominis* transcripts encoding more than one ORF were detected in the transcriptome, of which 113 overlap on the genome assembly. The remaining 27 do not overlap on the genome, but the intergenic region between them was spanned by RNAseq reads. This suggests that overlapping transcription occurs in *T. hominis,* as previously reported for the small genome species *E. cuniculi* and *A. locustae,* where a similar number of multi-ORF transcripts (144) was identified (Corradi et al., 2008; Williams et al., 2005). Interestingly, the data suggests that overlapping transcription is not necessarily linked with genome compaction (Corradi et al., 2008; Gill et al., 2008), because gene density in *T. hominis* is actually lower than for yeast (Heinz et al., 2012). One possibility is that overlapping transcription provides a mechanism for co-regulating the expression of particular genes (Zorio et al., 1994). If so, then this mode of regulation is poorly conserved over evolutionary time, because transcriptional overlap is conserved for only one gene pair across *E. cuniculi*, *A. locustae*, and *T. hominis* (Corradi et al., 2008): ribosomal protein L6 (THOM_0162) and RNA polymerase III transcription factor IIIC subunit 5 (THOM_0163), which overlap in the 3' UTR.

4.3.4 Low levels of splicing in T. hominis

A total of 85 introns were predicted in *T. hominis* based upon the presence of conserved *E. cuniculi* intron motifs (Heinz et al., 2012). Surprisingly, transcriptomic evidence was obtained for the splicing of only a single gene – 40S ribosomal protein S23 – at this conserved intron motif (JUNC00000002 in Table 4.1; this gene was spliced efficiently, with 93% of detected transcripts being spliced, higher than the splicing efficiency detected for any spliced gene in the *E. cuniculi* transcriptome (Grisdale et al., 2013). This gene was also one of only two genes for which splicing was detected in transcripts from the microsporidian *Spraguea lophii*, and the intron has a similar length (Campbell et al., 2013). Splicing in general in Microsporidia appears to be inefficient for short introns (Campbell et al., 2013), with splicing rates of less than 15% identified for several *E. cuniculi* transcripts (Grisdale et al., 2013). This potentially explains the inability to detect splicing at the great majority of characterised intron motifs in the *T. hominis* transcriptome. By contrast, evidence was obtained evidence for 13 introns where RNA sequencing reads suggest a spliced exon boundary. One of these novel junctions (JUNC00000048 in Table 4.1) is supported by a greater number of reads than the originally

predicted 40S ribosomal protein S23. Surprisingly, the remaining new experimentally identified introns lack the classical intron motif previously described in *E. cuniculi* (R. C. H. Lee et al., 2010), and an alignment revealed no unique novel motif common to the group (Appendix B).

***T. hominis* Genome Scaffold**	**Start Position**	**Stop Position**	**Junction ID**	**Sequencing Depth**	**Strand**
gi|440491300|gb|JH994095.1|	43594	43861	JUNC00000002	921	+
gi|440491618|gb|JH994056.1|	3451	3706	JUNC00000006	3	-
gi|440492242|gb|JH994017.1|	23199	23362	JUNC00000009	2	-
gi|440492544|gb|JH993988.1|	17612	18063	JUNC00000011	2	-
gi|440492778|gb|JH993971.1|	91029	91289	JUNC00000013	2	-
gi|440493277|gb|JH993926.1|	2085	2738	JUNC00000019	3	+
gi|440493277|gb|JH993926.1|	2085	2425	JUNC00000020	2	-
gi|440493277|gb|JH993926.1|	2131	2328	JUNC00000021	2	+
gi|440493277|gb|JH993926.1|	2131	2388	JUNC00000022	2	+
gi|440493277|gb|JH993926.1|	2131	2520	JUNC00000023	2	+
gi|440493277|gb|JH993926.1|	2131	2652	JUNC00000024	2	+
gi|440493277|gb|JH993926.1|	2496	2763	JUNC00000027	2	+
gi|440493277|gb|JH993926.1|	2529	2761	JUNC00000028	3	+
gi|440493278|gb|JH993925.1|	82566	83152	JUNC00000031	27	+
gi|440493278|gb|JH993925.1|	83012	83731	JUNC00000032	4	-
gi|440493278|gb|JH993925.1|	100673	100827	JUNC00000034	2	+
gi|440493278|gb|JH993925.1|	100783	101133	JUNC00000036	10	+
gi|440493278|gb|JH993925.1|	100783	101237	JUNC00000037	17	+
gi|440493278|gb|JH993925.1|	100823	101027	JUNC00000039	19	+
gi|440493278|gb|JH993925.1|	100856	101286	JUNC00000040	5	+
gi|440493278|gb|JH993925.1|	100896	101103	JUNC00000041	21	+
gi|440493278|gb|JH993925.1|	100952	101340	JUNC00000042	7	-
gi|440493278|gb|JH993925.1|	101021	101203	JUNC00000044	23	+
gi|440493725|gb|JH993866.1|	13021	13291	JUNC00000048	11873	-
gi|440493910|gb|JH993854.1|	41033	41735	JUNC00000050	2	+
gi|440494328|gb|JH993826.1|	20620	20847	JUNC00000056	3	-
gi|440494357|gb|JH993819.1|	5850	6040	JUNC00000058	3	-
gi|440494511|gb|JH993806.1|	30536	30732	JUNC00000060	3	+
gi|440494511|gb|JH993806.1|	30603	30803	JUNC00000061	2	-
gi|440494550|gb|JH993805.1|	9190	9434	JUNC00000062	30	-

Table 4.1: Predicted *T. hominis* intron junctions.

The genomic location and sequencing depth of all intron junctions identified in the *T. hominis* genome by TopHat (see Methods).

4.3.5 Highly expressed T. hominis genes

The top 5% (170 genes) of genes accounted for over half (58%) of all detected transcription in *T. hominis (*Figure 4.6). Fifty three percent of these highly transcribed ORFs belong to a core conserved set of microsporidian genes defined in chapter 3 as those encoded by 9 of the analysed 11 sequenced microsporidian genomes (Nakjang et al., 2013). Of these highly expressed core genes 32% encode rRNA or ribosomal proteins, and 31% encode other essential elements of eukaryotic cell biology including cytoskeletal proteins, transcription and translation factors, cell division proteins (e.g. Nuclear distribution protein (NudC)), histones, and molecular chaperones. Similar functional gene groups (e.g. Ribosome biogenesis and protein translation factors) were significantly enriched in highly expressed genes during proliferative growth of fission yeast (*Schizosaccharomyces pombe*) (Marguerat et al., 2012), suggesting the pattern of expression observed in *T. hominis* may reflect the signatures of its rapid growth and replication in the host cell. The highly expressed core microsporidian genes also include a large number of microsporidian hypothetical proteins of unknown function (37%). In fission yeast, groups of functionally related genes tend to be expressed at similar levels (Marguerat et al. 2012), suggesting that if the same pattern applies to Microsporidia these uncharacterised proteins may also play important and as yet unknown roles in core parasite biology and proliferation.

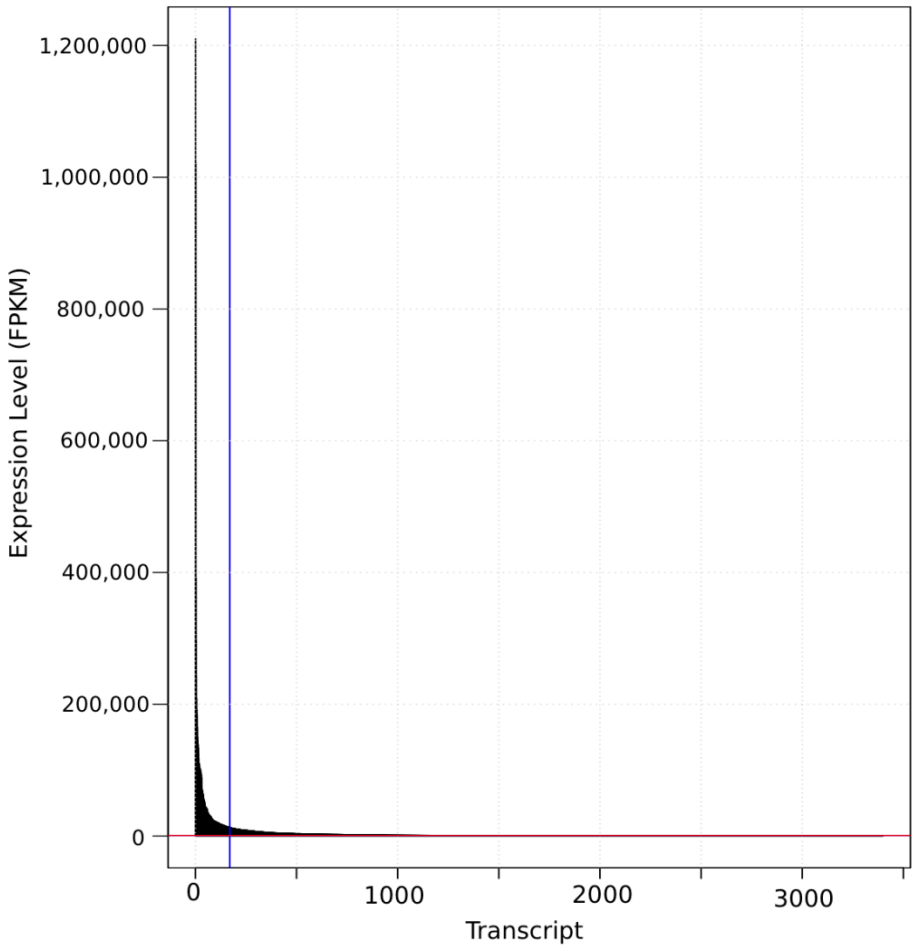

Figure 4.6: Overall expression profile of the *T. hominis* transcriptome.

Distribution of ranked FPKM values for the *T. hominis* transcriptome. The 95th percentile (2240 FPKM) is marked by a blue line and the mean expression value (705 FPKM) is marked by a red line.

The inclusion of molecular chaperones of the HSP40/DNAJ and HSP70 families and protein disulfide isomerase among highly expressed core *T. hominis* genes is intriguing. High expression of HSP70 has been identified in several different microsporidian clades (Gill et al., 2008), suggesting it is a common feature of the group. Chaperones have been identified as important virulence factors in bacterial and eukaryotic pathogens, including intracellular bacteria (Henderson et al., 2006). Published work has demonstrated that intracellular bacteria and bacteria cultured under conditions that introduce a population bottleneck often over-express chaperones to maintain functionality under an increased mutational load (Bogumil and Dagan, 2012; Fares et al., 2002; Liberek et al., 2008; McCutcheon and Moran, 2012; Williams and Fares, 2010). The high levels of chaperonin expression in several

microsporidians, which also experience bottlenecks during transmission and show high rates of sequence evolution (Heinz et al., 2012; Hollister et al., 1996), suggest that these intracellular eukaryotes are behaving in the same way (Gill et al., 2008).

Replication and biosynthesis are energy-requiring processes and hence *T. hominis* must either make or acquire ATP and GTP during proliferation. Genome analyses suggest that *T. hominis* has a complete glycolytic pathway (Heinz et al., 2012) and expression was detected for all of the relevant enzymes in the transcriptome, but only glyceraldehyde 3-phosphate dehydrogenase was in the top 5% of transcripts. The most highly expressed glycolytic enzymes were PBA, GAPDH and PGK, with GAPDH and PGK respectively providing NAD^+ reduction and ATP synthesis. These data suggest that *T. hominis* is potentially making some of the ATP it needs, but the cell stage where this occurs is not resolved by our data. Quantitative immuno-localisation of PGK protein, the first ATP-generating step of glycolysis, suggests that the protein is mainly, but not exclusively, inside *T. hominis* spores rather than vegetative cells (Heinz et al., 2012). It has also been previously suggested that glycolysis occurs mainly in the spores of another microsporidian, *Paranosema grylli* (Dolgikh et al., 1997). Interestingly, transcripts for the most abundant protein identified in spores, Polar Tube Protein 3, were detected at only modest levels in the RNA sequencing data, with an average of 18.1 FPKM ±12.3 SD (within the 30^{th} percentile for expressed genes in the dataset). Indeed, no genes known to be associated with spore wall formation (spore wall proteins, polar tube proteins and chitin synthases) were found in the top 5% of highly transcribed genes; while in the later stages of a time course of *E. cuniculi* infection, during spore formation, PTP2 is the 17^{th} most highly expressed gene in the organism (Grisdale et al., 2013). Conversely, high levels of expression were observed for a number of genes involved in DNA replication and proliferation, consistent with an enrichment of transcripts from the actively proliferating stages of the parasite, and suggesting that some ATP production by glycolysis may occur in these stages of the parasite lifecycle.

Few metabolic enzymes appeared in the top 5% of expressed transcripts, consistent with genomic predictions that *T. hominis* must import many of the substrates it needs for biosynthesis directly from the infected host cell (Heinz et al., 2012; Nakjang et al., 2013). One highly expressed enzyme is nucleotide diphosphate kinase (YNK) (Tsunehiro et al., 1993), which was also highly abundant in proteomic analyses of highly purified spores (Heinz

et al., 2012), YNK is predicted to play a key role in supporting *T. hominis* intracellular proliferation by converting nucleotides or nucleoside diphosphates to their triphosphate forms, the precursors for both RNA and DNA synthesis and sources of cellular energy. High levels of expression were also observed for dUTPase, another enzyme predicted to be involved in nucleotide biosynthesis (Vértessy and Tóth, 2009). The most highly transcribed metabolic enzyme was an asparagine synthetase A (asnA, THOM_2136, InterPro ID: IPR004618). Among Microsporidia, coding sequences for this protein are found on the genomes of *T. hominis, V. culicis, Enterocytozoon bieneusi, N. ceranae* and *Nosema pernyi*, and were likely acquired by lateral gene transfer from bacteria (Heinz et al., 2012; Nakjang et al., 2013). Among eukaryotes, AsnA is almost exclusively found in parasites (Heinz et al., 2012) including *Typanosoma brucei* and *Leishmania donovani*, where it is essential for survival (Loureiro et al., 2013; Manhas et al., 2014). In bacteria, AsnA is responsible for the reversible transamination of aspartate to asparagine in the presence of ATP and ammonia. *Leishmania and Trypanosoma* AsnA, the only characterised eukaryotic homologues, have a broader specificity, and are able to use glutamine as a nitrogen donor to generate glutamate (Loureiro et al., 2013; Manhas et al., 2014). One possibility is that microsporidian AsnA may play important roles in interconversion between essential amino acids, including glutamine, an important precursor to both chitin biosythensis for spore wall formation and glutathione (GSH) biosynthesis required in parasite detoxification systems. This ORF contains an aminoacyl-tRNA synthetase (class II) domain (InterPro ID: IPR004364) suggesting that it may also function to add asparagine to its cognate tRNA. Its specificity to parasitic eukaryotes, coupled with its functional importance, high expression level, and the availability of an AsnA crystal structure make the protein a promising potential drug target (Manhas et al. 2014).

Maintaining supplies of glutamine is important for the generation of GSH, a detoxifying molecule required for the prevention of damage by reactive oxygen species (Lu 2009). The *T. hominis* detoxification system also includes thioredoxin reductases, peroxidases, glutathione reductases and superoxide dismutase (Heinz et al., 2012). While all identified components of this pathway are expressed in *T. hominis*, the highest expressed in our dataset, and only component in the 95th percentile of overall expression levels, was iron/manganese superoxide dismutase (SOD), which reduces and detoxifies superoxide molecules (O_2^-) (Heinz et al., 2012). The largest biological source of superoxide species is as a

by-product in the production of ATP by oxidative phosphorylation, which *T. hominis* does not carry out but which we show is upregulated in host cells during infection by *T. hominis* (see below). *T. hominis* SOD may protect against oxidative stress generated by the host cell as it supports both its own survival and parasite proliferation. Previous work (Biron et al., 2005; Duncan et al., 2012; Panek et al., 2014) has indicated that oxidative stress in the host cell is elevated during infection; therefore, a robust detoxification system is likely to be important for parasite survival, as observed in some bacterial infections (Vanaporn et al., 2011).

One metabolic pathway that is likely to be essential and that has been functionally characterised in Microsporidia is iron-sulphur cluster biogenesis (Goldberg et al., 2008). Iron-sulphur clusters are required for the activity of key proteins needed for microsporidian replication, including DNA polymerase. The metabolic pathway for the biogenesis of iron-sulphur clusters is compartmentalised, starting in the microsporidian mitosome (remnant mitochondrion) and ending in the cytosol (Goldberg et al., 2008). This allows the examination of the variability in levels of transcript abundance between different compartments in a single linked pathway that should be required throughout the parasite lifecycle. The only highly expressed gene in the pathway (in the top 5% of expressed transcripts) was Dre2, a cytosolic component of iron-sulphur cluster biogenesis (Zhang et al., 2008). Interestingly, Dre2 also plays a role in inhibiting free radical-induced apoptosis (Zhang et al., 2008); given that other detoxifying enzymes are also highly expressed in *T. hominis*, it may be this function of Dre2 that drives its high expression level. Consistent with this idea, the other components of iron-sulphur cluster biogenesis are expressed at significantly lower and similar levels, suggesting that genes in the same pathway may be generally expressed at similar levels in *T. hominis*, as observed in fission yeast (Marguerat et al., 2012).

Surface-located transport proteins are predicted by genome analyses to be fundamental for supporting the replication of *T. hominis* and other microsporidians by importing substrates from infected host cells (Heinz et al., 2014, 2012; Nakjang et al., 2013; Tsaousis et al., 2008; Vávra and Lukeš, 2013). The expression of *T. hominis* proteins related to known transporters, or annotated as potential transporters, is very heterogeneous within structural types. Only three predicted transport proteins are found in the top 5% (> 2210 FKPM) of expressed genes and these do not include any of the *T. hominis* nucleotide (NTT1-4) transporters for which functional data is available (Heinz et al. 2014).The most highly

expressed of these - NTT4 - appears in the 92nd percentile of expression levels. NTT4 is one of four paralogous nucleotide transporters that are expressed on the surface of replicating parasites (Heinz et al., 2014), where they function to transport purine nucleotides including ATP and GTP, for energy and/or biosynthesis (Heinz et al., 2014). Of the three highly expressed transporters, the first and third in terms of expression are hypothetical transporters of unknown specificity while the second is a putative inorganic phosphate transport protein. Given the potential importance of the NTT transporters it seems possible that these more highly transcribed transporters also support important, albeit currently uncharacterised, cellular functions.

The most highly transcribed of the three membrane proteins (THOM_1886) appears to be specific to *T. hominis* and its closest sequenced relative, *V. culicis,* as determined by sensitive PSI-BLAST (Altschul, 1997) and HMMER (Finn et al., 2011) based searches. The THOM_1886 protein is predicted to include 7 transmembrane domains and was annotated as a putative transport protein (Heinz et al., 2012). Its expression level is more than 1500x that of the average transporter in our study (22209 FPKM ± 5483 SD) suggesting that, in addition to the conserved common core of microsporidian genes, lineage-specific innovation is also important for parasite biology.

4.3.6 Levels of T. hominis gene expression are correlated with gene history and conservation among microsporidians

Comparative analyses of the genome of *T. hominis* with other microsporidian genomes have demonstrated that genome evolution has been a dynamic process, in which the loss of ancestral gene families has been partially offset by the gain of new microsporidia-specific genes (Campbell et al., 2013; Cornman et al., 2009; Corradi et al., 2010; Cuomo et al., 2012; Heinz et al., 2012; Katinka et al., 2001; Nakjang et al., 2013). In this broader evolutionary context, *T. hominis* genes can be classified into three major groups: core eukaryotic genes – that is, core microsporidian genes defined in chapter 3 (Nakjang et al., 2013) that were also found in most or all eukaryotes; ancestral microsporidian innovations, or core microsporidian genes that evolved in the common ancestor of all microsporidia (and thus are not identified in other eukaryotes); and recent innovations (for example THOM_1886) that are only found in *T. hominis*, or that are shared between *T. hominis* and its close relative *V. culicis.* To evaluate the relationship between evolutionary conservation and expression

level in *T. hominis*, the expression levels of the genes in these three classes were compared using a linear mixed-effects model (Figure 4.7).

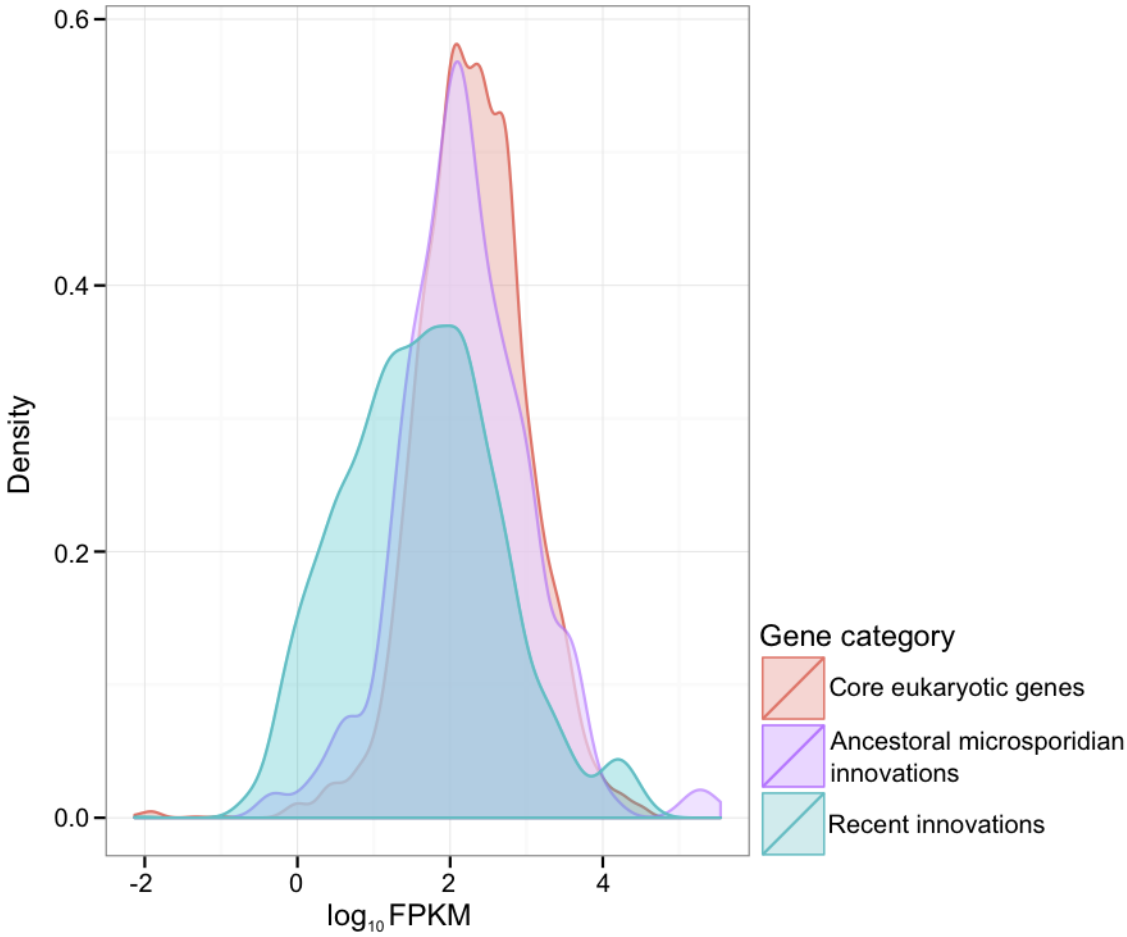

Figure 4.7: Levels of *T. hominis* gene expression are correlated with gene history and conservation among microsporidians.

T. hominis genes can be classified according to the period in evolutionary history when they first arose: core eukaryotic genes, shared with most or all other eukaryotes and encoding fundamental features of eukaryotic cell biology; ancestral microsporidian innovations, found only in *T. hominis* and other microsporidians; and recent innovations, genes found only in *T. hominis* and its close relative *V. culicis*. This density plot shows the distribution of expression levels (as $\log_{10}$FPKM) for *T. hominis* genes in each of these three categories. Mixed-effects modelling indicates that core eukaryotic genes and ancestral microsporidian innovations are expressed at significantly higher levels than recently-evolved *T. hominis* genes (P = 0), but that there is no significant difference in expression patterns between the former two classes (P = 0.166); the recently-evolved genes also show a much broader range of expression than the older gene classes, perhaps reflecting greater variation in functional constraints within this group.

Analysis indicated that core eukaryotic genes and ancestral microsporidian innovations were both expressed at significantly higher levels than recently-evolved genes specific to the *T. hominis*/*V. culicis* lineage (P = 0), but that there was no significant difference in expression levels between the two more highly-expressed classes (P = 0.166). The consistently high expression levels for core eukaryotic genes are not, in themselves, particularly surprising: this category includes genes involved in basic cellular processes such as DNA replication and repair, mitochondrial iron-sulphur cluster assembly, intracellular trafficking and in some metabolic pathways such as glycolysis and the pentose phosphate pathway. However, the equally high level of expression observed for ancestral microsporidian innovations is interesting because it implies that genes which first evolved in the common ancestor of microsporidia, and which were then conserved across the group, are as important to microsporidians – by the measure of transcript abundance - as genes encoding the fundamental eukaryotic cellular componentry.

By contrast, genes specific to the *T. hominis*/*V. culicis* lineage are expressed at significantly lower levels than other genes in the parasite (P = 0); genes shared between these close relatives were used to minimise the impact of *T. hominis* specific false ORF calls on our analyses. Most of these genes are expressed (735 out of 862, or 85%), but not necessarily at high levels; as can be seen from Figure 4.7, this class of recently evolved genes displays a broad range of expression levels. The more heterogeneous distribution of expression levels for recently evolved genes is consistent with a recently proposed model (Carvunis et al., 2012) for the gradual emergence of proto-genes from previously non-coding sequence. Under this model, some new, fortuitously expressed genes acquire important functions and are maintained by selection, while others do not and will eventually be lost to drift and pseudogenisation. It is possible that this process of genomic innovation underpins recently evolved host-parasite interactions for these two species, both of which are thought to infect insects as their natural hosts (Becnel and Andreadis, 2014; Heinz et al., 2012). Consistent with this hypothesis, the *T. hominis/V. culicis*-specific families are enriched for signal peptides (P = 1.2 x 10^{-10}, Fisher's exact test) (Nakjang et al., 2013), suggesting that the proteins in these families may be localised to the parasite cell surface, part of the infective polar tube, or secreted into the host cell.

4.3.7 Expression divergence in expanded T. hominis gene families

In contrast to the general trend of reductive evolution among microsporidians, a number of *T. hominis* gene families have expanded through gene duplication. Gene duplication is important in the evolution of gene family function, because duplication events can relax selective constraints allowing the functions of one or both paralogues to change (Force et al., 1999; Ohno, 1970). Consistent with a role for duplication and functional divergence in microsporidian evolution, (Nakjang et al., 2013) and (Heinz et al., 2014) found evidence of sequence divergence at conserved amino acid residues following microsporidia-specific duplications in the Hsp90 chaperone, Ste24 metalloprotease, NTT nucleotide transporter, ZiP zinc ion permease, SulP sulphate permease and NupG nucleoside transporter families. Intriguingly, members of expanded gene families tend to be expressed at above-average levels in *T. hominis* ($P = 3 \times 10^{-4}$, linear mixed-effects model).

Figure 4.8 summarises expression levels for the functionally characterised *T. hominis* nucleotide (NTT) transport proteins (Heinz et al. 2014) and *T. hominis* members of five additional microsporidian gene families investigated by in Nakjang et al. (2013) (Nakjang et al., 2013) that were identified as having undergone sequence divergence following gene duplication in Microsporidia. The variation in expression level is clearly correlated with the evolutionary history of the gene family: in all of these cases, the most highly conserved family member, in terms of conservation of critical residues or branch length in gene family trees (Heinz et al., 2014; Nakjang et al., 2013), is also the most highly expressed. These data are consistent with a model of functional divergence whereby one conserved, highly-expressed paralogue continues to carry out the ancestral function, while other duplicates experiencing reduced selective constraint can gain new functions (Conant and Wagner, 2003; Conant and Wolfe, 2008; Kellis et al., 2004). Any new functions, which could include stage-specific expression, different cellular location or substrate affinity or specificity, will need to be identified through experiment. For example, proteomics data already suggest that NTT4, the most highly expressed member of the gene family (Figure 4.8), is the main NTT transporter located within the *T. hominis* spore (Heinz et al., 2012). In the *Encephalitozoon* lineage the NTT transporter family has undergone an independent expansion (Heinz et al., 2014). In *E. cuniculi* this expansion was followed by divergence in both sequence and localisation, with one family member (EcNTT3) localised to the mitosome while the other three are located on the surface of replicating parasites (Tsaousis et al.,

2008). The correlation between sequence divergence and transcript abundance observed in *T. hominis* is maintained in *E. cuniculi* (Grisdale et al., 2013), with divergent family members (EcNTT3 and EcNTT4) expressed at lower levels (mean FPKM 139 for EcNTT3, 96 for EcNTT4) than the more highly conserved family members (EcNTT1 and EcNTT2 – 402 and 977 FPKM respectively).

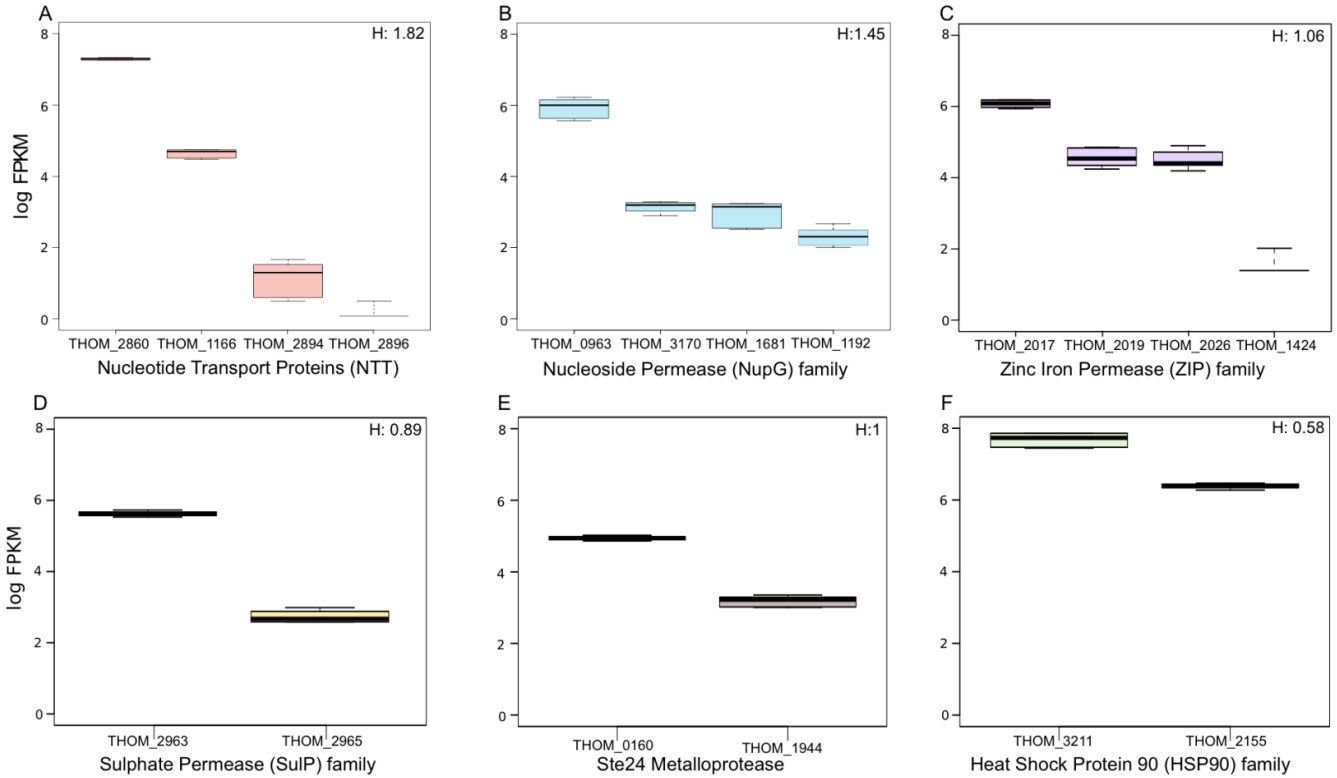

Figure 4.8: Members of gene families with evidence of sequence divergence also show variable levels of gene expression.

Expression levels ($\log_{10}$ FPKM) for the members of gene families in which functional divergence was previously detected at the sequence level (Nakjang et al. 2013). In each case, the most highly expressed paralogue is also the most highly conserved based on single gene trees. H, the heterogeneity index calculated for each gene family, is also shown (see Materials and Methods). A) Nucleotide transport proteins (NTTs). B) NupG-related nucleoside permeases. C) Zinc iron permase (Zip) family. D) Sulphate permease (SulP) family. E) Ste24 metalloprotease family. F) Heat shock protein 90 (HSP90) family.

To evaluate variation in expression among microsporidian gene duplicates more systematically, expression was analysed for all duplicate families identified by the phylogenetic screen of Nakjang et al. 2013 (Nakjang et al., 2013) which contained at least two paralogues in *T. hominis*. We calculated the standard deviation of FPKM values within each family, and normalised by the per-family mean (see Materials and Methods) (Table 4.2; Appendix C). Expanded *T. hominis* families were then ranked by this metric to identify the families showing the most extreme expression divergence. Plotting these scores revealed an inflection point in the distribution of the metric, above which we considered within-family expression to be the most highly heterogeneous (Figure 4.9). The most heterogeneous family identified by this approach included a family of retrotransposon-encoded reverse transcriptase; some family members had no detectable expression, suggesting ongoing pseudogenisation as might be expected for transposable elements. The group of *T. hominis* families showing the greatest expression divergence also includes the hexokinase gene family, whose paralogues in the microsporidian *N. parisii* have been suggested to manipulate host metabolism following secretion into the host cell (Cuomo et al., 2012). *T. hominis* encodes four hexokinases of which two include predicted signal peptides (Nakjang et al., 2013), consistent with the hypothesis that they may be secreted into the host cell. One hexokinase lacking a signal peptide (XLOC_001491) is the most highly expressed member of the family, again consistent with the idea that the most highly conserved member of a duplicated family continues to perform the ancestral function.

Gene Family	Heterogeneity Index	Annotation	KOG Category
c_563_	1.863932	RNA-directed DNA polymerase (reverse transcriptase)	[A]
c_474_	1.547009	Haloacid dehalogenase-like hydrolase (similar to SDT1; PHM8;)	[R]
c_456_	1.449592	MFS transport protein family	-
c_31765_	1.414214	hypothetical protein	-
c_201_	1.34656	Hexokinase (similar to HXK2; HXK1; GLK1; EMI2;)	[G]

Table 4.2: Heterogeneity in expression of duplicated gene families

Top ranked duplicated gene families (Nakjang et al., 2013) containing at least two paralogues in *T. hominis* according to their expression heterogeneity index. See Appendix C for full table.

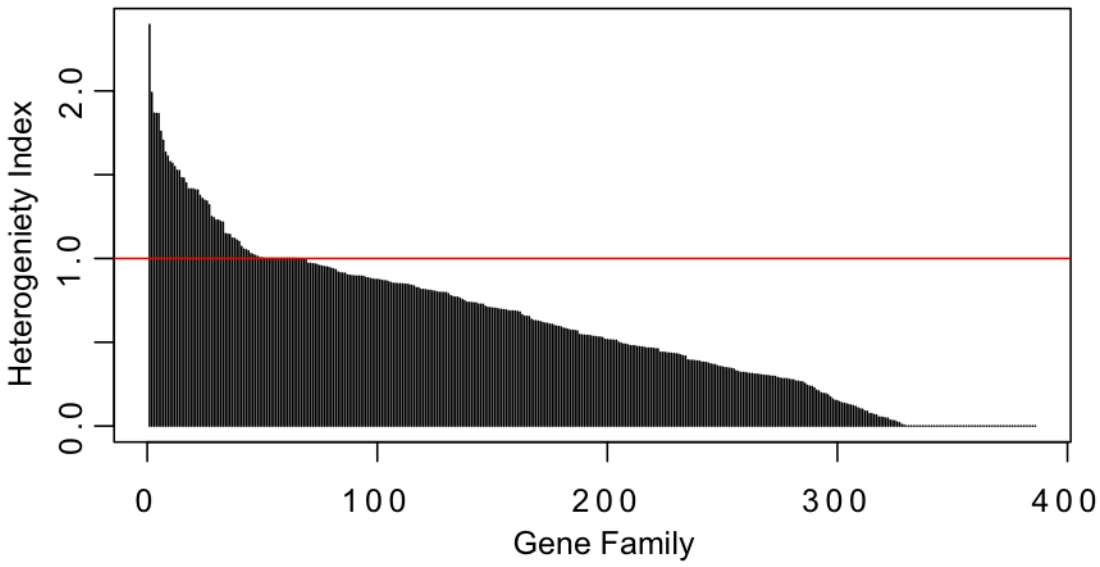

Figure 4.9: Heterogeneous expression in expanded microsporidian gene families.

Distribution of ranked heterogeneity index (see Methods). The red line denotes the inflection point above which we considered gene families to show relatively high levels of expression heterogeneity.

4.3.8 Parallel horizontal transfers of transposons implicate an insect host in the lifecycle of T. hominis

T. hominis is one of several microsporidians that retain elements of the RNA interference machinery (Heinz et al., 2012). The core components of this machinery, Dicer and Argonaute, are both expressed by *T. hominis* during infection but are not in the top 5% of expression. The RNAi machinery is hypothesised to play a role in defence against transposon activity in Microsporidia (Heinz et al., 2012). Consistent with this hypothesis, evidence was obtained for the expression of 58 of the 110 annotated transposons in the *T. hominis* genome. Combined with evidence for transcription of transposons in *Edhazardia aedis* (Gill et al., 2008), these data suggest that active transposons pose an ongoing threat to genome integrity in microsporidians more generally.

Although *T. hominis* is an opportunistic parasite of immunocompromised humans, its natural host remains unknown. *T. hominis* can proliferate within artificially infected mosquitoes under experimental conditions, but these infections have not been observed in nature (Weidner et al., 1999). One of the novel transcripts identified in this study showed similarity to a PiggyBac transposase (Cary et al., 1989). This transcript maps to a previously unannotated portion of the *T. hominis* genome, and is therefore distinct from the PiggyBac

element reported in the original genome annotation (Heinz et al., 2012). The best BLAST hits to the novel PiggyBac element include transposable elements from insects but not other Microsporidia, raising the possibility that *T. hominis* gained the element in a recent horizontal transfer that occurred after the divergence of *T. hominis* from its close relative *V. culicis*. A PiggyBac element identified as recently acquired in bats has been demonstrated to retain activity when inserted into both human and yeast cells, highlighting the capacity of this particular family of transposons for inter-species transfer (Mitra et al., 2013). Phylogenetic analysis of the novel *T. hominis* element strongly suggests that it was recently acquired from an insect, and probably a member of the Hymenoptera (ants, bees and wasps; Figure 4.10). The *T. hominis* sequence forms a strongly supported clade with PiggyBac elements from bees (*Bombus impatiens* and *Megachile rotundata*) and the ant *Harpegnathos saltator* (Figure 4.10, Clade B). Interestingly, this transfer appears to have occurred independently of the previously identified PiggyBac acquisition from insects in *T. hominis*, which branches in a separate insect clade with maximal posterior support (1.0 posterior probability; Figure 4.10, Clade A). In both cases, the most closely related sequence is from Jerdon's jumping ant (*Harpegnathos saltator*), although the posterior support for this relationship is variable (0.99 in Clade A, and 0.77 in Clade B). The phylogeny of the two separate *T. hominis* PiggyBac elements provides consistent support for the hypothesis that *T. hominis* infections of humans may represent opportunistic zoonosis from a natural hymenopteran host. Interestingly, a separate novel horizontal transfer from insects into the microsporidian *Nosema apis*, a honeybee parasite (Zander, 1909), was also identified, providing further support for the horizontal transfer of host-derived transposable elements into Microsporidia (Figure 4.10, Clade C) (Guo et al., 2014; Pan et al., 2013; Parisot et al., 2014).

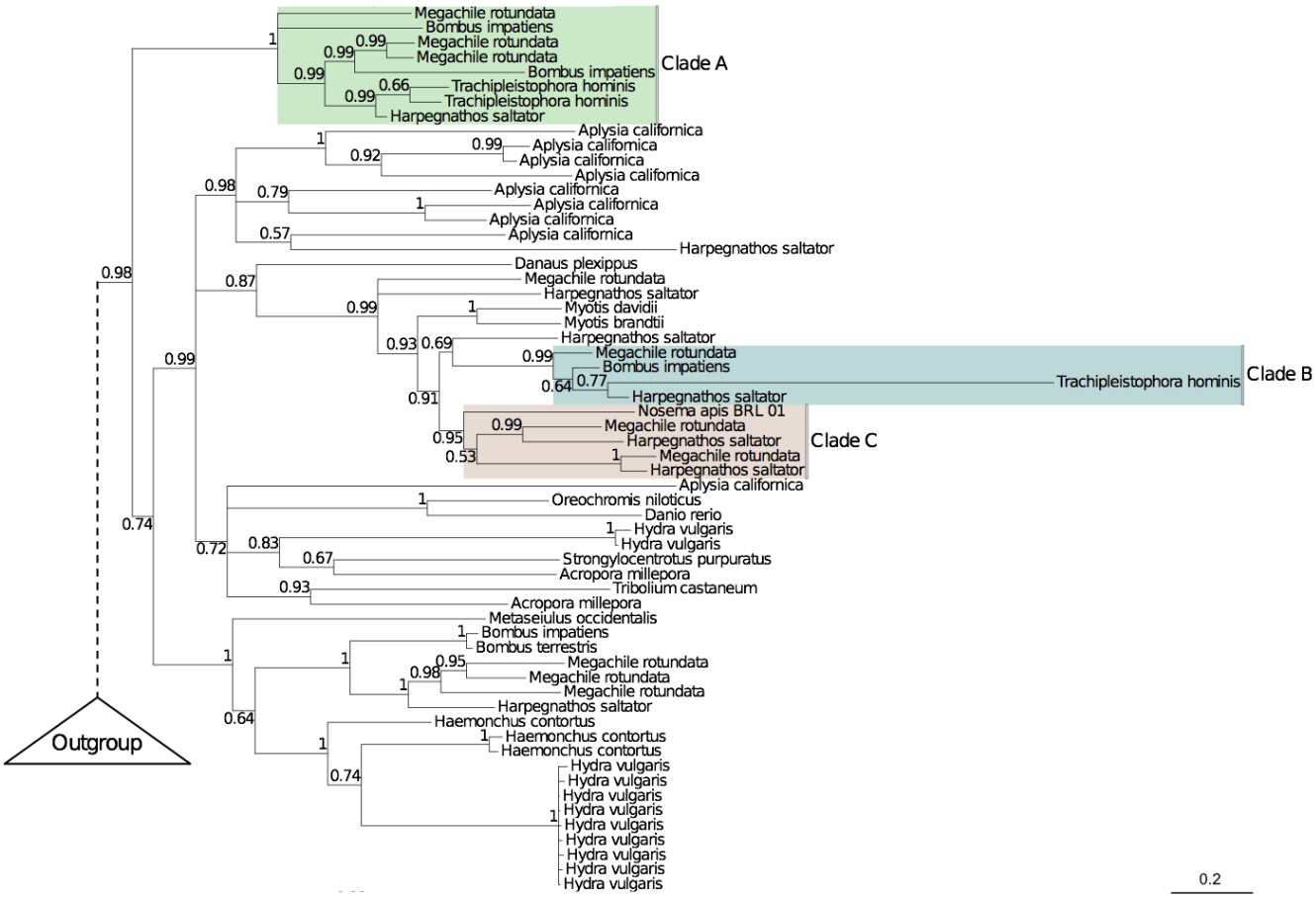

Figure 4.10: Phylogenetic analysis of PiggyBac transposons suggests a natural insect host for *T. hominis*.

A Bayesian phylogeny of *T. hominis* PiggyBac transposases inferred under the C20 model (Quang et al., 2007) in PhyloBayes (Lartillot et al., 2009). Support values are Bayesian posterior probabilities, and branch lengths are proportional to the expected number of substitutions per site. The tree topology supports two recent, independent transfers of PiggyBac elements from hymenopteran insects into *T. hominis.* In both cases, the ant *Harpegnathos saltator* is recovered as the closest relative of the *T. hominis* sequence, although with variable posterior support. We also identify a transfer from insects into the microsporidian *Nosema apis*, a honeybee parasite. Clade A – An insect clade including two *T. hominis* PiggyBac elements, as identified in (Heinz et al., 2012). Clade B – A distinct clade of insect elements, including the newly discovered *T. hominis* PiggyBac element. Clade C – Clade including *Nosema apis* and insect PiggyBac elements.

4.3.9 Patterns of single nucleotide polymorphisms reveal that T. hominis is diploid

Microsporidia replicate inside their host cell, and can only exist outside it as a resistant and infectious spore (Vávra and Lukeš, 2013). This would be a barrier to sex between two different parasite cells, which would require multiple independent infections of a single host cell. Nonetheless, limited evidence for a sexual reproduction cycle has been identified in several microsporidians (Ironside, 2007). The early morphological characterisation of *Ambylospora* identified a meiosis-like stage of division including karyogamy the fusion of two haploid nuclei to form a single diploid nucleus (Hazard and Brookbank, 1984). Recent studies of the *Nosema/Vairimorpha* lineage have also provided some evidence for sex and recombination (Ironside, 2007). Although proliferating *T. hominis* cells can contain multiple nuclei, nuclear fusion has never been observed (Field et al., 1996; Hollister et al., 1996). Our RNAseq data presents an opportunity to investigate the ploidy of *T. hominis* and to test whether sexual reproduction may be possible.

7596 variant sites (polymorphisms) were identified in the *T. hominis* transcriptome, with a total of 7654 possible variants. These included 7120 single nucleotide polymorphisms (SNPs), 314 insertions and 220 deletions. Plotting the allele frequency spectrum of the variations reveals a clear peak at a frequency of 0.5 (50% reference genome allele, 50% alternative allele) (Figure 4.11A). The *T. hominis* populations in this study are likely to be clonal, both because their obligate intracellular lifecycle results in a population bottleneck in each generation, and also because our experimental isolate has been passaged repeatedly in cell culture. In addition, population-level variation would not be expected to give rise to a peak at 0.5, unless two distinct populations had somehow been maintained in a 50:50 ratio. Given these considerations, the simplest interpretation of the observed allele frequency spectrum is that the genome of *T. hominis* is diploid in at least some stages of its lifecycle and that, at least in the majority of cases, both alleles are expressed. *T. hominis* is unikaryotic – that is, it has one nucleus per spore – and so the results are consistent with analyses suggesting that other unikaryotic microsporidians are also diploid (Cuomo et al., 2012; Haag et al., 2013; Selman et al., 2013). The diploidy of *T. hominis* and other unikaryotic Microsporidia supports the notion that diplokaryotic Microsporidia are likely to be tetraploid (Pelin et al., 2015), containing two diploid nuclei as observed in the diplomonad *Giardia lamblia* (Bernander et al., 2001). The diploidy of *T. hominis* raises the possibility that it

occasionally has sex, although the density of SNPs in our dataset was not sufficiently high to evaluate the possibility of recombination or linkage disequilibrium. Although the *T. hominis* spore is unikaryotic, the intracellular stages of its lifecycle divide by a combination of binary division and plasmotomy, the division of a single cell producing multinucleate progeny (Field et al., 1996; Hollister et al., 1996). This raises the possibility that meiosis could still be triggered in multinuclear intracellular stages of the parasite lifecycle.

A total of 5496 SNPs were identified within annotated *T. hominis* ORFs, with 2175 non-synonymous and 2933 synonymous changes. SNPs were identified in 1551 ORFs in total, with 1071 of these ORFs including non-synonymous changes, leading to possible protein variants. Although the possibility that some non-synonymous mutations might be beneficial cannot be excluded, we expect the majority to be deleterious, particularly given the frequent genetic bottlenecks experienced by our artificially maintained experimental population. 388 changes were more severe in nature, either including frameshifts or alterations to start and stop codons. In principle, the deleterious effects of these mutations could be suppressed in a diploid organism by preferential expression of the reference allele. However, the peak at 0.5 is still observed in the frequency spectrum for non-synonymous alleles (Figure 4.11B), implying that synonymous, non-synonymous and reference alleles are all expressed at similar levels. 34% of all SNPs occurred in “core” microsporidian genes – those shared among at least 9 of 11 sequenced Microsporidia and predicted to play an important role in the parasite. The expression of these variants is perhaps surprising due to their potential impact on protein function. However, it is important to remember that this study examines a single population of *T. hominis,* and that many of these SNPs may be en route to elimination by negative selection. Another possibility is that the high levels of expression observed for key molecular chaperones may help to suppress the phenotypic effect of these deleterious mutations, as has previously been reported for intracellular bacteria (Fares et al., 2002).

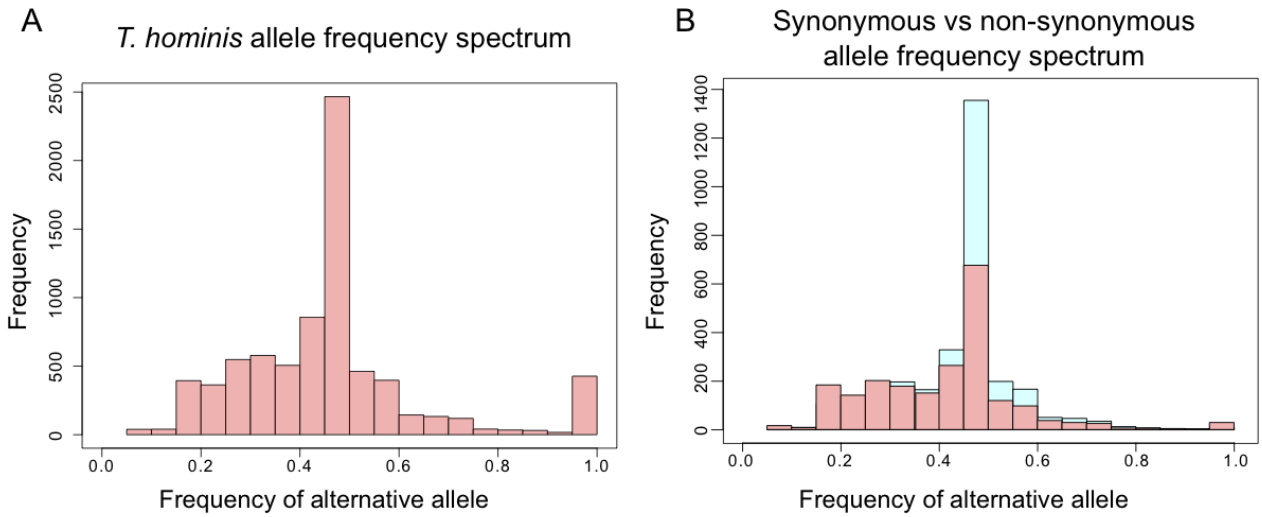

Figure 4.11: The allele frequency spectrum of SNPs in expressed *T. hominis* transcripts suggests a diploid phase to the parasite lifecycle.

A) The allele frequency spectrum (reference and alternative alleles) for *T. hominis* SNPs. The clear peak at an allele frequency of 0.5 suggests that *T. hominis* is diploid. B) Allele frequency spectra with synonymous and non-synonymous SNPs plotted separately. The distributions are similar, providing no evidence for reduced expression of non-synonymous alleles.

4.3.10 Response of the RK-13 cell line to infection with T. hominis

Recent studies have begun to shed light on the mechanisms by which microsporidians exploit their hosts (Estes et al., 2011; Heinz et al., 2014; Troemel et al., 2008; Tsaousis et al., 2008), but little is known about the host response to infection at the molecular level. Host gene expression was quantified to identify genes and pathways that were differentially expressed in RK-13 cells during infection with *T. hominis* compared to uninfected cells (Appendix D). These analyses provide a first snapshot of the impact of *T. hominis* infection on the host cell transcriptome. 1734 transcripts were identified that showed significant changes in expression in the RK-13 cell line during infection with *T. hominis* (Table 4.3; Appendix E). KEGG categories (Kanehisa and Goto, 2000) were assigned to these transcripts using the KOBAS annotation pipeline (Xie et al., 2011); nine KEGG categories were enriched for differentially expressed transcripts (Table 4.4; Appendix F); that is, these categories contained more genes whose expression levels changed in response to infection than would be expected by chance, allowing us to explore the general effects of infection on the host cell.

Transcriptome Gene ID	Uninfected RK-13 Mean FPKM	T. hominis infected RK-13 Mean FPKM	Fold Change	Log2 Fold Change	Test stat	P value	Q value	Ensembl Gene Name / Gene ID
XLOC_013192	0.12	1.99	16.71	4.06	3.77	3.40E-03	3.83E-02	NA
XLOC_019479	13.43	154.74	11.52	3.53	17.99	5.00E-05	1.41E-03	NA
XLOC_006353	0.46	3.79	8.17	3.03	5.05	5.00E-05	1.41E-03	NA
XLOC_014575	0.20	1.50	7.62	2.93	3.32	9.00E-04	1.42E-02	TMIGD1
XLOC_005410	0.45	3.05	6.84	2.77	4.64	5.00E-05	1.41E-03	NA
XLOC_010795	0.77	5.16	6.73	2.75	4.28	4.50E-04	8.42E-03	NA
XLOC_020722	4.85	30.16	6.22	2.64	7.69	5.00E-05	1.41E-03	KL
XLOC_011043	0.96	5.75	5.99	2.58	3.30	5.00E-05	1.41E-03	AGT
XLOC_031144	2.18	13.01	5.97	2.58	5.63	2.00E-04	4.42E-03	NA
XLOC_031145	0.37	2.09	5.72	2.52	3.23	8.00E-04	1.30E-02	NA
XLOC_008693	12.24	2.03	0.17	-2.59	-6.26	2.95E-03	3.44E-02	RPL35A
XLOC_016769	28.06	4.29	0.15	-2.71	-8.95	1.00E-04	2.52E-03	LBH
XLOC_032831	45.21	6.90	0.15	-2.71	-6.22	5.00E-05	1.41E-03	PAI1
XLOC_015300	7.71	1.02	0.13	-2.91	-8.04	5.00E-05	1.41E-03	HDAC5
XLOC_038191	12.15	1.47	0.12	-3.05	-6.04	1.30E-03	1.87E-02	ENSOCUG00000001791
XLOC_009703	5.23	0.57	0.11	-3.20	-5.80	5.00E-05	1.41E-03	NA
XLOC_007088	5.62	0.55	0.10	-3.35	-5.78	5.00E-05	1.41E-03	NTNG1
XLOC_024890	919.29	74.05	0.08	-3.63	-107.60	1.75E-03	2.35E-02	NA
XLOC_011178	20.97	1.61	0.08	-3.71	-4.40	5.00E-05	1.41E-03	U6
XLOC_027036	57.50	4.29	0.07	-3.75	-15.26	2.80E-03	3.32E-02	NA

Table 4.3: RK-13 transcripts identified as significantly differentially expressed during infection.

The top ten genes with the highest positive and negative fold change identified by cuffdiff (Trapnell et al., 2013) as significantly differentially expressed in the RK-13 host cell during *T. hominis* infection. Q-values are P-values that have been corrected for multiple testing using the false discovery rate. See attached CD, appendix E or table S5 at http://bmcgenomics.biomedcentral.com/articles/10.1186/s12864-015-1989-z for full table.

KEGG pathway name	KEGG id	% of gene modulated	Number of differentially expressed trancripts in pathway	Total number of rabbit genes in pathway	P-Value	Corrected P-Value
Ribosome	ko03010	0.2460137	108	439	2.61E-11	7.12E-09
DNA replication	ko03030	0.4166667	15	36	0.000133671	0.015926366
Pyrimidine metabolism	ko00240	0.2636364	29	110	0.000175015	0.015926366
Oxidative phosphorylation	ko00190	0.2323944	33	142	0.000470803	0.024954057
Meiosis - yeast	ko04113	0.3064516	19	62	0.000483241	0.024954057
Cell cycle - yeast	ko04111	0.2837838	21	74	0.000587157	0.024954057
Renal cell carcinoma	ko05211	0.28	21	75	0.000679558	0.024954057
Amino sugar and nucleotide sugar metabolism	ko00520	0.3148148	17	54	0.000731254	0.024954057
Focal adhesion	ko04510	0.1990741	43	216	0.001207557	0.036629238
ECM-receptor interaction	ko04512	0.25	22	88	0.001789389	0.048850311

Table 4.4: Testing for enrichment of differentially expressed genes in KEGG pathways

Fischer's exact test with Benjamini and Hochberg correction (Benjamini and Hochberg, 1995) for the enrichment of genes identified as significantly differentially expressed in KEGG pathways in the RK-13 cell line. See attached CD, appendix F, or table S6 at http://bmcgenomics.biomedcentral.com/articles/10.1186/s12864-015-1989-z for full table.

. The pathways enriched in differentially expressed genes in RK-13 cells during infection can be broadly divided in to three categories: metabolism, cell cycle related proteins, and genes involved in cell - cell interactions. The analysis suggests that the host experiences a generalised cellular shutdown in response to *T. hominis* infection, with the down-regulation of the great majority of genes involved in the KEGG pathways for the cell cycle, meiosis, DNA replication, and ribosome biogenesis (Appendix G). A shutdown in the cell cycle has previously been observed in the response to infection with *E. cuniculi* (Scanlon et al., 2000), as well as complex multinucleation phenotypes for host cells *in vivo* for *E. cuniculi infections* (Fuentealba et al., 1992), or *in vitro* for *Vittaforma corneae* infections

(Leitch et al., 2005), suggesting that changes to the host cell cycle are a common response to microsporidian infection.

Pathways for metabolism or cell-cell interactions show a mixture of both up-regulated and down-regulated genes relative to the uninfected control; these pathways are clearly disrupted during *T. hominis* infection, but the overall effect on the host is difficult to predict from changes in transcript abundance. Although these patterns are complex and difficult to interpret, they were also consistent across three biological replicates, and therefore represent reproducible perturbations of host cell pathways. The pathways included those involved in focal adhesion, extracellular matrix-receptor interactions, oxidative phosphorylation, and pyrimidine biosynthesis In a review of differentially regulated host pathways in other microsporidian host-parasite systems identified metabolism as the common feature identified as differentially expressed in all studies (Szumowski and Troemel, 2015). Proteins involved in cell-cell interactions in the form of lectins were differentially expressed in two host-parasite systems (Szumowski and Troemel, 2015). These results demonstrate that similar host pathways are differentially expressed in multiple different microsporidian host-parasite systems, suggesting there may be common features of the response to infection. Contrasting this finding, differences in the expression of several genes in the ubiquitination pathway that have been implicated in the immune response of *C. elegans* to *N. parisii* infection (Bakowski et al., 2014) were not identified in RK-13 cells infected by *T. hominis*. Although the expression levels of several host ubiquitination genes were altered upon *T. hominis* infection, the pathway as a whole was not enriched in differentially expressed genes in our analysis. Further study would be required to explore whether the ubiquitin system may be part of a general host response to microsporidian infection.

The only host cell pathways in which the majority of changes were up-regulations relative to the control were amino sugar and nucleotide sugar metabolism (Appendix G), potentially leading to increased production of nucleotide sugars by the host. Similar changes to silkworm metabolism were observed during infection with *Nosema bombycis*, suggesting that this may be common feature of microsporidian infection (Ma et al., 2013). Candidate nucleotide sugar importers have been identified in *T. hominis* (Heinz et al., 2012) and other Microsporidia, consistent with the idea that microsporidians might manipulate host

metabolism to increase production of required substrates. One potential mechanism for the manipulation of host metabolism that has already been proposed is the secretion of hexokinase into the host cell (Cuomo et al., 2012). As in mammalian cancer cells (Mathupala et al., 2010), Microsporidia infected RK-13 cells had a modulated hexokinase expression profile compared to healthy cells, possibly to the benefit of the intracellular parasite. The two hexokinase isozymes (HKI and HKII) with the highest affinity for glucose in mammals (Wilson, 2003) were significantly differentially expressed in the host during infection, with an increase in HKI and a decrease in HKII. HKI is believed to have a primarily catabolic function, driving glycolysis and ATP production (Wilson, 2003) - an essential molecule for *T. hominis* growth and replication. These changes in gene expression draw striking parallels to other host-parasite systems, where complex changes in host energy metabolism (Martin et al., 2006; Wang et al., 2004) and pyrimidine biosynthesis (Munger et al., 2006) are associated with infection.

A number of pathway regulators were also differentially expressed in RK-13 cells during *T. hominis* infection, providing insights into the potential mechanisms that might underpin some of the observed changes in transcript levels of metabolic genes. Significant up-regulation of host 5'-AMP-activated protein kinase catalytic subunit alpha-2 (PRKAA2) and peroxisome proliferator-activated receptor gamma co-activator 1-alpha (PPARGC1A) was observed during *T. hominis* infection, both of which are reported to promote energy metabolism and mitochondrial biogenesis (Lin et al., 2005; Towler and Hardie, 2007). PRKAA2 is additionally implicated in shutting down ATP-consuming pathways including cell proliferation (Towler and Hardie, 2007), consistent with our observation of decreased expression of genes in this pathway.

Linked to the above inference of increased host ATP production coupled with reduced consumption, a significant decrease in the expression of host pyruvate dehydrogenase lipoamide kinase isozyme 4 (PDK4) was also observed during infection. This kinase represses metabolism through the phosphorylation and inactivation of pyruvate dehydrogenase, the enzyme that converts pyruvate to acetyl-coA, thereby linking glycolysis and the citric acid cycle (Kim et al., 2006). Decreased expression of PDK4 would lead to increased activity of pyruvate dehydrogenase, promoting citric acid cycle-based metabolism and, under normal oxygen conditions, increased ATP production (Holness and Sugden, 2003;

Kim et al., 2006). The increased glucose required to support the elevated metabolic demand might be acquired by increased import since the glucose transporter GLUT9 (Doblado and Moley, 2009) is highly up-regulated transporter during infection by *T. hominis*.

4.4 Conclusions

Our transcriptomics data was highly reproducible for parasite and host, and confirmed that *T. hominis*, with ~3150 genes, has one of the largest coding capacities among microsporidians (Heinz et al., 2012; Peyretaillade et al., 2014). Although our data does not support some of the shortest predicted gene models, this was compensated by the identification of genes that were previously missed by the genome annotation. Some of these, including transporters that may acquire pyrimidines and enzymes that function in chitin biosynthesis, may plug what were previously considered to be gaps in the metabolic capacity of the parasite.

Gene expression for the parasite was highly biased towards growth and replication, consistent with published microscopic data (Field et al., 1996; Hollister et al., 1996) demonstrating rapid parasite proliferation after infection. Intriguingly, a proportion of the highly expressed transcripts are encoded by conserved microsporidian genes of unknown function, suggesting there is much still to discover about the core biology of these highly successful parasites. Expression within expanded gene families, including key transport proteins, was highly variable. In most cases the most highly conserved members of gene families were also the most highly expressed, consistent with evolutionary models in which duplication can free individual paralogues to diversify in function while preserving the ancestral function in the conserved copy. The expression of genes confined to *T. hominis* and its close relative *Vavraia culicus* was also more heterogeneous than was observed for core genes. Some of this lineage-specific innovation was highly expressed – in particular a membrane protein of unknown function - but much of it was not. This class of genes is also enriched for signal peptides (Nakjang et al., 2013) suggesting that some may be secreted or exposed on the surface of the parasite where they can interact with host targets. Our results contribute to a growing body of work supporting the idea that the evolution of contemporary microsporidian genomes is highly dynamic and innovative, and that while the initial transition to intracellular parasitism catalysed a drastic reduction in genome size and

coding capacity shared by all microsporidians, important lineage-specific differences continue to evolve.

Our data strongly suggest that *T. hominis* is diploid and demonstrate the presence of a large number of non-synonymous SNPs, many of which are expected to be deleterious, that are equally distributed between alleles. Many of these SNPs may eventually be eliminated by negative selection but, as already suggested for intracellular bacteria (Bogumil and Dagan, 2012; Fares et al., 2002; McCutcheon and Moran, 2012; Williams and Fares, 2010), the high levels of chaperonin expression that we observed may also suppress the phenotypic effects of these deleterious mutations in Microsporidia (Gill et al., 2008). It has been demonstrated that artificially infected mosquitoes can support the replication of *T. hominis* (Weidner et al., 1999), but the natural host of this opportunistic pathogen of humans is currently unknown. We identified transcripts from a novel PiggyBac element that, together with a previously identified element of insect origin (Heinz et al., 2012), strongly suggest that the natural host for *T. hominis* belongs to the hymenoptera.

The response of eukaryotic host cells to microsporidian infection is only just beginning to be investigated. Our data, which were highly reproducible between biological and technical replicates, suggest a generalized cellular shutdown by infected cells compared to uninfected rabbit kidney cells. Several other host pathways displayed a reproducible mixture of up-regulated and down-regulated genes relative to the uninfected control; these pathways are clearly disrupted but the overall effect on the host and its relationship to the activities of the parasite are difficult to predict based solely upon these data. We did observe an up-regulation of host amino and nucleotide sugar metabolism: this has also been reported for silkworms infected with *Nosema bombycis*. These are among substrates predicted to be imported by microsporidians to plug gaps in their reduced metabolism (Cuomo et al., 2012; Nakjang et al., 2013), so it is possible that these changes are to the benefit of the parasites. There is some evidence that host ATP production might be increased in combination with reduced host energy consumption. This could potentially benefit a parasite that is dependent on the host cell for most of its ATP and purine nucleotides for DNA and RNA biosynthesis (Heinz et al., 2014).

Chapter 5 : Characterising the progression of *T. hominis* infection in rabbit kidney cells

5.1 Introduction

Trachipleistophora hominis was first isolated from an HIV/AIDs patient in 1995 (Field et al., 1996; Hollister et al., 1996). Since this time it has been used as a model microsporidian for the study of zoonosis (Weidner et al., 1999), for the discovery of the microsporidian mitosome and identification of its functions (Goldberg et al., 2008; Hjort et al., 2010; Williams et al., 2002), as a model for studying how large microsporidian genomes evolve (Heinz et al., 2012), and for detailed study of the plasma membrane transporters used by all microsporidians to steal nucleotides and energy from their hosts (Heinz et al., 2014). Work discussed in this thesis has already provided more detailed information on the genes conserved on the *T. hominis* genome (chapter 3) and for their expression from a pooled sample of lifecycle stages infecting a rabbit kidney (RK-13) host cell line (chapter 4). In this chapter I describe my attempts to synchronise the infection cycle of *T. hominis* in rabbit kidney cells while following the infection cycle in detail at the level of light microscopy.

To understand the role of a gene or protein in the context of the lifecycle of *T. hominis* it would be beneficial to be able to synchronise infection in a reproducible manner. The initial studies characterising *T. hominis* explored the progression of the infectious cycle in individual cells across a post inoculation time course and focused on parasite ultrastructure using transmission electron microscopy (TEM) (Field et al., 1996; Hollister et al., 1996). This provided an extremely useful qualitative overview of the lifecycle of the parasite and the structure of the *T. hominis* cell (discussed in chapter I). However, it can be challenging to trace infection in a quantitative manner using only TEM because individual TEM sections sample only very thin sections of individual parasites. By contrast, light and fluorescence microscopy allow easier examination of whole cells and populations, making them useful complimentary techniques for quantitative analysis. Moreover, there are a number of published antibodies that are targeted against specific *T. hominis* proteins and compartments that have been characterised by immunofluorescence (Goldberg et al., 2008; Heinz et al., 2014; Williams et al., 2002). These include markers for the *T. hominis* mitosome

and for its plasma membrane located nucleotide transport proteins. These markers can also be used to follow the progression and synchronicity of the *T. hominis* infection in the RK-13 cell line during the proliferative stages of the parasite lifecycle.

5.2 Aims

To provide a semi-quantitative overview of the infectious cycle of *T. hominis* using a combination of light microscopy and immunofluorescence to investigate:

- The timing for the progression of the parasite lifecycle after inoculation, as well as the level of synchronicity in the overall parasite population.
- The localisation, division and role of mitosomes during the parasite lifecycle.
- The expression of nucleotide transport proteins across the *T. hominis* lifecycle.

5.2 Results

Here, the results of two separate time course studies are presented; a time course spanning from 0.5h to 40h post infection was used for semi-quantitative analysis of different features of parasite biology, including the number of parasites per host cell, parasite cell size and division status, number of nuclei and number of HSP70 signals and the localisation of MPS3 as markers for the *T. hominis* mitosome. This was complemented by the qualitative analysis of the expression of nucleotide transport proteins and HSP70 across the lifecycle of the parasite; between 2h and 69h post infection. The initiation of infection by the addition of spores to uninfected RK-13 cells is time 0 in each study (see materials and methods).

5.2.1 The early stages of the T. hominis lifecycle: 0h to 15h post infection

The start of microsporidian infection marks a major transition in its lifestyle from an extracellular spore to an active and dividing intracellular parasite. To enter a new host cell the microsporidium sporoplasm must pass through the everted polar tube. In *T. hominis* the estimated diameter of this tube is 0.1µm (Hollister et al., 1996), ~18x smaller than the diameter of the smallest intracellular stage of *T. hominis* that I observed in my experiments (1.75µm). Polar tube germination and initiation of infection was taken to occur at time 0 after the inoculation of RK-13 cells with *T. hominis* spores. The newly injected parasite at 0.5h post infection had a length of 2.3µm (0.2 standard error (SE)) and width of 2.0µm

(0.1SE), measured using phase contrast. The parasites were approximately spherical, and contain a single nucleus. By 12 hours post infection the average parasite diameter had increased to 2.81µm (0.11 SE), with a spherical morphology and a single nucleus. Only a few *T. hominis* infected RK-13 cells were infected with multiple uninucleate meronts between 0 and 12h post infection. The presence of multiple parasites inside a single host cell may be indicative of either multiple independent infections of a single host cell, or – less likely based upon my observations - of binary fission of meronts in this time period. Thus, there was no evidence of either cell or nuclear division forming binucleate parasites surrounded by a single continuous plasma membrane in any samples up to 15h post infection. In summary, my observations suggest that *T. hominis* is not actively dividing during the first 15h hours of infection, but is increasing in cell size. The average length of the parasite increased from 2.3µm to 2.8µm from 0.5 to 12h post infection, while retaining its overall spherical morphology.

The localisation of mitochondrial HSP70 to the *T. hominis* mitosome is well characterised(Williams et al., 2002). The average number of HSP70 signals per parasite at 0.5h post infection was 4 (SE2), and two of these signals were typically detected flanking the early parasite nucleus (Figure 5.1A); suggesting that at least two mitosomes localised near to the nucleus. This is supported by TEM of *T. hominis* during the infection of RK-13 cells (Figure 5.1B; Figure 5.1 C). The number of HSP70 signals increased by 12h post infection, with an average of 10 (SE2) per meront; suggesting that mitosomal division had occurred between 0h and 12h post infection (Figure 5.1A). The microsporidian mitosome retains its ancestral function in the biosynthesis of iron-sulphur clusters (Hjort et al., 2010; Lill and Mühlenhoff, 2008; Tsaousis et al., 2008). These clusters are required for the correct folding and function of a number of proteins that are essential to eukaryotes (Lill and Mühlenhoff, 2008) and some of these function in replication. The observed increase in the number of mitosomes in early stages of *T. hominis* infection is thus consistent with a preparation for parasite nuclear division later in infection. Division of mitosomes is required for their segregation to daughter cells during cell division; however it is not clear from published data whether mitosomes divide independently of nuclear division in *T. hominis*. The increase in the number of mitosomes in early non-dividing parasites suggests that at least some mitosomal division is linked to cell growth without cell division.

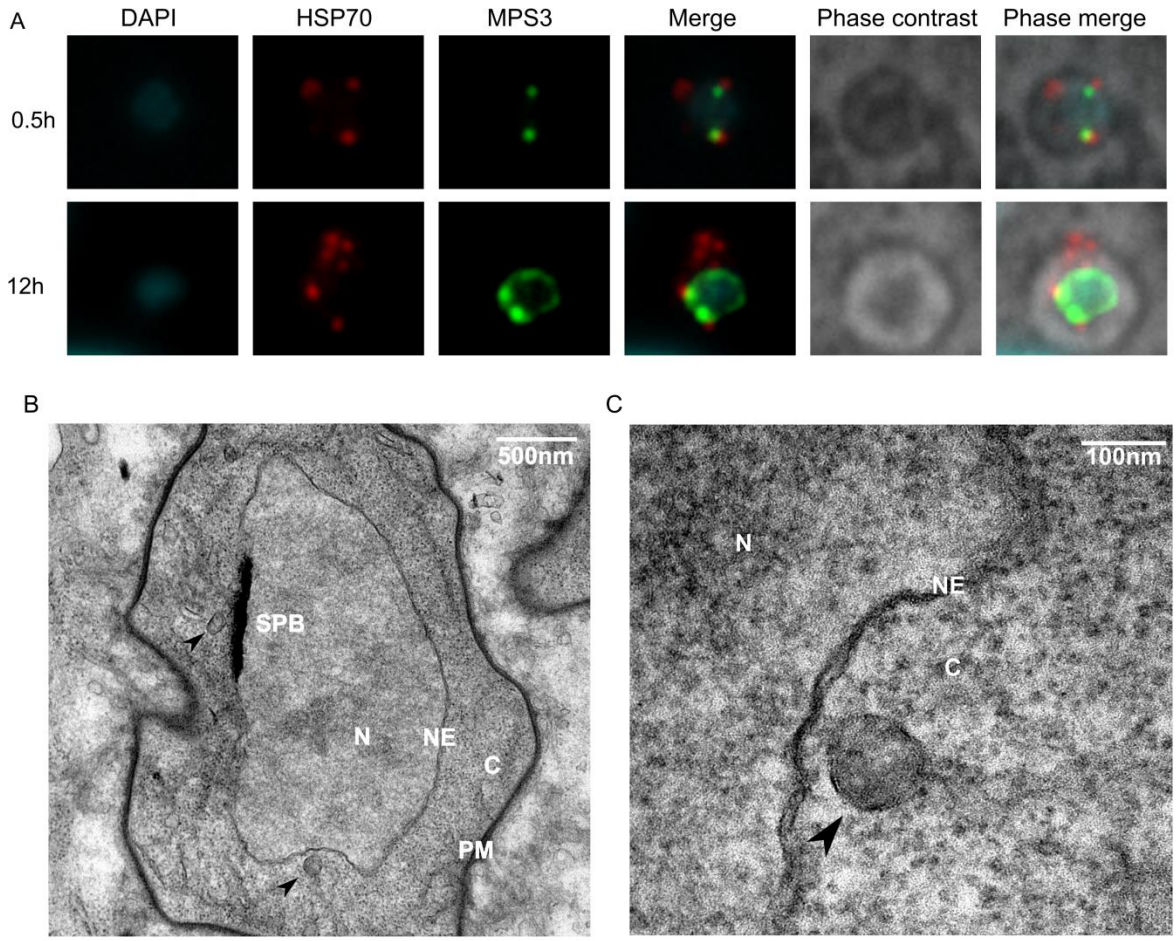

Figure 5.1: The localisation of mitosomes to spindle pole bodies in *T. hominis*.

A) At 0.5 hours post infection MPS3 (green) localises to two foci close to the parasite nucleus, consistent with its localisation to the spindle pole body. By 12h post infection the MPS3 signal surrounds the entire nucleus; however two foci are still present. The two nuclear adjacent MPS3 loci co-localise with HSP70 (red), suggesting that mitosomes may be associated with the spindle pole body. The total number of HSP70 signals increases between 0.5h and 12h post infection. B) TEM of *T. hominis* during infection of an RK-13 cell. Mitosomes are indicated with arrows. The electron dense structure at the parasite nucleus is similar to the spindle pole body (SPB) previously identified in *E. cuniculi* (Tsaousis et al., 2008). Abbreviations: SPB- spindle pole body, N - nucleus, NE - nuclear envelope, C – cytoplasm, PM – Plasma membrane. C) TEM showing the lower of the two mitosomes labelled in B) at higher magnification.

In *E. cuniculi,* mitosomes localise to a structure similar to the spindle pole body of yeast (Tsaousis et al., 2008), which is part of the nuclear division apparatus (Zheng et al., 2007). MPS3 is a nuclear envelope protein that interacts with the spindle pole body in yeast (Jaspersen et al., 2002), and antibodies against its homologue in *T. hominis* have been raised by Kacper Sendra. At 0.5h post infection MPS3 localised at two distinct foci at the nuclear envelop (Figure 5.1A). By 12h and 1h post infection MPS3 signal was detected surrounding the parasite nucleus, however the intensity continued to peak at two foci flanking the parasite nucleus (Figure 5.1A). HSP70 co-localises with MPS3 at these foci throughout the first 15 hours of infection (Figure 5.1A), suggesting that at least two mitosomes are associated with the spindle pole bodies in *T. hominis*. An electron dense structure with similarity to the spindle pole body in *E. cuniculi* (Tsaousis et al., 2008) was identified in TEM of *T. hominis* infected RK-13 cells (Figure 5.1B). A putative mitosome was localised adjacent to this structure (Figure 5.1B); consistent with an association between mitosomes and the spindle pole body. In model eukaryotes the association of mitochondria to spindle poles is hypothesised to aid in both the segregation of mitochondria to daughter cells and the alignment of spindles during cell division (Krüger and Tolić-Nørrelykke, 2008).

Nucleotides are essential both for providing energy for cell growth, which is observed in these early stages of the parasite lifecycle, and for DNA synthesis for nuclear division in later stages of infection. Without the ability to produce nucleotides *de novo*, Microsporidia including *T. hominis* are hypothesised to acquire purines using their nucleotide transport proteins (Heinz et al., 2014; Tsaousis et al., 2008). Signal for all three *T. hominis* nucleotide transport proteins for which antibodies were available (NTT1, NTT2 and NTT3) were detected at the parasite plasma membrane at 2h post infection and this was maintained at 15h post infection (Figure 5.2). These data suggest that the parasites are actively importing ATP and other nucleotides from the earliest phases of the infection. Previously NTT4 has been identified in *T. hominis* spore proteomics (Heinz et al., 2012), suggesting that the protein may already be present in the plasma membrane of the injected sporoplasm.

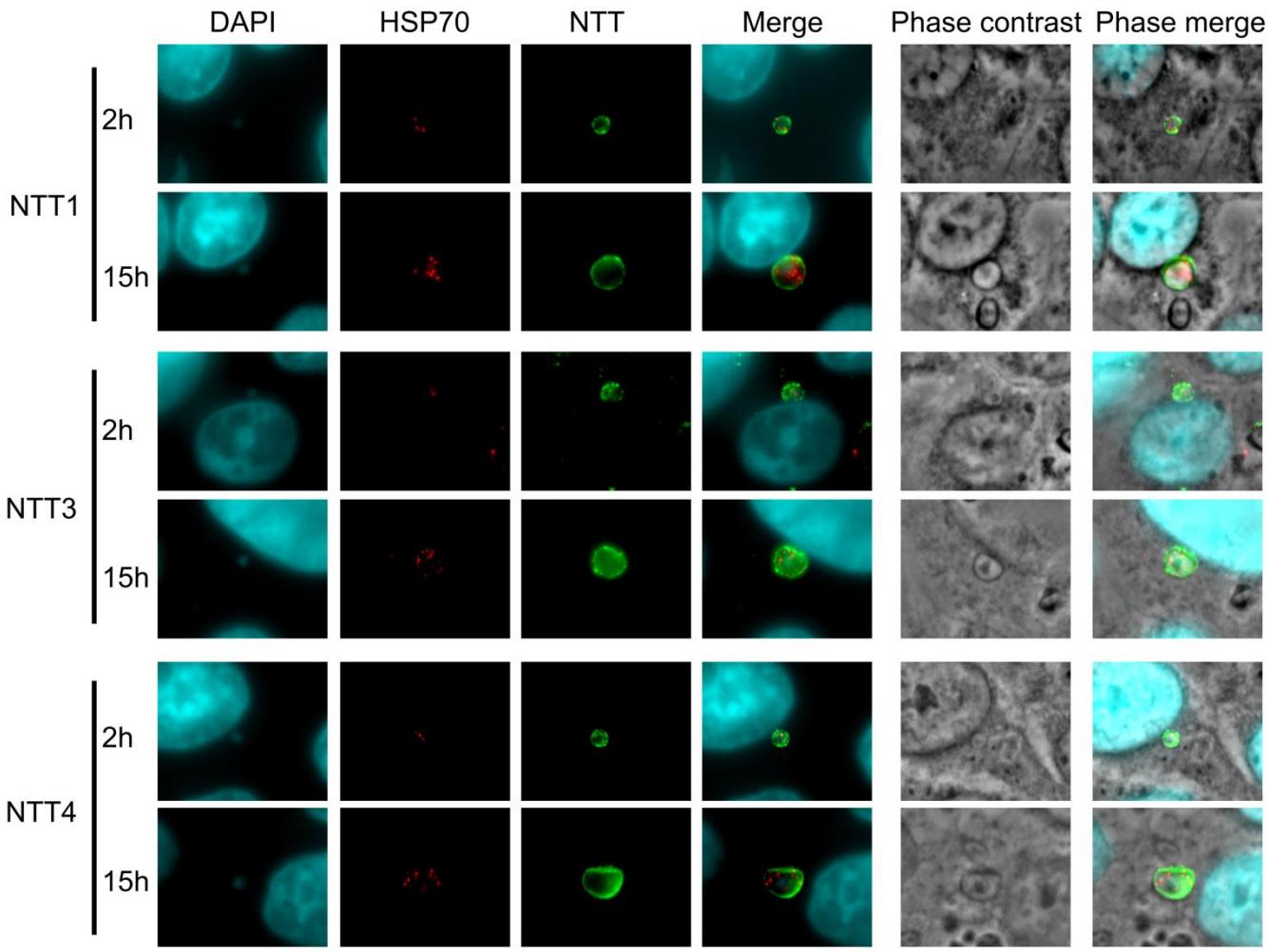

Figure 5.2: Localisation of NTT1, NTT3 and NTT4 to the plasma membrane of uninucleate *T. hominis* meronts at 2h and 15h post infection.

All three NTTs (green) are detected at the plasma membrane of the parasite in the early stages of the *T. hominis* infectious cycle. HSP70 signals are also detected throughout this period. As in the MPS3 time course, the number of HSP70 signals increases as the time course progresses.

5.2.2 T. hominis meronts divide by plasmotomy: 18h to 40h post infection

At 18 hours post infection I observed the first binucleate stage of the *T. hominis* lifecycle (Figure 5.3; 18h), and at 22 hours post infection the 23 of 27 parasites examined were binucleate, suggesting that a single nuclear division had occurred in most parasites between 16h and 22h post infection. The size of the parasites continued to increase during 18 and 22h post infection compared to 16h post infection; however the average length of the cell (5.3µm) at 22h post infection is 1.4µm larger than the average width (3.8µm); consistent with the observed loss of spherical morphology following the first nuclear division (Figure 5.3). Tetranuclear and octanuclear meronts were first observed at 28h and 32h post infection respectively (Figure 5.3; 28h and 32h), suggesting that a second and third round of nuclear division had occurred in *T. hominis*. Defining a single meront as a parasite contained within a single continuous cell membrane, the majority of host cells continued to only contain one multinucleate meront from 16h to 32h post infection, suggesting that cells do not divide until after 32h post infection. The 18 hour gap from inoculation to the first observation of nuclear division, and the much shorter gap between the second and third nuclear divisions, supports the hypothesis that the initial phase of parasite growth following inoculation is required for establishing infection prior to proliferation. In summary the data suggest that between 18h and 32h post infection *T. hominis* undergoes at least three rounds of nuclear division. The parasite continues to grow, without cell division, eventually leading to the formation of a large multinucleate meront.

In the initial characterisation of the *T. hominis* lifecycle using TEM (Hollister et al., 1996) it was suggested that the majority of meronts contained one to two nuclei, and that binucleate meronts divided by binary fission to produce uninucleate daughter cells. Rare exceptions to this contained four nuclei, and these divided to two binucleate daughter cells (Hollister et al., 1996). The division of a multinucleate cell to two multinucleate daughter cells is called plasmotomy. Our findings do not support this hypothesis, but suggest that the majority of meronts undergo at least two rounds of nuclear division without cell division until they contain four or eight nuclei, and that binary fission of a binucleate meront to two uninucleate daughter cells occurs during merogony is a rare event that we did not observe. Interestingly, my own observations are consistent with the development of meronts in characterised *Pleistophora*, a close microsporidian relatives of *Trachipleistophora*. The

differences between the results from my work and published data for *T. hominis* may be due in part to the limitations of TEM previously discussed. Examining a single TEM cross section through a meront may make it difficult to accurately predict the number of nuclei and define the limits of a single cell, whereas the use of Z-stacks in the present study allowed exploration of the entire meront. In chapter 4 we found that *T. hominis*, like other unikaryotic microsporidians (Cuomo et al., 2012; Haag et al., 2013; Selman et al., 2013), was a diploid, raising the possibility that the parasite may have sex at some stage in its lifecycle. In Microsporidia where potential stages of meiotic division have been identified, it is hypothesised to be initiated by the fusion of two nuclei in a multinucleate stage of the parasite lifecycle(Hazard and Brookbank, 1984; Ironside, 2007; Lee et al., 2014). While we saw no evidence of meiotic division in the *T. hominis* lifecycle, the multinucleate nature of the parasite after 18 hours post infection provides a window of time during which nuclear fusion and meiosis could occur.

The number of HSP70 signals detected in the parasites continued to increase from 16h to 32h post infection (Figure 5.3), suggesting continued division of mitosomes throughout this period. HSP70 signals were distributed throughout the cytoplasm in multinucleate meronts, but also continued to co-localise with two foci of MPS3 signal at the parasite nuclear envelope (Figure 5.3); suggesting that mitosomal association with nuclei at the spindle pole body is maintained throughout nuclear division. At 22h post infection NTT1, NTT3 and NTT4 were all detected localised to the parasite plasma membrane (Figure 5.4), suggesting that they continue to play an active role in the acquisition of ATP and other nucleotides during the proliferative stages of the lifecycle. This is a stage of the lifecycle where the requirement for nucleotides might be expected to be particularly high due to DNA synthesis.

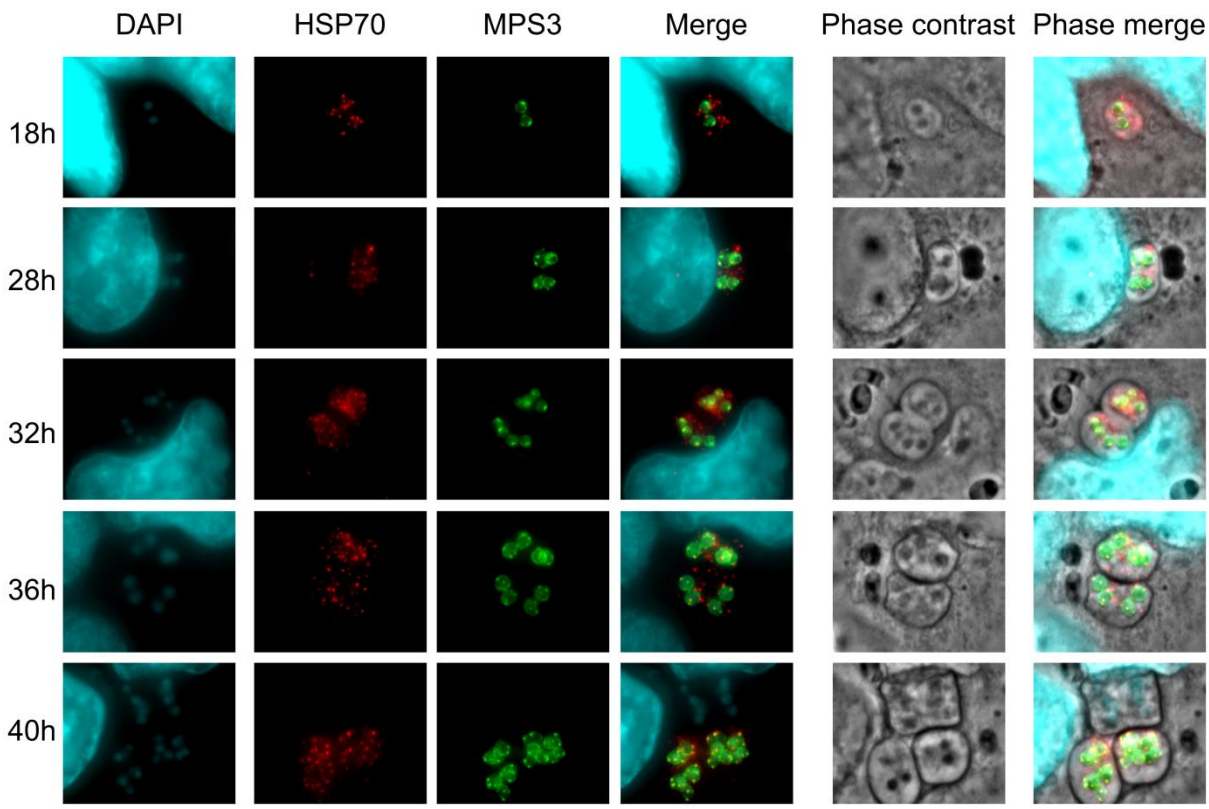

Figure 5.3: Localisation of HSP70 and MPS3 in parasites at 18h, 28h, 32h and 40h post infection; with key stages of the progression of infection represented in the dataset.

The number of HSP70 signals (red) continues to increase as the infectious cycle progressed from 18h to 40h post infection. MPS3 signal continues to localise to the *T. hominis* nuclear envelope. While the majority of HSP70s are distributed throughout the *T. hominis* cytoplasm, ~2 HSP70 signals continue to co-localise with MPS3 at the nucleus.

The stages of infection represented in this figure include: 18h) A binucleate meront. 28h) A tetranuclear meront. 32h) An octanuclear meront that is pinched in the centre, suggesting ongoing cell division. 36h) Two tetranuclear meronts in the same host cell, potentially resulting from the division of an octanuclear meront. 40h) Two tetranuclear meronts alongside putative sporonts. The sporonts is identified based on a change in morphology compared to meronts and the lack of either MPS3 of HSP70 signal.

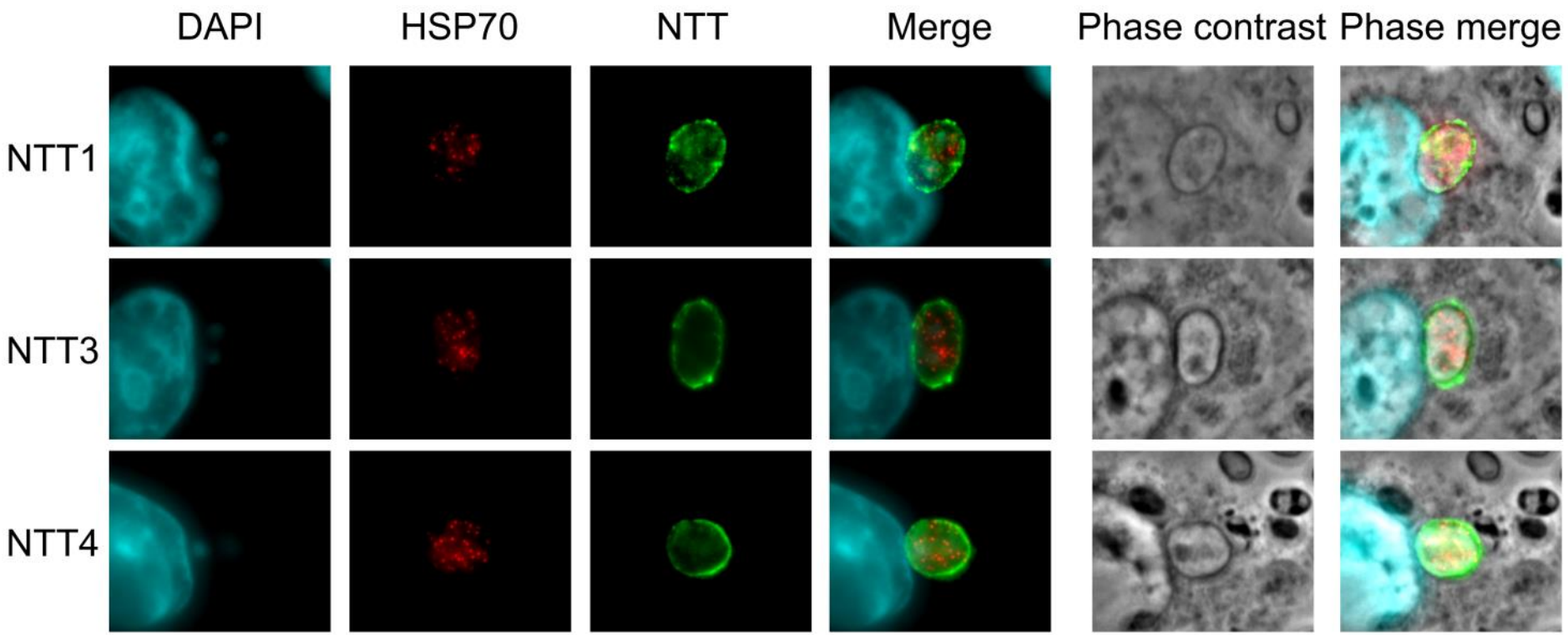

Figure 5.4: Localisation of nucleotide transport proteins to binucleate meronts at 22h post infection.

NTTs (green) continue to localise to the parasite membrane in binucleate meronts at 22h post infection. This is the phase of nuclear proliferation in the parasite, where nucleotides are required for the DNA synthesis as well as energy.

At 36h and 40h post infection there was a switch in the most frequently observed number of parasite cells per host cell from one to two (Figure 5.5), suggesting that the majority of meronts had undergone cell division. Few uninucleate or binucleate meronts were observed, and the parasite population was dominated by octanuclear and tetranuclear parasites. This suggests that the first *T. hominis* cell division is a plasmotomy of an octanuclear meront to generate two tetranuclear daughter cells. This suggestion is supported by the morphology of octanuclear meronts; which were often pinched in the centre, with four nuclei arranged either side of the pinch point, suggesting ongoing cell division (Figure 5.3; 32h post infection). In those host cells which contain multiple parasites at 36h and 40h post infection, the majority of which would be predicted to include the products of recent parasite cell division, HSP70 signals are found in both daughter cells (Figure 5.3; 32h and 36h). This demonstrates that mitosomes are distributed to these daughter cells during cell division; however it is unclear whether this is a passive result of the overall distribution of mitosomes throughout the parasite cytoplasm or a controlled process. The continued co-localisation of some HSP70 signals with MPS3 at the spindle pole body near the nucleus (Figure 5.3) suggests that the segregation of at least these mitosomes may be linked directly to cell division.

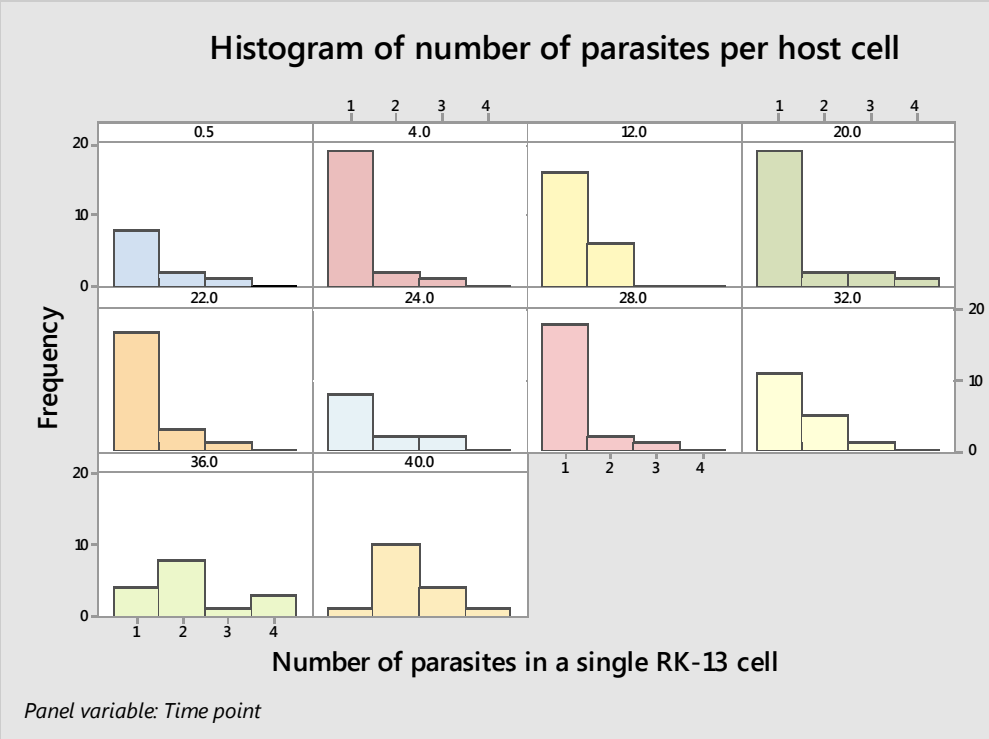

Figure 5.5: Histogram of the number of parasites per host cell for time points from 0.5 to 40h post infection.

From 0.5h to 32h post infection the majority of host cells contain only one meront. This shifts to two meronts for 36h and 40h post infection, suggesting that binary cell division has begun in meronts between 32h and 36h post infection. By 40h post infection very few host cells only contained one meront, suggesting that the majority of meronts have undergone binary cell division by this time.

5.2.3 T. hominis spore formation occurs alongside merogony: 40h post infection onwards

36h to 40 hours post infection was the first time point in which I observed evidence for sporont formation as defined by a change in cell morphology and the loss of HSP70 and DAPI signal (discussed below). By 69h post infection the majority of host cells contain a mixture of both meronts and sporonts, consistent with the findings of Hollister et al. (Hollister et al., 1996) in the initial characterisation of the *T. hominis* lifecycle that these two stages of the lifecycle occur concurrently. Following 40h post infection it is likely that at least one further meront cell division occurs; however the number of individual parasites and parasite nuclei per host cell in these stages of infection is difficult to ascertain accurately using current methods. The resolution of the Z-plane of a Z-stack is not as high as the XY planes, making it difficult to distinguish cell and nuclei boundaries in a crowded cell where parasites are more likely to be stacked on top of one another during later stages of infection. The lack of DAPI

staining of sporont nuclei means that the number of nuclei cannot be counted in this stage of the parasite lifecycle.

No signal is detected for HSP70 in sporonts, intracellular spores, or extracellular spores outside of spore bags (Figure 5.6; 69h, NTT1 and NTT3). HSP70 has previously been detected in *T. hominis* spore proteomics (Heinz et al., 2012)(Heinz et al. 2012) and in western blots from purified spores (Williams et al., 2002) suggesting that mitosomes are present in these stages of the parasite lifecycle despite the lack of signal. The nuclei of these lifecycle stages were also not stained with DAPI (Figure 5.6; 69h, NTT1 and NTT3). These results suggest that both DAPI and antibodies are excluded from the later stages of the parasite lifecycle. There are two changes in parasite biology during these stages of infection that may form a barrier to labelling - the formation of the spore wall around the parasite, or the formation of the parasitophorous vacuole. The lack of staining of isolated mature spores by either DAPI or HSP70 antibodies suggests that the microsporidian spore wall is sufficient by itself to limit antibody and DAPI access to the parasite cytoplasm; and that its formation may prevent the staining of intracellular sporonts.

Signal for all *T. hominis* NTTs continued to be detected at 46h and 69h post infection (Figure 5.6). Using the strict definition of complete loss of DAPI and HSP70 signal and a change in parasite morphology in the differentiation of sporonts and meronts in the same *T. hominis* infected RK-13 cell, only NTT1 and NTT3 were confirmed to label sporonts. However, it is tempting to speculate that the leftmost parasite cells in Figure 5.6 (NTT4 69h) are early sporonts based on their morphology. NTT4 was previously detected in the proteomics of *T. hominis* spores (Heinz et al., 2012). The signal to noise ratio was much lower for NTT1 during the later stages of infection than early in the parasite lifecycle (Figure 5.6), and this was reproducible in other time course or mixed infection experiments, suggesting that its expression may be reduced in later stages of the parasite lifecycle.

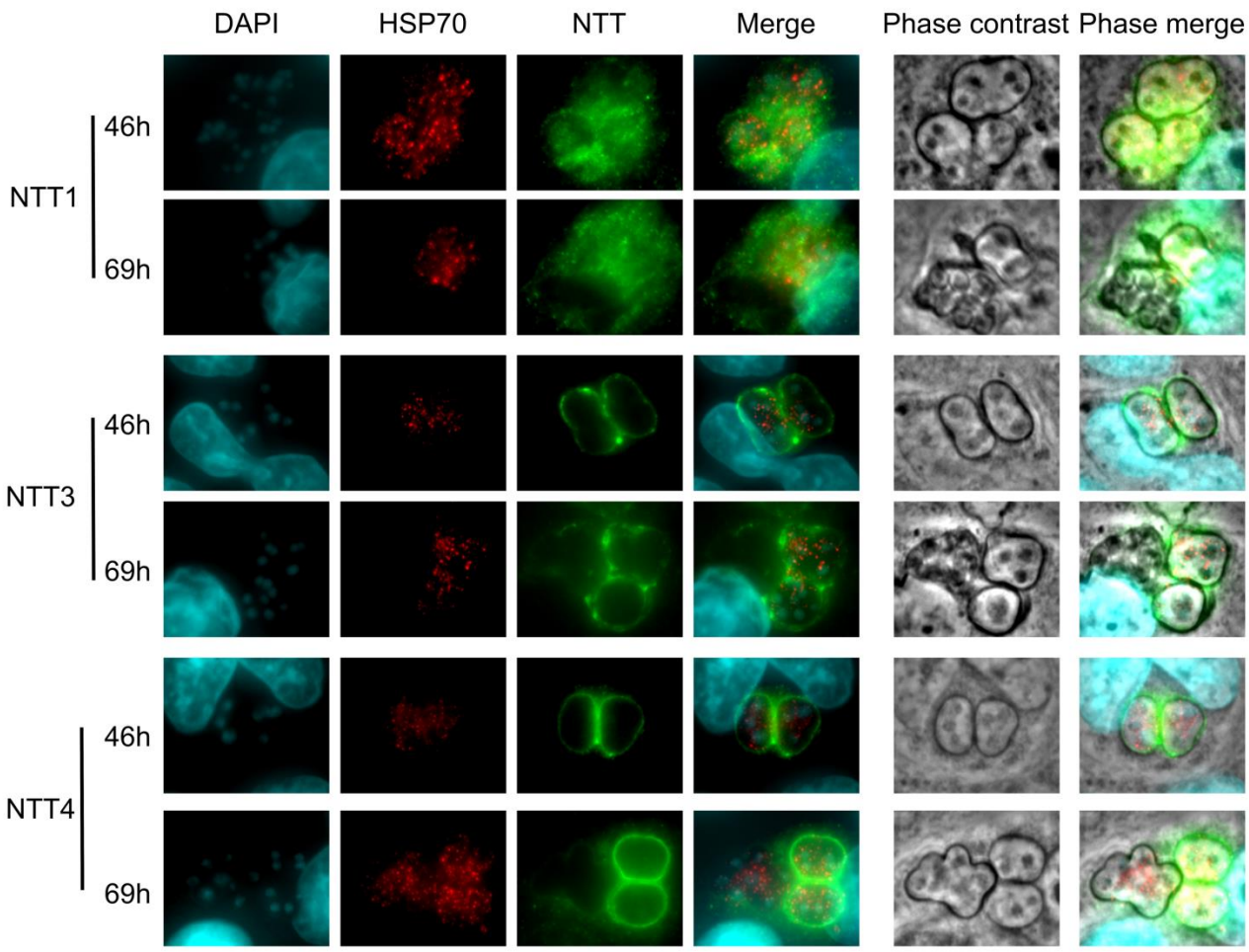

Figure 5.6: Localisation of NTT1, NTT3 and NTT4 to the plasma membrane of *T. hominis* at 46h and 69h post infection.

Signal for all three NTTs is detected at the plasma membrane of parasites during the later stages of infection at 46h and 69h post infection. At 69h post infection the majority of cells include a mixture of meronts and sporonts; though this is less clearly defined for NTT4. These data suggests that the NTTs may continue to localise to the parasite membrane and import nucleotides from the host cell in the sporont stages of the parasite lifecycle. Signal for NTT1 in the later stages of the infectious cycle of the parasite was consistently weaker, suggesting that its levels at the parasite membrane may be reduced during later stages of infection. Comparing signal for NTT1 in a mixed infection including different stages of the parasite lifecycle in the same image may help to support this finding.

5.2.4 A semi-quantitative overview of the T. hominis infectious cycle from 0h-40h post infection

In previous sections I have discussed different features of the biology of *T. hominis* at specific time points; however exploring trends across the infectious cycle as a whole can be a more informative way to explore these features. From 0h to 40h post infection, plotting the length and width of the parasite against time was indicative of a general trend for cell growth (Figure 5.7A and B). In terms of width, the rate of growth was relatively constant throughout the studied period of infection, as indicated by the relatively constant gradient of the LOESS regression line (Figure 5.7B). In contrast the rate of parasite growth in terms of length was higher between 12h and 28h post infection (Figure 5.7A), indicated by the increase in gradient at this time point. This suggests that elongation of the cell was occurring between these time points. The elongation of *T. hominis* between 10 and 28h hours post infection is consistent with the timing of nuclear division (Figure 5.8). The plot of parasite length against width (Figure 5.7C) revealed an inflection point at a length of ~4.5µm supporting this. It is important to remember that the samples were made up of a population of *T. hominis* cells which may vary in rates of growth and development. Separately plotting the length against the width of the parasite at each individual time point can be useful in comparing the level of variation in the population at these time points. The level of variation was greater during the later stages of infection, especially at 36h and 40h post infection indicated by the wider 95% confidence interval surrounding the LOESS regression line (Figure 5.7D). This was around the timing for the first cell division (Figure 5.5), and the population at this stage of the parasite lifecycle contained a mixture of tetranuclear and octanuclear meronts at different stages of development.

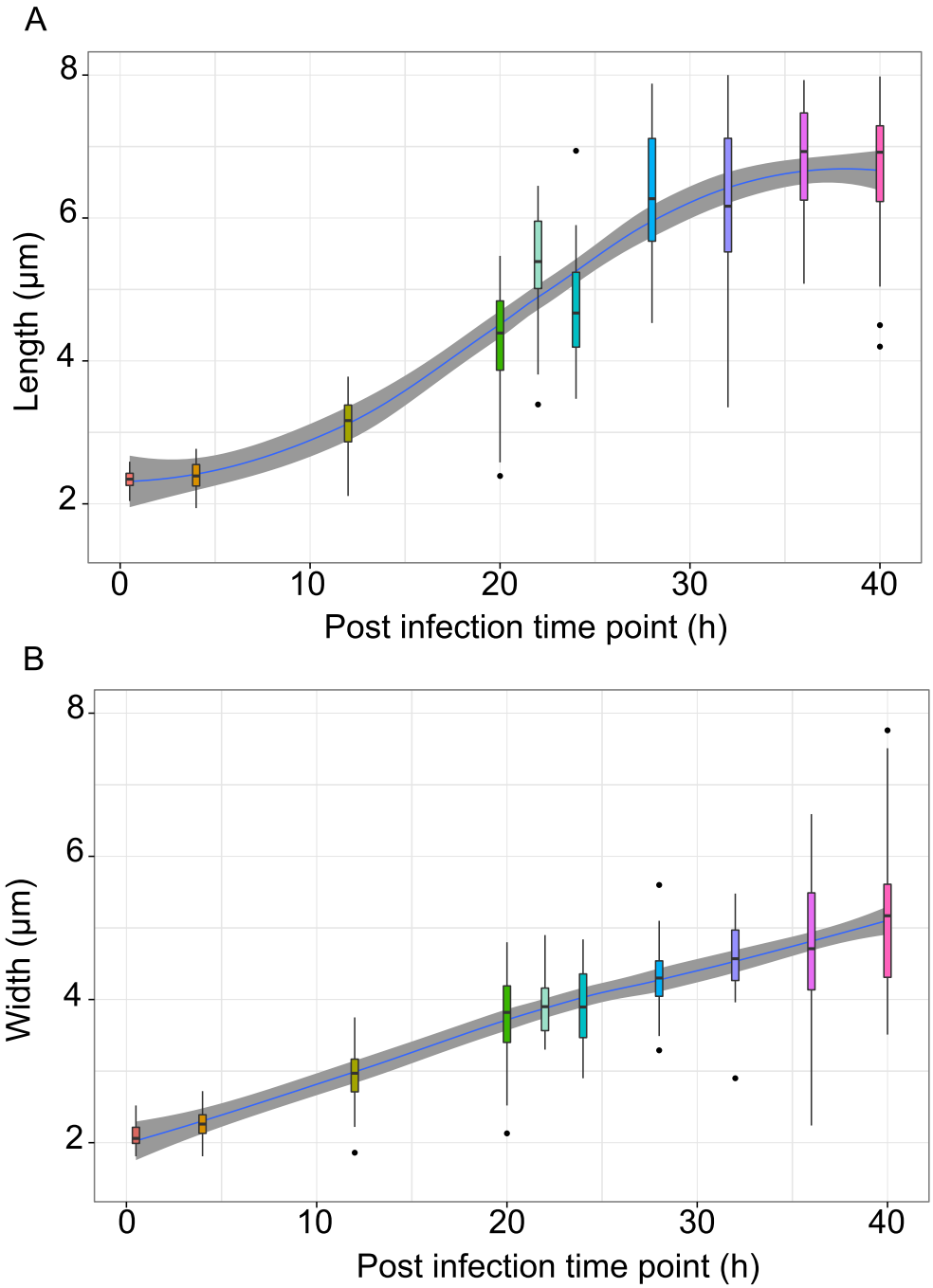

Figure 5.7 Growth of T. hominis

A and B: Boxplot of the size of *T. hominis* from 0 to 40h post infection. A LOESS regression line is fitted to the data, and the shaded area around the line shows the 95% confidence interval of the regression for: A) The length of *T. hominis*, defined as its longest axis on the XY plane in a Z-stack of the parasite. B) The width of *T. hominis*, defined as its shortest axis on the XY plane in a Z-stack of the parasite. The parasite grows in both length and width throughout infection. The rate of growth in terms of parasite width stays relatively constant from 0h to 40h post infection, as indicated by the relatively constant gradient of the regression line; the rate of growth in length accelerates between 12h and 28h post infection, consistent with the observed elongation during cell division.

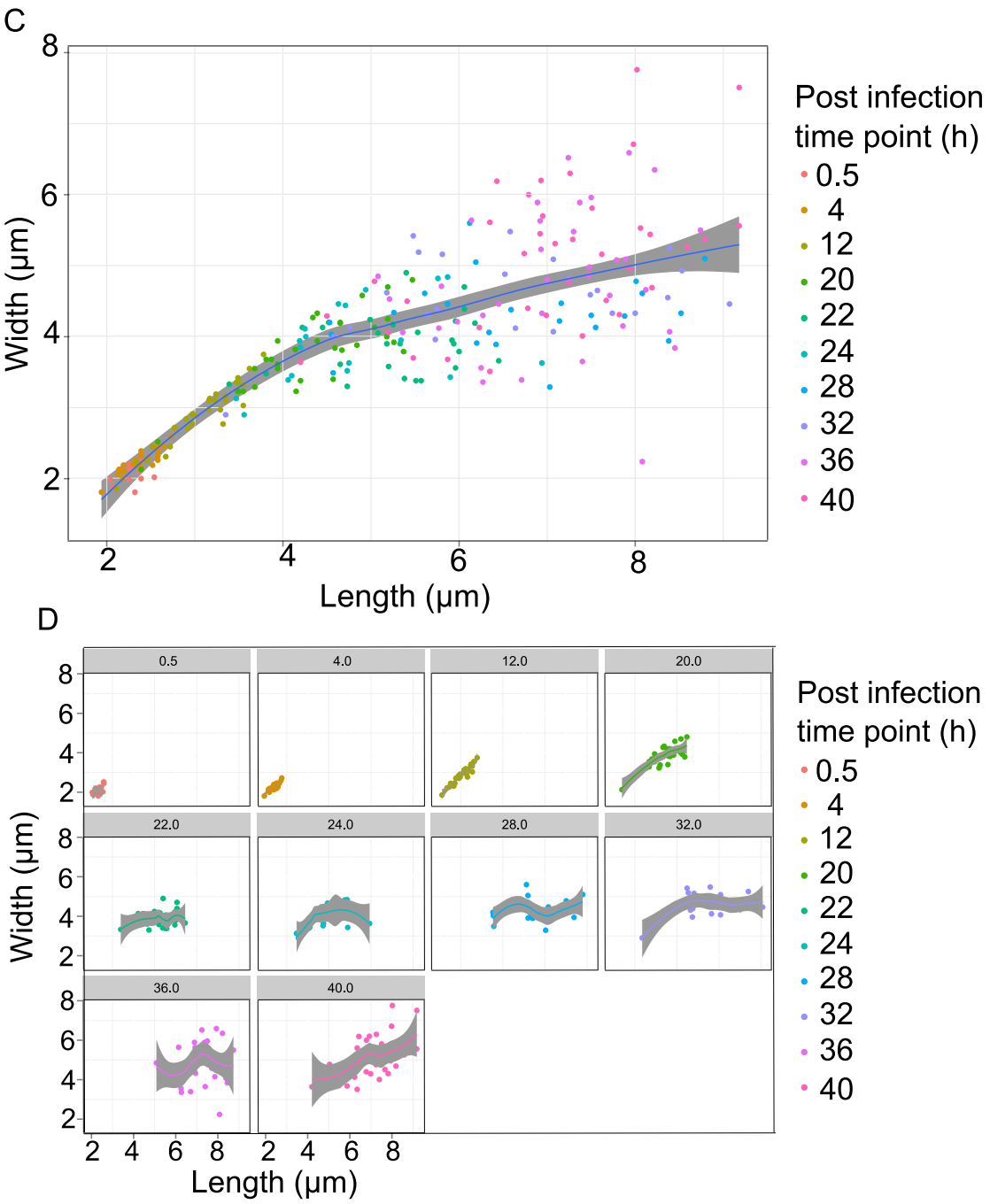

Figure 5.7 continued:

Plotting the length of the parasite against its width, with a LOESS regression line fit to the data: C) In all post infection time points. D) With post infection time points plotted separately. From 0h to 20h post infection, at each time point parasites in the population vary in total size, but have roughly equal length and width, reflecting their spherical morphology. After 20 hours post infection the width of parasites continue to vary, however the predominant source of variation is in parasite length, as indicated by the changing gradient of LOESS regression lines in both C and D following this point.

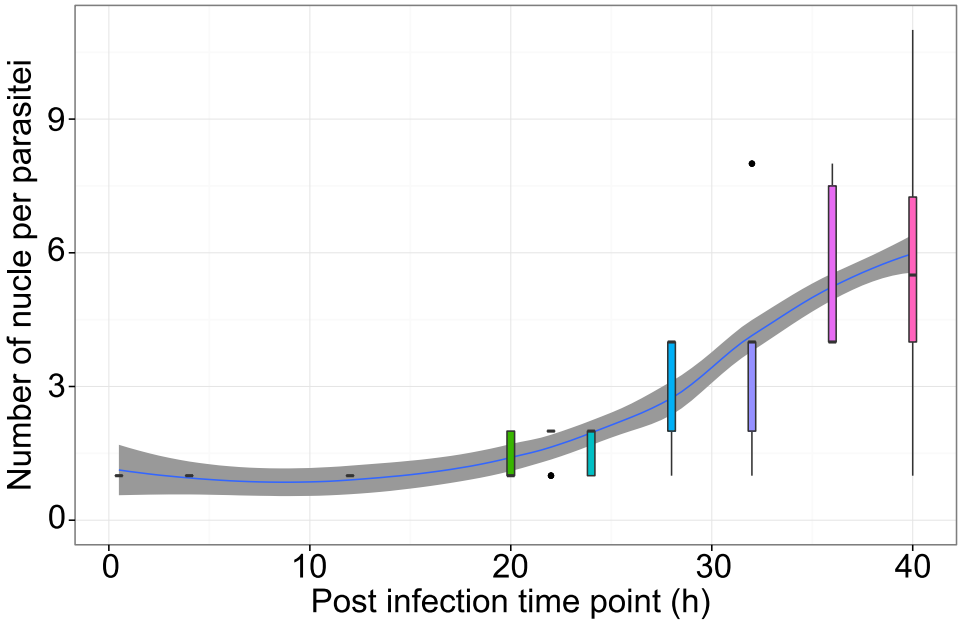

Figure 5.8: The number of nuclei per host parasite across the parasite infectious cycle.

The number of nuclei detected in meronts at each stage of the parasite lifecycle. The first nuclear division did not occur until 18 hours post infection, and by 20h post infection the majority of parasites were binucleate. Tetranuclear meronts were first observed at 32h post infection, and octanuclear meronts at 36h post infection, however the error bars in the dataset reflect that the variability in the number of nuclei per parasite within the population as a whole is more variable at these time points; likely due to the onset of cell division.

A punctate signal for HSP70 was observed in all meront stages of the parasite lifecycle, consistent with its published localisation to the mitosome (Williams et al., 2002). There was a general trend for an increase in the number of HSP70 signals throughout the infectious cycle of the parasite (Figure 5.9A). The increase in the number of HSP70 suggests mitosome division occurred throughout the studied stages of the parasite lifecycle. The number of HSP70 signals correlated positively with the size of the parasite (spearman correlation coefficient - 0.904) (Figure 5.9B). The increase in the number of HSP70 signals included the early stages of infection, prior to both *T. hominis* nuclear and cell division (Figure 5.9C). Fitting a mixed effects linear model to this data indicates that HSP70 signal number increased significantly with both time and parasite diameter (P = 0.0004). Together these data support our previous suggestion that mitosomal division occurred throughout the parasite lifecycle and was not solely linked to proliferation. As with parasite size, the number

of HSP70 signals in parasites in the population was more variable during the later stages of infection (Figure 5.9B) however the correlation with parasite size was retained (Figure 5.9C).

During the early stages of infection, the progression of infection retained strong synchronicity throughout the initial parasite growth phase, the first rounds of nuclear division and cell division of the parasite. This is supported both by the similarity in sizes of the size of the parasite (Figure 5.7D), the number of nuclear divisions (Figure 5.8), and the number of parasites per host cell, indicative of cell division (Figure 5.5C) at each time point. In the later stages of infection many of these features became more difficult to measure, however merogony and sporogony often occur concurrently in the same host cell making the infection a mixture of different parasite lifecycle stages by nature. The majority of infected cells observed at 69h post infection included a combination of both meronts and sporonts. The level of synchronicity observed suggests that it is possible to identify samples that are enriched for different stages of the *T. hominis* lifecycle; for example, sampling at 22h post infection to enrich for binucleate meronts shortly following the first nuclear division. Studying samples enriched for these different lifecycle stages could help to understand the molecular mechanisms underlining transitions in stages of the microsporidian lifecycle and intracellular infection as a whole.

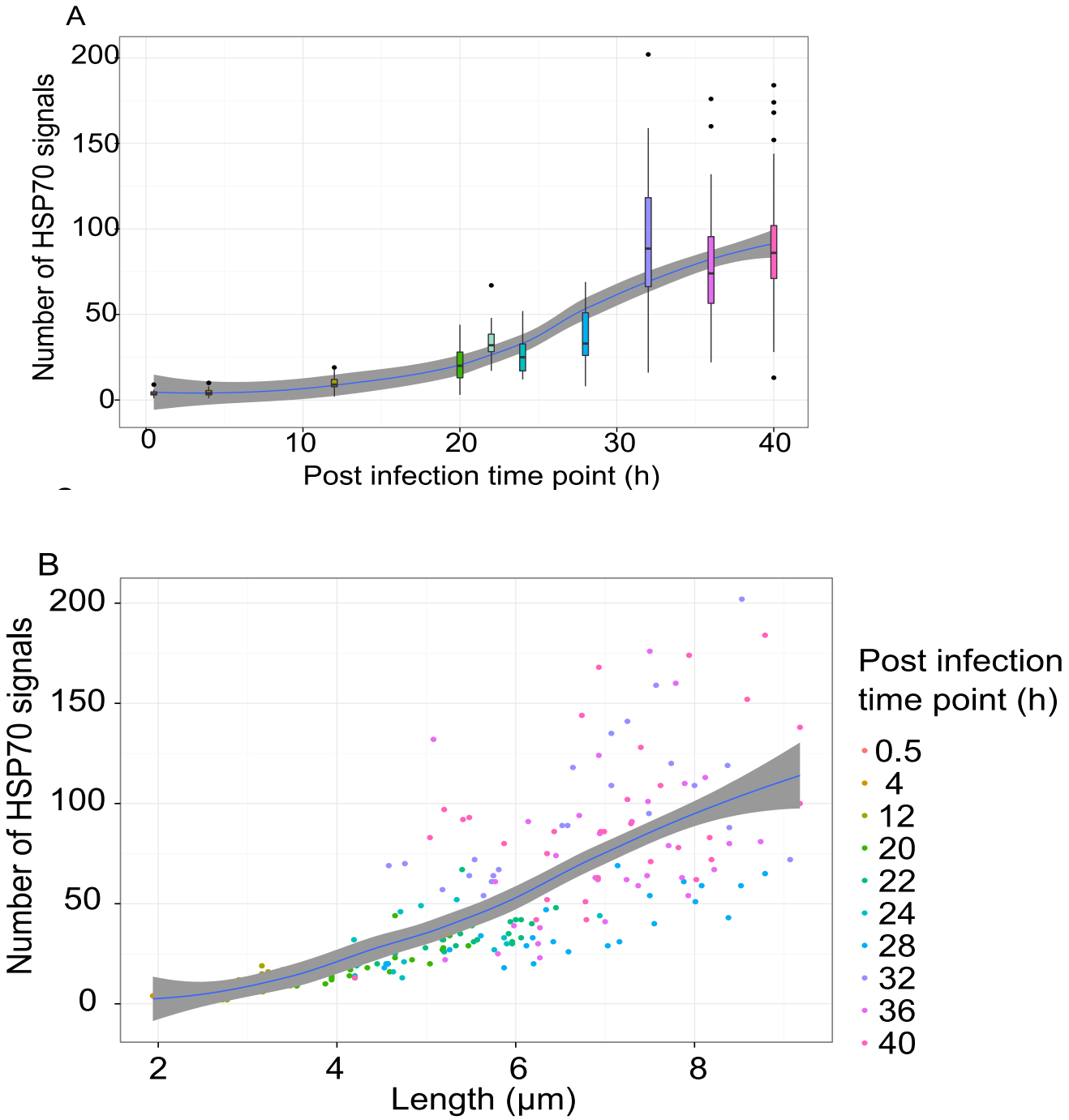

Figure 5.9: The increase in HSP70 signals across the lifecycle of *T. hominis*.

A) Bloxplot of the number of HSP70 signals at each post infection time point, with a LOESS regression curve fit to the data. B) Plot of parasite length against the number of HSP70 signals with a LOESS regression curve fit to the data. The number of HSP70 signals increases with parasite size (Spearman's correlation coefficient (0.904)).

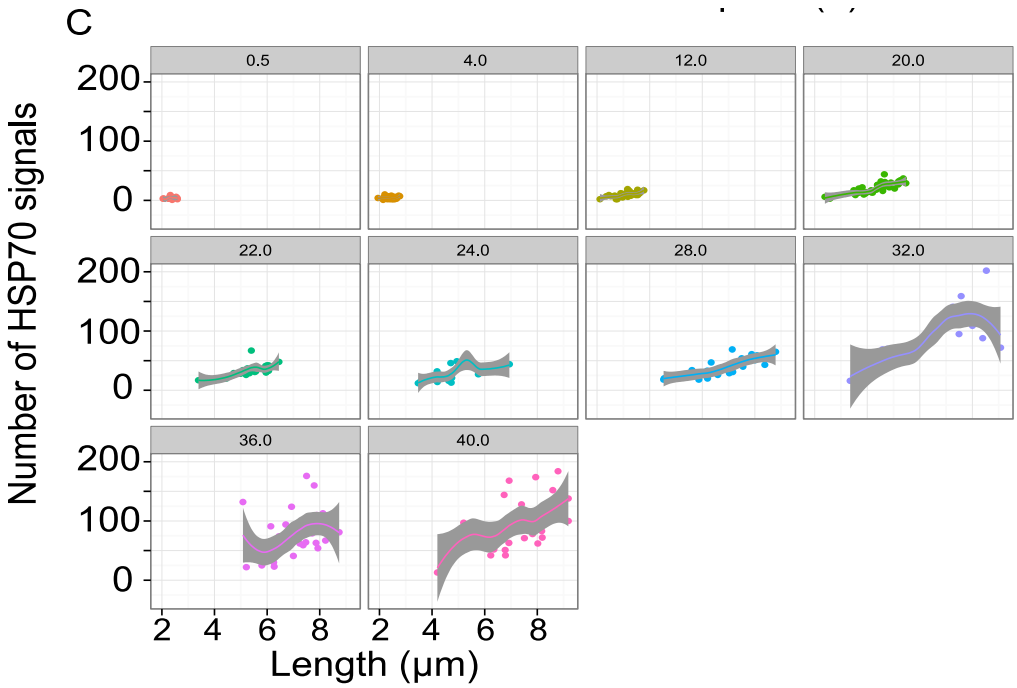

Figure 5.9 continued: C) Plot of number of HSP70 signals against parasite length at each time point.

5.3 Conclusions

The data presented in this chapter represents the first semi-quantitative profiling of the lifecycle of *T. hominis* during its infection of RK-13 cells. In my cultures there was a phase of cell growth without proliferation from 0.5h to 16h post infection that may be an important period of transition between the spore and replicative stages of the parasite lifecycle. Three rounds of nuclear division are hypothesised to have occurred in *T. hominis* between 16h and 32h post infection, prior to the first cell division (Figure 5.10). The increase in the number of HSP70 signals across this time period suggests that mitosomes divide throughout this period of parasite growth (Figure 5.11). This is consistent with the essential function of mitosomes in the production of iron sulphur clusters for the biosynthesis of proteins required for proliferation and DNA and RNA biosynthesis. The co-localisation of MPS3 with some mitosomal signals at the periphery of the nucleus throughout infection suggests that segregation of some mitosomes may be linked directly to parasite and nuclear division; ensuring that daughter cells retain the organelle after division. Sporogony began at 40h post infection, and after this point merogony and sporogony often occurred concurrently in the same host cell. Crucially, time points enriched for different stages of parasite development were identified in this study; raising the possibility of molecular characterisation of these lifecycle stages in future work.

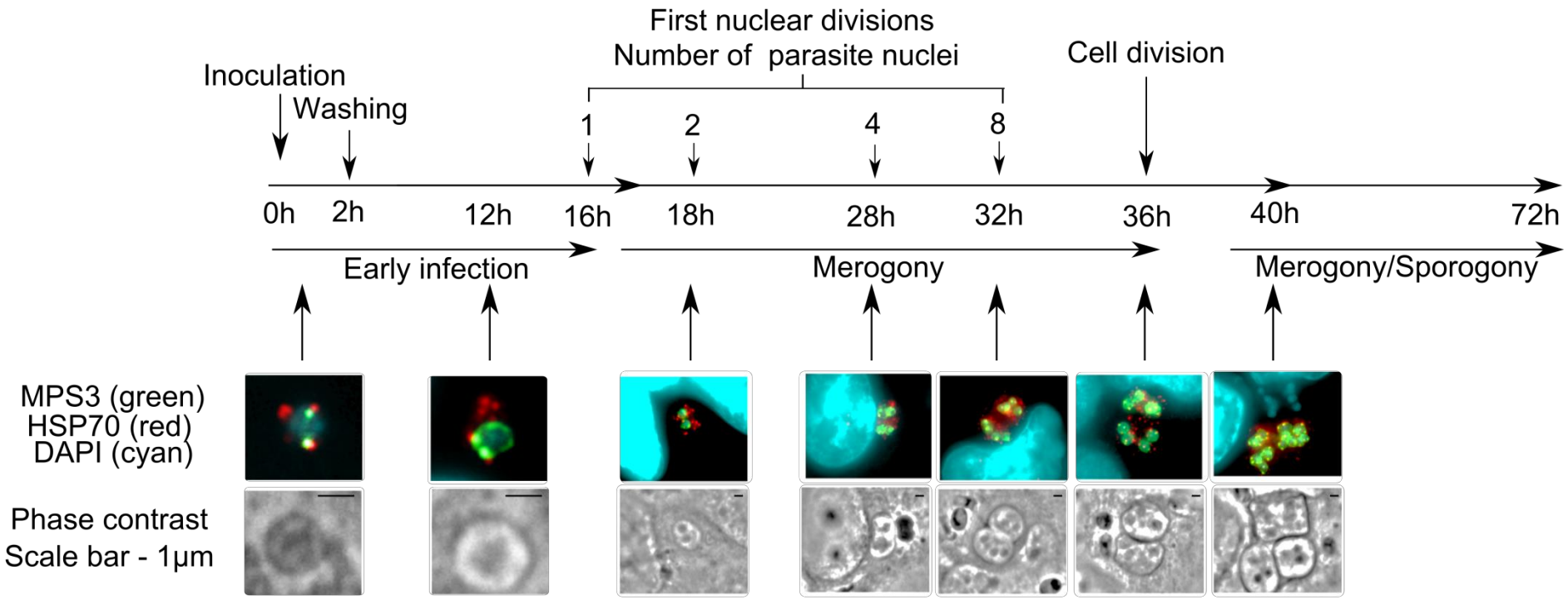

Figure 5.10: Summary of the progression of the *T. hominis* cell cycle in RK-13 cells.

The timeline of *T. hominis* infection in the RK-13 cell line, including the times that nuclear and cell division were observed, and reference images from 0.5h, 12h, 18h, 28h, 32h, 36h and 40h post infection showing some of the major events in the early parasite lifecycle. MPS3 (green) is a nuclear marker that is enriched at the spindle pole body (SPB) and used as a marker for this structure. HSP70 (red) localises to the parasite mitosome. DAPI (cyan) is a general nucleic acid stain that labels host and parasite nuclei.

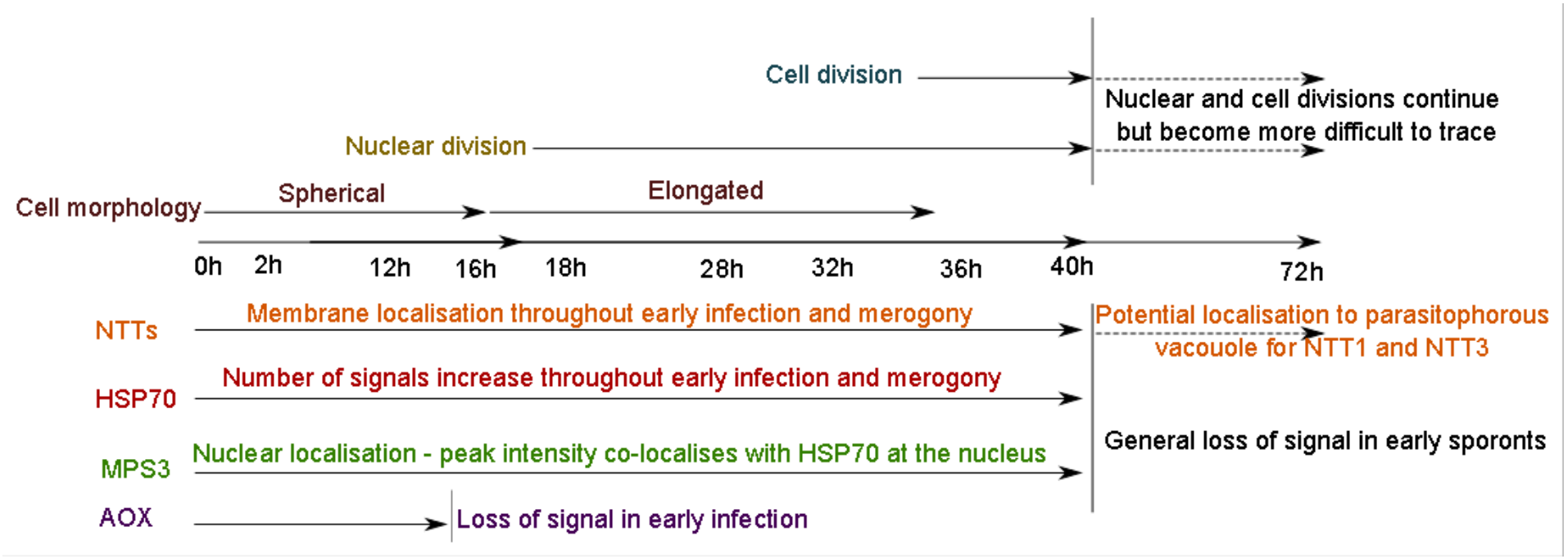

Figure 5.11: Summary of observations in the *T. hominis* infectious cycle.

The timeline of *T. hominis* infection in the RK-13 cell line summarising the timing of major observations during the parasite lifecycle, including the start of nuclear division and cell division, changes in parasite morphology, and localisation of different markers. The NTTs localise to the parasite plasma membrane where they are hypothesised to steal ATP from the host cell and are detected throughout the replicative stages of the parasite lifecycle. HSP70 is a marker for the mitosome, and the number of mitosome HSP70 signals is hypothesised to correlate with division of the organelle.

Chapter 6 : Conclusions

6.1 General conclusions

The overarching goal of my project was to advance the molecular characterisation of host-parasite interactions for *T. hominis* and for microsporidians more generally. To achieve this I have analysed and compared microsporidian genomes to identify which gene families have been conserved, gained, or expanded by gene duplication during the transition of the group to parasitism, sequenced the transcriptome of *Trachipleistophora hominis* in a rabbit kidney cell line, and provided a description of the *T. hominis* intracellular lifecycle at the level of light microscopy.

Microsporidia as a group had historically been characterised by their extremely reduced genomes compared to free-living relatives (Corradi et al., 2010; Katinka et al., 2001). Genome reduction is also observed in a number of bacterial intracellular pathogens or symbionts (McCutcheon and Moran, 2012; Moran, 2002). Beyond microbial evolution, a broad reconstruction of the protein domain repertoires of ancestral species in major eukaryotic divisions points has suggested that genome reduction is a general feature of eukaryotic evolution (Zmasek and Godzik, 2011), contributing to the suggestion that reduction may be the dominant mode of genome evolution, in which short and explosive periods of genome expansion and increasing complexity are followed by longer term reductive phase (Wolf and Koonin, 2013). The results presented in chapter III demonstrate that Microsporidia are an extreme example of reduction in protein coding capacity, with a huge loss of gene families inferred in the common ancestor of the group, and only 767 gene families shared with other opisthokonts that are conserved across the group. Microsporidia as a group are hypothesised to have radiated rapidly to generate new microsporidian lineages, in part, due to their occupation of an ecological niche that includes a wide range of different potential host species and tissues (Vávra and Lukeš, 2013). Our results follow on from previous studies (Heinz et al., 2012; Peyretaillade et al., 2014) to demonstrate that the extreme reduction in the microsporidian common ancestor is balanced by extensive innovations in protein coding capacity in individual lineages following the microsporidian radiation. Further, the results identified the gene families associated with different kinds of genome expansion, including the gain of genes by gene duplication, *de novo* gene formation, and by lateral gene transfer.

The “core” microsporidian genes, predicted to have been retained in the common ancestor of Microsporidia against the backdrop of extreme genome reduction, are hypothesised to play important roles in the biology of the parasites. Consistent with this idea, the core genes include many housekeeping genes that are shared with other eukaryotes. Many of these genes play roles in essential eukaryotic processes such as DNA and protein synthesis or iron-sulphur cluster biogenesis; but they also include a subset of genes that are found in microsporidians but not in their close relatives. Several of these proteins have already been demonstrated to play important roles in the Microsporidia. The polar tube proteins are an integral part of the polar tube structure, which is unique to microsporidians and essential to their mode of infection (Delbac et al., 2001; Peuvel et al., 2002; Polonais et al., 2005; Weiss et al., 2014), and are hypothesised to have been acquired in the group by *de novo* gene formation due to their lack of sequence similarity to any proteins outside the Microsporidia.

The core conserved microsporidian genes also include a gene family gained by lateral gene transfer. The nucleotide transport proteins (NTTs) are currently the only functionally characterised microsporidian transport protein family, and were likely acquired by lateral gene transfer from intracellular bacteria (Heinz et al., 2014; Richards et al., 2003; Tsaousis et al., 2008). The NTTs transport purines, but not pyrimidines (Heinz et al., 2014; Tsaousis et al., 2008). Throughout the *T. hominis* lifecycle the consistent presence of NTT1, NTT3 and NTT4 was observed in the plasma membrane of the parasite where they can provide purine nucleotides for DNA and RNA replication and ATP for energy; however immunofluorescence results suggest a reduction in NTT1 levels in later stages of infection. This strategy for the acquisition of nucleotides from a host cell is shared with the most likely candidates for donating the NTTs to the microsporidian common ancestors, intracellular bacteria such as *Chlamydia* (Haferkamp et al., 2004; Knab et al., 2011). In addition to being acquired in the common ancestor of Microsporidia, the nucleotide transport proteins have expanded by gene duplication independently in multiple microsporidian lineages against the backdrop for genome reduction (Heinz et al., 2014). The systematic identification of gene families that have expanded in Microsporidia has generated a dataset that can be useful in exploring the dynamics of genome evolution at the functional level, and identifying genes with similar evolutionary histories will help to prioritise future studies.

Prior to this project relatively few RNA sequencing studies had been carried out in Microsporidia (Campbell et al., 2013; Cuomo et al., 2012; Gill et al., 2008; Grisdale et al., 2013), and none that explored the gene expression in both host and parasite for a natural human pathogen. The sequencing of the *T. hominis* transcriptome has complimented the parasite genome study in a number of ways; including confirming and extending the *T. hominis* genome annotation. Based upon the published genome data *T. hominis* was reported to have a larger coding capacity than other microsporidians, but this was questioned by some because of the number of relatively short genes reported (Peyretaillade et al., 2014). The transcriptome data allowed identification of some of these genes as potential false positive inferences based on an absence of detectable transcription, however these genes may simply be expressed in different conditions or times in the parasite lifecycle to those used in the study, so cannot be confirmed as false annotations. Importantly, the transcriptome data confirmed the majority of *T. hominis* gene models and also identified new genes that were missed in the original genome analysis. Based upon the new data it appears that *T. hominis*, at ~3,153 genes, has one of the largest protein coding capacities of any sequenced microsporidian. Intriguingly, this identified a new potential UDP-N-acetylglucosamine transport protein. In many eukaryotes members of this family of transport proteins localise to the golgi, where they are involved in glycosylation reactions (Saier, 2000), including pathogens such as *Toxoplasma gondii* or *Typanosoma brucei* (Caffaro et al., 2013; Liu et al., 2013). If they are instead localised to the surface of the parasite cell in Microsporidia, these transporters could instead play a role in the acquisition of nucleoside-sugars from the host cell, potentially filling the gap in the metabolism and characterised transport protein repertoire of *T. hominis* by allowing the acquisition of pyrimidines and important chitin precursors from the host cell. Consistent with the idea that *T. hominis* is acquiring nucleoside-sugars from its host; data for host RNA expression suggested an increase in the expression of host genes in the pathways that produce these nucleoside-sugars. This was against a background of an overall reduction in host gene expression in other essential pathways such as ribosome biosynthesis. Recently the NupG family of putative nucleoside transport proteins was also highlighted as a potential source of pyrimidines in Microsporidia (Cuomo et al., 2012). This gene family has a similar evolutionary history to the NTTs in that it appears to have expanded independently in multiple

microsporidian lineages, supporting the idea that identifying gene families with these kinds of evolutionary histories may be useful in identifying important targets for characterisation.

Work presented in chapter III allowed the transcriptome of *T. hominis* to be explored in respect to the evolutionary history of its genes, and explore the varying roles of genes with different histories. In particular, core microsporidian genes, including some microsporidian innovations, are generally expressed at higher levels than other genes in the transcriptomes of *E. cuniculi* (Grisdale et al., 2013), *N. parisii* (Cuomo et al., 2012), and *T. hominis*; consistent with our prediction that these may play vital roles in the parasite lifecycle. By contrast, *T. hominis* and *V. culicis* lineage-specific genes show greater variation in expression level in *T. hominis* than core genes; while some are poorly expressed, others are among the most highly expressed genes in the organism. The generally lower level of expression of lineage specific genes is consistent with a model for *de novo* gene formation whereby fortuitously transcribed non-coding DNA acquires novel function (Carvunis et al., 2012); while the subset of highly expressed lineage specific innovations may play important roles in the biology of the parasite. This is particularly interesting when considering the extent of lineage specific variation between different microsporidians highlighted in chapter III, and may help to identify important clade specific innovations, as have been previously been discussed in *T. hominis* (Heinz et al., 2012) and *S. lophii* (Williams et al., 2016).

Another important source of innovation in microsporidian evolution is gene duplication; highlighted by the expanded gene families identified in chapter III. In the typical model for evolution following gene duplication, one gene may retain its important ancestral function, while new copies diverge at the sequence and functional level (Ohno, 1970). In chapter IV the variation in transcription of genes within gene families which have undergone expansion by duplication in Microsporidia was explored. Currently, the only gene family that has been characterised and has undergone expansion in Microsporidia is the previously discussed NTT family (Heinz et al., 2014; Tsaousis et al., 2008). These have undergone divergence at the sequence level following independent expansions by gene duplication in multiple microsporidian lineages; suggesting functional divergence. While the *T. hominis* NTTs have diverged at the sequence level, the published characterisation of this gene family suggests that they each localise to the cell surface where they transport the same substrates (ATP/ADP) at different affinities (Heinz et al., 2014), however whether the NTTs localise to

the parasite plasma membrane, the parasitophorous vacuole, or both remains unclear. The NTT family have independently expanded by gene duplication and undergone sequence divergence in *E. cuniculi* (Heinz et al., 2014; Tsaousis et al., 2008). Unlike *T. hominis*, there is evidence for differences in the spatial localisation of *E. cuniculi* NTTs, with one NTT localising to the mitosome of the parasite (Tsaousis et al., 2008). This NTT is expressed a the lowest level in the published transcriptome of *E. cuniculi* (Grisdale et al., 2013), perhaps reflecting its role in a small compartment and suggesting that differences in the level of expression of paralogues may reflect different cellular roles. It is possible that further characterisation of the *T. hominis* nucleotide transport proteins with respect to the lifecycle of the parasite may help to reveal any potential differences in their function, such as in spatial or temporal expression, and unpublished work in the host-laboratory for this study suggests that some NTTs may localise to the *T. hominis* parasitophorous vacuole rather than the parasite plasma membrane. The level of expression in the NTTs, and other expanded gene families, was correlated negatively with the sequence divergence. Previous studies have found that gene expression at the protein level is an important determinant of the rate of sequence evolution, with highly expressed genes evolving more slowly than those expressed at lower levels due to increased selection pressure (Drummond et al., 2006, 2005; Krylov et al., 2003; Zhang and Yang, 2015). Our results suggest that genes in Microsporidia may be subject to the same kind of expression related selective pressure.

To enable the study of the variation in expression of different genes across the parasite lifecycle, and to enhance understanding of the biology of *T. hominis*, a method was established for synchronising the *T. hominis* infection. The observations suggest that the infection proceeds in a predictable and reproducible pattern under the experimental conditions used. While data is presented here from two separate time course studies, this has since been repeated in the host laboratory multiple times with qualitatively consistent results. The system allows the dynamics of the host-parasite interaction to be followed across the infectious cycle of the parasite using light microscopy and antibodies to *T. hominis* proteins, and raises the possibility of molecular characterisation of different stages of infection by RNA sequencing or proteomics. This has already provided insights into basic microsporidian cell biology. Early studies into the *T. hominis* lifecycle suggested that in the early stages of infection merogony predominantly occurs by binary division of binucleate

meronts, and that in the later stages of infection sporogony and merogony are concurrent (Field et al., 1996; Hollister et al., 1996). Results in chapter V indicate that in the earliest stages of infection, from 0.5h to 15h after inoculation, the infection generally took the form of single small meronts resulting from a single infection per host cell that gradually increased in size without dividing. This phase of growth without division may allow the parasite to establish itself inside its host environment, thus its study may be useful in exploring host-parasite interactions. At 0.5h post infection the signals for mitochondrial HSP70 were limited to a small number of mitosomes close to the parasite nucleus; however by 18h post infection the number of signals had increased, suggesting mitosomes had divided during this period concomitantly with cell size increase. Mitosomes are essential as the sites for iron-sulphur cluster biogenesis (Goldberg et al., 2008), so understanding their division and distribution to daughter cells during parasite cell division is crucial to understanding the parasites cell biology. During the next time stage of 18-36h post infection, parasites underwent three rounds of nuclear division without cell division. The increase in parasite size and the number of HSP70 signals continued throughout the period, leading to the formation of single large meronts containing up to eight nuclei. This contrasts the idea of merogony as a series of binary cell divisions of binucleate meronts (Hollister et al., 1996) and suggests that plasmotomy, the division of a multinucleate parent cell to multinucleate daughter cells without mitosis, is the predominant form of cell division. While in chapter V we begin to explore changes in *T. hominis* across its infectious cycle in the RK-13 cell, we do not explore changes in the host cells themselves. A number of host phenotypes have been associated with microsporidian infection. These include disruption of the host cell cycle (Scanlon et al., 2000). Data in chapter 4 suggests a similar disruption of the RK-13 cell cycle during *T. hominis* infection. Outside of the Microsporidia, active pathogen induced disruption of host cell cycle has been observed in viral (Jault et al., 1995; Lu and Shenk, 1996) and bacterial (Nougayrède et al., 2005) infections. The ability to monitor changes in the host cell cycle within the context of a synchronised infection system in Microsporidia may help to explore whether these fungal pathogens also have a system for active disruption of the host cell cycle.

The allele frequency spectrum of SNPs identified in the *T. hominis* transcriptome suggests that the parasite is likely to have a diploid genome, highlighting this as a common

feature for unikaryotic microsporidians (Cuomo et al., 2012; Haag et al., 2013; Selman et al., 2013) and raising the possibility of sex in these species. In other species of Microsporidia the sexual cycle is hypothesised to include the fusion of two nuclei during multinucleate stages of the parasite lifecycle (Lee et al., 2014). The identification of a stage of the *T. hominis* lifecycle with 8 nuclei supports the possibility of a sexual cycle in the parasite. Study of the sexual lifecycle has provided useful insights into the pathogenicity and transmission of several parasitic protists, including the intracellular parasite *Toxoplasma gondii* (Weedall and Hall, 2015). Understanding what role, if any, sex plays in the lifecycle of Microsporidia would represent a major advance in our understanding of the basic cell biology of the group.

6.2 Future work

The results of my thesis suggest a number of ideas for future work. For example, the ability to synchronise the infection of *T. hominis* provides an opportunity for investigating both the spatial and temporal expression of genes at the protein and RNA level in *T. hominis*. This may yield insights into the dynamics of host and parasite gene expression across the parasite lifecycle. The results of my *T. hominis* transcriptome analyses already suggest that some genes of unknown function are very highly expressed in the parasite. Identifying at which stage in the *T. hominis* lifecycle these genes are expressed may help us to better understand their role during the parasite lifecycle. Antibodies to the most highly expressed of these proteins could then be used to identify the cellular localisation of the proteins. My preliminary data for NTT transport proteins and mitosome marker proteins already suggest that this can yield interesting biological insights. Focusing these studies on proteins that my analyses demonstrate are conserved on most microsporidian genomes would potentially yield insights of more general value for understanding how microsporidians mediate their lifecycle and exploit their hosts.

Thinking even further into the future, one of the main barriers to studying the function of genes in Microsporidia is the lack of any method for genetic manipulation for the group. My analyses show that a number of microsporidians, including *T. hominis*, possess the RNAi machinery, suggesting that gene knockdown by RNAi induction is possible in theory for these species. By exploring the co-distribution of genes with the core elements of the RNAi machinery Dicer and Argonaute in chapter III we identified QDE-1; a gene involved in the initiation of RNAi in response to DNA damage in yeast (H. C. Lee et al., 2010). A long term

goal is to explore whether these observations can contribute to the development of a workable system for the manipulation of gene expression in *T. hominis* using RNAi. *T. hominis* has an advantage over many other species because it can be maintained in tissue culture and it is large enough for light microscopy to yield useful data, and the partially synchronous progression of the parasite life cycle could be used for detailed investigation of the role of genes at different points in the parasite lifecycle. Initial experiments might include targeting the knockdown of essential components of the Fe/S pathway or specific NTTs, and monitoring the progression of infection in response to these challenges. The availability of antibodies to these key proteins and the demonstrated utility of RNAseq would allow the effects of these challenges to be followed at the molecular level.

Bibliography

Altschul, S., 1997. Gapped BLAST and PSI-BLAST: a new generation of protein database search programs. Nucleic Acids Research 25, 3389–3402. doi:10.1093/nar/25.17.3389

Altschul, S.F., Gish, W., Miller, W., Myers, E.W., Lipman, D.J., 1990. Altschul et al.. 1990. Basic Local Alignment Search Tool.pdf. Journal of Molecular Biology. doi:10.1016/S0022-2836(05)80360-2

Alvarez-Ponce, D., Lopez, P., Bapteste, E., McInerney, J.O., 2013. Gene similarity networks provide tools for understanding eukaryote origins and evolution. Proceedings of the National Academy of Sciences of the United States of America 110, E1594–603. doi:10.1073/pnas.1211371110

Andrews, S., 2010. FastQC: A quality control tool for high throughput sequence data. [WWW Document]. URL http://www.bioinformatics.babraham.ac.uk/projects/fastqc/ (accessed 9.1.14).

Aronesty, E., 2011. Command-line tools for processing biological sequencing data [WWW Document]. ea-utils. URL https://code.google.com/p/ea-utils/ (accessed 7.1.14).

Bakowski, M.A., Desjardins, C.A., Smelkinson, M.G., Dunbar, T.A., Lopez-Moyado, I.F., Rifkin, S.A., Cuomo, C.A., Troemel, E.R., 2014. Ubiquitin-Mediated Response to Microsporidia and Virus Infection in C. elegans. PLoS Pathogens 10, e1004200. doi:10.1371/journal.ppat.1004200

Bass, R.B., Strop, P., Barclay, M., Rees, D.C., 2002. Crystal structure of Escherichia coli MscS, a voltage-modulated and mechanosensitive channel. Science (New York, N.Y.) 298, 1582–7. doi:10.1126/science.1077945

Bassler, J., Kallas, M., Pertschy, B., Ulbrich, C., Thoms, M., Hurt, E., 2010. The AAA-ATPase Rea1 drives removal of biogenesis factors during multiple stages of 60S ribosome assembly. Molecular cell 38, 712–21. doi:10.1016/j.molcel.2010.05.024

Becnel, J.J., Andreadis, T.J., 2014. Microsporidia in Insects, in: Weiss, L.M., Becnel, J.J. (Eds.), Microsporidia : Pathogens of Opportunity. John Wiley & Sons, Inc, pp. 521–570.

Benjamini, Y., Hochberg, Y., 1995. Controlling the False Discovery Rate: A Practical and Powerful Approach to Multiple Testing. Journal of the Royal Statistical Society. Series B (Methodological) 57, 289 – 300. doi:10.2307/2346101

Bernander, R., Palm, J.E.D., Svard, S.G., 2001. Genome ploidy in different stages of the Giardia lamblia life cycle. Cellular Microbiology 3, 55–62. doi:10.1046/j.1462-5822.2001.00094.x

Biglardi, E., Selmi, M., Lupetti, P., Corona, S., Gatti, S., Scaglia, M., Sacchi, L., 1996. Microsporidian Spore Wall: Ultrastructural Findings on Encephalitozoon hellem Exospore. The Journal of Eukaryotic Microbiology 43, 181–186. doi:10.1111/j.1550-7408.1996.tb01388.x

Biron, D.G., Agnew, P., Marché, L., Renault, L., Sidobre, C., Michalakis, Y., 2005. Proteome of Aedes aegypti larvae in response to infection by the intracellular parasite Vavraia culicis. International Journal for Parasitology 35, 1385–1397. doi:http://dx.doi.org/10.1016/j.ijpara.2005.05.015

Bogumil, D., Dagan, T., 2012. Cumulative impact of chaperone-mediated folding on genome evolution. Biochemistry 51, 9941–53. doi:10.1021/bi3013643

Bouzahzah, B., Nagajyothi, F., Ghosh, K., Takvorian, P.M., Cali, A., Tanowitz, H.B., Weiss, L.M., 2010. Interactions of Encephalitozoon cuniculi polar tube proteins. Infection and immunity 78, 2745–53. doi:10.1128/IAI.01205-09

Bradley, R.K., Roberts, A., Smoot, M., Juvekar, S., Do, J., Dewey, C., Holmes, I., Pachter, L., 2009. Fast statistical alignment. PLoS computational biology 5, e1000392. doi:10.1371/journal.pcbi.1000392

Brendel, M., Bonatto, D., Strauss, M., Revers, L.F., Pungartnik, C., Saffi, J., Henriques, J.A.P., 2003. Role of PSO genes in repair of DNA damage of Saccharomyces cerevisiae. Mutation Research/Reviews in Mutation Research 544, 179–193. doi:10.1016/j.mrrev.2003.06.018

Brosson, D., Kuhn, L., Delbac, F., Garin, J., Vivarès, C.P., Texier, C., 2006. Proteomic analysis of the eukaryotic parasite Encephalitozoon cuniculi (microsporidia): A reference map for proteins expressed in late sporogonial stages. Proteomics 6, 3625–3635. doi:10.1002/pmic.200500796

Burge, S.W., Daub, J., Eberhardt, R., Tate, J., Barquist, L., Nawrocki, E.P., Eddy, S.R., Gardner, P.P., Bateman, A., 2013. Rfam 11.0: 10 years of RNA families. Nucleic acids research 41, D226–32. doi:10.1093/nar/gks1005

Caffaro, C.E., Koshy, A.A., Liu, L., Zeiner, G.M., Hirschberg, C.B., Boothroyd, J.C., 2013. A Nucleotide Sugar Transporter Involved in Glycosylation of the Toxoplasma Tissue Cyst Wall Is Required for Efficient Persistence of Bradyzoites. PLoS Pathogens 9. doi:10.1371/journal.ppat.1003331

Calendar, R., Berg, P., 1967. d-Tyrosyl RNA: Formation, hydrolysis and utilization for protein synthesis. Journal of Molecular Biology 26, 39–54. doi:10.1016/0022-2836(67)90259-8

Calfon, M., Zeng, H., Urano, F., Till, J.H., Hubbard, S.R., Harding, H.P., Clark, S.G., Ron, D., 2002. IRE1 couples endoplasmic reticulum load to secretory capacity by processing the XBP-1 mRNA. Nature 415, 92–6. doi:10.1038/415092a

Cali, A., Owen, R.L., 1990. Intracellular development of Enterocytozoon, a unique microsporidian found in the intestine of AIDS patients. The Journal of protozoology 37, 145–55.

Cali, A., Takvorian, P.M., 2014. Developmental Morphology and Life Cycles of Microsporidia, in: Weiss, L.M., Becnel, J.J. (Eds.), Microsporidia : Pathogens of Opportunity. John Wiley & Sons, Inc, pp. 71–134.

Callebaut, I., Mornon, J.P., 1997. The human EBNA-2 coactivator p100: multidomain organization and relationship to the staphylococcal nuclease fold and to the tudor protein involved in Drosophila melanogaster development. The Biochemical journal 321 (Pt 1, 125–32.

Campbell, S.E., Williams, T.A., Yousuf, A., Soanes, D.M., Paszkiewicz, K.H., Williams, B.A.P., 2013. The genome of Spraguea lophii and the basis of host-microsporidian interactions. PLoS genetics 9, e1003676. doi:10.1371/journal.pgen.1003676

Capella-Gutiérrez, S., Silla-Martínez, J.M., Gabaldón, T., 2009. trimAl: a tool for automated alignment trimming in large-scale phylogenetic analyses. Bioinformatics (Oxford, England) 25, 1972–3. doi:10.1093/bioinformatics/btp348

Carman, G.M., Han, G.-S., 2011. Regulation of phospholipid synthesis in the yeast Saccharomyces cerevisiae. Annual review of biochemistry 80, 859–83. doi:10.1146/annurev-biochem-060409-092229

Carvunis, A.-R., Rolland, T., Wapinski, I., Calderwood, M.A., Yildirim, M.A., Simonis, N., Charloteaux, B., Hidalgo, C.A., Barbette, J., Santhanam, B., Brar, G.A., Weissman, J.S., Regev, A., Thierry-Mieg, N., Cusick, M.E., Vidal, M., 2012. Proto-genes and de novo gene birth. Nature 487, 370–374. doi:10.1038/nature11184

Cary, L.C., Goebel, M., Corsaro, B.G., Wang, H.-G., Rosen, E., Fraser, M.J., 1989. Transposon mutagenesis of baculoviruses: Analysis of Trichoplusia ni transposon IFP2 insertions within the FP-locus of nuclear polyhedrosis viruses. Virology 172, 156–169. doi:10.1016/0042-6822(89)90117-7

Castel, S.E., Martienssen, R.A., 2013. RNA interference in the nucleus: roles for small RNAs in transcription, epigenetics and beyond. Nature reviews. Genetics 14, 100–12. doi:10.1038/nrg3355

Cattell, E., Sengerová, B., McHugh, P.J., 2010. The SNM1/Pso2 family of ICL repair nucleases: from yeast to man. Environmental and molecular mutagenesis 51, 635–45. doi:10.1002/em.20556

Cavalier-Smith, T., 1987a. Eukaryotes with no mitochondria. Nature 326, 332–333.

Cavalier-Smith, T., 1987b. The origin of eukaryotic and archaebacterial cells. Annals of the New York Academy of Sciences 503, 17–54.

Chavant, P., Taupin, V., El Alaoui, H., Wawrzyniak, I., Chambon, C., Prensier, G., Méténier, G., Vivarès, C.P., 2005. Proteolytic activity in Encephalitozoon cuniculi sporogonial stages: Predominance of metallopeptidases including an aminopeptidase-P-like enzyme. International Journal for Parasitology 35, 1425–1433. doi:10.1016/j.ijpara.2005.05.009

Cherry, J.M., Hong, E.L., Amundsen, C., Balakrishnan, R., Binkley, G., Chan, E.T., Christie, K.R., Costanzo, M.C., Dwight, S.S., Engel, S.R., Fisk, D.G., Hirschman, J.E., Hitz, B.C., Karra, K., Krieger, C.J., Miyasato, S.R., Nash, R.S., Park, J., Skrzypek, M.S., Simison, M., Weng, S., Wong, E.D., 2012. Saccharomyces Genome Database: the genomics resource of budding yeast. Nucleic acids research 40, D700–5. doi:10.1093/nar/gkr1029

Cingolani, P., Patel, V.M., Coon, M., Nguyen, T., Land, S.J., Ruden, D.M., Lu, X., 2012a. Using Drosophila melanogaster as a Model for Genotoxic Chemical Mutational Studies with a New Program, SnpSift. Frontiers in Genetics 3, 35. doi:10.3389/fgene.2012.00035

Cingolani, P., Platts, A., Wang, L.L.L., Coon, M., Nguyen, T., Wang, L.L.L., Land, S.J., Lu, X., Ruden, D.M., 2012b. A program for annotating and predicting the effects of single nucleotide polymorphisms, SnpEff: SNPs in the genome of Drosophila melanogaster strain w(1118); iso-2; iso-3. Fly 6, 80–92. doi:10.4161/fly.19695

Cohen, O., Gophna, U., Pupko, T., 2011. The complexity hypothesis revisited: connectivity rather than function constitutes a barrier to horizontal gene transfer. Molecular biology and evolution 28, 1481–9. doi:10.1093/molbev/msq333

Conant, G.C., Wagner, A., 2003. Asymmetric sequence divergence of duplicate genes. Genome research 13, 2052–8. doi:10.1101/gr.1252603

Conant, G.C., Wolfe, K.H., 2008. Turning a hobby into a job: how duplicated genes find new functions. Nature reviews. Genetics 9, 938–50. doi:10.1038/nrg2482

Consortium, H.G.S., 2006. Insights into social insects from the genome of the honeybee Apis mellifera. Nature 443, 931–949. doi:10.1038/nature05260

Cornman, R.S., Chen, Y.P., Schatz, M.C., Street, C., Zhao, Y., Desany, B., Egholm, M., Hutchison, S., Pettis, J.S., Lipkin, W.I., Evans, J.D., 2009. Genomic analyses of the microsporidian Nosema ceranae, an emergent pathogen of honey bees. PLoS pathogens 5, e1000466. doi:10.1371/journal.ppat.1000466

Corradi, N., Gangaeva, A., Keeling, P.J., 2008. Comparative profiling of overlapping transcription in the compacted genomes of microsporidia Antonospora locustae and Encephalitozoon cuniculi. Genomics 91, 388–93. doi:10.1016/j.ygeno.2007.12.006

Corradi, N., Haag, K.L., Pombert, J.-F., Ebert, D., Keeling, P.J., 2009. Draft genome sequence of the Daphnia pathogen Octosporea bayeri: insights into the gene content of a large microsporidian genome and a model for host-parasite interactions. Genome biology 10, R106. doi:10.1186/gb-2009-10-10-r106

Corradi, N., Pombert, J.-F., Farinelli, L., Didier, E.S., Keeling, P.J., 2010. The complete sequence of the smallest known nuclear genome from the microsporidian Encephalitozoon intestinalis. Nature communications 1, 77. doi:10.1038/ncomms1082

Corradi, N., Slamovits, C.H., 2011. The intriguing nature of microsporidian genomes. Briefings in functional genomics 10, 115–24. doi:10.1093/bfgp/elq032

Costa, V., Angelini, C., De Feis, I., Ciccodicola, A., 2010. Uncovering the complexity of transcriptomes with RNA-Seq. Journal of biomedicine & biotechnology 2010, 853916. doi:10.1155/2010/853916

Crollius, H.R., Jaillon, O., Dasilva, C., Ozouf-Costaz, C., Fizames, C., Fischer, C., Bouneau, L., Billault, A., Quetier, F., Saurin, W., Bernot, A., Weissenbach, J., 2000. Characterization and repeat analysis of the compact genome of the freshwater pufferfish Tetraodon nigroviridis. Genome Research 10, 939–949. doi:10.1101/gr.10.7.939

Csurös, M., 2010. Count: Evolutionary analysis of phylogenetic profiles with parsimony and likelihood. Bioinformatics 26, 1910–1912. doi:10.1093/bioinformatics/btq315

Cuomo, C.A., Becknel, J., Sanscrainte, N., Young, S.K., Zeng, Q., Gargeya, S., Fitzgerald, M., Haas, B., Abouelleil, A., Alvarado, L., Arachchi, H.M., Berlin, A., Chapman, S.B., Gearin, G., Goldberg, J., Griggs, A., Gujja, S., Hansen, M., Heiman, D., Howarth, C., Larimer, J., Lui, A., MacDonald, P.J.P., McCowen, C., Montmayeur, A., Murphy, C., Neiman, D., Pearson, M., Priest, M., Roberts, A., Saif, S., Shea, T., Sisk, P., Stolte, C., Sykes, S., Wortman, J., Nusbaum, C., Birren, B., 2011. The Genome Sequence of Vavraia culicis strain floridensis. NCBI Bioproject Genome - PRJNA242548.

Cuomo, C.A., Desjardins, C.A., Bakowski, M.A., Goldberg, J., Ma, A.T., Becnel, J.J., Didier, E.S., Fan, L., Heiman, D.I., Levin, J.Z., Young, S., Zeng, Q., Troemel, E.R., 2012. Microsporidian genome analysis reveals evolutionary strategies for obligate intracellular growth. Genome research 22, 2478–88. doi:10.1101/gr.142802.112

Danecek, P., Auton, A., Abecasis, G., Albers, C.A., Banks, E., DePristo, M.A., Handsaker, R.E., Lunter, G., Marth, G.T., Sherry, S.T., McVean, G., Durbin, R., 2011. The variant call format and VCFtools. Bioinformatics (Oxford, England) 27, 2156–8. doi:10.1093/bioinformatics/btr330

Decraene, V., Lebbad, M., Botero-Kleiven, S., Gustavsson, A., Lofdahl, M., 2012. First reported foodborne outbreak associated with microsporidia, Sweden, October 2009. Epidemiology and Infection 140, 519–527. doi:10.1017/S095026881100077X

DeLabre, M.L., Kessl, J., Karamanou, S., Trumpower, B.L., 2002. RPL29 codes for a non-essential protein of the 60S ribosomal subunit in Saccharomyces cerevisiae and exhibits synthetic lethality with mutations in genes for proteins required for subunit coupling. Biochimica et biophysica acta 1574, 255–61.

Delbac, F., David, D., Méténier, G., Vivarès, C., 1997. First complete amino acid sequence of a polar tube protein in a microsporidian species, Encephalitozoon cuniculi. The Journal of eukaryotic microbiology 44, 77S.

Delbac, F., Peuvel, I., Metenier, G., Peyretaillade, E., Vivares, C.P., 2001. Microsporidian invasion apparatus: identification of a novel polar tube protein and evidence for clustering of ptp1 and ptp2 genes in three Encephalitozoon species. Infection and immunity 69, 1016–24. doi:10.1128/IAI.69.2.1016-1024.2001

Desjardins, C.A., Sanscrainte, N.D., Goldberg, J.M., Heiman, D., Young, S., Zeng, Q., Madhani, H.D., Becnel, J.J., Cuomo, C.A., 2015. Contrasting host-pathogen interactions and genome evolution in two generalist and specialist microsporidian pathogens of mosquitoes. Nature communications 6, 7121. doi:10.1038/ncomms8121

Didier, E.S., 2005. Microsporidiosis: an emerging and opportunistic infection in humans and animals. Acta tropica 94, 61–76. doi:10.1016/j.actatropica.2005.01.010

Didier, E.S., Weiss, L.M., 2011. Microsporidiosis: not just in AIDS patients. Current opinion in infectious diseases 24, 490–495. doi:10.1097/QCO.0b013e32834aa152

Didier, E.S., Weiss, L.M., 2006. Microsporidiosis: current status. Current opinion in infectious diseases 19, 485–492. doi:10.1097/01.qco.0000244055.46382.23

Do, C.B., Mahabhashyam, M.S.P., Brudno, M., Batzoglou, S., 2005. ProbCons: Probabilistic consistency-based multiple sequence alignment. Genome research 15, 330–40. doi:10.1101/gr.2821705

Doblado, M., Moley, K.H., 2009. Facilitative glucose transporter 9, a unique hexose and urate transporter. American journal of physiology. Endocrinology and metabolism 297, E831–5. doi:10.1152/ajpendo.00296.2009

Dolgikh, V. V, Senderskiy, I. V, Pavlova, O.A., Naumov, A.M., Beznoussenko, G. V, 2011. Immunolocalization of an alternative respiratory chain in Antonospora (Paranosema) locustae spores: mitosomes retain their role in microsporidial energy metabolism. Eukaryotic cell 10, 588–93. doi:10.1128/EC.00283-10

Dolgikh, V. V, Sokolova, J.J., Issi, I. V, 1997. Activities of enzymes of carbohydrate and energy metabolism of the spores of the microsporidian, Nosema grylli. The Journal of eukaryotic microbiology 44, 246–249.

Drummond, D.A., Bloom, J.D., Adami, C., Wilke, C.O., Arnold, F.H., 2005. Why highly expressed proteins evolve slowly. Proc Natl Acad Sci U S A 102, 14338–14343. doi:10.1073/pnas.0504070102

Drummond, D.A., Raval, A., Wilke, C.O., 2006. A single determinant dominates the rate of yeast protein evolution. Molecular Biology and Evolution 23, 327–337. doi:10.1093/molbev/msj038

Duncan, A.B., Agnew, P., Noel, V., Demettre, E., Seveno, M., Brizard, J.-P., Michalakis, Y., 2012. Proteome of Aedes aegypti in response to infection and coinfection with microsporidian parasites. Ecology and Evolution 2, 681–694. doi:10.1002/ece3.199

Edgar, R.C., 2004. MUSCLE: a multiple sequence alignment method with reduced time and space complexity. BMC bioinformatics 5, 113. doi:10.1186/1471-2105-5-113

Edwards, M.D., Li, Y., Kim, S., Miller, S., Bartlett, W., Black, S., Dennison, S., Iscla, I., Blount, P., Bowie, J.U., Booth, I.R., 2005. Pivotal role of the glycine-rich TM3 helix in gating the MscS mechanosensitive channel. Nature structural & molecular biology 12, 113–9. doi:10.1038/nsmb895

Enright, A.J., Van Dongen, S., Ouzounis, C.A., 2002. An efficient algorithm for large-scale detection of protein families. Nucleic acids research 30, 1575–84. doi:10.1093/nar/30.7.1575

Estes, K.A., Szumowski, S.C., Troemel, E.R., 2011. Non-Lytic, Actin-Based Exit of Intracellular Parasites from C. elegans Intestinal Cells. PLoS Pathog 7, e1002227. doi:10.1371/journal.ppat.1002227

Fares, M.A., Ruiz-González, M.X., Moya, A., Elena, S.F., Barrio, E., 2002. Endosymbiotic bacteria: groEL buffers against deleterious mutations. Nature 417, 398. doi:10.1038/417398a

Field, a S., Marriott, D.J., Milliken, S.T., Brew, B.J., Canning, E.U., Kench, J.G., Darveniza, P., Harkness, J.L., 1996. Myositis associated with a newly described microsporidian, Trachipleistophora hominis, in a patient with AIDS. Journal of clinical microbiology 34, 2803–11.

Finn, R.D., Clements, J., Eddy, S.R., 2011. HMMER web server: interactive sequence similarity searching. Nucleic acids research 39, W29–37. doi:10.1093/nar/gkr367

Force, A., Lynch, M., Pickett, F.B., Amores, A., Yan, Y.L., Postlethwait, J., 1999. Preservation of duplicate genes by complementary, degenerative mutations. Genetics 151, 1531–45.

Forrest, E.C., Cogoni, C., Macino, G., 2004. The RNA-dependent RNA polymerase, QDE-1, is a rate-limiting factor in post-transcriptional gene silencing in Neurospora crassa. Nucleic acids research 32, 2123–8. doi:10.1093/nar/gkh530

Franzen, C., 2008. Microsporidia: A Review of 150 Years of Research. The Open Parasitology Journal. doi:10.2174/1874421400802010001

Fuentealba, I.C., Mahoney, N.T., Shadduck, J. a., Harvill, J., Wicher, V., Wicher, K., 1992. Hepatic Lesions in Rabbits Infected with Encephalitozoon cuniculi Administered per Rectum. Veterinary Pathology 29, 536–540. doi:10.1177/030098589202900608

Galagan, J.E., Calvo, S.E., Borkovich, K.A., Selker, E.U., Read, N.D., Jaffe, D., FitzHugh, W., Ma, L.-J., Smirnov, S., Purcell, S., Rehman, B., Elkins, T., Engels, R., Wang, S., Nielsen, C.B., Butler, J., Endrizzi, M., Qui, D., Ianakiev, P., Bell-Pedersen, D., Nelson, M.A., Werner-Washburne, M., Selitrennikoff, C.P., Kinsey, J.A., Braun, E.L., Zelter, A., Schulte, U., Kothe, G.O., Jedd, G., Mewes, W., Staben, C., Marcotte, E., Greenberg, D., Roy, A., Foley, K., Naylor, J., Stange-Thomann, N., Barrett, R., Gnerre, S., Kamal, M., Kamvysselis, M., Mauceli, E., Bielke, C., Rudd, S., Frishman, D., Krystofova, S., Rasmussen, C., Metzenberg, R.L., Perkins, D.D., Kroken, S., Cogoni, C., Macino, G., Catcheside, D., Li, W., Pratt, R.J., Osmani, S.A., DeSouza, C.P.C., Glass, L., Orbach, M.J., Berglund, J.A., Voelker, R., Yarden, O., Plamann, M., Seiler, S., Dunlap, J., Radford, A., Aramayo, R., Natvig, D.O., Alex, L.A., Mannhaupt, G., Ebbole, D.J., Freitag, M., Paulsen, I., Sachs, M.S., Lander, E.S., Nusbaum, C., Birren, B., 2003. The genome sequence of the filamentous fungus Neurospora crassa. Nature 422, 859–868. doi:10.1038/nature01554

Germot, A., Philippe, H., Le Guyader, H., 1997. Evidence for loss of mitochondria in Microsporidia from a mitochondrial-type HSP70 in Nosema locustae1Note: Nucleotide sequence data reported in this paper has been submitted to the GenBank™ data base under the accession number U97520.1. Molecular and Biochemical Parasitology 87, 159–168. doi:10.1016/S0166-6851(97)00064-9

Ghaemmaghami, S., Huh, W.-K., Bower, K., Howson, R.W., Belle, A., Dephoure, N., O'Shea, E.K., Weissman, J.S., 2003. Global analysis of protein expression in yeast. Nature 425, 737–41. doi:10.1038/nature02046

Gill, E.E., Becnel, J.J., Fast, N.M., 2008. ESTs from the microsporidian Edhazardia aedis. BMC genomics 9, 296. doi:10.1186/1471-2164-9-296

Girard, A., Hannon, G.J., 2008. Conserved themes in small-RNA-mediated transposon control. Trends in Cell Biology 18, 136–148. doi:10.1016/j.tcb.2008.01.004

Goffeau, A., Barrell, B.G., Bussey, H., Davis, R.W., Dujon, B., Feldmann, H., Galibert, F., Hoheisel, J.D., Jacq, C., Johnston, M., Louis, E.J., Mewes, H.W., Murakami, Y., Philippsen, P., Tettelin, H., Oliver, S.G., 1996. Life with 6000 Genes. Science 274, 546–567. doi:10.1126/science.274.5287.546

Goldberg, A.L., 2003. Protein degradation and protection against misfolded or damaged proteins. Nature 426, 895–9. doi:10.1038/nature02263

Goldberg, A. V, Molik, S., Tsaousis, A.D., Neumann, K., Kuhnke, G., Delbac, F., Vivares, C.P., Hirt, R.P., Lill, R., Embley, T.M., 2008. Localization and functionality of microsporidian iron-sulphur cluster assembly proteins. Nature 452, 624–8. doi:10.1038/nature06606

Gouy, M., Guindon, S., Gascuel, O., 2010. SeaView version 4: A multiplatform graphical user interface for sequence alignment and phylogenetic tree building. Molecular biology and evolution 27, 221–4. doi:10.1093/molbev/msp259

Grisdale, C.J., Bowers, L.C., Didier, E.S., Fast, N.M., 2013. Transcriptome analysis of the parasite Encephalitozoon cuniculi: an in-depth examination of pre-mRNA splicing in a reduced eukaryote. BMC genomics 14, 207. doi:10.1186/1471-2164-14-207

Guo, X., Gao, J., Li, F., Wang, J., 2014. Evidence of horizontal transfer of non-autonomous Lep1 Helitrons facilitated by host-parasite interactions. Scientific reports 4, 5119. doi:10.1038/srep05119

Haag, K.L., Traunecker, E., Ebert, D., 2013. Single-nucleotide polymorphisms of two closely related microsporidian parasites suggest a clonal population expansion after the last glaciation. Molecular ecology 22, 314–26. doi:10.1111/mec.12126

Haferkamp, I., Schmitz-Esser, S., Linka, N., Urbany, C., Collingro, A., Wagner, M., Horn, M., Neuhaus, H.E., 2004. A candidate NAD+ transporter in an intracellular bacterial symbiont related to Chlamydiae. Nature 432, 622–5. doi:10.1038/nature03131

Haswell, E.S., Phillips, R., Rees, D.C., 2011. Mechanosensitive channels: what can they do and how do they do it? Structure (London, England : 1993) 19, 1356–69. doi:10.1016/j.str.2011.09.005

Hayman, J.R., Southern, T.R., Nash, T.E., Mmun, I.N.I., 2005. Role of Sulfated Glycans in Adherence of the Microsporidian Encephalitozoon intestinalis to Host Cells In Vitro 73, 841–848. doi:10.1128/IAI.73.2.841

Hazard, E.I., Brookbank, J.W., 1984. Karyogamy and meiosis in an Amblyospora sp. (Microspora) in the mosquito Culex salinarius. Journal of Invertebrate Pathology 44, 3–11. doi:10.1016/0022-2011(84)90039-9

Heinz, E., Hacker, C., Dean, P., Mifsud, J., Goldberg, A. V, Williams, T.A., Nakjang, S., Gregory, A., Hirt, R.P., Lucocq, J.M., Kunji, E.R.S., Embley, T.M., 2014. Plasma Membrane-Located Purine Nucleotide Transport Proteins Are Key Components for Host Exploitation by Microsporidian Intracellular Parasites. PLoS Pathog 10, e1004547.

Heinz, E., Williams, T.A., Nakjang, S., Noël, C.J., Swan, D.C., Goldberg, A. V, Harris, S.R., Weinmaier, T., Markert, S., Becher, D., Bernhardt, J., Dagan, T., Hacker, C., Lucocq, J.M., Schweder, T., Rattei, T., Hall, N., Hirt, R.P., Embley, T.M., 2012. The genome of the obligate intracellular parasite Trachipleistophora hominis: new insights into microsporidian genome dynamics and reductive evolution. PLoS pathogens 8, e1002979. doi:10.1371/journal.ppat.1002979

Henderson, B., Allan, E., Coates, A.R.M., 2006. Stress wars: the direct role of host and bacterial molecular chaperones in bacterial infection. Infection and immunity 74, 3693–706. doi:10.1128/IAI.01882-05

Hirt, R.P., Healy, B., Vossbrinck, C.R., Canning, E.U., Embley, T.M., 1997. A mitochondrial Hsp70 orthologue in Vairimorpha necatrix: molecular evidence that microsporidia once contained mitochondria. Current biology : CB 7, 995–8.

Hirt, R.P., Logsdon, J.M., Healy, B., Dorey, M.W., Doolittle, W.F., Embley, T.M., 1999. Microsporidia are related to Fungi: Evidence from the largest subunit of RNA polymerase II and other proteins. Proceedings of the National Academy of Sciences 96, 580–585. doi:10.1073/pnas.96.2.580

Hjort, K., Goldberg, A. V, Tsaousis, A.D., Hirt, R.P., Embley, T.M., 2010. Diversity and reductive evolution of mitochondria among microbial eukaryotes. Philosophical transactions of the Royal Society of London. Series B, Biological sciences 365, 713–27. doi:10.1098/rstb.2009.0224

Hollister, W.S., Canning, E.U., Weidner, E., Field, a S., Kench, J., Marriott, D.J., 1996. Development and ultrastructure of Trachipleistophora hominis n.g., n.sp. after in vitro isolation from an AIDS patient and inoculation into athymic mice. Parasitology 112 (Pt 1), 143–54.

Holness, M.J., Sugden, M.C., 2003. Regulation of pyruvate dehydrogenase complex activity by reversible phosphorylation. Biochemical Society transactions 31, 1143–1151. doi:10.1042/

Inglis, D.O., Arnaud, M.B., Binkley, J., Shah, P., Skrzypek, M.S., Wymore, F., Binkley, G., Miyasato, S.R., Simison, M., Sherlock, G., 2012. The Candida genome database incorporates multiple Candida species:

Multispecies search and analysis tools with curated gene and protein information for Candida albicans and Candida glabrata. Nucleic Acids Research 40. doi:10.1093/nar/gkr945

Ironside, J.E., 2007. Multiple losses of sex within a single genus of Microsporidia. BMC evolutionary biology 7, 48. doi:10.1186/1471-2148-7-48

Jain, R., Rivera, M.C., Lake, J.A., 1999. Horizontal gene transfer among genomes: the complexity hypothesis. Proceedings of the National Academy of Sciences of the United States of America 96, 3801–6.

James, T.Y., Pelin, A., Bonen, L., Ahrendt, S., Sain, D., Corradi, N., Stajich, J.E., 2013. Shared signatures of parasitism and phylogenomics unite Cryptomycota and microsporidia. Current biology : CB 23, 1548–53. doi:10.1016/j.cub.2013.06.057

Jaspersen, S.L., Giddings, T.H., Winey, M., 2002. Mps3p is a novel component of the yeast spindle pole body that interacts with the yeast centrin homologue Cdc31p. The Journal of cell biology 159, 945–56. doi:10.1083/jcb.200208169

Jault, F.M., Jault, J.M., Ruchti, F., Fortunato, E.A., Clark, C., Corbeil, J., Richman, D.D., Spector, D.H., 1995. Cytomegalovirus infection induces high levels of cyclins, phosphorylated Rb, and p53, leading to cell cycle arrest. Journal of virology 69, 6697–704.

Kanehisa, M., Goto, S., 2000. KEGG: kyoto encyclopedia of genes and genomes. Nucleic acids research 28, 27–30.

Katinka, M.D., Duprat, S., Cornillot, E., Méténier, G., Thomarat, F., Prensier, G., Barbe, V., Peyretaillade, E., Brottier, P., Wincker, P., Delbac, F., El Alaoui, H., Peyret, P., Saurin, W., Gouy, M., Weissenbach, J., Vivarès, C.P., 2001. Genome sequence and gene compaction of the eukaryote parasite Encephalitozoon cuniculi. Nature 414, 450–3. doi:10.1038/35106579

Katoh, K., 2002. MAFFT: a novel method for rapid multiple sequence alignment based on fast Fourier transform. Nucleic Acids Research 30, 3059–3066. doi:10.1093/nar/gkf436

Kellis, M., Birren, B.W., Lander, E.S., 2004. Proof and evolutionary analysis of ancient genome duplication in the yeast Saccharomyces cerevisiae. Nature 428, 617–24. doi:10.1038/nature02424

Kent, M.L., 2000. Marine netpen farming leads to infections with some unusual parasites, in: International Journal for Parasitology. pp. 321–326. doi:10.1016/S0020-7519(00)00018-7

Kim, D., Pertea, G., Trapnell, C., Pimentel, H., Kelley, R., Salzberg, S.L., 2013. TopHat2: accurate alignment of transcriptomes in the presence of insertions, deletions and gene fusions. Genome biology 14, R36. doi:10.1186/gb-2013-14-4-r36

Kim, J., Tchernyshyov, I., Semenza, G.L., Dang, C. V, 2006. HIF-1-mediated expression of pyruvate dehydrogenase kinase: a metabolic switch required for cellular adaptation to hypoxia. Cell metabolism 3, 177–85. doi:10.1016/j.cmet.2006.02.002

Knab, S., Mushak, T.M., Schmitz-Esser, S., Horn, M., Haferkamp, I., 2011. Nucleotide parasitism by Simkania negevensis (Chlamydiae). Journal of bacteriology 193, 225–35. doi:10.1128/JB.00919-10

Koprowski, P., Kubalski, A., 2003. C termini of the Escherichia coli mechanosensitive ion channel (MscS) move apart upon the channel opening. The Journal of biological chemistry 278, 11237–45. doi:10.1074/jbc.M212073200

Korbel, J.O., Kim, P.M., Chen, X., Urban, A.E., Weissman, S., Snyder, M., Gerstein, M.B., 2008. The current excitement about copy-number variation: how it relates to gene duplications and protein families. Current opinion in structural biology 18, 366–74. doi:10.1016/j.sbi.2008.02.005

Krogh, A., Larsson, B., von Heijne, G., Sonnhammer, E.L., 2001. Predicting transmembrane protein topology with a hidden Markov model: application to complete genomes. Journal of molecular biology 305, 567–80. doi:10.1006/jmbi.2000.4315

Krüger, N., Tolić-Nørrelykke, I.M., 2008. Association of mitochondria with spindle poles facilitates spindle alignment. Current Biology 18, R646–R647. doi:10.1016/j.cub.2008.06.069

Krylov, D.M., Wolf, Y.I., Rogozin, I.B., Koonin, E. V., 2003. Gene loss, protein sequence divergence, gene dispensability, expression level, and interactivity are correlated in eukaryotic evolution. Genome Research 13, 2229–2235. doi:10.1101/gr.1589103

Kung, C., Martinac, B., Sukharev, S., 2010. Mechanosensitive channels in microbes. Annual review of microbiology 64, 313–29. doi:10.1146/annurev.micro.112408.134106

Langmead, B., Salzberg, S.L., 2012. Fast gapped-read alignment with Bowtie 2. Nature methods 9, 357–9. doi:10.1038/nmeth.1923

Lartillot, N., Lepage, T., Blanquart, S., 2009. PhyloBayes 3: a Bayesian software package for phylogenetic reconstruction and molecular dating. Bioinformatics (Oxford, England) 25, 2286–8. doi:10.1093/bioinformatics/btp368

Le, S.Q., Lartillot, N., Gascuel, O., 2008. Phylogenetic mixture models for proteins. Philosophical transactions of the Royal Society of London. Series B, Biological sciences 363, 3965–76. doi:10.1098/rstb.2008.0180

Lee, H.C., Aalto, A.P., Yang, Q., Chang, S.-S., Huang, G., Fisher, D., Cha, J., Poranen, M.M., Bamford, D.H., Liu, Y., 2010. The DNA/RNA-dependent RNA polymerase QDE-1 generates aberrant RNA and dsRNA for RNAi in a process requiring replication protein A and a DNA helicase. PLoS biology 8. doi:10.1371/journal.pbio.1000496

Lee, H.-C., Chang, S.-S., Choudhary, S., Aalto, A.P., Maiti, M., Bamford, D.H., Liu, Y., 2009. qiRNA is a new type of small interfering RNA induced by DNA damage. Nature 459, 274–7. doi:10.1038/nature08041

Lee, R.C.H., Gill, E.E., Roy, S.W., Fast, N.M., 2010. Constrained intron structures in a microsporidian. Molecular biology and evolution 27, 1979–82. doi:10.1093/molbev/msq087

Lee, S.C., Heitman, J., Ironside, J.E., 2014. Sex and the Microsporidia, in: Weiss, L.M., Becnel, J.J. (Eds.), Microsporidia : Pathogens of Opportunity. John Wiley & Sons, Inc, pp. 231–244.

Leitch, G.J., Shaw, A.P., Colden-Stanfield, M., Scanlon, M., Visvesvara, G.S., 2005. Multinucleate host cells induced by Vittaforma corneae (Microsporidia). Folia parasitologica 52, 103–10.

Li, H., Handsaker, B., Wysoker, A., Fennell, T., Ruan, J., Homer, N., Marth, G., Abecasis, G., Durbin, R., 2009. The Sequence Alignment/Map format and SAMtools. Bioinformatics (Oxford, England) 25, 2078–9. doi:10.1093/bioinformatics/btp352

Li, Z., Pan, G., Li, T., Huang, W., Chen, J., Geng, L., Yang, D., Wang, L., Zhou, Z., 2012. SWP5, a spore wall protein, interacts with polar tube proteins in the parasitic microsporidian Nosema bombycis. Eukaryotic cell 11, 229–37. doi:10.1128/EC.05127-11

Liberek, K., Lewandowska, A., Zietkiewicz, S., 2008. Chaperones in control of protein disaggregation. The EMBO journal 27, 328–35. doi:10.1038/sj.emboj.7601970

Lill, R., Mühlenhoff, U., 2008. Maturation of iron-sulfur proteins in eukaryotes: mechanisms, connected processes, and diseases. Annual review of biochemistry 77, 669–700. doi:10.1146/annurev.biochem.76.052705.162653

Lin, J., Handschin, C., Spiegelman, B.M., 2005. Metabolic control through the PGC-1 family of transcription coactivators. Cell metabolism 1, 361–70. doi:10.1016/j.cmet.2005.05.004

Liu, L., Xu, Y.X., Caradonna, K.L., Kruzel, E.K., Burleigh, B.A., Bangs, J.D., Hirschberg, C.B., 2013. Inhibition of nucleotide sugar transport in Trypanosoma brucei alters surface Glycosylation. Journal of Biological Chemistry 288, 10599–10615. doi:10.1074/jbc.M113.453597

Long, O.S., Benson, J.A., Kwak, J.H., Luke, C.J., Gosai, S.J., O'Reilly, L.P., Wang, Y., Li, J., Vetica, A.C., Miedel, M.T., Stolz, D.B., Watkins, S.C., Züchner, S., Perlmutter, D.H., Silverman, G.A., Pak, S.C., 2014. A C. elegans model of human α1-antitrypsin deficiency links components of the RNAi pathway to misfolded protein turnover. Human molecular genetics 23, 5109–22. doi:10.1093/hmg/ddu235

Loureiro, I., Faria, J., Clayton, C., Ribeiro, S.M., Roy, N., Santarém, N., Tavares, J., Cordeiro-da-Silva, A., 2013. Knockdown of Asparagine Synthetase A Renders Trypanosoma brucei Auxotrophic to Asparagine. PLoS Neglected Tropical Diseases 7, e2578. doi:10.1371/journal.pntd.0002578

Lu, M., Shenk, T., 1996. Human cytomegalovirus infection inhibits cell cycle progression at multiple points, including the transition from G1 to S. Journal of virology 70, 8850–7.

Lunn, D., Spiegelhalter, D., Thomas, A., Best, N., 2009. The BUGS project: Evolution, critique and future directions. Statistics in Medicine 28, 3049–3067. doi:10.1002/sim.3680

Ma, L.J., Ibrahim, A.S., Skory, C., Grabherr, M.G., Burger, G., Butler, M., Elias, M., Idnurm, A., Lang, B.F., Sone, T., Abe, A., Calvo, S.E., Corrochano, L.M., Engels, R., Fu, J., Hansberg, W., Kim, J.M., Kodira, C.D., Koehrsen, M.J., Liu, B., Miranda-Saavedra, D., O'Leary, S., Ortiz-Castellanos, L., Poulter, R., Rodriguez-Romero, J., Ruiz-Herrera, J., Shen, Y.Q., Zeng, Q., Galagan, J., Birren, B.W., Cuomo, C.A., Wickes, B.L., 2009. Genomic analysis of the basal lineage fungus Rhizopus oryzae reveals a whole-genome duplication. PLoS Genetics 5. doi:10.1371/journal.pgen.1000549

Ma, Z., Li, C., Pan, G., Li, Z., Han, B., Xu, J., Lan, X., Chen, J., Yang, D., Chen, Q., Sang, Q., Ji, X., Li, T., Long, M., Zhou, Z., 2013. Genome-wide transcriptional response of silkworm (Bombyx mori) to infection by the microsporidian Nosema bombycis. PloS one 8, e84137. doi:10.1371/journal.pone.0084137

Manhas, R., Tripathi, P., Khan, S., Sethu Lakshmi, B., Lal, S.K., Gowri, V.S., Sharma, A., Madhubala, R., 2014. Identification and functional characterization of a novel bacterial type asparagine synthetase A: a tRNA synthetase paralog from Leishmania donovani. The Journal of biological chemistry 289, 12096–108. doi:10.1074/jbc.M114.554642

Marguerat, S., Schmidt, A., Codlin, S., Chen, W., Aebersold, R., Bähler, J., 2012. Quantitative Analysis of Fission Yeast Transcriptomes and Proteomes in Proliferating and Quiescent Cells. Cell 151, 671–683. doi:10.1016/j.cell.2012.09.019

Martin, F.-P.J., Verdu, E.F., Wang, Y., Dumas, M.-E., Yap, I.K.S., Cloarec, O., Bergonzelli, G.E., Corthesy-Theulaz, I., Kochhar, S., Holmes, E., Lindon, J.C., Collins, S.M., Nicholson, J.K., 2006. Transgenomic metabolic interactions in a mouse disease model: interactions of Trichinella spiralis infection with dietary Lactobacillus paracasei supplementation. Journal of proteome research 5, 2185–93. doi:10.1021/pr060157b

Mathupala, S.P., Ko, Y.H., Pedersen, P.L., 2010. The pivotal roles of mitochondria in cancer: Warburg and beyond and encouraging prospects for effective therapies. Biochimica et biophysica acta 1797, 1225–30. doi:10.1016/j.bbabio.2010.03.025

McCutcheon, J.P., Moran, N.A., 2012. Extreme genome reduction in symbiotic bacteria. Nature reviews. Microbiology 10, 13–26. doi:10.1038/nrmicro2670

Meissner, D., Odman-Naresh, J., Vogelpohl, I., Merzendorfer, H., 2010. A novel role of the yeast CaaX protease Ste24 in chitin synthesis. Molecular biology of the cell 21, 2425–33. doi:10.1091/mbc.E10-01-0080

Mitra, R., Li, X., Kapusta, A., Mayhew, D., Mitra, R.D., Feschotte, C., Craig, N.L., 2013. Functional characterization of piggyBat from the bat Myotis lucifugus unveils an active mammalian DNA transposon. Proceedings of the National Academy of Sciences of the United States of America 110, 234–9. doi:10.1073/pnas.1217548110

Moran, N.A., 2002. Microbial minimalism: Genome reduction in bacterial pathogens. Cell. doi:10.1016/S0092-8674(02)00665-7

Mortazavi, A., Williams, B., McCue, K., 2008. Mapping and quantifying mammalian transcriptomes by RNA-Seq. Nature.

Munger, J., Bajad, S.U., Coller, H.A., Shenk, T., Rabinowitz, J.D., 2006. Dynamics of the cellular metabolome during human cytomegalovirus infection. PLoS pathogens 2, e132. doi:10.1371/journal.ppat.0020132

Muralidharan, V., Goldberg, D.E., 2013. Asparagine repeats in Plasmodium falciparum proteins: good for nothing? PLoS pathogens 9, e1003488. doi:10.1371/journal.ppat.1003488

Nagalakshmi, U., Wang, Z., Waern, K., Shou, C., Raha, D., Gerstein, M., Snyder, M., 2008. The transcriptional landscape of the yeast genome defined by RNA sequencing. Science (New York, N.Y.) 320, 1344–9. doi:10.1126/science.1158441

Nakjang, S., Williams, T.A., Heinz, E., Watson, A.K., Foster, P.G., Sendra, K.M., Heaps, S.E., Hirt, R.P., Martin Embley, T., 2013. Reduction and expansion in microsporidian genome evolution: new insights from comparative genomics. Genome biology and evolution 5, 2285–303. doi:10.1093/gbe/evt184

Nawrocki, E.P., Kolbe, D.L., Eddy, S.R., 2009. Infernal 1.0: inference of RNA alignments. Bioinformatics (Oxford, England) 25, 1335–7. doi:10.1093/bioinformatics/btp157

Nkinin, S.W., Asonganyi, T., Didier, E.S., Kaneshiro, E.S., 2007. Microsporidian Infection Is Prevalent in Healthy People in Cameroon. Journal of Clinical Microbiology 45, 2841–2846. doi:10.1128/JCM.00328-07

Notredame, C., Higgins, D.G., Heringa, J., 2000. T-Coffee: A novel method for fast and accurate multiple sequence alignment. Journal of molecular biology 302, 205–17. doi:10.1006/jmbi.2000.4042

Nougayrède, J.-P., Taieb, F., De Rycke, J., Oswald, E., 2005. Cyclomodulins: bacterial effectors that modulate the eukaryotic cell cycle. Trends in microbiology 13, 103–10. doi:10.1016/j.tim.2005.01.002

Obbard, D.J., Gordon, K.H.J., Buck, A.H., Jiggins, F.M., 2009. The evolution of RNAi as a defence against viruses and transposable elements. Philosophical transactions of the Royal Society of London. Series B, Biological sciences 364, 99–115. doi:10.1098/rstb.2008.0168

Ohno, S., 1970. Evolution by gene duplication. Springer-Verlag., New York.

Paccanaro, A., Casbon, J.A., Saqi, M.A.S., 2006. Spectral clustering of protein sequences. Nucleic Acids Research 34, 1571–1580. doi:10.1093/nar/gkj515

Paldi, N., Glick, E., Oliva, M., Zilberberg, Y., Aubin, L., Pettis, J., Chen, Y., Evans, J.D., 2010. Effective gene silencing in a microsporidian parasite associated with honeybee (Apis mellifera) colony declines. Applied and environmental microbiology 76, 5960–4. doi:10.1128/AEM.01067-10

Pan, G., Xu, J., Li, T., Xia, Q., Liu, S.-L., Zhang, G., Li, S., Li, C., Liu, H., Yang, L., Liu, T., Zhang, X., Wu, Z., Fan, W., Dang, X., Xiang, H., Tao, M., Li, Y., Hu, J., Li, Z., Lin, L., Luo, J., Geng, L., Wang, L., Long, M., Wan, Y., He, N., Zhang, Z., Lu, C., Keeling, P.J., Wang, J., Xiang, Z., Zhou, Z., 2013. Comparative genomics of parasitic silkworm microsporidia reveal an association between genome expansion and host adaptation. BMC genomics 14, 186. doi:10.1186/1471-2164-14-186

Panek, J., El Alaoui, H., Mone, A., Urbach, S., Demettre, E., Texier, C., Brun, C., Zanzoni, A., Peyretaillade, E., Parisot, N., Lerat, E., Peyret, P., Delbac, F., Biron, D.G., 2014. Hijacking of Host Cellular Functions by an Intracellular Parasite, the Microsporidian Anncaliia algerae. PloS one 9, e100791. doi:10.1371/journal.pone.0100791

Parisot, N., Pelin, A., Gasc, C., Polonais, V., Belkorchia, A., Panek, J., El Alaoui, H., Biron, D.G., Brasset, E., Vaury, C., Peyret, P., Corradi, N., Peyretaillade, É., Lerat, E., 2014. Microsporidian genomes harbor a diverse array of transposable elements that demonstrate an ancestry of horizontal exchange with metazoans. Genome biology and evolution 6, 2289–300. doi:10.1093/gbe/evu178

Park, M.H., Wolff, E.C., Folk, J.E., 1993. Hypusine: its post-translational formation in eukaryotic initiation factor 5A and its potential role in cellular regulation. BioFactors (Oxford, England) 4, 95–104.

Pei, J., Sadreyev, R., Grishin, N. V, 2003. PCMA: fast and accurate multiple sequence alignment based on profile consistency. Bioinformatics (Oxford, England) 19, 427–8.

Pelin, A., Selman, M., Aris-Brosou, S., Farinelli, L., Corradi, N., 2015. Genome analyses suggest the presence of polyploidy and recent human-driven expansions in eight global populations of the honeybee pathogen Nosema ceranae. Environmental microbiology. doi:10.1111/1462-2920.12883

Petersen, T.N., Brunak, S., von Heijne, G., Nielsen, H., 2011. SignalP 4.0: discriminating signal peptides from transmembrane regions. Nature Methods. doi:10.1038/nmeth.1701

Peuvel, I., Peyret, P., Méténier, G., Vivarès, C.P., Delbac, F., 2002. The microsporidian polar tube: evidence for a third polar tube protein (PTP3) in Encephalitozoon cuniculi. Molecular and biochemical parasitology 122, 69–80.

Peuvel-Fanget, I., Polonais, V., Brosson, D., Texier, C., Kuhn, L., Peyret, P., Vivarès, C., Delbac, F., 2006. EnP1 and EnP2, two proteins associated with the Encephalitozoon cuniculi endospore, the chitin-rich inner layer of the microsporidian spore wall. International journal for parasitology 36, 309–18. doi:10.1016/j.ijpara.2005.10.005

Peyretaillade, E., Boucher, D., Parisot, N., Gasc, C., Butler, R., Pombert, J.-F., Lerat, E., Peyret, P., 2014. Exploiting the architecture and the features of the microsporidian genomes to investigate diversity and impact of these parasites on ecosystems. Heredity ePub. doi:10.1038/hdy.2014.78

Peyretaillade, E., Broussolle, V., Peyret, P., Méténier, G., Gouy, M., Vivarès, C.P., 1998. Microsporidia, amitochondrial protists, possess a 70-kDa heat shock protein gene of mitochondrial evolutionary origin. Molecular biology and evolution 15, 683–9.

Polonais, V., Prensier, G., Méténier, G., Vivarès, C.P., Delbac, F., 2005. Microsporidian polar tube proteins: Highly divergent but closely linked genes encode PTP1 and PTP2 in members of the evolutionarily distant Antonospora and Encephalitozoon groups. Fungal Genetics and Biology 42, 791–803. doi:10.1016/j.fgb.2005.05.005

Ponting, C.P., 1997. P100, a transcriptional coactivator, is a human homologue of staphylococcal nuclease. Protein science : a publication of the Protein Society 6, 459–63. doi:10.1002/pro.5560060224

Quang, L.S., Gascuel, O., Lartillot, N., Lirmm, B., Cedex, M., 2007. Empirical profile mixture models for phylogenetic reconstruction. Bioinformatics (Oxford, England) 1–7.

Richards, T.A., Hirt, R.P., Williams, B.A.P., Embley, T.M., 2003. Horizontal gene transfer and the evolution of parasitic protozoa. Protist 154, 17–32. doi:10.1078/143446103764928468

Rönnebäumer, K., Gross, U., Bohne, W., 2008. The nascent parasitophorous vacuole membrane of Encephalitozoon cuniculi is formed by host cell lipids and contains pores which allow nutrient uptake. Eukaryotic cell 7, 1001–8. doi:10.1128/EC.00004-08

Saier, M.H., 2000. Families of transmembrane sugar transport proteins. Molecular Microbiology. doi:10.1046/j.1365-2958.2000.01759.x

Sak, B., Kváč, M., Kučerová, Z., Květoňová, D., Saková, K., 2011. Latent microsporidial infection in immunocompetent individuals - a longitudinal study. PLoS Neglected Tropical Diseases 5. doi:10.1371/journal.pntd.0001162

Scanlon, M., Shaw, a P., Zhou, C.J., Visvesvara, G.S., Leitch, G.J., 2000. Infection by microsporidia disrupts the host cell cycle. The Journal of eukaryotic microbiology 47, 525–531.

Schindelin, J., Arganda-Carreras, I., Frise, E., Kaynig, V., Longair, M., Pietzsch, T., Preibisch, S., Rueden, C., Saalfeld, S., Schmid, B., Tinevez, J.-Y., White, D.J., Hartenstein, V., Eliceiri, K., Tomancak, P., Cardona, A., 2012. Fiji: an open-source platform for biological-image analysis. Nature methods 9, 676–82. doi:10.1038/nmeth.2019

Selman, M., Corradi, N., 2011. Microsporidia: Horizontal gene transfers in vicious parasites. Mobile genetic elements 1, 251–255. doi:10.4161/mge.18611

Selman, M., Sak, B., Kváč, M., Farinelli, L., Weiss, L.M., Corradi, N., 2013. Extremely reduced levels of heterozygosity in the vertebrate pathogen Encephalitozoon cuniculi. Eukaryotic cell 12, 496–502. doi:10.1128/EC.00307-12

Slawson, C., Housley, M.P., Hart, G.W., 2006. O-GlcNAc cycling: how a single sugar post-translational modification is changing the way we think about signaling networks. Journal of cellular biochemistry 97, 71–83. doi:10.1002/jcb.20676

Smith, J.E., 2009. The ecology and evolution of microsporidian parasites. Parasitology 136, 1901. doi:10.1017/S0031182009991818

Söding, J., 2005. Protein homology detection by HMM-HMM comparison. Bioinformatics (Oxford, England) 21, 951–60. doi:10.1093/bioinformatics/bti125

Söding, J., Biegert, A., Lupas, A.N., 2005. The HHpred interactive server for protein homology detection and structure prediction. Nucleic acids research 33, W244–8. doi:10.1093/nar/gki408

Sonnhammer, E.L., von Heijne, G., Krogh, A., 1998. A hidden Markov model for predicting transmembrane helices in protein sequences. Proceedings / ... International Conference on Intelligent Systems for Molecular Biology ; ISMB. International Conference on Intelligent Systems for Molecular Biology 6, 175–82.

Southern, T.R., Jolly, C.E., Lester, M.E., Hayman, J.R., 2007. EnP1, a microsporidian spore wall protein that enables spores to adhere to and infect host cells in vitro. Eukaryotic cell 6, 1354–62. doi:10.1128/EC.00113-07

Soutourina, J., 2000. D-Tyrosyl-tRNATyr Metabolism in Saccharomyces cerevisiae. Journal of Biological Chemistry 275, 11626–11630. doi:10.1074/jbc.275.16.11626

Stajich, J.E., Wilke, S.K., Ahrén, D., Hang, C., Birren, B.W., Borodovsky, M., Burns, C., James, T.Y., Kamada, T., Kilaru, S., Kodira, C., Kües, U., Kupfer, D., Kwan, H.S., 2010. Insights into evolution of multicellular fungi from the assembled chromosomes of the mushroom Coprinopsis cinerea (Coprinus cinereus). Pnas 107, 11889–11894. doi:10.1073/pnas.1003391107

Stokes, M.J., Güther, M.L.S., Turnock, D.C., Prescott, A.R., Martin, K.L., Alphey, M.S., Ferguson, M.A.J., 2008. The synthesis of UDP-N-acetylglucosamine is essential for bloodstream form trypanosoma brucei in vitro and in vivo and UDP-N-acetylglucosamine starvation reveals a hierarchy in parasite protein glycosylation. The Journal of biological chemistry 283, 16147–61. doi:10.1074/jbc.M709581200

Szumowski, S.C., Troemel, E.R., 2015. Microsporidia-host interactions. Current Opinion in Microbiology. doi:10.1016/j.mib.2015.03.006

Tam, A., Schmidt, W.K., Michaelis, S., 2001. The multispanning membrane protein Ste24p catalyzes CAAX proteolysis and NH2-terminal processing of the yeast a-factor precursor. The Journal of biological chemistry 276, 46798–806. doi:10.1074/jbc.M106150200

Tatusov, R.L., Galperin, M.Y., Natale, D.A., Koonin, E. V, 2000. The COG database: a tool for genome-scale analysis of protein functions and evolution. Nucleic acids research 28, 33–36. doi:10.1093/nar/28.1.33

Taupin, V., Metenier, G., Delbac, F., Vivares, C., 2006. Expression of two cell wall proteins during the intracellular development of Encephalitozoon cuniculi: an immunocytochemical and in situ hybridization study with ultrathin frozen sections. Parasitology 815–825. doi:10.1017/S0031182005009777

Tiefenbach, T., Junop, M., 2012. Pso2 (SNM1) is a DNA structure-specific endonuclease. Nucleic acids research 40, 2131–9. doi:10.1093/nar/gkr1059

Towler, M.C., Hardie, D.G., 2007. AMP-activated protein kinase in metabolic control and insulin signaling. Circulation research 100, 328–41. doi:10.1161/01.RES.0000256090.42690.05

Trapnell, C., Hendrickson, D.G., Sauvageau, M., Goff, L., Rinn, J.L., Pachter, L., 2013. Differential analysis of gene regulation at transcript resolution with RNA-seq. Nature biotechnology 31, 46–53. doi:10.1038/nbt.2450

Trapnell, C., Roberts, A., Goff, L., Pertea, G., Kim, D., Kelley, D.R., Pimentel, H., Salzberg, S.L., Rinn, J.L., Pachter, L., 2012. Differential gene and transcript expression analysis of RNA-seq experiments with TopHat and Cufflinks. Nature protocols 7, 562–78. doi:10.1038/nprot.2012.016

Trapnell, C., Williams, B.A., Pertea, G., Mortazavi, A., Kwan, G., van Baren, M.J., Salzberg, S.L., Wold, B.J., Pachter, L., 2010. Transcript assembly and quantification by RNA-Seq reveals unannotated transcripts and isoform switching during cell differentiation. Nature biotechnology 28, 511–5. doi:10.1038/nbt.1621

Troemel, E.R., Félix, M.-A., Whiteman, N.K., Barrière, A., Ausubel, F.M., 2008. Microsporidia are natural intracellular parasites of the nematode Caenorhabditis elegans. PLoS biology 6, 2736–2752. doi:10.1371/journal.pbio.0060309

Tsaousis, A.D., Kunji, E.R.S., Goldberg, A. V, Lucocq, J.M., Hirt, R.P., Embley, T.M., 2008. A novel route for ATP acquisition by the remnant mitochondria of Encephalitozoon cuniculi. Nature 453, 553–6. doi:10.1038/nature06903

Tsunehiro, F., Junichi, N., Narimichi, K., Kazutada, W., 1993. Isolation, overexpression and disruption of a Saccharomyces cerevisiae YNK gene encoding nucleoside diphosphate kinase. Gene 129, 141–146. doi:10.1016/0378-1119(93)90710-K

Urbaniak, M.D., Collie, I.T., Fang, W., Aristotelous, T., Eskilsson, S., Raimi, O.G., Harrison, J., Navratilova, I.H., Frearson, J.A., van Aalten, D.M.F., Ferguson, M.A.J., 2013. A novel allosteric inhibitor of the uridine diphosphate N-acetylglucosamine pyrophosphorylase from Trypanosoma brucei. ACS chemical biology 8, 1981–7. doi:10.1021/cb400411x

Van het Hoog, M., Rast, T.J., Martchenko, M., Grindle, S., Dignard, D., Hogues, H., Cuomo, C., Berriman, M., Scherer, S., Magee, B.B., Whiteway, M., Chibana, H., Nantel, A., Magee, P.T., 2007. Assembly of the Candida albicans genome into sixteen supercontigs aligned on the eight chromosomes. Genome Biol 8, R52. doi:10.1186/gb-2007-8-4-r52

Vanaporn, M., Wand, M., Michell, S.L., Sarkar-Tyson, M., Ireland, P., Goldman, S., Kewcharoenwong, C., Rinchai, D., Lertmemongkolchai, G., Titball, R.W., 2011. Superoxide dismutase C is required for

intracellular survival and virulence of Burkholderia pseudomallei. Microbiology (Reading, England) 157, 2392–400. doi:10.1099/mic.0.050823-0

Vávra, J., Becnel, J.J., 2007. Vavraia culicis (Weiser, 1947) Weiser, 1977 revisited: cytological characterisation of a Vavraia culicis-like microsporidium isolated from mosquitoes in Florida and the establishment of Vavraia culicis floridensis subsp. n. Folia parasitologica 54, 259–71.

Vávra, J., Lukeš, J., 2013. Microsporidia and "the art of living together". Advances in parasitology 82, 253–319. doi:10.1016/B978-0-12-407706-5.00004-6

Venter, J.C., Adams, M.D., Myers, E.W., Li, P.W., Mural, R.J., Sutton, G.G., Smith, H.O., Yandell, M., Evans, C.A., Holt, R.A., Gocayne, J.D., Amanatides, P., Ballew, R.M., Huson, D.H., Wortman, J.R., Zhang, Q., Kodira, C.D., Zheng, X.H., Chen, L., Skupski, M., Subramanian, G., Thomas, P.D., Zhang, J., Gabor Miklos, G.L., Nelson, C., Broder, S., Clark, A.G., Nadeau, J., McKusick, V.A., Zinder, N., Levine, A.J., Roberts, R.J., Simon, M., Slayman, C., Hunkapiller, M., Bolanos, R., Delcher, A., Dew, I., Fasulo, D., Flanigan, M., Florea, L., Halpern, A., Hannenhalli, S., Kravitz, S., Levy, S., Mobarry, C., Reinert, K., Remington, K., Abu-Threideh, J., Beasley, E., Biddick, K., Bonazzi, V., Brandon, R., Cargill, M., Chandramouliswaran, I., Charlab, R., Chaturvedi, K., Deng, Z., Di Francesco, V., Dunn, P., Eilbeck, K., Evangelista, C., Gabrielian, A.E., Gan, W., Ge, W., Gong, F., Gu, Z., Guan, P., Heiman, T.J., Higgins, M.E., Ji, R.R., Ke, Z., Ketchum, K.A., Lai, Z., Lei, Y., Li, Z., Li, J., Liang, Y., Lin, X., Lu, F., Merkulov, G. V, Milshina, N., Moore, H.M., Naik, A.K., Narayan, V.A., Neelam, B., Nusskern, D., Rusch, D.B., Salzberg, S., Shao, W., Shue, B., Sun, J., Wang, Z., Wang, A., Wang, X., Wang, J., Wei, M., Wides, R., Xiao, C., Yan, C., Yao, A., Ye, J., Zhan, M., Zhang, W., Zhang, H., Zhao, Q., Zheng, L., Zhong, F., Zhong, W., Zhu, S., Zhao, S., Gilbert, D., Baumhueter, S., Spier, G., Carter, C., Cravchik, A., Woodage, T., Ali, F., An, H., Awe, A., Baldwin, D., Baden, H., Barnstead, M., Barrow, I., Beeson, K., Busam, D., Carver, A., Center, A., Cheng, M.L., Curry, L., Danaher, S., Davenport, L., Desilets, R., Dietz, S., Dodson, K., Doup, L., Ferriera, S., Garg, N., Gluecksmann, A., Hart, B., Haynes, J., Haynes, C., Heiner, C., Hladun, S., Hostin, D., Houck, J., Howland, T., Ibegwam, C., Johnson, J., Kalush, F., Kline, L., Koduru, S., Love, A., Mann, F., May, D., McCawley, S., McIntosh, T., McMullen, I., Moy, M., Moy, L., Murphy, B., Nelson, K., Pfannkoch, C., Pratts, E., Puri, V., Qureshi, H., Reardon, M., Rodriguez, R., Rogers, Y.H., Romblad, D., Ruhfel, B., Scott, R., Sitter, C., Smallwood, M., Stewart, E., Strong, R., Suh, E., Thomas, R., Tint, N.N., Tse, S., Vech, C., Wang, G., Wetter, J., Williams, S., Williams, M., Windsor, S., Winn-Deen, E., Wolfe, K., Zaveri, J., Zaveri, K., Abril, J.F., Guigó, R., Campbell, M.J., Sjolander, K. V, Karlak, B., Kejariwal, A., Mi, H., Lazareva, B., Hatton, T., Narechania, A., Diemer, K., Muruganujan, A., Guo, N., Sato, S., Bafna, V., Istrail, S., Lippert, R., Schwartz, R., Walenz, B., Yooseph, S., Allen, D., Basu, A., Baxendale, J., Blick, L., Caminha, M., Carnes-Stine, J., Caulk, P., Chiang, Y.H., Coyne, M., Dahlke, C., Mays, A., Dombroski, M., Donnelly, M., Ely, D., Esparham, S., Fosler, C., Gire, H., Glanowski, S., Glasser, K., Glodek, A., Gorokhov, M., Graham, K., Gropman, B., Harris, M., Heil, J., Henderson, S., Hoover, J., Jennings, D., Jordan, C., Jordan, J., Kasha, J., Kagan, L., Kraft, C., Levitsky, A., Lewis, M., Liu, X., Lopez, J., Ma, D., Majoros, W., McDaniel, J., Murphy, S., Newman, M., Nguyen, T., Nguyen, N., Nodell, M., Pan, S., Peck, J., Peterson, M., Rowe, W., Sanders, R., Scott, J., Simpson, M., Smith, T., Sprague, A., Stockwell, T., Turner, R., Venter, E., Wang, M., Wen, M., Wu, D., Wu, M., Xia, A., Zandieh, A., Zhu, X., 2001. The sequence of the human genome. Science (New York, N.Y.) 291, 1304–51. doi:10.1126/science.1058040

Vértessy, B.G., Tóth, J., 2009. Keeping uracil out of DNA: physiological role, structure and catalytic mechanism of dUTPases. Accounts of chemical research 42, 97–106. doi:10.1021/ar800114w

Vidau, C., Diogon, M., Aufauvre, J., Fontbonne, R., Viguès, B., Brunet, J.-L., Texier, C., Biron, D.G., Blot, N., El Alaoui, H., Belzunces, L.P., Delbac, F., 2011. Exposure to sublethal doses of fipronil and thiacloprid highly increases mortality of honeybees previously infected by Nosema ceranae. PloS one 6, e21550. doi:10.1371/journal.pone.0021550

Vogel, C., Chothia, C., 2006. Protein family expansions and biological complexity. PLoS Computational Biology 2, 370–382. doi:10.1371/journal.pcbi.0020048

Wallace, I.M., O'Sullivan, O., Higgins, D.G., Notredame, C., 2006. M-Coffee: combining multiple sequence alignment methods with T-Coffee. Nucleic acids research 34, 1692–9. doi:10.1093/nar/gkl091

Wang, Y., Holmes, E., Nicholson, J.K., Cloarec, O., Chollet, J., Tanner, M., Singer, B.H., Utzinger, J., 2004. Metabonomic investigations in mice infected with Schistosoma mansoni: an approach for biomarker identification. Proceedings of the National Academy of Sciences of the United States of America 101, 12676–81. doi:10.1073/pnas.0404878101

Watson, A.K., Williams, T.A., Williams, B.A.P., Moore, K.A., Hirt, R.P., Embley, T.M., 2015. Transcriptomic profiling of host-parasite interactions in the microsporidian Trachipleistophora hominis. BMC genomics 16, 983. doi:10.1186/s12864-015-1989-z

Weber, S., 2005. Light-driven enzymatic catalysis of DNA repair: a review of recent biophysical studies on photolyase. Biochimica et biophysica acta 1707, 1–23. doi:10.1016/j.bbabio.2004.02.010

Weedall, G.D., Hall, N., 2015. Sexual reproduction and genetic exchange in parasitic protists. Parasitology 142 Suppl, S120–7. doi:10.1017/S0031182014001693

Weidner, E., Canning, E.U., Rutledge, C.R., Meek, C.L., 1999. Mosquito (Diptera: Culicidae) Host Compatibility and Vector Competency for the Human Myositic Parasite Trachipleistophora hominis (Phylum Microspora). Journal of Medical Entomology 36, 522–525.

Weiss, L.M., Delbac, F., Hayman, J.R., Pan, G., Dang, X., Zhou, Z., 2014. The Microsporidian Polar Tube and Spore Wall, in: Weiss, L.M., Becnel, J.J. (Eds.), Microsporidia: Pathogens of Opportunity. John Wiley & Sons, Inc, Iowa, pp. 261–306.

Williams, B.A.P., 2009. Unique physiology of host-parasite interactions in microsporidia infections. Cellular microbiology 11, 1551–60. doi:10.1111/j.1462-5822.2009.01362.x

Williams, B.A.P., Elliot, C., Burri, L., Kido, Y., Kita, K., Moore, A.L., Keeling, P.J., 2010. A broad distribution of the alternative oxidase in microsporidian parasites. PLoS pathogens 6, e1000761. doi:10.1371/journal.ppat.1000761

Williams, B.A.P., Hirt, R.P., Lucocq, J.M., Embley, T.M., 2002. A mitochondrial remnant in the microsporidian Trachipleistophora hominis. Nature 418, 865–9. doi:10.1038/nature00949

Williams, B.A.P., Slamovits, C.H., Patron, N.J., Fast, N.M., Keeling, P.J., 2005. A high frequency of overlapping gene expression in compacted eukaryotic genomes. Proceedings of the National Academy of Sciences of the United States of America 102, 10936–41. doi:10.1073/pnas.0501321102

Williams, T.A., Fares, M.A., 2010. The effect of chaperonin buffering on protein evolution. Genome biology and evolution 2, 609–19. doi:10.1093/gbe/evq045

Williams, T.A., Foster, P.G., Cox, C.J., Embley, T.M., 2013. An archaeal origin of eukaryotes supports only two primary domains of life. Nature 504, 231–6. doi:10.1038/nature12779

Williams, T.A., Nakjang, S., Campbell, S.E., Freeman, M.A., Eydal, M., Moore, K., Hirt, R.P., Embley, T.M., Williams, B.A.P., 2016. A recent whole-genome duplication divides populations of a globally-distributed microsporidian. Molecular Biology and Evolution . doi:10.1093/molbev/msw083

Wilson, J.E., 2003. Isozymes of mammalian hexokinase: structure, subcellular localization and metabolic function. Journal of Experimental Biology 206, 2049–2057. doi:10.1242/jeb.00241

Wilson, M., Haswell, E., 2012. A role for mechanosensitive channels in chloroplast and bacterial fission. Plant signaling & behavior 7, 157–60. doi:10.4161/psb.18735

Wolf, Y.I., Koonin, E. V., 2013. Genome reduction as the dominant mode of evolution. BioEssays 35, 829–837. doi:10.1002/bies.201300037

Wood, V., Gwilliam, R., Rajandream, M., Lyne, M., Lyne, R., Stewart, a, Sgouros, J., Peat, N., Hayles, J., Baker, S., Basham, D., Bowman, S., Brooks, K., Brown, D., Brown, S., Chillingworth, T., Churcher, C., Collins, M., Connor, R., Cronin, a, Davis, P., Feltwell, T., Fraser, a, Gentles, S., Goble, a, Hamlin, N., Harris, D., Hidalgo, J., Hodgson, G., Holroyd, S., Hornsby, T., Howarth, S., Huckle, E.J., Hunt, S., Jagels, K., James, K., Jones, L., Jones, M., Leather, S., McDonald, S., McLean, J., Mooney, P., Moule, S., Mungall, K., Murphy, L., Niblett, D., Odell, C., Oliver, K., O'Neil, S., Pearson, D., Quail, M. a, Rabbinowitsch, E., Rutherford, K., Rutter, S., Saunders, D., Seeger, K., Sharp, S., Skelton, J., Simmonds, M., Squares, R., Squares, S., Stevens, K., Taylor, K., Taylor, R.G., Tivey, a, Walsh, S., Warren, T., Whitehead, S., Woodward, J., Volckaert, G., Aert, R., Robben, J., Grymonprez, B., Weltjens, I., Vanstreels, E., Rieger, M., Schäfer, M., Müller-Auer, S., Gabel, C., Fuchs, M., Düsterhöft, a, Fritzc, C., Holzer, E., Moestl, D., Hilbert, H., Borzym, K., Langer, I., Beck, a, Lehrach, H., Reinhardt, R., Pohl, T.M., Eger, P., Zimmermann, W., Wedler, H., Wambutt, R., Purnelle, B., Goffeau, a, Cadieu, E., Dréano, S., Gloux, S., Lelaure, V., Mottier, S., Galibert, F., Aves, S.J., Xiang, Z., Hunt, C., Moore, K., Hurst, S.M., Lucas, M., Rochet, M., Gaillardin, C., Tallada, V. a, Garzon, a, Thode, G., Daga, R.R., Cruzado, L., Jimenez, J., Sánchez, M., del Rey, F., Benito, J., Domínguez, a, Revuelta, J.L., Moreno, S., Armstrong, J., Forsburg, S.L., Cerutti, L., Lowe, T., McCombie, W.R., Paulsen, I., Potashkin, J., Shpakovski, G. V, Ussery, D., Barrell, B.G., Nurse, P., 2002. The genome sequence of Schizosaccharomyces pombe. Nature 415, 871–880. doi:10.1038/nature724

Xie, C., Mao, X., Huang, J., Ding, Y., Wu, J., Dong, S., Kong, L., Gao, G., Li, C.-Y., Wei, L., 2011. KOBAS 2.0: a web server for annotation and identification of enriched pathways and diseases. Nucleic acids research 39, W316–22. doi:10.1093/nar/gkr483

Xu, Y., Takvorian, P., Cali, A., Wang, F., Zhang, H., Orr, G., Weiss, L.M., 2006. Identification of a new spore wall protein from Encephalitozoon cuniculi. Infection and immunity 74, 239–47. doi:10.1128/IAI.74.1.239-247.2006

Yike, I., 2011. Fungal proteases and their pathophysiological effects. Mycopathologia 171, 299–323. doi:10.1007/s11046-010-9386-2

Zachara, N.E., Hart, G.W., 2004. O-GlcNAc a sensor of cellular state: the role of nucleocytoplasmic glycosylation in modulating cellular function in response to nutrition and stress. Biochimica et biophysica acta 1673, 13–28. doi:10.1016/j.bbagen.2004.03.016

Zander, E., 1909. Tierische Parasiten als Krankenheitserreger bei der Biene. Münchener Bienenzeitung 31, 196 – 204.

Zhang, J., Yang, J.-R., 2015. Determinants of the rate of protein sequence evolution. Nature reviews. Genetics 16, 409–420. doi:10.1038/nrg3950

Zhang, Y., Lyver, E.R., Nakamaru-Ogiso, E., Yoon, H., Amutha, B., Lee, D.-W., Bi, E., Ohnishi, T., Daldal, F., Pain, D., Dancis, A., 2008. Dre2, a Conserved Eukaryotic Fe/S Cluster Protein, Functions in Cytosolic Fe/S Protein Biogenesis. Molecular and Cellular Biology 28, 5569–5582. doi:10.1128/MCB.00642-08

Zheng, L., Schwartz, C., Magidson, V., Khodjakov, A., Oliferenko, S., 2007. The spindle pole bodies facilitate nuclear envelope division during closed mitosis in fission yeast. PLoS biology 5, e170. doi:10.1371/journal.pbio.0050170

Zmasek, C.M., Godzik, A., 2011. Strong functional patterns in the evolution of eukaryotic genomes revealed by the reconstruction of ancestral protein domain repertoires. Genome biology 12, R4. doi:10.1186/gb-2011-12-1-r4

Zorio, D.A., Cheng, N.N., Blumenthal, T., Spieth, J., 1994. Operons as a common form of chromosomal organization in C. elegans. Nature 372, 270–272. doi:10.1038/372270a0

Appendix A

Expression levels of T. hominis transcripts.

These include novel transcripts identified in this study (Locus tag labelled as "NA"). Genes annotated in the *T. hominis* genome but not detected during this study are also included for reference. In some cases multiple locus tags map to a single transcript, as discussed in the main text.

This table is too large to include in the text, but is available in xlsx format on the CD supplied with this thesis, or from http://bmcgenomics.biomedcentral.com/articles/10.1186/s12864-015-1989-z, Table S1 (Watson et al., 2015).

Appendix B

An alignment of novel *T. hominis* intron sequences predicted from our transcriptome, suggesting no conserved intron motif. The alignment was generated using MUSCLE (Edgar, 2004) and visualised using SeaView (Gouy et al., 2010).

Alignment: /Users/Andrew/junctions_files_TH_only/Sup_Figure_Junctions.fasta_aln
Seaview [blocks=10 fontsize=10 A4] on Mon Jun 30 03:55:06 2014

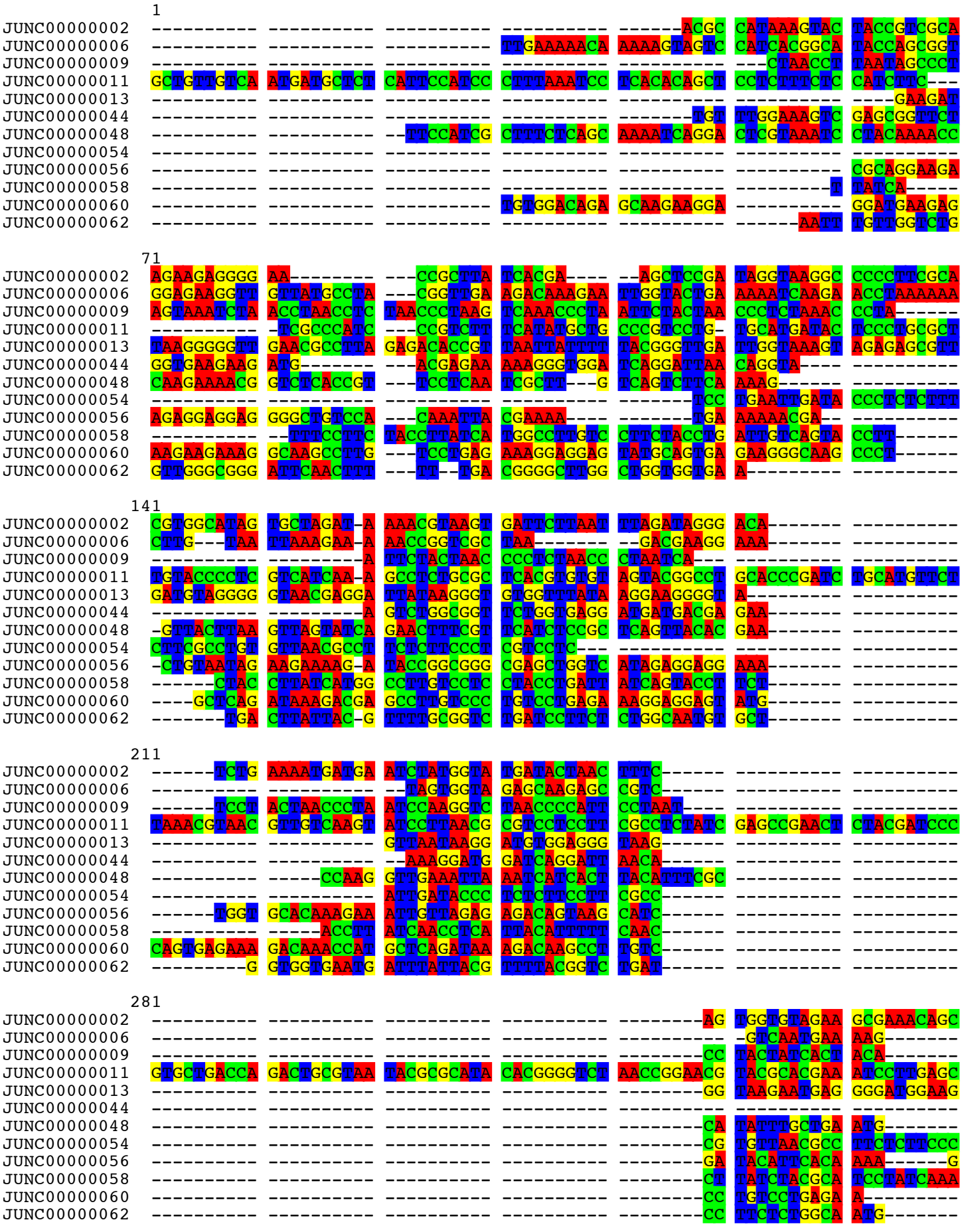

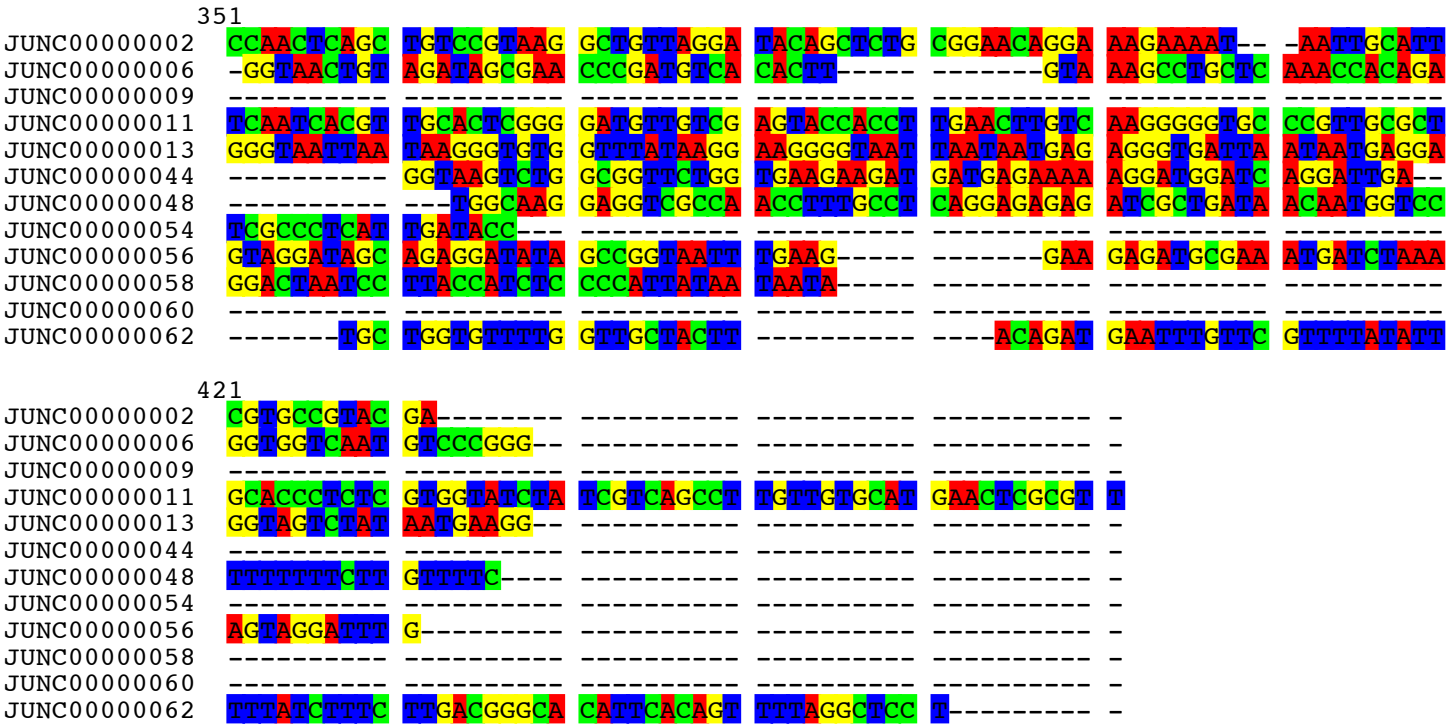
351
JUNC00000002 CCAACTCAGC TGTCCGTAAG GCTGTTAGGA TACAGCTCTG CGGAACAGGA AAGAAAAT-- -AATTGCATT
JUNC00000006 -GGTAACTGT AGATAGCGAA CCCGATGTCA CACTT----- -------GTA AAGCCTGCTC AAACCACAGA
JUNC00000009 ---------- ---------- ---------- ---------- ---------- ---------- ----------
JUNC00000011 TCAATCACGT TGCACTCGGG GATGTTGTCG AGTACCACCT TGAACTTGTC AAGGGGGTGC CCGTTGCGCT
JUNC00000013 GGGTAATTAA TAAGGGTGTG GTTTATAAGG AAGGGGTAAT TAATAATGAG AGGGTGATTA ATAATGAGGA
JUNC00000044 ---------- GGTAAGTCTG GCGGTTCTGG TGAAGAAGAT GATGAGAAAA AGGATGGATC AGGATTGA--
JUNC00000048 ---------- ---TGGCAAG GAGGTCGCCA ACCTTTGCCT CAGGAGAGAG ATCGCTGATA ACAATGGTCC
JUNC00000054 TCGCCCTCAT TGATACC--- ---------- ---------- ---------- ---------- ----------
JUNC00000056 GTAGGATAGC AGAGGATATA GCCGGTAATT TGAAG----- -------GAA GAGATGCGAA ATGATCTAAA
JUNC00000058 GGACTAATCC TTACCATCTC CCCATTATAA TAATA----- ---------- ---------- ----------
JUNC00000060 ---------- ---------- ---------- ---------- ---------- ---------- ----------
JUNC00000062 -------TGC TGGTGTTTTG GTTGCTACTT ---------- ----ACAGAT GAATTTGTTC GTTTTATATT
421
JUNC00000002 CGTGCCGTAC GA-------- ---------- ---------- ---------- -
JUNC00000006 GGTGGTCAAT GTCCCGGG-- ---------- ---------- ---------- -
JUNC00000009 ---------- ---------- ---------- ---------- ---------- -
JUNC00000011 GCACCCTCTC GTGGTATCTA TCGTCAGCCT TGTTGTGCAT GAACTCGCGT T
JUNC00000013 GGTAGTCTAT AATGAAGG-- ---------- ---------- ---------- -
JUNC00000044 ---------- ---------- ---------- ---------- ---------- -
JUNC00000048 TTTTTTTCTT GTTTTC---- ---------- ---------- ---------- -
JUNC00000054 ---------- ---------- ---------- ---------- ---------- -
JUNC00000056 AGTAGGATTT G--------- ---------- ---------- ---------- -
JUNC00000058 ---------- ---------- ---------- ---------- ---------- -
JUNC00000060 ---------- ---------- ---------- ---------- ---------- -
JUNC00000062 TTTATCTTTC TTGACGGGCA CATTCACAGT TTTAGGCTCC T--------- -

Appendix C

Heterogeneity in expression of duplicated gene families

Duplicated gene families (Nakjang et al., 2013) containing at least two paralogues in *T. hominis* ranked according to their expression heterogeneity index.

This table is additionally available in xlsx format for excel on the CD supplied with this thesis, or from http://bmcgenomics.biomedcentral.com/articles/10.1186/s12864-015-1989-z, table S3 (Watson et al., 2015).

Gene Family	*T. hominis* Locus Tags in Gene Family	FPKM Value	Heterogeneity Index	Annotation	KOG Functional Category
c_563_	['THOM_1060', 'THOM_1159', 'THOM_1160', 'THOM_1429', 'THOM_1598', 'THOM_1870', 'THOM_1988', 'THOM_2285', 'THOM_2304', 'THOM_2305', 'THOM_0238', 'THOM_2547', 'THOM_2644', 'THOM_2836', 'THOM_2856', 'THOM_2969', 'THOM_3075', 'THOM_0348', 'THOM_0349', 'THOM_0444', 'THOM_0454', 'THOM_0059', 'THOM_0680', 'THOM_0733', 'THOM_0083', 'THOM_0906', 'THOM_0941', 'THOM_0942']	[2.4223833333333333, 42.544649999999997, 3.2567900000000001, 1.6757083333333334, 20.554716666666668, 162.91653333333332, 0.0, 11.983716666666666, 4.8786383333333339, 0.0, 4.1026683333333329, 7.9724000000000004, 106.59913333333333, 0.95707850000000005, 10.857271666666668, 92.296183333333332, 2.58663, 0.0, 16.499848333333333, 6.2602816666666667, 10.401653333333334, 6.9825300000000006, 35.661466666666662, 1.6879783333333334, 0.53262666666666669, 0.0, 0.0]	1.86	RNA-directed DNA polymerase (reverse transcriptase)	[A]
c_474_	['THOM_1305', 'THOM_1449', 'THOM_1839', 'THOM_2072', 'THOM_0876']	[143.54650000000001, 0.0, 1251.3666666666666, 73.248883333333325, 65.459383333333335]	1.55	Haloacid dehalogenase-like hydrolase (similar to SDT1; PHM8;)	[R]
c_456_	['THOM_1192', 'THOM_1681', 'THOM_3170', 'THOM_0963']	[388.589, 10.370223333333334, 20.475183333333334, 23.449816666666667]	1.45	MFS	-
c_31765_	['THOM_1416', 'THOM_1417', 'THOM_1522']	[1.6609316666666667, 0.0, 0.0]	1.41	hypothetical protein	-
c_201_	['THOM_1847', 'THOM_1848', 'THOM_0443', 'THOM_0897', 'THOM_0898', 'THOM_0937']	[32.942866666666667, 3.3656383333333331, 10.47761, 989.16733333333332, 989.16733333333332, 18.642616666666665]	1.35	Hexokinase (similar to HXK2; HXK1; GLK1; EMI2;)	[G]
c_747_	['THOM_1496', 'THOM_2692', 'THOM_2693']	[1483.7640000000001, 31.930866666666663, 21.131666666666668]	1.34	60S ribosomal protein L10A (similar to RPL1B; RPL1A;)	[J]
c_279_	['THOM_2161', 'THOM_3247', 'THOM_0834']	[2.6969933333333334, 127.88778333333333, 3.28464]	1.32	Gluconate transport-inducing protein	[TG]
c_1828_	['THOM_1011', 'THOM_2537', 'THOM_2538']	[3.1810533333333333, 75.569550000000007, 3.1810533333333333]	1.25	Glycosyltransferase (similar to ALG2;)	[M]
c_68_	['THOM_1220', 'THOM_2066', 'THOM_2067', 'THOM_2261', 'THOM_2262', 'THOM_2678', 'THOM_2679']	[18.704550000000001, 18.704550000000001, 14.40077, 28.041266666666669, 394.69400000000002, 519.19883333333337, 104.05603333333333]	1.24	Helicase	[L][A]
c_525_	['THOM_1832', 'THOM_2053', 'THOM_0890']	[0.0, 1129.665, 111.8402]	1.23	Endoplasmic reticulum membrane-associated oxidoreductin involved in disulfide bond formation (similar to ERO1;)	[OU]
c_54_	['THOM_1563', 'THOM_2609', 'THOM_3070', 'THOM_3237']	[3990.0966666666668, 30548.25, 861.02550000000008, 5819.0266666666676]	1.15	ubiquitin	[J]
c_12_	['THOM_1236', 'THOM_1562', 'THOM_2276', 'THOM_2311', 'THOM_2341', 'THOM_0241', 'THOM_2579', 'THOM_2798', 'THOM_0432', 'THOM_0462', 'THOM_0561', 'THOM_0839']	[26.092466666666667, 28.12585, 225.41733333333332, 615.30899999999997, 127.2865, 205.80516666666665, 120.90751666666667, 201.25683333333333, 481.90000000000003, 29.903866666666669, 1070.7429999999999, 73.881583333333325]	1.12	RNA helicase	[J][A][L]
c_284_	['THOM_1424', 'THOM_2017', 'THOM_2019', 'THOM_2026']	[437.94149999999996, 92.319033333333337, 97.995916666666673, 2.0748353333333331]	1.06	The Zinc (Zn2+)-Iron (Fe2+) Permease (ZIP) Family	[P]
c_137_	['THOM_2139', 'THOM_2216', 'THOM_0510']	[533.62116666666668, 106.03331666666666, 21.693149999999999]	1.02	Vesicle trafficking protein Sec1/Vacuolar sorting protein (Sec1 family)	[U]
c_7939_	['THOM_1219', 'THOM_1629', 'THOM_1737', 'THOM_2163', 'THOM_0489', 'THOM_0499', 'THOM_1134', 'THOM_1960', 'THOM_2200', 'THOM_2588', 'THOM_0804']	[105.04143333333333, 1185.665, 1354.3171666666667, 324.10766666666666, 311.26499999999999, 191.10683333333336, 308.38550000000004, 95.983166666666662, 404.24166666666662, 131.2141, 151.21000000000001]	1.00	Small Nuclear ribonucleoprotein	[A],[K]
c_225_	['THOM_2439', 'THOM_2773']	[1495.2233333333334, 0.0]	1.00	Glyoxylase (similar to GLO4; GLO2;)/ hydroxyacylglutathione hydrolase	[R]
c_580_	['THOM_2391', 'THOM_0452']	[3338.3866666666668, 14.024766666666666]	0.99	60S ribosomal protein L14E/L6E/L27E	[J]
c_406_	['THOM_1721', 'THOM_1773']	[18.869816666666669, 1254.0083333333334]	0.97	Transcription initiation factor	[K]
c_1122_	['THOM_2697', 'THOM_0627']	[934.14833333333343, 14.197391666666666]	0.97	hypothetical protein	-
c_264_	['THOM_1460', 'THOM_1461', 'THOM_1699']	[4.7800183333333335, 533.38166666666666, 1679.2433333333331]	0.95	DNA polymerase sigma (similar to TRF5; PAP2;)	[L]
c_147_	['THOM_1618', 'THOM_1619', 'THOM_1684', 'THOM_1922', 'THOM_2792', 'THOM_2793', 'THOM_0524', 'THOM_0527']	[34.782683333333331, 19.157233333333334, 199.87916666666669, 51.517783333333334, 37.226333333333336, 41.068300000000001, 46.831349999999993]	0.93	The Small Conductance Mechanosensitive Ion Channel (MscS) Family	[M]
c_694_	['THOM_1237', 'THOM_2111', 'THOM_2574']	[0.42615833333333336, 123.56599999999999, 46.043016666666666]	0.90	protein containing Rho GTPase activation protein	[TZ]
c_153_	['THOM_1707', 'THOM_2040', 'THOM_3134']	[219.98016666666669, 2081.8200000000002, 465.54683333333332]	0.90	Glutamyl/Prolyl-tRNA synthetase	[J]
c_560_	['THOM_2963', 'THOM_2965']	[277.95266666666663, 15.517183333333334]	0.89	The Sulfate Permease (SulP) transporter Family	[P]
c_237_	['THOM_1208', 'THOM_3296']	[38.243283333333331, 579.0575]	0.88	Pseudouridylate synthase (similar to PUS2; PUS1;)	[J]
c_981_	['THOM_1569', 'THOM_0690']	[1565.0783333333331, 105.12518333333333]	0.87	protein containing Nucleotide-binding, alpha-beta plait, RNA recognition motif domain	-
c_40_	['THOM_1736', 'THOM_2392', 'THOM_0245']	[1332.0150000000001, 488.15883333333335, 38.3902]	0.87	cis-trans isomerase	[O][U]

Gene Family	*T. hominis* Locus Tags in Gene Family	FPKM Value	Heterogeneity Index	Annotation	KOG Functional Category
c_118_	['THOM_0251', 'THOM_0752']	[860.54899999999998, 65.140566666666658]	0.86	Puromycin-sensitive aminopeptidase and related aminopeptidases (similar to TMA108; APE2;); Protein containing Peptidase M1 (APA), membrane alanine aminopeptidase	[EO]
c_3052_	['THOM_2089', 'THOM_0252', 'THOM_3015', 'THOM_0754']	[2.8003250000000004, 42.985583333333331, 27.566400000000002, 5.0034999999999998]	0.85	hypothetical protein	-
c_109_	['THOM_1154', 'THOM_0971']	[60.408766666666672, 733.02633333333335]	0.85	SNARE protein YKT6, synaptobrevin/VAMP superfamily (similar to YKT6;)o	[U]
c_197_	['THOM_1734', 'THOM_2049', 'THOM_2923']	[513.1873333333333, 100.77898333333333, 88.952216666666672]	0.84	Putative_ATP_binding_protein	-
c_269_	['THOM_2876', 'THOM_2953']	[181.57016666666667, 2020.0]	0.84	U3 small nucleolar ribonucleoprotein (snoRNP) component /Ribosomal protein S4 (similar to RPS9B; RPS9A;)	[A] ,[J]
c_13_	['THOM_1388', 'THOM_1397', 'THOM_1398', 'THOM_0153', 'THOM_1620', 'THOM_1831', 'THOM_2043', 'THOM_2583', 'THOM_3230', 'THOM_0590', 'THOM_0658', 'THOM_0772', 'THOM_0840']	[142.792, 42.770466666666664, 424.94999999999999, 631.10866666666664, 1.7263615000000001, 597.77233333333334, 54.963433333333334, 88.692516666666663, 1090.675, 525.64783333333332, 1076.5378333333333, 648.99900000000002, 400.66949999999997]	0.81	proteasome regulatory complex	[O]
c_760_	['THOM_1135', 'THOM_2592']	[38.132116666666668, 337.17733333333337]	0.80	CDP-diacylglycerol insitol-3-phosphatidyltransferase /Phosphatidylinositol synthase (similar to PIS1;)	[I]
c_23_	['THOM_1155', 'THOM_1189', 'THOM_1231', 'THOM_1679', 'THOM_1728', 'THOM_2483', 'THOM_2484', 'THOM_2485', 'THOM_3292', 'THOM_0736', 'THOM_0737']	[192.25649999999999, 0.0, 226.16999999999999, 226.16999999999999, 224.67949999999999, 61.866350000000004, 47.691015, 48.502266666666664, 36.661116666666665, 47.691015]	0.80	helicase DNA-binding protein family	[KL] ,[B]
c_25_	['THOM_2236', 'THOM_2286', 'THOM_2829', 'THOM_2945', 'THOM_3076', 'THOM_0732']	[1.1735629999999999, 3.2665333333333333, 3.493395, 6.2602816666666667, 1.3013710000000001, 0.16121133333333335]	0.77	RNA-directed DNA polymerase	[R]
c_856_	['THOM_0360', 'THOM_0412']	[254.18499999999997, 1937.3083333333334]	0.77	Zinc finger protein C4-type Zn-finger protein (similar to ZPR1;)	[R]
c_7968_	['THOM_1525', 'THOM_1820', 'THOM_1907', 'THOM_0235', 'THOM_0321']	[347.11233333333331, 2028.2700000000002, 749.64566666666667, 135.90163333333334, 1064.1245000000001]	0.77	Myosin regulatory light chain/ Ca2+/calmodulin-dependent protein phosphatase/ EF-Hand superfamily protein	[Z] ,[T]
c_660_	['THOM_0883', 'THOM_0884']	[62.215533333333333, 442.63783333333339]	0.75	Predicted membrane protein (similar to PER1;)	[S]
c_5757_	['THOM_2406', 'THOM_1234', 'THOM_0625']	[1919.665, 157.38649999999998, 3531.4283333333333]	0.74	Thioredoxin/protein disulfide isomerase	[O]
c_1606_	['THOM_0293', 'THOM_0294', 'THOM_0295']	[116.92035, 769.04283333333331]	0.74	Serine/threonine protein kinaseorf_295 Serine/threonine protein kinase	[R]
c_112_	['THOM_2241', 'THOM_0346']	[37.560833333333335, 237.60799999999998]	0.73	GTPase-activating protein	[R][U]
c_176_	['THOM_1404', 'THOM_1405', 'THOM_2437', 'THOM_0067']	[37.224650000000004, 52.97698333333333, 20.052116666666667, 0.69318666666666662]	0.70	DNA mismatch repair protein	[L]
c_6131_	['THOM_2827', 'THOM_0699', 'THOM_0635', 'THOM_2524', 'THOM_1625', 'THOM_1682', 'THOM_1791', 'THOM_2112', 'THOM_2113', 'THOM_1485', 'THOM_1486']	[95.253150000000005, 106.23183333333333, 521.48866666666663, 839.70566666666673, 839.70566666666673, 374.37933333333331, 487.20599999999996, 430.96583333333336, 349.22816666666671, 1124.9913333333334, 42.191683333333337]	0.69	vesicular transport protein	[O] ,[Z] ,[TU]
c_130_	['THOM_1889', 'THOM_2375', 'THOM_0592']	[230.00616666666667, 20.763366666666666, 124.87950000000001]	0.68	putative methyltransferase/nucleolar proteins	[J] ,[A] ,[D]
c_450_	['THOM_2650', 'THOM_2651']	[408.67650000000003, 2139.5883333333336]	0.68	Lectin VIP36, involved in the transport of glycoproteins carrying high mannose-type glycans/hypothetical protein	[U]
c_1061_	['THOM_1803', 'THOM_1997', 'THOM_3127', 'THOM_0892']	[145.14183333333332, 246.26166666666666, 375.68950000000001, 24.308666666666667]	0.65	RhoGAP domain-containing protein	-
c_2636_	['THOM_1804', 'THOM_1805']	[10.935193333333332, 2.4931533333333333]	0.63	Predicted cell surface protein homologous to bacterial outer membrane proteins (similar to SAM50;)	[R]
c_1124_	['THOM_1050', 'THOM_1051']	[48.581949999999999, 11.710138333333333]	0.61	RNA-directed RNA polymerase QDE-1 required for posttranscriptional gene silencing and RNA interference	[A]
c_1438_	['THOM_2176', 'THOM_2177', 'THOM_0895']	[30.086433333333332, 24.833500000000001, 88.902966666666671]	0.61	protein containing Protein of unknown function DUF2404, transmembrane	-
c_745_	['THOM_2689', 'THOM_2690']	[201.68133333333333, 50.564999999999998]	0.60	Predicted RNA-binding protein	[R]

Gene Family	*T. hominis* Locus Tags in Gene Family	FPKM Value	Heterogeneity Index	Annotation	KOG Functional Category
c_510_	['THOM_2081', 'THOM_2270']	[351.97049999999996, 89.440049999999999]	0.59	protein containing FY-rich, N-terminal	-
c_442_	['THOM_1935', 'THOM_2774']	[485.8921666666667, 124.086]	0.59	Cholin/ethanolamine kinase	[M]
c_29_	['THOM_1058', 'THOM_1059', 'THOM_1955', 'THOM_2242', 'THOM_0660']	[291.59033333333332, 244.04116666666667, 45.526466666666664, 434.16949999999997, 125.7685]	0.59	Ubiquitin-specific protease (similar to UBP8; UBP1;); Protein containing Peptidase C19, ubiquitin carboxyl-terminal hydrolase	[O]
c_182_	['THOM_1164', 'THOM_1169', 'THOM_1170', 'THOM_2208', 'THOM_2209']	[195.67983333333333, 87.500916666666669, 44.954483333333336]	0.58	mRNA cleavage and polyadenylation specificity factor (CPSF subunit)	[A]
c_259_	['THOM_2155', 'THOM_3241']	[2203.1816666666668, 592.92750000000001]	0.58	Molecular chaperone (HSP90 family) (similar to HSP82; HSC82;)	[O]
c_614_	['THOM_2578', 'THOM_2581']	[102.62976666666667, 337.04900000000004]	0.53	Inosine triphosphate pyrophosphatase (similar to HAM1;)	[F]
c_167_	['THOM_0010', 'THOM_0920', 'THOM_0921']	[107.37291666666665, 352.31816666666668]	0.53	Valyl/Isoleucyl-tRNA synthetase	[J]
c_1135_	['THOM_1829', 'THOM_1830']	[312.06366666666668, 95.879116666666675]	0.53	Phosphatidylglycerolphosphate synthase (similar to PGS1;)	[I]
c_19_	['THOM_1029', 'THOM_1261', 'THOM_1806', 'THOM_1942', 'THOM_1943', 'THOM_1952', 'THOM_0207', 'THOM_2343', 'THOM_2344', 'THOM_2490', 'THOM_2599', 'THOM_2864', 'THOM_2910', 'THOM_3239', 'THOM_0762']	[2156.3516666666669, 646.5381666666666, 682.60666666666668, 704.64766666666674, 576.27266666666662, 644.38133333333337, 1441.0883333333334, 965.50466666666671, 895.45866666666677, 513.39583333333337, 682.10833333333335, 748.12549999999999, 1457.8983333333333, 392.53483333333332, 505.4666666666667]	0.53	20S proteasome, regulatory subunits	[O]
c_146_	['THOM_0002', 'THOM_0271', 'THOM_0272', 'THOM_0273', 'THOM_0003', 'THOM_0463']	[12.760471666666668, 60.389150000000001, 72.295366666666666, 65.884100000000004, 139.90983333333332, 89.757349999999988]	0.51	RNA polymerase	[K]
c_21_	['THOM_1136', 'THOM_1288', 'THOM_2162', 'THOM_2254', 'THOM_0228', 'THOM_3060', 'THOM_3166', 'THOM_0078']	[539.93449999999996, 391.94633333333331, 283.75650000000002, 717.88200000000006, 129.45133333333334, 329.31649999999996, 311.84083333333336, 150.72516666666667]	0.51	Ubiquitin-protein ligase/Ubiquitin conjugating enzyme	[O]
c_92_	['THOM_1201', 'THOM_2804', 'THOM_3114']	[1069.7868333333333, 648.38383333333331, 264.21783333333332]	0.50	tRNA synthetase	[J]
c_425_	['THOM_2148', 'THOM_2149']	[138.54443333333333, 46.928100000000001]	0.49	Cell cycle control protein (crooked neck) (similar to CLF1;)	[D]
c_275_	['THOM_1720', 'THOM_3014']	[209.83816666666667, 594.05650000000003]	0.48	Signal recognition particle receptors	[U]
c_661_	['THOM_0398', 'THOM_0399', 'THOM_0400']	[39.370799999999996, 158.79766666666666, 158.79766666666666]	0.47	Negative regulator of transcription (similar to CDC39;)	[K]
c_579_	['THOM_0927', 'THOM_0928']	[108.81405000000001, 303.75283333333334]	0.47	Ubiquitin-specific protease UBP14 (similar to UBP14;); Protein containing Peptidase C19,	[O]
c_352_	['THOM_2824', 'THOM_0688']	[314.11533333333335, 113.52683333333333]	0.47	encu_19074135|ref|NP_584741.1| hypothetical protein ECU04_0590 [Encephalitozoon cuniculi GB-M1] encu_19173595|ref|NP_597398.1| hypothetical protein ECU05_0560 [Encephalitozoon cuniculi GB-M1] enin_303388938|ref|XP_003072702.1| hypothetical protein Eint_040520 [Encephalitozoon intestinalis ATCC 50506] enin_303389267|ref|XP_003072866.1| hypothetical protein Eint_050570 [Encephalitozoon intestinalis ATCC 50506] noce_300707709|ref|XP_002996052.1 hypothetical protein NCER_100911 [Nosema ceranae BRL01] splo_NODE7039length2600cov17_69307d_46_570_Strand__1_FCF1_family_protein splo_NODE8939length11985cov49_31731d_4637_5320_Str	[R]
c_216_	['THOM_2722', 'THOM_0917']	[112.86873333333334, 41.305366666666664]	0.46	WD40 domain-containing putative histone transcription regulator	[DK]
c_48_	['THOM_1356', 'THOM_1380', 'THOM_2796', 'THOM_0319', 'THOM_3223', 'THOM_3257', 'THOM_3258', 'THOM_0589', 'THOM_0800']	[315.46533333333332, 136.54050000000001, 93.590533333333326, 176.16943333333333, 130.20716666666667, 192.68799999999999, 67.488133333333337, 176.16943333333333, 86.740083333333345]	0.46	DNA replication licensing factor	[L]
c_172_	['THOM_1797', 'THOM_1798', 'THOM_3240', 'THOM_0357']	[85.409666666666666, 25.194550000000003, 77.176266666666663, 40.03456666666667]	0.44	Helicase of the DEAD superfamily (similar to CHL1;)	[KL]

Gene Family	*T. hominis* Locus Tags in Gene Family	FPKM Value	Heterogeneity Index	Annotation	KOG Functional Category
c_207_	['THOM_3285', 'THOM_0388']	[111.01963333333333, 282.29416666666668]	0.44	Trehalose-6-phosphate synthase component TPS1 and related subunits (similar to TPS3; TPS2; TPS1;)	[G]
c_254_	['THOM_1528', 'THOM_0193', 'THOM_0200']	[110.32358333333333, 150.90133333333333, 44.287399999999998]	0.43	1-acyl-sn-glycerol-3-phosphate acyltransferase (SCL1)/ Lysophosphatidic acid acyltransferase LPAAT and related acyltransferases	[I]
c_1716_	['THOM_1151', 'THOM_1152', 'THOM_1153']	[361.04333333333335, 361.04333333333335, 108.37015000000001]	0.43	Dopey and related predicted leucine zipper transcription factors (similar to DOP1;)	[K]
c_872_	['THOM_1900', 'THOM_2449']	[149.29300000000001, 61.503016666666667]	0.42	Vacuolar H+-ATPase V1 sector, subunit H (similar to VMA13;)	[C]
c_2252_	['THOM_2283', 'THOM_0479']	[107.13948333333333, 46.642416666666662]	0.39	CutA-like, Divalent cation tolerance-related protein	[P]
c_114_	['THOM_0104', 'THOM_1903']	[60.023983333333327, 129.46663333333333]	0.37	G2/mitotic specific cyclin	[D]
c_426_	['THOM_3106', 'THOM_3107']	[92.76403333333333, 43.188766666666673]	0.36	Putative_membrane_bound_O_acyl_transferase/Predicted membrane protein (similar to ALE1;)	[S]
c_2635_	['THOM_0362', 'THOM_0363']	[116.16590000000001, 55.018599999999999]	0.36	protein containing Armadillo-type fold	-
c_179_	['THOM_1792', 'THOM_2367', 'THOM_0529']	[205.79830000000001, 353.80933333333337, 514.86766666666665]	0.35	The H+- or Na+-translocating F-type, V-type and A-type ATPase (F-ATPase) Superfamily [3.A.3]	[C]
c_37_	['THOM_1430', 'THOM_1600', 'THOM_1695', 'THOM_1696', 'THOM_2450', 'THOM_2451', 'THOM_2634', 'THOM_2635', 'THOM_3004', 'THOM_0320', 'THOM_3265']	[696.3416666666667, 413.61883333333338, 449.52583333333337, 863.45899999999995, 814.26850000000002, 655.45749999999998, 388.34483333333333, 963.86783333333335, 406.71766666666667, 586.69783333333328]	0.32	Chaperonin complex component, TCP-1 gamma subunit (CCT3) (similar to CCT3;)	[O]
c_127_	['THOM_2063', 'THOM_2753', 'THOM_3229']	[123.50416666666666, 224.59916666666666, 283.89499999999998]	0.31	Vesicle coat complex COPII, subunit SEC24/subunit SFB2 (similar to SFB2; SEC24;)	[U]
c_408_	['THOM_0166', 'THOM_0167', 'THOM_2625', 'THOM_0980']	[148.81283333333332, 72.248633333333331, 93.194416666666669]	0.31	Glycine/serine hydroxymethyltransferase (similar to SHM2; SHM1;)	[E]
c_1986_	['THOM_1671', 'THOM_1672']	[144.17933333333335, 77.622916666666669]	0.30	protein containing Actin-binding FH2	-
c_6082_	['THOM_2364', 'THOM_0270']	[148.44866666666667, 273.79183333333333]	0.30	Component of the U4/U6.U5 snRNP/mitosis protein DIM1 (similar to DIB1;)	[AD]
c_89_	['THOM_1067', 'THOM_2925', 'THOM_0687']	[134.46416666666667, 83.237533333333332, 68.523983333333334]	0.30	putative SKT5-like protein /similarity to HYPOTHETICAL PROTEIN YBET_ECOLI	[MOT]
c_862_	['THOM_1283', 'THOM_1284']	[120.39916666666666, 214.87516666666667]	0.28	Chromosome condensation complex Condensin, subunit D2 (similar to YCS4;)	[BD]
c_962_	['THOM_1210', 'THOM_1211']	[518.87366666666674, 295.61183333333332]	0.27	Phenylalanyl-tRNA synthetase beta subunit (similar to FRS1;)	[J]
c_1515_	['THOM_3288', 'THOM_0727']	[167.79916666666665, 287.76299999999998]	0.26	Transcription initiation factor	[U] ,[K]
c_1701_	['THOM_2622', 'THOM_2393', 'THOM_2394']	[74.287516666666662, 45.382149999999996]	0.24	Gamma-tubulin complex, DGRIP91/SPC98 component (similar to SPC98;)	[Z]
c_38_	['THOM_2222', 'THOM_2271', 'THOM_0708']	[811.72299999999996, 1109.6283333333333, 622.29466666666667]	0.24	Acyl-CoA synthetase	[I]
c_753_	['THOM_0249', 'THOM_0250']	[178.19866666666667, 287.88238333333334]	0.24	Exopolyphosphatases and related proteins (similar to PPX1;)	[C]
c_922_	['THOM_1462', 'THOM_1463']	[32.819683333333337, 48.844633333333327]	0.20	protein containing WD40/YVTN repeat-like-containing domain,	-
c_1597_	['THOM_3044', 'THOM_0675', 'THOM_0676']	[201.57666666666668, 271.5891666666667, 283.44049999999999]	0.14	hypothetical protein	-
c_2209_	['THOM_0827', 'THOM_0828']	[55.04591666666667, 41.843399999999995]	0.14	protein-tyrosine-phosphatase	[T]
c_224_	['THOM_0194', 'THOM_0195', 'THOM_0196', 'THOM_0198', 'THOM_0490', 'THOM_0491']	[413.95949999999999, 413.95949999999999, 413.95949999999999, 413.95949999999999, 297.11500000000001]	0.12	Structural maintenance of chromosome protein, SMC superfamily	[BDL]
c_304_	['THOM_1071', 'THOM_1501']	[110.36253333333333, 138.98333333333332]	0.11	DNA-binding cell division cycle control protein (similar to CDC27;/ Anaphase-promoting complex (APC), Cdc23 subunit (similar to CDC23;)	[DO]
c_887_	['THOM_1232', 'THOM_1934']	[391.51683333333335, 479.4495]	0.10	Acyl-CoA thioesterase (similar to TES1;)	[I]
c_805_	['THOM_1259', 'THOM_0555']	[62.649683333333336, 52.638033333333333]	0.09	Deoxyhypusine synthase (similar to DYS1;)	[O]
c_90_	['THOM_1733', 'THOM_3214']	[90.697966666666673, 78.345816666666664]	0.07	helicase	[A]
c_990_	['THOM_2403', 'THOM_2404']	[1534.7391666666665, 1342.7555]	0.07	U3 small nucleolar ribonucleoprotein (snoRNP) subunit - Mpp10p (similar to MPP10;)	[A]

Gene Family	*T. hominis* Locus Tags in Gene Family	FPKM Value	Heterogeneity Index	Annotation	KOG Functional Category
c_1150_	['THOM_0049', 'THOM_0050']	[615.10500000000002, 683.12233333333336]	0.05	similar to saccharopine dehydrogenase	[S]
c_1603_	['THOM_2141', 'THOM_2142']	[109.67146666666667, 100.11326666666668]	0.05	Chromosome condensation complex Condensin, subunit G (similar to YCG1;)	[BD]
c_1040_	['THOM_1357', 'THOM_1358']	[180.21716666666669, 169.77666666666667]	0.03	tRNA uracil-5-methyltransferase and related tRNA-modifying enzymes (similar to TRM2;	[J]
c_588_	['THOM_1294', 'THOM_1295']	[398.94450000000001, 384.24816666666669]	0.02	Arginyl-tRNA synthetase (similar to MSR1;)	[J]
c_743_	['THOM_0372', 'THOM_0373']	[207.73083333333332, 204.44149999999999]	0.01	Predicted methyltransferase (similar to ABP140;)	[R]
c_3425_	['THOM_1419', 'THOM_1420']	[341.24266666666665, 337.96583333333336]	0.00	Adaptor complexes medium subunit family (similar to APM2; APM1;)	[U]
c_6285_	['THOM_0643', 'THOM_0644', 'THOM_0645']	[53.297016666666671]	0.00	N-arginine dibasic convertase NRD1 and related Zn2+-dependent endopeptidases, insulinase superfamily	[O]
c_267_	['THOM_0673', 'THOM_0674']	[44.207349999999998]	0.00	Uncharacterized conserved protein (similar to SPO75; RSN1; PHM7;)	[R]
c_1118_	['THOM_1254', 'THOM_1255']	[266.5625, 266.5625]	0.00	Protein involved in vacuole import and degradation (similar to VID27;)	[U]
c_185_	['THOM_2401', 'THOM_2402']	[116.43296666666667, 116.43296666666667]	0.00	NADPH_cytochrome_p450_reductase	[C]
c_415_	['THOM_1030', 'THOM_1031']	[478.32199999999995]	0.00	26S proteasome regulatory complex, subunit RPN1/PSMD2 (similar to RPN1;)	[O]
c_925_	['THOM_0918', 'THOM_0919']	[32.716349999999998]	0.00	Eukaryotic-type DNA primase, catalytic (small) subunit (similar to PRI1;)	[L]
c_920_	['THOM_2331', 'THOM_2332', 'THOM_2333']	[478.91249999999997, 478.91249999999997, 478.91249999999997]	0.00	DNA repair protein RAD50, ABC-type ATPase/SMC superfamily (similar to RAD50;)	[L]
c_1202_	['THOM_1072', 'THOM_1073']	[148.28966666666668, 148.28966666666668]	0.00	protein containing WD40/YVTN repeat-like-containing domain, WD40 repeat	-
c_1170_	['THOM_0307', 'THOM_0308']	[17.038349999999998, 17.038349999999998]	0.00	Splicing factor 3a, subunit 3 (similar to PRP9;)	[A]
c_1598_	['THOM_0802', 'THOM_0803']	[298.08483333333334, 298.08483333333334]	0.00	ER to golgi transport protein/RAD50-interacting protein 1 (similar to TIP20;) OR hypothetical protein	[UD]
c_481_	['THOM_2531', 'THOM_2532']	[135.24503333333334]	0.00	Phenylalanyl-tRNA synthetase, beta subunit (similar to FRS2;)	[J]
c_877_	['THOM_1079', 'THOM_1080']	[44.503183333333332]	0.00	Histone acetyltransferase SAGA, TRRAP/TRA1 component, PI-3 kinase superfamily (similar to TRA1;)	[TBLD]
c_956_	['THOM_2595', 'THOM_2596']	[44.320866666666667, 44.320866666666667]	0.00	hypothetical protein	-
c_1711_	['THOM_0072', 'THOM_0073']	[291.4425, 291.4425]	0.00	predicted thioredoxin binding protein/Vacuolar protein sorting-associated protein	[R]
c_570_	['THOM_1738', 'THOM_1739']	[42.964616666666664]	0.00	Predicted DNA damage inducible protein	[L]
c_865_	['THOM_1615', 'THOM_1616']	[673.43916666666667, 673.43916666666667]	0.00	Centromere-associated protein HEC1 (similar to TID3;)	[D]
c_272_	['THOM_0815', 'THOM_0816']	[496.20100000000002, 496.20100000000002]	0.00	carboxylesterase	[R]

Appendix D

Expression levels of RK-13 transcripts.

Table showing the expression level of all *Oryctolagus cuniculus* genes in all samples expressed as FPKM – fragments per kilobase per million mapped reads. Where possible these genes were annotated with Ensembl gene names. For unannotated transcripts identified in this study Ensembl Gene IDs are labelled as "NA". Genes annotated in the *O. cuniculus* genome with no detectable expression during this study are also included for reference. Due to overlapping genes and alternative splicing, some transcriptome gene IDs are associated with multiple Ensembl gene IDs and/or multiple Ensembl Protein IDs.

This table is too large to include in the text, but is available in xlsx format for excel on the CD supplied with this thesis, or from http://bmcgenomics.biomedcentral.com/articles/10.1186/s12864-015-1989-z, table S4 (Watson et al., 2015).

Appendix E

RK-13 transcripts identified as significantly differentially expressed during infection.

Genes identified by cuffdiff (Trapnell et al., 2013) as significantly differentially expressed in the RK-13 host cell during *T. hominis* infection. Q-values are P-values that have been corrected for multiple testing using the false discovery rate method.

This table is additionally available in xlsx format for excel on the CD supplied with this thesis, or from http://bmcgenomics.biomedcentral.com/articles/10.1186/s12864-015-1989-z, table S5 (Watson et al., 2015).

Transcriptome Gene ID	Uninfected RK-13 Mean FPKM	T. hominis infected RK-13 Mean FPKM	Fold Change	Log2 Fold Change	Test stat	P value	Q value	Ensembl Gene Name / Gene ID	Gene Locus (Chromosome/scaffold:position)
XLOC_013192	0.12	1.99	16.71	4.06	3.77	3.40E-03	3.83E-02	NA	17:50320395-50321991
XLOC_019479	13.43	154.74	11.52	3.53	17.99	5.00E-05	1.41E-03	NA	3:79130412-79130758
XLOC_006353	0.46	3.79	8.17	3.03	5.05	5.00E-05	1.41E-03	NA	13:86906062-86908001
XLOC_014575	0.20	1.50	7.62	2.93	3.32	9.00E-04	1.42E-02	TMIGD1	19:17927667-17941959
XLOC_005410	0.45	3.05	6.84	2.77	4.64	5.00E-05	1.41E-03	NA	12:58113748-58115856
XLOC_010795	0.77	5.16	6.73	2.75	4.28	4.50E-04	8.42E-03	NA	15:67112396-67113014
XLOC_020722	4.85	30.16	6.22	2.64	7.69	5.00E-05	1.41E-03	KL	4:67489124-67575835
XLOC_011043	0.96	5.75	5.99	2.58	3.30	5.00E-05	1.41E-03	AGT	16:37238353-37316909
XLOC_031144	2.18	13.01	5.97	2.58	5.63	2.00E-04	4.42E-03	NA	GL018773:764333-764821
XLOC_031145	0.37	2.09	5.72	2.52	3.23	8.00E-04	1.30E-02	NA	GL018773:765702-766859
XLOC_032156	0.51	2.77	5.40	2.43	3.30	1.05E-03	1.60E-02	NA	GL018805:255477-256411
XLOC_018848	0.58	3.10	5.38	2.43	3.15	3.60E-03	3.99E-02	NA	3:57920585-57924012
XLOC_028945	0.76	4.01	5.30	2.41	5.00	5.00E-05	1.41E-03	NA	GL018720:456522-458692
XLOC_007257	0.24	1.25	5.28	2.40	2.97	7.00E-04	1.18E-02	PRKAA2	13:110265877-110332377
XLOC_031143	0.63	3.34	5.27	2.40	3.43	2.60E-03	3.17E-02	NA	GL018773:761555-762251
XLOC_031087	1.26	6.61	5.24	2.39	4.30	7.50E-04	1.24E-02	NA	GL018769:935546-936083
XLOC_036016	0.38	1.99	5.24	2.39	3.33	2.00E-04	4.42E-03	NA	GL019114:63942-65419
XLOC_027448	0.33	1.73	5.20	2.38	3.16	5.00E-04	9.12E-03	NA	GL018699:4656804-4658389
XLOC_016218	0.32	1.64	5.18	2.37	2.90	5.00E-05	1.41E-03	SLC2A9	2:423376-565836
XLOC_025819	7.98	41.33	5.18	2.37	1.77	8.50E-04	1.36E-02	ESCO1	9:62861689-62928949
XLOC_026348	32.19	162.17	5.04	2.33	31.39	1.35E-03	1.93E-02	NA	9:92491662-92491820
XLOC_038482	0.69	3.48	5.04	2.33	3.52	3.00E-04	6.09E-03	NA	X:80692608-80751007
XLOC_005734	2.24	11.20	5.00	2.32	5.53	5.00E-05	1.41E-03	NA	12:106317600-106318427
XLOC_038926	0.67	3.31	4.95	2.31	4.33	5.00E-05	1.41E-03	NA	X:46745175-46747031
XLOC_030865	1.24	6.12	4.95	2.31	4.13	3.20E-03	3.67E-02	NA	GL018763:1027123-1027571
XLOC_037488	0.32	1.53	4.84	2.27	2.76	3.10E-03	3.59E-02	NA	GL019772:19384-20576
XLOC_007187	0.47	2.25	4.76	2.25	4.88	5.00E-05	1.41E-03	PTGFR	13:86859728-86904578
XLOC_012577	6.76	31.35	4.64	2.21	9.17	3.65E-03	4.03E-02	ENSOCUG00000021585	17:37646374-37759057
XLOC_026200	117.72	534.64	4.54	2.18	83.95	3.90E-03	4.24E-02	NA	9:50017983-50018085
XLOC_007159	0.23	1.05	4.52	2.18	2.66	1.45E-03	2.04E-02	ENSOCUG00000008656	13:75602341-75621193
XLOC_005409	1.72	7.65	4.46	2.16	4.60	5.00E-05	1.41E-03	NA	12:58112710-58113484
XLOC_005105	1.40	6.19	4.44	2.15	5.07	5.00E-05	1.41E-03	PLAGL1	12:134681491-134701672
XLOC_029775	0.80	3.53	4.41	2.14	4.64	5.00E-05	1.41E-03	ANPEP	GL018738:1829889-1842909
XLOC_004838	121.86	522.51	4.29	2.10	7.14	5.00E-05	1.41E-03	ENSOCUG00000011952,ENSOCUG00000021171,ENSOCUG00000029486	12:42355145-42507924
XLOC_038278	0.92	3.95	4.28	2.10	2.14	2.10E-03	2.71E-02	ZNF630	X:33011348-33035372
XLOC_032974	39.64	168.72	4.26	2.09	36.20	4.80E-03	4.91E-02	NA	GL018838:518461-518598
XLOC_034869	0.60	2.54	4.22	2.08	2.89	4.30E-03	4.54E-02	NA	GL018967:118759-119489
XLOC_021956	0.77	3.23	4.21	2.08	4.18	5.00E-05	1.41E-03	ANKS4B	6:12114182-12133453
XLOC_019581	0.95	3.98	4.19	2.07	3.25	2.90E-03	3.41E-02	NA	3:98227459-98228054
XLOC_027952	0.86	3.60	4.18	2.06	3.21	2.30E-03	2.88E-02	NA	GL018704:6573509-6574200
XLOC_014164	0.81	3.28	4.03	2.01	3.79	5.00E-05	1.41E-03	NA	18:27890309-27891833
XLOC_007528	0.44	1.77	4.01	2.00	3.01	4.00E-04	7.69E-03	NA	13:1235499-1237037
XLOC_016250	4.88	19.42	3.98	1.99	6.86	5.00E-05	1.41E-03	PPARGC1A	2:14395692-14502163
XLOC_016279	0.36	1.43	3.97	1.99	2.04	2.95E-03	3.44E-02	TMEM156	2:28353940-28391980
XLOC_027962	1.48	5.87	3.97	1.99	2.45	1.65E-03	2.24E-02	ENSOCUG00000024145	GL018705:1939799-2059107
XLOC_024934	66.90	264.07	3.95	1.98	11.73	5.00E-05	1.41E-03	NA	8:87770973-87771387
XLOC_028851	33.53	131.88	3.93	1.98	2.28	1.20E-03	1.78E-02	NA	GL018719:1303459-1308485
XLOC_011786	287.21	1126.35	3.92	1.97	97.86	5.00E-05	1.41E-03	NA	16:47977927-47978037
XLOC_023808	0.74	2.88	3.91	1.97	3.47	1.50E-04	3.53E-03	NA	7:141337117-141338484
XLOC_011963	3.38	13.20	3.90	1.96	4.76	5.00E-04	9.12E-03	NA	17:429810-521192
XLOC_002245	1.98	7.69	3.89	1.96	4.22	5.50E-04	9.84E-03	NA	1:114189214-114189746
XLOC_028179	0.52	2.03	3.88	1.96	2.92	8.00E-04	1.30E-02	NA	GL018707:1120901-1122184
XLOC_038428	0.31	1.18	3.88	1.96	2.38	5.50E-04	9.84E-03	AKAP17A	X:67976298-67988069
XLOC_025699	1.43	5.50	3.84	1.94	2.77	1.50E-04	3.53E-03	NA	9:24354939-24356495
XLOC_027500	0.71	2.72	3.83	1.94	3.98	5.00E-05	1.41E-03	AFF2	GL018700:12062822-12650191
XLOC_008393	1.88	7.20	3.83	1.94	2.97	9.50E-04	1.48E-02	NA	14:1987899-2007659
XLOC_038803	0.72	2.74	3.82	1.93	3.06	8.00E-04	1.30E-02	NA	X:23771419-23772450
XLOC_038729	0.50	1.91	3.81	1.93	2.98	7.50E-04	1.24E-02	NA	X:10424433-10425885
XLOC_007817	0.79	3.01	3.80	1.93	3.16	5.50E-04	9.84E-03	NA	13:54655217-54656225
XLOC_003470	0.47	1.78	3.79	1.92	3.08	5.00E-05	1.41E-03	AGXT2	11:56320214-56363142
XLOC_024132	1.77	6.69	3.78	1.92	4.96	5.00E-05	1.41E-03	GALNT8	8:30814744-30863819
XLOC_037901	0.47	1.76	3.77	1.91	2.76	1.10E-03	1.66E-02	GJB1	X:49697297-49698685
XLOC_014896	6.40	23.70	3.71	1.89	5.18	5.00E-05	1.41E-03	KCNJ16	19:53822415-53885847
XLOC_035430	17.72	65.10	3.67	1.88	15.06	1.35E-03	1.93E-02	NA	GL019041:32904-33108
XLOC_023411	5.56	20.36	3.66	1.87	7.00	1.55E-03	2.14E-02	NA	7:41289157-41289450
XLOC_016398	2.01	7.37	3.66	1.87	4.55	5.00E-05	1.41E-03	ACSL1	2:62247812-62298540
XLOC_001401	0.57	2.07	3.65	1.87	2.57	5.00E-04	9.12E-03	C11orf70	1:114710914-114745039
XLOC_018102	0.97	3.53	3.64	1.86	3.60	5.00E-05	1.41E-03	NA	21:12591087-12592440
XLOC_015607	1.91	6.94	3.63	1.86	3.88	2.65E-03	3.21E-02	NA	19:53886356-53886804
XLOC_014294	0.45	1.64	3.62	1.86	2.57	3.25E-03	3.71E-02	NA	18:48813029-48814237
XLOC_023424	1.38	4.95	3.58	1.84	3.44	6.50E-04	1.12E-02	NA	7:44980549-44981217
XLOC_021348	0.41	1.47	3.57	1.84	2.92	5.00E-05	1.41E-03	CX3CL1	5:13525855-13538730
XLOC_011248	6.49	22.91	3.53	1.82	3.95	5.00E-05	1.41E-03	ENKUR	16:1313012-1336660
XLOC_035397	5.48	19.28	3.52	1.81	5.54	5.00E-05	1.41E-03	NA	GL019037:191697-192316
XLOC_023379	0.91	3.20	3.51	1.81	3.19	3.00E-04	6.09E-03	NA	7:32370751-32371806
XLOC_015616	0.60	2.10	3.51	1.81	2.74	1.75E-03	2.35E-02	NA	19:56085680-56086782
XLOC_002269	0.70	2.47	3.51	1.81	2.64	4.50E-03	4.70E-02	NA	1:126694598-126695407
XLOC_002348	0.53	1.83	3.47	1.80	2.89	2.00E-04	4.42E-03	NA	1:147734343-147736009
XLOC_028966	1.23	4.27	3.47	1.80	2.91	1.00E-04	2.52E-03	COLEC11	GL018721:261522-305189
XLOC_005231	4.98	17.15	3.44	1.78	5.14	5.00E-05	1.41E-03	NA	12:10885659-10886432
XLOC_000507	10.46	35.99	3.44	1.78	5.77	5.00E-05	1.41E-03	SYTL2	1:130928304-131068598
XLOC_001166	19.10	65.33	3.42	1.77	6.69	5.00E-05	1.41E-03	ALDH1A1	1:59416688-59478488
XLOC_022600	0.57	1.93	3.41	1.77	3.12	5.00E-05	1.41E-03	AOX1	7:141217105-141289366
XLOC_005217	0.72	2.45	3.40	1.77	2.66	2.85E-03	3.37E-02	NA	12:10398307-10399217
XLOC_017205	0.37	1.25	3.39	1.76	2.31	3.70E-03	4.07E-02	NA	2:112766377-112767845
XLOC_030409	6.29	21.28	3.38	1.76	6.93	2.30E-03	2.88E-02	NA	GL018752:1851007-1851291
XLOC_032131	0.95	3.20	3.36	1.75	2.94	1.05E-03	1.60E-02	NA	GL018804:926299-927193
XLOC_038045	0.45	1.50	3.34	1.74	3.46	5.00E-05	1.41E-03	ENSOCUG00000003437	X:83593303-83682260
XLOC_001113	1.61	5.38	3.34	1.74	4.31	5.00E-05	1.41E-03	LURAP1L	1:41234306-41276911
XLOC_006235	1.88	6.28	3.34	1.74	3.72	5.00E-05	1.41E-03	SLC16A4	13:53792521-53815810
XLOC_033751	0.87	2.90	3.33	1.74	2.91	1.35E-03	1.93E-02	NA	GL018883:90288-91206
XLOC_035091	28.66	95.38	3.33	1.73	19.34	2.45E-03	3.02E-02	NA	GL018992:164513-164690
XLOC_021261	1.39	4.63	3.33	1.73	3.79	5.00E-05	1.41E-03	NA	4:91029382-91030709
XLOC_033643	1.17	3.88	3.32	1.73	3.35	2.00E-04	4.42E-03	NA	GL018879:96981-97969
XLOC_023536	1.00	3.33	3.32	1.73	3.09	4.00E-04	7.69E-03	NA	7:62097650-62098651
XLOC_020502	1.17	3.87	3.32	1.73	4.86	5.00E-05	1.41E-03	SPTLC3	4:23027242-23189669
XLOC_022653	2.71	8.94	3.30	1.72	5.20	5.00E-05	1.41E-03	MAP2	7:150243424-150556321
XLOC_024839	1.51	4.96	3.29	1.72	3.48	5.00E-05	1.41E-03	NA	8:44781229-44782061
XLOC_010174	0.52	1.70	3.29	1.72	2.67	1.65E-03	2.24E-02	ADH2-1	15:50651975-50668716
XLOC_028828	0.57	1.88	3.28	1.72	2.70	8.50E-04	1.36E-02	NA	GL018718:710957-713817
XLOC_032320	0.32	1.06	3.28	1.71	2.75	1.50E-04	3.53E-03	ENSOCUG00000029241	GL018812:539452-544766
XLOC_009664	0.69	2.26	3.27	1.71	3.27	1.00E-04	2.52E-03	NA	14:83401468-83403482
XLOC_011259	0.94	3.06	3.27	1.71	2.78	2.95E-03	3.44E-02	NA	16:3798680-3803445
XLOC_028953	0.67	2.19	3.26	1.70	2.59	3.50E-03	3.92E-02	NA	GL018720:1148969-1149919
XLOC_019042	8.73	28.36	3.25	1.70	5.94	5.00E-05	1.41E-03	ANGPT1	3:122696118-122945695
XLOC_007105	4.19	13.59	3.24	1.70	1.68	2.35E-03	2.93E-02	CDC14A	13:63639835-63826034
XLOC_030720	10.41	33.56	3.23	1.69	4.74	5.00E-05	1.41E-03	ENSOCUG00000027138	GL018762:509857-555218
XLOC_014098	1.22	3.94	3.22	1.69	3.21	2.00E-04	4.42E-03	NA	18:18835148-18836030
XLOC_006493	2.34	7.54	3.22	1.69	4.35	5.00E-05	1.41E-03	PIK3R3	13:120346503-120541996
XLOC_005406	0.59	1.90	3.22	1.69	2.59	1.85E-03	2.44E-02	NA	12:58064904-58066188

Transcriptome Gene ID	Uninfected RK-13 Mean FPKM	T. hominis infected RK-13 Mean FPKM	Fold Change	Log2 Fold Change	Test stat	P value	Q value	Ensembl Gene Name / Gene ID	Gene Locus (Chromosome/scaffold:position)
XLOC_021260	0.80	2.57	3.22	1.68	3.10	1.50E-04	3.53E-03	NA	4:91027742-91029284
XLOC_005240	0.91	2.94	3.21	1.68	2.69	3.30E-03	3.75E-02	NA	12:12797431-12798228
XLOC_020854	0.95	3.07	3.21	1.68	3.53	5.00E-05	1.41E-03	NA	4:8219938-8221837
XLOC_019610	0.91	2.92	3.20	1.68	2.96	8.50E-04	1.36E-02	NA	3:99610548-99611612
XLOC_021397	2.81	8.91	3.18	1.67	4.69	5.00E-05	1.41E-03	HSD11B2	5:23014000-23020581
XLOC_002838	0.50	1.59	3.17	1.66	3.43	5.00E-05	1.41E-03	ZNF804B	10:39211106-39221001
XLOC_022861	28.19	88.97	3.16	1.66	6.00	5.00E-05	1.41E-03	CD36	7:35299518-35367222
XLOC_038804	0.77	2.43	3.15	1.66	3.45	5.00E-05	1.41E-03	NA	X:23772504-23774928
XLOC_001638	3.66	11.52	3.15	1.65	1.93	2.90E-03	3.41E-02	NA	1:151202315-151209170
XLOC_019672	0.31	0.96	3.13	1.65	2.35	2.40E-03	2.97E-02	NA	3:116710589-116712905
XLOC_021877	0.95	2.96	3.11	1.64	2.86	1.10E-03	1.66E-02	NA	5:33716272-33717223
XLOC_017345	1.31	4.07	3.10	1.63	3.08	9.50E-04	1.48E-02	NA	2:146767630-146768398
XLOC_022893	7.66	23.73	3.10	1.63	1.72	3.40E-03	3.83E-02	NA	7:44560585-44586471
XLOC_001000	2.52	7.78	3.09	1.63	2.00	5.00E-04	9.12E-03	ZNF189	1:11593410-11609109
XLOC_007529	1.97	6.08	3.09	1.63	3.60	3.00E-04	6.09E-03	NA	13:1238057-1238803
XLOC_018952	1.41	4.32	3.07	1.62	3.10	5.00E-05	1.41E-03	IL7	3:94496941-94585618
XLOC_001462	3.23	9.89	3.06	1.61	4.40	5.00E-05	1.41E-03	ENSOCUG00000021600	1:134727885-134729038
XLOC_018985	0.50	1.52	3.05	1.61	2.90	5.00E-05	1.41E-03	TMEM55A	3:106596017-106667024
XLOC_007908	2.74	8.36	3.05	1.61	4.13	5.00E-05	1.41E-03	NA	13:75840553-75841699
XLOC_013128	0.71	2.16	3.04	1.60	2.91	1.00E-04	2.52E-03	NA	17:37924660-37926312
XLOC_014889	3.21	9.74	3.03	1.60	3.73	5.00E-05	1.41E-03	AMZ2	19:52192339-52203777
XLOC_008533	26.33	79.70	3.03	1.60	5.59	5.00E-05	1.41E-03	MME	14:49293435-49395270
XLOC_032220	1.11	3.35	3.02	1.60	2.71	3.60E-03	3.99E-02	NA	GL018806:921963-922694
XLOC_033150	3.78	11.37	3.01	1.59	4.47	5.00E-05	1.41E-03	SLC16A5	GL018845:596489-606692
XLOC_030242	1.28	3.85	3.00	1.58	3.11	3.50E-04	6.91E-03	NA	GL018750:1345205-1346201
XLOC_021259	0.71	2.14	3.00	1.58	3.66	5.00E-05	1.41E-03	NA	4:91023348-91027329
XLOC_035429	1.56	4.67	2.99	1.58	3.56	5.00E-05	1.41E-03	NA	GL019040:56609-57990
XLOC_016277	0.57	1.71	2.98	1.58	2.91	5.00E-05	1.41E-03	TLR1	2:28215233-28217624
XLOC_023054	8.13	24.09	2.96	1.57	3.25	5.00E-05	1.41E-03	SLC25A12	7:111490168-111594160
XLOC_017266	10.60	31.24	2.95	1.56	6.64	5.00E-05	1.41E-03	NA	2:122538332-122538683
XLOC_006684	1.83	5.39	2.94	1.56	3.13	3.40E-03	3.83E-02	NA	13:142932260-142936396
XLOC_027132	10.54	30.99	2.94	1.56	5.88	5.00E-05	1.41E-03	NA	AAGW02083174:497-1002
XLOC_025878	3.42	10.04	2.93	1.55	4.62	5.00E-05	1.41E-03	PSTPIP2	9:87412590-87492166
XLOC_036742	3.14	9.20	2.93	1.55	4.22	5.00E-05	1.41E-03	NA	GL019321:2484-3664
XLOC_032117	2.44	7.12	2.93	1.55	3.67	1.50E-04	3.53E-03	NA	GL018804:114361-115122
XLOC_028658	64.94	190.01	2.93	1.55	28.63	1.75E-03	2.35E-02	NA	GL018716:3484473-3484626
XLOC_030218	2.74	8.01	2.92	1.55	3.29	5.00E-05	1.41E-03	ENSOCUG00000012841,PGER8	GL018750:547414-603740
XLOC_015688	1.36	3.98	2.92	1.54	2.83	5.00E-05	1.41E-03	N4BP2	2:29323988-29377878
XLOC_013808	1.43	4.16	2.92	1.54	4.02	5.00E-05	1.41E-03	SLC16A12	18:37369948-37432444
XLOC_035955	0.34	0.98	2.92	1.54	1.86	3.60E-03	3.99E-02	RSPH1	GL019109:150127-169962
XLOC_029696	0.68	1.98	2.91	1.54	3.07	5.00E-05	1.41E-03	NEU2	GL018736:549001-571185
XLOC_035782	1.67	4.86	2.91	1.54	3.03	3.60E-03	3.99E-02	NA	GL019086:224097-224684
XLOC_038802	1.51	4.38	2.90	1.54	3.86	5.00E-05	1.41E-03	NA	X:23768908-23771178
XLOC_000221	0.31	0.90	2.89	1.53	2.93	5.00E-05	1.41E-03	RFX3	1:50987294-51191661
XLOC_025301	21.87	63.22	2.89	1.53	3.81	5.00E-05	1.41E-03	LAMA1	9:54750449-54894693
XLOC_021140	1.18	3.39	2.88	1.53	2.81	1.20E-03	1.78E-02	NA	4:48789516-48790411
XLOC_036328	1.10	3.18	2.87	1.52	2.67	3.25E-03	3.71E-02	NA	GL019195:78687-79485
XLOC_027137	0.99	2.85	2.87	1.52	2.82	5.00E-04	9.12E-03	NA	AAGW02083187:1988-3200
XLOC_014785	0.63	1.79	2.86	1.52	2.73	1.50E-04	3.53E-03	ENSOCUG00000013236	19:42816235-42843600
XLOC_038165	4.90	14.01	2.86	1.51	4.74	5.00E-05	1.41E-03	PIR	X:1244574-1332621
XLOC_027403	1.68	4.80	2.86	1.51	3.04	1.30E-03	1.87E-02	ENSOCUG00000017167	GL018699:9342456-9343118
XLOC_038457	1.92	5.48	2.86	1.51	2.97	3.90E-03	4.24E-02	NA	X:72461477-72503341
XLOC_014756	0.68	1.93	2.85	1.51	2.36	4.00E-03	4.31E-02	NA	19:40813548-40815300
XLOC_025312	0.55	1.56	2.85	1.51	3.49	5.00E-05	1.41E-03	MYOM1	9:58833632-58987720
XLOC_027217	6.38	18.14	2.84	1.51	5.66	2.25E-03	2.84E-02	NA	AAGW02083529:5629-5948
XLOC_034055	3.14	8.92	2.84	1.51	3.72	7.00E-04	1.18E-02	NA	GL018899:446871-447391
XLOC_022930	3.53	9.94	2.82	1.49	4.24	5.00E-05	1.41E-03	ENSOCUG00000023503	7:62227354-62280029
XLOC_033234	1.09	3.06	2.81	1.49	2.56	5.00E-05	1.41E-03	NA	GL018851:474490-478151
XLOC_030397	279.52	781.68	2.80	1.48	56.02	5.00E-05	1.41E-03	NA	GL018752:598911-599042
XLOC_028668	4.76	13.28	2.79	1.48	4.51	5.00E-05	1.41E-03	NA	GL018717:417216-430057
XLOC_004267	11.60	32.35	2.79	1.48	6.18	5.00E-05	1.41E-03	NA	12:64467691-64530226
XLOC_004848	16.48	45.95	2.79	1.48	5.12	5.00E-05	1.41E-03	GCLC	12:43272558-43321078
XLOC_014418	0.50	1.38	2.77	1.47	2.04	2.25E-03	2.84E-02	ENSOCUG00000015802	19:4332442-4394208
XLOC_023807	0.99	2.72	2.75	1.46	2.75	5.00E-04	9.12E-03	NA	7:141335789-141337062
XLOC_037688	0.47	1.30	2.75	1.46	2.48	1.00E-04	2.52E-03	CDKL5	X:4271483-4505068
XLOC_024066	2.59	7.10	2.75	1.46	3.15	5.00E-05	1.41E-03	CASC1	8:14893245-15023321
XLOC_031108	5.74	15.75	2.74	1.46	4.48	5.00E-05	1.41E-03	NA	GL018771:474440-475198
XLOC_027423	0.74	2.02	2.73	1.45	2.85	2.50E-04	5.26E-03	NA	GL018699:735255-737426
XLOC_012351	6.57	17.89	2.72	1.45	3.55	5.00E-05	1.41E-03	STYX	17:71572511-71603221
XLOC_002499	15.11	41.13	2.72	1.44	9.75	4.65E-03	4.81E-02	NA	1:191472297-191472523
XLOC_002011	0.48	1.32	2.72	1.44	2.37	8.50E-04	1.36E-02	NA	1:35875846-35877994
XLOC_025289	0.44	1.18	2.72	1.44	2.62	2.50E-04	5.26E-03	ENSOCUG00000010254	9:50740448-51088848
XLOC_031617	0.73	1.98	2.71	1.44	2.31	3.70E-03	4.07E-02	NA	GL018788:823307-824494
XLOC_018176	0.97	2.62	2.70	1.43	2.87	5.00E-05	1.41E-03	PHF15	3:17281471-17317162
XLOC_006325	23.53	63.41	2.69	1.43	5.51	5.00E-05	1.41E-03	ENSOCUG00000017251	13:75635644-75650152
XLOC_013861	0.97	2.62	2.69	1.43	2.69	4.50E-04	8.42E-03	CPN1	18:47988543-48019553
XLOC_011404	0.38	1.03	2.69	1.43	2.23	1.40E-03	1.98E-02	TMEM63A	16:47803083-47831652
XLOC_005148	3.10	8.29	2.68	1.42	3.71	5.00E-05	1.41E-03	SLC22A2	12:149926383-149956141
XLOC_027135	11.43	30.56	2.67	1.42	2.03	2.75E-03	3.29E-02	NA	AAGW02083187:3319-5177
XLOC_018981	0.78	2.07	2.67	1.42	2.73	5.00E-05	1.41E-03	CALB1	3:105510593-105534337
XLOC_012532	0.43	1.14	2.66	1.41	2.43	1.50E-04	3.53E-03	GANC	17:29835958-29914449
XLOC_016856	144.69	382.71	2.65	1.40	42.28	1.35E-03	1.93E-02	NA	2:9168089-9168219
XLOC_011748	18.42	48.64	2.64	1.40	7.87	1.00E-04	2.52E-03	NA	16:41759487-41759792
XLOC_000904	1.95	5.15	2.64	1.40	4.23	5.00E-05	1.41E-03	DTX4	1:192029933-192104481
XLOC_026546	7.97	21.00	2.63	1.40	2.49	3.00E-04	6.09E-03	ENSOCUG00000023353	AAGW02080821:13544-15602
XLOC_002672	1.19	3.14	2.63	1.39	2.56	2.20E-03	2.80E-02	NA	10:44221234-44224425
XLOC_021146	1.56	4.10	2.63	1.39	2.91	6.50E-04	1.12E-02	NA	4:49206486-49207443
XLOC_017575	3.37	8.85	2.62	1.39	2.62	2.00E-04	4.42E-03	ENTPD5	20:31003155-31072897
XLOC_023109	1.64	4.31	2.62	1.39	3.92	5.00E-05	1.41E-03	SLC40A1	7:129930834-129952629
XLOC_001679	0.81	2.12	2.62	1.39	2.30	3.85E-03	4.21E-02	FANCF	1:161749429-161750509
XLOC_034054	1.00	2.61	2.61	1.38	2.73	2.50E-04	5.26E-03	NA	GL018899:443975-445525
XLOC_022020	9.73	25.33	2.60	1.38	3.78	1.00E-04	2.52E-03	XPO6	6:18907720-19029932
XLOC_007444	6.24	16.16	2.59	1.37	4.51	5.00E-05	1.41E-03	ENSOCUG00000014622	13:133616910-133624878
XLOC_011366	1.81	4.70	2.59	1.37	3.21	5.00E-05	1.41E-03	CAPN9	16:37164987-37209983
XLOC_011271	1.27	3.27	2.58	1.37	2.14	1.85E-03	2.44E-02	ENSOCUG00000014318	16:10630686-10661237
XLOC_028188	0.52	1.35	2.58	1.37	2.14	4.05E-03	4.35E-02	NA	GL018707:1190636-1192272
XLOC_010959	0.51	1.31	2.57	1.36	2.93	5.00E-05	1.41E-03	ITI-HC2	16:12055883-12101847
XLOC_005955	2.24	5.76	2.57	1.36	3.23	5.00E-05	1.41E-03	C1orf110	13:30135686-30142352
XLOC_010213	2.48	6.37	2.57	1.36	3.77	5.00E-05	1.41E-03	HPSE	15:67074644-67111687
XLOC_016127	33.54	85.84	2.56	1.36	7.77	5.00E-05	1.41E-03	ENSOCUG00000029517	2:146895539-147010054
XLOC_027716	1.17	3.00	2.56	1.35	3.17	5.00E-05	1.41E-03	SMAD9	GL018702:7766920-7838621
XLOC_003123	0.96	2.44	2.55	1.35	2.54	1.20E-03	1.78E-02	NA	10:45654104-45655485
XLOC_028620	1.62	4.13	2.55	1.35	2.98	2.50E-04	5.26E-03	NA	GL018715:1958102-1959296
XLOC_018280	0.56	1.41	2.54	1.35	2.40	6.50E-04	1.12E-02	PAT1	3:32927618-32966337
XLOC_037388	0.70	1.78	2.53	1.34	2.14	4.65E-03	4.81E-02	NA	GL019700:18882-20278
XLOC_002735	1.79	4.53	2.53	1.34	1.80	1.30E-03	1.87E-02	FKBP14	10:14432834-14445151
XLOC_016200	5.81	14.58	2.51	1.33	3.66	1.30E-03	1.87E-02	KCNS3	2:166914642-166965925
XLOC_016776	0.36	0.90	2.51	1.33	2.49	2.50E-04	5.26E-03	PLB1	2:157459246-157583846
XLOC_009024	0.74	1.85	2.51	1.33	3.32	5.00E-05	1.41E-03	PLCH1	14:49750746-49970925
XLOC_030243	0.85	2.14	2.51	1.33	2.30	3.00E-03	3.49E-02	NA	GL018750:1346465-1347681
XLOC_009967	2.19	5.50	2.51	1.33	2.86	3.45E-03	3.88E-02	NA	14:135983385-135983959
XLOC_033402	1.48	3.71	2.50	1.32	2.68	1.00E-03	1.55E-02	NA	GL018862:432661-433639

Transcriptome Gene ID	Uninfected RK-13 Mean FPKM	T. hominis infected RK-13 Mean FPKM	Fold Change	Log2 Fold Change	Test stat	P value	Q value	Ensembl Gene Name / Gene ID	Gene Locus (Chromosome/scaffold:position)
XLOC_023992	1.13	2.82	2.50	1.32	2.52	1.80E-03	2.39E-02	NA	7:172319460-172320623
XLOC_033618	185.00	461.40	2.49	1.32	39.32	7.50E-04	1.24E-02	NA	GL018878:128150-128288
XLOC_019201	0.98	2.44	2.49	1.32	2.83	5.00E-05	1.41E-03	NA	3:17954173-17956327
XLOC_010078	1.36	3.39	2.49	1.32	3.13	5.00E-05	1.41E-03	INPP4B	15:21871664-22539205
XLOC_032343	1.22	3.05	2.49	1.32	2.42	4.25E-03	4.50E-02	NA	GL018812:536306-537180
XLOC_037029	3.38	8.42	2.49	1.31	3.36	1.05E-03	1.60E-02	NA	GL019451:3839-4399
XLOC_007796	0.89	2.21	2.49	1.31	2.59	5.50E-04	9.84E-03	NA	13:53026376-53028182
XLOC_013817	1.38	3.43	2.48	1.31	2.34	1.00E-04	2.52E-03	CPEB3	18:39951113-40166497
XLOC_034020	15.00	37.19	2.48	1.31	4.93	1.40E-03	1.98E-02	NA	GL018899:337885-339968
XLOC_003391	9.20	22.79	2.48	1.31	3.29	5.00E-05	1.41E-03	ST8SIA4	11:20360739-20461942
XLOC_010244	657.40	1625.79	2.47	1.31	7.72	5.00E-05	1.41E-03	CXCL10	15:74369016-74370722
XLOC_024609	2.16	5.35	2.47	1.31	2.74	1.10E-03	1.66E-02	NA	8:78945183-78977923
XLOC_023046	4.25	10.51	2.47	1.30	4.69	5.00E-05	1.41E-03	LRP2	7:108888119-109114341
XLOC_016316	4.59	11.30	2.46	1.30	3.06	5.00E-05	1.41E-03	ENSOCUG00000015419	2:38191512-38209597
XLOC_024204	22.06	54.17	2.46	1.30	3.14	5.00E-05	1.41E-03	RNF6	8:38989682-39000672
XLOC_035315	0.62	1.53	2.45	1.29	2.08	3.25E-03	3.71E-02	NA	GL019028:22398-27200
XLOC_037882	2.45	5.99	2.44	1.29	3.89	5.00E-05	1.41E-03	STARD8	X:47301051-47341912
XLOC_029946	1.13	2.76	2.44	1.29	2.63	6.00E-04	1.06E-02	NA	GL018741:1895201-1896771
XLOC_031125	1.05	2.54	2.43	1.28	2.85	5.00E-05	1.41E-03	NA	GL018773:75697-77969
XLOC_014019	1.99	4.83	2.43	1.28	3.09	5.00E-05	1.41E-03	NA	18:5071672-5073112
XLOC_036600	1.12	2.70	2.41	1.27	2.54	7.00E-04	1.18E-02	NA	GL019276:66439-67942
XLOC_008958	1.15	2.77	2.41	1.27	2.07	9.00E-04	1.42E-02	NME9	14:31954326-31975179
XLOC_027619	2.99	7.20	2.41	1.27	3.59	5.00E-05	1.41E-03	NA	GL018701:7854065-7866994
XLOC_006170	0.72	1.73	2.41	1.27	2.61	5.00E-05	1.41E-03	FMO5	13:43918642-43949807
XLOC_036747	56.17	135.19	2.41	1.27	12.44	5.00E-05	1.41E-03	NA	GL019326:23064-23305
XLOC_014078	0.86	2.06	2.40	1.26	2.15	4.25E-03	4.50E-02	NA	18:15077745-15078932
XLOC_026039	1.59	3.82	2.39	1.26	2.72	8.00E-04	1.30E-02	NA	9:12659924-12661057
XLOC_022495	0.65	1.55	2.39	1.26	1.86	1.80E-03	2.39E-02	B3GALT1	7:107471354-107473230
XLOC_022648	1.65	3.95	2.39	1.26	2.14	5.00E-04	9.12E-03	NA	7:148712138-148714281
XLOC_034031	1.02	2.44	2.39	1.26	2.33	2.65E-03	3.21E-02	NA	GL018899:193999-195267
XLOC_030543	0.93	2.23	2.39	1.26	2.25	2.70E-03	3.25E-02	NA	GL018757:590877-592149
XLOC_010209	12.21	29.15	2.39	1.26	4.02	5.00E-05	1.41E-03	ARHGAP24	15:65289797-65750911
XLOC_029440	0.79	1.90	2.39	1.26	2.16	3.65E-03	4.03E-02	NA	GL018730:2756662-2758042
XLOC_037526	0.95	2.27	2.39	1.26	2.77	1.50E-04	3.53E-03	ENSOCUG00000029565	GL019821:2758-8690
XLOC_030528	1.08	2.57	2.38	1.25	2.35	2.65E-03	3.21E-02	NA	GL018757:353565-354748
XLOC_006264	4.08	9.71	2.38	1.25	4.31	5.00E-05	1.41E-03	VAV3	13:56144497-56550635
XLOC_020302	0.68	1.61	2.38	1.25	1.82	2.25E-03	2.84E-02	ENSOCUG00000003924	4:85497275-85501939
XLOC_005433	3.15	7.49	2.37	1.25	3.46	5.00E-05	1.41E-03	NA	12:58177894-58179283
XLOC_025122	20.98	49.68	2.37	1.24	2.07	9.50E-04	1.48E-02	NA	9:11402843-11408233
XLOC_006167	33.20	78.60	2.37	1.24	2.61	1.00E-04	2.52E-03	PDZK1	13:43032012-43138880
XLOC_006728	0.42	1.00	2.37	1.24	2.08	5.00E-04	9.12E-03	ABL2	13:6198172-6219786
XLOC_016725	7.12	16.84	2.36	1.24	2.66	1.00E-04	2.52E-03	SLC3A1	2:141886987-141980585
XLOC_020976	11.24	26.58	2.36	1.24	5.21	4.50E-04	8.42E-03	NA	4:35199989-35200344
XLOC_003049	0.91	2.15	2.36	1.24	2.73	1.00E-04	2.52E-03	NA	10:34869325-34872294
XLOC_021779	59.76	141.02	2.36	1.24	17.78	1.85E-03	2.44E-02	NA	5:14375485-14375664
XLOC_005086	15.02	35.40	2.36	1.24	3.18	5.00E-05	1.41E-03	MAP3K5	12:126997369-127248332
XLOC_000792	1.99	4.69	2.35	1.23	1.83	1.80E-03	2.39E-02	C11orf49	1:186291584-186537600
XLOC_038805	2.26	5.32	2.35	1.23	3.27	5.00E-05	1.41E-03	NA	X:23775129-23777043
XLOC_011490	2.47	5.80	2.35	1.23	2.92	5.00E-05	1.41E-03	MFSD4	16:66560903-66584843
XLOC_033866	0.63	1.47	2.34	1.23	2.27	1.30E-03	1.87E-02	NA	GL018889:280076-282466
XLOC_021134	1.06	2.46	2.33	1.22	2.61	3.00E-04	6.09E-03	NA	4:48282124-48284161
XLOC_023151	1.07	2.49	2.33	1.22	2.89	5.00E-05	1.41E-03	NA	7:142009527-142014975
XLOC_018303	1.31	3.04	2.33	1.22	2.30	1.50E-04	3.53E-03	ADRA1B	3:41338643-41396620
XLOC_022864	7.72	17.95	2.32	1.22	4.25	5.00E-05	1.41E-03	GNAI1	7:35800453-35912590
XLOC_027339	1.40	3.25	2.32	1.21	1.96	2.45E-03	3.02E-02	AMBP	GL018699:13513512-13521327
XLOC_010403	1.06	2.46	2.32	1.21	3.35	5.00E-05	1.41E-03	EDNRA	15:17109143-17191949
XLOC_022097	3.02	7.00	2.32	1.21	3.22	5.00E-05	1.41E-03	CRYM	6:12137414-12156602
XLOC_024610	2.14	4.95	2.31	1.21	2.88	3.50E-04	6.91E-03	NA	8:78978888-78994255
XLOC_010318	1.84	4.24	2.31	1.21	3.06	5.00E-05	1.41E-03	CLOCK	15:93327110-93398734
XLOC_004271	72.75	167.60	2.30	1.20	1.75	2.90E-03	3.41E-02	SH3BGRL2	12:66519724-66588218
XLOC_031304	21.21	48.78	2.30	1.20	3.85	5.00E-05	1.41E-03	FAM175B	GL018780:459789-494624
XLOC_006489	14.12	32.37	2.29	1.20	2.78	2.75E-03	3.29E-02	MKNK1	13:119980966-120021110
XLOC_033689	2.22	5.09	2.29	1.20	2.91	2.00E-04	4.42E-03	NA	GL018880:354050-355257
XLOC_004529	7.42	16.99	2.29	1.19	2.66	5.00E-05	1.41E-03	SLC22A3	12:150017670-150152958
XLOC_010127	4.17	9.53	2.29	1.19	3.32	4.50E-04	8.42E-03	NA	15:38888992-38900756
XLOC_037105	1.31	3.00	2.28	1.19	1.84	2.40E-03	2.97E-02	BIRC7	GL019502:20963-24501
XLOC_030156	0.80	1.82	2.27	1.18	2.40	4.00E-04	7.69E-03	ENSOCUG00000024756	GL018748:963243-969450
XLOC_001230	2.09	4.74	2.27	1.18	1.79	1.90E-03	2.49E-02	CDC14B	1:75329702-75394138
XLOC_025600	1.25	2.83	2.27	1.18	2.09	8.50E-04	1.36E-02	PFKFB4	9:16230092-16257527
XLOC_017518	0.70	1.59	2.26	1.18	1.80	3.85E-03	4.21E-02	GPR68	20:14478110-14489333
XLOC_007802	1.30	2.93	2.26	1.18	2.47	5.50E-04	9.84E-03	NA	13:53039085-53040542
XLOC_008369	0.70	1.57	2.25	1.17	2.05	3.95E-03	4.28E-02	NA	13:141847840-141849585
XLOC_003541	9.79	22.06	2.25	1.17	2.23	2.50E-04	5.26E-03	NA	11:77197363-77198168
XLOC_026952	0.49	1.11	2.25	1.17	2.22	6.00E-04	1.06E-02	NA	AAGW02082676:1443-4908
XLOC_025747	1.16	2.61	2.25	1.17	2.25	3.30E-03	3.75E-02	ENSOCUG00000022648	9:43393585-43404910
XLOC_037160	2.29	5.15	2.25	1.17	2.99	5.00E-05	1.41E-03	ENSOCUG00000029491	GL019539:25004-26606
XLOC_017507	8.11	18.21	2.25	1.17	4.52	3.30E-03	3.75E-02	NA	20:13487984-13491760
XLOC_008865	1.15	2.57	2.24	1.17	2.93	5.00E-05	1.41E-03	HUNK	14:161997085-162103378
XLOC_010610	1.71	3.81	2.23	1.16	2.25	2.25E-03	2.84E-02	NA	15:81208657-81223247
XLOC_017555	6.26	13.97	2.23	1.16	2.47	3.00E-04	6.09E-03	NA	20:28369084-28382425
XLOC_032687	3.34	7.44	2.23	1.15	3.01	5.00E-04	9.12E-03	NA	GL018827:505989-506755
XLOC_009031	1.12	2.49	2.22	1.15	1.91	2.25E-03	2.84E-02	VEPH1	14:51663527-51913966
XLOC_011734	0.88	1.96	2.22	1.15	2.11	4.15E-03	4.42E-02	NA	16:38112142-38113610
XLOC_025583	6.01	13.30	2.21	1.15	3.80	5.00E-05	1.41E-03	NA	9:15107444-15111554
XLOC_035100	5.31	11.74	2.21	1.15	2.64	3.00E-04	6.09E-03	NA	GL018994:19605-25511
XLOC_028660	0.75	1.66	2.21	1.14	2.02	3.80E-03	4.17E-02	NA	GL018716:3499509-3501185
XLOC_011154	2.77	6.12	2.21	1.14	3.44	5.00E-05	1.41E-03	PIGR	16:65441052-65458867
XLOC_025451	1.82	4.01	2.21	1.14	2.91	5.00E-05	1.41E-03	CNDP1	9:114681592-114723824
XLOC_022896	4.26	9.38	2.20	1.14	2.42	5.00E-05	1.41E-03	PNPLA8	7:45064692-45122839
XLOC_023255	2.87	6.31	2.20	1.14	2.45	1.00E-04	2.52E-03	TM4SF20	7:169147882-169162942
XLOC_006667	19.79	43.56	2.20	1.14	4.99	5.00E-05	1.41E-03	NA	13:139870581-139874421
XLOC_022134	1.29	2.84	2.20	1.14	2.76	5.00E-05	1.41E-03	APOBR	6:18601895-18609621
XLOC_027511	8.65	18.97	2.19	1.13	3.90	1.05E-03	1.60E-02	NA	GL018700:2379941-2431087
XLOC_009566	1.47	3.21	2.19	1.13	3.00	5.00E-05	1.41E-03	NA	14:55555285-55558736
XLOC_022461	5.15	11.28	2.19	1.13	3.00	5.00E-05	1.41E-03	GALNT13	7:92772637-93304931
XLOC_025310	4.01	8.78	2.19	1.13	2.83	5.00E-05	1.41E-03	NA	9:58657827-58675019
XLOC_026704	2.60	5.69	2.19	1.13	2.61	1.00E-04	2.52E-03	ENSOCUG00000012133	AAGW02081976:4112-14539
XLOC_020458	1.25	2.73	2.19	1.13	2.89	5.00E-05	1.41E-03	FERMT1	4:12489663-12544292
XLOC_021882	27.53	60.08	2.18	1.13	8.66	1.40E-03	1.98E-02	NA	5:34062318-34062564
XLOC_003476	3.06	6.66	2.18	1.12	2.89	5.00E-05	1.41E-03	LMBRD2	11:57276103-57324282
XLOC_012522	1.30	2.81	2.17	1.12	3.50	5.00E-05	1.41E-03	MAP1A	17:28723902-28744832
XLOC_012111	1.03	2.24	2.17	1.12	2.81	5.00E-05	1.41E-03	TTBK2	17:29315325-29473813
XLOC_034324	11.10	24.02	2.16	1.11	5.18	4.80E-03	4.91E-02	NA	GL018920:411721-412022
XLOC_029957	1.16	2.51	2.16	1.11	2.28	1.50E-03	2.09E-02	NA	GL018741:1924117-1925709
XLOC_021913	0.52	1.12	2.16	1.11	1.75	3.95E-03	4.28E-02	SNX29	6:5391739-5867076
XLOC_035108	0.73	1.57	2.16	1.11	2.01	3.35E-03	3.79E-02	NA	GL018995:40088-41937
XLOC_010179	11.16	24.09	2.16	1.11	3.40	5.00E-05	1.41E-03	TSPAN5	15:51330749-51493789
XLOC_005206	1.36	2.92	2.16	1.11	2.56	2.50E-04	5.26E-03	NA	12:9468045-9470039
XLOC_005449	0.82	1.76	2.15	1.10	2.14	2.85E-03	3.37E-02	NA	12:59566621-59568618
XLOC_001106	14.44	30.99	2.15	1.10	4.24	4.50E-04	8.42E-03	NA	1:36976627-37080521
XLOC_032621	0.61	1.31	2.15	1.10	2.23	3.50E-04	6.91E-03	ENSOCUG00000029570	GL018825:496379-503168
XLOC_033576	51.77	111.03	2.14	1.10	10.88	2.00E-04	4.42E-03	NA	GL018876:20531-20767

Transcriptome Gene ID	Uninfected RK-13 Mean FPKM	T. hominis infected RK-13 Mean FPKM	Fold Change	Log2 Fold Change	Test stat	P value	Q value	Ensembl Gene Name / Gene ID	Gene Locus (Chromosome/scaffold:position)
XLOC_027923	0.90	1.92	2.14	1.10	2.17	2.80E-03	3.32E-02	NA	GL018704:2270060-2272018
XLOC_031201	5.24	11.21	2.14	1.10	2.07	2.00E-03	2.60E-02	ZNF564	GL018776:565954-590008
XLOC_033199	3.02	6.46	2.14	1.10	3.19	5.00E-05	1.41E-03	NA	GL018847:463339-465446
XLOC_028084	34.62	73.96	2.14	1.09	1.94	2.75E-03	3.29E-02	NA	GL018706:1141046-1141620
XLOC_010755	4.57	9.76	2.13	1.09	3.09	1.40E-03	1.98E-02	NA	15:45908480-45909071
XLOC_011004	17.82	37.99	2.13	1.09	2.42	1.00E-04	2.52E-03	LGALS8	16:26248704-26337399
XLOC_010062	3.00	6.40	2.13	1.09	3.36	5.00E-05	1.41E-03	ENSOCUG00000008453	15:13432716-13614513
XLOC_025488	0.83	1.76	2.13	1.09	2.61	5.00E-05	1.41E-03	ALDH1L1	9:5584308-5712102
XLOC_009493	4.49	9.55	2.13	1.09	3.17	1.00E-04	2.52E-03	NA	14:35596351-35597399
XLOC_018184	2.91	6.20	2.13	1.09	3.12	5.00E-05	1.41E-03	NA	3:17897185-17904417
XLOC_008562	6.31	13.43	2.13	1.09	3.63	5.00E-05	1.41E-03	PPM1L	14:55201190-55552777
XLOC_014507	5.29	11.25	2.13	1.09	2.68	5.00E-05	1.41E-03	RABEP1	19:12577160-12818776
XLOC_024857	1.39	2.95	2.12	1.09	2.32	1.35E-03	1.93E-02	NA	8:50996842-50998242
XLOC_028178	2.80	5.94	2.12	1.09	3.03	5.00E-05	1.41E-03	NA	GL018707:1086071-1120385
XLOC_006277	1.42	3.01	2.12	1.08	2.51	1.50E-04	3.53E-03	FRRS1	13:64367355-64424819
XLOC_030534	1.31	2.77	2.12	1.08	2.53	1.50E-04	3.53E-03	NA	GL018757:472239-474430
XLOC_026175	1.27	2.68	2.12	1.08	2.20	3.05E-03	3.54E-02	NA	9:47428944-47430233
XLOC_038233	5.97	12.64	2.12	1.08	2.64	2.50E-04	5.26E-03	NA	X:22795401-22804748
XLOC_038353	1.50	3.16	2.11	1.08	2.40	4.00E-04	7.69E-03	NA	X:49172677-49388553
XLOC_030496	0.82	1.72	2.11	1.08	2.61	5.00E-05	1.41E-03	KIAA2022	GL018757:903067-1093157
XLOC_034019	5.95	12.54	2.11	1.08	3.38	1.25E-03	1.82E-02	NA	GL018899:8252-10351
XLOC_006205	6.96	14.65	2.11	1.07	2.90	5.00E-05	1.41E-03	PHTF1	13:50456551-50511156
XLOC_005074	5.26	11.06	2.10	1.07	3.64	5.00E-05	1.41E-03	VNN2	12:123000300-123021600
XLOC_030231	1.99	4.18	2.10	1.07	2.32	1.00E-04	2.52E-03	TUBAL3	GL018750:1356086-1376689
XLOC_038924	2.05	4.29	2.10	1.07	2.30	4.90E-03	4.98E-02	NA	X:46743929-46744753
XLOC_034053	3.54	7.43	2.10	1.07	2.79	6.50E-04	1.12E-02	NA	GL018899:443131-443881
XLOC_010073	2.00	4.18	2.10	1.07	2.42	1.50E-04	3.53E-03	OTUD4	15:19479717-19524849
XLOC_036843	1.93	4.03	2.09	1.07	2.94	5.00E-05	1.41E-03	ENSOCUG00000029363	GL019370:34833-42746
XLOC_026545	11.17	23.39	2.09	1.07	1.92	1.75E-03	2.35E-02	ENSOCUG00000023353	AAGW02080821:13544-15602
XLOC_012128	7.44	15.57	2.09	1.07	2.62	1.00E-04	2.52E-03	RHOV	17:31200099-31201538
XLOC_033423	4.47	9.35	2.09	1.06	3.05	2.00E-04	4.42E-03	FN3K	GL018866:272548-287307
XLOC_022347	0.78	1.62	2.09	1.06	1.94	1.75E-03	2.35E-02	FGL2	7:38978984-39155699
XLOC_033790	1.21	2.52	2.09	1.06	2.53	1.00E-04	2.52E-03	NA	GL018887:372191-374886
XLOC_030852	0.79	1.65	2.09	1.06	2.08	2.75E-03	3.29E-02	NA	GL018763:359205-361353
XLOC_010252	13.55	28.26	2.09	1.06	3.57	5.00E-05	1.41E-03	CDKL2	15:74745496-74804112
XLOC_018965	39.32	81.87	2.08	1.06	3.47	5.00E-05	1.41E-03	IMPA1	3:97297563-97323830
XLOC_016028	1.61	3.35	2.08	1.06	2.81	5.00E-05	1.41E-03	AAK1	2:116550130-116723840
XLOC_021448	0.84	1.74	2.08	1.06	1.79	3.20E-03	3.67E-02	FTSJD1	5:28254751-28261483
XLOC_025290	2.59	5.38	2.08	1.06	1.67	2.90E-03	3.41E-02	PIEZO2	9:51092602-51195059
XLOC_032808	0.63	1.32	2.08	1.05	2.06	2.30E-03	2.88E-02	NA	GL018830:688586-691415
XLOC_032340	1.84	3.83	2.08	1.05	2.34	2.10E-03	2.71E-02	NA	GL018812:426832-427901
XLOC_028653	2.77	5.74	2.07	1.05	2.83	2.00E-04	4.42E-03	NA	GL018716:238332-239849
XLOC_023028	1.55	3.21	2.07	1.05	2.56	5.00E-05	1.41E-03	GRB14	7:103859664-103986957
XLOC_019985	2.94	6.09	2.07	1.05	2.86	5.00E-05	1.41E-03	KIF16B	4:19567860-19883460
XLOC_021668	3.16	6.53	2.07	1.05	2.59	5.00E-05	1.41E-03	NA	5:34041637-34049032
XLOC_017567	4.12	8.51	2.07	1.05	2.25	1.05E-03	1.60E-02	AREL1	20:30398944-30457175
XLOC_018002	1.14	2.35	2.06	1.05	2.02	4.50E-03	4.70E-02	TMEM120B	21:5918408-5959567
XLOC_014521	0.82	1.69	2.06	1.05	2.72	5.00E-05	1.41E-03	ZZEF1	19:14417633-14530454
XLOC_038168	1.39	2.86	2.06	1.04	2.25	2.50E-04	5.26E-03	TMEM27	X:1478214-1535889
XLOC_014748	0.83	1.71	2.06	1.04	2.04	2.00E-03	2.60E-02	SOCS7	19:39875445-39916169
XLOC_022417	16.94	34.96	2.06	1.04	2.70	5.00E-05	1.41E-03	CCDC93	7:64873681-64980030
XLOC_002729	1.28	2.63	2.06	1.04	1.97	6.50E-04	1.12E-02	HOXA13	10:11914097-11916957
XLOC_011295	32.03	66.05	2.06	1.04	3.78	5.00E-05	1.41E-03	FRMD4A	16:18525431-18862958
XLOC_003386	0.56	1.15	2.06	1.04	1.99	2.80E-03	3.32E-02	ERAP1	11:16484132-16599046
XLOC_027954	1.94	3.99	2.06	1.04	2.30	3.95E-03	4.28E-02	NA	GL018704:6575394-6576365
XLOC_016729	1.19	2.45	2.06	1.04	2.91	5.00E-05	1.41E-03	PLEKHH2	2:142497105-142609212
XLOC_011547	2.87	5.89	2.05	1.04	2.22	2.00E-04	4.42E-03	CFH	16:74224440-74347589
XLOC_018089	2.16	4.44	2.05	1.04	2.66	5.00E-05	1.41E-03	NA	21:8780439-8782136
XLOC_009259	13.29	27.18	2.05	1.03	3.77	5.00E-05	1.41E-03	PHLDB2	14:107223233-107461531
XLOC_002782	34.01	69.52	2.04	1.03	3.08	5.00E-05	1.41E-03	C7orf25	10:25816585-25819836
XLOC_013690	1.22	2.49	2.04	1.03	2.30	1.00E-03	1.55E-02	NA	18:4748126-4752813
XLOC_011003	6.13	12.51	2.04	1.03	3.22	2.25E-03	2.84E-02	ENSOCUG00000025911	16:26236690-26237173
XLOC_005731	76.77	156.25	2.04	1.03	14.20	7.50E-04	1.24E-02	NA	12:101757458-101757657
XLOC_035551	1.64	3.34	2.03	1.02	2.37	7.50E-04	1.24E-02	ENSOCUG00000026493	GL019057:198816-200430
XLOC_032438	21.10	42.91	2.03	1.02	2.52	5.00E-05	1.41E-03	SLC6A8	GL018816:730340-738670
XLOC_012367	9.58	19.45	2.03	1.02	2.08	7.50E-04	1.24E-02	TMEM260	17:75046668-75107508
XLOC_034930	2.69	5.45	2.03	1.02	2.42	4.00E-03	4.31E-02	NA	GL018971:116188-116934
XLOC_014079	1.46	2.96	2.03	1.02	2.13	3.45E-03	3.88E-02	NA	18:15079454-15080717
XLOC_027323	6.06	12.28	2.03	1.02	3.43	5.00E-05	1.41E-03	MEGF9	GL018699:6547454-6658444
XLOC_015895	1.22	2.47	2.02	1.02	2.43	3.00E-04	6.09E-03	ENSOCUG00000006028	2:94929950-94939538
XLOC_031936	11.41	23.08	2.02	1.02	2.29	4.00E-04	7.69E-03	DMTN	GL018798:559624-604230
XLOC_007230	0.90	1.81	2.02	1.02	2.59	5.00E-05	1.41E-03	DNAJC6	13:100963486-101144759
XLOC_020274	79.38	160.43	2.02	1.02	3.54	5.00E-05	1.41E-03	TXNRD1	4:83334802-83462653
XLOC_028728	1.07	2.16	2.02	1.01	1.89	1.70E-03	2.29E-02	ENSOCUG00000025543	GL018717:500024-526185
XLOC_035432	2.83	5.71	2.02	1.01	2.27	1.00E-04	2.52E-03	ENSOCUG00000022101	GL019042:192470-238132
XLOC_022570	1.56	3.14	2.02	1.01	2.97	5.00E-05	1.41E-03	FAM171B	7:127097339-127175277
XLOC_010034	6.66	13.42	2.02	1.01	2.71	5.00E-05	1.41E-03	NAT1	15:3023743-3187729
XLOC_013873	3.80	7.66	2.02	1.01	2.27	5.00E-05	1.41E-03	NA	18:48817301-48824636
XLOC_010043	3.08	6.20	2.01	1.01	2.62	5.00E-05	1.41E-03	CTSO	15:8107002-8140141
XLOC_017901	1.33	2.68	2.01	1.01	2.62	1.00E-04	2.52E-03	NA	21:5199580-5206049
XLOC_004956	1.93	3.88	2.01	1.01	3.20	5.00E-05	1.41E-03	SIM1	12:88173540-88254718
XLOC_002788	22.04	44.28	2.01	1.01	2.33	5.00E-05	1.41E-03	TMEM106B	10:26858435-26886092
XLOC_017051	9.87	19.82	2.01	1.01	3.52	5.00E-05	1.41E-03	NA	2:66157228-66157980
XLOC_013238	7.59	15.24	2.01	1.01	3.30	6.50E-04	1.12E-02	NA	17:60702094-60702653
XLOC_016143	0.93	1.87	2.01	1.00	2.11	4.50E-04	8.42E-03	EIF2AK2	2:149149229-149190877
XLOC_001476	4.92	9.87	2.01	1.00	2.99	5.00E-05	1.41E-03	UVRAG	1:140655864-140979183
XLOC_009191	18.10	36.29	2.00	1.00	2.65	5.00E-05	1.41E-03	PIGX	14:92053704-92084268
XLOC_021396	0.64	1.29	2.00	1.00	1.98	1.30E-03	1.87E-02	LRRC36	5:22920427-22980125
XLOC_013469	7.19	14.41	2.00	1.00	3.07	5.00E-05	1.41E-03	PAPSS2	18:35544452-35631880
XLOC_001104	3.57	7.14	2.00	1.00	2.82	5.00E-05	1.41E-03	SH3GL2	1:36228382-36462226
XLOC_018512	0.82	1.65	2.00	1.00	2.28	2.00E-04	4.42E-03	MATN2	3:113696144-113844332
XLOC_007158	28.11	56.21	2.00	1.00	3.57	5.00E-05	1.41E-03	ENSOCUG00000012502	13:75514220-75565008
XLOC_005056	6.52	13.03	2.00	1.00	3.27	5.00E-05	1.41E-03	ARHGAP18	12:119573158-119747625
XLOC_036202	9.21	18.41	2.00	1.00	2.30	5.00E-05	1.41E-03	ENSOCUG00000023555	GL019156:25540-28753
XLOC_015044	0.95	1.89	2.00	1.00	1.93	1.50E-03	2.09E-02	PIPOX	19:19120640-19135595
XLOC_013492	11.47	22.88	2.00	1.00	2.38	3.00E-04	6.09E-03	PCGF5	18:39214696-39283327
XLOC_035901	2.09	4.16	1.99	1.00	2.52	2.00E-04	4.42E-03	NA	GL019101:98015-99730
XLOC_021735	1.55	3.10	1.99	0.99	2.21	1.80E-03	2.39E-02	NA	5:1642920-1644430
XLOC_007439	3.88	7.72	1.99	0.99	2.25	1.00E-04	2.52E-03	OTUD3	13:133066046-133098422
XLOC_028479	6.34	12.63	1.99	0.99	1.70	4.10E-03	4.39E-02	NA	GL018713:480719-492212
XLOC_021916	0.78	1.56	1.99	0.99	1.91	1.65E-03	2.24E-02	ERCC4	6:7055458-7081512
XLOC_008215	2.06	4.10	1.99	0.99	2.55	2.00E-04	4.42E-03	NA	13:118937681-118939563
XLOC_005764	6.58	13.05	1.98	0.99	3.17	5.00E-05	1.41E-03	NA	12:126995596-126996965
XLOC_037207	2.03	4.03	1.98	0.99	2.23	2.90E-03	3.41E-02	NA	GL019565:33536-34568
XLOC_013837	194.58	385.48	1.98	0.99	5.42	5.00E-05	1.41E-03	ENSOCUG00000024251	18:44406851-44407440
XLOC_024380	7.77	15.35	1.98	0.98	3.43	5.00E-05	1.41E-03	BICD1	8:8898930-9118441
XLOC_026684	3.23	6.37	1.97	0.98	3.05	5.00E-05	1.41E-03	ENSOCUG00000029670	AAGW02081834:7420-15388
XLOC_016011	12.94	25.50	1.97	0.98	2.41	5.00E-05	1.41E-03	PAIP2B	2:115119343-115161151
XLOC_026161	1.13	2.23	1.97	0.98	2.00	3.20E-03	3.67E-02	NA	9:43338168-43339997
XLOC_012757	1.16	2.29	1.97	0.98	2.02	1.30E-03	1.87E-02	KLHL28	17:64339121-64368051
XLOC_014666	13.20	25.98	1.97	0.98	2.58	1.00E-04	2.52E-03	TRIM37	19:29176803-29763354
XLOC_011354	4.14	8.13	1.97	0.98	3.13	5.00E-05	1.41E-03	ENSOCUG00000010372	16:34638353-34715576

Transcriptome Gene ID	Uninfected RK-13 Mean FPKM	T. hominis infected RK-13 Mean FPKM	Fold Change	Log2 Fold Change	Test stat	P value	Q value	Ensembl Gene Name / Gene ID	Gene Locus (Chromosome/scaffold:position)
XLOC_008815	48.99	96.21	1.96	0.97	3.43	5.00E-05	1.41E-03	GBE1	14:135668274-135975127
XLOC_013803	9.15	17.96	1.96	0.97	2.27	5.00E-05	1.41E-03	ANKRD22	18:36745889-36775904
XLOC_021899	1.33	2.62	1.96	0.97	2.70	5.00E-05	1.41E-03	ABAT	6:2684974-2737869
XLOC_027125	3.19	6.26	1.96	0.97	2.49	1.70E-03	2.29E-02	NA	AAGW02083155:6651-7553
XLOC_015758	1.45	2.85	1.96	0.97	2.79	5.00E-05	1.41E-03	PALLD	2:46554581-47011009
XLOC_006952	10.21	20.01	1.96	0.97	2.60	5.00E-05	1.41E-03	SNX27	13:40474714-40560172
XLOC_033547	1.04	2.03	1.96	0.97	1.87	1.90E-03	2.49E-02	ENSOCUG00000022342	GL018873:369504-408335
XLOC_001720	0.42	0.83	1.96	0.97	1.82	2.70E-03	3.25E-02	ELF5	1:173764070-173797132
XLOC_008719	20.27	39.63	1.95	0.97	3.47	5.00E-05	1.41E-03	GOLGB1	14:97244171-97326781
XLOC_023067	9.66	18.85	1.95	0.96	2.93	4.20E-03	4.46E-02	NA	7:114772040-114815153
XLOC_027312	2.21	4.32	1.95	0.96	2.47	5.00E-05	1.41E-03	STOM	GL018699:5817602-5852437
XLOC_011107	87.62	170.85	1.95	0.96	1.92	1.10E-03	1.66E-02	BPNT1	16:52834634-53022886
XLOC_003987	4.84	9.43	1.95	0.96	3.00	5.00E-05	1.41E-03	NA	12:10958682-10963295
XLOC_008697	10.25	19.97	1.95	0.96	1.91	8.00E-04	1.30E-02	ZNF148	14:93672606-93793248
XLOC_016283	72.37	140.98	1.95	0.96	3.29	5.00E-05	1.41E-03	UGDH	2:28788113-28930175
XLOC_016420	1.09	2.12	1.95	0.96	1.74	3.10E-03	3.59E-02	MICU3	2:68785423-68916470
XLOC_000444	2.58	5.03	1.95	0.96	1.93	1.30E-03	1.87E-02	PDGFD	1:112364650-112640550
XLOC_015033	9.31	18.12	1.95	0.96	2.27	4.50E-04	8.42E-03	GOSR1	19:17732837-17783805
XLOC_001135	11.87	23.07	1.94	0.96	2.13	1.05E-03	1.60E-02	CDC37L1	1:49527858-49667886
XLOC_013013	1.12	2.18	1.94	0.96	2.22	6.00E-04	1.06E-02	NA	17:8750785-8753435
XLOC_035392	1.18	2.29	1.94	0.96	2.04	3.40E-03	3.83E-02	NA	GL019036:216790-218616
XLOC_014240	6.26	12.15	1.94	0.96	2.97	2.30E-03	2.88E-02	NA	18:40399820-40400390
XLOC_026004	1.63	3.16	1.94	0.95	2.18	1.80E-03	2.39E-02	NA	9:8101347-8102890
XLOC_020434	1.00	1.94	1.94	0.95	2.01	2.30E-03	2.88E-02	ENSOCUG00000004066	4:10114816-10117990
XLOC_038098	5.09	9.87	1.94	0.95	2.98	5.00E-05	1.41E-03	XIAP	X:98360660-98408443
XLOC_019738	1.26	2.45	1.94	0.95	2.33	2.50E-04	5.26E-03	NA	3:138911118-138914033
XLOC_038333	2.72	5.27	1.94	0.95	2.04	2.55E-03	3.12E-02	ENSOCUG00000001613	X:42688299-42862986
XLOC_005010	18.59	35.96	1.93	0.95	2.59	5.00E-05	1.41E-03	ENSOCUG00000024678	12:102031776-102218900
XLOC_023019	6.99	13.47	1.93	0.95	3.24	5.00E-05	1.41E-03	DPP4	7:101114291-101202606
XLOC_028009	0.48	0.93	1.93	0.95	1.88	1.70E-03	2.29E-02	ATP7B	GL018705:5680100-5786595
XLOC_033926	1.64	3.16	1.93	0.95	2.24	9.50E-04	1.48E-02	NA	GL018891:139667-141539
XLOC_012491	15.21	29.29	1.93	0.95	3.51	5.00E-05	1.41E-03	GALK2	17:22871799-23262132
XLOC_027028	1.20	2.31	1.93	0.94	2.07	1.45E-03	2.04E-02	NA	AAGW02082876:6893-8969
XLOC_009298	11.12	21.38	1.92	0.94	3.95	3.30E-03	3.75E-02	NA	14:120369387-120392914
XLOC_009848	1.32	2.53	1.92	0.94	2.12	1.70E-03	2.29E-02	NA	14:111575956-111577984
XLOC_010616	4.45	8.55	1.92	0.94	2.63	2.25E-03	2.84E-02	ENSOCUG00000024506	15:86219946-86220681
XLOC_012788	14.57	27.97	1.92	0.94	1.69	4.70E-03	4.84E-02	NA	17:71608612-71610143
XLOC_022945	14.83	28.45	1.92	0.94	2.19	1.00E-04	2.52E-03	INSIG2	7:64781938-64806436
XLOC_038456	3.43	6.59	1.92	0.94	2.95	5.00E-05	1.41E-03	BRWD3	X:72399263-72457591
XLOC_036739	1.90	3.65	1.92	0.94	2.28	8.00E-04	1.30E-02	NA	GL019320:35583-37348
XLOC_027121	2.48	4.76	1.92	0.94	2.34	1.85E-03	2.44E-02	NA	AAGW02083155:3046-4319
XLOC_032872	0.63	1.21	1.92	0.94	2.07	8.50E-04	1.36E-02	ZNF699	GL018833:749023-754348
XLOC_030671	22.24	42.63	1.92	0.94	2.50	5.00E-05	1.41E-03	CNPY4	GL018760:80368-86291
XLOC_006049	44.32	84.93	1.92	0.94	2.21	3.00E-04	6.09E-03	RIT1	13:36944747-36956463
XLOC_012232	18.89	36.18	1.92	0.94	3.26	5.00E-05	1.41E-03	ABHD4	17:42879457-42892908
XLOC_035336	1.10	2.11	1.91	0.94	2.23	8.00E-04	1.30E-02	NA	GL019028:30138-33222
XLOC_002642	21.66	41.45	1.91	0.94	3.34	5.00E-05	1.41E-03	SAMD9L	10:35684274-35704736
XLOC_008316	2.25	4.31	1.91	0.94	2.40	4.00E-04	7.69E-03	NA	13:133610475-133612145
XLOC_017589	1.04	1.99	1.91	0.93	1.95	1.15E-03	1.72E-02	RDH12	20:4526960-4542334
XLOC_029870	6.91	13.20	1.91	0.93	2.20	1.00E-04	2.52E-03	ENSOCUG00000029686	GL018740:608175-617626
XLOC_011037	11.07	21.13	1.91	0.93	2.61	5.00E-05	1.41E-03	EGLN1	16:36568632-36623559
XLOC_010347	3.73	7.12	1.91	0.93	2.89	5.00E-05	1.41E-03	HSPA4L	15:103602625-103667535
XLOC_007145	2.29	4.37	1.91	0.93	2.80	5.00E-05	1.41E-03	KIAA1107	13:72265782-72366937
XLOC_029455	14.09	26.83	1.91	0.93	4.01	1.20E-03	1.78E-02	NA	GL018731:6177-10127
XLOC_027160	1.96	3.73	1.90	0.93	2.73	5.00E-05	1.41E-03	NA	AAGW02083264:1197-6228
XLOC_028343	34.44	65.56	1.90	0.93	2.95	5.00E-05	1.41E-03	ENSOCUG00000009337	GL018710:823239-869290
XLOC_022775	20.14	38.30	1.90	0.93	2.87	5.00E-05	1.41E-03	TMEM139	7:8813603-8815964
XLOC_035169	5.77	10.96	1.90	0.93	2.85	2.00E-04	4.42E-03	FOSB	GL019006:121962-124101
XLOC_003183	6.10	11.59	1.90	0.92	1.92	2.80E-03	3.32E-02	FER	11:28315238-28735374
XLOC_031956	2.37	4.50	1.90	0.92	2.30	1.20E-03	1.78E-02	NA	GL018799:790019-791404
XLOC_028908	1.86	3.52	1.89	0.92	2.02	2.85E-03	3.37E-02	NA	GL018720:521515-549820
XLOC_006418	7.08	13.41	1.89	0.92	1.93	1.05E-03	1.60E-02	CYP2J1	13:106785834-106832218
XLOC_022433	1.42	2.69	1.89	0.92	2.16	3.50E-04	6.91E-03	THSD7B	7:74453601-75364651
XLOC_018528	3.76	7.11	1.89	0.92	2.46	1.75E-03	2.35E-02	NA	3:118277324-118279384
XLOC_013692	2.02	3.81	1.89	0.92	2.81	5.00E-05	1.41E-03	ENSOCUG00000029316	18:5311076-5350654
XLOC_013929	7.68	14.53	1.89	0.92	2.41	5.00E-05	1.41E-03	C10orf118	18:61707844-61756565
XLOC_018935	30.10	56.88	1.89	0.92	3.47	5.00E-05	1.41E-03	LACTB2	3:86543703-86657209
XLOC_021135	1.02	1.93	1.89	0.92	1.90	4.70E-03	4.84E-02	NA	4:48309435-48311441
XLOC_004980	1.12	2.10	1.88	0.91	2.25	2.50E-04	5.26E-03	PPIL6	12:97353724-97392637
XLOC_020470	13.60	25.63	1.88	0.91	3.12	1.00E-04	2.52E-03	NA	4:14527198-14551595
XLOC_007189	7.79	14.67	1.88	0.91	2.16	5.00E-05	1.41E-03	DNAJB4	13:87448060-87462218
XLOC_025380	0.84	1.58	1.88	0.91	2.30	3.00E-04	6.09E-03	SETBP1	9:86160788-86539965
XLOC_013689	3.34	6.27	1.88	0.91	2.74	1.50E-04	3.53E-03	NA	18:4594099-4617644
XLOC_010579	125.52	236.02	1.88	0.91	3.76	5.00E-05	1.41E-03	IL8	15:76368975-76371927
XLOC_036253	4.32	8.12	1.88	0.91	2.04	2.00E-04	4.42E-03	KCNAB2	GL019171:9039-91582
XLOC_013300	0.59	1.11	1.88	0.91	1.78	4.90E-03	4.98E-02	NA	17:77569670-77572966
XLOC_010066	0.97	1.82	1.88	0.91	2.58	5.00E-05	1.41E-03	NR3C2	15:16126443-16521206
XLOC_022445	3.02	5.65	1.87	0.90	2.11	4.50E-04	8.42E-03	ACVR2A	7:86489295-86581515
XLOC_038493	3.53	6.60	1.87	0.90	2.00	1.30E-03	1.87E-02	NAP1L3	X:85317519-85319855
XLOC_029379	7.68	14.34	1.87	0.90	3.07	5.00E-05	1.41E-03	ZNF879	GL018730:324515-345570
XLOC_029522	1.21	2.25	1.87	0.90	1.73	2.45E-03	3.02E-02	ENSOCUG00000017633	GL018733:2258714-2300470
XLOC_000257	2.42	4.52	1.87	0.90	2.97	5.00E-05	1.41E-03	VPS13A	1:63590620-63838606
XLOC_006419	15.07	28.10	1.86	0.90	3.06	5.00E-05	1.41E-03	C-JUN	13:107996049-107999057
XLOC_029997	37.76	70.33	1.86	0.90	3.20	5.00E-05	1.41E-03	NA	GL018743:2158453-2165877
XLOC_018520	3.53	6.58	1.86	0.90	2.92	5.00E-05	1.41E-03	VPS13B	3:114744931-115464276
XLOC_004007	6.44	11.99	1.86	0.90	2.79	3.00E-04	6.09E-03	ENSOCUG00000001123	12:12867712-12868602
XLOC_020168	110.95	206.26	1.86	0.89	2.34	5.00E-05	1.41E-03	KCNMB4	4:49389823-49467345
XLOC_007247	5.43	10.10	1.86	0.89	2.41	1.00E-04	2.52E-03	HOOK1	13:106842908-107462117
XLOC_022190	1.62	3.01	1.86	0.89	2.01	4.05E-03	4.35E-02	NA	6:11624564-11626068
XLOC_000072	0.95	1.76	1.86	0.89	1.71	3.95E-03	4.28E-02	ZBTB5	1:16597283-16599998
XLOC_015041	5.59	10.37	1.86	0.89	2.73	5.00E-05	1.41E-03	TAOK1	19:18648467-18815827
XLOC_029955	1.81	3.36	1.85	0.89	2.07	2.90E-03	3.41E-02	NA	GL018741:1921813-1923254
XLOC_033620	30.96	57.36	1.85	0.89	5.89	1.20E-03	1.78E-02	NA	GL018878:422431-422728
XLOC_008780	1.55	2.86	1.85	0.89	2.20	5.00E-05	1.41E-03	SENP7	14:118958511-119149983
XLOC_003998	4.66	8.61	1.85	0.89	2.19	1.00E-04	2.52E-03	ENSOCUG00000004430	12:11758745-11962470
XLOC_003699	1.36	2.51	1.85	0.89	2.02	1.70E-03	2.29E-02	NA	11:29160572-29162697
XLOC_008653	4.60	8.49	1.85	0.89	2.33	1.05E-03	1.60E-02	NA	14:83395446-83401340
XLOC_019065	6.44	11.88	1.85	0.88	2.72	5.00E-05	1.41E-03	ENPP2	3:135388833-135507133
XLOC_010416	5.22	9.64	1.85	0.88	2.84	5.00E-05	1.41E-03	GAB1	15:20959684-21092482
XLOC_000733	2.00	3.69	1.84	0.88	2.68	5.00E-05	1.41E-03	PRRG4	1:172198553-172230840
XLOC_030467	4.91	9.05	1.84	0.88	2.43	5.00E-05	1.41E-03	FAM217B	GL018755:1140614-1146600
XLOC_031022	1.27	2.34	1.84	0.88	2.17	4.00E-04	7.69E-03	PNPLA6	GL018767:883180-901740
XLOC_015141	4.83	8.90	1.84	0.88	2.61	5.00E-05	1.41E-03	PCTP	19:32193826-32221369
XLOC_013807	56.05	103.01	1.84	0.88	3.21	5.00E-05	1.41E-03	LIPA	18:37157992-37198652
XLOC_028376	124.45	228.64	1.84	0.88	14.66	1.30E-03	1.87E-02	NA	GL018710:4147609-4147800
XLOC_026923	1.26	2.31	1.84	0.88	2.08	1.70E-03	2.29E-02	NA	AAGW02082574:3061-5829
XLOC_033095	4.49	8.25	1.84	0.88	2.66	5.00E-05	1.41E-03	NA	GL018844:116469-118330
XLOC_006588	3.42	6.27	1.84	0.88	2.73	5.00E-05	1.41E-03	ECE1	13:131866337-131914801
XLOC_025352	14.21	26.08	1.84	0.88	3.30	5.00E-05	1.41E-03	DSG2	9:72753409-72816308
XLOC_022557	45.58	83.57	1.83	0.87	3.08	5.00E-05	1.41E-03	ENSOCUG00000029255	7:122815790-122832824
XLOC_030283	14.93	27.36	1.83	0.87	2.81	5.00E-05	1.41E-03	WDR20	GL018751:1265557-1323689
XLOC_006298	26.70	48.91	1.83	0.87	2.19	5.00E-05	1.41E-03	GCLM	13:70585864-70613366

Transcriptome Gene ID	Uninfected RK-13 Mean FPKM	T. hominis infected RK-13 Mean FPKM	Fold Change	Log2 Fold Change	Test stat	P value	Q value	Ensembl Gene Name / Gene ID	Gene Locus (Chromosome/scaffold:position)
XLOC_003804	6.85	12.55	1.83	0.87	2.75	3.55E-03	3.95E-02	NA	11:72154156-72154690
XLOC_013599	18.88	34.56	1.83	0.87	2.31	2.50E-04	5.26E-03	SLK	18:51855953-51944092
XLOC_016825	3.48	6.36	1.83	0.87	2.06	5.50E-04	9.84E-03	HS1BP3	2:169635961-169751464
XLOC_024563	17.96	32.80	1.83	0.87	3.10	5.00E-05	1.41E-03	LACC1	8:51138293-51203413
XLOC_032572	11.49	20.97	1.83	0.87	1.99	5.00E-04	9.12E-03	ENSOCUG00000025228	GL018823:92560-113745
XLOC_022210	2.33	4.25	1.82	0.87	2.36	1.50E-04	3.53E-03	NA	6:18100725-18103141
XLOC_006420	2.18	3.97	1.82	0.86	2.09	2.00E-04	4.42E-03	ENSOCUG00000029356	13:108083767-108118001
XLOC_003185	19.59	35.63	1.82	0.86	1.95	6.50E-04	1.12E-02	SLC25A46	11:30441305-30467845
XLOC_003409	18.48	33.59	1.82	0.86	2.32	2.00E-04	4.42E-03	EFNA5	11:26857224-27169236
XLOC_007710	1.49	2.72	1.82	0.86	2.07	1.05E-03	1.60E-02	NA	13:41363867-41366197
XLOC_028928	0.51	0.93	1.82	0.86	1.75	1.95E-03	2.55E-02	ZNF366	GL018720:1052894-1075556
XLOC_008914	2.60	4.73	1.82	0.86	1.63	3.70E-03	4.07E-02	NEK10	14:13807832-14183822
XLOC_006344	19.58	35.53	1.81	0.86	2.43	5.00E-05	1.41E-03	SSX2IP	13:80228991-80282500
XLOC_037830	1.79	3.25	1.81	0.86	2.02	2.80E-03	3.32E-02	USP27X	X:34098748-34100638
XLOC_011986	4.31	7.82	1.81	0.86	2.37	5.00E-05	1.41E-03	DENND4A	17:6526226-6654143
XLOC_013924	2.70	4.90	1.81	0.86	1.82	4.05E-03	4.35E-02	GPAM	18:59823399-59858803
XLOC_019029	11.08	20.06	1.81	0.86	2.23	5.00E-04	9.12E-03	RRM2B	3:117723094-117762990
XLOC_018329	2.77	5.02	1.81	0.86	1.85	2.25E-03	2.84E-02	RANBP17	3:52186052-52553232
XLOC_003402	11.00	19.87	1.81	0.85	2.61	1.00E-04	2.52E-03	NA	11:24003865-24036340
XLOC_014720	1.55	2.80	1.81	0.85	1.86	1.55E-03	2.14E-02	ZNF652	19:38244889-38272604
XLOC_007109	8.78	15.84	1.80	0.85	2.46	5.00E-05	1.41E-03	TRMT13	13:64004099-64023173
XLOC_032134	11.69	21.04	1.80	0.85	2.52	1.00E-04	2.52E-03	ZNF248	GL018805:38899-85663
XLOC_029886	179.02	322.11	1.80	0.85	9.04	5.00E-05	1.41E-03	NA	GL018740:1495503-1495771
XLOC_029059	1.59	2.86	1.80	0.85	2.21	4.50E-04	8.42E-03	LIF	GL018723:3396571-3412864
XLOC_013510	5.95	10.68	1.79	0.84	2.82	5.00E-05	1.41E-03	TBC1D12	18:42166494-42251906
XLOC_027850	461.09	827.42	1.79	0.84	1.79	2.50E-03	3.07E-02	PTP4A2	GL018704:6223435-6251125
XLOC_025299	7.05	12.64	1.79	0.84	2.61	5.00E-05	1.41E-03	NA	9:54578812-54583755
XLOC_031355	10.69	19.16	1.79	0.84	2.95	3.00E-04	6.09E-03	ENSOCUG00000022820	GL018782:643522-645544
XLOC_023133	1.01	1.80	1.79	0.84	1.96	8.00E-04	1.30E-02	ENSOCUG00000009183	7:137467393-137693932
XLOC_002540	9.67	17.32	1.79	0.84	2.92	5.00E-05	1.41E-03	GPNMB	10:8328033-8362824
XLOC_007665	3.95	7.06	1.79	0.84	2.40	8.00E-04	1.30E-02	NA	13:35924538-35925911
XLOC_021385	1.73	3.10	1.79	0.84	2.00	3.15E-03	3.63E-02	CES3	5:22600078-22612249
XLOC_032441	0.97	1.72	1.78	0.84	1.84	2.10E-03	2.71E-02	ATP2B3	GL018816:828935-848040
XLOC_016145	7.44	13.27	1.78	0.84	2.05	6.50E-04	1.12E-02	STRN	2:149407338-149489129
XLOC_005901	18.04	32.19	1.78	0.83	2.68	5.00E-05	1.41E-03	GALNT11	13:13412710-13472087
XLOC_012059	3.95	7.04	1.78	0.83	2.62	5.00E-05	1.41E-03	MYO5A	17:20043529-20260920
XLOC_036949	4.70	8.38	1.78	0.83	2.43	1.05E-03	1.60E-02	NA	GL019412:217-1347
XLOC_001091	13.21	23.53	1.78	0.83	2.55	5.00E-05	1.41E-03	KLHL9	1:32385246-32395554
XLOC_010246	1.39	2.47	1.78	0.83	1.85	1.60E-03	2.20E-02	CXCL9	15:74394601-74401482
XLOC_027606	1.84	3.26	1.78	0.83	2.05	4.00E-04	7.69E-03	TMEM144	GL018701:763611-807868
XLOC_003513	24.00	42.64	1.78	0.83	2.29	2.00E-04	4.42E-03	ENSOCUG00000011406	11:69141490-69152579
XLOC_014612	26.56	47.13	1.77	0.83	2.49	5.00E-05	1.41E-03	SUZ12	19:21489676-21606093
XLOC_036024	8.06	14.31	1.77	0.83	2.44	5.00E-05	1.41E-03	NA	GL019117:46201-63359
XLOC_000036	4.64	8.24	1.77	0.83	2.92	5.00E-05	1.41E-03	ABCA1	1:8128275-8266414
XLOC_025409	2.34	4.15	1.77	0.83	2.58	5.00E-05	1.41E-03	WDR7	9:97249812-97606816
XLOC_013747	59.87	106.21	1.77	0.83	2.76	5.00E-05	1.41E-03	C10orf35	18:17218189-17219950
XLOC_014020	6.54	11.59	1.77	0.83	2.88	5.00E-05	1.41E-03	NA	18:5074065-5078359
XLOC_022505	11.24	19.92	1.77	0.83	2.46	5.00E-05	1.41E-03	UBR3	7:109610784-109797833
XLOC_024568	3.76	6.67	1.77	0.83	2.81	5.00E-05	1.41E-03	AKAP11	8:52749480-52792348
XLOC_023185	144.65	256.08	1.77	0.82	2.89	5.00E-05	1.41E-03	IDH1	7:149124019-149153481
XLOC_001376	1.06	1.88	1.77	0.82	1.88	1.45E-03	2.04E-02	ZC3H12C	1:106331417-106376392
XLOC_006115	2.59	4.58	1.77	0.82	2.35	2.00E-04	4.42E-03	SELENBP1	13:40811373-40821635
XLOC_036555	2.29	4.04	1.77	0.82	2.00	4.70E-03	4.84E-02	NA	GL019259:1-1353
XLOC_033041	2.76	4.88	1.77	0.82	1.76	2.55E-03	3.12E-02	FOXJ1	GL018843:539110-541883
XLOC_012715	22.32	39.47	1.77	0.82	1.89	3.45E-03	3.88E-02	STRN3	17:50782495-50939815
XLOC_038972	2.44	4.30	1.77	0.82	2.23	4.00E-04	7.69E-03	NA	X:53392586-53394872
XLOC_018196	2.60	4.58	1.77	0.82	1.94	8.00E-04	1.30E-02	REEP2	3:20719169-20725700
XLOC_029344	7.93	14.01	1.77	0.82	2.23	1.00E-04	2.52E-03	DNAJC28	GL018729:307174-310393
XLOC_006430	24.59	43.41	1.77	0.82	2.91	5.00E-05	1.41E-03	PPAP2B	13:110415993-110497437
XLOC_007226	2.55	4.50	1.77	0.82	2.50	5.00E-05	1.41E-03	PDE4B	13:99883784-99930147
XLOC_009205	2.65	4.68	1.76	0.82	2.68	5.00E-05	1.41E-03	PARP14	14:96395560-96446674
XLOC_031959	3.42	6.03	1.76	0.82	2.30	6.50E-04	1.12E-02	NA	GL018799:830482-832145
XLOC_013428	10.23	18.03	1.76	0.82	1.97	9.50E-04	1.48E-02	RUFY2	18:18259082-18302423
XLOC_013127	2.67	4.70	1.76	0.82	2.42	1.50E-04	3.53E-03	NA	17:37920980-37924286
XLOC_015802	17.82	31.34	1.76	0.81	2.86	5.00E-05	1.41E-03	FAM149A	2:63552907-63605447
XLOC_014438	1.89	3.32	1.76	0.81	1.99	7.00E-04	1.18E-02	GAS7	19:9476031-9574843
XLOC_008687	2.73	4.81	1.76	0.81	2.13	2.50E-04	5.26E-03	TNK2	14:92681252-92720012
XLOC_003249	5.14	9.03	1.76	0.81	2.16	2.00E-04	4.42E-03	C5orf51	11:62789985-62806989
XLOC_001498	42.92	75.38	1.76	0.81	3.56	5.00E-05	1.41E-03	ENSOCUG00000024033	1:142869960-142870766
XLOC_013590	6.46	11.35	1.76	0.81	2.24	2.00E-04	4.42E-03	ENSOCUG00000021890	18:50711257-50782852
XLOC_015318	0.53	0.93	1.76	0.81	1.71	4.05E-03	4.35E-02	ADAM11	19:45538983-45557160
XLOC_010258	17.13	30.06	1.75	0.81	2.78	5.00E-05	1.41E-03	NA	15:76878904-76954807
XLOC_039073	1.54	2.70	1.75	0.81	1.92	4.65E-03	4.81E-02	NA	X:78929695-78931756
XLOC_033681	2.31	4.05	1.75	0.81	2.24	1.00E-04	2.52E-03	ENSOCUG00000029290	GL018880:359334-387392
XLOC_018699	1.23	2.16	1.75	0.81	1.76	3.40E-03	3.83E-02	SLC23A1	3:21621080-21631302
XLOC_003488	34.14	59.83	1.75	0.81	2.96	5.00E-05	1.41E-03	DAB2	11:60401298-60465144
XLOC_026390	7.88	13.81	1.75	0.81	2.67	5.00E-05	1.41E-03	ENSOCUG00000026453	AAGW02076170:121141-122516
XLOC_010998	1.59	2.78	1.75	0.81	1.89	1.35E-03	1.93E-02	CHML	16:25764791-25768964
XLOC_028826	4.14	7.25	1.75	0.81	2.82	5.00E-05	1.41E-03	ZHX3	GL018718:578631-647961
XLOC_010125	1.49	2.61	1.75	0.81	2.13	6.00E-04	1.06E-02	PITX2	15:38870886-38880690
XLOC_015338	57.32	100.23	1.75	0.81	3.03	5.00E-05	1.41E-03	CCDC47	19:48596499-48619960
XLOC_000765	35.06	61.30	1.75	0.81	4.10	2.00E-04	4.42E-03	NA	1:182985772-182988104
XLOC_022865	6.30	11.01	1.75	0.81	2.49	2.50E-03	3.07E-02	NA	7:36888681-36889595
XLOC_018279	0.51	0.89	1.75	0.80	1.69	4.35E-03	4.57E-02	ENSOCUG00000015837	3:32805128-32821490
XLOC_018866	27.76	48.47	1.75	0.80	3.96	1.00E-04	2.52E-03	ENSOCUG00000023403	3:64100521-64100950
XLOC_004954	68.04	118.80	1.75	0.80	2.68	1.50E-04	3.53E-03	CCNC	12:87177386-87216587
XLOC_028018	6.90	12.02	1.74	0.80	2.39	4.50E-04	8.42E-03	NA	GL018705:1939799-2059107
XLOC_007038	1.13	1.96	1.74	0.80	1.99	8.50E-04	1.36E-02	MAGI3	13:50514666-50809781
XLOC_001755	1.32	2.31	1.74	0.80	1.75	2.05E-03	2.65E-02	HARBI1	1:185969386-185982671
XLOC_007776	3.83	6.67	1.74	0.80	2.23	2.15E-03	2.76E-02	NA	13:51048985-51050188
XLOC_011300	3.90	6.79	1.74	0.80	2.26	1.00E-04	2.52E-03	ADCK3	16:20468536-20511862
XLOC_038387	6.36	11.05	1.74	0.80	2.56	5.00E-05	1.41E-03	RBM41	X:55704941-55758350
XLOC_010334	5.31	9.22	1.74	0.80	2.55	5.00E-05	1.41E-03	KIAA1109	15:97973697-98198715
XLOC_030808	1.79	3.10	1.73	0.79	2.01	2.05E-03	2.65E-02	NA	GL018763:1314316-1316699
XLOC_025930	4.83	8.36	1.73	0.79	2.65	5.00E-05	1.41E-03	BCL2	9:103402664-103572189
XLOC_008726	16.43	28.40	1.73	0.79	2.88	5.00E-05	1.41E-03	LRRC58	14:98488400-98513003
XLOC_015845	43.55	75.28	1.73	0.79	2.81	5.00E-05	1.41E-03	GSR	2:77025666-77072296
XLOC_018018	4.70	8.13	1.73	0.79	1.76	3.20E-03	3.67E-02	NA	21:7794135-7795767
XLOC_021426	1.52	2.62	1.73	0.79	2.16	2.50E-04	5.26E-03	NFAT5	5:24980880-25125785
XLOC_008733	17.68	30.52	1.73	0.79	2.19	2.00E-04	4.42E-03	B4GALT4	14:99529442-99571143
XLOC_024019	48.06	82.90	1.73	0.79	2.25	1.50E-04	3.53E-03	TWF1	8:2511396-2524345
XLOC_034388	2.48	4.28	1.73	0.79	2.36	1.00E-04	2.52E-03	NA	GL018926:92251-98352
XLOC_000686	26.66	45.96	1.72	0.79	2.74	5.00E-05	1.41E-03	USP47	1:153589541-153704833
XLOC_018910	7.65	13.18	1.72	0.79	2.66	1.00E-04	2.52E-03	GGH	3:78802066-78831793
XLOC_004148	3.60	6.20	1.72	0.79	2.42	5.00E-05	1.41E-03	UBR2	12:32130557-32250068
XLOC_008770	69.49	119.73	1.72	0.78	2.05	5.00E-04	9.12E-03	ENSOCUG00000003966	14:111914913-111977506
XLOC_037270	2.38	4.09	1.72	0.78	1.94	3.65E-03	4.03E-02	NA	GL019605:101-1637
XLOC_010257	1.20	2.06	1.72	0.78	2.13	8.00E-04	1.30E-02	RASSF6	15:76472819-76526900
XLOC_024440	1.80	3.09	1.72	0.78	1.98	3.50E-04	6.91E-03	CREBL2	8:27090961-27118298
XLOC_034864	39.53	67.92	1.72	0.78	2.54	5.00E-05	1.41E-03	PIK3AP1	GL018967:52671-116708
XLOC_001144	3.27	5.62	1.72	0.78	2.08	2.70E-03	3.25E-02	ENSOCUG00000023438	1:52983081-52984269
XLOC_022554	7.15	12.29	1.72	0.78	2.64	5.00E-05	1.41E-03	SSFA2	7:121974741-122016388

Transcriptome Gene ID	Uninfected RK-13 Mean FPKM	T. hominis infected RK-13 Mean FPKM	Fold Change	Log2 Fold Change	Test stat	P value	Q value	Ensembl Gene Name / Gene ID	Gene Locus (Chromosome/scaffold:position)
XLOC_005207	3.48	5.98	1.72	0.78	2.49	1.00E-04	2.52E-03	NA	12:9470132-9474197
XLOC_023052	36.09	61.92	1.72	0.78	1.99	5.50E-04	9.84E-03	TLK1	7:110680003-110827197
XLOC_027209	2.97	5.09	1.71	0.78	2.05	2.50E-03	3.07E-02	ENSOCUG00000011698	AAGW02083514:20-6374
XLOC_038604	3.71	6.35	1.71	0.78	2.41	5.00E-05	1.41E-03	ARHGEF6	X:111234686-111369675
XLOC_015939	1.11	1.91	1.71	0.78	1.83	2.40E-03	2.97E-02	EIF2AK3	2:99052912-99118142
XLOC_012021	4.21	7.22	1.71	0.78	1.81	2.30E-03	2.88E-02	VPS13C	17:10208066-10410049
XLOC_008835	6.25	10.69	1.71	0.78	2.46	3.00E-04	6.09E-03	NA	14:146999015-147003517
XLOC_002615	17.83	30.51	1.71	0.77	2.32	1.75E-03	2.35E-02	NDUFA4	10:28056470-28063461
XLOC_011999	0.70	1.19	1.71	0.77	1.83	3.50E-03	3.92E-02	PIF1	17:7440503-7450112
XLOC_017864	7.03	12.03	1.71	0.77	2.37	1.00E-04	2.52E-03	TCN2	21:3176606-3189733
XLOC_008710	6.04	10.31	1.71	0.77	2.33	5.00E-05	1.41E-03	PARP9	14:96519375-96551683
XLOC_031957	1.52	2.60	1.71	0.77	2.01	1.65E-03	2.24E-02	NA	GL018799:804887-808544
XLOC_014585	9.29	15.88	1.71	0.77	2.69	5.00E-05	1.41E-03	MYO18A	19:19007348-19104605
XLOC_008520	5.37	9.18	1.71	0.77	1.64	4.30E-03	4.54E-02	AADACL2	14:45744125-45785470
XLOC_025237	2.36	4.03	1.71	0.77	1.87	9.00E-04	1.42E-02	PXK	9:25116770-25212206
XLOC_017793	25.21	43.00	1.71	0.77	3.85	1.00E-03	1.55E-02	NA	20:12898307-12898705
XLOC_025730	12.10	20.63	1.70	0.77	2.57	5.00E-05	1.41E-03	TMF1	9:36424691-36461072
XLOC_022624	2.10	3.58	1.70	0.77	1.88	1.05E-03	1.60E-02	CARF	7:143576976-143641541
XLOC_016438	74.71	127.27	1.70	0.77	2.18	8.00E-04	1.30E-02	DCTN6	2:77560398-77581076
XLOC_038424	22.03	37.50	1.70	0.77	2.30	2.80E-03	3.32E-02	KLHL13	X:66534197-66723536
XLOC_001322	11.08	18.87	1.70	0.77	2.85	5.00E-05	1.41E-03	UBASH3B	1:95256941-95404398
XLOC_025243	6.72	11.44	1.70	0.77	2.71	5.00E-05	1.41E-03	PTPRG	9:28871173-29192733
XLOC_024526	9.12	15.51	1.70	0.77	2.25	1.00E-04	2.52E-03	CDK8	8:38814503-38959248
XLOC_007114	2.31	3.93	1.70	0.77	2.28	3.50E-04	6.91E-03	PALMD	13:64434140-64505444
XLOC_001472	3.01	5.12	1.70	0.77	1.98	2.50E-04	5.26E-03	ACER3	1:139900942-140062568
XLOC_025209	4.14	7.03	1.70	0.76	1.89	7.50E-04	1.24E-02	PHF7	9:19485838-19499443
XLOC_012010	2.63	4.46	1.70	0.76	1.97	7.00E-04	1.18E-02	DAPK2	17:8200052-8320781
XLOC_034318	1.43	2.42	1.70	0.76	1.91	2.55E-03	3.12E-02	ENSOCUG00000017750	GL018920:163066-178732
XLOC_026672	4.12	6.99	1.70	0.76	2.25	1.20E-03	1.78E-02	NA	AAGW02081749:10291-11977
XLOC_005553	6.62	11.22	1.69	0.76	2.34	4.75E-03	4.87E-02	NA	12:71270638-71271331
XLOC_029526	1.43	2.42	1.69	0.76	1.69	3.85E-03	4.21E-02	SOX6	GL018733:60436-700128
XLOC_009463	1.99	3.37	1.69	0.76	1.96	2.85E-03	3.37E-02	NA	14:20757063-20759254
XLOC_021489	3.46	5.86	1.69	0.76	1.88	1.15E-03	1.72E-02	OSGIN1	5:37974505-37983991
XLOC_028524	131.55	222.59	1.69	0.76	3.63	5.00E-05	1.41E-03	NA	GL018714:2619-4132
XLOC_008821	1.20	2.02	1.69	0.76	1.76	1.80E-03	2.39E-02	RBM11	14:142004497-142025226
XLOC_004254	7.91	13.36	1.69	0.76	2.56	5.00E-05	1.41E-03	ENSOCUG00000006338	12:60271199-60287374
XLOC_031221	1.05	1.78	1.69	0.76	1.99	1.25E-03	1.82E-02	CALR3	GL018776:960259-979809
XLOC_023113	17.82	30.10	1.69	0.76	2.29	1.00E-04	2.52E-03	HIBCH	7:130592371-130701828
XLOC_004006	46.76	78.99	1.69	0.76	2.65	5.00E-05	1.41E-03	DCDC2	12:12614288-12793302
XLOC_002798	38.65	65.28	1.69	0.76	2.62	5.00E-05	1.41E-03	ENSOCUG00000000464	10:31074324-31076551
XLOC_012259	22.00	37.17	1.69	0.76	2.56	5.00E-05	1.41E-03	DCAF11	17:44166761-44175207
XLOC_018975	8.62	14.56	1.69	0.76	1.76	2.20E-03	2.80E-02	RMDN1	3:101929510-101964390
XLOC_028008	6.77	11.42	1.69	0.75	2.21	2.00E-04	4.42E-03	INTS6	GL018705:5106644-5229077
XLOC_000764	32.68	55.11	1.69	0.75	3.56	3.00E-04	6.09E-03	NA	1:182975785-182985337
XLOC_019609	4.78	8.06	1.69	0.75	2.18	2.35E-03	2.93E-02	NA	3:99585786-99586900
XLOC_013913	5.65	9.52	1.69	0.75	1.91	1.95E-03	2.55E-02	WDR96	18:52060541-52172272
XLOC_016071	29.02	48.88	1.68	0.75	2.73	5.00E-05	1.41E-03	EFEMP1	2:130178306-130244873
XLOC_018336	1.01	1.71	1.68	0.75	1.65	3.75E-03	4.12E-02	NEURL1B	3:53731738-53765648
XLOC_024816	616.19	1036.39	1.68	0.75	16.31	5.00E-05	1.41E-03	NA	8:34889349-34889547
XLOC_005027	1.19	2.00	1.68	0.75	2.15	2.00E-04	4.42E-03	CEP85L	12:107443755-107612783
XLOC_037935	2.32	3.90	1.68	0.75	2.31	2.00E-04	4.42E-03	TBC1D8B	X:55377243-55463417
XLOC_019997	11.52	19.36	1.68	0.75	2.57	5.00E-05	1.41E-03	JAG1	4:25555795-25596254
XLOC_016002	62.11	104.35	1.68	0.75	1.94	1.15E-03	1.72E-02	TPRKB	2:112771063-112782962
XLOC_011510	6.99	11.74	1.68	0.75	1.89	9.50E-04	1.48E-02	MYOG	16:68670261-68682369
XLOC_022630	5.00	8.40	1.68	0.75	2.10	1.65E-03	2.24E-02	NA	7:144231456-144263427
XLOC_014915	11.15	18.73	1.68	0.75	1.61	4.75E-03	4.87E-02	COX10	19:5586727-5734821
XLOC_033986	4.14	6.95	1.68	0.75	2.46	1.00E-04	2.52E-03	NA	GL018895:478498-483188
XLOC_031975	1.74	2.92	1.68	0.75	2.13	6.50E-04	1.12E-02	NA	GL018799:1096882-1102170
XLOC_003765	3.13	5.24	1.68	0.74	2.36	1.00E-04	2.52E-03	NA	11:56372466-56377178
XLOC_015630	2.91	4.88	1.68	0.74	2.30	5.00E-05	1.41E-03	CPEB2	2:5510722-5577662
XLOC_027543	59.04	98.84	1.67	0.74	3.46	5.00E-05	1.41E-03	NA	GL018700:792356-792965
XLOC_007177	3.18	5.32	1.67	0.74	1.79	3.30E-03	3.75E-02	DNAJB8	13:80610509-80669269
XLOC_014003	3.45	5.77	1.67	0.74	2.11	1.60E-03	2.20E-02	NA	18:4592299-4594005
XLOC_013863	29.49	49.29	1.67	0.74	2.31	5.00E-05	1.41E-03	ERLIN1	18:48086098-48127058
XLOC_018508	9.60	16.03	1.67	0.74	2.38	5.00E-05	1.41E-03	SDC2	3:112249388-112374232
XLOC_031381	8.84	14.74	1.67	0.74	2.05	6.00E-04	1.06E-02	TMLHE	GL018783:351324-462045
XLOC_015816	69.91	116.53	1.67	0.74	2.46	5.00E-05	1.41E-03	ASAH1	2:67538460-67574274
XLOC_029404	1.80	3.00	1.67	0.74	2.05	7.00E-04	1.18E-02	NA	GL018730:559845-563771
XLOC_003142	15.78	26.28	1.67	0.74	2.50	5.00E-04	9.12E-03	XRCC4	11:3308265-3650155
XLOC_034326	426.34	709.53	1.66	0.73	4.00	1.00E-04	2.52E-03	ENSOCUG00000026860	GL018921:256791-257312
XLOC_009839	1.88	3.12	1.66	0.73	1.88	2.60E-03	3.17E-02	NA	14:108071615-108074007
XLOC_031366	9.20	15.29	1.66	0.73	2.45	5.00E-05	1.41E-03	ENSOCUG00000008383	GL018782:604522-624896
XLOC_029357	15.50	25.74	1.66	0.73	2.95	2.55E-03	3.12E-02	NA	GL018729:492584-493091
XLOC_010247	20.14	33.39	1.66	0.73	2.23	2.50E-04	5.26E-03	SDAD1	15:74422871-74454053
XLOC_021761	7.50	12.41	1.66	0.73	2.51	5.00E-05	1.41E-03	NA	5:9470452-9474041
XLOC_008769	43.91	72.61	1.65	0.73	2.81	5.00E-05	1.41E-03	IFT57	14:111770327-111837564
XLOC_000989	5.15	8.51	1.65	0.73	2.19	1.25E-03	1.82E-02	NIPSNAP3A	1:8272814-8287523
XLOC_004416	10.62	17.55	1.65	0.72	2.52	5.00E-05	1.41E-03	HINT3	12:115431347-115461129
XLOC_025994	287.56	474.99	1.65	0.72	9.98	2.50E-04	5.26E-03	NA	9:7579118-7579355
XLOC_004846	30.00	49.55	1.65	0.72	2.38	5.00E-05	1.41E-03	ELOVL5	12:43007929-43092060
XLOC_010251	68.80	113.51	1.65	0.72	2.00	8.00E-04	1.30E-02	G3BP2	15:74699148-74732510
XLOC_015731	1.65	2.73	1.65	0.72	2.28	1.00E-04	2.52E-03	KIF13B	2:40235654-40430464
XLOC_004184	2.14	3.53	1.65	0.72	2.01	7.50E-04	1.24E-02	ENPP4	12:35356000-35397084
XLOC_016014	2.19	3.62	1.65	0.72	1.67	4.75E-03	4.87E-02	CD207	2:115326305-115352331
XLOC_035124	2.08	3.44	1.65	0.72	1.94	2.45E-03	3.02E-02	NA	GL018997:343604-346369
XLOC_007157	5.36	8.83	1.65	0.72	1.78	3.50E-03	3.92E-02	ENSOCUG00000003764	13:75163777-75512122
XLOC_010750	6.45	10.62	1.65	0.72	2.15	3.80E-03	4.17E-02	NA	15:40002647-40003607
XLOC_021424	6.48	10.66	1.65	0.72	1.99	3.25E-03	3.71E-02	NIP7	5:24738105-24746707
XLOC_029748	3.14	5.16	1.64	0.72	2.19	2.00E-04	4.42E-03	ARNT2	GL018737:2128618-2275588
XLOC_000202	38.25	62.86	1.64	0.72	2.61	5.00E-05	1.41E-03	ERMP1	1:48315068-48564939
XLOC_006271	19.27	31.66	1.64	0.72	2.07	7.50E-04	1.24E-02	EXTL2	13:63282867-63308152
XLOC_007287	39.16	64.31	1.64	0.72	1.72	2.65E-03	3.21E-02	OSBPL9	13:114840365-115123570
XLOC_034756	1.14	1.86	1.64	0.72	1.85	2.75E-03	3.29E-02	NA	GL018959:86762-91474
XLOC_004612	35.98	59.08	1.64	0.72	2.17	2.00E-04	4.42E-03	MRS2	12:12491906-12586156
XLOC_024020	2.17	3.56	1.64	0.72	1.93	1.10E-03	1.66E-02	PUS7L	8:2553100-2584957
XLOC_030054	6.52	10.71	1.64	0.71	1.95	5.50E-04	9.84E-03	CTSH	GL018746:337816-354620
XLOC_000054	9.12	14.96	1.64	0.71	2.01	6.50E-04	1.12E-02	ALG2	1:14003195-14006600
XLOC_012070	5.67	9.31	1.64	0.71	2.45	5.00E-05	1.41E-03	TRPM7	17:21812586-21926225
XLOC_008689	31.77	52.07	1.64	0.71	1.67	2.65E-03	3.21E-02	FYTTD1	14:92959804-92993359
XLOC_015365	13.76	22.55	1.64	0.71	2.42	5.00E-05	1.41E-03	ABCA5	19:53047081-53140211
XLOC_021547	7.48	12.25	1.64	0.71	1.82	1.40E-03	1.98E-02	ENSOCUG00000006737	5:12027797-12052517
XLOC_028382	9.64	15.77	1.64	0.71	2.25	2.00E-04	4.42E-03	TPMT	GL018711:1959779-1980034
XLOC_036294	2.87	4.69	1.64	0.71	2.17	2.00E-04	4.42E-03	NA	GL019185:9113-13500
XLOC_016086	1.82	2.97	1.63	0.71	1.87	1.15E-03	1.72E-02	GPR75	2:132368582-132372532
XLOC_017862	4.86	7.94	1.63	0.71	1.78	1.75E-03	2.35E-02	ENSOCUG00000002313	21:3011637-3034476
XLOC_003526	2.73	4.46	1.63	0.71	1.72	2.30E-03	2.88E-02	SLC38A9	11:71522008-71606357
XLOC_023610	448.19	731.91	1.63	0.71	2.85	2.50E-04	5.26E-03	NA	7:90331254-90332220
XLOC_008855	1.52	2.48	1.63	0.71	1.61	4.85E-03	4.95E-02	BACH1	14:158704516-158847226
XLOC_031885	3.77	6.16	1.63	0.71	1.73	3.00E-03	3.49E-02	GRK4	GL018796:895711-961082
XLOC_036693	2.34	3.82	1.63	0.71	1.69	3.95E-03	4.28E-02	CATSPERD	GL019306:845-31307
XLOC_004899	13.09	21.36	1.63	0.71	2.23	2.50E-04	5.26E-03	ME1	12:70185999-70432998
XLOC_038928	30.22	49.29	1.63	0.71	3.26	1.20E-03	1.78E-02	NA	X:47712709-47713240

Transcriptome Gene ID	Uninfected RK-13 Mean FPKM	T. hominis infected RK-13 Mean FPKM	Fold Change	Log2 Fold Change	Test stat	P value	Q value	Ensembl Gene Name / Gene ID	Gene Locus (Chromosome/scaffold:position)
XLOC_015908	1.68	2.74	1.63	0.71	1.96	1.70E-03	2.29E-02	MERTK	2:96884738-96984978
XLOC_015681	16.87	27.50	1.63	0.70	2.65	5.00E-05	1.41E-03	KLHL5	2:28452796-28486529
XLOC_024640	11.51	18.76	1.63	0.70	2.09	7.50E-04	1.24E-02	DOCK9	8:100526205-100725132
XLOC_000029	20.87	33.98	1.63	0.70	2.27	2.00E-04	4.42E-03	CTNNAL1	1:4154041-4222660
XLOC_027290	6.68	10.88	1.63	0.70	1.94	1.05E-03	1.60E-02	GOLGA1	GL018699:2387853-2456585
XLOC_000440	13.34	21.71	1.63	0.70	2.41	1.00E-04	2.52E-03	MSANTD4	1:110652025-110664893
XLOC_013730	3.02	4.91	1.63	0.70	1.94	6.50E-04	1.12E-02	NUDT13	18:14291350-14313728
XLOC_029371	35.93	58.43	1.63	0.70	2.51	5.00E-05	1.41E-03	RUFY1	GL018730:1036646-1092564
XLOC_003492	19.87	32.31	1.63	0.70	1.83	1.55E-03	2.14E-02	PRKAA1	11:61663248-61695400
XLOC_020721	5.09	8.27	1.63	0.70	2.18	1.00E-04	2.52E-03	CEP290	4:67087784-67196398
XLOC_036383	3.86	6.27	1.62	0.70	1.99	2.75E-03	3.29E-02	NA	GL019211:15983-62119
XLOC_013897	97.41	158.22	1.62	0.70	2.37	5.00E-05	1.41E-03	NT5C2	18:51045259-51154603
XLOC_023073	83.28	135.24	1.62	0.70	2.12	9.50E-04	1.48E-02	NFE2L2	7:116890363-117216332
XLOC_021350	26.00	42.21	1.62	0.70	2.75	5.00E-05	1.41E-03	COQ9	5:13584072-13596745
XLOC_028102	4.65	7.55	1.62	0.70	2.27	4.00E-04	7.69E-03	PLEKHA2	GL018706:4436799-4509814
XLOC_008326	1.88	3.06	1.62	0.70	1.84	4.05E-03	4.35E-02	NA	13:136791730-136794411
XLOC_037713	521.75	846.54	1.62	0.70	2.25	1.00E-04	2.52E-03	SAT1	X:9714312-9718085
XLOC_032125	14.53	23.57	1.62	0.70	2.59	2.80E-03	3.32E-02	NA	GL018804:405884-406542
XLOC_037931	11.40	18.48	1.62	0.70	2.15	2.50E-04	5.26E-03	MUM1L1	X:54897307-54906052
XLOC_022587	9.23	14.97	1.62	0.70	2.09	6.00E-04	1.06E-02	SLC39A10	7:136075716-136528449
XLOC_024632	4.90	7.94	1.62	0.70	2.40	1.00E-04	2.52E-03	ABCC4	8:96944296-97213670
XLOC_016131	15.00	24.29	1.62	0.70	1.96	1.05E-03	1.60E-02	SOS1	2:147290463-147379295
XLOC_006309	5.25	8.51	1.62	0.70	2.13	1.50E-03	2.09E-02	ENSOCUG00000021982	13:72231926-72233513
XLOC_031954	2.84	4.60	1.62	0.69	2.12	8.00E-04	1.30E-02	NA	GL018799:445282-449780
XLOC_030858	2.13	3.44	1.62	0.69	1.90	2.00E-03	2.60E-02	NA	GL018763:927058-930013
XLOC_004812	5.50	8.90	1.62	0.69	2.08	3.00E-04	6.09E-03	CYP39A1	12:35903584-35996422
XLOC_015782	4.22	6.82	1.62	0.69	2.41	5.00E-05	1.41E-03	ENSOCUG00000007616	2:59809081-60171034
XLOC_019394	7.75	12.53	1.62	0.69	2.41	1.00E-04	2.52E-03	NA	3:62569830-62572831
XLOC_020793	25.69	41.51	1.62	0.69	2.69	5.00E-05	1.41E-03	HO1	4:86060984-86066691
XLOC_018490	19.23	31.01	1.61	0.69	1.80	1.25E-03	1.82E-02	OTUD6B	3:106705284-106725458
XLOC_020700	11.64	18.77	1.61	0.69	2.45	1.45E-03	2.04E-02	ENSOCUG00000000726	4:55945157-55945967
XLOC_016796	28.01	45.17	1.61	0.69	2.60	4.00E-04	7.69E-03	MAPRE3	2:159023772-159073246
XLOC_009345	19.63	31.66	1.61	0.69	1.98	1.45E-03	2.04E-02	ENSOCUG00000020937,NRIP1	14:142546389-142933853
XLOC_001142	27.68	44.58	1.61	0.69	2.05	4.00E-04	7.69E-03	VLDLR	1:51846740-51891847
XLOC_038757	1.67	2.69	1.61	0.69	1.94	1.75E-03	2.35E-02	NA	X:13262333-13267137
XLOC_013295	2.18	3.51	1.61	0.69	1.96	1.90E-03	2.49E-02	NA	17:75713743-75717708
XLOC_018920	16.70	26.85	1.61	0.69	1.87	1.50E-03	2.09E-02	VCPIP1	3:82496768-82542954
XLOC_030900	3.33	5.35	1.61	0.69	1.96	8.00E-04	1.30E-02	TSC1	GL018764:1450441-1469879
XLOC_018234	24.87	39.96	1.61	0.68	2.42	5.00E-05	1.41E-03	RNF14	3:24004848-24025426
XLOC_004893	11.54	18.55	1.61	0.68	2.38	3.00E-04	6.09E-03	LCA5	12:66360916-66407894
XLOC_032445	11.74	18.85	1.61	0.68	2.52	5.00E-05	1.41E-03	NA	GL018816:2224-6807
XLOC_021479	3.21	5.16	1.61	0.68	1.95	9.00E-04	1.42E-02	GAN	5:35719978-35781821
XLOC_014905	1.98	3.17	1.61	0.68	1.66	4.15E-03	4.42E-02	AKAP10	19:3233957-3313230
XLOC_000987	1.90	3.05	1.60	0.68	1.85	1.25E-03	1.82E-02	FSD1L	1:7503511-7599054
XLOC_012089	4.05	6.49	1.60	0.68	1.88	1.00E-03	1.55E-02	SLC30A4	17:27078652-27114684
XLOC_010566	37.71	60.48	1.60	0.68	2.48	5.00E-05	1.41E-03	USO1	15:74565266-74654373
XLOC_038551	1.92	3.07	1.60	0.68	1.87	1.15E-03	1.72E-02	SMARCA1	X:103841981-103941637
XLOC_005026	14.73	23.55	1.60	0.68	1.92	1.25E-03	1.82E-02	GOPC	12:106516849-106564747
XLOC_020544	1.46	2.34	1.60	0.68	1.94	1.45E-03	2.04E-02	BCDIN3D	4:34012661-34022123
XLOC_010530	4.05	6.48	1.60	0.68	2.39	5.00E-05	1.41E-03	WDFY3	15:64351450-64649539
XLOC_017546	14.15	22.61	1.60	0.68	1.92	2.30E-03	2.88E-02	SPTLC2	20:27802901-27897911
XLOC_024047	1.38	2.21	1.60	0.68	1.70	2.85E-03	3.37E-02	TMTC1	8:10605855-10839057
XLOC_024666	5.54	8.85	1.60	0.68	1.95	1.00E-03	1.55E-02	LIG4	8:109975527-109983218
XLOC_001912	6.69	10.68	1.60	0.67	2.13	3.45E-03	3.88E-02	NA	1:1955835-1956937
XLOC_024724	2.16	3.44	1.60	0.67	1.82	4.65E-03	4.81E-02	NA	8:9784730-9787296
XLOC_008718	7.34	11.71	1.60	0.67	2.30	5.00E-05	1.41E-03	IQCB1	14:97169585-97231505
XLOC_001928	47.63	75.95	1.59	0.67	3.71	2.95E-03	3.44E-02	NA	1:10273511-10273895
XLOC_019215	28.21	44.95	1.59	0.67	2.87	6.00E-04	1.06E-02	NA	3:20832560-20833194
XLOC_012114	5.89	9.38	1.59	0.67	2.26	5.00E-05	1.41E-03	ZNF106	17:29694094-29779497
XLOC_007241	5.89	9.39	1.59	0.67	1.77	2.25E-03	2.84E-02	ATG4C	13:103632869-103731243
XLOC_017704	9.07	14.44	1.59	0.67	1.64	4.90E-03	4.98E-02	PSEN1	20:31805430-31892112
XLOC_017594	9.46	15.06	1.59	0.67	2.03	4.00E-04	7.69E-03	MPP5	20:4951816-5032164
XLOC_009263	6.22	9.90	1.59	0.67	2.18	6.00E-04	1.06E-02	ENSOCUG00000017796	14:108003021-108005195
XLOC_003798	5.30	8.43	1.59	0.67	2.19	3.50E-04	6.91E-03	NA	11:69003008-69006434
XLOC_000470	14.95	23.79	1.59	0.67	1.78	1.50E-03	2.09E-02	CCDC82	1:120397223-120440652
XLOC_021890	1.86	2.96	1.59	0.67	1.86	2.65E-03	3.21E-02	NA	5:35784178-35787877
XLOC_024408	55.30	87.93	1.59	0.67	2.42	5.00E-05	1.41E-03	CMAS	8:18040225-18058985
XLOC_030967	1.33	2.12	1.59	0.67	1.91	8.00E-04	1.30E-02	ENSOCUG00000017339	GL018766:470086-606057
XLOC_016435	8.96	14.25	1.59	0.67	1.93	7.50E-04	1.24E-02	ENSOCUG00000005223	2:76974196-77007658
XLOC_022586	17.97	28.52	1.59	0.67	2.42	5.00E-05	1.41E-03	NABP1	7:132158384-132171195
XLOC_028632	60.48	95.95	1.59	0.67	1.82	1.15E-03	1.72E-02	FAM213A	GL018716:143023-237809
XLOC_029032	16.24	25.76	1.59	0.67	2.32	2.00E-04	4.42E-03	NF2	GL018723:2795413-2886084
XLOC_006336	9.84	15.60	1.59	0.67	1.82	2.00E-03	2.60E-02	BCL10	13:79599403-79618649
XLOC_032324	3.81	6.04	1.59	0.67	2.09	3.00E-04	6.09E-03	CLTCL1	GL018812:770495-880503
XLOC_034041	2.64	4.19	1.59	0.66	1.81	4.35E-03	4.57E-02	NA	GL018899:260408-262506
XLOC_006275	33.21	52.65	1.59	0.66	2.54	4.00E-04	7.69E-03	ENSOCUG00000011973	13:64126473-64200696
XLOC_004311	2.92	4.63	1.58	0.66	2.02	9.00E-04	1.42E-02	FHL5	12:83828019-83884601
XLOC_001512	3.48	5.52	1.58	0.66	1.74	2.20E-03	2.80E-02	ENSOCUG00000000162	1:144262799-144270657
XLOC_023153	10.12	16.04	1.58	0.66	2.45	5.00E-05	1.41E-03	TRAK2	7:142123677-142195035
XLOC_003134	5.46	8.64	1.58	0.66	1.77	2.50E-03	3.07E-02	FAM151B	11:1079143-1112864
XLOC_009017	241.39	382.36	1.58	0.66	2.90	1.50E-04	3.53E-03	ENSOCUG00000024788	14:46854539-46855538
XLOC_006227	3.77	5.97	1.58	0.66	2.14	4.50E-04	8.42E-03	DENND2D	13:52939540-52955080
XLOC_012774	10.38	16.42	1.58	0.66	2.15	1.50E-04	3.53E-03	SOS2	17:69210171-69315634
XLOC_002706	2.88	4.55	1.58	0.66	1.73	2.50E-03	3.07E-02	FAM126A	10:8006947-8093416
XLOC_036501	57.94	91.61	1.58	0.66	3.05	5.00E-05	1.41E-03	ENSOCUG00000026614	GL019248:96097-96983
XLOC_004214	5.15	8.15	1.58	0.66	2.14	6.50E-04	1.12E-02	LRRC1	12:43763512-43815372
XLOC_014704	21.49	33.96	1.58	0.66	1.99	1.15E-03	1.72E-02	SPAG9	19:36691678-36859151
XLOC_015948	167.29	264.38	1.58	0.66	2.13	2.50E-04	5.26E-03	ENSOCUG00000029277	2:99793509-99860680
XLOC_029171	8.28	13.08	1.58	0.66	2.30	5.00E-05	1.41E-03	ARFGEF2	GL018725:2919057-3032821
XLOC_001441	7.94	12.55	1.58	0.66	2.00	3.00E-04	6.09E-03	FOLH1	1:127101259-127166683
XLOC_030219	53.06	83.83	1.58	0.66	2.33	5.00E-05	1.41E-03	PGER4	GL018750:622215-641740
XLOC_011964	5.99	9.46	1.58	0.66	1.95	1.25E-03	1.82E-02	MYO9A	17:576657-668727
XLOC_015380	47.92	75.65	1.58	0.66	2.83	5.00E-05	1.41E-03	NA	19:8737961-8738897
XLOC_018476	7.93	12.50	1.58	0.66	2.02	3.50E-04	6.91E-03	ATP6V0D2	3:101581451-101636320
XLOC_018477	11.68	18.40	1.58	0.66	1.83	1.45E-03	2.04E-02	WWP1	3:101821195-101922504
XLOC_020164	46.59	73.42	1.58	0.66	2.31	5.00E-05	1.41E-03	ENSOCUG00000002977	4:48803766-48840585
XLOC_026919	43.08	67.84	1.57	0.66	2.70	1.00E-04	2.52E-03	NA	AAGW02082567:554-11116
XLOC_032965	5.68	8.94	1.57	0.66	1.64	4.75E-03	4.87E-02	RAB4A	GL018838:187277-231045
XLOC_038413	10.25	16.14	1.57	0.65	2.35	5.00E-05	1.41E-03	AMOT	X:61346625-61417027
XLOC_033357	3.36	5.29	1.57	0.65	1.66	4.00E-03	4.31E-02	ENSOCUG00000029330	GL018859:476186-498059
XLOC_032102	2.14	3.36	1.57	0.65	1.86	3.20E-03	3.67E-02	CHFR	GL018804:770654-814047
XLOC_015943	104.41	164.08	1.57	0.65	1.97	8.50E-04	1.36E-02	KRCC1	2:99496945-99520486
XLOC_028053	1.33	2.08	1.57	0.65	1.70	3.70E-03	4.07E-02	KAT6A	GL018706:1212380-1324322
XLOC_028587	3.73	5.85	1.57	0.65	2.00	8.00E-04	1.30E-02	SLC22A23	GL018715:2243675-2407900
XLOC_019109	34.35	53.86	1.57	0.65	2.35	5.00E-05	1.41E-03	NDRG1	3:148946640-148991702
XLOC_015709	3.38	5.29	1.57	0.65	2.03	6.50E-04	1.12E-02	ATP10D	2:36063632-36176665
XLOC_014249	3.65	5.72	1.57	0.65	2.11	2.50E-04	5.26E-03	NA	18:42151597-42156527
XLOC_008401	12.61	19.74	1.57	0.65	2.31	7.00E-04	1.18E-02	ENSOCUG00000027919	14:5779588-5780753
XLOC_016364	9.65	15.11	1.57	0.65	2.29	5.00E-05	1.41E-03	NEK1	2:47477019-47679163
XLOC_015115	14.50	22.70	1.57	0.65	1.91	9.00E-04	1.42E-02	NA	19:28787067-28803939
XLOC_010518	12.29	19.25	1.57	0.65	2.34	5.00E-05	1.41E-03	PKD2	15:61948934-62134728
XLOC_004793	1.81	2.83	1.56	0.65	1.95	9.50E-04	1.48E-02	ZNF318	12:32783773-32823789

Transcriptome Gene ID	Uninfected RK-13 Mean FPKM	T. hominis infected RK-13 Mean FPKM	Fold Change	Log2 Fold Change	Test stat	P value	Q value	Ensembl Gene Name / Gene ID	Gene Locus (Chromosome/scaffold:position)
XLOC_029263	6.46	10.11	1.56	0.65	1.95	1.30E-03	1.87E-02	MORC3	GL018727:502688-558900
XLOC_006731	4.98	7.79	1.56	0.65	1.86	1.85E-03	2.44E-02	TOR1AIP2	13:6872592-6887893
XLOC_012483	5.32	8.31	1.56	0.64	2.15	1.00E-04	2.52E-03	AP4E1	17:21506024-21593854
XLOC_024554	13.70	21.40	1.56	0.64	1.77	4.25E-03	4.50E-02	SLC25A30	8:49695148-49722692
XLOC_037601	21.33	33.26	1.56	0.64	2.44	4.50E-04	8.42E-03	NA	GL019898:3-6839
XLOC_022614	12.32	19.21	1.56	0.64	2.02	1.10E-03	1.66E-02	STRADB	7:142196366-142411884
XLOC_022294	2.95	4.59	1.56	0.64	1.66	4.45E-03	4.66E-02	ZNF800	7:16929246-16963255
XLOC_020167	92.00	143.13	1.56	0.64	1.77	2.40E-03	2.97E-02	CNOT2	4:49255088-49377759
XLOC_029385	309.65	481.41	1.55	0.64	1.84	2.30E-03	2.88E-02	HNRNPH1	GL018730:1095709-1104837
XLOC_025896	136.26	211.76	1.55	0.64	2.30	5.00E-05	1.41E-03	ACAA2	9:90615950-90650492
XLOC_020314	4.14	6.44	1.55	0.64	1.87	1.35E-03	1.93E-02	CRY1	4:89376414-89471178
XLOC_008987	6.56	10.19	1.55	0.63	2.12	8.00E-04	1.30E-02	ENSOCUG00000026392	14:42429544-42432265
XLOC_038000	4.74	7.36	1.55	0.63	2.18	1.50E-04	3.53E-03	ATP7A	X:69646774-69764638
XLOC_003133	9.02	13.99	1.55	0.63	2.21	1.50E-04	3.53E-03	ZFYVE16	11:1009821-1072091
XLOC_030799	1.66	2.57	1.55	0.63	1.77	2.40E-03	2.97E-02	ZNF134	GL018763:811677-824790
XLOC_035570	11.94	18.52	1.55	0.63	1.94	9.00E-04	1.42E-02	PPP2R2C	GL019060:13237-46868
XLOC_002693	11.98	18.57	1.55	0.63	2.25	1.00E-04	2.52E-03	SNX13	10:3024002-3165574
XLOC_025417	79.85	123.78	1.55	0.63	3.14	1.00E-04	2.52E-03	SEC11C	9:99518473-99533092
XLOC_036274	2.29	3.56	1.55	0.63	1.70	3.10E-03	3.59E-02	NA	GL019181:24961-29123
XLOC_009286	11.30	17.51	1.55	0.63	1.90	1.25E-03	1.82E-02	NXPE3	14:118719165-118768553
XLOC_037772	60.65	93.91	1.55	0.63	1.99	9.50E-04	1.48E-02	USP9X	X:26462330-26597260
XLOC_026272	5.10	7.90	1.55	0.63	2.05	6.50E-04	1.12E-02	NA	9:58827056-58829945
XLOC_027842	40.98	63.42	1.55	0.63	1.82	1.65E-03	2.24E-02	ZBTB8OS	GL018704:5605335-5623749
XLOC_020737	9.56	14.79	1.55	0.63	2.00	7.00E-04	1.18E-02	CCDC41	4:73645292-73799703
XLOC_009171	4.77	7.37	1.55	0.63	2.02	1.25E-03	1.82E-02	MB21D2	14:88637234-88765326
XLOC_010161	2.35	3.63	1.54	0.63	1.86	1.25E-03	1.82E-02	MANBA	15:46851368-46984996
XLOC_008550	9.94	15.34	1.54	0.63	1.80	1.65E-03	2.24E-02	MFSD1	14:53258479-53286332
XLOC_017511	5.56	8.57	1.54	0.62	2.22	2.00E-04	4.42E-03	TRIP11	20:13863895-13944604
XLOC_010937	1.74	2.69	1.54	0.62	1.67	3.40E-03	3.83E-02	MYO3A	16:2045690-2270488
XLOC_024452	35.97	55.41	1.54	0.62	2.05	5.50E-04	9.84E-03	GABARAPL1	8:28630981-28640010
XLOC_016831	2.68	4.13	1.54	0.62	1.83	1.70E-03	2.29E-02	ATAD2B	2:172867228-173087676
XLOC_036824	7.12	10.97	1.54	0.62	2.14	5.50E-04	9.84E-03	NA	GL019362:53129-56280
XLOC_006502	1.90	2.92	1.54	0.62	1.83	3.15E-03	3.63E-02	ZSWIM5	13:121549117-121614580
XLOC_004234	17.08	26.29	1.54	0.62	2.30	1.00E-04	2.52E-03	PHF3	12:50390718-50880949
XLOC_013886	5.39	8.29	1.54	0.62	1.69	3.45E-03	3.88E-02	C10orf76	18:49898475-50111935
XLOC_006710	3.42	5.25	1.54	0.62	2.03	4.00E-04	7.69E-03	SERPINC1	13:1239079-1261312
XLOC_013547	13.88	21.33	1.54	0.62	1.96	7.50E-04	1.24E-02	ANKRD2,HOGA1	18:45754794-45792019
XLOC_006981	5.89	9.05	1.54	0.62	1.81	2.70E-03	3.25E-02	VPS45	13:41894050-41973731
XLOC_006442	46.96	72.15	1.54	0.62	2.09	1.00E-04	2.52E-03	TMEM59	13:112632671-112775536
XLOC_008446	25.53	39.22	1.54	0.62	2.18	1.50E-04	3.53E-03	GOLGA4	14:24069148-24194998
XLOC_027373	25.13	38.59	1.54	0.62	2.19	4.00E-04	7.69E-03	RABGAP1	GL018699:4076812-4266792
XLOC_016665	5.26	8.07	1.53	0.62	1.66	4.20E-03	4.46E-02	UGP2	2:122471492-122537593
XLOC_009243	37.15	57.00	1.53	0.62	2.19	5.00E-05	1.41E-03	ATP6V1A,GRAMD1C	14:105275837-105492082
XLOC_021369	3.93	6.03	1.53	0.62	1.73	2.75E-03	3.29E-02	NA	5:21904188-21908012
XLOC_004075	6.80	10.43	1.53	0.62	1.85	1.90E-03	2.49E-02	BRD2	12:23497494-23503080
XLOC_014526	8.58	13.16	1.53	0.62	1.89	8.50E-04	1.36E-02	C17orf85	19:14664013-14694628
XLOC_029878	3.75	5.75	1.53	0.62	1.89	3.05E-03	3.54E-02	NA	GL018740:585023-587790
XLOC_002560	280.14	429.42	1.53	0.62	2.04	5.00E-04	9.12E-03	TAX1BP1	10:12407933-12498154
XLOC_010943	12.39	18.99	1.53	0.62	1.71	1.90E-03	2.49E-02	ENSOCUG00000025856,EPC1	16:3256424-3332078
XLOC_036354	6.85	10.49	1.53	0.61	2.03	4.50E-04	8.42E-03	KIAA0232	GL019201:62997-111558
XLOC_000145	3.27	5.01	1.53	0.61	1.79	2.25E-03	2.84E-02	C9orf72	1:25947084-25982869
XLOC_011274	5.02	7.69	1.53	0.61	2.06	3.00E-04	6.09E-03	ITIH5	16:11908204-12014636
XLOC_027218	140.06	214.30	1.53	0.61	5.30	9.50E-04	1.48E-02	NA	AAGW02083531:3321-3630
XLOC_020357	7.22	11.04	1.53	0.61	2.17	2.50E-04	5.26E-03	CEP250	4:4285727-4342890
XLOC_022475	4.09	6.24	1.53	0.61	1.73	3.20E-03	3.67E-02	TANK	7:100261256-100339238
XLOC_027981	26.12	39.89	1.53	0.61	1.92	8.00E-04	1.30E-02	VPS36	GL018705:5964358-6000633
XLOC_015889	6.66	10.17	1.53	0.61	2.01	6.50E-04	1.12E-02	ACTR1B	2:94463696-94472779
XLOC_011227	9.33	14.24	1.53	0.61	2.19	5.00E-05	1.41E-03	ASPM	16:74079943-74132538
XLOC_022610	4.90	7.48	1.53	0.61	1.66	4.20E-03	4.46E-02	CFLAR	7:141862536-141910302
XLOC_012380	4.37	6.67	1.53	0.61	1.96	6.50E-04	1.12E-02	ENSOCUG00000006754	17:77775344-78011859
XLOC_017697	20.06	30.59	1.52	0.61	1.89	1.10E-03	1.66E-02	ENSOCUG00000006785	20:31124120-31154085
XLOC_014930	3.14	4.79	1.52	0.61	1.85	1.50E-03	2.09E-02	NDEL1	19:10836622-10882857
XLOC_010432	8.26	12.59	1.52	0.61	2.00	3.40E-03	3.83E-02	ENSOCUG00000002051	15:26535175-26536458
XLOC_016848	37.87	57.72	1.52	0.61	2.48	2.50E-04	5.26E-03	NA	2:4595057-4596411
XLOC_015134	30.17	45.99	1.52	0.61	2.00	4.00E-04	7.69E-03	MSI2	19:30464842-30862371
XLOC_030699	4.31	6.57	1.52	0.61	1.82	4.70E-03	4.84E-02	NA	GL018760:707009-709066
XLOC_018486	13.04	19.87	1.52	0.61	1.69	4.50E-03	4.70E-02	ENSOCUG00000006333	3:105454614-105505383
XLOC_003932	5.03	7.66	1.52	0.61	2.04	7.50E-04	1.24E-02	NA	12:4828736-4855616
XLOC_007281	4.42	6.72	1.52	0.61	2.05	2.50E-04	5.26E-03	ZYG11B	13:113904603-113985346
XLOC_031510	20.93	31.81	1.52	0.60	1.99	5.00E-04	9.12E-03	NA	GL018786:1048636-1050807
XLOC_014778	42.73	64.92	1.52	0.60	2.08	4.50E-04	8.42E-03	ENSOCUG00000021896	19:42151610-42226613
XLOC_014577	13.17	19.99	1.52	0.60	2.22	5.00E-05	1.41E-03	BLMH	19:17964685-18018751
XLOC_001171	2.32	3.52	1.52	0.60	1.75	1.70E-03	2.29E-02	ENSOCUG00000003734	1:61168371-61242200
XLOC_011006	3.28	4.98	1.52	0.60	1.98	4.50E-04	8.42E-03	MTR	16:26513593-26662604
XLOC_036901	5.40	8.19	1.52	0.60	2.00	6.00E-04	1.06E-02	PIGG	GL019396:37680-65193
XLOC_020647	4.86	7.37	1.52	0.60	2.09	4.00E-04	7.69E-03	PPM1H	4:41608748-41904980
XLOC_034380	64.47	97.70	1.52	0.60	3.34	1.55E-03	2.14E-02	NA	GL018925:205000-205457
XLOC_022611	7.76	11.75	1.51	0.60	1.98	4.50E-04	8.42E-03	CASP10	7:141928496-141970801
XLOC_028854	7.10	10.74	1.51	0.60	1.83	1.15E-03	1.72E-02	NHLRC3	GL018719:2017714-2030577
XLOC_008609	16.24	24.58	1.51	0.60	1.73	3.50E-03	3.92E-02	MFN1	14:74793983-74843101
XLOC_015798	4.03	6.10	1.51	0.60	1.99	7.50E-04	1.24E-02	SNX25	2:62675835-62845357
XLOC_006371	22.54	34.03	1.51	0.59	1.68	2.25E-03	2.84E-02	CRYZ	13:90946563-90999565
XLOC_025852	5.23	7.89	1.51	0.59	1.99	9.00E-04	1.42E-02	KLHL14	9:74008963-74110027
XLOC_012671	8.87	13.39	1.51	0.59	1.74	3.50E-03	3.92E-02	PPP1R3E	17:43497795-43503665
XLOC_012466	21.89	33.01	1.51	0.59	2.07	5.50E-04	9.84E-03	CGNL1	17:14920720-15098322
XLOC_038204	3.69	5.56	1.51	0.59	1.85	1.30E-03	1.87E-02	PCYT1B	X:10441366-10538886
XLOC_006421	4.33	6.52	1.51	0.59	1.91	7.50E-04	1.24E-02	ENSOCUG00000013464	13:108118463-108134495
XLOC_000533	64.14	96.62	1.51	0.59	1.81	1.80E-03	2.39E-02	CLNS1A	1:139079463-139102878
XLOC_014560	1.67	2.52	1.51	0.59	1.68	3.55E-03	3.95E-02	SLC43A2	19:16504329-16552799
XLOC_019870	13.60	20.47	1.50	0.59	1.95	9.50E-04	1.48E-02	NDRG3	4:3285524-3363639
XLOC_010751	221.72	333.64	1.50	0.59	4.00	4.50E-04	8.42E-03	NA	15:43098537-43098948
XLOC_006932	12.14	18.27	1.50	0.59	2.06	3.50E-04	6.91E-03	NPR1	13:38785273-38799262
XLOC_014791	20.83	31.34	1.50	0.59	1.93	8.50E-04	1.36E-02	ATP6V0A1	19:43229962-43285129
XLOC_025313	105.14	158.17	1.50	0.59	1.98	5.00E-04	9.12E-03	LPIN2	9:59066943-59135724
XLOC_029840	1.22	1.84	1.50	0.59	1.89	1.25E-03	1.82E-02	VPS13D	GL018739:1611060-1888268
XLOC_021509	5.05	7.59	1.50	0.59	1.65	4.05E-03	4.35E-02	ZNF570	5:1319125-1339544
XLOC_013642	11.56	17.38	1.50	0.59	2.10	9.50E-04	1.48E-02	EMX2	18:64946420-64952478
XLOC_010080	8.47	12.73	1.50	0.59	2.13	3.50E-04	6.91E-03	TBC1D9	15:23844435-23968920
XLOC_003174	45.60	68.53	1.50	0.59	2.74	1.95E-03	2.55E-02	FAM174A	11:20044649-20091121
XLOC_007449	101.72	152.82	1.50	0.59	1.76	3.10E-03	3.59E-02	ENSOCUG00000014599	13:134849946-134924705
XLOC_016295	20.00	30.01	1.50	0.59	1.78	1.95E-03	2.55E-02	GNPDA2	2:33464769-33489327
XLOC_006338	2.41	3.62	1.50	0.59	1.67	4.05E-03	4.35E-02	SYDE2	13:79686698-79743254
XLOC_003564	13.01	19.51	1.50	0.58	1.64	4.65E-03	4.81E-02	ENSOCUG00000008816	11:85405102-85406718
XLOC_028384	3.02	4.54	1.50	0.58	1.64	4.90E-03	4.98E-02	KIF13A	GL018711:2115582-2358343
XLOC_016452	4.49	6.74	1.50	0.58	1.97	3.50E-04	6.91E-03	GCC2	2:84074976-84131842
XLOC_013749	28.11	42.14	1.50	0.58	2.14	1.00E-04	2.52E-03	HK1,HKDC1	18:17372619-17530654
XLOC_036212	15.44	23.14	1.50	0.58	1.81	2.15E-03	2.76E-02	ENSOCUG00000022668	GL019158:36108-38077
XLOC_009087	12.53	18.77	1.50	0.58	2.16	6.00E-04	1.06E-02	NCEH1	14:67603840-67676966
XLOC_032004	7.34	10.99	1.50	0.58	1.77	2.80E-03	3.32E-02	SWT1	GL018801:545960-619021
XLOC_000292	2.89	4.33	1.50	0.58	1.80	2.20E-03	2.80E-02	ERCC6L2	1:74835758-74957232
XLOC_006798	4.61	6.90	1.50	0.58	1.67	2.95E-03	3.44E-02	DCAF6	13:24953788-25050076
XLOC_027837	13.45	20.13	1.50	0.58	1.80	1.40E-03	1.98E-02	RNF19B	GL018704:5333258-5348355

Transcriptome Gene ID	Uninfected RK-13 Mean FPKM	T. hominis infected RK-13 Mean FPKM	Fold Change	Log2 Fold Change	Test stat	P value	Q value	Ensembl Gene Name / Gene ID	Gene Locus (Chromosome/scaffold:position)
XLOC_009160	13.17	19.70	1.50	0.58	2.17	5.00E-04	9.12E-03	LEPREL1	14:85620532-85789266
XLOC_020116	1.68	2.51	1.50	0.58	1.63	4.70E-03	4.84E-02	ERBB3	4:39637900-39661715
XLOC_000039	44.99	67.23	1.49	0.58	1.86	1.15E-03	1.72E-02	SPCS2	1:9273482-9274861
XLOC_002773	99.61	148.87	1.49	0.58	2.02	6.50E-04	1.12E-02	VPS41	10:21832449-22020791
XLOC_000924	25.34	37.82	1.49	0.58	2.06	4.25E-03	4.50E-02	MS4A13	1:193103946-193219028
XLOC_013405	77.09	115.06	1.49	0.58	1.75	1.95E-03	2.55E-02	MICU1	18:14847445-15077649
XLOC_018733	6.52	9.73	1.49	0.58	2.00	4.50E-04	8.42E-03	NR3C1	3:25227137-25330671
XLOC_011465	15.35	22.89	1.49	0.58	1.70	3.20E-03	3.67E-02	RCOR3	16:61520355-61576093
XLOC_002663	8.06	12.01	1.49	0.58	1.92	7.00E-04	1.18E-02	STEAP4	10:40164965-40189629
XLOC_034640	8.13	12.12	1.49	0.58	1.94	2.65E-03	3.21E-02	NA	GL018945:114632-116622
XLOC_006843	961.65	1433.64	1.49	0.58	1.80	2.00E-03	2.60E-02	ENSOCUG00000022552	13:32506243-32508413
XLOC_014248	3.68	5.48	1.49	0.58	1.78	3.50E-03	3.92E-02	NA	18:42148249-42151542
XLOC_015712	10.28	15.31	1.49	0.58	1.77	2.20E-03	2.80E-02	SLAIN2	2:36957485-37046127
XLOC_016211	5.92	8.82	1.49	0.58	1.97	9.00E-04	1.42E-02	NCOA1	2:173705372-173903170
XLOC_010538	6.85	10.19	1.49	0.57	1.84	1.55E-03	2.14E-02	KLHL8	15:66903715-66960325
XLOC_011114	8.03	11.94	1.49	0.57	1.78	2.05E-03	2.65E-02	GPATCH2	16:55628311-55809178
XLOC_023417	5.09	7.57	1.49	0.57	1.80	4.35E-03	4.57E-02	NA	7:43176466-43178889
XLOC_019012	30.64	45.51	1.49	0.57	2.03	5.00E-04	9.12E-03	STK3	3:114199448-114522250
XLOC_025337	4.16	6.18	1.49	0.57	1.86	2.30E-03	2.88E-02	IMPACT	9:65574360-65601989
XLOC_012492	32.63	48.35	1.48	0.57	1.80	1.90E-03	2.49E-02	EID1	17:23456271-23597597
XLOC_011459	100.58	149.02	1.48	0.57	2.12	3.00E-04	6.09E-03	PPP2R5A	16:60648098-60726439
XLOC_035756	327.38	484.78	1.48	0.57	3.80	4.00E-04	7.69E-03	NA	GL019084:180362-198453
XLOC_013501	32.99	48.80	1.48	0.56	1.92	8.50E-04	1.36E-02	EXOC6	18:40502768-40825297
XLOC_018436	22.25	32.90	1.48	0.56	2.07	3.00E-04	6.09E-03	RDH10	3:89061371-89092334
XLOC_024306	86.35	127.58	1.48	0.56	2.57	6.50E-04	1.12E-02	ENSOCUG00000027015	8:91210495-91211338
XLOC_026409	86.17	127.21	1.48	0.56	1.75	2.40E-03	2.97E-02	NA	AAGW02078537:84694-90117
XLOC_027612	4.59	6.77	1.48	0.56	1.84	1.60E-03	2.20E-02	RAPGEF2	GL018701:1726994-2003275
XLOC_037974	42.62	62.88	1.48	0.56	2.08	4.00E-04	7.69E-03	PLS3	X:64068859-64161379
XLOC_037788	59.88	88.32	1.48	0.56	2.44	1.05E-03	1.60E-02	ENSOCUG00000022444	X:31213802-31214834
XLOC_029056	54.66	80.60	1.47	0.56	1.93	6.00E-04	1.06E-02	NIPSNAP1	GL018723:2758686-2778302
XLOC_023035	8.33	12.28	1.47	0.56	1.96	6.50E-04	1.12E-02	TTC21B	7:105289931-105397796
XLOC_016826	27.35	40.30	1.47	0.56	2.05	3.50E-04	6.91E-03	C2orf43	2:169762605-169912749
XLOC_038237	47.26	69.59	1.47	0.56	2.04	4.00E-04	7.69E-03	DYNLT3	X:23429000-23442795
XLOC_023506	7.59	11.17	1.47	0.56	1.93	1.45E-03	2.04E-02	NA	7:53373002-53376256
XLOC_038128	16.80	24.68	1.47	0.56	1.61	4.15E-03	4.42E-02	CCDC160	X:108570647-108584524
XLOC_022538	13.00	19.08	1.47	0.55	1.99	7.00E-04	1.18E-02	MTX2	7:115826077-115909184
XLOC_038184	14.28	20.97	1.47	0.55	1.63	4.70E-03	4.84E-02	SH3KBP1	X:5231837-5560880
XLOC_008978	11.42	16.76	1.47	0.55	1.94	1.10E-03	1.66E-02	PLOD2	14:39741112-39840641
XLOC_024165	4.81	7.05	1.47	0.55	1.77	4.70E-03	4.84E-02	C1S	8:33038638-33047235
XLOC_000501	7.92	11.61	1.47	0.55	1.72	3.00E-03	3.49E-02	FZD4	1:129790799-129799769
XLOC_003446	75.31	110.45	1.47	0.55	1.95	8.50E-04	1.36E-02	FAM134B	11:41351070-41502821
XLOC_019033	73.45	107.67	1.47	0.55	1.90	1.05E-03	1.60E-02	NA	3:118297141-118315325
XLOC_012541	8.08	11.83	1.46	0.55	1.97	1.50E-03	2.09E-02	NA	17:30793553-30803849
XLOC_000697	5.17	7.57	1.46	0.55	1.80	1.80E-03	2.39E-02	PDE3B	1:156399239-156578578
XLOC_014627	592.51	867.37	1.46	0.55	1.95	7.50E-04	1.24E-02	CCL2	19:23692540-23722108
XLOC_025677	17.05	24.94	1.46	0.55	1.72	2.65E-03	3.21E-02	NEK4	9:19765435-19810300
XLOC_025726	74.87	109.51	1.46	0.55	2.16	3.00E-04	6.09E-03	SUCLG2	9:34574961-34875080
XLOC_029740	24.20	35.39	1.46	0.55	2.04	1.20E-03	1.78E-02	MESDC2	GL018737:1797633-1807022
XLOC_021938	3.77	5.51	1.46	0.55	1.93	6.50E-04	1.12E-02	SMG1	6:9138874-9225495
XLOC_001707	14.64	21.42	1.46	0.55	2.03	9.00E-04	1.42E-02	CSTF3	1:172443334-172534031
XLOC_034603	686.66	1004.06	1.46	0.55	2.93	1.05E-03	1.60E-02	ENSOCUG00000014878	GL018942:176950-178248
XLOC_023089	15.12	22.09	1.46	0.55	1.76	2.00E-03	2.60E-02	CWC22	7:119695483-119747839
XLOC_001994	57.40	83.84	1.46	0.55	2.91	3.00E-03	3.49E-02	NA	1:31962297-31962773
XLOC_015766	9.21	13.45	1.46	0.55	1.78	2.85E-03	3.37E-02	GALNT7	2:51110466-51183223
XLOC_016653	41.92	61.21	1.46	0.55	1.91	5.50E-04	9.84E-03	APLF	2:117556754-117691916
XLOC_000498	28.32	41.35	1.46	0.55	1.75	2.00E-03	2.60E-02	CTSC	1:128493079-128543008
XLOC_010622	9.18	13.41	1.46	0.55	1.81	2.00E-03	2.60E-02	REST	15:92078188-92102717
XLOC_012315	30.33	44.28	1.46	0.55	1.95	4.00E-04	7.69E-03	ENSOCUG00000004700	17:58817592-58935110
XLOC_018320	41.50	60.58	1.46	0.55	2.00	2.50E-04	5.26E-03	WWC1	3:49623291-49797972
XLOC_024110	3.77	5.50	1.46	0.55	1.82	1.55E-03	2.14E-02	LRP6	8:27457034-27632076
XLOC_016078	15.69	22.90	1.46	0.55	1.92	6.50E-04	1.12E-02	MTIF2	2:130857303-130887537
XLOC_002700	5.30	7.73	1.46	0.55	1.79	2.40E-03	2.97E-02	MACC1	10:5299002-5382926
XLOC_007384	9.04	13.19	1.46	0.54	1.83	1.70E-03	2.29E-02	RLF,TMCO2	13:126264578-126342666
XLOC_013616	25.14	36.66	1.46	0.54	1.98	7.00E-04	1.18E-02	SHOC2	18:58547538-58649953
XLOC_010628	15.54	22.66	1.46	0.54	1.82	1.20E-03	1.78E-02	EXOC1	15:92927805-92990921
XLOC_022266	98.61	143.73	1.46	0.54	1.95	7.50E-04	1.24E-02	AKR1B19	7:13030139-13044200
XLOC_008509	36.01	52.47	1.46	0.54	1.66	4.20E-03	4.46E-02	RNF13	14:43622098-43799075
XLOC_037979	16.81	24.48	1.46	0.54	1.93	9.00E-04	1.42E-02	WDR44	X:67029999-67127132
XLOC_013332	7.58	11.01	1.45	0.54	1.79	2.00E-03	2.60E-02	ENSOCUG00000029443	18:3172210-3257034
XLOC_021578	9.73	14.15	1.45	0.54	1.88	9.50E-04	1.48E-02	DYNC1LI2	5:22139415-22167617
XLOC_000529	36.87	53.59	1.45	0.54	2.31	2.90E-03	3.41E-02	ENSOCUG00000000958	1:138680186-138688605
XLOC_018660	13.36	19.39	1.45	0.54	1.95	5.50E-04	9.84E-03	RA_M002_JSMFBA6BR	3:15899475-15964540
XLOC_013558	5.84	8.48	1.45	0.54	1.83	1.25E-03	1.82E-02	ENTPD7	18:47622347-47670145
XLOC_006472	8.71	12.63	1.45	0.54	1.66	4.10E-03	4.39E-02	SPATA6	13:118228905-118358641
XLOC_006025	5.04	7.30	1.45	0.53	1.77	1.80E-03	2.39E-02	ETV3	13:35838488-35853525
XLOC_012105	3.28	4.74	1.45	0.53	1.68	4.70E-03	4.84E-02	ZSCAN29	17:28894492-28934358
XLOC_013383	77.89	112.63	1.45	0.53	2.29	2.50E-03	3.07E-02	COMTD1	18:12276206-12277744
XLOC_007083	15.85	22.91	1.45	0.53	1.69	4.20E-03	4.46E-02	GPSM2	13:55256905-55330910
XLOC_038469	66.32	95.83	1.44	0.53	2.21	1.50E-03	2.09E-02	ENSOCUG00000025426	X:76662995-76664269
XLOC_007607	227.08	327.87	1.44	0.53	3.35	1.25E-03	1.82E-02	NA	13:24111947-24112387
XLOC_028204	16.16	23.33	1.44	0.53	1.85	2.35E-03	2.93E-02	NR2F2	GL018708:1975651-1990317
XLOC_023211	2.66	3.84	1.44	0.53	1.66	3.95E-03	4.28E-02	TNS1	7:159252073-159340087
XLOC_012458	52.77	76.09	1.44	0.53	1.93	7.00E-04	1.18E-02	FAM81A	17:12913125-12986249
XLOC_021881	36.80	53.00	1.44	0.53	2.07	1.35E-03	1.93E-02	NA	5:34058576-34060975
XLOC_037670	7.48	10.77	1.44	0.53	1.72	4.60E-03	4.78E-02	MOSPD2	X:726180-838118
XLOC_004906	28.49	41.01	1.44	0.53	1.75	3.30E-03	3.75E-02	SNX14	12:72498909-72651089
XLOC_038221	14.16	20.38	1.44	0.52	1.79	2.15E-03	2.76E-02	DMD	X:17253674-17819468
XLOC_018543	17.20	24.69	1.44	0.52	1.85	1.45E-03	2.04E-02	OXR1	3:121966655-122070556
XLOC_028709	468.84	672.74	1.43	0.52	2.46	9.50E-04	1.48E-02	FTH1	GL018717:2788851-2802504
XLOC_006166	21.64	31.05	1.43	0.52	1.61	4.25E-03	4.50E-02	RNF115	13:42882117-42990372
XLOC_003537	15.79	22.65	1.43	0.52	1.77	1.95E-03	2.55E-02	ELOVL7	11:76788788-76871312
XLOC_004857	12.08	17.32	1.43	0.52	1.82	2.20E-03	2.80E-02	DST	12:46426547-46802699
XLOC_037940	74.20	106.36	1.43	0.52	1.90	4.55E-03	4.73E-02	ENSOCUG00000012391	X:56251778-56275664
XLOC_025330	10.21	14.64	1.43	0.52	1.67	3.90E-03	4.24E-02	RIOK3	9:64660027-64691009
XLOC_004210	12.15	17.40	1.43	0.52	1.63	3.95E-03	4.28E-02	FBXO9	12:42805639-42849605
XLOC_018021	13.71	19.64	1.43	0.52	1.63	4.25E-03	4.50E-02	NAA25	21:7963937-8051414
XLOC_013661	22.90	32.79	1.43	0.52	1.72	2.45E-03	3.02E-02	PLEKHA1	18:69195814-69261307
XLOC_023029	10.86	15.55	1.43	0.52	1.65	4.05E-03	4.35E-02	COBLL1	7:104064710-104251392
XLOC_022135	105.79	151.43	1.43	0.52	1.84	1.35E-03	1.93E-02	TUFM	6:18695700-18698857
XLOC_012641	11.68	16.72	1.43	0.52	1.90	1.25E-03	1.82E-02	CHD8	17:41661903-41725517
XLOC_020453	14.53	20.78	1.43	0.52	1.68	3.65E-03	4.03E-02	GPCPD1	4:12023022-12084713
XLOC_013791	132.52	189.40	1.43	0.52	1.78	1.85E-03	2.44E-02	CISD1	18:27892403-27913622
XLOC_010128	32.69	46.71	1.43	0.52	1.88	1.10E-03	1.66E-02	ELOVL6	15:39263606-39394624
XLOC_009026	11.93	17.03	1.43	0.51	1.63	4.70E-03	4.84E-02	SLC33A1	14:50060782-50079522
XLOC_013059	304.58	434.76	1.43	0.51	3.63	4.40E-03	4.61E-02	NA	17:18788797-18789177
XLOC_028203	3.37	4.80	1.42	0.51	1.68	4.50E-03	4.70E-02	ARRDC4	GL018708:404258-421962
XLOC_018727	5.36	7.64	1.42	0.51	1.70	3.90E-03	4.24E-02	GNPDA1	3:24031766-24043649
XLOC_009183	10.21	14.53	1.42	0.51	1.87	2.10E-03	2.71E-02	ACAP2	14:90981880-91139317
XLOC_021329	8.82	12.56	1.42	0.51	1.81	2.90E-03	3.41E-02	MMP2	5:11717914-11744859
XLOC_027130	45.14	64.22	1.42	0.51	1.68	3.75E-03	4.12E-02	NA	AAGW02083172:444-7098
XLOC_006556	13.92	19.80	1.42	0.51	1.88	2.10E-03	2.71E-02	RRAGC	13:127618976-127641923
XLOC_013431	32.49	46.20	1.42	0.51	1.85	1.00E-03	1.55E-02	HERC4	18:18535250-18686502

Transcriptome Gene ID	Uninfected RK-13 Mean FPKM	T. hominis infected RK-13 Mean FPKM	Fold Change	Log2 Fold Change	Test stat	P value	Q value	Ensembl Gene Name / Gene ID	Gene Locus (Chromosome/scaffold:position)
XLOC_022370	36.76	52.20	1.42	0.51	1.69	3.95E-03	4.28E-02	DLD	7:44419715-44454114
XLOC_017472	77.98	110.65	1.42	0.50	1.83	1.10E-03	1.66E-02	ATP6V1D	20:4928192-4949005
XLOC_012032	30.32	43.01	1.42	0.50	1.83	1.65E-03	2.24E-02	MYO1E	17:13051298-13277239
XLOC_016512	9.31	13.20	1.42	0.50	1.67	4.15E-03	4.42E-02	NPHP1	2:95597499-95659203
XLOC_029705	71.29	101.04	1.42	0.50	1.75	2.25E-03	2.84E-02	UGT1A1	GL018736:1153069-1282986
XLOC_003255	18.81	26.64	1.42	0.50	1.76	2.25E-03	2.84E-02	ZNF131	11:63963031-63999624
XLOC_028392	7.14	10.10	1.41	0.50	1.71	2.80E-03	3.32E-02	RNF144B	GL018711:1643877-1762871
XLOC_024071	16.86	23.79	1.41	0.50	1.74	2.65E-03	3.21E-02	C2CD5	8:17642925-17735848
XLOC_004258	5.54	7.81	1.41	0.50	1.73	2.75E-03	3.29E-02	CD109	12:60546041-60714300
XLOC_019893	15.24	21.47	1.41	0.49	1.62	4.15E-03	4.42E-02	PXMP4	4:5970347-5990618
XLOC_018647	7.85	11.05	1.41	0.49	1.76	2.20E-03	2.80E-02	FNIP1	3:14795226-14928401
XLOC_022884	18.36	25.82	1.41	0.49	1.71	3.35E-03	3.79E-02	PUS7	7:41837690-41897178
XLOC_016128	39.83	55.98	1.41	0.49	1.73	2.30E-03	2.88E-02	MAP4K3	2:147022083-147120539
XLOC_008725	74.13	104.18	1.41	0.49	1.71	2.35E-03	2.93E-02	FSTL1	14:98382769-98446132
XLOC_012079	4.93	6.91	1.40	0.49	1.67	3.20E-03	3.67E-02	SECISBP2L	17:23372672-23424469
XLOC_024659	38.62	54.11	1.40	0.49	1.69	3.50E-03	3.92E-02	KDELC1	8:104406492-104420707
XLOC_012376	13.70	19.17	1.40	0.48	1.75	2.65E-03	3.21E-02	KIAA0586	17:76752117-76870123
XLOC_016631	12.37	17.30	1.40	0.48	1.73	3.55E-03	3.95E-02	ZNF638	2:114911952-115026644
XLOC_003124	15.03	20.99	1.40	0.48	1.81	2.50E-03	3.07E-02	NA	10:45804059-45811077
XLOC_012484	24.54	34.25	1.40	0.48	1.69	3.40E-03	3.83E-02	USP8	17:21934436-22059360
XLOC_007119	37.13	51.69	1.39	0.48	1.87	3.75E-03	4.12E-02	SNX7	13:65551656-65706384
XLOC_037812	7.04	9.80	1.39	0.48	1.62	4.45E-03	4.66E-02	WDR13	X:33298006-33308542
XLOC_023176	13.08	18.19	1.39	0.48	1.72	2.50E-03	3.07E-02	FZD5	7:148642453-148649461
XLOC_009264	26.75	37.21	1.39	0.48	1.70	3.15E-03	3.63E-02	PVRL3	14:108146415-108222126
XLOC_008490	26.97	37.48	1.39	0.47	1.81	3.00E-03	3.49E-02	PLS1	14:35983444-36119975
XLOC_020137	22.46	31.21	1.39	0.47	1.63	3.95E-03	4.28E-02	TBK1	4:43251459-43303929
XLOC_011988	12.60	17.39	1.38	0.46	1.61	4.30E-03	4.54E-02	DPP8	17:6780311-6852628
XLOC_007279	45.46	62.58	1.38	0.46	1.68	3.25E-03	3.71E-02	SCP2	13:113709211-113821907
XLOC_030285	19.20	26.42	1.38	0.46	1.68	3.30E-03	3.75E-02	DYNC1H1	GL018751:1406974-1463041
XLOC_010979	21.05	28.92	1.37	0.46	1.66	3.60E-03	3.99E-02	AHCTF1	16:20701136-20774375
XLOC_022857	13.52	18.58	1.37	0.46	1.63	4.35E-03	4.57E-02	MDFIC	7:30350000-30451736
XLOC_008425	62.10	85.23	1.37	0.46	1.65	3.85E-03	4.21E-02	STT3B	14:18745525-18854869
XLOC_007067	46.60	63.95	1.37	0.46	1.67	3.85E-03	4.21E-02	AHCYL1	13:54134793-54175918
XLOC_007082	33.23	45.47	1.37	0.45	1.64	3.95E-03	4.28E-02	NA	13:55122419-55128471
XLOC_015888	13.93	19.05	1.37	0.45	1.65	4.35E-03	4.57E-02	TMEM131	2:94203769-94373423
XLOC_010154	9.84	13.46	1.37	0.45	1.60	4.30E-03	4.54E-02	CENPE	15:46423571-46506024
XLOC_030061	32.51	44.40	1.37	0.45	1.61	4.80E-03	4.91E-02	PSMA4	GL018746:844563-853328
XLOC_012716	26.34	35.94	1.36	0.45	1.65	4.70E-03	4.84E-02	HECTD1	17:50941791-51044502
XLOC_003184	28.22	38.10	1.35	0.43	1.59	4.85E-03	4.95E-02	MAN2A1	11:29263469-29416314
XLOC_025620	43.27	31.91	0.74	-0.44	-1.60	4.50E-03	4.70E-02	LAMB2	9:16736776-16748954
XLOC_023093	481.06	350.34	0.73	-0.46	-1.63	4.30E-03	4.54E-02	ENSOCUG00000012914	7:121433106-121714614
XLOC_021302	357.92	260.37	0.73	-0.46	-2.36	4.05E-03	4.35E-02	EIF3K	5:2582136-2591291
XLOC_017974	69.20	50.31	0.73	-0.46	-1.63	4.35E-03	4.57E-02	PES1	21:3138439-3151396
XLOC_019889	20.79	15.10	0.73	-0.46	-1.64	4.00E-03	4.31E-02	AHCY	4:5402620-5425722
XLOC_018498	22.92	16.64	0.73	-0.46	-1.63	4.40E-03	4.61E-02	PDP1	3:109537566-109551699
XLOC_029529	367.34	266.01	0.72	-0.47	-1.67	3.15E-03	3.63E-02	RPS13	GL018733:1083663-1086802
XLOC_012343	27.68	20.02	0.72	-0.47	-1.69	3.20E-03	3.67E-02	FRMD6	17:70565480-70671815
XLOC_010645	131.25	94.67	0.72	-0.47	-1.72	2.85E-03	3.37E-02	ANXA5	15:97109286-97152727
XLOC_016777	16.97	12.17	0.72	-0.48	-1.71	2.75E-03	3.29E-02	FOSL2	2:157648807-157669335
XLOC_023099	145.25	104.10	0.72	-0.48	-2.41	4.45E-03	4.66E-02	ENSOCUG00000001267	7:123221334-123221980
XLOC_033299	54.46	39.02	0.72	-0.48	-1.71	2.95E-03	3.44E-02	F2RL1	GL018855:46923-61319
XLOC_015159	101.04	72.35	0.72	-0.48	-1.77	2.15E-03	2.76E-02	ACSF2	19:37247657-37301019
XLOC_020682	123.09	88.06	0.72	-0.48	-1.90	1.25E-03	1.82E-02	TSPAN8	4:50157279-50190354
XLOC_008995	246.11	175.91	0.71	-0.48	-1.67	3.75E-03	4.12E-02	WWTR1	14:43311903-43457181
XLOC_018666	201.63	144.07	0.71	-0.48	-1.77	2.40E-03	2.97E-02	SKP1	3:16977804-16994064
XLOC_022273	12.84	9.17	0.71	-0.49	-1.68	4.10E-03	4.39E-02	NUP205	7:13962943-14048555
XLOC_037992	76.12	54.24	0.71	-0.49	-1.76	1.75E-03	2.35E-02	RNF113A	X:68569480-68576480
XLOC_025469	1145.03	815.63	0.71	-0.49	-1.73	2.20E-03	2.80E-02	RPL14	9:3477782-3481280
XLOC_017463	57.43	40.89	0.71	-0.49	-1.80	1.70E-03	2.29E-02	ACTN1	20:3286538-3390355
XLOC_034882	42.05	29.93	0.71	-0.49	-1.92	2.30E-03	2.88E-02	RNPS1	GL018968:21683-30526
XLOC_014752	205.04	145.93	0.71	-0.49	-1.68	3.55E-03	3.95E-02	PSMB3	19:40214676-40224172
XLOC_029122	583.16	414.90	0.71	-0.49	-4.39	2.95E-03	3.44E-02	NA	GL018724:377459-377789
XLOC_004056	38.80	27.58	0.71	-0.49	-1.88	2.95E-03	3.44E-02	PPP1R11	12:22060747-22067122
XLOC_030667	10.67	7.58	0.71	-0.49	-1.59	4.90E-03	4.98E-02	SMURF1	GL018760:1179313-1199844
XLOC_016924	289.13	205.35	0.71	-0.49	-4.12	4.55E-03	4.73E-02	NA	2:36918419-36918751
XLOC_020878	16.54	11.74	0.71	-0.49	-1.78	4.10E-03	4.39E-02	NA	4:11798235-11800699
XLOC_010407	11.31	8.03	0.71	-0.49	-1.60	4.75E-03	4.87E-02	SMAD1	15:19092522-19178534
XLOC_016720	52.45	37.20	0.71	-0.50	-1.89	1.45E-03	2.04E-02	EPAS1	2:139861491-139942118
XLOC_003353	17.23	12.21	0.71	-0.50	-1.72	3.10E-03	3.59E-02	EDIL3	11:4179975-4668948
XLOC_026796	179.55	126.93	0.71	-0.50	-1.81	1.45E-03	2.04E-02	ENSOCUG00000003613	AAGW02082242:3403-12145
XLOC_013583	25.68	18.15	0.71	-0.50	-1.80	4.00E-03	4.31E-02	NFKB2	18:50403638-50425193
XLOC_022569	23.98	16.94	0.71	-0.50	-1.85	1.20E-03	1.78E-02	ITGAV	7:126961509-127066231
XLOC_022966	128.30	90.61	0.71	-0.50	-1.95	1.65E-03	2.24E-02	MCM6	7:73385012-73432818
XLOC_020529	41.90	29.57	0.71	-0.50	-1.77	3.05E-03	3.54E-02	ARF3	4:33207549-33251576
XLOC_006362	269.15	189.94	0.71	-0.50	-1.67	4.15E-03	4.42E-02	ENSOCUG00000015239	13:87913289-88116842
XLOC_021284	43.70	30.81	0.71	-0.50	-1.66	3.35E-03	3.79E-02	ENSOCUG00000021288	5:1262241-1266547
XLOC_013951	115.33	81.28	0.70	-0.50	-1.63	4.40E-03	4.61E-02	RGS10	18:66667792-66695605
XLOC_014582	12.67	8.92	0.70	-0.51	-1.67	4.10E-03	4.39E-02	GIT1	19:18615171-18623770
XLOC_015987	55.47	39.04	0.70	-0.51	-1.77	1.95E-03	2.55E-02	AUP1	2:112011826-112015209
XLOC_000730	42.75	30.08	0.70	-0.51	-1.93	1.60E-03	2.20E-02	RCN1	1:171420802-171437524
XLOC_035643	9.40	6.61	0.70	-0.51	-1.74	4.15E-03	4.42E-02	NA	GL019067:122464-127449
XLOC_019881	96.45	67.79	0.70	-0.51	-1.65	3.60E-03	3.99E-02	EIF6	4:4522827-4528679
XLOC_029773	72.36	50.85	0.70	-0.51	-1.98	1.50E-03	2.09E-02	IDH2	GL018738:1555434-1570808
XLOC_010625	165.21	115.89	0.70	-0.51	-1.75	1.85E-03	2.44E-02	ENSOCUG00000012216	15:92423330-92441697
XLOC_035660	105.03	73.67	0.70	-0.51	-1.81	1.65E-03	2.24E-02	BNIP3	GL019068:90429-95667
XLOC_002622	177.49	124.48	0.70	-0.51	-1.84	1.35E-03	1.93E-02	ASNS	10:31564639-31585382
XLOC_033704	14.91	10.46	0.70	-0.51	-1.64	4.55E-03	4.73E-02	CADM4	GL018881:64270-79588
XLOC_025950	34.84	24.40	0.70	-0.51	-2.01	2.95E-03	3.44E-02	CYB5A	9:114441610-114477083
XLOC_031101	95.88	67.11	0.70	-0.51	-1.87	9.00E-04	1.42E-02	ENSOCUG00000027746	GL018771:821417-823126
XLOC_031325	206.45	144.46	0.70	-0.52	-1.83	1.50E-03	2.09E-02	YBX3	GL018781:653547-678533
XLOC_029557	137.49	96.07	0.70	-0.52	-1.68	3.40E-03	3.83E-02	CYB5R3	GL018734:80732-91096
XLOC_033404	133.31	93.14	0.70	-0.52	-2.15	1.35E-03	1.93E-02	ENSOCUG00000026167	GL018863:277193-278781
XLOC_031109	256.59	179.26	0.70	-0.52	-3.77	2.80E-03	3.32E-02	ENSOCUG00000005148	GL018772:563233-563608
XLOC_006700	90.06	62.73	0.70	-0.52	-1.64	4.40E-03	4.61E-02	SNORD24	13:1208516-1211661
XLOC_029709	7.90	5.50	0.70	-0.52	-1.70	3.00E-03	3.49E-02	SH3BP4	GL018736:2226395-2264270
XLOC_002625	1003.54	697.87	0.70	-0.52	-1.62	4.75E-03	4.87E-02	ENSOCUG00000026246	10:32485957-32554333
XLOC_014454	22.24	15.45	0.69	-0.53	-1.73	2.80E-03	3.32E-02	AURKB	19:11052806-11058938
XLOC_025115	8.42	5.84	0.69	-0.53	-1.76	2.20E-03	2.80E-02	PLXND1	9:10971718-11012143
XLOC_035052	21.39	14.84	0.69	-0.53	-1.93	2.10E-03	2.71E-02	MRPL40	GL018985:178330-184671
XLOC_035586	68.87	47.77	0.69	-0.53	-1.87	6.00E-04	1.06E-02	USP36	GL019063:1114-84202
XLOC_031655	228.29	158.30	0.69	-0.53	-1.91	2.10E-03	2.71E-02	AXL,HNRNPUL1	GL018789:641995-708372
XLOC_033420	5.42	3.75	0.69	-0.53	-1.63	4.50E-03	4.70E-02	NARF	GL018866:47945-76061
XLOC_015066	47.33	32.76	0.69	-0.53	-1.87	2.40E-03	2.97E-02	WSB1	19:20562461-20576224
XLOC_032764	7.92	5.48	0.69	-0.53	-1.73	2.80E-03	3.32E-02	WIZ	GL018829:505644-530658
XLOC_001654	9.98	6.90	0.69	-0.53	-1.79	4.15E-03	4.42E-02	GALNT18	1:153013943-153362015
XLOC_005706	1615.47	1117.22	0.69	-0.53	-3.32	1.35E-03	1.93E-02	NA	12:92041539-92042015
XLOC_007099	101.56	70.23	0.69	-0.53	-2.30	1.40E-03	1.98E-02	ENSOCUG00000029734	13:62637584-62638724
XLOC_003197	365.84	252.66	0.69	-0.53	-2.74	7.50E-04	1.24E-02	ENSOCUG00000027984	11:36688854-36689541
XLOC_003536	9.56	6.60	0.69	-0.53	-1.77	4.90E-03	4.98E-02	DEPDC1B	11:76635166-76742728
XLOC_016806	96.30	66.44	0.69	-0.54	-1.95	7.50E-04	1.24E-02	RAB10	2:159756027-159853696
XLOC_024616	13.93	9.61	0.69	-0.54	-1.78	2.70E-03	3.25E-02	SPRY2	8:82253032-82259173
XLOC_014970	23.32	16.06	0.69	-0.54	-1.63	4.40E-03	4.61E-02	ELP5	19:11881261-11891179

Transcriptome Gene ID	Uninfected RK-13 Mean FPKM	T. hominis infected RK-13 Mean FPKM	Fold Change	Log2 Fold Change	Test stat	P value	Q value	Ensembl Gene Name / Gene ID	Gene Locus (Chromosome/scaffold:position)
XLOC_036131	12.42	8.55	0.69	-0.54	-1.67	4.15E-03	4.42E-02	LRRC8A	GL019142:123080-143778
XLOC_027985	1033.47	711.10	0.69	-0.54	-3.48	4.50E-04	8.42E-03	ENSOCUG00000014699	GL018705:1171161-1171620
XLOC_016757	24.36	16.75	0.69	-0.54	-1.90	1.20E-03	1.78E-02	LTBP1	2:152968662-153408718
XLOC_008794	44.33	30.46	0.69	-0.54	-2.24	3.55E-03	3.95E-02	ENSOCUG00000022615	14:124198670-124199490
XLOC_024668	20.82	14.30	0.69	-0.54	-1.95	8.00E-04	1.30E-02	COL4A1	8:111524928-111654735
XLOC_027207	17.44	11.97	0.69	-0.54	-1.65	3.90E-03	4.24E-02	ARHGEF1	AAGW02083505:20-6046
XLOC_030974	7.62	5.23	0.69	-0.54	-1.67	3.90E-03	4.24E-02	GIT2	GL018766:72179-127221
XLOC_021657	18.67	12.80	0.69	-0.54	-1.96	8.00E-04	1.30E-02	BCAR1	5:29937748-29977726
XLOC_030150	12.01	8.24	0.69	-0.54	-1.88	2.70E-03	3.25E-02	ENSOCUG00000016686	GL018748:1511403-1519153
XLOC_026774	9.46	6.49	0.69	-0.54	-1.91	1.25E-03	1.82E-02	NA	AAGW02082159:5370-11047
XLOC_011518	13.81	9.46	0.69	-0.55	-1.97	1.30E-03	1.87E-02	ELF3	16:69597840-69604723
XLOC_010734	38.46	26.34	0.68	-0.55	-2.15	1.20E-03	1.78E-02	NA	15:33313351-33314814
XLOC_037475	19.07	13.05	0.68	-0.55	-1.95	3.55E-03	3.95E-02	FAM20C	GL019765:0-16738
XLOC_003566	94.18	64.44	0.68	-0.55	-2.06	7.00E-04	1.18E-02	ENSOCUG00000020970	11:85526615-85547255
XLOC_034256	90.31	61.76	0.68	-0.55	-2.02	6.50E-04	1.12E-02	ILF3	GL018914:280051-309811
XLOC_030273	6.64	4.54	0.68	-0.55	-1.72	3.00E-03	3.49E-02	TRMT61A	GL018751:355514-364442
XLOC_015182	4.62	3.16	0.68	-0.55	-1.64	3.55E-03	3.95E-02	SP2	19:39408618-39444669
XLOC_032042	12.61	8.61	0.68	-0.55	-1.66	4.00E-03	4.31E-02	MTMR14	GL018802:453125-494138
XLOC_035794	18.79	12.82	0.68	-0.55	-1.93	1.05E-03	1.60E-02	LIG1	GL019089:917-24350
XLOC_022520	25.87	17.65	0.68	-0.55	-2.00	3.50E-04	6.91E-03	ITGA6	7:112180182-112224751
XLOC_021338	22.58	15.40	0.68	-0.55	-1.98	6.50E-04	1.12E-02	NUP93	5:12967125-13092338
XLOC_023120	49.91	34.04	0.68	-0.55	-1.76	2.00E-03	2.60E-02	TMEFF2	7:132442125-132714573
XLOC_007172	416.38	283.96	0.68	-0.55	-2.19	1.10E-03	1.66E-02	CYR61	13:79255236-79257963
XLOC_037808	87.01	59.34	0.68	-0.55	-1.69	3.15E-03	3.63E-02	EBP	X:33228623-33234550
XLOC_029466	134.94	91.83	0.68	-0.56	-2.00	5.50E-04	9.84E-03	ENSOCUG00000005986	GL018731:1608069-1613276
XLOC_011415	8.65	5.89	0.68	-0.56	-1.83	3.25E-03	3.71E-02	ENSOCUG00000023942	16:49110841-49116246
XLOC_020723	17.50	11.90	0.68	-0.56	-1.82	1.05E-03	1.60E-02	DUSP6	4:68380272-68384053
XLOC_032399	17.25	11.73	0.68	-0.56	-1.99	4.50E-04	8.42E-03	G6PD	GL018816:26542-44761
XLOC_022014	28.52	19.40	0.68	-0.56	-1.99	6.50E-04	1.12E-02	ATXN2L	6:18682855-18694495
XLOC_022820	19.57	13.30	0.68	-0.56	-1.98	3.35E-03	3.79E-02	ENSOCUG00000014136	7:15706295-15709542
XLOC_011205	123.27	83.78	0.68	-0.56	-1.87	1.20E-03	1.78E-02	CSRP1	16:70031762-70049217
XLOC_023253	27.25	18.51	0.68	-0.56	-2.04	8.00E-04	1.30E-02	IRS1	7:168485180-168544806
XLOC_034172	917.64	622.59	0.68	-0.56	-6.69	7.00E-04	1.18E-02	ENSOCUG00000023984	GL018907:316644-316917
XLOC_028952	209.08	141.78	0.68	-0.56	-4.41	3.35E-03	3.79E-02	NA	GL018720:1041534-1041862
XLOC_004496	156.53	106.14	0.68	-0.56	-1.90	7.00E-04	1.18E-02	AKAP12	12:141220132-141335193
XLOC_036359	29.44	19.96	0.68	-0.56	-1.84	1.50E-03	2.09E-02	TUBB4A	GL019202:101998-106857
XLOC_014781	212.53	144.09	0.68	-0.56	-2.04	4.50E-04	8.42E-03	EIF1	19:42627272-42630178
XLOC_007350	76.71	52.00	0.68	-0.56	-1.69	3.50E-03	3.92E-02	CDC20	13:123291091-123310121
XLOC_008862	561.26	380.36	0.68	-0.56	-1.86	1.55E-03	2.14E-02	SOD1	14:161796298-161804964
XLOC_032356	165.46	112.07	0.68	-0.56	-1.80	1.45E-03	2.04E-02	BUB3	GL018813:336444-346755
XLOC_010230	10.95	7.42	0.68	-0.56	-1.83	1.65E-03	2.24E-02	ANTXR2	15:70309510-70464132
XLOC_001132	16.48	11.16	0.68	-0.56	-1.79	1.55E-03	2.14E-02	RCL1	1:49372260-49453664
XLOC_025073	39.34	26.62	0.68	-0.56	-2.01	6.00E-04	1.06E-02	MCM2	9:6677973-6697588
XLOC_021405	117.83	79.68	0.68	-0.56	-2.19	4.50E-04	8.42E-03	ENSOCUG00000006322	5:23430043-23436361
XLOC_021583	23.86	16.13	0.68	-0.57	-2.09	9.50E-04	1.48E-02	RRAD	5:22311514-22315347
XLOC_037522	130.88	88.33	0.67	-0.57	-1.95	4.00E-04	7.69E-03	UBE2S	GL019814:14699-18040
XLOC_008458	9.42	6.36	0.67	-0.57	-1.67	4.10E-03	4.39E-02	PCCB	14:30038506-30113285
XLOC_028049	9.78	6.60	0.67	-0.57	-1.83	1.25E-03	1.82E-02	SLC20A2	GL018706:844828-885980
XLOC_017489	7.04	4.75	0.67	-0.57	-1.85	1.35E-03	1.93E-02	RHOJ	20:10904462-10998410
XLOC_006380	45.00	30.35	0.67	-0.57	-2.05	8.00E-04	1.30E-02	NEGR1	13:94057349-94611443
XLOC_034208	28.23	19.02	0.67	-0.57	-2.02	1.50E-04	3.53E-03	USP10	GL018911:181623-219935
XLOC_006818	12.90	8.68	0.67	-0.57	-1.85	1.25E-03	1.82E-02	UAP1	13:30415541-30456055
XLOC_021490	669.65	450.71	0.67	-0.57	-2.35	5.50E-04	9.84E-03	ENSOCUG00000013117	5:4539-5835
XLOC_006906	95.23	64.09	0.67	-0.57	-1.96	8.50E-04	1.36E-02	FDPS	13:37377899-37397037
XLOC_002867	4.28	2.88	0.67	-0.57	-1.78	1.90E-03	2.49E-02	TBRG4	10:45302531-45312841
XLOC_012371	171.58	115.29	0.67	-0.57	-2.80	3.00E-04	6.09E-03	CDC34	17:76221614-76222331
XLOC_029793	23.79	15.98	0.67	-0.57	-1.64	3.90E-03	4.24E-02	NGRN	GL018738:1419284-1424486
XLOC_000275	3.86	2.59	0.67	-0.57	-1.69	3.60E-03	3.99E-02	PHF2	1:71162547-71201960
XLOC_005127	8.02	5.39	0.67	-0.57	-1.83	4.00E-03	4.31E-02	FBXO5	12:143098858-143108925
XLOC_004835	38.12	25.59	0.67	-0.57	-2.19	3.00E-04	6.09E-03	MCM3	12:41762710-41784435
XLOC_014977	2.48	1.67	0.67	-0.58	-1.76	2.70E-03	3.25E-02	PELP1	19:12206904-12236890
XLOC_034725	36.62	24.57	0.67	-0.58	-2.29	1.75E-03	2.35E-02	NA	GL018957:38382-39335
XLOC_003284	29.65	19.89	0.67	-0.58	-1.87	1.25E-03	1.82E-02	MAP3K1	11:72713459-72776125
XLOC_021649	16.12	10.80	0.67	-0.58	-1.98	1.40E-03	1.98E-02	RFWD3	5:29474917-29726436
XLOC_027203	14.39	9.64	0.67	-0.58	-1.71	2.70E-03	3.25E-02	LTBP3	AAGW02083472:20-6389
XLOC_014974	14.25	9.54	0.67	-0.58	-1.82	1.95E-03	2.55E-02	ENSOCUG00000025664	19:12026394-12031075
XLOC_012651	251.50	168.40	0.67	-0.58	-1.72	2.70E-03	3.25E-02	ENSOCUG00000024959	17:42020850-42021942
XLOC_021366	34.40	23.03	0.67	-0.58	-2.30	2.25E-03	2.84E-02	ENSOCUG00000022105	5:19310910-19311810
XLOC_004233	30.51	20.42	0.67	-0.58	-2.08	4.00E-04	7.69E-03	PTP4A1	12:50335247-50341849
XLOC_005675	93.91	62.85	0.67	-0.58	-2.91	1.20E-03	1.78E-02	NA	12:77070062-77070628
XLOC_036492	31.11	20.82	0.67	-0.58	-1.92	9.50E-04	1.48E-02	TEAD2	GL019240:19400-40570
XLOC_036190	25.76	17.22	0.67	-0.58	-2.20	3.35E-03	3.79E-02	PIH1D1	GL019152:35343-38194
XLOC_016341	49.95	33.37	0.67	-0.58	-2.12	2.00E-04	4.42E-03	SCARA3	2:41995633-42039522
XLOC_020592	17.01	11.36	0.67	-0.58	-1.80	1.10E-03	1.66E-02	AAAS	4:37134753-37145063
XLOC_018839	11.57	7.72	0.67	-0.58	-1.90	1.10E-03	1.66E-02	RNF44	3:57039072-57048275
XLOC_027280	305.57	203.89	0.67	-0.58	-2.06	2.50E-04	5.26E-03	RPL12	GL018699:202411-205739
XLOC_015091	11.27	7.52	0.67	-0.58	-1.67	3.25E-03	3.71E-02	MMP23B	19:24823883-24850485
XLOC_031659	5.96	3.98	0.67	-0.58	-1.82	2.15E-03	2.76E-02	EGLN2	GL018789:1004399-1015351
XLOC_000101	8.04	5.36	0.67	-0.58	-1.76	2.20E-03	2.80E-02	FAM214B	1:18775041-18778546
XLOC_026607	92.58	61.74	0.67	-0.58	-2.30	1.50E-04	3.53E-03	GSTP1	AAGW02081305:20347-24268
XLOC_008896	32.69	21.80	0.67	-0.58	-1.97	1.95E-03	2.55E-02	RFTN1	14:2340874-2566661
XLOC_007292	19.87	13.24	0.67	-0.59	-2.16	4.50E-04	8.42E-03	RNF11	13:115471389-115521542
XLOC_033609	1219.52	812.63	0.67	-0.59	-1.83	1.65E-03	2.24E-02	ACTG1	GL018878:124755-127236
XLOC_023228	59.04	39.33	0.67	-0.59	-2.38	5.50E-04	9.84E-03	TUBA4A	7:160492836-160496451
XLOC_004010	24.14	16.07	0.67	-0.59	-2.00	4.50E-04	8.42E-03	MBOAT1	12:16875987-16994909
XLOC_018763	460.99	306.76	0.67	-0.59	-1.91	7.00E-04	1.18E-02	ENSOCUG00000011509	3:32175995-32180443
XLOC_014753	86.32	57.38	0.66	-0.59	-1.74	2.45E-03	3.02E-02	LASP1	19:40313538-40355416
XLOC_002240	7.73	5.13	0.66	-0.59	-1.84	3.50E-03	3.92E-02	NA	1:113509196-113511318
XLOC_035809	23.35	15.50	0.66	-0.59	-1.78	4.75E-03	4.87E-02	RRP1B	GL019091:97403-108299
XLOC_011599	4121.95	2735.63	0.66	-0.59	-8.56	1.50E-04	3.53E-03	NA	16:7509590-7509842
XLOC_032072	3.77	2.50	0.66	-0.59	-1.80	2.25E-03	2.84E-02	KLF11	GL018803:164-9287
XLOC_004945	11.38	7.55	0.66	-0.59	-1.62	4.70E-03	4.84E-02	MMS22L	12:84512912-84632252
XLOC_034212	127.77	84.75	0.66	-0.59	-2.14	3.00E-04	6.09E-03	COTL1	GL018911:65032-101365
XLOC_028965	214.40	142.18	0.66	-0.59	-2.15	5.00E-05	1.41E-03	ENSOCUG00000008507	GL018721:247342-253370
XLOC_029063	75.47	50.01	0.66	-0.59	-2.08	2.00E-04	4.42E-03	SF3A1	GL018723:3483415-3503031
XLOC_000518	565.75	374.48	0.66	-0.60	-5.44	4.00E-04	7.69E-03	ENSOCUG00000021220	1:134691136-134691454
XLOC_003447	14.18	9.38	0.66	-0.60	-2.11	2.00E-04	4.42E-03	MYO10	11:41506873-41772958
XLOC_004620	10.03	6.64	0.66	-0.60	-2.08	6.50E-04	1.12E-02	E2F3	12:16561609-16648266
XLOC_021421	67.88	44.90	0.66	-0.60	-2.13	1.00E-04	2.52E-03	CIRH1A	5:24546988-24577146
XLOC_032434	173.37	114.66	0.66	-0.60	-3.29	4.00E-04	7.69E-03	SSR4	GL018816:627569-630218
XLOC_029482	19.38	12.81	0.66	-0.60	-1.95	8.00E-04	1.30E-02	SIAH1	GL018732:2276790-2282563
XLOC_033408	8.50	5.61	0.66	-0.60	-1.80	1.80E-03	2.39E-02	TMEM132B	GL018864:169155-589412
XLOC_034715	9.82	6.48	0.66	-0.60	-1.95	2.60E-03	3.17E-02	NA	GL018957:98045-109865
XLOC_013872	168.65	111.27	0.66	-0.60	-1.81	1.80E-03	2.39E-02	ENSOCUG00000000989	18:48629086-48637148
XLOC_004020	56.44	37.19	0.66	-0.60	-2.15	1.50E-04	3.53E-03	CSNK2B	12:20478475-20484020
XLOC_032415	95.77	63.10	0.66	-0.60	-2.13	3.00E-04	6.09E-03	IDH3G	GL018816:630490-637876
XLOC_024488	27.44	18.08	0.66	-0.60	-2.11	2.50E-04	5.26E-03	MLF2	8:32769464-32776478
XLOC_022268	17.42	11.47	0.66	-0.60	-2.07	3.50E-04	6.91E-03	CALD1	7:13255398-13449154
XLOC_021496	10.08	6.64	0.66	-0.60	-1.98	9.50E-04	1.48E-02	PLEKHG2	5:545104-553599
XLOC_035328	57.33	37.74	0.66	-0.60	-2.11	3.00E-04	6.09E-03	RUVBL2	GL019028:51897-68026
XLOC_018988	2.61	1.72	0.66	-0.60	-1.81	2.60E-03	3.17E-02	RUNX1T1	3:107542767-107697440
XLOC_031644	91.91	60.49	0.66	-0.60	-2.22	3.00E-04	6.09E-03	ENSOCUG00000006441	GL018789:144947-161786

Transcriptome Gene ID	Uninfected RK-13 Mean FPKM	T. hominis infected RK-13 Mean FPKM	Fold Change	Log2 Fold Change	Test stat	P value	Q value	Ensembl Gene Name / Gene ID	Gene Locus (Chromosome/scaffold:position)
XLOC_025181	17.23	11.34	0.66	-0.60	-1.93	1.25E-03	1.82E-02	SEMA3F	9:17630555-17657785
XLOC_020041	23.08	15.19	0.66	-0.60	-1.73	2.80E-03	3.32E-02	C12orf44	4:36214851-36227163
XLOC_002704	39.95	26.29	0.66	-0.60	-2.40	1.70E-03	2.29E-02	NA	10:7829250-7834836
XLOC_018376	72.96	48.00	0.66	-0.60	-2.34	5.00E-05	1.41E-03	MCM4	3:62473469-62494806
XLOC_032401	8.90	5.86	0.66	-0.60	-1.76	2.45E-03	3.02E-02	NA	GL018816:62036-66186
XLOC_014827	33.61	22.11	0.66	-0.60	-2.08	1.50E-04	3.53E-03	GRN	19:44627273-44635805
XLOC_022684	13.80	9.06	0.66	-0.61	-1.74	2.95E-03	3.44E-02	BCS1L	7:159934570-159938324
XLOC_025683	142.33	93.40	0.66	-0.61	-2.44	2.00E-04	4.42E-03	TKT	9:20184802-20207587
XLOC_003342	38.59	25.31	0.66	-0.61	-2.21	1.30E-03	1.87E-02	ENSOCUG00000005127	11:1175452-1367053
XLOC_016184	15.15	9.93	0.66	-0.61	-2.09	2.95E-03	3.44E-02	NA	2:159944936-159947357
XLOC_014841	6.02	3.94	0.65	-0.61	-1.77	2.35E-03	2.93E-02	KIF18B	19:45370778-45393551
XLOC_011389	2370.37	1551.95	0.65	-0.61	-1.67	3.70E-03	4.07E-02	VIM	16:44090199-44101692
XLOC_028731	45.26	29.63	0.65	-0.61	-2.13	2.00E-04	4.42E-03	SLC3A2	GL018717:1482541-1507689
XLOC_035177	10.46	6.85	0.65	-0.61	-1.73	1.75E-03	2.35E-02	ERCC1	GL019006:72235-90284
XLOC_021481	12.63	8.26	0.65	-0.61	-2.20	1.00E-04	2.52E-03	CMIP	5:35964467-36046805
XLOC_000260	77.65	50.76	0.65	-0.61	-2.44	1.00E-04	2.52E-03	PSAT1	1:64697634-64728069
XLOC_006846	28.88	18.88	0.65	-0.61	-2.30	2.00E-04	4.42E-03	NCSTN	13:32736051-32751567
XLOC_000129	6.81	4.45	0.65	-0.61	-2.03	5.00E-04	9.12E-03	NOL6	1:20001248-20012385
XLOC_021337	797.23	521.02	0.65	-0.61	-2.19	1.50E-04	3.53E-03	ENSOCUG00000029235	5:12935092-12937197
XLOC_035024	6.67	4.36	0.65	-0.61	-1.80	2.05E-03	2.65E-02	LENG8	GL018981:282242-288926
XLOC_011548	692.54	452.50	0.65	-0.61	-1.80	2.55E-03	3.12E-02	ENSOCUG00000024544	16:75998014-75999171
XLOC_006611	7.31	4.77	0.65	-0.62	-1.94	1.90E-03	2.49E-02	ALDH4A1	13:133985548-134011065
XLOC_034933	2.04	1.33	0.65	-0.62	-1.76	2.40E-03	2.97E-02	TRIOBP	GL018972:34111-82176
XLOC_014775	39.17	25.54	0.65	-0.62	-2.15	2.00E-04	4.42E-03	CDC6	19:41452487-41467746
XLOC_014422	32.13	20.94	0.65	-0.62	-2.10	4.50E-04	8.42E-03	PMP22	19:4699506-4732995
XLOC_009132	77.15	50.27	0.65	-0.62	-1.91	8.00E-04	1.30E-02	POLR2H	14:81347860-81353387
XLOC_003254	3792.20	2470.74	0.65	-0.62	-1.97	7.00E-04	1.18E-02	NA	11:63697942-63698805
XLOC_036009	155.97	101.60	0.65	-0.62	-1.92	8.00E-04	1.30E-02	GUK1	GL019112:32057-42336
XLOC_028505	23.63	15.39	0.65	-0.62	-2.19	5.00E-05	1.41E-03	SHMT2	GL018714:398504-406172
XLOC_036782	138.57	90.24	0.65	-0.62	-2.16	2.00E-04	4.42E-03	C19orf43	GL019346:20050-23032
XLOC_018835	20.99	13.66	0.65	-0.62	-2.25	5.50E-04	9.84E-03	THOC3	3:56693009-56708375
XLOC_037972	95.72	62.31	0.65	-0.62	-2.69	2.50E-04	5.26E-03	ENSOCUG00000026035	X:63774953-63775980
XLOC_025647	12.23	7.96	0.65	-0.62	-1.73	2.35E-03	2.93E-02	HYAL2	9:17785455-17790355
XLOC_021392	20.79	13.52	0.65	-0.62	-1.73	3.15E-03	3.63E-02	ENSOCUG00000010022	5:22769640-22831282
XLOC_036187	163.34	106.21	0.65	-0.62	-2.24	1.00E-04	2.52E-03	PRMT1	GL019152:174226-181662
XLOC_014968	432.30	280.93	0.65	-0.62	-2.22	5.00E-05	1.41E-03	EIF5AL1	19:11834251-11837736
XLOC_013104	5.43	3.53	0.65	-0.62	-1.82	4.85E-03	4.95E-02	NA	17:31695035-31697230
XLOC_015048	1050.49	681.99	0.65	-0.62	-2.13	2.00E-04	4.42E-03	RPL23A	19:19438322-19445440
XLOC_003440	9.56	6.20	0.65	-0.63	-1.99	4.50E-04	8.42E-03	ANKH	11:39550939-39695579
XLOC_014908	74.78	48.46	0.65	-0.63	-2.08	4.50E-04	8.42E-03	CENPV	19:4058385-4086567
XLOC_013500	30.07	19.48	0.65	-0.63	-2.01	5.00E-04	9.12E-03	HHEX	18:40477599-40483993
XLOC_012404	12.21	7.91	0.65	-0.63	-2.06	3.00E-04	6.09E-03	CHSY1	17:84741923-84802926
XLOC_011802	5.87	3.80	0.65	-0.63	-1.83	4.80E-03	4.91E-02	NA	16:51341244-51343051
XLOC_011353	606.14	392.13	0.65	-0.63	-4.11	5.00E-05	1.41E-03	ENSOCUG00000021269	16:34578315-34578765
XLOC_000235	6.14	3.97	0.65	-0.63	-2.07	1.00E-03	1.55E-02	PGM5	1:54570516-54802335
XLOC_033554	5.01	3.24	0.65	-0.63	-1.96	1.45E-03	2.04E-02	CYTL1	GL018874:376125-383584
XLOC_006079	55.58	35.88	0.65	-0.63	-2.66	1.55E-03	2.14E-02	JTB	13:38549080-38556493
XLOC_013746	12.91	8.33	0.65	-0.63	-1.88	7.50E-04	1.24E-02	COL13A1	18:16952441-17034190
XLOC_024290	3.27	2.11	0.65	-0.63	-1.66	3.90E-03	4.24E-02	SCEL	8:79326688-79441905
XLOC_004140	132.64	85.58	0.65	-0.63	-1.83	2.20E-03	2.80E-02	OBTP	12:31401897-31405938
XLOC_038369	490.52	316.47	0.65	-0.63	-2.22	1.00E-04	2.52E-03	ENSOCUG00000015749	X:50991252-50996670
XLOC_012145	410.65	264.93	0.65	-0.63	-3.61	2.00E-04	4.42E-03	ENSOCUG00000027082	17:36007914-36008469
XLOC_022831	33.69	21.73	0.65	-0.63	-2.69	4.25E-03	4.50E-02	ARF5	7:16706554-16708934
XLOC_020299	24.48	15.78	0.64	-0.63	-2.18	4.00E-04	7.69E-03	EIF3D	4:85281952-85295993
XLOC_031862	116.94	75.39	0.64	-0.63	-2.27	2.50E-04	5.26E-03	RRM2	GL018795:3519-223881
XLOC_016369	36.69	23.64	0.64	-0.63	-1.69	4.90E-03	4.98E-02	HMGB2	2:51194487-51197694
XLOC_021362	28.14	18.12	0.64	-0.64	-2.18	1.50E-04	3.53E-03	NDRG4	5:14378959-14387241
XLOC_002476	1.94	1.25	0.64	-0.64	-1.81	2.95E-03	3.44E-02	NA	1:182906857-182914628
XLOC_016687	56.93	36.65	0.64	-0.64	-3.06	1.60E-03	2.20E-02	ENSOCUG00000011673	2:130843046-130845244
XLOC_003534	4.34	2.79	0.64	-0.64	-2.00	4.50E-04	8.42E-03	PDE4D	11:74907734-75270661
XLOC_035095	2.25	1.45	0.64	-0.64	-1.72	1.90E-03	2.49E-02	PASK	GL018993:45-29598
XLOC_034466	7.56	4.86	0.64	-0.64	-1.87	4.55E-03	4.73E-02	NA	GL018932:210-1803
XLOC_029926	39.97	25.68	0.64	-0.64	-2.25	5.00E-05	1.41E-03	GINS1	GL018741:725178-763310
XLOC_021451	4.54	2.92	0.64	-0.64	-1.75	2.20E-03	2.80E-02	MTSS1L	5:28837987-28856048
XLOC_012258	43.26	27.78	0.64	-0.64	-2.22	1.00E-04	2.52E-03	PCK2	17:44144638-44159479
XLOC_030009	353.61	226.95	0.64	-0.64	-3.55	1.00E-04	2.52E-03	NA	GL018744:1123959-1133212
XLOC_028815	14.68	9.41	0.64	-0.64	-2.07	5.00E-04	9.12E-03	MYBL2	GL018718:3033680-3064828
XLOC_032747	35.50	22.75	0.64	-0.64	-2.02	5.00E-04	9.12E-03	DNASE1	GL018828:849277-858039
XLOC_004404	577.79	370.05	0.64	-0.64	-6.24	2.50E-04	5.26E-03	ENSOCUG00000022825	12:111635784-111636118
XLOC_011017	10.55	6.75	0.64	-0.64	-2.20	1.50E-04	3.53E-03	ENSOCUG00000016007	16:32162417-32237747
XLOC_012357	23.51	15.05	0.64	-0.64	-2.02	5.00E-04	9.12E-03	SAMD4A	17:73273481-73499911
XLOC_023589	646.55	413.56	0.64	-0.64	-15.17	2.05E-03	2.65E-02	NA	7:77372055-77372237
XLOC_004009	72.31	46.23	0.64	-0.65	-2.37	5.00E-05	1.41E-03	SOX4	12:15382240-15386689
XLOC_021422	14.24	9.09	0.64	-0.65	-2.21	3.50E-04	6.91E-03	SNTB2	5:24590942-24709339
XLOC_011508	23.71	15.13	0.64	-0.65	-2.41	1.00E-04	2.52E-03	BTG2	16:68471082-68475713
XLOC_031351	37.61	23.99	0.64	-0.65	-2.47	1.50E-04	3.53E-03	ENSOCUG00000029455	GL018782:465650-474793
XLOC_025674	10.64	6.78	0.64	-0.65	-1.70	4.00E-03	4.31E-02	NT5DC2	9:19565765-19598578
XLOC_001235	339.96	216.58	0.64	-0.65	-4.69	1.50E-04	3.53E-03	ENSOCUG00000008405	1:75739306-75739687
XLOC_005846	353.58	225.24	0.64	-0.65	-1.94	1.05E-03	1.60E-02	PRDX6	13:888674-901838
XLOC_009157	11.16	7.11	0.64	-0.65	-1.85	2.90E-03	3.41E-02	BCL6	14:83371541-83395083
XLOC_011198	17.90	11.40	0.64	-0.65	-2.19	1.50E-04	3.53E-03	ENSOCUG00000022112	16:68896641-68909008
XLOC_009302	61.86	39.37	0.64	-0.65	-3.84	4.55E-03	4.73E-02	ANAPC15	14:121419516-121419873
XLOC_037824	27.21	17.30	0.64	-0.65	-2.31	5.00E-05	1.41E-03	CCDC120	X:33678626-33693928
XLOC_000152	848.74	539.79	0.64	-0.65	-3.17	5.00E-05	1.41E-03	ENSOCUG00000003706	1:26785336-26786110
XLOC_008651	8.76	5.57	0.64	-0.65	-1.90	1.55E-03	2.14E-02	RTP4	14:83034410-83038322
XLOC_020566	20.57	13.07	0.64	-0.65	-2.22	5.00E-05	1.41E-03	KRT80	4:36253025-36271637
XLOC_014563	55.52	35.23	0.63	-0.66	-2.38	5.00E-05	1.41E-03	MYO1C	19:16629617-16650525
XLOC_013378	26.56	16.84	0.63	-0.66	-2.00	7.00E-04	1.18E-02	DLG5	18:9684878-9765673
XLOC_016135	84.75	53.72	0.63	-0.66	-1.99	4.00E-04	7.69E-03	SRSF7	2:147600116-147643411
XLOC_014935	3.19	2.02	0.63	-0.66	-2.12	1.50E-04	3.53E-03	PFAS	19:10996821-11022433
XLOC_017904	23.61	14.96	0.63	-0.66	-2.40	1.50E-04	3.53E-03	UBE2L3	21:5433677-5513053
XLOC_031019	8.21	5.20	0.63	-0.66	-2.20	3.00E-04	6.09E-03	STXBP2	GL018767:814098-822309
XLOC_007687	26.14	16.55	0.63	-0.66	-2.50	7.50E-04	1.24E-02	NA	13:38703269-38704146
XLOC_024501	7.56	4.78	0.63	-0.66	-2.11	5.50E-04	9.84E-03	FOXJ2	8:33629084-33654376
XLOC_005094	1.15	0.73	0.63	-0.66	-1.65	4.45E-03	4.66E-02	NHSL1	12:128828668-128990458
XLOC_037872	10.55	6.67	0.63	-0.66	-2.02	3.50E-04	6.91E-03	ENSOCUG00000024108	X:44202195-44207225
XLOC_001775	4.39	2.78	0.63	-0.66	-2.09	3.00E-04	6.09E-03	NUP160	1:187068437-187132558
XLOC_002805	917.21	579.98	0.63	-0.66	-4.71	5.00E-05	1.41E-03	ENSOCUG00000025551	10:32350916-32351331
XLOC_038268	106.39	67.26	0.63	-0.66	-2.24	5.00E-05	1.41E-03	NDUFB11	X:32259377-32264340
XLOC_014374	9000.31	5689.48	0.63	-0.66	-10.72	1.00E-04	2.52E-03	NA	18:66434587-66582033
XLOC_033126	28.64	18.10	0.63	-0.66	-2.49	2.50E-04	5.26E-03	GALK1	GL018845:49072-53189
XLOC_034505	5.79	3.66	0.63	-0.66	-1.91	1.15E-03	1.72E-02	MFGE8	GL018934:45647-58724
XLOC_017492	23.48	14.83	0.63	-0.66	-2.09	1.65E-03	2.24E-02	NA	20:11893575-11912115
XLOC_009039	3.78	2.39	0.63	-0.66	-1.92	1.60E-03	2.20E-02	NA	14:54214378-54218037
XLOC_007068	14.53	9.17	0.63	-0.66	-2.19	1.50E-04	3.53E-03	CSF1	13:54245540-54264758
XLOC_008908	6.38	4.03	0.63	-0.66	-2.23	3.00E-04	6.09E-03	THRB	14:10447744-10676392
XLOC_035291	2.98	1.88	0.63	-0.66	-1.88	9.00E-04	1.42E-02	STX6	GL019023:29000-66180
XLOC_024125	17.51	11.04	0.63	-0.67	-2.33	5.00E-05	1.41E-03	TEAD4	8:29175741-29464015
XLOC_017606	8.64	5.45	0.63	-0.67	-2.16	6.00E-04	1.06E-02	ENSOCUG00000014268	20:8229769-8234257
XLOC_038040	186.70	117.63	0.63	-0.67	-4.16	2.50E-04	5.26E-03	ENSOCUG00000014194	X:81654160-81654584
XLOC_002791	52.12	32.83	0.63	-0.67	-2.86	2.00E-04	4.42E-03	ENSOCUG00000009140	10:28688948-28689816
XLOC_010138	40.17	25.30	0.63	-0.67	-2.56	5.00E-05	1.41E-03	PAPSS1	15:41803373-41912629

Transcriptome Gene ID	Uninfected RK-13 Mean FPKM	T. hominis infected RK-13 Mean FPKM	Fold Change	Log2 Fold Change	Test stat	P value	Q value	Ensembl Gene Name / Gene ID	Gene Locus (Chromosome/scaffold:position)
XLOC_025127	11.08	6.98	0.63	-0.67	-1.93	1.15E-03	1.72E-02	VGLL4	9:12142737-12295276
XLOC_032535	30.60	19.24	0.63	-0.67	-2.52	1.50E-04	3.53E-03	ENSOCUG00000026506	GL018821:709070-712440
XLOC_034689	16.24	10.21	0.63	-0.67	-2.22	1.00E-04	2.52E-03	MED15	GL018951:138984-190960
XLOC_032479	5.36	3.37	0.63	-0.67	-1.79	2.50E-03	3.07E-02	ALKBH5	GL018817:905886-927414
XLOC_031476	36.39	22.85	0.63	-0.67	-2.31	5.00E-05	1.41E-03	LSR	GL018786:165302-185766
XLOC_036977	1.76	1.10	0.63	-0.67	-1.69	3.30E-03	3.75E-02	PRDM16	GL019427:12620-48949
XLOC_021906	22.06	13.84	0.63	-0.67	-2.44	2.00E-04	4.42E-03	ENSOCUG00000021942	6:4472235-4473534
XLOC_005922	9.77	6.13	0.63	-0.67	-1.82	1.85E-03	2.44E-02	C1orf112	13:21914141-22018209
XLOC_017641	99.22	62.20	0.63	-0.67	-2.40	1.00E-04	2.52E-03	TDP1	20:15451836-15537809
XLOC_028831	175.43	109.96	0.63	-0.67	-4.08	1.50E-04	3.53E-03	ENSOCUG00000025431	GL018718:1306248-1306695
XLOC_034304	36.18	22.65	0.63	-0.68	-2.61	3.00E-04	6.09E-03	NA	GL018918:268918-270215
XLOC_006037	5.14	3.22	0.63	-0.68	-2.12	4.00E-04	7.69E-03	MEF2D	13:36426563-36444809
XLOC_012589	11.89	7.43	0.63	-0.68	-1.99	6.50E-04	1.12E-02	LPCAT4	17:39590355-39597558
XLOC_010047	16.66	10.41	0.62	-0.68	-1.87	1.35E-03	1.93E-02	MND1	15:9545675-9635691
XLOC_013735	13.86	8.66	0.62	-0.68	-2.02	2.50E-04	5.26E-03	DDIT4	18:15149446-15151531
XLOC_008813	23.18	14.48	0.62	-0.68	-2.48	2.00E-04	4.42E-03	ENSOCUG00000024114	14:134833854-134835311
XLOC_014836	5.21	3.25	0.62	-0.68	-1.97	6.00E-04	1.06E-02	PLCD3	19:45199942-45218301
XLOC_018273	5.72	3.56	0.62	-0.68	-1.98	9.00E-04	1.42E-02	SYNPO	3:32308722-32357552
XLOC_027873	2.49	1.55	0.62	-0.68	-1.83	2.55E-03	3.12E-02	NCDN	GL018704:2755191-2764734
XLOC_032934	10.40	6.47	0.62	-0.68	-2.12	3.50E-04	6.91E-03	MEIS3	GL018835:637015-645010
XLOC_006158	45.23	28.16	0.62	-0.68	-2.46	5.00E-05	1.41E-03	TXNIP	13:42736056-42740027
XLOC_016235	12.69	7.88	0.62	-0.69	-2.27	5.00E-05	1.41E-03	PROM1	2:6570948-6681319
XLOC_016346	30.94	19.22	0.62	-0.69	-2.48	1.00E-04	2.52E-03	DPYSL2	2:43044811-43120018
XLOC_014547	6.11	3.80	0.62	-0.69	-1.72	4.85E-03	4.95E-02	MNT	19:15774567-15828066
XLOC_000415	20.67	12.84	0.62	-0.69	-2.01	5.50E-04	9.84E-03	IL18	1:104201273-104234940
XLOC_018538	5.56	3.46	0.62	-0.69	-1.86	1.40E-03	1.98E-02	RIMS2	3:119260426-119645961
XLOC_004658	3.82	2.37	0.62	-0.69	-2.00	7.50E-04	1.24E-02	ATF6B	12:20900076-20912540
XLOC_030622	84.62	52.50	0.62	-0.69	-2.01	8.50E-04	1.36E-02	NA	GL018759:139428-160649
XLOC_029868	735.12	456.03	0.62	-0.69	-2.43	5.00E-05	1.41E-03	ENSOCUG00000007825	GL018740:307699-308476
XLOC_032472	3.84	2.38	0.62	-0.69	-1.74	2.85E-03	3.37E-02	MAPK7	GL018817:323190-327527
XLOC_025396	6.23	3.86	0.62	-0.69	-2.25	3.00E-04	6.09E-03	SKA1	9:91095294-91115561
XLOC_032073	4.01	2.48	0.62	-0.69	-1.67	4.60E-03	4.78E-02	GRHL1	GL018803:46196-89333
XLOC_000689	24.15	14.96	0.62	-0.69	-2.28	2.00E-04	4.42E-03	PARVA	1:154083408-154248605
XLOC_030471	1145.21	708.41	0.62	-0.69	-2.32	1.00E-04	2.52E-03	ENSOCUG00000001042	GL018755:407750-419457
XLOC_034088	36.84	22.78	0.62	-0.69	-3.28	4.75E-03	4.87E-02	TECR	GL018901:480704-499164
XLOC_032878	107.95	66.69	0.62	-0.69	-2.51	5.00E-05	1.41E-03	ICAM1	GL018833:97979-106837
XLOC_011509	7.52	4.64	0.62	-0.70	-1.85	1.45E-03	2.04E-02	ADORA1	16:68612154-68642478
XLOC_036875	15.48	9.56	0.62	-0.70	-2.34	4.50E-04	8.42E-03	NA	GL019385:46738-48241
XLOC_036227	1.94	1.20	0.62	-0.70	-1.91	1.75E-03	2.35E-02	ZNF516	GL019165:85486-127530
XLOC_027677	23.90	14.75	0.62	-0.70	-2.59	5.00E-05	1.41E-03	RFC3	GL018702:4595341-4615895
XLOC_028701	37.43	23.09	0.62	-0.70	-2.21	5.00E-05	1.41E-03	EEF1G	GL018717:1747650-1758871
XLOC_032388	6.25	3.85	0.62	-0.70	-1.87	1.45E-03	2.04E-02	CD276	GL018815:17486-29849
XLOC_019896	5.43	3.35	0.62	-0.70	-1.78	2.30E-03	2.88E-02	SNTA1	4:6191076-6220529
XLOC_020284	6.94	4.28	0.62	-0.70	-1.95	8.50E-04	1.36E-02	SUN2	4:84443977-84449935
XLOC_028935	5.96	3.67	0.62	-0.70	-2.14	1.50E-04	3.53E-03	ENC1	GL018720:3267369-3275893
XLOC_031211	4.98	3.06	0.62	-0.70	-1.67	3.70E-03	4.07E-02	HAUS8	GL018776:1142933-1150494
XLOC_004115	56.69	34.85	0.61	-0.70	-2.48	5.00E-05	1.41E-03	CDKN1A	12:26614085-26621169
XLOC_018954	61.99	38.07	0.61	-0.70	-3.19	5.00E-05	1.41E-03	MRPS28	3:95623108-95774056
XLOC_009020	32.06	19.69	0.61	-0.70	-1.79	3.60E-03	3.99E-02	RAP2B	14:47357938-47381468
XLOC_028867	15.27	9.37	0.61	-0.70	-2.50	5.00E-05	1.41E-03	FOXO1	GL018719:3590941-3644865
XLOC_015825	125.85	77.17	0.61	-0.71	-4.48	3.00E-04	6.09E-03	ENSOCUG00000025641	2:69386169-69386553
XLOC_033707	5.45	3.34	0.61	-0.71	-1.74	2.95E-03	3.44E-02	KCNN4	GL018881:157212-169613
XLOC_017872	10.82	6.63	0.61	-0.71	-2.13	2.50E-04	5.26E-03	LIMK2	21:3658718-3740229
XLOC_030012	32.88	20.14	0.61	-0.71	-2.61	5.00E-05	1.41E-03	NA	GL018744:1989413-2016586
XLOC_029399	110.17	67.41	0.61	-0.71	-3.02	5.00E-05	1.41E-03	ENSOCUG00000025196	GL018730:2576983-2578186
XLOC_037550	3.76	2.30	0.61	-0.71	-1.87	3.35E-03	3.79E-02	NA	GL019840:18674-20743
XLOC_013899	58.14	35.55	0.61	-0.71	-2.44	1.00E-04	2.52E-03	ENSOCUG00000020100	18:51298117-51321088
XLOC_033910	722.64	441.77	0.61	-0.71	-2.58	5.00E-05	1.41E-03	ENSOCUG00000021964	GL018890:440577-441252
XLOC_031978	12.08	7.38	0.61	-0.71	-2.16	2.00E-04	4.42E-03	NUP43	GL018800:158206-175813
XLOC_034879	32.06	19.58	0.61	-0.71	-2.36	6.00E-04	1.06E-02	ATP6V0C,ENSOCUG00000021194	GL018968:236625-247571
XLOC_038709	2.23	1.36	0.61	-0.71	-1.78	4.40E-03	4.61E-02	NA	X:3542863-3546172
XLOC_034591	19.08	11.64	0.61	-0.71	-2.32	1.00E-04	2.52E-03	POLA2	GL018942:272558-297509
XLOC_035651	2.59	1.58	0.61	-0.71	-1.89	1.55E-03	2.14E-02	NA	GL019067:178653-182511
XLOC_032580	7.47	4.55	0.61	-0.71	-2.11	3.50E-04	6.91E-03	DPAGT1	GL018823:567092-572884
XLOC_033154	5.74	3.50	0.61	-0.71	-1.68	4.65E-03	4.81E-02	CDR2L	GL018845:676469-681863
XLOC_017975	55.81	34.00	0.61	-0.71	-1.78	2.20E-03	2.80E-02	ENSOCUG00000009987	21:3218818-3222305
XLOC_010907	290.86	177.18	0.61	-0.72	-6.32	2.00E-04	4.42E-03	NA	15:101010723-101011032
XLOC_037483	5.35	3.26	0.61	-0.72	-1.99	3.20E-03	3.67E-02	NA	GL019771:16708-18345
XLOC_039174	5.15	3.14	0.61	-0.72	-2.12	1.10E-03	1.66E-02	NA	X:109576858-109579845
XLOC_001892	13.91	8.46	0.61	-0.72	-1.72	3.55E-03	3.95E-02	RBM4	1:194276026-194286832
XLOC_012048	127.04	77.27	0.61	-0.72	-2.05	5.00E-04	9.12E-03	NA	17:17223305-17224842
XLOC_003266	6.99	4.25	0.61	-0.72	-2.46	5.00E-05	1.41E-03	ITGA2	11:69030569-69139625
XLOC_011337	9.47	5.76	0.61	-0.72	-2.08	1.30E-03	1.87E-02	ENSOCUG00000021494	16:31438120-31464040
XLOC_031205	216.42	131.42	0.61	-0.72	-2.62	5.00E-05	1.41E-03	TPM4	GL018776:769119-789646
XLOC_020587	401.82	243.57	0.61	-0.72	-2.39	5.00E-05	1.41E-03	KRT8	4:36812952-36820567
XLOC_034432	4.69	2.84	0.61	-0.72	-2.27	1.50E-04	3.53E-03	CELSR1	GL018928:339268-397924
XLOC_018208	85.45	51.72	0.61	-0.72	-1.61	4.90E-03	4.98E-02	CYSTM1	3:22324022-22387488
XLOC_036181	892.46	540.10	0.61	-0.72	-2.58	5.00E-05	1.41E-03	RPL13A,SNORD33	GL019152:63672-64988
XLOC_029822	4.57	2.77	0.60	-0.73	-2.01	1.55E-03	2.14E-02	NA	GL018738:2452693-2454861
XLOC_027861	8.98	5.43	0.60	-0.73	-1.88	2.25E-03	2.84E-02	ZC3H12A	GL018704:980379-989309
XLOC_011739	684.67	414.00	0.60	-0.73	-4.73	5.00E-05	1.41E-03	NA	16:39164018-39164472
XLOC_006140	33.85	20.46	0.60	-0.73	-2.34	5.00E-05	1.41E-03	SF3B4	13:42105016-42110263
XLOC_005834	2520.44	1523.81	0.60	-0.73	-4.17	5.00E-05	1.41E-03	NA	12:145311725-145312242
XLOC_015151	61.74	37.31	0.60	-0.73	-1.97	6.50E-04	1.12E-02	NME1	19:36653277-36662332
XLOC_031024	8.39	5.07	0.60	-0.73	-2.04	6.00E-04	1.06E-02	ZNF358	GL018767:914107-926915
XLOC_033603	43.14	26.07	0.60	-0.73	-2.43	5.00E-05	1.41E-03	FSCN1	GL018878:166736-168710
XLOC_021264	730.42	441.32	0.60	-0.73	-2.64	5.00E-05	1.41E-03	RPS16	5:537595-540034
XLOC_025801	200.49	120.98	0.60	-0.73	-2.29	5.00E-05	1.41E-03	TGIF1	9:58604066-58622396
XLOC_012061	9.81	5.92	0.60	-0.73	-2.12	5.50E-04	9.84E-03	GNB5	17:20396492-20423406
XLOC_027911	2.97	1.79	0.60	-0.73	-1.98	1.55E-03	2.14E-02	NA	GL018704:975529-978724
XLOC_037415	9.26	5.57	0.60	-0.73	-1.85	1.10E-03	1.66E-02	ENSOCUG00000023981	GL019715:15118-18767
XLOC_020622	18.60	11.19	0.60	-0.73	-2.55	2.00E-04	4.42E-03	WIBG	4:39455630-39516240
XLOC_018374	35.49	21.34	0.60	-0.73	-2.50	5.00E-05	1.41E-03	SPIDR	3:61829138-62285681
XLOC_004725	35.09	21.10	0.60	-0.73	-2.09	3.50E-04	6.91E-03	RPS10	12:24580427-24586488
XLOC_024462	3.92	2.36	0.60	-0.73	-1.86	9.00E-04	1.42E-02	FOXM1	8:29084504-29098591
XLOC_029572	49.88	29.97	0.60	-0.74	-2.44	5.00E-05	1.41E-03	NHP2L1	GL018734:820427-840780
XLOC_004689	32.22	19.36	0.60	-0.74	-2.13	3.50E-04	6.91E-03	NRM	12:22721191-22724047
XLOC_024057	10.46	6.28	0.60	-0.74	-1.86	2.15E-03	2.76E-02	NA	8:13915546-13916985
XLOC_014763	4.75	2.85	0.60	-0.74	-1.97	3.85E-03	4.21E-02	GRB7	19:40979143-40982961
XLOC_024751	79.74	47.86	0.60	-0.74	-2.82	5.00E-05	1.41E-03	NA	8:14057045-14061706
XLOC_036533	26.28	15.77	0.60	-0.74	-2.70	5.00E-05	1.41E-03	NA	GL019254:19355-46730
XLOC_006809	81.72	49.00	0.60	-0.74	-2.63	5.00E-05	1.41E-03	MGST3	13:27242692-27262554
XLOC_006804	7.75	4.64	0.60	-0.74	-2.03	4.50E-04	8.42E-03	POGK	13:26145936-26158379
XLOC_018684	18.30	10.97	0.60	-0.74	-2.08	1.10E-03	1.66E-02	HNRNPA0	3:19926305-20087435
XLOC_036404	120.26	72.06	0.60	-0.74	-2.24	1.50E-04	3.53E-03	ENSOCUG00000023609	GL019215:73625-83888
XLOC_030810	882.85	528.86	0.60	-0.74	-2.63	5.00E-05	1.41E-03	RPS5	GL018763:1361228-1368282
XLOC_005840	35.60	21.31	0.60	-0.74	-2.94	1.50E-04	3.53E-03	NA	12:151753066-151753867
XLOC_035278	13.84	8.28	0.60	-0.74	-2.29	5.00E-05	1.41E-03	UBE2G2	GL019021:12869-40637
XLOC_020778	14.91	8.92	0.60	-0.74	-2.32	1.50E-04	3.53E-03	SMCR7L	4:84044722-84061310
XLOC_038656	2.92	1.74	0.60	-0.74	-1.94	2.40E-03	2.97E-02	NA	X:3377423-3380326
XLOC_023730	303.79	181.45	0.60	-0.74	-5.18	5.00E-05	1.41E-03	NA	7:122659291-122659687

Transcriptome Gene ID	Uninfected RK-13 Mean FPKM	T. hominis infected RK-13 Mean FPKM	Fold Change	Log2 Fold Change	Test stat	P value	Q value	Ensembl Gene Name / Gene ID	Gene Locus (Chromosome/scaffold:position)
XLOC_006214	104.72	62.52	0.60	-0.74	-3.24	5.00E-05	1.41E-03	ENSOCUG00000027213	13:51451522-51457153
XLOC_027291	766.00	457.01	0.60	-0.75	-2.69	5.00E-05	1.41E-03	ENSOCUG00000002996	GL018699:2466656-2469337
XLOC_031660	15.99	9.53	0.60	-0.75	-2.38	1.00E-04	2.52E-03	ENSOCUG00000006680,ENSOCUG00000022977	GL018789:1016251-1029025
XLOC_010964	17.23	10.27	0.60	-0.75	-2.65	5.00E-05	1.41E-03	CELF2	16:15371099-15968959
XLOC_028432	3.94	2.35	0.60	-0.75	-2.30	5.00E-05	1.41E-03	ZNF217	GL018712:2829760-2844210
XLOC_030367	120.78	71.97	0.60	-0.75	-2.71	5.00E-05	1.41E-03	NA	GL018752:849824-855196
XLOC_036159	19.63	11.68	0.60	-0.75	-2.29	1.00E-04	2.52E-03	IL9R,POLR3K	GL019146:18665-42874
XLOC_030031	16.89	10.04	0.59	-0.75	-2.18	1.50E-04	3.53E-03	UPP1	GL018745:170254-185349
XLOC_035270	34.16	20.30	0.59	-0.75	-2.34	7.00E-04	1.18E-02	MAP2K3	GL019019:41822-112016
XLOC_023742	17.84	10.60	0.59	-0.75	-2.63	1.50E-04	3.53E-03	NA	7:126275610-126277003
XLOC_003731	40.16	23.86	0.59	-0.75	-2.98	5.00E-05	1.41E-03	NA	11:37365956-37366965
XLOC_038380	756.12	448.39	0.59	-0.75	-4.13	5.00E-05	1.41E-03	ENSOCUG00000014764	X:52633615-52636417
XLOC_024282	121.98	72.32	0.59	-0.75	-2.14	2.50E-04	5.26E-03	BTEB2	8:74494634-74511648
XLOC_011467	7.33	4.34	0.59	-0.75	-2.55	5.00E-05	1.41E-03	SERTAD4	16:62420598-62429035
XLOC_028509	22.22	13.17	0.59	-0.75	-2.55	5.00E-05	1.41E-03	MARS	GL018714:646796-670945
XLOC_004141	7.27	4.31	0.59	-0.75	-1.76	2.85E-03	3.37E-02	BYSL	12:31517404-31534986
XLOC_038062	203.41	120.50	0.59	-0.76	-3.32	5.00E-05	1.41E-03	NA	X:87171498-87173973
XLOC_034228	354.35	209.87	0.59	-0.76	-2.76	5.00E-05	1.41E-03	FBL	GL018912:362329-371229
XLOC_003219	1.51	0.89	0.59	-0.76	-2.02	3.50E-04	6.91E-03	PDZD2	11:53531890-53935197
XLOC_026608	10.30	6.09	0.59	-0.76	-2.02	3.90E-03	4.24E-02	ENSOCUG00000025066	AAGW02081306:5826-25343
XLOC_032562	31.59	18.68	0.59	-0.76	-2.12	2.00E-04	4.42E-03	ENSOCUG00000017261	GL018823:493884-496799
XLOC_029528	6.70	3.96	0.59	-0.76	-1.88	2.25E-03	2.84E-02	PLEKHA7	GL018733:827213-964650
XLOC_018850	83.81	49.49	0.59	-0.76	-2.55	5.00E-05	1.41E-03	PDLIM7	3:57989096-58004029
XLOC_000935	18.10	10.68	0.59	-0.76	-2.62	5.00E-05	1.41E-03	TMEM109	1:193539338-193549353
XLOC_025828	311.07	183.39	0.59	-0.76	-2.24	2.00E-04	4.42E-03	ENSOCUG00000002862	9:64211991-64296744
XLOC_025664	2.52	1.49	0.59	-0.76	-1.99	1.80E-03	2.39E-02	DUSP7	9:19153373-19159153
XLOC_007320	19.61	11.55	0.59	-0.76	-2.08	1.00E-03	1.55E-02	ENSOCUG00000005945,ENSOCUG00000017363	13:121036927-121097230
XLOC_020237	16.54	9.74	0.59	-0.76	-2.26	1.50E-04	3.53E-03	NA	4:75418502-75466001
XLOC_012185	224.89	132.35	0.59	-0.76	-3.08	5.00E-05	1.41E-03	APEX1	17:40910515-40917602
XLOC_005097	48.43	28.50	0.59	-0.77	-2.64	5.00E-05	1.41E-03	ENSOCUG00000023408	12:129792288-129794038
XLOC_017128	5334.27	3138.61	0.59	-0.77	-100.56	9.00E-04	1.42E-02	NA	2:86080969-86081061
XLOC_029835	203.10	119.50	0.59	-0.77	-2.74	5.00E-05	1.41E-03	PDPN	GL018739:1237810-1269612
XLOC_000419	106.35	62.56	0.59	-0.77	-3.93	5.00E-05	1.41E-03	CRYAB	1:104462697-104465651
XLOC_014794	9.66	5.68	0.59	-0.77	-1.93	9.50E-04	1.48E-02	COASY	19:43310093-43314137
XLOC_020001	175.34	103.11	0.59	-0.77	-2.58	5.00E-05	1.41E-03	ENSOCUG00000024676	4:28047912-28150575
XLOC_027084	318.61	187.32	0.59	-0.77	-2.66	5.00E-05	1.41E-03	NA	AAGW02083030:367-3010
XLOC_035188	32.77	19.27	0.59	-0.77	-2.98	5.00E-05	1.41E-03	NA	GL019007:125103-126097
XLOC_038303	22.28	13.09	0.59	-0.77	-2.63	5.00E-05	1.41E-03	ENSOCUG00000005034	X:34892473-34911539
XLOC_020351	7.84	4.60	0.59	-0.77	-1.85	1.55E-03	2.14E-02	AAR2	4:3663754-3679909
XLOC_022287	28.62	16.81	0.59	-0.77	-2.29	1.00E-04	2.52E-03	IMPDH1	7:15955329-15974447
XLOC_025629	11.04	6.48	0.59	-0.77	-2.50	1.50E-04	3.53E-03	NICN1	9:16959257-16963100
XLOC_001481	503.03	294.89	0.59	-0.77	-2.96	5.00E-05	1.41E-03	ENSOCUG00000022412	1:141307966-141313359
XLOC_013781	41.48	24.32	0.59	-0.77	-2.83	5.00E-05	1.41E-03	CDK1	18:25384669-25403733
XLOC_015150	615.15	360.11	0.59	-0.77	-2.70	5.00E-05	1.41E-03	NME2	19:36641171-36647821
XLOC_017683	3.73	2.18	0.58	-0.77	-2.13	7.50E-04	1.24E-02	FOS	20:29860026-29864096
XLOC_000956	2.31	1.35	0.58	-0.77	-1.72	4.15E-03	4.42E-02	RCE1	1:194439623-194444763
XLOC_027279	22.39	13.08	0.58	-0.78	-2.53	5.00E-05	1.41E-03	FAM129B	GL018699:120722-166352
XLOC_012419	18.47	10.78	0.58	-0.78	-2.71	5.00E-05	1.41E-03	SMAD3	17:5343805-5366146
XLOC_004950	543.91	317.58	0.58	-0.78	-7.49	5.00E-05	1.41E-03	LSM3	12:86876000-86876309
XLOC_019561	3.84	2.24	0.58	-0.78	-2.15	1.00E-03	1.55E-02	NA	3:96778573-96781316
XLOC_001502	9.34	5.45	0.58	-0.78	-2.11	3.50E-04	6.91E-03	P2RY2	1:143227554-143242518
XLOC_018830	36.51	21.30	0.58	-0.78	-2.96	5.00E-05	1.41E-03	DUSP1	3:53837408-53841158
XLOC_014469	51.78	30.16	0.58	-0.78	-2.66	5.00E-05	1.41E-03	TP53	19:11519969-11531427
XLOC_029270	15.86	9.24	0.58	-0.78	-2.76	5.00E-05	1.41E-03	ETS2	GL018727:2808337-2822042
XLOC_017981	11.35	6.61	0.58	-0.78	-2.54	5.00E-05	1.41E-03	PATZ1	21:3785123-3802889
XLOC_026825	9.87	5.75	0.58	-0.78	-1.69	3.35E-03	3.79E-02	ARHGEF16	AAGW02082356:12340-14228
XLOC_035051	13.76	8.00	0.58	-0.78	-2.64	5.00E-05	1.41E-03	ENSOCUG00000006396	GL018985:112012-150636
XLOC_000748	4.20	2.44	0.58	-0.78	-1.90	1.20E-03	1.78E-02	ENSOCUG00000026770	1:174934219-174936465
XLOC_022402	20.03	11.65	0.58	-0.78	-1.84	1.50E-03	2.09E-02	IMP4	7:59985705-59990658
XLOC_012318	655.41	380.91	0.58	-0.78	-3.32	5.00E-05	1.41E-03	ENSOCUG00000010443	17:60707702-60708828
XLOC_025892	1.51	0.88	0.58	-0.78	-1.80	4.65E-03	4.81E-02	SMAD7	9:89924493-89950849
XLOC_008667	90.84	52.77	0.58	-0.78	-2.23	1.50E-04	3.53E-03	HES1	14:89962124-89964999
XLOC_038372	11.50	6.67	0.58	-0.79	-2.64	5.00E-05	1.41E-03	PHKA1	X:51317197-51437727
XLOC_021387	48.56	28.17	0.58	-0.79	-2.81	5.00E-05	1.41E-03	NA	5:22656605-22720368
XLOC_029999	5.96	3.46	0.58	-0.79	-2.36	5.00E-05	1.41E-03	GPT2	GL018743:1016877-1057455
XLOC_032270	258.41	149.80	0.58	-0.79	-2.25	5.00E-05	1.41E-03	SNRPD3	GL018810:625034-651716
XLOC_008484	11.87	6.88	0.58	-0.79	-2.21	2.80E-03	3.32E-02	ZBTB38	14:34827910-34882991
XLOC_031222	11.44	6.62	0.58	-0.79	-2.49	5.50E-04	9.84E-03	NA	GL018776:1010873-1012646
XLOC_031493	47.90	27.65	0.58	-0.79	-1.63	3.00E-03	3.49E-02	ENSOCUG00000013445	GL018786:573909-575273
XLOC_025767	36.10	20.84	0.58	-0.79	-2.47	5.00E-05	1.41E-03	PSMG2	9:49414260-49438288
XLOC_006046	10.46	6.04	0.58	-0.79	-2.57	5.00E-05	1.41E-03	ARHGEF2	13:36868880-36897296
XLOC_000936	4.29	2.48	0.58	-0.79	-1.90	1.65E-03	2.24E-02	TMEM132A	1:193550486-193575083
XLOC_004081	9.28	5.35	0.58	-0.79	-2.39	1.20E-03	1.78E-02	RING1	12:23635788-23638339
XLOC_007497	6.71	3.87	0.58	-0.79	-2.14	2.00E-04	4.42E-03	SEPN1	13:139464122-139471284
XLOC_024930	8.49	4.90	0.58	-0.79	-2.50	2.50E-04	5.26E-03	NA	8:82250498-82252748
XLOC_018364	120.90	69.55	0.58	-0.80	-2.62	5.00E-05	1.41E-03	ENSOCUG00000002779	3:57816707-57823500
XLOC_010716	86.89	49.92	0.57	-0.80	-5.40	4.00E-04	7.69E-03	NA	15:21734685-21735011
XLOC_027832	18.52	10.64	0.57	-0.80	-2.82	5.00E-05	1.41E-03	PHC2	GL018704:4889073-5011916
XLOC_004092	53.66	30.82	0.57	-0.80	-1.95	8.50E-04	1.36E-02	HMGA1	12:24437171-24439978
XLOC_012332	9.22	5.30	0.57	-0.80	-2.33	1.00E-04	2.52E-03	LRR1	17:68756936-68769661
XLOC_019054	636.29	364.80	0.57	-0.80	-9.62	5.00E-05	1.41E-03	ENSOCUG00000022022	3:127677497-127677764
XLOC_000665	132.11	75.69	0.57	-0.80	-2.85	5.00E-05	1.41E-03	EIF3F	1:149719930-149768396
XLOC_038143	47.34	27.08	0.57	-0.81	-1.76	2.75E-03	3.29E-02	NA	X:110169071-110195458
XLOC_028713	72.09	41.19	0.57	-0.81	-2.04	7.50E-04	1.24E-02	TMEM258	GL018717:3017434-3022015
XLOC_037226	15.23	8.69	0.57	-0.81	-2.72	5.50E-04	9.84E-03	NA	GL019575:9401-10286
XLOC_033415	32.50	18.55	0.57	-0.81	-3.65	1.40E-03	1.98E-02	NA	GL018864:150526-150947
XLOC_005875	164.21	93.70	0.57	-0.81	-5.74	5.00E-05	1.41E-03	ENSOCUG00000023710	13:7157656-7158012
XLOC_038452	171.48	97.84	0.57	-0.81	-9.07	5.50E-04	9.84E-03	CKS2	X:71420756-71420996
XLOC_001659	25.26	14.41	0.57	-0.81	-3.01	5.00E-05	1.41E-03	RRAS2	1:156014769-156050337
XLOC_016479	83.98	47.91	0.57	-0.81	-2.18	2.50E-04	5.26E-03	ENSOCUG00000002392	2:91339549-91344844
XLOC_034241	9.38	5.35	0.57	-0.81	-1.92	1.60E-03	2.20E-02	YIPF2	GL018914:136996-154877
XLOC_001917	17.74	10.11	0.57	-0.81	-2.87	1.00E-03	1.55E-02	NA	1:5987471-5988095
XLOC_008059	4.19	2.39	0.57	-0.81	-2.33	3.50E-04	6.91E-03	NA	13:93886584-93889963
XLOC_034525	40.46	23.01	0.57	-0.81	-2.78	5.00E-05	1.41E-03	LOXL2	GL018937:273005-353669
XLOC_038839	38.40	21.82	0.57	-0.82	-4.38	2.80E-03	3.32E-02	NA	X:30495481-30495817
XLOC_018519	4.12	2.34	0.57	-0.82	-1.80	2.40E-03	2.97E-02	OSR2	3:114655952-114663800
XLOC_006714	247.13	140.32	0.57	-0.82	-2.67	5.00E-05	1.41E-03	ENSOCUG00000026497	13:2247362-2274564
XLOC_004436	2.57	1.46	0.57	-0.82	-1.63	4.55E-03	4.73E-02	NA	12:122369531-122371739
XLOC_000480	41.02	23.28	0.57	-0.82	-2.89	5.00E-05	1.41E-03	ENSOCUG00000001096	1:123180322-123185547
XLOC_037828	5.65	3.20	0.57	-0.82	-2.11	6.00E-04	1.06E-02	PPP1R3F	X:33836373-33853797
XLOC_019342	65.63	37.19	0.57	-0.82	-4.98	8.00E-04	1.30E-02	NA	3:52185445-52185787
XLOC_000908	26.35	14.92	0.57	-0.82	-3.06	5.00E-05	1.41E-03	ENSOCUG00000022710	1:192259960-192260836
XLOC_029105	296.66	167.99	0.57	-0.82	-3.90	5.00E-05	1.41E-03	ENSOCUG00000021352	GL018724:2793160-2814295
XLOC_014754	65.03	36.80	0.57	-0.82	-3.68	5.00E-05	1.41E-03	RPL19	19:40523281-40526475
XLOC_011521	14.20	8.03	0.57	-0.82	-2.67	5.00E-05	1.41E-03	SHISA4	16:69693885-69699451
XLOC_014624	14.20	8.03	0.57	-0.82	-2.36	1.50E-04	3.53E-03	TMEM98	19:22461237-22472121
XLOC_025693	52.17	29.50	0.57	-0.82	-3.00	5.00E-05	1.41E-03	ARHGEF3	9:23620035-23951867
XLOC_002885	414.86	234.50	0.57	-0.82	-15.58	4.50E-04	8.42E-03	NA	10:4898905-4899100
XLOC_006511	5.56	3.14	0.57	-0.82	-1.75	2.15E-03	2.76E-02	ENSOCUG00000024452	13:121943051-121959599
XLOC_031475	84.47	47.73	0.57	-0.82	-2.94	5.00E-05	1.41E-03	FXYD5	GL018786:96453-106923

Transcriptome Gene ID	Uninfected RK-13 Mean FPKM	T. hominis infected RK-13 Mean FPKM	Fold Change	Log2 Fold Change	Test stat	P value	Q value	Ensembl Gene Name / Gene ID	Gene Locus (Chromosome/scaffold:position)
XLOC_024863	7.65	4.32	0.57	-0.82	-2.62	5.00E-05	1.41E-03	NA	8:52830668-52834116
XLOC_036652	38.07	21.50	0.56	-0.82	-3.35	2.00E-04	4.42E-03	RABAC1	GL019289:3770-5526
XLOC_024355	20.36	11.49	0.56	-0.82	-2.94	5.00E-05	1.41E-03	COL4A2	8:111654940-111791971
XLOC_018174	113.14	63.86	0.56	-0.83	-2.72	5.00E-05	1.41E-03	UBE2B	3:17154092-17165288
XLOC_019009	127.03	71.69	0.56	-0.83	-3.61	5.00E-05	1.41E-03	ENSOCUG00000017386,SNORA72	3:113845451-113855784
XLOC_027277	16.22	9.15	0.56	-0.83	-1.84	2.80E-03	3.32E-02	TOR2A	GL018699:285-19364
XLOC_011201	54.90	30.95	0.56	-0.83	-2.88	5.00E-05	1.41E-03	UBE2T	16:69339427-69348013
XLOC_011070	4.91	2.77	0.56	-0.83	-1.82	2.35E-03	2.93E-02	NMT2	16:46195764-46232843
XLOC_011203	64.31	36.21	0.56	-0.83	-1.96	1.35E-03	1.93E-02	ARL8A	16:69518392-69522736
XLOC_008518	309.22	174.05	0.56	-0.83	-2.95	5.00E-05	1.41E-03	ENSOCUG00000021109	14:45695154-45725298
XLOC_016272	17.09	9.62	0.56	-0.83	-2.99	5.00E-05	1.41E-03	RELL1	2:27137390-27198488
XLOC_023611	20.09	11.30	0.56	-0.83	-2.89	1.00E-04	2.52E-03	NA	7:90488123-90489274
XLOC_032460	3.59	2.02	0.56	-0.83	-1.79	2.80E-03	3.32E-02	B9D1	GL018817:336852-344433
XLOC_001584	27.25	15.32	0.56	-0.83	-3.03	5.00E-05	1.41E-03	PRKCDBP	1:147333108-147335429
XLOC_018998	129.48	72.80	0.56	-0.83	-4.18	5.00E-05	1.41E-03	ENSOCUG00000003392	3:110241611-110242214
XLOC_028605	234.73	131.95	0.56	-0.83	-5.41	5.00E-05	1.41E-03	PSMG4	GL018715:2410409-2420073
XLOC_034688	36.80	20.65	0.56	-0.83	-2.12	3.00E-04	6.09E-03	ENSOCUG00000011182	GL018951:93334-129930
XLOC_020056	2.25	1.26	0.56	-0.83	-2.37	5.00E-05	1.41E-03	ESPL1	4:37101053-37123381
XLOC_002354	22.36	12.55	0.56	-0.83	-3.00	1.00E-04	2.52E-03	NA	1:150745928-150746838
XLOC_027224	82.79	46.43	0.56	-0.83	-2.52	5.00E-05	1.41E-03	LRRC47	AAGW02083553:3898-6260
XLOC_000787	34.75	19.49	0.56	-0.83	-3.14	5.00E-05	1.41E-03	NA	1:185672850-185675475
XLOC_027418	5.95	3.33	0.56	-0.84	-2.22	1.70E-03	2.29E-02	NA	GL018699:36861-38032
XLOC_031489	516.33	289.13	0.56	-0.84	-5.64	5.00E-05	1.41E-03	COX6B1	GL018786:497700-506657
XLOC_022163	9.79	5.48	0.56	-0.84	-2.50	1.10E-03	1.66E-02	ENSOCUG00000025881	6:27292005-27293014
XLOC_028109	196.44	109.92	0.56	-0.84	-6.04	5.00E-05	1.41E-03	EIF4EBP1	GL018706:5335424-5354625
XLOC_027164	7.49	4.19	0.56	-0.84	-2.41	5.00E-05	1.41E-03	INTS1	AAGW02083290:15-6834
XLOC_010808	2.28	1.28	0.56	-0.84	-2.14	1.05E-03	1.60E-02	NA	15:73767815-73771334
XLOC_022585	83.48	46.65	0.56	-0.84	-2.90	5.00E-05	1.41E-03	MYO1B	7:131681524-131871528
XLOC_014658	3.32	1.85	0.56	-0.84	-2.23	8.00E-04	1.30E-02	TBX2	19:27598881-27607454
XLOC_034587	4.60	2.57	0.56	-0.84	-2.10	5.00E-04	9.12E-03	TM7SF2,VPS51	GL018942:149291-172195
XLOC_020234	1233.24	688.92	0.56	-0.84	-1.75	1.65E-03	2.24E-02	SNRPF	4:75061837-75068476
XLOC_034649	5.18	2.89	0.56	-0.84	-2.57	5.00E-05	1.41E-03	COL6A1	GL018946:25285-45866
XLOC_032882	4.12	2.30	0.56	-0.84	-2.12	1.50E-04	3.53E-03	C19orf66	GL018833:217265-222379
XLOC_022184	14.44	8.05	0.56	-0.84	-2.76	5.00E-05	1.41E-03	NA	6:8880497-8881641
XLOC_029193	9.89	5.51	0.56	-0.84	-2.60	1.00E-04	2.52E-03	ACOT8	GL018725:846883-859030
XLOC_037021	9.37	5.22	0.56	-0.84	-2.01	1.55E-03	2.14E-02	ENSOCUG00000024569	GL019444:55087-60688
XLOC_035181	253.18	140.67	0.56	-0.85	-4.58	5.00E-05	1.41E-03	SNRPD2	GL019006:258107-270482
XLOC_032610	2.98	1.65	0.55	-0.85	-2.45	2.50E-04	5.26E-03	BCL7A	GL018824:621652-651037
XLOC_037231	8.31	4.61	0.55	-0.85	-2.27	1.00E-04	2.52E-03	COL5A1	GL019578:28547-49246
XLOC_037650	29.34	16.28	0.55	-0.85	-4.08	4.55E-03	4.73E-02	MT-ND3	MT:9490-9837
XLOC_021316	14.44	8.01	0.55	-0.85	-2.18	2.00E-04	4.42E-03	PDCD2L	5:4202511-4223179
XLOC_037503	816.61	452.90	0.55	-0.85	-3.09	5.00E-05	1.41E-03	PSMA7	GL019793:10-2342
XLOC_034146	3.91	2.17	0.55	-0.85	-2.10	2.50E-04	5.26E-03	SBF1	GL018905:366442-375383
XLOC_016779	29.70	16.45	0.55	-0.85	-2.14	8.00E-04	1.30E-02	NA	2:157715198-158360933
XLOC_015351	7.01	3.88	0.55	-0.85	-2.51	3.50E-04	6.91E-03	KPNA2	19:49592432-49602809
XLOC_021240	15.72	8.69	0.55	-0.85	-2.84	5.00E-05	1.41E-03	NA	4:84512458-84513888
XLOC_013382	39.12	21.63	0.55	-0.85	-3.04	5.00E-05	1.41E-03	ZNF503	18:12124740-12129364
XLOC_027238	16.05	8.87	0.55	-0.86	-2.84	1.00E-04	2.52E-03	PSCA	AAGW02083648:3534-5937
XLOC_020792	22.80	12.58	0.55	-0.86	-3.12	5.00E-05	1.41E-03	MCM5	4:86038162-86058078
XLOC_018230	24.75	13.66	0.55	-0.86	-2.27	5.00E-05	1.41E-03	PCDHGB1,PCDHGB7,PCDHGC5	3:23379863-23541420
XLOC_037113	1.47	0.81	0.55	-0.86	-1.80	2.35E-03	2.93E-02	PKNOX1	GL019508:29229-51166
XLOC_027611	4.38	2.41	0.55	-0.86	-2.68	5.00E-05	1.41E-03	ENSOCUG00000006859	GL018701:1361853-1633039
XLOC_013737	4.78	2.63	0.55	-0.86	-2.76	5.00E-05	1.41E-03	C6ST	18:15365035-15395723
XLOC_022176	14.68	8.07	0.55	-0.86	-2.89	8.50E-04	1.36E-02	NA	6:5282925-5283560
XLOC_026220	158.01	86.84	0.55	-0.86	-4.47	5.00E-05	1.41E-03	NA	9:52821409-52821977
XLOC_006808	72.44	39.80	0.55	-0.86	-3.87	5.00E-05	1.41E-03	UCK2	13:26987888-26999994
XLOC_032422	0.96	0.53	0.55	-0.86	-2.05	9.50E-04	1.48E-02	PLXNA3	GL018816:87964-103410
XLOC_024149	195.77	107.47	0.55	-0.87	-3.09	5.00E-05	1.41E-03	NA	8:32787710-32790355
XLOC_020043	162.36	89.09	0.55	-0.87	-2.67	5.00E-05	1.41E-03	KRT7	4:36275381-36323529
XLOC_001041	3.13	1.72	0.55	-0.87	-2.42	5.00E-05	1.41E-03	TESK1	1:18292770-18303015
XLOC_016117	466.50	255.51	0.55	-0.87	-2.75	5.00E-05	1.41E-03	ENSOCUG00000027683	2:143398250-143618573
XLOC_037150	58.94	32.21	0.55	-0.87	-4.07	5.00E-05	1.41E-03	NA	GL019531:29285-29814
XLOC_032350	2.04	1.12	0.55	-0.87	-1.96	1.10E-03	1.66E-02	ENSOCUG00000024624	GL018813:121248-138184
XLOC_037384	28.89	15.77	0.55	-0.87	-2.13	7.00E-04	1.18E-02	VPS28	GL019699:20453-24563
XLOC_031631	22.88	12.48	0.55	-0.87	-1.85	9.00E-04	1.42E-02	EXOSC5	GL018789:442390-452972
XLOC_017053	16.64	9.07	0.54	-0.88	-2.98	2.50E-04	5.26E-03	NA	2:67346382-67347133
XLOC_020349	126.06	68.70	0.54	-0.88	-2.06	6.00E-04	1.06E-02	MYL9	4:3439511-3448504
XLOC_019319	4.24	2.31	0.54	-0.88	-2.12	3.35E-03	3.79E-02	NA	3:44062204-44063397
XLOC_037497	4.45	2.43	0.54	-0.88	-2.15	2.40E-03	2.97E-02	NA	GL019782:44-1333
XLOC_037811	1753.54	954.35	0.54	-0.88	-23.90	5.00E-05	1.41E-03	USMG5	X:33280221-33297593
XLOC_027504	789.70	429.70	0.54	-0.88	-8.25	5.00E-05	1.41E-03	ENSOCUG00000003584	GL018700:704659-704977
XLOC_020588	5.74	3.12	0.54	-0.88	-2.10	3.00E-04	6.09E-03	SPRYD3	4:36927541-36957529
XLOC_019124	6.22	3.38	0.54	-0.88	-2.54	5.00E-05	1.41E-03	NA	3:387455-389320
XLOC_026262	4.32	2.35	0.54	-0.88	-2.10	3.60E-03	3.99E-02	NA	9:58598388-58599513
XLOC_006496	2.11	1.14	0.54	-0.88	-1.68	3.95E-03	4.28E-02	CCDC17	13:120981823-120985624
XLOC_032984	20.59	11.18	0.54	-0.88	-3.10	5.00E-05	1.41E-03	COL6A3	GL018840:384609-433502
XLOC_016601	11.64	6.31	0.54	-0.88	-2.04	2.30E-03	2.88E-02	HK2	2:111595304-111721018
XLOC_013914	9.20	4.99	0.54	-0.88	-2.67	1.00E-04	2.52E-03	ITPRIP	18:52236240-52261080
XLOC_026810	2.00	1.09	0.54	-0.88	-1.89	4.75E-03	4.87E-02	NA	AAGW02082284:12925-14996
XLOC_010740	4.81	2.61	0.54	-0.88	-2.18	3.55E-03	3.95E-02	NA	15:36269881-36270964
XLOC_039156	32.38	17.54	0.54	-0.88	-3.70	5.00E-05	1.41E-03	NA	X:103019218-103019749
XLOC_018886	21.70	11.75	0.54	-0.89	-2.12	1.50E-04	3.53E-03	RPS20	3:71607724-71609256
XLOC_018633	6.71	3.63	0.54	-0.89	-2.24	3.40E-03	3.83E-02	NA	3:8820511-8824682
XLOC_004066	305.62	165.16	0.54	-0.89	-3.11	5.00E-05	1.41E-03	TUBB	12:22748029-22752315
XLOC_014475	102.14	55.07	0.54	-0.89	-1.93	1.80E-03	2.39E-02	ENSOCUG00000005534	19:11767433-11770377
XLOC_036468	3.52	1.90	0.54	-0.89	-2.14	1.85E-03	2.44E-02	MMP11	GL019236:34356-42550
XLOC_032667	34.70	18.67	0.54	-0.89	-2.89	5.00E-05	1.41E-03	COMT	GL018826:718960-746470
XLOC_004174	12.98	6.97	0.54	-0.90	-2.65	5.00E-05	1.41E-03	SLC29A1	12:33601686-33615197
XLOC_012119	16.74	8.99	0.54	-0.90	-2.43	5.00E-05	1.41E-03	EHD4	17:30179089-30255452
XLOC_031427	3.40	1.83	0.54	-0.90	-2.02	4.55E-03	4.73E-02	NA	GL018785:327840-329137
XLOC_035171	79.23	42.56	0.54	-0.90	-2.62	5.00E-05	1.41E-03	VASP	GL019006:124484-233041
XLOC_023976	8.25	4.43	0.54	-0.90	-2.66	2.50E-04	5.26E-03	NA	7:165553493-165554898
XLOC_003901	1.51	0.81	0.54	-0.90	-1.88	4.35E-03	4.57E-02	NA	11:82726652-82729427
XLOC_014386	55.16	29.56	0.54	-0.90	-3.77	5.00E-05	1.41E-03	NA	18:67590066-67590921
XLOC_029758	8.43	4.52	0.54	-0.90	-2.70	5.00E-05	1.41E-03	ENSOCUG00000026694	GL018738:148362-247744
XLOC_000176	9.01	4.83	0.54	-0.90	-2.40	1.00E-04	2.52E-03	RPS6	1:34527155-34531340
XLOC_013832	100.78	53.97	0.54	-0.90	-3.80	5.00E-05	1.41E-03	PDLIM1	18:43944161-44010361
XLOC_015391	9.58	5.12	0.53	-0.90	-2.09	5.00E-04	9.12E-03	SPNS3	19:14117224-14166609
XLOC_006754	4.56	2.44	0.53	-0.90	-1.93	2.20E-03	2.80E-02	SMARCD3	13:12642765-12657349
XLOC_027763	153.37	82.03	0.53	-0.90	-2.94	5.00E-05	1.41E-03	BHLHE40	GL018703:3264229-3270423
XLOC_028122	59.90	32.02	0.53	-0.90	-5.62	7.00E-04	1.18E-02	NA	GL018706:332859-333169
XLOC_038691	2.91	1.55	0.53	-0.91	-2.36	2.50E-04	5.26E-03	NA	X:3482601-3485929
XLOC_032390	11.08	5.91	0.53	-0.91	-2.74	5.00E-05	1.41E-03	ENSOCUG00000029514	GL018815:367865-380661
XLOC_033443	18.73	9.99	0.53	-0.91	-2.42	1.00E-04	2.52E-03	ZMYND19	GL018867:473767-478951
XLOC_026427	18.13	9.66	0.53	-0.91	-3.22	6.00E-04	1.06E-02	ENSOCUG00000027889	AAGW02079242:70261-70846
XLOC_006735	36.08	19.21	0.53	-0.91	-3.10	5.00E-05	1.41E-03	ENSOCUG00000000064	13:9909565-9974628
XLOC_012005	12042.70	6410.38	0.53	-0.91	-2.57	5.00E-05	1.41E-03	ENSOCUG00000014619	17:7869795-8081638
XLOC_011457	59.20	31.51	0.53	-0.91	-3.15	5.00E-05	1.41E-03	ATF3	16:60421623-60434540
XLOC_030930	65.44	34.82	0.53	-0.91	-2.73	1.50E-04	3.53E-03	CLDN4	GL018765:813992-953393
XLOC_025463	22.72	12.09	0.53	-0.91	-2.66	5.00E-05	1.41E-03	NA	9:1684906-1689763
XLOC_009681	38.25	20.35	0.53	-0.91	-3.61	5.00E-05	1.41E-03	NA	14:86029191-86029993

Transcriptome Gene ID	Uninfected RK-13 Mean FPKM	T. hominis infected RK-13 Mean FPKM	Fold Change	Log2 Fold Change	Test stat	P value	Q value	Ensembl Gene Name / Gene ID	Gene Locus (Chromosome/scaffold:position)
XLOC_015507	2.94	1.56	0.53	-0.91	-2.15	1.60E-03	2.20E-02	NA	19:39918708-39920611
XLOC_031282	193.38	102.82	0.53	-0.91	-4.44	5.00E-05	1.41E-03	NA	GL018778:1080347-1081082
XLOC_019026	62.98	33.48	0.53	-0.91	-1.90	1.65E-03	2.24E-02	ENSOCUG00000008661	3:116741404-116747004
XLOC_017085	2.70	1.43	0.53	-0.91	-1.98	3.20E-03	3.67E-02	NA	2:74979760-74981340
XLOC_037896	9.15	4.85	0.53	-0.91	-2.93	5.00E-05	1.41E-03	GDPD2	X:48983414-48997529
XLOC_005831	26.35	13.97	0.53	-0.92	-4.07	2.05E-03	2.65E-02	NA	12:142766942-142767315
XLOC_020467	15.67	8.30	0.53	-0.92	-1.93	2.70E-03	3.25E-02	NXT1	4:13605712-13608849
XLOC_037513	4.23	2.24	0.53	-0.92	-2.31	5.00E-04	9.12E-03	NA	GL019802:5855-7449
XLOC_023204	97.73	51.77	0.53	-0.92	-3.24	5.00E-05	1.41E-03	FN1	7:156703348-156770766
XLOC_004884	31.91	16.85	0.53	-0.92	-3.60	5.00E-05	1.41E-03	NA	12:62141564-62145223
XLOC_034938	142.54	75.19	0.53	-0.92	-5.88	5.00E-05	1.41E-03	POLR2F	GL018972:212612-236536
XLOC_014513	568.63	299.82	0.53	-0.92	-4.43	5.00E-05	1.41E-03	ENSOCUG00000022355	19:13630899-13631767
XLOC_002852	37.26	19.62	0.53	-0.93	-2.97	5.00E-05	1.41E-03	POLD2	10:44664283-44681336
XLOC_030651	176.96	93.19	0.53	-0.93	-3.02	5.00E-05	1.41E-03	MCM7	GL018760:97013-108035
XLOC_000192	27.77	14.61	0.53	-0.93	-3.56	5.00E-05	1.41E-03	ENSOCUG00000005565	1:42055787-42056832
XLOC_006664	226.03	118.90	0.53	-0.93	-3.31	5.00E-05	1.41E-03	ENSOCUG00000006493	13:139370111-139373388
XLOC_036587	34.02	17.87	0.53	-0.93	-2.93	5.00E-05	1.41E-03	MED25	GL019272:8089-17814
XLOC_028939	8.46	4.44	0.53	-0.93	-2.65	2.00E-04	4.42E-03	CBX3	GL018720:3534604-3536661
XLOC_013656	129.92	68.18	0.52	-0.93	-6.59	5.00E-05	1.41E-03	TCEB1	18:68415602-68415938
XLOC_002662	950.15	498.45	0.52	-0.93	-6.64	5.00E-05	1.41E-03	ENSOCUG00000005304	10:40065950-40066358
XLOC_017601	3.70	1.94	0.52	-0.93	-2.24	1.00E-04	2.52E-03	ENSOCUG00000014429	20:7031747-7121597
XLOC_037800	55.55	29.11	0.52	-0.93	-3.30	5.00E-05	1.41E-03	TIMP1	X:32645153-32703324
XLOC_029052	6.02	3.15	0.52	-0.93	-2.51	5.50E-04	9.84E-03	NA	GL018723:2583466-2585978
XLOC_017308	7.81	4.09	0.52	-0.93	-2.53	3.05E-03	3.54E-02	NA	2:139637012-139637708
XLOC_021755	4.35	2.28	0.52	-0.93	-2.28	1.40E-03	1.98E-02	NA	5:3972954-3974272
XLOC_029162	5.35	2.80	0.52	-0.93	-2.66	1.00E-04	2.52E-03	CD40	GL018725:1087564-1098803
XLOC_004104	53.01	27.75	0.52	-0.93	-3.43	5.00E-05	1.41E-03	ENSOCUG00000004065	12:25543354-25559581
XLOC_031569	8.81	4.61	0.52	-0.93	-2.93	5.00E-05	1.41E-03	TFAP4	GL018787:520277-533396
XLOC_037172	2.24	1.17	0.52	-0.94	-2.18	1.40E-03	1.98E-02	NA	GL019545:39615-42242
XLOC_036680	7.47	3.90	0.52	-0.94	-2.05	8.00E-04	1.30E-02	NA	GL019300:85445-86687
XLOC_027571	12.72	6.63	0.52	-0.94	-2.95	1.30E-03	1.87E-02	NA	GL018700:8439816-8440444
XLOC_034179	142.19	74.11	0.52	-0.94	-2.89	5.00E-05	1.41E-03	NA	GL018908:228052-229767
XLOC_009627	133.28	69.39	0.52	-0.94	-7.76	5.00E-05	1.41E-03	NA	14:74351773-74352066
XLOC_028235	1.87	0.97	0.52	-0.94	-2.33	1.50E-04	3.53E-03	ENSOCUG00000026949	GL018709:3068786-3101821
XLOC_026789	10.48	5.45	0.52	-0.94	-1.64	3.55E-03	3.95E-02	HIP1R	AAGW02082218:0-4530
XLOC_037450	34.11	17.74	0.52	-0.94	-2.75	5.00E-05	1.41E-03	NME4	GL019754:7762-10291
XLOC_005191	3.19	1.66	0.52	-0.94	-2.25	1.10E-03	1.66E-02	NA	12:6094152-6096005
XLOC_020715	229.21	119.18	0.52	-0.94	-4.60	5.00E-05	1.41E-03	ENSOCUG00000024686	4:64523701-64524430
XLOC_011877	27.52	14.31	0.52	-0.94	-3.76	2.50E-04	5.26E-03	NA	16:68041006-68041520
XLOC_009161	268.01	139.28	0.52	-0.94	-3.50	5.00E-05	1.41E-03	CLDN1	14:85971156-85989565
XLOC_008468	9.72	5.05	0.52	-0.94	-2.99	5.00E-05	1.41E-03	MRAS	14:32018723-32046246
XLOC_016273	244.45	126.94	0.52	-0.95	-5.11	5.00E-05	1.41E-03	ENSOCUG00000022888	2:27709551-27710106
XLOC_004209	56.68	29.42	0.52	-0.95	-5.36	6.00E-04	1.06E-02	7SK	12:42739159-42739490
XLOC_019971	9.03	4.68	0.52	-0.95	-2.68	5.00E-05	1.41E-03	FOXA2	4:14204088-14207440
XLOC_026513	235.22	121.69	0.52	-0.95	-8.69	5.00E-05	1.41E-03	PPP1R14B	AAGW02080442:46427-46718
XLOC_029678	2.73	1.41	0.52	-0.95	-2.59	5.00E-05	1.41E-03	SLC7A1	GL018735:2510296-2536658
XLOC_021238	17.04	8.81	0.52	-0.95	-3.23	5.00E-05	1.41E-03	NA	4:84467045-84468144
XLOC_022159	43.24	22.34	0.52	-0.95	-2.93	1.50E-04	3.53E-03	GNB2	6:27122584-27201248
XLOC_011568	69.75	36.04	0.52	-0.95	-5.88	2.00E-04	4.42E-03	NA	16:102817-103148
XLOC_029797	1.01	0.52	0.52	-0.95	-2.05	1.30E-03	1.87E-02	ZNF710	GL018738:1571079-1580727
XLOC_019894	23.28	12.01	0.52	-0.95	-3.14	5.00E-05	1.41E-03	E2F1	4:6002820-6012567
XLOC_030500	83.52	43.09	0.52	-0.95	-7.76	6.00E-04	1.06E-02	ENSOCUG00000022885	GL018757:1239538-1239801
XLOC_025657	9.59	4.95	0.52	-0.96	-2.75	1.85E-03	2.44E-02	NA	9:18740000-18740871
XLOC_009131	1.76	0.91	0.52	-0.96	-2.07	1.15E-03	1.72E-02	CHORDIN	14:81327038-81334113
XLOC_008831	34.93	17.99	0.52	-0.96	-4.33	1.50E-04	3.53E-03	ENSOCUG00000013322	14:144822955-144823383
XLOC_034066	3.90	2.01	0.51	-0.96	-2.25	1.55E-03	2.14E-02	NA	GL018900:35354-36611
XLOC_034037	7.92	4.07	0.51	-0.96	-2.59	3.90E-03	4.24E-02	NA	GL018899:250071-250679
XLOC_012028	4317.13	2219.83	0.51	-0.96	-2.48	1.00E-04	2.52E-03	ANXA2	17:11979743-12028244
XLOC_010224	2.11	1.09	0.51	-0.96	-2.09	3.50E-04	6.91E-03	RASGEF1B	15:68716393-68875629
XLOC_020480	27.90	14.34	0.51	-0.96	-3.44	5.00E-05	1.41E-03	RIN2	4:16541037-16664159
XLOC_018426	164.43	84.47	0.51	-0.96	-5.74	5.00E-05	1.41E-03	RPS23	3:83730860-83731292
XLOC_010726	188.53	96.83	0.51	-0.96	-15.12	1.30E-03	1.87E-02	NA	15:27951534-27951723
XLOC_032442	94.99	48.76	0.51	-0.96	-3.47	5.00E-05	1.41E-03	BGN	GL018816:868233-879291
XLOC_001898	45.14	23.17	0.51	-0.96	-2.83	5.00E-05	1.41E-03	PPP1CA	1:194828533-194837468
XLOC_014476	4.54	2.33	0.51	-0.96	-2.17	5.00E-05	1.41E-03	PLSCR3	19:11774658-11778811
XLOC_003493	399.65	204.98	0.51	-0.96	-3.47	5.00E-05	1.41E-03	RPL37,SNORD72	11:61718796-61722341
XLOC_018482	95.38	48.90	0.51	-0.96	-5.17	5.00E-05	1.41E-03	ENSOCUG00000016091	3:104784724-104785186
XLOC_022154	2.05	1.05	0.51	-0.96	-2.15	2.00E-04	4.42E-03	SLC12A9	6:27001285-27010068
XLOC_025613	6.04	3.10	0.51	-0.96	-2.09	9.00E-04	1.42E-02	DALRD3	9:16635460-16648488
XLOC_023542	40.12	20.56	0.51	-0.96	-5.46	2.65E-03	3.21E-02	NA	7:65225940-65226241
XLOC_011537	52.15	26.70	0.51	-0.97	-2.50	1.00E-04	2.52E-03	NEK7	16:72918151-73007444
XLOC_004026	30.38	15.52	0.51	-0.97	-1.80	3.65E-03	4.03E-02	SNORD48,SNORD52	12:20684711-20687125
XLOC_030055	1.61	0.82	0.51	-0.97	-2.31	2.50E-04	5.26E-03	ADAMTS7	GL018746:435320-474341
XLOC_020026	118.99	60.74	0.51	-0.97	-4.91	5.00E-05	1.41E-03	NA	4:34267836-34271344
XLOC_031487	10.77	5.50	0.51	-0.97	-2.74	5.00E-05	1.41E-03	HAUS5	GL018786:394608-480597
XLOC_000264	230.16	117.46	0.51	-0.97	-4.36	5.00E-05	1.41E-03	GAPDH	1:67461814-67462816
XLOC_006500	2.96	1.51	0.51	-0.97	-1.92	8.00E-04	1.30E-02	MUTYH	13:121316472-121325177
XLOC_018680	30.79	15.70	0.51	-0.97	-3.81	5.00E-05	1.41E-03	ENSOCUG00000021117	3:19170973-19171623
XLOC_032962	130.11	66.33	0.51	-0.97	-4.85	5.00E-05	1.41E-03	ENSOCUG00000023673	GL018838:112876-113479
XLOC_024287	73.18	37.30	0.51	-0.97	-3.47	5.00E-05	1.41E-03	LMO7	8:77229933-77459254
XLOC_029880	2.79	1.42	0.51	-0.97	-2.02	4.70E-03	4.84E-02	NA	GL018740:641276-642561
XLOC_019246	3.19	1.63	0.51	-0.97	-2.17	1.80E-03	2.39E-02	NA	3:23217478-23218838
XLOC_038260	7.96	4.05	0.51	-0.97	-1.64	7.50E-04	1.24E-02	ENSOCUG00000018016,ENSOCUG00000018035	X:30971638-30973645
XLOC_029352	127.45	64.86	0.51	-0.97	-3.81	5.00E-05	1.41E-03	RCAN1	GL018729:1284717-1292493
XLOC_030683	8.27	4.21	0.51	-0.97	-2.91	5.00E-05	1.41E-03	ZSCAN25	GL018760:674513-692569
XLOC_029145	38.49	19.58	0.51	-0.98	-1.85	2.25E-03	2.84E-02	DBNDD2	GL018725:548844-553417
XLOC_005777	436.53	222.03	0.51	-0.98	-6.12	5.00E-05	1.41E-03	NA	12:131312438-131312907
XLOC_013932	135.29	68.68	0.51	-0.98	-3.46	5.00E-05	1.41E-03	ABLIM1	18:62008155-62195848
XLOC_017977	16.44	8.34	0.51	-0.98	-1.68	4.65E-03	4.81E-02	SMTN	21:3539611-3565413
XLOC_017215	14.78	7.50	0.51	-0.98	-3.21	5.00E-05	1.41E-03	NA	2:115506063-115507141
XLOC_037233	32.04	16.25	0.51	-0.98	-2.09	4.00E-04	7.69E-03	ASF1B	GL019579:26646-29448
XLOC_020280	2.21	1.12	0.51	-0.98	-2.51	5.00E-05	1.41E-03	PDGFB	4:84240585-84257745
XLOC_015257	19.14	9.70	0.51	-0.98	-3.21	5.00E-05	1.41E-03	JUP	19:42674673-42696773
XLOC_001888	24.48	12.41	0.51	-0.98	-2.41	5.00E-05	1.41E-03	MRPL11	1:194078173-194080897
XLOC_012545	1.32	0.67	0.51	-0.98	-2.04	1.40E-03	1.98E-02	CHAC1	17:31128126-31132281
XLOC_001057	21.72	11.00	0.51	-0.98	-3.81	1.25E-03	1.82E-02	ENSOCUG00000028075	1:19709776-19710187
XLOC_032838	88.47	44.80	0.51	-0.98	-2.92	5.00E-05	1.41E-03	ZNHIT1	GL018831:253468-258987
XLOC_036702	200.39	101.43	0.51	-0.98	-10.35	5.00E-05	1.41E-03	NA	GL019309:38762-40100
XLOC_003383	20.40	10.32	0.51	-0.98	-3.25	5.00E-05	1.41E-03	ENSOCUG00000007162	11:15520518-15588463
XLOC_020713	4.83	2.44	0.51	-0.98	-2.32	2.95E-03	3.44E-02	NA	4:61974992-61976134
XLOC_009593	3.41	1.72	0.51	-0.99	-2.47	2.00E-04	4.42E-03	NA	14:65955133-65957258
XLOC_034184	28.66	14.48	0.51	-0.99	-3.37	5.00E-05	1.41E-03	GPRC5C	GL018908:374917-386606
XLOC_008053	15.04	7.59	0.50	-0.99	-3.33	5.00E-05	1.41E-03	NA	13:93848153-93849840
XLOC_034221	12.95	6.53	0.50	-0.99	-2.74	5.00E-05	1.41E-03	SERTAD1	GL018912:109785-112817
XLOC_013611	4.01	2.02	0.50	-0.99	-2.69	1.00E-04	2.52E-03	DUSP5	18:58114242-58128665
XLOC_000322	35.65	17.96	0.50	-0.99	-3.58	5.00E-05	1.41E-03	ETS1	1:88323118-88459437
XLOC_032282	21.50	10.82	0.50	-0.99	-3.73	2.50E-04	5.26E-03	MIF	GL018810:947035-947691
XLOC_008508	3.32	1.67	0.50	-0.99	-2.01	1.00E-03	1.55E-02	ENSOCUG00000026009	14:43553259-43591116
XLOC_032080	5.65	2.84	0.50	-0.99	-2.42	3.00E-03	3.49E-02	NA	GL018803:911430-914326
XLOC_012002	78.34	39.39	0.50	-0.99	-2.39	5.00E-05	1.41E-03	NA	17:7844344-7869469
XLOC_010361	26.14	13.14	0.50	-0.99	-4.29	1.30E-03	1.87E-02	ENSOCUG00000001516	15:4434502-4434881

Transcriptome Gene ID	Uninfected RK-13 Mean FPKM	T. hominis infected RK-13 Mean FPKM	Fold Change	Log2 Fold Change	Test stat	P value	Q value	Ensembl Gene Name / Gene ID	Gene Locus (Chromosome/scaffold:position)
XLOC_037648	38.16	19.17	0.50	-0.99	-3.91	5.00E-05	1.41E-03	MT-CO3	MT:8636-9420
XLOC_002920	2.99	1.50	0.50	-0.99	-2.42	2.50E-04	5.26E-03	NA	10:13611648-13613950
XLOC_008088	4.35	2.18	0.50	-1.00	-2.23	4.85E-03	4.95E-02	NA	13:94001091-94001915
XLOC_004325	96.51	48.33	0.50	-1.00	-5.83	5.00E-05	1.41E-03	ENSOCUG00000022257	12:90642913-90643309
XLOC_004818	374.40	187.38	0.50	-1.00	-3.12	5.00E-05	1.41E-03	ENSOCUG00000002821	12:37055035-37072872
XLOC_009452	2.92	1.46	0.50	-1.00	-2.65	5.00E-05	1.41E-03	NA	14:17063957-17067459
XLOC_036604	4.25	2.12	0.50	-1.00	-2.18	1.30E-03	1.87E-02	NA	GL019277:45180-76619
XLOC_028347	41.16	20.52	0.50	-1.00	-3.85	5.00E-05	1.41E-03	SOSTDC1	GL018710:1254278-1259030
XLOC_008895	3094.65	1541.10	0.50	-1.01	-5.87	5.00E-05	1.41E-03	RPS19	14:2333404-2333898
XLOC_013482	70.55	35.10	0.50	-1.01	-3.69	5.00E-05	1.41E-03	IFIT2	18:37228149-37236410
XLOC_035055	21.79	10.83	0.50	-1.01	-3.72	2.00E-04	4.42E-03	ENSOCUG00000027725	GL018986:265109-265627
XLOC_032030	79.04	39.27	0.50	-1.01	-4.22	5.00E-05	1.41E-03	NA	GL018802:144109-155159
XLOC_021244	11.45	5.68	0.50	-1.01	-3.16	5.00E-05	1.41E-03	NA	4:85017426-85018949
XLOC_035677	7.13	3.54	0.50	-1.01	-2.90	1.00E-04	2.52E-03	UCKL1	GL019070:121678-126951
XLOC_006999	86.36	42.77	0.50	-1.01	-2.58	5.00E-05	1.41E-03	ENSOCUG00000028209	13:42823056-42840852
XLOC_036236	8.00	3.96	0.49	-1.01	-2.57	5.00E-05	1.41E-03	IRF2BP1	GL019168:48246-50334
XLOC_019287	19.19	9.50	0.49	-1.01	-3.60	5.00E-05	1.41E-03	NA	3:32357695-32359786
XLOC_033712	1.58	0.78	0.49	-1.02	-1.81	2.35E-03	2.93E-02	ZNF180	GL018881:450771-453128
XLOC_020048	106.76	52.77	0.49	-1.02	-3.59	5.00E-05	1.41E-03	ENSOCUG00000027691	4:36850181-36854502
XLOC_035724	1.45	0.72	0.49	-1.02	-2.00	3.25E-03	3.71E-02	TELO2	GL019077:16495-27942
XLOC_020787	5.75	2.84	0.49	-1.02	-1.89	1.25E-03	1.82E-02	MPST	4:84923143-84929813
XLOC_006378	2.12	1.05	0.49	-1.02	-2.16	1.60E-03	2.20E-02	NA	13:93663507-93665634
XLOC_018043	248.18	122.53	0.49	-1.02	-3.50	5.00E-05	1.41E-03	COX6A1	21:12132326-12134925
XLOC_019859	1.09	0.54	0.49	-1.02	-1.82	1.40E-03	1.98E-02	TGM2	4:2164488-2194122
XLOC_009431	2.23	1.10	0.49	-1.02	-2.18	1.80E-03	2.39E-02	NA	14:10743869-10745940
XLOC_011042	13.17	6.49	0.49	-1.02	-3.19	5.00E-05	1.41E-03	C1orf198	16:37090881-37127224
XLOC_015891	1.24	0.61	0.49	-1.02	-1.90	3.65E-03	4.03E-02	SEMA4C	2:94617321-94623671
XLOC_027416	4.15	2.04	0.49	-1.02	-2.40	5.00E-05	1.41E-03	RGS3	GL018699:13951855-14079782
XLOC_027257	92.09	45.35	0.49	-1.02	-9.67	7.00E-04	1.18E-02	RABL6	AAGW02083801:838-4497
XLOC_018111	11.19	5.51	0.49	-1.02	-2.60	1.50E-04	3.53E-03	ENSOCUG00000009273	3:633466-693168
XLOC_004068	26.15	12.87	0.49	-1.02	-3.52	5.00E-05	1.41E-03	DDR1	12:22889923-22905659
XLOC_012792	25.70	12.62	0.49	-1.03	-3.83	5.00E-05	1.41E-03	ENSOCUG00000010333	17:72164391-72164954
XLOC_023376	576.30	282.69	0.49	-1.03	-42.77	4.35E-03	4.57E-02	NA	7:31442822-31442943
XLOC_011678	3.56	1.75	0.49	-1.03	-2.28	2.15E-03	2.76E-02	NA	16:25369476-25370677
XLOC_021432	401.05	196.58	0.49	-1.03	-3.38	5.00E-05	1.41E-03	ENSOCUG00000027459	5:26202189-26203634
XLOC_033125	279.18	136.82	0.49	-1.03	-3.12	5.00E-05	1.41E-03	ENSOCUG00000014989	GL018845:40634-43013
XLOC_022774	17.20	8.43	0.49	-1.03	-3.08	5.00E-05	1.41E-03	CASP2	7:8793315-8812804
XLOC_013743	1.31	0.64	0.49	-1.03	-2.09	6.50E-04	1.12E-02	PALD1	18:16451592-16509405
XLOC_002619	317.01	154.78	0.49	-1.03	-2.40	3.00E-04	6.09E-03	RPA3	10:30565879-31006153
XLOC_003484	36.50	17.82	0.49	-1.03	-3.75	5.00E-05	1.41E-03	LIFR	11:59531356-59598354
XLOC_002732	2.66	1.30	0.49	-1.03	-2.51	5.00E-05	1.41E-03	ENSOCUG00000026897	10:13618753-13622724
XLOC_034309	2.07	1.01	0.49	-1.03	-2.68	5.00E-05	1.41E-03	ENSOCUG00000013645	GL018919:148073-190140
XLOC_000287	18.44	9.00	0.49	-1.04	-2.33	1.50E-04	3.53E-03	C9orf3	1:73722847-74103561
XLOC_000688	1.16	0.57	0.49	-1.04	-2.15	5.50E-04	9.84E-03	MICALCL	1:154012611-154073667
XLOC_021304	51.91	25.30	0.49	-1.04	-5.28	5.00E-05	1.41E-03	NA	5:2659837-2661112
XLOC_032864	2.57	1.25	0.49	-1.04	-2.92	5.00E-05	1.41E-03	COL5A3	GL018833:271671-309666
XLOC_020051	5.35	2.60	0.49	-1.04	-1.83	2.05E-03	2.65E-02	IGFBP6	4:36970454-36976170
XLOC_020195	8.67	4.21	0.49	-1.04	-2.46	2.00E-04	4.42E-03	TMTC2	4:61976785-62423084
XLOC_036432	461.72	223.81	0.48	-1.04	-4.87	5.00E-05	1.41E-03	ENSOCUG00000025604	GL019220:108780-109812
XLOC_028694	38.12	18.48	0.48	-1.04	-3.24	5.00E-05	1.41E-03	C11orf48	GL018717:1669149-1674716
XLOC_020063	49.50	23.99	0.48	-1.05	-3.47	5.00E-05	1.41E-03	ENSOCUG00000022490	4:37279306-37304317
XLOC_013250	2.24	1.09	0.48	-1.05	-2.27	1.10E-03	1.66E-02	NA	17:68986775-68988838
XLOC_015305	45.31	21.95	0.48	-1.05	-3.50	5.00E-05	1.41E-03	SLC25A39	19:44613756-44617186
XLOC_029041	12.88	6.24	0.48	-1.05	-3.34	5.00E-05	1.41E-03	TPST2	GL018723:148769-188116
XLOC_025813	27.47	13.30	0.48	-1.05	-3.43	5.00E-05	1.41E-03	TYMS	9:61682510-61695932
XLOC_013824	5.64	2.73	0.48	-1.05	-2.75	1.50E-04	3.53E-03	RBP4	18:41282997-41288870
XLOC_020115	14.34	6.94	0.48	-1.05	-2.92	2.60E-03	3.17E-02	NA	4:39591638-39593409
XLOC_017956	295.99	142.98	0.48	-1.05	-3.68	5.00E-05	1.41E-03	ENSOCUG00000005749	21:12357000-12361094
XLOC_015968	187.16	90.25	0.48	-1.05	-6.86	5.00E-05	1.41E-03	ENSOCUG00000006135	2:104510693-104511080
XLOC_000182	3.70	1.78	0.48	-1.05	-2.67	5.00E-05	1.41E-03	BNC2	1:37165357-37623468
XLOC_037111	307.68	148.34	0.48	-1.05	-22.78	5.00E-04	9.12E-03	NA	GL019507:84-251
XLOC_002807	12.73	6.14	0.48	-1.05	-2.54	2.55E-03	3.12E-02	NA	10:32605202-32626013
XLOC_007692	55.44	26.70	0.48	-1.05	-5.70	5.00E-05	1.41E-03	NA	13:38858477-38858847
XLOC_027566	12.42	5.98	0.48	-1.05	-3.28	8.50E-04	1.36E-02	NA	GL018700:2983461-2983973
XLOC_036704	28.40	13.66	0.48	-1.06	-3.60	5.00E-05	1.41E-03	TK1	GL019309:12082-33521
XLOC_020118	304.69	146.49	0.48	-1.06	-3.83	5.00E-05	1.41E-03	NA	4:39675788-39677846
XLOC_037657	37.64	18.09	0.48	-1.06	-3.99	5.00E-05	1.41E-03	MT-CYB	MT:14174-15313
XLOC_012570	128.18	61.59	0.48	-1.06	-5.84	5.00E-05	1.41E-03	RPS14	17:33026319-33026775
XLOC_010040	44.65	21.45	0.48	-1.06	-3.66	5.00E-05	1.41E-03	FAM198B	15:5587987-5646842
XLOC_012704	2.38	1.14	0.48	-1.06	-2.66	5.00E-05	1.41E-03	STXBP6	17:44743833-45029571
XLOC_008545	23.79	11.42	0.48	-1.06	-3.92	5.00E-05	1.41E-03	NA	14:52976581-52977805
XLOC_018561	56.57	27.02	0.48	-1.07	-4.35	5.00E-05	1.41E-03	MED30	3:133296075-133322478
XLOC_009052	121.71	58.04	0.48	-1.07	-4.81	5.00E-05	1.41E-03	ENSOCUG00000022742	14:58128508-58129679
XLOC_006585	7.84	3.74	0.48	-1.07	-3.73	5.00E-05	1.41E-03	HSPG2	13:131388582-131517371
XLOC_007467	28.01	13.35	0.48	-1.07	-1.80	3.70E-03	4.07E-02	ENSOCUG00000017932	13:137305426-137311278
XLOC_016706	1693.66	806.99	0.48	-1.07	-7.80	5.00E-05	1.41E-03	ENSOCUG00000024873	2:138529888-138530290
XLOC_003204	134.90	64.27	0.48	-1.07	-3.89	5.00E-05	1.41E-03	BASP1	11:42023272-42064337
XLOC_022198	6.53	3.11	0.48	-1.07	-2.69	1.55E-03	2.14E-02	NA	6:13884819-13885600
XLOC_029694	27.07	12.90	0.48	-1.07	-3.91	5.00E-05	1.41E-03	EFHD1	GL018736:218081-268189
XLOC_002999	5.56	2.65	0.48	-1.07	-2.59	1.80E-03	2.39E-02	NA	10:23067881-23068703
XLOC_038697	3.14	1.50	0.48	-1.07	-2.99	5.00E-05	1.41E-03	NA	X:3495999-3500379
XLOC_015039	6.16	2.93	0.48	-1.07	-3.00	5.00E-05	1.41E-03	ANKRD13B	19:18586146-18606103
XLOC_032075	717.13	340.46	0.47	-1.07	-15.43	5.00E-05	1.41E-03	ENSOCUG00000028159	GL018803:179132-179372
XLOC_014411	138.38	65.67	0.47	-1.08	-3.47	5.00E-05	1.41E-03	UBB	19:4086997-4089227
XLOC_018645	319.78	151.68	0.47	-1.08	-3.80	5.00E-05	1.41E-03	HINT1	3:14380729-14393593
XLOC_030669	151.42	71.82	0.47	-1.08	-3.17	5.00E-05	1.41E-03	COX20	GL018760:3663-49449
XLOC_011538	8.97	4.25	0.47	-1.08	-2.72	5.00E-05	1.41E-03	NA	16:73056375-73072279
XLOC_019766	6.68	3.16	0.47	-1.08	-2.68	3.15E-03	3.63E-02	NA	3:144688765-144689391
XLOC_021909	3.65	1.73	0.47	-1.08	-2.79	5.00E-05	1.41E-03	RMI2	6:4885172-4891420
XLOC_025059	1.42	0.67	0.47	-1.08	-2.64	5.00E-05	1.41E-03	CSRNP1	9:4501242-4509750
XLOC_007489	27.01	12.77	0.47	-1.08	-4.04	5.00E-05	1.41E-03	SH3BGRL3	13:139058017-139059383
XLOC_020145	6.56	3.10	0.47	-1.08	-3.24	5.00E-05	1.41E-03	HMGA2	4:44653158-44850411
XLOC_034950	10.46	4.94	0.47	-1.08	-3.18	5.00E-05	1.41E-03	CDC42EP1	GL018973:291146-293032
XLOC_025804	3765.51	2017.78	0.54	-1.08	-1.67	9.00E-04	1.42E-02	MYL12B	9:58773287-58826963
XLOC_005024	22.68	10.70	0.47	-1.08	-3.95	5.00E-05	1.41E-03	ENSOCUG00000013444	12:105770757-105771381
XLOC_035944	15.70	7.40	0.47	-1.08	-2.48	2.50E-04	5.26E-03	LOXL1	GL019108:1683-85767
XLOC_036821	67.00	31.59	0.47	-1.08	-2.81	5.00E-05	1.41E-03	ENSOCUG00000022297	GL019361:573-11888
XLOC_033939	18.52	8.73	0.47	-1.09	-3.68	5.00E-05	1.41E-03	UNG	GL018892:27153-38466
XLOC_012689	705.02	332.23	0.47	-1.09	-2.39	2.50E-04	5.26E-03	NEDD8	17:44259472-44270892
XLOC_011028	26.30	12.39	0.47	-1.09	-2.00	7.50E-04	1.24E-02	IRF2BP2	16:33612533-33616987
XLOC_021430	33.32	15.68	0.47	-1.09	-4.37	1.25E-03	1.82E-02	NA	5:25439990-25543385
XLOC_001724	565.54	265.99	0.47	-1.09	-2.25	1.50E-04	3.53E-03	CD44	1:174450771-174543842
XLOC_022772	55.64	26.14	0.47	-1.09	-3.60	5.00E-05	1.41E-03	ZYX	7:8711384-8719668
XLOC_017690	21.14	9.93	0.47	-1.09	-2.29	4.00E-04	7.69E-03	ISCA2	20:30596460-30597925
XLOC_021597	15.09	7.08	0.47	-1.09	-3.01	5.00E-05	1.41E-03	ACD	5:23207880-23222915
XLOC_037487	1.28	0.60	0.47	-1.09	-2.23	1.00E-03	1.55E-02	ENSOCUG00000003316	GL019772:20-16334
XLOC_018333	2.10	0.98	0.47	-1.09	-2.06	3.90E-03	4.24E-02	FGF18	3:52642279-52676438
XLOC_037394	78.61	36.81	0.47	-1.09	-4.82	5.00E-05	1.41E-03	AEN,ISG20	GL019705:882-10769
XLOC_014823	1.01	0.47	0.47	-1.09	-2.12	4.50E-04	8.42E-03	C17orf53	19:44473058-44488081
XLOC_028221	2.37	1.11	0.47	-1.09	-3.05	5.00E-05	1.41E-03	DLC1	GL018709:2628131-2676466
XLOC_024244	103.87	48.57	0.47	-1.10	-3.97	5.00E-05	1.41E-03	TSC22D1	8:50453802-50576474
XLOC_010951	2.23	1.04	0.47	-1.10	-2.23	2.50E-04	5.26E-03	MAP3K8	16:5196768-5223091

Transcriptome Gene ID	Uninfected RK-13 Mean FPKM	T. hominis infected RK-13 Mean FPKM	Fold Change	Log2 Fold Change	Test stat	P value	Q value	Ensembl Gene Name / Gene ID	Gene Locus (Chromosome/scaffold:position)
XLOC_025176	533.06	249.16	0.47	-1.10	-3.16	5.00E-05	1.41E-03	RPL28	9:17205069-17315797
XLOC_014451	387.06	180.36	0.47	-1.10	-3.85	5.00E-05	1.41E-03	RPL26	19:10915723-10920732
XLOC_021237	7.09	3.30	0.47	-1.10	-2.80	2.70E-03	3.25E-02	NA	4:84239219-84239855
XLOC_007999	11.64	5.41	0.46	-1.11	-1.69	4.20E-03	4.46E-02	NA	13:93665732-93819698
XLOC_034064	15.96	7.41	0.46	-1.11	-3.65	5.00E-05	1.41E-03	ENSOCUG00000021132	GL018900:555131-556237
XLOC_010999	422.61	196.21	0.46	-1.11	-8.62	5.00E-05	1.41E-03	ENSOCUG00000028015	16:25786775-25787123
XLOC_017936	7.49	3.48	0.46	-1.11	-2.68	5.00E-05	1.41E-03	OAS3	21:8711532-8743763
XLOC_010720	42.24	19.60	0.46	-1.11	-6.99	3.45E-03	3.88E-02	NA	15:23096048-23096312
XLOC_022046	9.20	4.27	0.46	-1.11	-1.71	2.45E-03	3.02E-02	CARHSP1	6:2775159-2778256
XLOC_034509	688.34	319.07	0.46	-1.11	-14.54	5.00E-05	1.41E-03	ENSOCUG00000027307	GL018934:30037-30289
XLOC_000716	18.75	8.69	0.46	-1.11	-3.84	1.50E-04	3.53E-03	HMGB3	1:163247969-163249725
XLOC_032528	5.74	2.66	0.46	-1.11	-2.96	5.00E-05	1.41E-03	DDX51	GL018821:77685-80545
XLOC_021601	1.02	0.47	0.46	-1.11	-2.32	5.50E-04	9.84E-03	CENPT	5:23379907-23403963
XLOC_037645	156.36	72.37	0.46	-1.11	-5.37	5.00E-05	1.41E-03	MT-CO2	MT:7038-7722
XLOC_001896	13.60	6.29	0.46	-1.11	-2.39	1.50E-04	3.53E-03	POLD4	1:194802178-194803973
XLOC_031284	9.09	4.20	0.46	-1.11	-3.54	5.00E-05	1.41E-03	BDKRB2	GL018779:457542-485522
XLOC_000104	2.79	1.29	0.46	-1.11	-2.30	5.00E-05	1.41E-03	FANCG	1:18802441-18808101
XLOC_035310	1.32	0.61	0.46	-1.11	-2.05	2.60E-03	3.17E-02	NAGPA	GL019027:41024-46927
XLOC_000687	12.02	5.54	0.46	-1.12	-3.58	5.00E-05	1.41E-03	MICAL2	1:153859881-153986744
XLOC_027879	22.17	10.21	0.46	-1.12	-2.91	5.00E-05	1.41E-03	ENSOCUG00000007467	GL018704:3560390-3563688
XLOC_039148	37.53	17.25	0.46	-1.12	-6.91	4.60E-03	4.78E-02	NA	X:97173885-97174140
XLOC_032007	8.42	3.87	0.46	-1.12	-3.11	5.00E-05	1.41E-03	NA	GL018801:978936-993016
XLOC_019640	3.45	1.58	0.46	-1.12	-2.31	3.70E-03	4.07E-02	NA	3:110258681-110259652
XLOC_029126	3.12	1.43	0.46	-1.12	-2.36	1.65E-03	2.24E-02	NA	GL018724:1352577-1353827
XLOC_022083	12.87	5.91	0.46	-1.12	-3.23	5.00E-05	1.41E-03	ABCC1	6:10811673-10900291
XLOC_001223	183.14	83.99	0.46	-1.12	-5.28	5.00E-05	1.41E-03	ENSOCUG00000008778	1:74527929-74528673
XLOC_006088	2526.65	1155.42	0.46	-1.13	-3.81	5.00E-05	1.41E-03	S100A3,S100A4	13:38908306-38913909
XLOC_002521	11.60	5.30	0.46	-1.13	-3.34	6.50E-04	1.12E-02	NA	1:194750979-194751553
XLOC_006035	13.09	5.98	0.46	-1.13	-2.40	2.50E-04	5.26E-03	IQGAP3	13:36294614-36387552
XLOC_002688	79.44	36.29	0.46	-1.13	-3.79	5.00E-05	1.41E-03	SEC61G	10:45981041-45996457
XLOC_000047	503.14	229.84	0.46	-1.13	-8.41	5.00E-05	1.41E-03	ENSOCUG00000025109	1:12513146-12513524
XLOC_013256	5.48	2.50	0.46	-1.13	-2.58	2.40E-03	2.97E-02	NA	17:69201924-69202662
XLOC_009432	2.81	1.28	0.46	-1.13	-2.55	2.00E-04	4.42E-03	NA	14:10746641-10748655
XLOC_024713	2.39	1.09	0.46	-1.13	-2.23	1.80E-03	2.39E-02	NA	8:8886620-8888065
XLOC_007550	21.96	10.03	0.46	-1.13	-3.96	5.00E-05	1.41E-03	NA	13:5657292-5658897
XLOC_025991	3.24	1.48	0.46	-1.13	-2.30	2.55E-03	3.12E-02	NA	9:7110702-7111704
XLOC_027654	123.48	56.28	0.46	-1.13	-12.25	2.50E-04	5.26E-03	NA	GL018701:4636177-4636399
XLOC_002683	1537.89	700.84	0.46	-1.13	-3.94	5.00E-05	1.41E-03	ENSOCUG00000016662	10:45134906-45138511
XLOC_002932	52.55	23.94	0.46	-1.13	-5.52	5.00E-05	1.41E-03	NA	10:14899723-14900147
XLOC_002789	13.77	6.27	0.46	-1.14	-3.08	2.75E-03	3.29E-02	NA	10:27857338-27951307
XLOC_018637	1.94	0.88	0.46	-1.14	-2.73	5.00E-05	1.41E-03	Mar-03	3:10587271-10745571
XLOC_033310	1.71	0.78	0.46	-1.14	-2.09	2.85E-03	3.37E-02	NA	GL018855:93413-95201
XLOC_034205	4.02	1.82	0.45	-1.14	-2.19	2.50E-04	5.26E-03	ENSOCUG00000006248	GL018910:269862-316649
XLOC_022787	14.15	6.42	0.45	-1.14	-2.33	5.00E-05	1.41E-03	NA	7:9539502-9544458
XLOC_031470	15.55	7.04	0.45	-1.14	-3.81	5.00E-05	1.41E-03	NA	GL018786:81-6515
XLOC_024436	17.47	7.91	0.45	-1.14	-3.97	5.00E-05	1.41E-03	GPRC5A	8:26842202-26857460
XLOC_006558	35.17	15.92	0.45	-1.14	-2.56	5.00E-05	1.41E-03	NA	13:128341232-128345955
XLOC_027685	28.16	12.74	0.45	-1.14	-4.34	5.00E-05	1.41E-03	RPL18A	GL018702:7680308-7680882
XLOC_020449	584.21	264.04	0.45	-1.15	-4.08	5.00E-05	1.41E-03	PCNA	4:11721711-11726500
XLOC_037292	13.64	6.16	0.45	-1.15	-2.96	5.00E-05	1.41E-03	MRPL38	GL019624:26373-30977
XLOC_027627	19.32	8.72	0.45	-1.15	-3.17	1.00E-04	2.52E-03	C4orf46	GL018701:1259828-1263447
XLOC_007516	267.32	120.57	0.45	-1.15	-2.98	5.00E-05	1.41E-03	NA	13:142803356-142870641
XLOC_001655	3.22	1.45	0.45	-1.15	-2.29	3.00E-04	6.09E-03	DKK3	1:153711081-153755748
XLOC_031009	383.80	172.71	0.45	-1.15	-3.58	5.00E-05	1.41E-03	RPS28	GL018767:375747-384626
XLOC_002271	162.71	73.12	0.45	-1.15	-14.95	5.00E-04	9.12E-03	NA	1:127249107-127249312
XLOC_030259	2113.74	949.35	0.45	-1.15	-2.52	2.00E-04	4.42E-03	C14orf2	GL018751:18336-136581
XLOC_009960	552.11	247.84	0.45	-1.16	-31.27	5.00E-05	1.41E-03	NA	14:133060038-133060198
XLOC_027936	2.79	1.25	0.45	-1.16	-2.21	4.65E-03	4.81E-02	NA	GL018704:3557066-3558144
XLOC_030460	285.81	128.12	0.45	-1.16	-4.16	5.00E-05	1.41E-03	GNAS	GL018755:296095-315917
XLOC_027188	4.97	2.23	0.45	-1.16	-2.74	3.00E-04	6.09E-03	NA	AAGW02083402:5106-6166
XLOC_004773	40.70	18.22	0.45	-1.16	-3.31	5.00E-05	1.41E-03	CCND3	12:31535764-31635927
XLOC_004454	1.00	0.45	0.45	-1.16	-2.26	8.50E-04	1.36E-02	MYB	12:125582166-125617099
XLOC_037566	33.59	15.02	0.45	-1.16	-1.84	4.05E-03	4.35E-02	MRPL21	GL019863:14705-20303
XLOC_019795	4.29	1.91	0.45	-1.16	-2.45	3.70E-03	4.07E-02	NA	3:150324954-150325693
XLOC_013571	15.57	6.95	0.45	-1.16	-3.61	5.00E-05	1.41E-03	LZTS2	18:49092518-49101220
XLOC_028239	5.00	2.23	0.45	-1.17	-3.63	5.00E-05	1.41E-03	DUSP4	GL018709:4381341-4396904
XLOC_032751	11.86	5.29	0.45	-1.17	-3.59	5.00E-05	1.41E-03	NA	GL018828:256834-257935
XLOC_037826	65.35	29.08	0.45	-1.17	-5.69	5.00E-05	1.41E-03	PLP2	X:33750798-33753194
XLOC_027153	22.56	10.04	0.44	-1.17	-4.06	5.00E-05	1.41E-03	SNORD23	AAGW02083242:5547-7289
XLOC_011561	50.31	22.36	0.44	-1.17	-4.13	5.00E-05	1.41E-03	PLA2G4A	16:83420674-83582381
XLOC_021613	22.24	9.88	0.44	-1.17	-3.12	5.00E-05	1.41E-03	ENSOCUG00000016924	5:24531309-24546422
XLOC_026562	10.33	4.58	0.44	-1.17	-3.33	2.00E-04	4.42E-03	NA	AAGW02080975:27065-27697
XLOC_027844	89.88	39.80	0.44	-1.18	-2.17	3.90E-03	4.24E-02	MARCKSL1	GL018704:5862294-5898556
XLOC_005371	4.88	2.16	0.44	-1.18	-2.60	2.65E-03	3.21E-02	NA	12:36565354-36566135
XLOC_014393	2.37	1.05	0.44	-1.18	-2.34	9.50E-04	1.48E-02	NA	18:68573050-68574585
XLOC_037235	20.08	8.88	0.44	-1.18	-5.01	4.45E-03	4.66E-02	NA	GL019579:19332-19638
XLOC_024147	92.23	40.74	0.44	-1.18	-3.43	5.00E-05	1.41E-03	IFFO1	8:32581139-32603783
XLOC_004688	3.61	1.59	0.44	-1.19	-2.86	5.00E-05	1.41E-03	PPP1R18	12:22711132-22719961
XLOC_017255	5.19	2.28	0.44	-1.19	-3.09	1.00E-04	2.52E-03	NA	2:121067231-121068826
XLOC_019520	2.67	1.17	0.44	-1.19	-2.60	2.00E-04	4.42E-03	NA	3:89593430-89595446
XLOC_024005	3.07	1.34	0.44	-1.20	-2.97	5.00E-05	1.41E-03	RAPGEF3	8:20672-36353
XLOC_039152	203.84	88.63	0.43	-1.20	-19.76	4.50E-04	8.42E-03	NA	X:101161688-101161869
XLOC_016664	8.78	3.81	0.43	-1.20	-3.55	5.00E-05	1.41E-03	LGALSL	2:121887093-121894730
XLOC_027103	8.07	3.50	0.43	-1.21	-2.48	5.00E-05	1.41E-03	ORAOV1	AAGW02083102:3472-7475
XLOC_035297	30.74	13.33	0.43	-1.21	-4.43	5.00E-05	1.41E-03	NA	GL019024:8836-15361
XLOC_025037	4.30	1.86	0.43	-1.21	-3.13	5.00E-05	1.41E-03	NA	8:111304375-111306535
XLOC_022223	5.36	2.32	0.43	-1.21	-2.83	7.50E-04	1.24E-02	NA	6:27014583-27015423
XLOC_038269	13.42	5.79	0.43	-1.21	-3.76	5.00E-05	1.41E-03	ENSOCUG00000028092	X:32399687-32400254
XLOC_034890	6.73	2.90	0.43	-1.21	-3.01	4.00E-04	7.69E-03	NA	GL018969:115875-117993
XLOC_038648	3.04	1.31	0.43	-1.21	-2.82	1.00E-04	2.52E-03	NA	X:3325172-3327214
XLOC_021299	1.36	0.58	0.43	-1.22	-2.68	1.00E-04	2.52E-03	SPRED3	5:2419904-2430041
XLOC_004011	2.34	1.01	0.43	-1.22	-2.83	5.00E-05	1.41E-03	TCF19	12:20163914-20168635
XLOC_033705	42.26	18.16	0.43	-1.22	-3.69	5.00E-05	1.41E-03	PLAUR	GL018881:85741-98960
XLOC_037144	69.07	29.64	0.43	-1.22	-5.66	5.00E-05	1.41E-03	AURKAIP1	GL019531:42286-43007
XLOC_034931	57.76	24.79	0.43	-1.22	-3.36	5.00E-05	1.41E-03	LGALS1	GL018972:7657-11154
XLOC_012385	9.38	4.02	0.43	-1.22	-4.18	5.00E-05	1.41E-03	ATP10A	17:80340542-80522603
XLOC_000971	272.58	116.45	0.43	-1.23	-10.52	5.00E-05	1.41E-03	ENSOCUG00000021292	1:1290345-1290646
XLOC_037581	2.18	0.93	0.43	-1.23	-2.05	1.15E-03	1.72E-02	PTP4A3	GL019882:5604-18306
XLOC_035226	11.65	4.96	0.43	-1.23	-3.64	5.00E-05	1.41E-03	NA	GL019011:219443-220328
XLOC_027236	4.88	2.07	0.43	-1.23	-2.44	5.00E-05	1.41E-03	PLVAP	AAGW02083628:20-3837
XLOC_022525	19.94	8.47	0.42	-1.23	-4.05	5.00E-05	1.41E-03	CDCA7	7:113037948-113049844
XLOC_011424	7.09	3.01	0.42	-1.24	-3.20	5.00E-05	1.41E-03	ENSOCUG00000003625	16:50669058-50669946
XLOC_029570	5.79	2.45	0.42	-1.24	-2.26	5.00E-05	1.41E-03	CENPM	GL018734:619866-634960
XLOC_018187	10.83	4.58	0.42	-1.24	-3.04	5.00E-05	1.41E-03	TGFBI	3:18397430-18557341
XLOC_027682	183.66	77.53	0.42	-1.24	-4.24	5.00E-05	1.41E-03	ENSOCUG00000022169	GL018702:7279895-7287790
XLOC_030455	2.09	0.88	0.42	-1.25	-2.16	4.35E-03	4.57E-02	NA	GL018754:337759-338974
XLOC_000333	575.72	242.34	0.42	-1.25	-3.70	5.00E-05	1.41E-03	NA	1:91621920-91622237
XLOC_020645	93.45	39.31	0.42	-1.25	-5.48	5.00E-05	1.41E-03	NA	4:40211751-40212747
XLOC_019721	6.99	2.93	0.42	-1.25	-3.09	9.00E-04	1.42E-02	NA	3:133955906-133956618
XLOC_004430	212.60	89.14	0.42	-1.25	-6.47	5.00E-05	1.41E-03	ENSOCUG00000022399	12:120594514-120595150
XLOC_013713	256.10	107.32	0.42	-1.25	-4.56	5.00E-05	1.41E-03	ANXA8	18:8938032-8955097
XLOC_033252	1.34	0.56	0.42	-1.26	-2.46	3.50E-04	6.91E-03	TMEM213	GL018853:111516-118970

Transcriptome Gene ID	Uninfected RK-13 Mean FPKM	T. hominis infected RK-13 Mean FPKM	Fold Change	Log2 Fold Change	Test stat	P value	Q value	Ensembl Gene Name / Gene ID	Gene Locus (Chromosome/scaffold:position)
XLOC_017750	18.13	7.57	0.42	-1.26	-4.83	3.15E-03	3.63E-02	NA	20:8725305-8725633
XLOC_012768	14.24	5.93	0.42	-1.26	-4.26	4.15E-03	4.42E-02	RPS29	17:68747913-68749255
XLOC_010548	57.49	23.94	0.42	-1.26	-5.12	5.00E-05	1.41E-03	ENSOCUG00000026627	15:70508155-70509168
XLOC_012144	17.60	7.33	0.42	-1.26	-4.52	7.00E-04	1.18E-02	ENSOCUG00000027076	17:35869650-35870037
XLOC_008070	2.01	0.84	0.42	-1.27	-2.21	2.65E-03	3.21E-02	NA	13:93939315-93940716
XLOC_015290	16.40	6.82	0.42	-1.27	-2.33	1.00E-04	2.52E-03	ETV4	19:44023930-44037525
XLOC_012276	140.19	58.25	0.42	-1.27	-6.79	5.00E-05	1.41E-03	ENSOCUG00000026942	17:46054214-46054712
XLOC_008082	3.93	1.63	0.42	-1.27	-2.64	1.55E-03	2.14E-02	NA	13:93990227-93991154
XLOC_008849	4.88	2.03	0.41	-1.27	-2.91	4.50E-04	8.42E-03	NA	14:157484284-157487951
XLOC_008510	19.16	7.95	0.41	-1.27	-4.13	5.00E-05	1.41E-03	TSC22D2	14:44271326-44345944
XLOC_038678	5.01	2.08	0.41	-1.27	-3.02	1.50E-04	3.53E-03	NA	X:3445428-3446545
XLOC_017943	6.81	2.82	0.41	-1.27	-2.59	1.50E-04	3.53E-03	NA	21:11528745-11537813
XLOC_035126	29.61	12.22	0.41	-1.28	-3.70	5.00E-05	1.41E-03	ENSOCUG00000007536	GL018998:208702-211013
XLOC_018784	863.53	356.19	0.41	-1.28	-16.84	5.00E-05	1.41E-03	ENSOCUG00000024002	3:36354510-36354762
XLOC_018788	2.84	1.17	0.41	-1.28	-3.01	5.00E-05	1.41E-03	HAVCR2	3:38562190-38589132
XLOC_011552	3.99	1.64	0.41	-1.28	-3.18	5.00E-05	1.41E-03	ENSOCUG00000027066	16:77985042-77988470
XLOC_036608	5.71	2.35	0.41	-1.28	-3.30	5.00E-05	1.41E-03	NA	GL019277:41878-43283
XLOC_028958	6.68	2.75	0.41	-1.28	-3.10	3.50E-04	6.91E-03	NA	GL018720:1416328-1417089
XLOC_021872	2.21	0.91	0.41	-1.28	-2.41	1.15E-03	1.72E-02	NA	5:33258508-33259992
XLOC_019397	2.80	1.15	0.41	-1.29	-2.45	1.85E-03	2.44E-02	NA	3:62937989-62939136
XLOC_038538	36.20	14.83	0.41	-1.29	-5.50	5.00E-05	1.41E-03	SSB	X:98660003-98660450
XLOC_012737	31.93	13.07	0.41	-1.29	-4.73	5.00E-05	1.41E-03	NFKBIA	17:55105726-55109740
XLOC_037333	8.83	3.62	0.41	-1.29	-2.56	1.00E-04	2.52E-03	ENSOCUG00000021612	GL019656:11366-24001
XLOC_037225	7.11	2.91	0.41	-1.29	-3.13	4.70E-03	4.84E-02	NA	GL019575:11051-33460
XLOC_016084	318.97	130.16	0.41	-1.29	-7.58	5.00E-05	1.41E-03	ENSOCUG00000027435	2:132090105-132090582
XLOC_026454	6.08	2.48	0.41	-1.29	-3.89	5.00E-05	1.41E-03	NA	AAGW02079667:56051-60052
XLOC_005064	519.78	211.84	0.41	-1.29	-4.43	5.00E-05	1.41E-03	CTGF	12:122182435-122186258
XLOC_026372	2.96	1.21	0.41	-1.30	-2.77	1.50E-04	3.53E-03	NA	9:104821773-104823410
XLOC_033771	18.31	7.46	0.41	-1.30	-2.04	1.60E-03	2.20E-02	NA	GL018886:252565-253462
XLOC_018549	26.70	10.87	0.41	-1.30	-2.82	4.00E-04	7.69E-03	NA	3:124864966-124871881
XLOC_015168	4.89	1.99	0.41	-1.30	-2.11	5.00E-04	9.12E-03	NXPH3	19:38039758-38041451
XLOC_011846	3.18	1.29	0.41	-1.30	-2.96	1.50E-04	3.53E-03	NA	16:60436741-60438605
XLOC_025705	37.24	15.14	0.41	-1.30	-4.57	5.00E-05	1.41E-03	FAM107A	9:25319199-25347044
XLOC_031068	5.15	2.09	0.41	-1.30	-3.44	5.00E-05	1.41E-03	NA	GL018768:476714-478800
XLOC_037112	60.68	24.62	0.41	-1.30	-4.53	5.00E-05	1.41E-03	CBS	GL019508:12819-24467
XLOC_034893	8.06	3.27	0.41	-1.30	-3.74	5.00E-05	1.41E-03	KLHL30	GL018969:197653-203883
XLOC_007466	5.15	2.09	0.41	-1.30	-3.46	5.00E-05	1.41E-03	SESN2	13:137259403-137282265
XLOC_009166	376.63	152.59	0.41	-1.30	-9.45	5.00E-05	1.41E-03	ENSOCUG00000013247	14:87023625-87023994
XLOC_002821	1.95	0.79	0.40	-1.31	-1.89	3.70E-03	4.07E-02	NA	10:35950690-35954504
XLOC_019649	1586.41	641.52	0.40	-1.31	-13.16	5.00E-05	1.41E-03	NA	3:111957787-111958092
XLOC_009225	21.78	8.78	0.40	-1.31	-4.21	5.00E-05	1.41E-03	PLA1A	14:99141046-99174167
XLOC_036814	4.79	1.93	0.40	-1.31	-2.32	5.00E-04	9.12E-03	C17orf70	GL019359:64204-67210
XLOC_024139	44.05	17.71	0.40	-1.31	-4.99	5.00E-05	1.41E-03	CD9	8:32289512-32309928
XLOC_024836	5.53	2.22	0.40	-1.31	-3.01	6.50E-04	1.12E-02	NA	8:43887197-43887982
XLOC_033803	3.49	1.40	0.40	-1.32	-2.51	3.15E-03	3.63E-02	NA	GL018887:513011-513821
XLOC_004718	45.61	18.32	0.40	-1.32	-6.13	5.00E-05	1.41E-03	MNF1	12:24015206-24029309
XLOC_013681	171.60	68.87	0.40	-1.32	-1.82	2.70E-03	3.25E-02	RPL15	18:3885289-4138074
XLOC_002127	9.85	3.95	0.40	-1.32	-3.64	4.40E-03	4.61E-02	NA	1:66118498-66118905
XLOC_011612	10.42	4.17	0.40	-1.32	-3.74	5.00E-05	1.41E-03	NA	16:15969130-15969928
XLOC_029204	6.50	2.60	0.40	-1.32	-1.87	3.40E-03	3.83E-02	NA	GL018725:1522438-1523357
XLOC_029821	5.18	2.07	0.40	-1.32	-2.83	3.55E-03	3.95E-02	NA	GL018738:2451495-2452114
XLOC_006102	1419.70	566.56	0.40	-1.33	-3.48	5.00E-05	1.41E-03	S100A11	13:40164771-40170626
XLOC_027657	207.89	82.90	0.40	-1.33	-7.68	5.00E-05	1.41E-03	NA	GL018701:7597144-7597582
XLOC_034370	41.71	16.63	0.40	-1.33	-4.27	5.00E-05	1.41E-03	MYADM	GL018924:158704-160866
XLOC_030879	1.38	0.55	0.40	-1.33	-1.76	4.85E-03	4.95E-02	PPAPDC3	GL018764:197258-215735
XLOC_014914	28.81	11.47	0.40	-1.33	-4.62	5.00E-05	1.41E-03	ENSOCUG00000012432	19:5502985-5548874
XLOC_017823	142.57	56.66	0.40	-1.33	-9.59	5.00E-05	1.41E-03	NA	20:23524698-23525019
XLOC_032656	3.50	1.39	0.40	-1.33	-2.71	5.00E-05	1.41E-03	C22orf29	GL018826:822419-825121
XLOC_024976	2.31	0.92	0.40	-1.33	-2.96	5.00E-05	1.41E-03	NA	8:95436028-95439260
XLOC_015165	41.40	16.43	0.40	-1.33	-3.62	5.00E-05	1.41E-03	ITGA3	19:37474893-37598932
XLOC_020568	24.13	9.54	0.40	-1.34	-2.11	1.85E-03	2.44E-02	KRT7	4:36275381-36323529
XLOC_025030	13.85	5.47	0.40	-1.34	-4.15	5.00E-05	1.41E-03	NA	8:101642747-101643765
XLOC_013724	121.65	48.07	0.40	-1.34	-4.80	5.00E-05	1.41E-03	PLAU	18:13594966-13601381
XLOC_032730	17.05	6.73	0.39	-1.34	-2.12	1.80E-03	2.39E-02	TCEB2	GL018828:143066-146972
XLOC_036609	2.03	0.80	0.39	-1.34	-2.38	1.50E-03	2.09E-02	NA	GL019277:43580-45033
XLOC_006513	2.50	0.99	0.39	-1.34	-2.70	5.00E-05	1.41E-03	SLC6A9	13:122675285-122695747
XLOC_001882	35.10	13.78	0.39	-1.35	-2.60	2.50E-04	5.26E-03	FOSL1	1:193696579-193723143
XLOC_012408	2.79	1.09	0.39	-1.35	-3.61	5.00E-05	1.41E-03	THSD4	17:681143-705682
XLOC_013459	9.34	3.66	0.39	-1.35	-3.62	5.00E-05	1.41E-03	ENSOCUG00000002408	18:28742591-28743337
XLOC_017838	9.34	3.66	0.39	-1.35	-3.58	9.50E-04	1.48E-02	NA	20:28060354-28060913
XLOC_032705	32.28	12.63	0.39	-1.35	-4.34	5.00E-05	1.41E-03	TNFRSF12A	GL018828:260678-268190
XLOC_020139	12.20	4.77	0.39	-1.35	-3.97	3.00E-04	6.09E-03	ENSOCUG00000021191	4:43558560-43559031
XLOC_037290	3.32	1.30	0.39	-1.35	-3.25	5.00E-05	1.41E-03	TRIM47	GL019624:7853-12135
XLOC_022933	1.42	0.55	0.39	-1.36	-2.58	1.50E-04	3.53E-03	INHBB	7:62748295-62753560
XLOC_026982	1.52	0.59	0.39	-1.36	-2.45	5.50E-04	9.84E-03	NA	AAGW02082738:7867-10010
XLOC_032709	1.43	0.56	0.39	-1.36	-1.56	4.80E-03	4.91E-02	CASP16	GL018828:348012-351941
XLOC_033495	13.40	5.21	0.39	-1.36	-4.18	8.00E-04	1.30E-02	NA	GL018872:18556-18978
XLOC_021129	2.14	0.83	0.39	-1.37	-2.53	9.00E-04	1.42E-02	NA	4:47821089-47822622
XLOC_002100	6.31	2.45	0.39	-1.37	-3.12	1.50E-03	2.09E-02	NA	1:54143091-54143702
XLOC_010537	301.86	117.05	0.39	-1.37	-19.06	5.00E-05	1.41E-03	ATP5I	15:66657333-66657549
XLOC_011528	4.59	1.78	0.39	-1.37	-3.82	5.00E-05	1.41E-03	C1orf106	16:70468662-70485652
XLOC_013046	11.46	4.43	0.39	-1.37	-3.92	5.00E-05	1.41E-03	NA	17:16738483-16739154
XLOC_036816	6.37	2.46	0.39	-1.37	-3.71	5.00E-05	1.41E-03	CDT1	GL019360:45840-48784
XLOC_035218	55.97	21.59	0.39	-1.37	-6.65	5.00E-05	1.41E-03	APOCI	GL019011:106233-108836
XLOC_000941	45.57	17.53	0.38	-1.38	-3.10	5.00E-05	1.41E-03	BANF1	1:193775833-193778040
XLOC_016755	51.30	19.73	0.38	-1.38	-4.94	5.00E-05	1.41E-03	CRIM1	2:149750674-149917711
XLOC_038889	391.55	150.57	0.38	-1.38	-41.62	1.70E-03	2.29E-02	NA	X:41558760-41558891
XLOC_008065	13.33	5.12	0.38	-1.38	-4.13	5.00E-05	1.41E-03	NA	13:93927638-93928217
XLOC_007902	39.45	15.11	0.38	-1.38	-5.89	5.00E-05	1.41E-03	NA	13:75089381-75089850
XLOC_016995	56.16	21.49	0.38	-1.39	-6.43	5.00E-05	1.41E-03	NA	2:57486223-57486688
XLOC_032848	50.36	19.20	0.38	-1.39	-5.70	5.00E-05	1.41E-03	FIS1	GL018831:267229-269820
XLOC_010042	7.17	2.73	0.38	-1.39	-4.40	5.00E-05	1.41E-03	PDGFC	15:7015698-7229005
XLOC_031334	26.75	10.18	0.38	-1.39	-5.41	5.00E-05	1.41E-03	ENSOCUG00000014416	GL018781:71019-71436
XLOC_007190	164.16	62.44	0.38	-1.39	-4.88	5.00E-05	1.41E-03	NEXN	13:87527752-87585006
XLOC_019942	41.65	15.76	0.38	-1.40	-4.32	5.00E-05	1.41E-03	ITPA	4:10147064-10160479
XLOC_010194	1.48	0.56	0.38	-1.40	-2.53	2.50E-04	5.26E-03	GPRIN3	15:60770180-60772472
XLOC_006635	328.63	124.16	0.38	-1.40	-14.18	9.00E-04	1.42E-02	SNORA16	13:136969831-136990696
XLOC_004363	18.10	6.84	0.38	-1.40	-4.58	5.00E-05	1.41E-03	MARCKS	12:101772750-101778971
XLOC_037114	111.27	42.00	0.38	-1.41	-10.62	5.00E-05	1.41E-03	NA	GL019508:515-804
XLOC_007253	73.61	27.78	0.38	-1.41	-4.34	5.00E-05	1.41E-03	TACSTD2	13:108170929-108198739
XLOC_036710	31.78	11.99	0.38	-1.41	-6.37	5.00E-05	1.41E-03	NA	GL019309:47392-47730
XLOC_036880	10.58	3.99	0.38	-1.41	-4.55	5.00E-05	1.41E-03	NA	GL019385:57926-63166
XLOC_003291	454.91	171.54	0.38	-1.41	-12.85	5.00E-05	1.41E-03	ENY2	11:74834913-74835219
XLOC_027653	614.54	231.38	0.38	-1.41	-59.18	1.10E-03	1.66E-02	NA	GL018701:4635396-4635511
XLOC_031591	37.01	13.93	0.38	-1.41	-5.26	5.00E-05	1.41E-03	ENSOCUG00000008732	GL018788:771694-776389
XLOC_002135	603.88	226.01	0.37	-1.42	-10.75	5.00E-05	1.41E-03	NA	1:74347941-74348306
XLOC_016430	48.00	17.95	0.37	-1.42	-4.03	5.00E-05	1.41E-03	NRG1	2:74984999-75233685
XLOC_004447	13.53	5.05	0.37	-1.42	-4.31	2.00E-04	4.42E-03	ENSOCUG00000022189	12:123469013-123469482
XLOC_012986	1.63	0.61	0.37	-1.42	-2.32	2.60E-03	3.17E-02	NA	17:5451726-5453316
XLOC_021368	3.63	1.35	0.37	-1.42	-3.28	5.00E-05	1.41E-03	CDH5	5:21866453-21901834
XLOC_026817	8.38	3.12	0.37	-1.42	-3.93	5.00E-05	1.41E-03	LTBP4	AAGW02082344:9483-14317
XLOC_034908	268.65	99.94	0.37	-1.43	-35.45	4.30E-03	4.54E-02	NA	GL018969:206231-206365

Transcriptome Gene ID	Uninfected RK-13 Mean FPKM	T. hominis infected RK-13 Mean FPKM	Fold Change	Log2 Fold Change	Test stat	P value	Q value	Ensembl Gene Name / Gene ID	Gene Locus (Chromosome/scaffold:position)
XLOC_031314	2.68	0.99	0.37	-1.43	-2.58	1.25E-03	1.82E-02	NA	GL018780:549137-550264
XLOC_024434	52.18	19.36	0.37	-1.43	-6.11	5.00E-05	1.41E-03	EMP1	8:26497032-26514500
XLOC_008992	341.42	126.61	0.37	-1.43	-5.75	5.00E-05	1.41E-03	TM4SF1	14:43161242-43193421
XLOC_037605	67.44	24.99	0.37	-1.43	-8.15	5.00E-05	1.41E-03	ENSOCUG00000023143	GL019908:12743-14102
XLOC_004723	23.55	8.72	0.37	-1.43	-4.19	5.00E-05	1.41E-03	ENSOCUG00000013398	12:24440987-24444203
XLOC_025604	3.86	1.43	0.37	-1.43	-2.73	5.00E-05	1.41E-03	SLC26A6	9:16316842-16324771
XLOC_031746	3.25	1.20	0.37	-1.44	-3.56	5.00E-05	1.41E-03	EPHA2	GL018791:240133-264789
XLOC_034956	7.24	2.67	0.37	-1.44	-3.47	5.00E-05	1.41E-03	CARD10	GL018973:238504-263001
XLOC_036005	60.89	22.50	0.37	-1.44	-2.66	5.00E-05	1.41E-03	ENSOCUG00000015380	GL019112:69436-72684
XLOC_006485	688.62	254.28	0.37	-1.44	-21.08	5.00E-05	1.41E-03	SNRPG	13:119851311-119851542
XLOC_037437	14.37	5.30	0.37	-1.44	-1.91	1.05E-03	1.60E-02	ENSOCUG00000026531	GL019741:23482-24627
XLOC_016885	415.46	153.01	0.37	-1.44	-49.95	3.65E-03	4.03E-02	NA	2:24775588-24775707
XLOC_008052	2.75	1.01	0.37	-1.44	-2.71	6.50E-04	1.12E-02	NA	13:93846728-93847972
XLOC_007014	56.53	20.74	0.37	-1.45	-4.92	5.00E-05	1.41E-03	PHGDH	13:44692970-44724788
XLOC_037675	56.71	20.80	0.37	-1.45	-5.21	5.00E-05	1.41E-03	CA5B	X:1536327-1639004
XLOC_013893	136.23	49.67	0.36	-1.46	-2.73	5.00E-05	1.41E-03	TRIM8	18:50615920-50629810
XLOC_031575	16.49	6.01	0.36	-1.46	-2.17	6.50E-04	1.12E-02	UBALD1	GL018787:855963-858412
XLOC_020297	9.83	3.58	0.36	-1.46	-3.16	5.00E-05	1.41E-03	IFT27	4:85099844-85125248
XLOC_006527	57.80	21.19	0.37	-1.46	-5.20	5.00E-05	1.41E-03	SLC2A1	13:123845143-123862841
XLOC_032886	54.73	19.79	0.36	-1.47	-3.45	5.00E-05	1.41E-03	UBL5	GL018833:401170-402796
XLOC_024750	13.16	4.76	0.36	-1.47	-4.25	5.00E-05	1.41E-03	NA	8:14056428-14056990
XLOC_029771	2.67	0.97	0.36	-1.47	-2.89	1.00E-04	2.52E-03	RCCD1	GL018738:1353401-1357847
XLOC_029184	256.64	92.50	0.36	-1.47	-5.31	5.00E-05	1.41E-03	SDC4	GL018725:472399-485394
XLOC_008090	3.48	1.25	0.36	-1.47	-2.74	1.50E-03	2.09E-02	NA	13:94018115-94018945
XLOC_005648	7.58	2.73	0.36	-1.47	-3.90	5.00E-05	1.41E-03	NA	12:72653756-72655058
XLOC_026989	38.79	13.96	0.36	-1.47	-2.31	3.50E-04	6.91E-03	NA	AAGW02082749:935-6655
XLOC_022257	17.52	6.30	0.36	-1.47	-3.39	5.00E-05	1.41E-03	NA	7:9682934-9686516
XLOC_017167	5.32	1.91	0.36	-1.48	-3.06	1.95E-03	2.55E-02	NA	2:96418472-96419108
XLOC_002779	27.80	9.98	0.36	-1.48	-2.57	5.00E-05	1.41E-03	INHBA	10:24643427-24708586
XLOC_015860	119.03	42.69	0.36	-1.48	-5.23	5.00E-05	1.41E-03	FHL2	2:86920534-87003591
XLOC_028722	177.92	63.80	0.36	-1.48	-8.25	5.00E-05	1.41E-03	ENSOCUG00000017388	GL018717:625-1859
XLOC_026918	49.33	17.66	0.36	-1.48	-5.80	5.00E-05	1.41E-03	ENSOCUG00000026724	AAGW02082565:3012-3897
XLOC_029538	151.91	54.40	0.36	-1.48	-6.08	5.00E-05	1.41E-03	SAA3	GL018733:2135171-2139996
XLOC_008093	2.14	0.76	0.36	-1.48	-2.56	1.20E-03	1.78E-02	NA	13:94038151-94039485
XLOC_038679	3.93	1.41	0.36	-1.48	-3.21	5.00E-05	1.41E-03	NA	X:3446807-3448081
XLOC_015479	1853.32	662.68	0.36	-1.48	-129.90	5.00E-04	9.12E-03	NA	19:33820169-33820259
XLOC_014378	6.27	2.23	0.36	-1.49	-3.86	5.00E-05	1.41E-03	NA	18:66708847-66710350
XLOC_018023	628.59	223.75	0.36	-1.49	-5.33	5.00E-05	1.41E-03	ENSOCUG00000003802	21:8325175-8328113
XLOC_001170	78.76	28.02	0.36	-1.49	-6.78	5.00E-05	1.41E-03	ENSOCUG00000026323	1:60521556-60522084
XLOC_018775	46.82	16.64	0.36	-1.49	-1.71	3.05E-03	3.54E-02	ATOX1	3:33187374-33199165
XLOC_019583	48.14	17.08	0.35	-1.49	-6.78	5.00E-05	1.41E-03	NA	3:98416239-98416648
XLOC_031285	6.31	2.23	0.35	-1.50	-2.99	5.00E-05	1.41E-03	BDKRB1	GL018779:486656-504538
XLOC_033055	154.27	54.55	0.35	-1.50	-3.36	5.00E-05	1.41E-03	UBALD2	GL018843:433029-434090
XLOC_027205	9.18	3.25	0.35	-1.50	-4.14	5.00E-05	1.41E-03	NA	AAGW02083485:1362-2492
XLOC_027755	8.39	2.96	0.35	-1.50	-4.30	5.00E-05	1.41E-03	LMCD1	GL018703:336269-376156
XLOC_006572	7.69	2.71	0.35	-1.50	-2.59	1.50E-04	3.53E-03	ID3	13:129667263-129668717
XLOC_026371	3.09	1.09	0.35	-1.50	-2.64	2.30E-03	2.88E-02	NA	9:104813938-104814802
XLOC_034919	18.86	6.61	0.35	-1.51	-5.65	2.95E-03	3.44E-02	NA	GL018970:78616-78923
XLOC_008054	8.54	2.98	0.35	-1.52	-4.45	5.00E-05	1.41E-03	NA	13:93850043-93852129
XLOC_001333	6.68	2.33	0.35	-1.52	-3.60	5.00E-05	1.41E-03	OAF	1:97774159-97787619
XLOC_010933	8.84	3.08	0.35	-1.52	-3.25	5.00E-05	1.41E-03	ENSOCUG00000029065	16:79834-81355
XLOC_025895	427.94	148.83	0.35	-1.52	-5.29	5.00E-05	1.41E-03	ENSOCUG00000012485,SNORD 58	9:90425593-90429195
XLOC_005960	6.92	2.40	0.35	-1.53	-4.43	5.00E-05	1.41E-03	OLFML2B	13:31039243-31072625
XLOC_030339	56.55	19.59	0.35	-1.53	-6.12	5.00E-05	1.41E-03	ENSOCUG00000022745	GL018752:1383611-1411028
XLOC_027134	15.27	5.28	0.35	-1.53	-4.70	5.00E-05	1.41E-03	NA	AAGW02083176:42-777
XLOC_035381	5.41	1.87	0.35	-1.53	-3.23	6.00E-04	1.06E-02	NA	GL019033:23691-27896
XLOC_016139	2.66	0.92	0.34	-1.54	-1.96	1.35E-03	1.93E-02	CDC42EP3	2:148584637-148606645
XLOC_036217	12.35	4.25	0.34	-1.54	-3.35	5.00E-05	1.41E-03	CEBPB	GL019159:126964-128649
XLOC_024059	17.34	5.95	0.34	-1.54	-4.58	5.00E-05	1.41E-03	NA	8:14030531-14052116
XLOC_027101	18.30	6.26	0.34	-1.55	-5.02	5.00E-05	1.41E-03	FBXL6	AAGW02083097:3-803
XLOC_037486	5.16	1.76	0.34	-1.55	-3.09	3.05E-03	3.54E-02	NA	GL019771:22619-23210
XLOC_025475	41.95	14.25	0.34	-1.56	-5.47	5.00E-05	1.41E-03	ENSOCUG00000007018	9:4323261-4328712
XLOC_009996	249.61	84.53	0.34	-1.56	-7.71	5.00E-05	1.41E-03	NA	14:154163237-154163908
XLOC_028207	627.82	212.13	0.34	-1.57	-63.96	7.50E-04	1.24E-02	NA	GL018708:797521-797637
XLOC_011494	39.96	13.47	0.34	-1.57	-3.06	5.00E-05	1.41E-03	ENSOCUG00000029728	16:67011510-67049870
XLOC_038769	2.86	0.96	0.34	-1.57	-2.63	3.50E-03	3.92E-02	NA	X:14086756-14087603
XLOC_024514	6.77	2.28	0.34	-1.57	-3.87	5.00E-05	1.41E-03	WNT5B	8:36029456-36046785
XLOC_037243	60.03	20.15	0.34	-1.58	-6.02	5.00E-05	1.41E-03	NA	GL019589:7893-11011
XLOC_034629	85.47	28.63	0.34	-1.58	-3.92	5.00E-05	1.41E-03	NA	GL018945:827-3849
XLOC_027698	3.81	1.28	0.33	-1.58	-2.08	2.80E-03	3.32E-02	B3GALTL	GL018702:1654948-1780851
XLOC_032933	26.92	9.00	0.33	-1.58	-3.06	5.00E-05	1.41E-03	NA	GL018835:531300-539512
XLOC_037056	52.04	17.39	0.33	-1.58	-7.69	5.00E-05	1.41E-03	IER2	GL019462:35054-35426
XLOC_003801	13.97	4.66	0.33	-1.58	-4.73	4.50E-04	8.42E-03	NA	11:69862705-69863105
XLOC_003097	105.86	35.22	0.33	-1.59	-11.63	5.00E-05	1.41E-03	NA	10:39988019-39988305
XLOC_008201	8.50	2.82	0.33	-1.59	-3.82	2.50E-04	5.26E-03	NA	13:116232231-116232843
XLOC_012387	19.24	6.39	0.33	-1.59	-5.57	5.00E-05	1.41E-03	ENSOCUG00000022682	17:81664270-81664649
XLOC_023739	198.64	65.89	0.33	-1.59	-32.67	4.10E-03	4.39E-02	NA	7:125615326-125615465
XLOC_032701	19.35	6.41	0.33	-1.59	-1.87	6.50E-04	1.12E-02	TCEB2	GL018828:143066-146972
XLOC_034992	6.17	2.04	0.33	-1.59	-3.65	5.00E-05	1.41E-03	NA	GL018976:283022-286352
XLOC_027071	13.28	4.39	0.33	-1.60	-4.74	3.50E-04	6.91E-03	ENSOCUG00000022364	AAGW02082989:7653-8447
XLOC_027796	40.27	13.32	0.33	-1.60	-8.47	1.00E-04	2.52E-03	NA	GL018703:6308370-6308655
XLOC_038280	3.77	1.24	0.33	-1.60	-2.30	1.00E-04	2.52E-03	SLC38A5	X:33165628-33175671
XLOC_030447	5.03	1.65	0.33	-1.61	-4.93	5.00E-05	1.41E-03	PDGFRA	GL018754:203438-237590
XLOC_016915	3.30	1.08	0.33	-1.61	-2.89	1.90E-03	2.49E-02	NA	2:32343994-32344852
XLOC_035702	9.15	2.99	0.33	-1.62	-4.07	4.90E-03	4.98E-02	NA	GL019074:150983-151370
XLOC_002733	4.37	1.43	0.33	-1.62	-2.58	1.50E-04	3.53E-03	CPVL	10:13663384-13792209
XLOC_005879	18.40	6.00	0.33	-1.62	-5.78	5.00E-05	1.41E-03	XPR1	13:7659570-7847247
XLOC_037082	3.69	1.20	0.33	-1.62	-2.00	7.00E-04	1.18E-02	TRPT1	GL019482:43796-46161
XLOC_034995	3.81	1.24	0.33	-1.62	-2.81	4.25E-03	4.50E-02	NA	GL018976:246883-247498
XLOC_029540	15.55	5.05	0.32	-1.62	-3.92	5.00E-05	1.41E-03	SAA1	GL018733:2188531-2191341
XLOC_011576	3.11	1.00	0.32	-1.63	-2.86	1.35E-03	1.93E-02	NA	16:3252259-3253188
XLOC_005179	2.65	0.86	0.32	-1.63	-3.06	2.00E-04	4.42E-03	NA	12:5757485-5758935
XLOC_008380	12.64	4.06	0.32	-1.64	-4.66	1.00E-04	2.52E-03	NA	13:142963227-142963689
XLOC_032996	18.08	5.81	0.32	-1.64	-5.08	5.00E-05	1.41E-03	NA	GL018840:441447-442118
XLOC_003627	3.13	1.00	0.32	-1.65	-3.33	5.00E-05	1.41E-03	NA	11:22653020-22654586
XLOC_025890	379.80	121.35	0.32	-1.65	-11.68	5.00E-05	1.41E-03	ENSOCUG00000026631	9:89494493-89494865
XLOC_008047	8.84	2.82	0.32	-1.65	-5.24	5.00E-05	1.41E-03	NA	13:93821710-93825918
XLOC_037256	22.30	7.07	0.32	-1.66	-2.87	5.00E-05	1.41E-03	NA	GL019599:41816-43567
XLOC_029628	25.27	8.01	0.32	-1.66	-5.83	5.00E-05	1.41E-03	NA	GL018734:1431201-1431704
XLOC_016020	365.80	115.87	0.32	-1.66	-2.71	5.00E-05	1.41E-03	ENSOCUG00000011214	2:115924483-115937121
XLOC_024171	3.39	1.07	0.32	-1.66	-4.50	5.00E-05	1.41E-03	ENSOCUG00000008575	8:33740675-33755403
XLOC_026460	72.71	22.96	0.32	-1.66	-7.54	5.00E-05	1.41E-03	NA	AAGW02079667:75803-76328
XLOC_039173	9.72	3.06	0.31	-1.67	-4.14	3.50E-04	6.91E-03	NA	X:109510776-109511304
XLOC_024559	23.20	7.29	0.31	-1.67	-5.75	5.00E-05	1.41E-03	ENSOCUG00000027968	8:50205914-50206370
XLOC_015378	4.02	1.26	0.31	-1.68	-3.10	9.50E-04	1.48E-02	NA	19:5549566-5550370
XLOC_008064	4.38	1.37	0.31	-1.68	-3.30	3.50E-04	6.91E-03	NA	13:93926637-93927587
XLOC_021335	58.52	18.29	0.31	-1.68	-13.49	3.45E-03	3.88E-02	MT3	5:12893441-12894623
XLOC_034222	5.04	1.57	0.31	-1.68	-4.53	5.00E-05	1.41E-03	PRX	GL018912:117296-129162
XLOC_021289	1224.86	381.75	0.31	-1.68	-18.12	5.00E-05	1.41E-03	RPL38	5:1616778-1642499
XLOC_021032	7.13	2.22	0.31	-1.68	-3.84	2.00E-04	4.42E-03	NA	4:39593498-39594205
XLOC_007842	20.97	6.51	0.31	-1.69	-5.58	5.00E-05	1.41E-03	NA	13:63014249-63014698

Transcriptome Gene ID	Uninfected RK-13 Mean FPKM	T. hominis infected RK-13 Mean FPKM	Fold Change	Log2 Fold Change	Test stat	P value	Q value	Ensembl Gene Name / Gene ID	Gene Locus (Chromosome/scaffold:position)
XLOC_025169	3.99	1.24	0.31	-1.69	-2.36	6.50E-04	1.12E-02	KLHDC8B	9:16772395-16788761
XLOC_022821	8.69	2.68	0.31	-1.70	-5.65	5.00E-05	1.41E-03	FLNC	7:15713363-15738228
XLOC_035921	5.30	1.63	0.31	-1.70	-3.48	3.50E-04	6.91E-03	NA	GL019105:5965-6679
XLOC_026391	11.23	3.44	0.31	-1.70	-4.61	5.00E-05	1.41E-03	ENSOCUG00000025688	AAGW02076170:229692-230442
XLOC_028333	2.05	0.63	0.31	-1.71	-2.49	4.00E-03	4.31E-02	NA	GL018709:3040358-3041369
XLOC_007027	1.82	0.55	0.31	-1.71	-3.36	5.00E-05	1.41E-03	MAB21L3	13:48145204-48199749
XLOC_023515	230.91	70.34	0.30	-1.71	-36.77	2.25E-03	2.84E-02	NA	7:53518125-53518265
XLOC_007916	248.19	75.50	0.30	-1.72	-10.32	5.00E-05	1.41E-03	NA	13:78633351-78633783
XLOC_010763	29.94	9.08	0.30	-1.72	-6.95	5.00E-05	1.41E-03	NA	15:47621026-47621391
XLOC_005517	15.18	4.59	0.30	-1.72	-5.16	1.00E-04	2.52E-03	NA	12:62137537-62137966
XLOC_038660	2.97	0.90	0.30	-1.73	-3.17	3.00E-04	6.09E-03	NA	X:3387823-3389104
XLOC_013489	20.53	6.20	0.30	-1.73	-5.60	5.00E-05	1.41E-03	ENSOCUG00000025563	18:37864429-37865654
XLOC_025837	274.77	82.99	0.30	-1.73	-18.00	5.00E-05	1.41E-03	COX7A2	9:67425157-67425409
XLOC_027610	3.86	1.16	0.30	-1.73	-3.14	5.00E-04	9.12E-03	NA	GL018701:1344207-1345186
XLOC_029862	4.38	1.32	0.30	-1.73	-3.20	8.00E-04	1.30E-02	ENSOCUG00000004760	GL018740:1707347-1708068
XLOC_032519	210.35	62.96	0.30	-1.74	-9.94	5.00E-05	1.41E-03	ENSOCUG00000024198	GL018820:708093-708529
XLOC_024062	9.20	2.75	0.30	-1.74	-2.06	3.30E-03	3.75E-02	RASSF8	8:14096773-14192355
XLOC_008806	13.96	4.15	0.30	-1.75	-4.97	5.00E-05	1.41E-03	ENSOCUG00000025046	14:129046116-129046759
XLOC_037452	9.07	2.70	0.30	-1.75	-4.25	1.00E-04	2.52E-03	NA	GL019755:13158-13760
XLOC_005369	10.08	2.99	0.30	-1.75	-4.56	2.00E-03	2.60E-02	NA	12:36119855-36120236
XLOC_032972	1026.74	303.70	0.30	-1.76	-96.43	3.00E-04	6.09E-03	NA	GL018838:452289-452391
XLOC_022149	24.49	7.24	0.30	-1.76	-4.28	5.00E-05	1.41E-03	ENSOCUG00000012690	6:26753072-26754365
XLOC_003434	4.93	1.45	0.30	-1.76	-3.89	5.00E-05	1.41E-03	NA	11:35666582-35668086
XLOC_018429	80.44	23.62	0.29	-1.77	-6.41	5.00E-05	1.41E-03	SULF1	3:85423722-85617040
XLOC_010864	173.56	50.55	0.29	-1.78	-21.55	5.00E-05	1.41E-03	NA	15:89339284-89339485
XLOC_029354	6.81	1.97	0.29	-1.79	-5.52	5.00E-05	1.41E-03	RUNX1	GL018729:1548088-1799866
XLOC_008402	20.79	6.01	0.29	-1.79	-6.44	3.50E-04	6.91E-03	ENSOCUG00000025838	14:5843984-5844308
XLOC_029359	4.25	1.22	0.29	-1.80	-3.15	2.55E-03	3.12E-02	NA	GL018729:1293052-1293671
XLOC_032427	19.93	5.71	0.29	-1.80	-5.73	5.00E-05	1.41E-03	ENSOCUG00000024511	GL018816:170573-176953
XLOC_019381	3.03	0.86	0.29	-1.81	-2.89	2.25E-03	2.84E-02	NA	3:57980123-57980887
XLOC_034467	3.00	0.85	0.29	-1.81	-3.23	2.00E-04	4.42E-03	NA	GL018932:15679-16857
XLOC_031860	5.78	1.65	0.28	-1.81	-3.55	3.70E-03	4.07E-02	NA	GL018794:251806-252302
XLOC_027327	347.18	98.85	0.28	-1.81	-25.27	5.00E-05	1.41E-03	ENSOCUG00000021402	GL018699:8523155-8523368
XLOC_023939	56.23	16.00	0.28	-1.81	-7.09	5.00E-05	1.41E-03	NA	7:157932037-157932841
XLOC_020011	1.43	0.40	0.28	-1.82	-2.50	7.50E-04	1.24E-02	WNT1	4:33265516-33280776
XLOC_026259	1.58	0.44	0.28	-1.83	-2.45	4.35E-03	4.57E-02	NA	9:58576573-58577748
XLOC_004995	155.33	43.34	0.28	-1.84	-13.39	5.00E-05	1.41E-03	NDUFA3	12:98666153-98666457
XLOC_027150	5.80	1.61	0.28	-1.85	-3.64	6.00E-04	1.06E-02	NA	AAGW02083233:10-719
XLOC_034581	5.40	1.50	0.28	-1.85	-3.59	4.50E-04	8.42E-03	NA	GL018941:360388-361047
XLOC_018080	2.82	0.78	0.28	-1.86	-2.78	3.90E-03	4.24E-02	NA	21:5688159-5688907
XLOC_013313	11.02	3.03	0.28	-1.86	-4.74	2.50E-04	5.26E-03	NA	17:82820003-82820457
XLOC_000158	17.05	4.68	0.27	-1.86	-5.63	5.00E-05	1.41E-03	ENSOCUG00000022465	1:30703574-30704109
XLOC_035149	7.61	2.09	0.27	-1.87	-4.03	5.00E-05	1.41E-03	NA	GL018999:97159-97745
XLOC_021269	5.48	1.49	0.27	-1.88	-3.66	4.50E-04	8.42E-03	FBXO27	5:824615-828207
XLOC_036216	35.72	9.65	0.27	-1.89	-2.94	5.00E-05	1.41E-03	CEBPB	GL019159:126964-128649
XLOC_009077	104.27	28.11	0.27	-1.89	-5.36	5.00E-05	1.41E-03	ENSOCUG00000014962	14:65758993-65762460
XLOC_037507	3.22	0.86	0.27	-1.90	-3.92	5.00E-05	1.41E-03	CD248	GL019795:14017-16693
XLOC_031474	51.39	13.70	0.27	-1.91	-4.42	1.50E-04	3.53E-03	FXYD1	GL018786:87385-91108
XLOC_003776	1.55	0.41	0.27	-1.91	-2.79	7.00E-04	1.18E-02	NA	11:60109405-60111062
XLOC_037241	36.70	9.73	0.27	-1.92	-7.06	5.00E-05	1.41E-03	NA	GL019589:3175-7600
XLOC_023990	161.28	42.70	0.26	-1.92	-13.74	5.00E-05	1.41E-03	NA	7:170465653-170465964
XLOC_000448	74.00	19.46	0.26	-1.93	-7.38	5.00E-05	1.41E-03	MMP13	1:113615790-113627810
XLOC_008157	21.77	5.70	0.26	-1.93	-7.75	2.15E-03	2.76E-02	NA	13:109267991-109268267
XLOC_034553	4.06	1.06	0.26	-1.94	-2.77	5.00E-05	1.41E-03	SNAI1	GL018940:12971-17461
XLOC_011241	16.00	4.13	0.26	-1.95	-6.06	5.00E-05	1.41E-03	PTGS2	16:83706415-83714496
XLOC_012588	105.83	27.12	0.26	-1.96	-1.75	4.75E-03	4.87E-02	ENSOCUG00000006173	17:39575337-39576290
XLOC_016878	34.08	8.67	0.25	-1.97	-8.92	5.00E-05	1.41E-03	NA	2:17816287-17816581
XLOC_018900	3.05	0.76	0.25	-2.01	-4.84	5.00E-05	1.41E-03	TOX	3:74291086-74624995
XLOC_008483	11.18	2.77	0.25	-2.01	-3.00	5.00E-05	1.41E-03	NA	14:34738779-34777042
XLOC_002021	2.90	0.72	0.25	-2.01	-3.06	1.30E-03	1.87E-02	NA	1:37628976-37629848
XLOC_002628	11.51	2.85	0.25	-2.01	-6.50	5.00E-05	1.41E-03	PDK4	10:33583465-33598844
XLOC_023000	6.46	1.59	0.25	-2.02	-5.27	5.00E-05	1.41E-03	NR4A2	7:95178064-95195850
XLOC_037383	14.76	3.44	0.23	-2.10	-5.79	5.00E-05	1.41E-03	NA	GL019699:19150-20399
XLOC_011900	7.45	1.70	0.23	-2.13	-4.32	5.00E-04	9.12E-03	NA	16:70879706-70880234
XLOC_007480	5.54	1.25	0.23	-2.15	-4.01	1.00E-04	2.52E-03	SFN	13:138502951-138503698
XLOC_005261	2.21	0.49	0.22	-2.19	-2.83	2.95E-03	3.44E-02	NA	12:15124024-15124983
XLOC_008669	6.96	1.52	0.22	-2.19	-5.64	5.00E-05	1.41E-03	FAM43A	14:90536999-90540547
XLOC_033229	68.68	14.81	0.22	-2.21	-8.60	5.00E-05	1.41E-03	ENSOCUG00000021938	GL018850:50898-67777
XLOC_010783	1.88	0.40	0.21	-2.22	-3.69	5.00E-05	1.41E-03	NA	15:60776882-60779257
XLOC_015636	155.66	32.77	0.21	-2.25	-11.28	5.00E-05	1.41E-03	ENSOCUG00000001331	2:7615568-7616037
XLOC_018928	5.19	1.09	0.21	-2.25	-2.41	4.20E-03	4.46E-02	ENSOCUG00000022920	3:84244628-84737352
XLOC_007864	2.10	0.42	0.20	-2.33	-3.43	1.00E-04	2.52E-03	NA	13:70197395-70198943
XLOC_035645	2.10	0.41	0.20	-2.35	-3.25	3.50E-04	6.91E-03	NA	GL019067:131088-132387
XLOC_036521	1.44	0.28	0.20	-2.36	-3.48	5.00E-05	1.41E-03	LFNG	GL019252:18828-25637
XLOC_003806	1.93	0.37	0.19	-2.37	-2.91	3.00E-03	3.49E-02	NA	11:72220337-72221350
XLOC_034602	2.26	0.44	0.19	-2.37	-3.02	4.80E-03	4.91E-02	ZNHIT2	GL018942:172338-173584
XLOC_010782	1.62	0.31	0.19	-2.38	-2.84	3.75E-03	4.12E-02	NA	15:60775219-60776305
XLOC_003009	27.85	5.21	0.19	-2.42	-10.25	1.80E-03	2.39E-02	NA	10:24086339-24086590
XLOC_002368	2.37	0.44	0.18	-2.44	-3.95	5.00E-05	1.41E-03	NA	1:153819333-153821222
XLOC_014076	2.73	0.47	0.17	-2.54	-3.10	4.35E-03	4.57E-02	NA	18:14759045-14759763
XLOC_008693	12.24	2.03	0.17	-2.59	-6.26	2.95E-03	3.44E-02	RPL35A	14:93169689-93172758
XLOC_016769	28.06	4.29	0.15	-2.71	-8.95	1.00E-04	2.52E-03	LBH	2:155874812-155897974
XLOC_032831	45.21	6.90	0.15	-2.71	-6.22	5.00E-05	1.41E-03	PAI1	GL018831:42756-50505
XLOC_015300	7.71	1.02	0.13	-2.91	-8.04	5.00E-05	1.41E-03	HDAC5	19:44423052-44453608
XLOC_038191	12.15	1.47	0.12	-3.05	-6.04	1.30E-03	1.87E-02	ENSOCUG00000001791	X:6049547-6049921
XLOC_009703	5.23	0.57	0.11	-3.20	-5.80	5.00E-05	1.41E-03	NA	14:90656480-90658261
XLOC_007088	5.62	0.55	0.10	-3.35	-5.78	5.00E-05	1.41E-03	NTNG1	13:56634994-57027409
XLOC_024890	919.29	74.05	0.08	-3.63	-107.60	1.75E-03	2.35E-02	NA	8:64779133-64779239
XLOC_011178	20.97	1.61	0.08	-3.71	-4.40	5.00E-05	1.41E-03	U6	16:67559682-67561220
XLOC_027036	57.50	4.29	0.07	-3.75	-15.26	2.80E-03	3.32E-02	NA	AAGW02082887:5144-5371
XLOC_003437	92.63	0.00	0.00	#NAME?	NA	5.00E-05	1.41E-03	U6	11:37140585-37140692
XLOC_005340	53.97	0.00	0.00	#NAME?	NA	3.50E-04	6.91E-03	NA	12:31948214-31948327
XLOC_005391	566.06	0.00	0.00	#NAME?	NA	5.00E-05	1.41E-03	NA	12:49603414-49603482
XLOC_005657	2.52	0.00	0.00	#NAME?	NA	1.00E-04	2.52E-03	NA	12:75124945-75125258
XLOC_005733	26.63	0.00	0.00	#NAME?	NA	5.00E-05	1.41E-03	NA	12:104558255-104558419
XLOC_005735	2107.69	0.00	0.00	#NAME?	NA	5.00E-05	1.41E-03	NA	12:106340561-106340621
XLOC_007560	2.49	0.00	0.00	#NAME?	NA	5.00E-05	1.41E-03	NA	13:7521051-7521406
XLOC_007562	160.06	0.00	0.00	#NAME?	NA	5.00E-05	1.41E-03	NA	13:8982602-8982702
XLOC_010677	171.31	0.00	0.00	#NAME?	NA	5.00E-05	1.41E-03	NA	15:6783760-6783862
XLOC_011930	1.36	0.00	0.00	#NAME?	NA	5.00E-05	1.41E-03	NA	16:72782770-72783277
XLOC_014182	27.85	0.00	0.00	#NAME?	NA	5.00E-05	1.41E-03	NA	18:33960080-33960238
XLOC_016973	45.63	0.00	0.00	#NAME?	NA	1.50E-04	3.53E-03	NA	2:51091424-51091550
XLOC_020885	2.75	0.00	0.00	#NAME?	NA	5.00E-05	1.41E-03	NA	4:13874887-13875234
XLOC_021737	2.23	0.00	0.00	#NAME?	NA	5.00E-05	1.41E-03	NA	5:1679327-1679732
XLOC_026322	1312.22	0.00	0.00	#NAME?	NA	5.00E-05	1.41E-03	NA	9:85365526-85365610
XLOC_034386	1419.94	0.00	0.00	#NAME?	NA	5.00E-05	1.41E-03	NA	GL018925:580790-580856
XLOC_036668	19.25	0.00	0.00	#NAME?	NA	5.00E-05	1.41E-03	NA	GL019294:7912-8089
XLOC_038653	3.67	0.00	0.00	#NAME?	NA	5.00E-05	1.41E-03	NA	X:3344703-3345013
XLOC_039177	215.87	0.00	0.00	#NAME?	NA	5.00E-05	1.41E-03	NA	X:111450112-111450201
XLOC_028133	0.00	412.12	#DIV/0!	Inf	NA	5.00E-05	1.41E-03	NA	GL018706:4129410-4129494
XLOC_002450	0.00	354.79	#DIV/0!	Inf	NA	5.00E-05	1.41E-03	NA	1:179274118-179274213
XLOC_028845	0.00	242.83	#DIV/0!	Inf	NA	5.00E-05	1.41E-03	NA	GL018718:2960551-2960651

Transcriptome Gene ID	Uninfected RK-13 Mean FPKM	T. hominis infected RK-13 Mean FPKM	Fold Change	Log2 Fold Change	Test stat	P value	Q value	Ensembl Gene Name / Gene ID	Gene Locus (Chromosome/scaffold:position)
XLOC_021168	0.00	215.94	#DIV/0!	Inf	NA	5.00E-05	1.41E-03	NA	4:53668264-53668365
XLOC_030161	0.00	144.45	#DIV/0!	Inf	NA	5.00E-05	1.41E-03	NA	GL018748:681796-681904
XLOC_037469	0.00	121.17	#DIV/0!	Inf	NA	5.00E-05	1.41E-03	NA	GL019760:17843-17944
XLOC_002177	0.00	70.04	#DIV/0!	Inf	NA	5.00E-05	1.41E-03	NA	1:92309072-92309197
XLOC_013118	0.00	65.55	#DIV/0!	Inf	NA	5.00E-05	1.41E-03	NA	17:36123009-36123140
XLOC_005822	0.00	63.88	#DIV/0!	Inf	NA	1.00E-04	2.52E-03	NA	12:138580748-138580865
XLOC_038993	0.00	51.19	#DIV/0!	Inf	NA	5.00E-05	1.41E-03	NA	X:53608452-53608579
XLOC_005810	0.00	46.20	#DIV/0!	Inf	NA	5.00E-05	1.41E-03	NA	12:134996052-134996183
XLOC_016912	0.00	29.15	#DIV/0!	Inf	NA	5.00E-05	1.41E-03	NA	2:32235989-32236179
XLOC_009395	0.00	18.60	#DIV/0!	Inf	NA	5.00E-05	1.41E-03	NA	14:162787085-162800086
XLOC_001910	0.00	17.66	#DIV/0!	Inf	NA	5.00E-05	1.41E-03	NA	1:1759210-1759407
XLOC_023460	0.00	16.20	#DIV/0!	Inf	NA	5.00E-05	1.41E-03	NA	7:48369753-48369933
XLOC_001938	0.00	14.62	#DIV/0!	Inf	NA	5.00E-05	1.41E-03	NA	1:15042186-15042370
XLOC_034817	0.00	9.54	#DIV/0!	Inf	NA	5.00E-05	1.41E-03	NA	GL018962:92385-92618
XLOC_031064	0.00	7.87	#DIV/0!	Inf	NA	5.00E-05	1.41E-03	NA	GL018768:212344-212567
XLOC_019706	0.00	6.53	#DIV/0!	Inf	NA	5.00E-05	1.41E-03	NA	3:127013334-127013599
XLOC_031536	0.00	5.41	#DIV/0!	Inf	NA	5.00E-05	1.41E-03	NA	GL018786:480758-481008
XLOC_005276	0.00	4.99	#DIV/0!	Inf	NA	5.00E-05	1.41E-03	NA	12:16863374-16863640
XLOC_019699	0.00	4.26	#DIV/0!	Inf	NA	5.00E-05	1.41E-03	NA	3:124236333-124236672
XLOC_026468	0.00	3.83	#DIV/0!	Inf	NA	5.00E-05	1.41E-03	NA	AAGW02079674:67751-68059
XLOC_027079	0.00	3.22	#DIV/0!	Inf	NA	5.00E-05	1.41E-03	NA	AAGW02083011:7511-7867
XLOC_026349	0.00	2.95	#DIV/0!	Inf	NA	5.00E-05	1.41E-03	NA	9:93074160-93074700
XLOC_038686	0.00	2.84	#DIV/0!	Inf	NA	4.00E-04	7.69E-03	NA	X:3469924-3470209
XLOC_029958	0.00	2.50	#DIV/0!	Inf	NA	5.00E-05	1.41E-03	NA	GL018741:1927370-1927794
XLOC_033350	0.00	2.38	#DIV/0!	Inf	NA	5.00E-05	1.41E-03	NA	GL018857:541990-542398
XLOC_024882	0.00	2.33	#DIV/0!	Inf	NA	5.00E-05	1.41E-03	NA	8:64178251-64178619
XLOC_017373	0.00	2.32	#DIV/0!	Inf	NA	5.00E-05	1.41E-03	NA	2:149922734-149923100
XLOC_010012	0.00	2.11	#DIV/0!	Inf	NA	1.00E-04	2.52E-03	NA	14:163176634-163176966
XLOC_023564	0.00	2.10	#DIV/0!	Inf	NA	1.00E-04	2.52E-03	NA	7:65506146-65506489

Appendix F

Testing for enrichment of differentially expressed genes in KEGG pathways.

Fischer's exact test with Benjamini and Hochberg correction (Benjamini and Hochberg, 1995) for the enrichment of genes identified as significantly differentially expressed in KEGG pathways in the RK-13 cell line.

This table is additionally available in xlsx format for excel on the CD supplied with this thesis, or from http://bmcgenomics.biomedcentral.com/articles/10.1186/s12864-015-1989-z, table S6 (Watson et al., 2015).

KEGG pathway name	KEGG id	% of gene modulated	Number of differentially expressed trancripts in pathway	Total number of rabbit genes in pathway	P-Value	Corrected P-Value
Ribosome	ko03010	0.25	108	439	2.61E-11	7.12E-09
DNA replication	ko03030	0.42	15	36	1.34E-04	1.59E-02
Pyrimidine metabolism	ko00240	0.26	29	110	1.75E-04	1.59E-02
Oxidative phosphorylation	ko00190	0.23	33	142	4.71E-04	2.50E-02
Meiosis - yeast	ko04113	0.31	19	62	4.83E-04	2.50E-02
Cell cycle - yeast	ko04111	0.28	21	74	5.87E-04	2.50E-02
Renal cell carcinoma	ko05211	0.28	21	75	6.80E-04	2.50E-02
Amino sugar and nucleotide sugar metabolism	ko00520	0.31	17	54	7.31E-04	2.50E-02
Focal adhesion	ko04510	0.20	43	216	1.21E-03	3.66E-02
ECM-receptor interaction	ko04512	0.25	22	88	1.79E-03	4.89E-02
Cell cycle	ko04110	0.21	30	142	2.93E-03	7.26E-02
Purine metabolism	ko00230	0.19	37	190	3.49E-03	7.94E-02
Small cell lung cancer	ko05222	0.22	22	100	6.64E-03	1.38E-01
TNF signaling pathway	ko04668	0.21	23	107	7.09E-03	1.38E-01
Pathways in cancer	ko05200	0.16	62	379	7.61E-03	1.39E-01
Glutathione metabolism	ko00480	0.25	15	60	8.96E-03	1.53E-01
Collecting duct acid secretion	ko04966	0.32	9	28	1.13E-02	1.81E-01
HIF-1 signaling pathway	ko04066	0.20	25	127	1.29E-02	1.96E-01
Mismatch repair	ko03430	0.33	8	24	1.40E-02	2.01E-01
Hippo signaling pathway	ko04390	0.18	29	160	1.96E-02	2.63E-01
Carbon metabolism	ko01200	0.20	21	106	2.02E-02	2.63E-01
Citrate cycle (TCA cycle)	ko00020	0.26	10	38	2.28E-02	2.73E-01
Fanconi anemia pathway	ko03460	0.23	13	56	2.30E-02	2.73E-01
One carbon pool by folate	ko00670	0.29	7	24	3.55E-02	3.86E-01
MicroRNAs in cancer	ko05206	0.17	28	163	3.64E-02	3.86E-01
Streptomycin biosynthesis	ko00521	0.44	4	9	3.78E-02	3.86E-01
Carbon fixation pathways in prokaryotes	ko00720	0.32	6	19	3.82E-02	3.86E-01
TGF-beta signaling pathway	ko04350	0.19	17	88	4.07E-02	3.89E-01
Butirosin and neomycin biosynthesis	ko00524	0.60	3	5	4.14E-02	3.89E-01
Regulation of actin cytoskeleton	ko04810	0.16	36	225	4.44E-02	4.04E-01
PI3K-Akt signaling pathway	ko04151	0.15	58	395	5.05E-02	4.45E-01
Huntington's disease	ko05016	0.16	32	199	5.26E-02	4.49E-01
Proteoglycans in cancer	ko05205	0.15	39	253	5.70E-02	4.71E-01
Nucleotide excision repair	ko03420	0.22	10	46	5.88E-02	4.72E-01
Hepatitis C	ko05160	0.17	23	137	6.44E-02	5.02E-01
Hippo signaling pathway - fly	ko04391	0.19	14	75	7.21E-02	5.47E-01
Gap junction	ko04540	0.18	17	97	7.73E-02	5.59E-01
Sphingolipid metabolism	ko00600	0.20	10	49	7.87E-02	5.59E-01
2-Oxocarboxylic acid metabolism	ko01210	0.28	5	18	8.15E-02	5.59E-01
MAPK signaling pathway - yeast	ko04011	0.25	6	24	8.26E-02	5.59E-01
Ubiquitin mediated proteolysis	ko04120	0.16	24	150	8.70E-02	5.59E-01
Base excision repair	ko03410	0.22	8	37	8.74E-02	5.59E-01
Vibrio cholerae infection	ko05110	0.19	11	57	8.80E-02	5.59E-01
Insulin signaling pathway	ko04910	0.16	24	152	9.60E-02	5.95E-01
Galactose metabolism	ko00052	0.21	8	39	1.07E-01	6.45E-01
Selenocompound metabolism	ko00450	0.25	5	20	1.09E-01	6.45E-01
Leukocyte transendothelial migration	ko04670	0.16	20	126	1.16E-01	6.62E-01
MAPK signaling pathway	ko04010	0.14	38	264	1.16E-01	6.62E-01
MAPK signaling pathway - fly	ko04013	0.27	4	15	1.25E-01	6.80E-01
Melanoma	ko05218	0.17	13	76	1.26E-01	6.80E-01
Circadian rhythm	ko04710	0.21	6	28	1.32E-01	6.80E-01
Fatty acid elongation	ko00062	0.21	6	28	1.32E-01	6.80E-01
Prostate cancer	ko05215	0.16	16	99	1.34E-01	6.80E-01
Epithelial cell signaling in Helicobacter pylori infection	ko05120	0.17	12	70	1.36E-01	6.80E-01
RNA polymerase	ko03020	0.20	7	35	1.37E-01	6.80E-01
Biosynthesis of amino acids	ko01230	0.17	13	78	1.43E-01	6.95E-01
Parkinson's disease	ko05012	0.15	22	147	1.52E-01	7.18E-01
Glycosaminoglycan biosynthesis - chondroitin sulfate / dermatan sulfate	ko00532	0.22	5	23	1.56E-01	7.18E-01
Dorso-ventral axis formation	ko04320	0.22	5	23	1.56E-01	7.18E-01
Polycyclic aromatic hydrocarbon degradation	ko00624	0.40	2	5	1.58E-01	7.18E-01
Ovarian steroidogenesis	ko04913	0.17	11	66	1.68E-01	7.50E-01
Cytosolic DNA-sensing pathway	ko04623	0.17	10	59	1.71E-01	7.53E-01
Homologous recombination	ko03440	0.19	6	31	1.77E-01	7.68E-01
Primary bile acid biosynthesis	ko00120	0.22	4	18	1.86E-01	7.74E-01
Glioma	ko05214	0.16	11	68	1.89E-01	7.74E-01
Epstein-Barr virus infection	ko05169	0.14	35	256	1.92E-01	7.74E-01
Glycine, serine and threonine metabolism	ko00260	0.18	7	39	1.92E-01	7.74E-01
Vitamin B6 metabolism	ko00750	0.33	2	6	1.97E-01	7.74E-01
Arrhythmogenic right ventricular cardiomyopathy (ARVC)	ko05412	0.15	13	84	1.99E-01	7.74E-01

KEGG pathway name	KEGG id	% of gene modulated	Number of differentially expressed trancripts in pathway	Total number of rabbit genes in pathway	P-Value	Corrected P-Value
Ribosome biogenesis in eukaryotes	ko03008	0.15	14	92	2.02E-01	7.74E-01
Hypertrophic cardiomyopathy (HCM)	ko05410	0.15	14	92	2.02E-01	7.74E-01
Endocytosis	ko04144	0.14	29	210	2.04E-01	7.74E-01
Bladder cancer	ko05219	0.18	7	40	2.07E-01	7.75E-01
Adipocytokine signaling pathway	ko04920	0.16	11	70	2.11E-01	7.76E-01
Notch signaling pathway	ko04330	0.17	8	48	2.17E-01	7.76E-01
HTLV-I infection	ko05166	0.13	41	309	2.17E-01	7.76E-01
Fructose and mannose metabolism	ko00051	0.17	7	41	2.23E-01	7.76E-01
Drug metabolism - other enzymes	ko00983	0.15	11	71	2.23E-01	7.76E-01
Folate biosynthesis	ko00790	0.23	3	13	2.25E-01	7.76E-01
Neurotrophin signaling pathway	ko04722	0.14	19	134	2.30E-01	7.84E-01
Caprolactam degradation	ko00930	0.29	2	7	2.36E-01	7.84E-01
Peroxisome	ko04146	0.15	12	80	2.38E-01	7.84E-01
Chronic myeloid leukemia	ko05220	0.15	12	80	2.38E-01	7.84E-01
ErbB signaling pathway	ko04012	0.15	14	96	2.43E-01	7.90E-01
p53 signaling pathway	ko04115	0.15	12	81	2.50E-01	8.00E-01
Acute myeloid leukemia	ko05221	0.16	9	58	2.52E-01	8.00E-01
Synaptic vesicle cycle	ko04721	0.15	10	66	2.56E-01	8.04E-01
Alzheimer's disease	ko05010	0.13	24	179	2.71E-01	8.42E-01
Toll-like receptor signaling pathway	ko04620	0.14	14	99	2.76E-01	8.46E-01
Tyrosine metabolism	ko00350	0.16	6	37	2.81E-01	8.48E-01
Renin-angiotensin system	ko04614	0.20	3	15	2.83E-01	8.48E-01
Sulfur metabolism	ko00920	0.17	4	23	3.02E-01	8.94E-01
Ether lipid metabolism	ko00565	0.15	7	46	3.05E-01	8.94E-01
Mucin type O-Glycan biosynthesis	ko00512	0.16	5	31	3.13E-01	9.08E-01
Vitamin digestion and absorption	ko04977	0.17	4	24	3.27E-01	9.39E-01
Nicotinate and nicotinamide metabolism	ko00760	0.16	5	32	3.34E-01	9.39E-01
Alanine, aspartate and glutamate metabolism	ko00250	0.16	5	32	3.34E-01	9.39E-01
Lysosome	ko04142	0.13	17	130	3.48E-01	9.69E-01
mTOR signaling pathway	ko04150	0.14	10	73	3.53E-01	9.72E-01
Dopaminergic synapse	ko04728	0.13	16	125	3.84E-01	1.00E+00
Mineral absorption	ko04978	0.14	7	51	3.91E-01	1.00E+00
Sulfur relay system	ko04122	0.18	2	11	3.94E-01	1.00E+00
Hepatitis B	ko05161	0.13	20	160	3.99E-01	1.00E+00
Steroid biosynthesis	ko00100	0.16	3	19	4.00E-01	1.00E+00
Tight junction	ko04530	0.13	18	144	4.08E-01	1.00E+00
Cardiac muscle contraction	ko04260	0.13	10	77	4.10E-01	1.00E+00
Aldosterone-regulated sodium reabsorption	ko04960	0.14	6	44	4.14E-01	1.00E+00
Cocaine addiction	ko05030	0.14	6	44	4.14E-01	1.00E+00
RIG-I-like receptor signaling pathway	ko04622	0.13	9	69	4.15E-01	1.00E+00
GnRH signaling pathway	ko04912	0.13	11	86	4.19E-01	1.00E+00
Amphetamine addiction	ko05031	0.13	8	61	4.21E-01	1.00E+00
Pentose phosphate pathway	ko00030	0.14	4	28	4.24E-01	1.00E+00
Glycerolipid metabolism	ko00561	0.13	8	64	4.69E-01	1.00E+00
Carbon fixation in photosynthetic organisms	ko00710	0.13	4	30	4.72E-01	1.00E+00
Influenza A	ko05164	0.12	21	176	4.72E-01	1.00E+00
Estrogen signaling pathway	ko04915	0.12	12	99	4.78E-01	1.00E+00
Caffeine metabolism	ko00232	0.20	1	5	4.80E-01	1.00E+00
Phosphonate and phosphinate metabolism	ko00440	0.20	1	5	4.80E-01	1.00E+00
Circadian rhythm - plant	ko04712	0.20	1	5	4.80E-01	1.00E+00
Valine, leucine and isoleucine degradation	ko00280	0.13	6	48	4.89E-01	1.00E+00
Pathogenic Escherichia coli infection	ko05130	0.12	8	66	5.01E-01	1.00E+00
Various types of N-glycan biosynthesis	ko00513	0.13	5	40	5.02E-01	1.00E+00
Non-homologous end-joining	ko03450	0.14	2	14	5.03E-01	1.00E+00
Type II diabetes mellitus	ko04930	0.12	6	49	5.08E-01	1.00E+00
Wnt signaling pathway	ko04310	0.12	17	145	5.10E-01	1.00E+00
Non-small cell lung cancer	ko05223	0.12	7	58	5.12E-01	1.00E+00
Starch and sucrose metabolism	ko00500	0.12	8	67	5.17E-01	1.00E+00
mRNA surveillance pathway	ko03015	0.12	12	102	5.17E-01	1.00E+00
Regulation of autophagy	ko04140	0.13	4	32	5.17E-01	1.00E+00
Oocyte meiosis	ko04114	0.12	13	111	5.20E-01	1.00E+00
Glycolysis / Gluconeogenesis	ko00010	0.12	9	76	5.20E-01	1.00E+00
Prolactin signaling pathway	ko04917	0.12	9	76	5.20E-01	1.00E+00
Cysteine and methionine metabolism	ko00270	0.12	5	41	5.22E-01	1.00E+00
Vasopressin-regulated water reabsorption	ko04962	0.12	5	41	5.22E-01	1.00E+00
Glycerophospholipid metabolism	ko00564	0.12	11	94	5.27E-01	1.00E+00
Protein digestion and absorption	ko04974	0.12	13	112	5.32E-01	1.00E+00
Phenylalanine metabolism	ko00360	0.13	2	15	5.36E-01	1.00E+00
Pantothenate and CoA biosynthesis	ko00770	0.13	2	15	5.36E-01	1.00E+00
Protein export	ko03060	0.13	3	24	5.38E-01	1.00E+00
Histidine metabolism	ko00340	0.12	3	25	5.63E-01	1.00E+00

KEGG pathway name	KEGG id	% of gene modulated	Number of differentially expressed trancripts in pathway	Total number of rabbit genes in pathway	P-Value	Corrected P-Value
Glycosaminoglycan biosynthesis - heparan sulfate / heparin	ko00534	0.12	3	25	5.63E-01	1.00E+00
Hematopoietic cell lineage	ko04640	0.11	14	124	5.69E-01	1.00E+00
Toxoplasmosis	ko05145	0.11	15	133	5.70E-01	1.00E+00
Complement and coagulation cascades	ko04610	0.11	9	80	5.77E-01	1.00E+00
Cyanoamino acid metabolism	ko00460	0.14	1	7	5.82E-01	1.00E+00
Maturity onset diabetes of the young	ko04950	0.12	3	26	5.88E-01	1.00E+00
beta-Alanine metabolism	ko00410	0.11	3	27	6.11E-01	1.00E+00
Glycosylphosphatidylinositol(GPI)-anchor biosynthesis	ko00563	0.11	3	27	6.11E-01	1.00E+00
Biosynthesis of unsaturated fatty acids	ko01040	0.11	3	27	6.11E-01	1.00E+00
Basal transcription factors	ko03022	0.11	5	46	6.16E-01	1.00E+00
Apoptosis	ko04210	0.11	10	92	6.17E-01	1.00E+00
Chagas disease (American trypanosomiasis)	ko05142	0.11	16	147	6.23E-01	1.00E+00
Circadian rhythm - fly	ko04711	0.13	1	8	6.25E-01	1.00E+00
Glycosphingolipid biosynthesis - ganglio series	ko00604	0.11	2	18	6.26E-01	1.00E+00
N-Glycan biosynthesis	ko00510	0.11	6	56	6.28E-01	1.00E+00
Nitrogen metabolism	ko00910	0.11	3	28	6.34E-01	1.00E+00
Methane metabolism	ko00680	0.11	4	38	6.42E-01	1.00E+00
VEGF signaling pathway	ko04370	0.10	7	67	6.53E-01	1.00E+00
Glyoxylate and dicarboxylate metabolism	ko00630	0.10	3	29	6.56E-01	1.00E+00
Morphine addiction	ko05032	0.10	9	86	6.57E-01	1.00E+00
Propanoate metabolism	ko00640	0.10	4	39	6.61E-01	1.00E+00
Carbohydrate digestion and absorption	ko04973	0.10	5	49	6.67E-01	1.00E+00
Insulin secretion	ko04911	0.10	9	87	6.69E-01	1.00E+00
Salmonella infection	ko05132	0.10	9	87	6.69E-01	1.00E+00
Phagosome	ko04145	0.11	22	207	6.72E-01	1.00E+00
Steroid hormone biosynthesis	ko00140	0.10	8	78	6.74E-01	1.00E+00
Chemokine signaling pathway	ko04062	0.11	18	171	6.76E-01	1.00E+00
Amoebiasis	ko05146	0.10	16	153	6.80E-01	1.00E+00
Basal cell carcinoma	ko05217	0.10	6	60	6.88E-01	1.00E+00
Ubiquinone and other terpenoid-quinone biosynthesis	ko00130	0.10	1	10	6.98E-01	1.00E+00
Benzoate degradation	ko00362	0.10	1	10	6.98E-01	1.00E+00
Terpenoid backbone biosynthesis	ko00900	0.10	2	21	7.03E-01	1.00E+00
Glycosaminoglycan degradation	ko00531	0.10	2	21	7.03E-01	1.00E+00
Pentose and glucuronate interconversions	ko00040	0.10	4	42	7.13E-01	1.00E+00
Hedgehog signaling pathway	ko04340	0.09	5	53	7.28E-01	1.00E+00
Endocrine and other factor-regulated calcium reabsorption	ko04961	0.09	4	43	7.29E-01	1.00E+00
ABC transporters	ko02010	0.09	4	43	7.29E-01	1.00E+00
B cell receptor signaling pathway	ko04662	0.10	11	112	7.36E-01	1.00E+00
Adherens junction	ko04520	0.10	9	93	7.38E-01	1.00E+00
Bacterial invasion of epithelial cells	ko05100	0.10	9	93	7.38E-01	1.00E+00
Other glycan degradation	ko00511	0.09	2	23	7.46E-01	1.00E+00
Proteasome	ko03050	0.09	5	55	7.55E-01	1.00E+00
SNARE interactions in vesicular transport	ko04130	0.09	4	45	7.59E-01	1.00E+00
Cell adhesion molecules (CAMs)	ko04514	0.10	18	182	7.64E-01	1.00E+00
Axon guidance	ko04360	0.10	14	144	7.65E-01	1.00E+00
Dilated cardiomyopathy	ko05414	0.10	13	135	7.69E-01	1.00E+00
Viral carcinogenesis	ko05203	0.10	21	213	7.82E-01	1.00E+00
Phototransduction - fly	ko04745	0.08	2	25	7.83E-01	1.00E+00
Pancreatic cancer	ko05212	0.09	7	78	7.87E-01	1.00E+00
Herpes simplex infection	ko05168	0.10	21	214	7.88E-01	1.00E+00
RNA transport	ko03013	0.10	19	196	7.95E-01	1.00E+00
Melanogenesis	ko04916	0.09	9	99	7.96E-01	1.00E+00
Colorectal cancer	ko05210	0.09	8	89	7.96E-01	1.00E+00
Cytokine-cytokine receptor interaction	ko04060	0.10	24	245	8.03E-01	1.00E+00
Endometrial cancer	ko05213	0.08	5	59	8.03E-01	1.00E+00
Glycosaminoglycan biosynthesis - keratan sulfate	ko00533	0.07	1	14	8.05E-01	1.00E+00
Pyruvate metabolism	ko00620	0.08	4	49	8.11E-01	1.00E+00
Fc gamma R-mediated phagocytosis	ko04666	0.09	12	131	8.14E-01	1.00E+00
Legionellosis	ko05134	0.09	7	81	8.16E-01	1.00E+00
Malaria	ko05144	0.09	7	81	8.16E-01	1.00E+00
Other types of O-glycan biosynthesis	ko00514	0.07	2	27	8.16E-01	1.00E+00
Thyroid hormone synthesis	ko04918	0.08	6	71	8.19E-01	1.00E+00
Rheumatoid arthritis	ko05323	0.09	16	171	8.19E-01	1.00E+00
Osteoclast differentiation	ko04380	0.09	11	122	8.21E-01	1.00E+00
Jak-STAT signaling pathway	ko04630	0.09	14	152	8.23E-01	1.00E+00
Protein processing in endoplasmic reticulum	ko04141	0.09	18	194	8.40E-01	1.00E+00
Transcriptional misregulation in cancer	ko05202	0.09	24	254	8.49E-01	1.00E+00
Porphyrin and chlorophyll metabolism	ko00860	0.08	5	64	8.53E-01	1.00E+00

KEGG pathway name	KEGG id	% of gene modulated	Number of differentially expressed trancripts in pathway	Total number of rabbit genes in pathway	P-Value	Corrected P-Value
Amyotrophic lateral sclerosis (ALS)	ko05014	0.08	5	64	8.53E-01	1.00E+00
Glycosphingolipid biosynthesis - lacto and neolacto series	ko00601	0.07	2	30	8.57E-01	1.00E+00
Vascular smooth muscle contraction	ko04270	0.09	12	138	8.60E-01	1.00E+00
Arachidonic acid metabolism	ko00590	0.09	11	128	8.61E-01	1.00E+00
Butanoate metabolism	ko00650	0.06	2	31	8.68E-01	1.00E+00
alpha-Linolenic acid metabolism	ko00592	0.06	2	31	8.68E-01	1.00E+00
NOD-like receptor signaling pathway	ko04621	0.07	4	55	8.71E-01	1.00E+00
GABAergic synapse	ko04727	0.08	7	88	8.71E-01	1.00E+00
Plant-pathogen interaction	ko04626	0.06	1	18	8.74E-01	1.00E+00
Fc epsilon RI signaling pathway	ko04664	0.08	9	110	8.77E-01	1.00E+00
PPAR signaling pathway	ko03320	0.08	6	78	8.77E-01	1.00E+00
Alcoholism	ko05034	0.09	14	162	8.80E-01	1.00E+00
Phosphatidylinositol signaling system	ko04070	0.08	6	79	8.84E-01	1.00E+00
Pertussis	ko05133	0.08	6	79	8.84E-01	1.00E+00
Chemical carcinogenesis	ko05204	0.08	10	122	8.86E-01	1.00E+00
NF-kappa B signaling pathway	ko04064	0.09	14	164	8.89E-01	1.00E+00
Bile secretion	ko04976	0.07	5	71	9.04E-01	1.00E+00
Progesterone-mediated oocyte maturation	ko04914	0.07	7	94	9.07E-01	1.00E+00
Cholinergic synapse	ko04725	0.08	8	105	9.08E-01	1.00E+00
Ascorbate and aldarate metabolism	ko00053	0.06	2	36	9.15E-01	1.00E+00
Proximal tubule bicarbonate reclamation	ko04964	0.05	1	22	9.18E-01	1.00E+00
Fatty acid degradation	ko00071	0.06	3	50	9.21E-01	1.00E+00
Drug metabolism - cytochrome P450	ko00982	0.08	9	120	9.26E-01	1.00E+00
Lysine degradation	ko00310	0.06	3	52	9.33E-01	1.00E+00
Two-component system	ko02020	0.04	1	24	9.34E-01	1.00E+00
Long-term depression	ko04730	0.06	4	65	9.35E-01	1.00E+00
Fat digestion and absorption	ko04975	0.06	3	53	9.38E-01	1.00E+00
T cell receptor signaling pathway	ko04660	0.08	12	157	9.41E-01	1.00E+00
Shigellosis	ko05131	0.06	4	67	9.44E-01	1.00E+00
Aminoacyl-tRNA biosynthesis	ko00970	0.05	2	42	9.50E-01	1.00E+00
Gastric acid secretion	ko04971	0.06	4	69	9.51E-01	1.00E+00
Salivary secretion	ko04970	0.06	5	82	9.53E-01	1.00E+00
Arginine and proline metabolism	ko00330	0.05	3	59	9.61E-01	1.00E+00
Retinol metabolism	ko00830	0.06	6	97	9.62E-01	1.00E+00
Linoleic acid metabolism	ko00591	0.05	3	61	9.67E-01	1.00E+00
Tryptophan metabolism	ko00380	0.04	2	47	9.68E-01	1.00E+00
Leishmaniasis	ko05140	0.06	7	112	9.68E-01	1.00E+00
Inositol phosphate metabolism	ko00562	0.05	3	62	9.70E-01	1.00E+00
Circadian entrainment	ko04713	0.06	5	89	9.71E-01	1.00E+00
Spliceosome	ko03040	0.07	12	172	9.72E-01	1.00E+00
Taste transduction	ko04742	0.03	1	32	9.73E-01	1.00E+00
RNA degradation	ko03018	0.05	4	79	9.77E-01	1.00E+00
Thyroid cancer	ko05216	0.03	1	34	9.78E-01	1.00E+00
Prion diseases	ko05020	0.03	1	34	9.78E-01	1.00E+00
Metabolism of xenobiotics by cytochrome P450	ko00980	0.06	8	130	9.78E-01	1.00E+00
Serotonergic synapse	ko04726	0.06	9	143	9.80E-01	1.00E+00
African trypanosomiasis	ko05143	0.04	3	72	9.87E-01	1.00E+00
Retrograde endocannabinoid signaling	ko04723	0.05	5	101	9.88E-01	1.00E+00
Primary immunodeficiency	ko05340	0.04	3	78	9.92E-01	1.00E+00
Long-term potentiation	ko04720	0.03	2	63	9.93E-01	1.00E+00
Glutamatergic synapse	ko04724	0.04	5	115	9.96E-01	1.00E+00
Viral myocarditis	ko05416	0.05	8	164	9.98E-01	1.00E+00
Measles	ko05162	0.05	11	209	9.99E-01	1.00E+00
Inflammatory bowel disease (IBD)	ko05321	0.03	3	98	9.99E-01	1.00E+00
Tuberculosis	ko05152	0.05	12	228	9.99E-01	1.00E+00
Calcium signaling pathway	ko04020	0.06	15	269	9.99E-01	1.00E+00
Staphylococcus aureus infection	ko05150	0.03	4	124	9.99E-01	1.00E+00
Intestinal immune network for IgA production	ko04672	0.03	4	125	9.99E-01	1.00E+00
Natural killer cell mediated cytotoxicity	ko04650	0.04	7	171	1.00E+00	1.00E+00
Asthma	ko05310	0.02	2	103	1.00E+00	1.00E+00
Pancreatic secretion	ko04972	0.02	2	116	1.00E+00	1.00E+00
Neuroactive ligand-receptor interaction	ko04080	0.04	14	313	1.00E+00	1.00E+00
Allograft rejection	ko05330	0.01	1	115	1.00E+00	1.00E+00
Systemic lupus erythematosus	ko05322	0.02	5	207	1.00E+00	1.00E+00
Autoimmune thyroid disease	ko05320	0.01	1	126	1.00E+00	1.00E+00

Appendix G

Changes in host cell gene expression in KEGG pathways enriched for differentially expressed genes. Genes highlighted in cyan are significantly up-regulated upon infection with *T. hominis*, genes in red are down-regulated, and the expression of genes in purple does not significantly change. Genes were assigned to KEGG pathways (Kanehisa & Goto 2000) using the KOBAS annotation pipeline (Xie et al. 2011), and colours representing differential expression were assigned using the KEGG web server (Kanehisa et al. 2014).

OXIDATIVE PHOSPHORYLATION

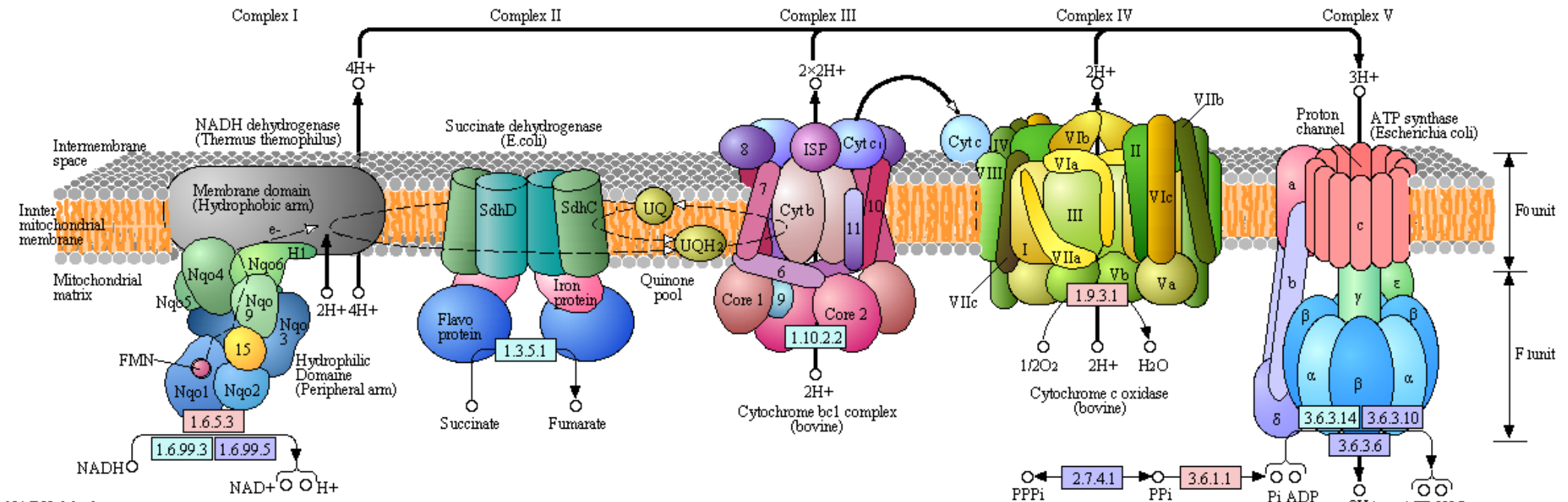

NADH dehydrogenase

E	ND1	ND2	ND3	ND4	ND4L	ND5	ND6										
E	Ndufs1	Ndufs2	Ndufs3	Ndufs4	Ndufs5	Ndufs6	Ndufs7	Ndufs8	Ndufv1	Ndufv2	Ndufv3						
B/A	NuoA	NuoB	NuoC	NuoD	NuoE	NuoF	NuoG	NuoH	NuoI	NuoJ	NuoK	NuoL	NuoM	NuoN			
B/A	NdhC	NdhK	NdhJ	NdhH	NdhA	NdhI	NdhG	NdhE	NdhF	NdhD	NdhB	NdhL	NdhM	NdhN	HoxE	HoxF	HoxU
E	Ndufa1	Ndufa2	Ndufa3	Ndufa4	Ndufa5	Ndufa6	Ndufa7	Ndufa8	Ndufa9	Ndufa10	Ndufab1	Ndufa11	Ndufa12	Ndufa13			
E	Ndufb1	Ndufb2	Ndufb3	Ndufb4	Ndufb5	Ndufb6	Ndufb7	Ndufb8	Ndufb9	Ndufb10	Ndufb11	Ndufc1	Ndufc2				

F-type ATPase (Bacteria)

alpha	beta	gamma	delta	epsilon	
a	b	c			

F-type ATPase (Eukaryotes)

alpha	beta	gamma	delta	epsilon	
OSCP	a	b	c	d	e
f	g	f6/h	j	k	8

Succinate dehydrogenase / Fumarate reductase

E	SDHC	SDHD	SDHA	SDHB	
B/A	SdhC	SdhD	SdhA	SdhB	
			FrdA	FrdB	FrdC	FrdD

Cytochrome c reductase

E/B/A	ISP	Cyt b	Cyt 1							
E				COR1	QCR2	QCR6	QCR7	QCR8	QCR9	QCR10

V/A-type ATPase (Bacteria, Archaeas)

A	B	C	D	E	F	G/H
I	K					

Cytochrome c oxidase

E	COX10		COX3	COX1	COX2	COX4	COX5A	COX5B	COX6A	COX6B	COX6C	COX7A	COX7B	COX7C	COX8	E/B/A
																COX11	COX15	COX17
B/A	CyoE	CyoD	CyoC	CyoB	CyoA													
		CoxD	CoxC	CoxA	CoxB													
		QoxD	QoxC	QoxB	QoxA													

Cytochrome c oxidase , cbb3-type

B	I	II	IV	III

Cytochrome bd complex

B/A	CydA	CydB

V-type ATPase (Eukaryotes)

A	B	C	D	E	F	G	H
a	c	d	e	S1			

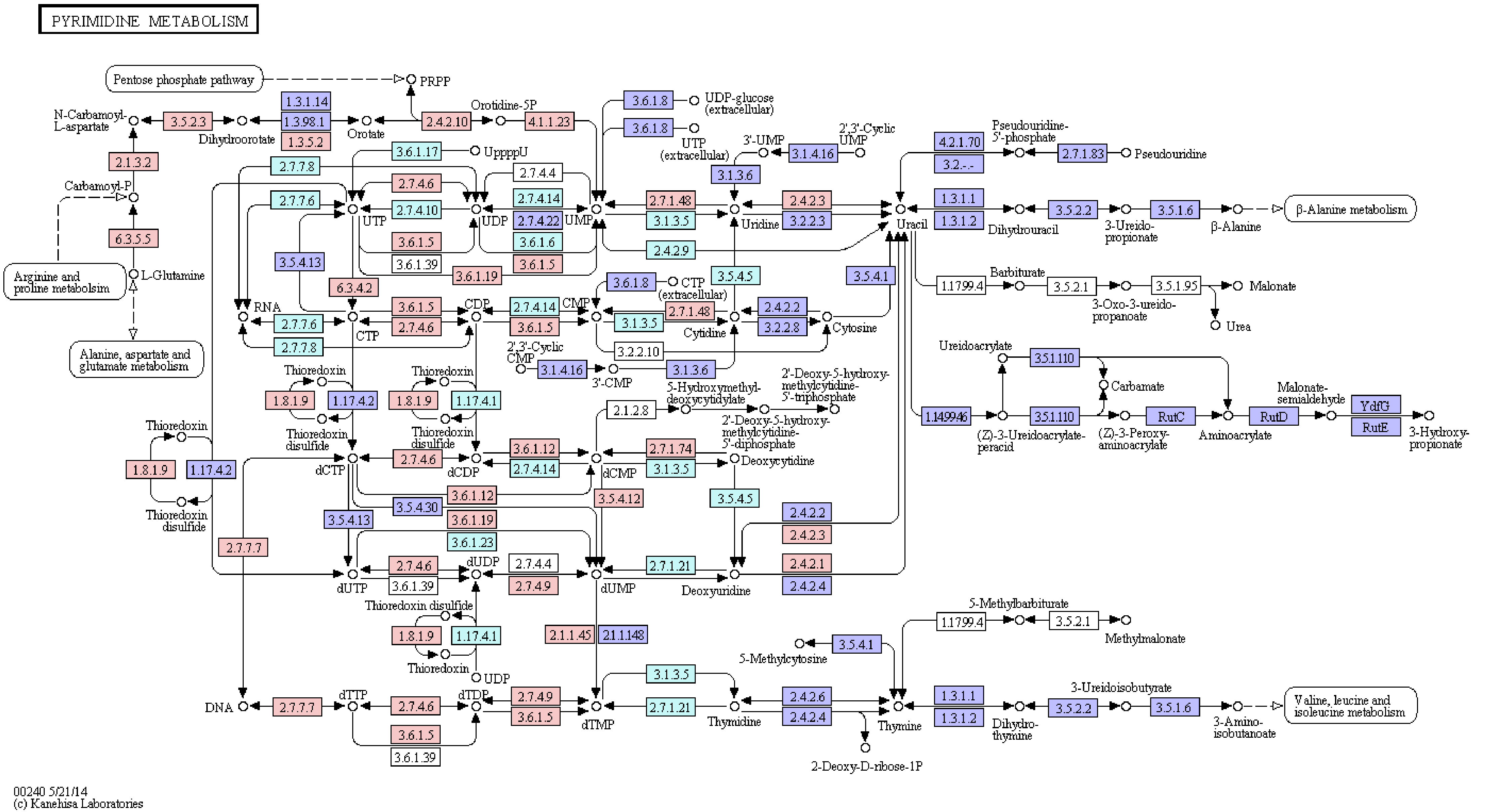
PYRIMIDINE METABOLISM
Pentose phosphate pathway
PRPP
N-Carbamoyl-L-aspartate
3.5.2.3
Dihydroorotate
1.3.1.14
1.3.98.1
1.3.5.2
Orotate
2.4.2.10
Orotidine-5P
4.1.1.23
2.1.3.2
Carbamoyl-P
6.3.5.5
L-Glutamine
Arginine and proline metabolsim
Alanine, aspartate and glutamate metabolism
3.6.1.17
UppppU
2.7.7.8
2.7.4.6
2.7.4.4
2.7.7.6
2.7.4.10
2.7.4.14
2.7.4.22
UTP
UDP
UMP
3.6.1.5
3.6.1.39
3.6.1.19
3.6.1.6
3.6.1.5
3.5.4.13
6.3.4.2
3.6.1.8
UDP-glucose (extracellular)
3.6.1.8
UTP (extracellular)
3'-UMP
3.1.4.16
2',3'-Cyclic UMP
3.1.3.6
2.7.1.48
3.1.3.5
Uridine
2.4.2.3
3.2.2.3
2.4.2.9
Uracil
4.2.1.70
3.2.-.-
Pseudouridine-5'-phosphate
2.7.1.83
Pseudouridine
1.3.1.1
1.3.1.2
Dihydrouracil
3.5.2.2
3-Ureido-propionate
3.5.1.6
β-Alanine
β-Alanine metabolism
RNA
2.7.7.6
2.7.7.8
CTP
3.6.1.5
2.7.4.6
CDP
2.7.4.14
3.6.1.5
CMP
3.6.1.8
CTP (extracellular)
2.7.1.48
3.1.3.5
Cytidine
3.5.4.5
2.4.2.2
3.2.2.8
Cytosine
3.5.4.1
3.2.2.10
2',3'-Cyclic CMP
3.1.4.16
3'-CMP
3.1.3.6
1.17.99.4
Barbiturate
3.5.2.1
3-Oxo-3-ureido-propanoate
3.5.1.95
Malonate
Urea
Ureidoacrylate
3.5.1.110
Carbamate
1.14.99.46
(Z)-3-Ureidoacrylate-peracid
3.5.1.110
(Z)-3-Peroxy-aminoacrylate
RutC
Aminoacrylate
RutD
Malonate-semialdehyde
YdfG
RutE
3-Hydroxy-propionate
Thioredoxin
1.8.1.9
1.17.4.2
Thioredoxin disulfide
Thioredoxin
1.8.1.9
1.17.4.1
Thioredoxin disulfide
5-Hydroxymethyl-deoxycytidylate
2.1.2.8
2'-Deoxy-5-hydroxy-methylcytidine-5'-triphosphate
2'-Deoxy-5-hydroxy-methylcytidine-5'-diphosphate
Thioredoxin
1.8.1.9
1.17.4.2
Thioredoxin disulfide
dCTP
2.7.4.6
dCDP
3.6.1.12
2.7.4.14
dCMP
2.7.1.74
3.1.3.5
Deoxycytidine
3.6.1.12
3.5.4.12
3.5.4.30
3.6.1.19
3.5.4.13
3.5.4.5
2.4.2.2
2.4.2.3
2.7.7.7
3.6.1.23
dUTP
2.7.4.6
3.6.1.39
dUDP
2.7.4.4
2.7.4.9
dUMP
2.7.1.21
Deoxyuridine
2.4.2.1
2.4.2.4
Thioredoxin disulfide
1.8.1.9
1.17.4.1
Thioredoxin
UDP
2.1.1.45
2.1.1.148
5-Methylbarbiturate
1.17.99.4
3.5.2.1
Methylmalonate
5-Methylcytosine
3.5.4.1
DNA
2.7.7.7
dTTP
2.7.4.6
dTDP
2.7.4.9
3.6.1.5
dTMP
3.6.1.5
3.6.1.39
3.1.3.5
2.7.1.21
Thymidine
2.4.2.6
2.4.2.4
2-Deoxy-D-ribose-1P
Thymine
1.3.1.1
1.3.1.2
Dihydro-thymine
3-Ureidoisobutyrate
3.5.2.2
3.5.1.6
3-Amino-isobutanoate
Valine, leucine and isoleucine metabolism
00240 5/21/14
(c) Kanehisa Laboratories

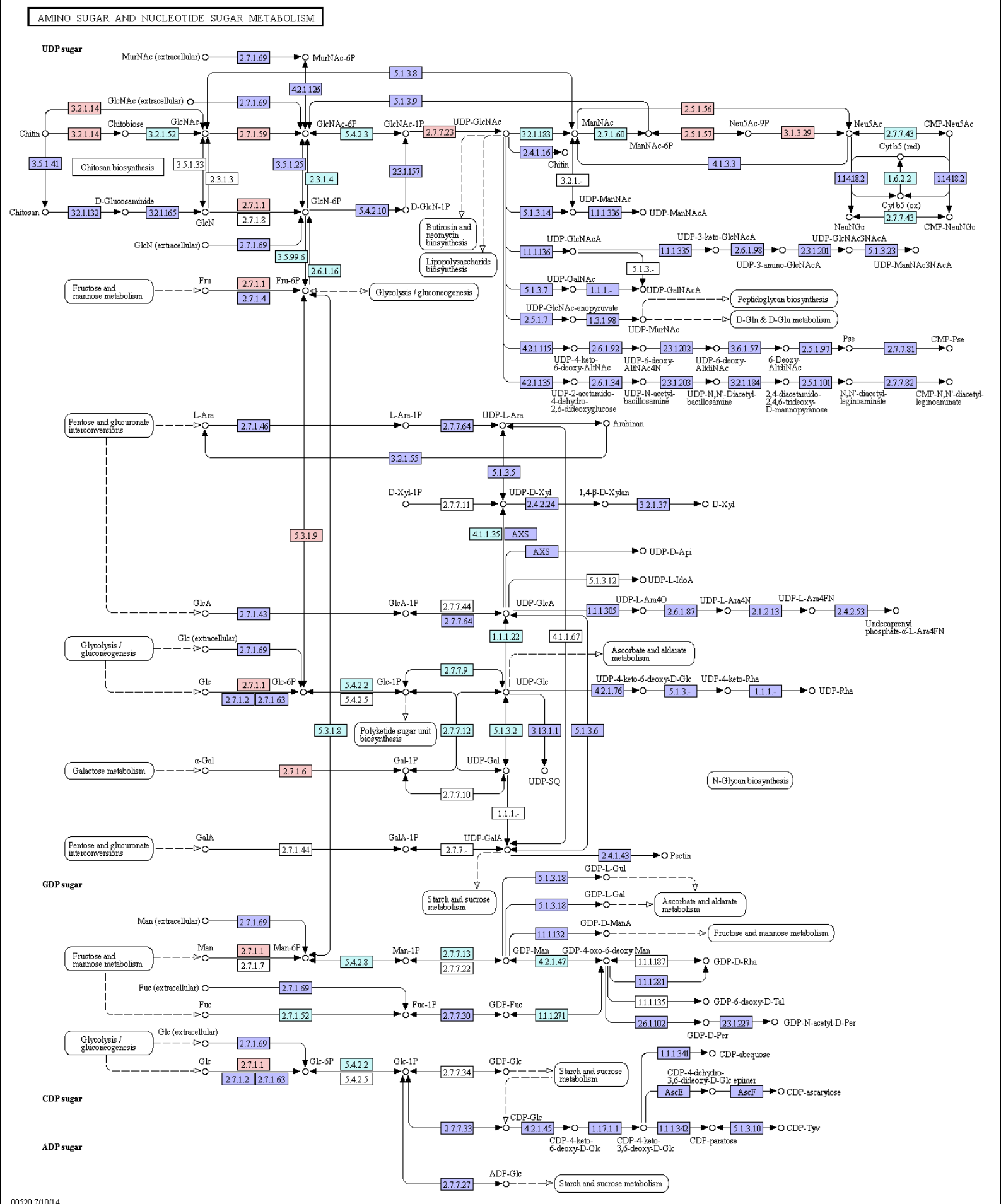
AMINO SUGAR AND NUCLEOTIDE SUGAR METABOLISM
UDP sugar
MurNAc (extracellular)
MurNAc-6P
GlcNAc (extracellular)
Chitobiose
GlcNAc
Chitin
Chitosan biosynthesis
D-Glucosaminide
Chitosan
GlcN
GlcN (extracellular)
GlcNAc-6P
GlcNAc-1P
UDP-GlcNAc
D-GlcN-1P
GlcN-6P
Butirosin and neomycin biosynthesis
Lipopolysaccharide biosynthesis
Fructose and mannose metabolism
Fru
Fru-6P
Glycolysis / gluconeogenesis
ManNAc
ManNAc-6P
Neu5Ac-9P
Neu5Ac
CMP-Neu5Ac
Cytb5 (red)
Cytb5 (ox)
NeuNGc
CMP-NeuNGc
UDP-ManNAc
UDP-ManNAcA
UDP-GlcNAcA
UDP-3-keto-GlcNAcA
UDP-GlcNAc3NAcA
UDP-3-amino-GlcNAcA
UDP-ManNAc3NAcA
UDP-GalNAc
UDP-GalNAcA
Peptidoglycan biosynthesis
UDP-GlcNAc-enopyruvate
UDP-MurNAc
D-Gln & D-Glu metabolism
UDP-4-keto-6-deoxy-AltNAc
UDP-6-deoxy-AltNAc4N
UDP-6-deoxy-AltdiNAc
6-Deoxy-AltdiNAc
Pse
CMP-Pse
UDP-2-acetamido-4-dehydro-2,6-dideoxyglucose
UDP-N-acetyl-bacillosamine
UDP-N,N'-Diacetyl-bacillosamine
2,4-diacetamido-2,4,6-trideoxy-D-mannopyranose
N,N'-diacetyl-leginoaminate
CMP-N,N'-diacetyl-leginoaminate
Pentose and glucuronate interconversions
L-Ara
L-Ara-1P
UDP-L-Ara
Arabinan
D-Xyl-1P
UDP-D-Xyl
1,4-β-D-Xylan
D-Xyl
AXS
UDP-D-Api
UDP-L-IdoA
GlcA
GlcA-1P
UDP-GlcA
UDP-L-Ara4O
UDP-L-Ara4N
UDP-L-Ara4FN
Undecaprenyl phosphate-α-L-Ara4FN
Glycolysis / gluconeogenesis
Glc (extracellular)
Glc
Glc-6P
Glc-1P
UDP-Glc
UDP-4-keto-6-deoxy-D-Glc
UDP-4-keto-Rha
UDP-Rha
Ascorbate and aldarate metabolism
Polyketide sugar unit biosynthesis
Galactose metabolism
α-Gal
Gal-1P
UDP-Gal
UDP-SQ
N-Glycan biosynthesis
Pentose and glucuronate interconversions
GalA
GalA-1P
UDP-GalA
Pectin
GDP sugar
GDP-L-Gul
GDP-L-Gal
Starch and sucrose metabolism
Man (extracellular)
Man
Man-6P
Man-1P
GDP-Man
GDP-4-oxo-6-deoxy Man
GDP-D-ManA
Fructose and mannose metabolism
GDP-D-Rha
Fuc (extracellular)
Fuc
Fuc-1P
GDP-Fuc
GDP-6-deoxy-D-Tal
GDP-N-acetyl-D-Per
GDP-D-Per
CDP sugar
CDP-abequose
CDP-4-dehydro-3,6-dideoxy-D-Glc epimer
AscE
AscF
CDP-ascarylose
CDP-Glc
CDP-4-keto-6-deoxy-D-Glc
CDP-4-keto-3,6-deoxy-D-Glc
CDP-paratose
CDP-Tyv
ADP sugar
ADP-Glc
00520 7/10/14
(c) Kanehisa Laboratories

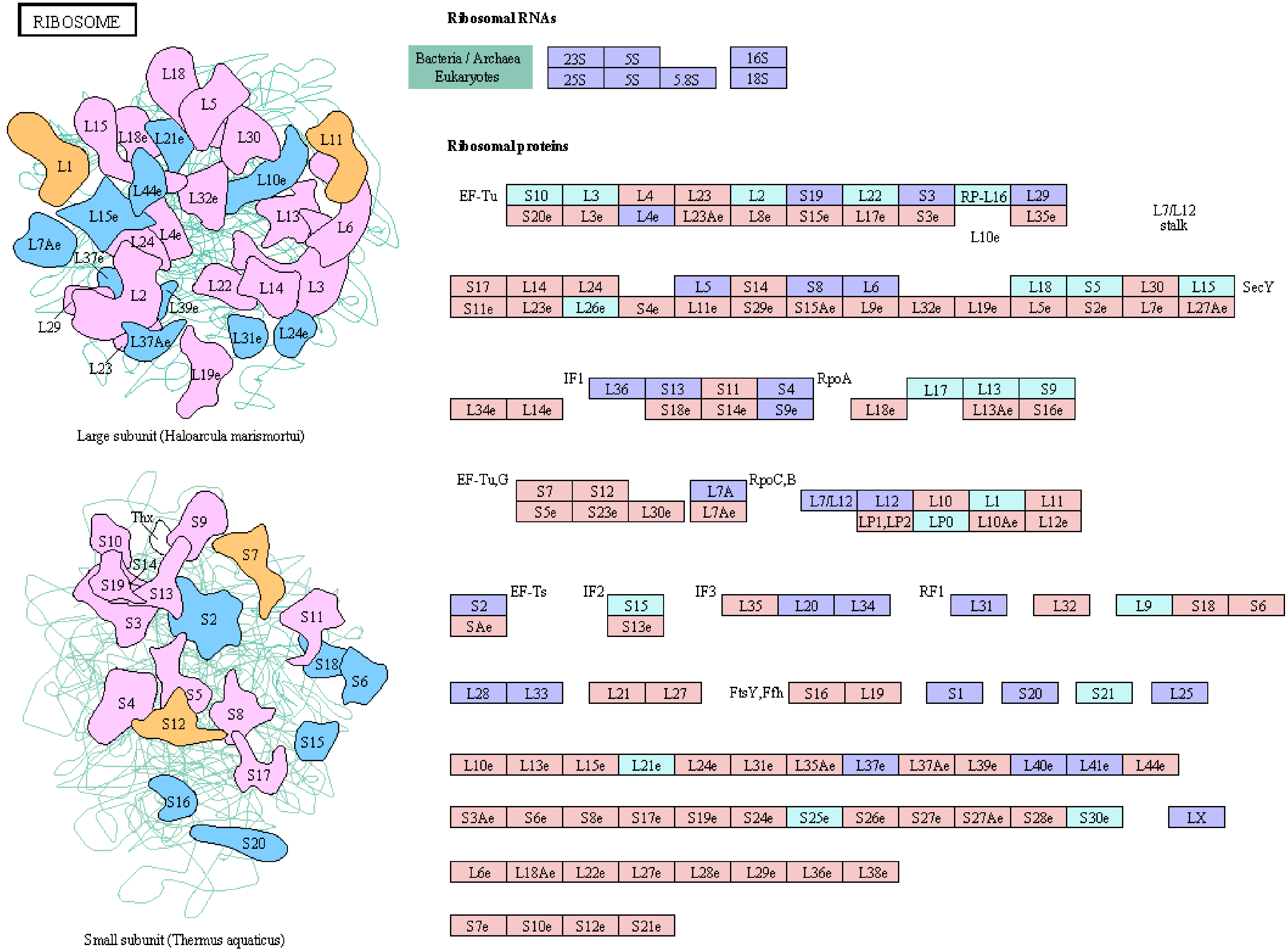

03010 7/29/13

DNA REPLICATION

Replication complex (Prokaryotes)

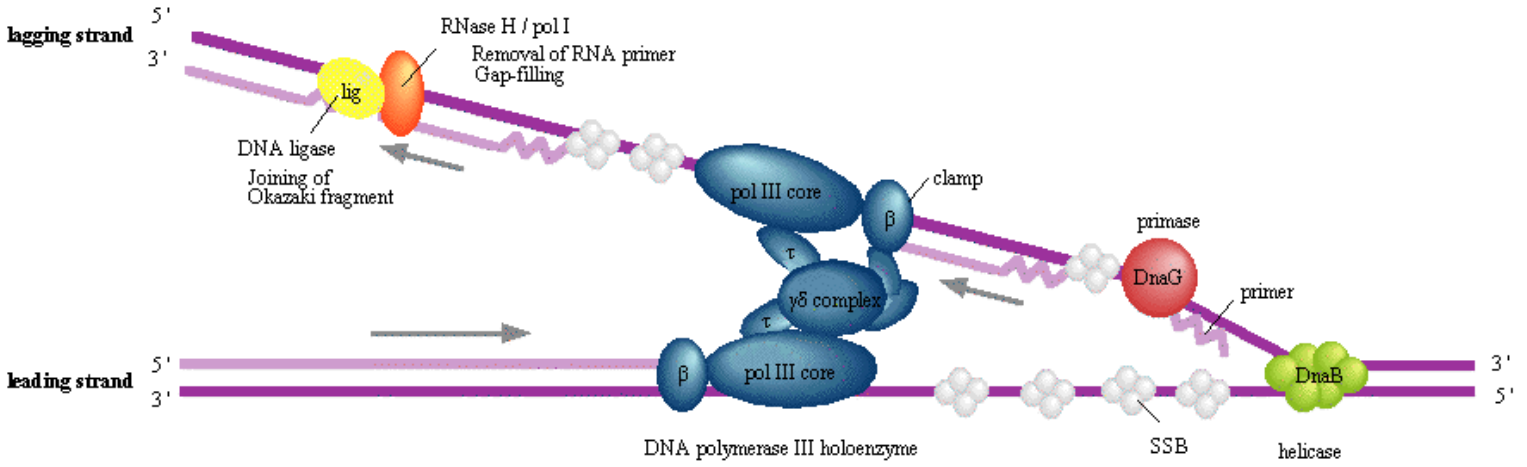

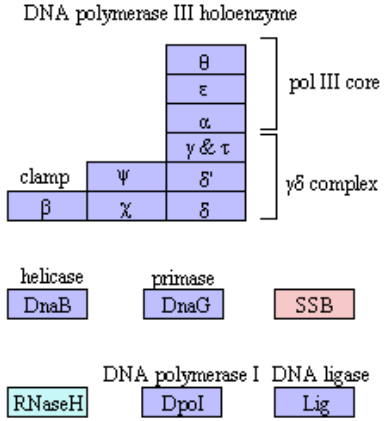

Replication complex (Eukaryotes)

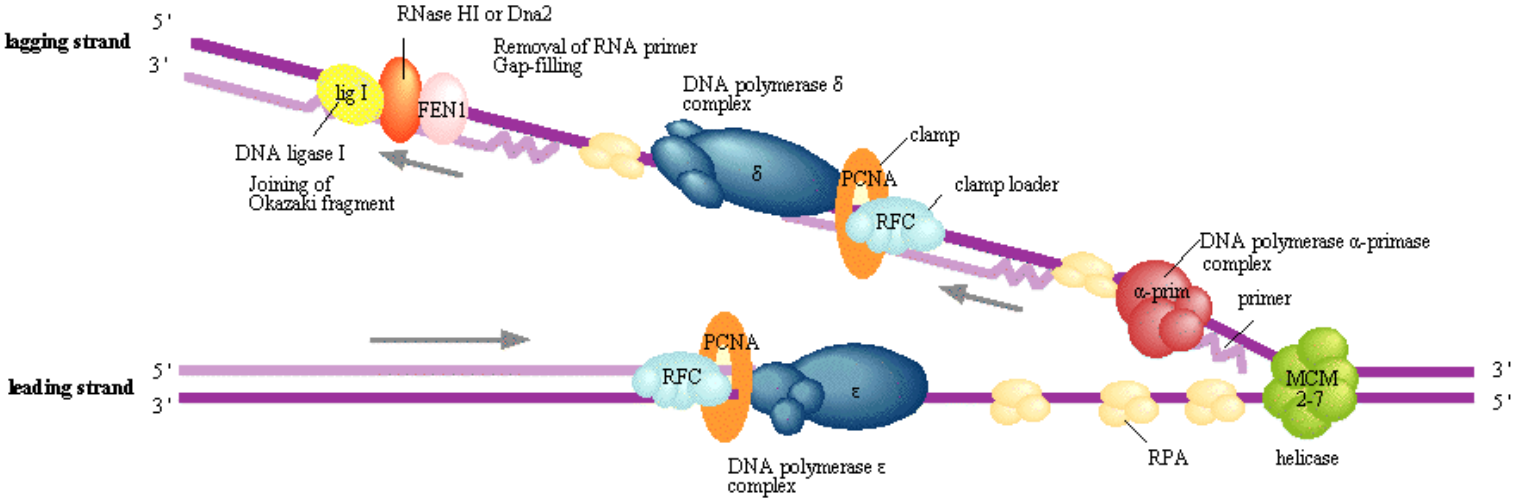

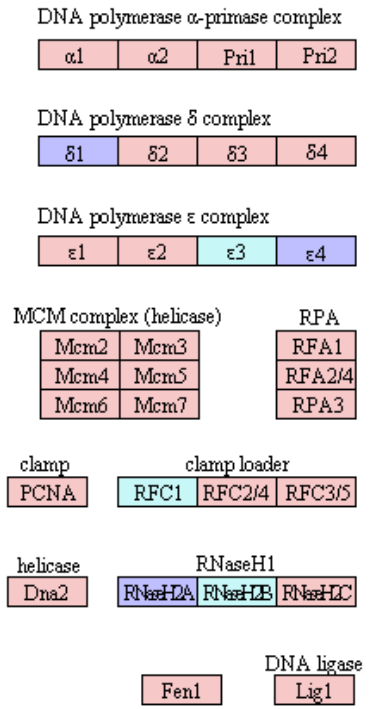

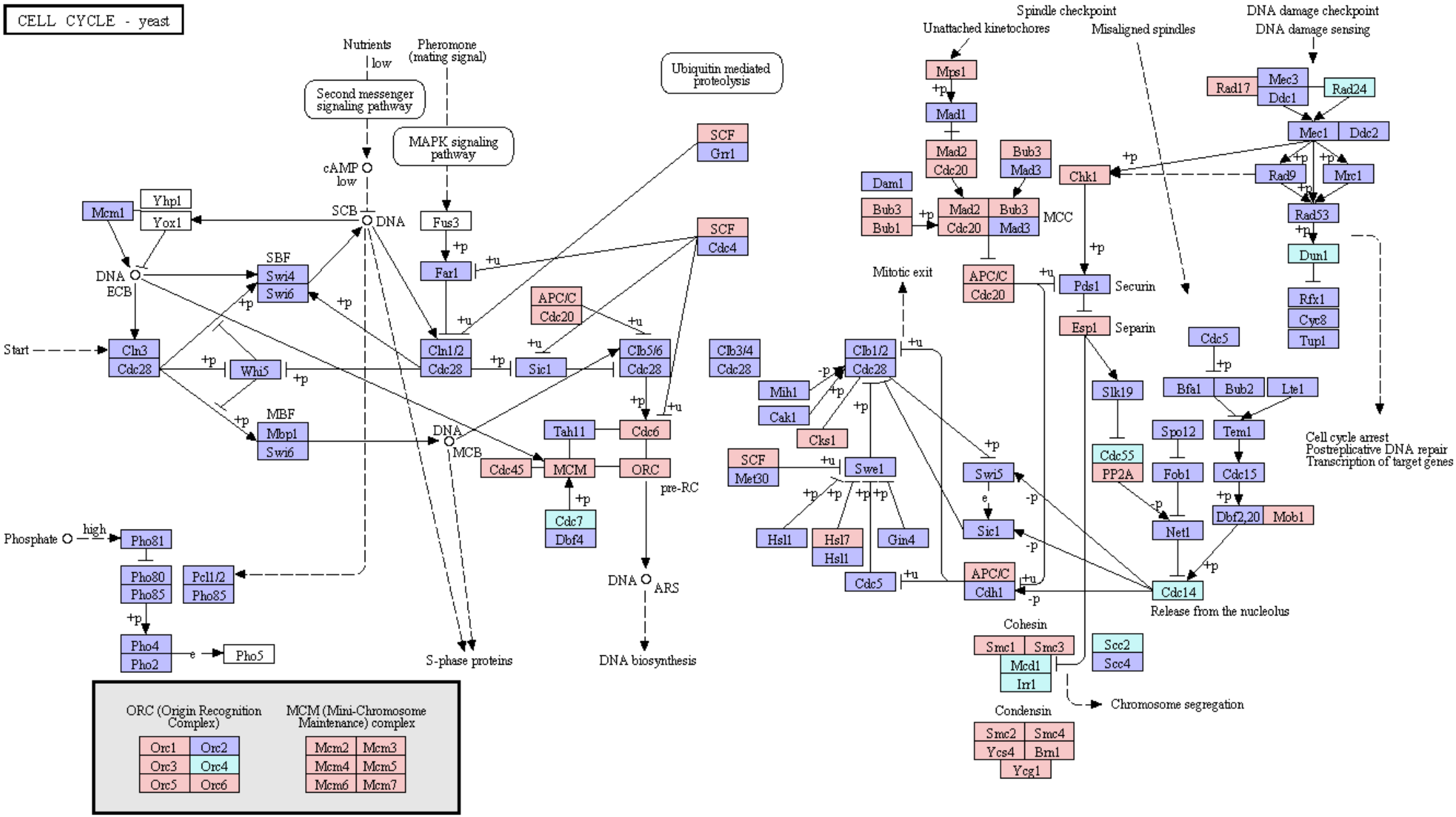

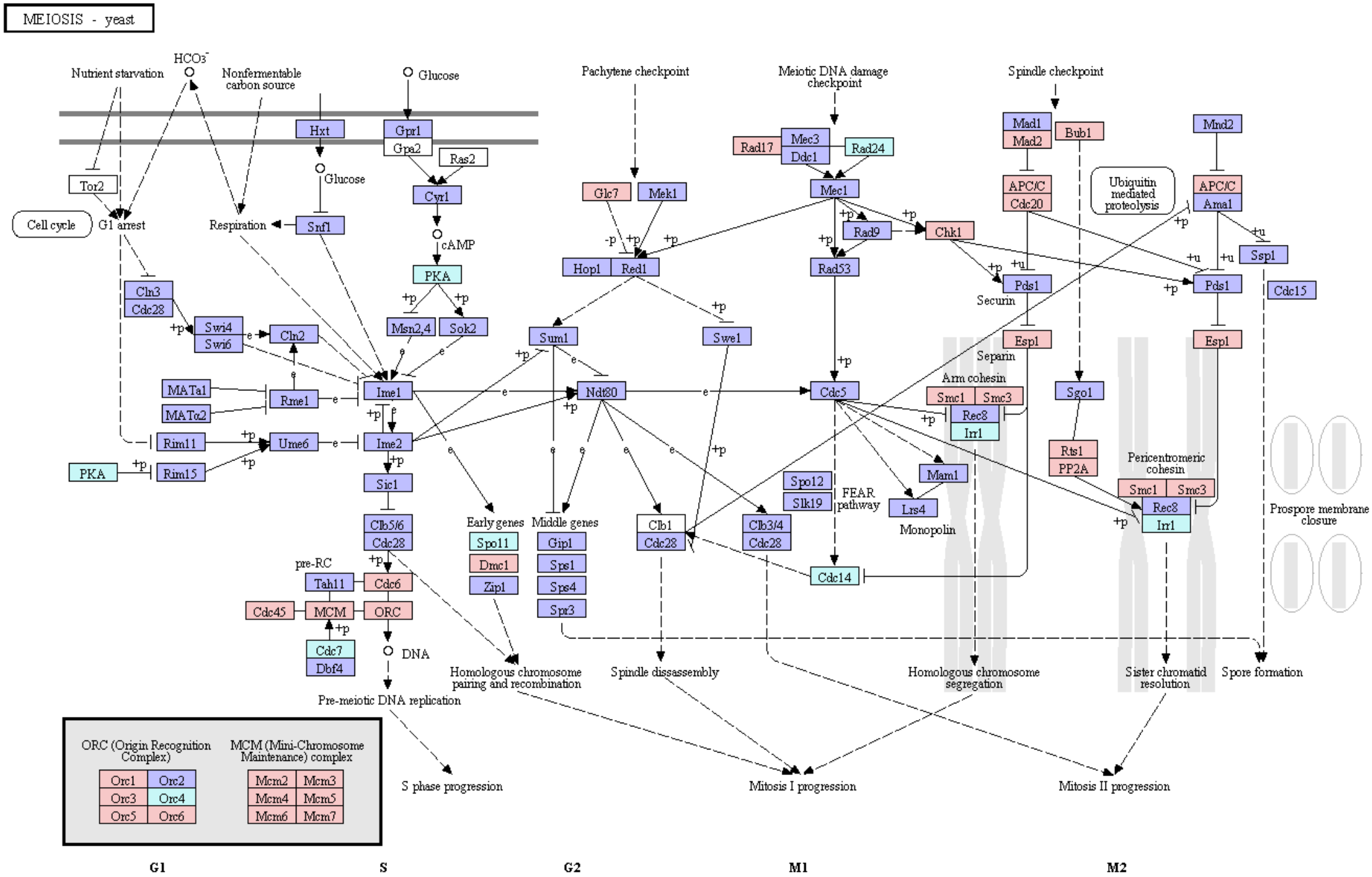
MEIOSIS - yeast
Nutrient starvation
HCO3-
Nonfermentable carbon source
Glucose
Pachytene checkpoint
Meiotic DNA damage checkpoint
Spindle checkpoint
Hxt
Gpr1
Gpa2
Ras2
Glucose
Tor2
Cell cycle
G1 arrest
Respiration
Snf1
Cyr1
cAMP
PKA
Cln3
Cdc28
Swi4
Swi6
Cln2
Msn2,4
Sok2
MATa1
MATα2
Rme1
Ime1
Rim11
Ume6
Ime2
PKA
Rim15
Sic1
Clb5/6
Cdc28
pre-RC
Tah11
Cdc6
Cdc45
MCM
ORC
Cdc7
Dbf4
DNA
Pre-meiotic DNA replication
Glc7
Mek1
Hop1
Red1
Sum1
Swe1
Ndt80
Early genes
Middle genes
Spo11
Dmc1
Zip1
Gip1
Sps1
Sps4
Spr3
Clb1
Cdc28
Clb3/4
Cdc28
Homologous chromosome pairing and recombination
Spindle dissassembly
Rad17
Mec3
Ddc1
Rad24
Mec1
Rad9
Rad53
Chk1
Hop1
Red1
Cdc5
Cdc14
Spo12
Slk19
FEAR pathway
Mam1
Lrs4
Monopolin
Homologous chromosome segregation
Mad1
Mad2
Bub1
APC/C
Cdc20
Ubiquitin mediated proteolysis
Pds1
Securin
Esp1
Separin
Arm cohesin
Smc1
Smc3
Rec8
Irr1
Sgo1
Rts1
PP2A
Pericentromeric cohesin
Mnd2
APC/C
Ama1
Ssp1
Cdc15
Prospore membrane closure
Sister chromatid resolution
Spore formation
ORC (Origin Recognition Complex)
Orc1
Orc2
Orc3
Orc4
Orc5
Orc6
MCM (Mini-Chromosome Maintenance) complex
Mcm2
Mcm3
Mcm4
Mcm5
Mcm6
Mcm7
S phase progression
Mitosis I progression
Mitosis II progression
G1
S
G2
M1
M2
04113 5/13/14
(c) Kanehisa Laboratories

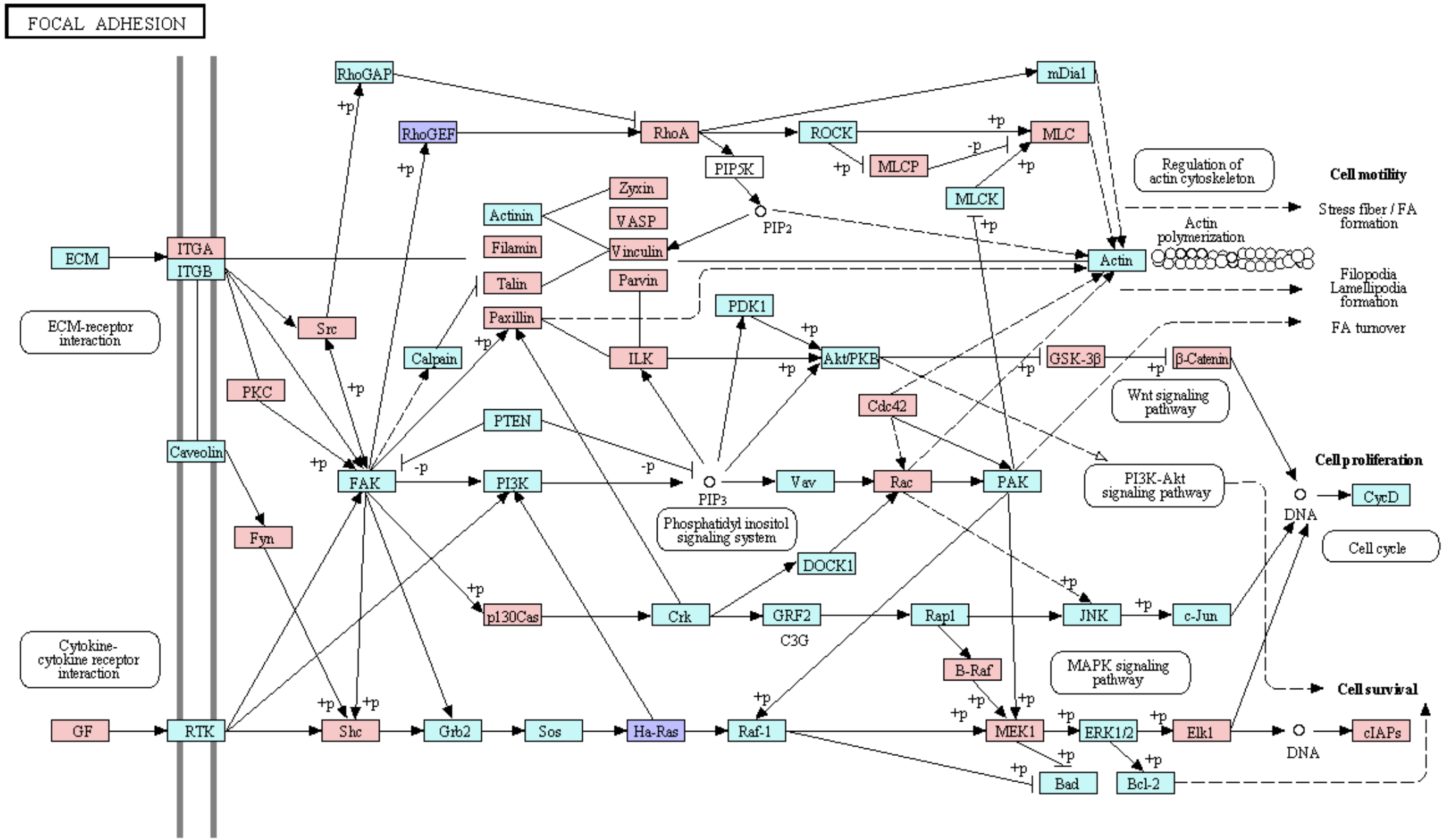

04510 8/8/13

ECM-RECEPTOR INTERACTION

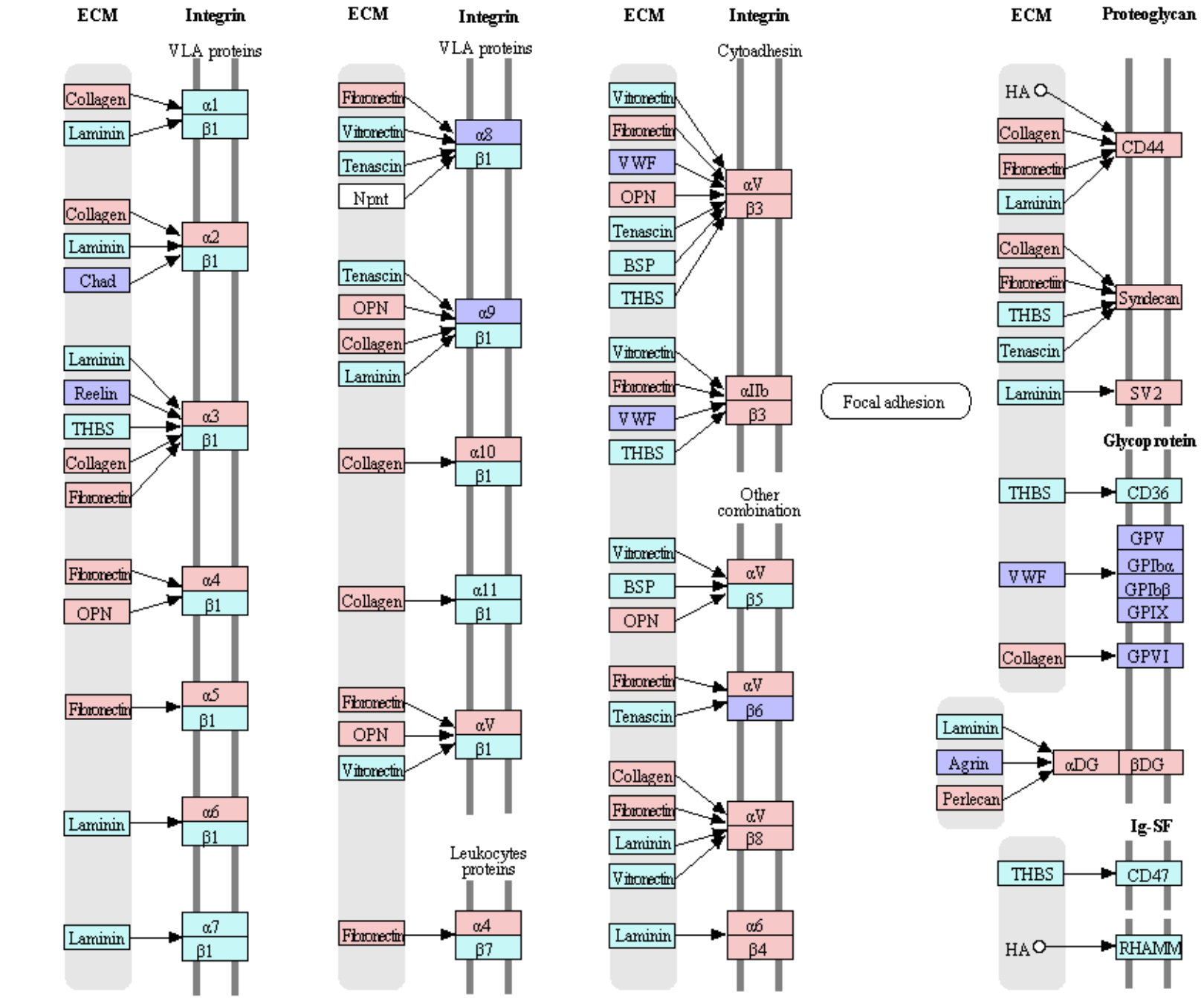

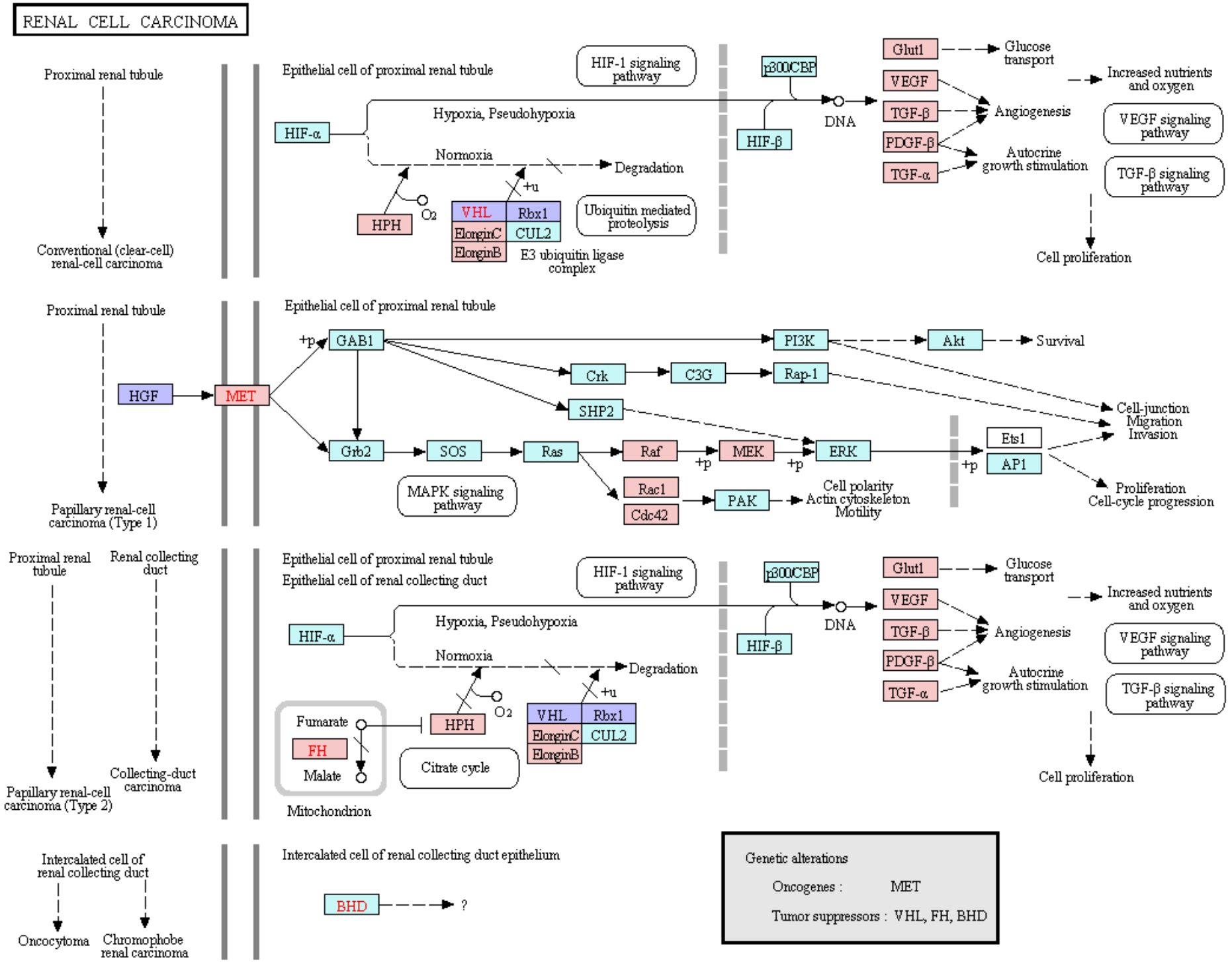
RENAL CELL CARCINOMA
Proximal renal tubule
Conventional (clear-cell) renal-cell carcinoma
Epithelial cell of proximal renal tubule
HIF-1 signaling pathway
HIF-α
Hypoxia, Pseudohypoxia
Normoxia
Degradation
HPH
O2
+u
VHL
Rbx1
ElonginC
CUL2
ElonginB
E3 ubiquitin ligase complex
Ubiquitin mediated proteolysis
p300/CBP
HIF-β
DNA
Glut1
VEGF
TGF-β
PDGF-β
TGF-α
Glucose transport
Angiogenesis
Autocrine growth stimulation
Increased nutrients and oxygen
VEGF signaling pathway
TGF-β signaling pathway
Cell proliferation
Proximal renal tubule
Papillary renal-cell carcinoma (Type 1)
Epithelial cell of proximal renal tubule
HGF
MET
+p
GAB1
PI3K
Akt
Survival
Crk
C3G
Rap-1
SHP2
Cell-junction Migration Invasion
Grb2
SOS
Ras
Raf
MEK
ERK
Ets1
AP1
Proliferation Cell-cycle progression
MAPK signaling pathway
Rac1
Cdc42
PAK
Cell polarity Actin cytoskeleton Motility
Proximal renal tubule
Renal collecting duct
Papillary renal-cell carcinoma (Type 2)
Collecting-duct carcinoma
Epithelial cell of proximal renal tubule
Epithelial cell of renal collecting duct
HIF-1 signaling pathway
HIF-α
Hypoxia, Pseudohypoxia
Normoxia
Degradation
Fumarate
FH
Malate
HPH
O2
+u
VHL
Rbx1
ElonginC
CUL2
ElonginB
Citrate cycle
Mitochondrion
p300/CBP
HIF-β
DNA
Glut1
VEGF
TGF-β
PDGF-β
TGF-α
Glucose transport
Angiogenesis
Autocrine growth stimulation
Increased nutrients and oxygen
VEGF signaling pathway
TGF-β signaling pathway
Cell proliferation
Intercalated cell of renal collecting duct
Oncocytoma
Chromophobe renal carcinoma
Intercalated cell of renal collecting duct epithelium
BHD
?
Genetic alterations
Oncogenes : MET
Tumor suppressors : VHL, FH, BHD
05211 7/24/13
(c) Kanehisa Laboratories